UAB
Universitat Autònoma de Barcelona

Universitat Autònoma de Barcelona

Department of Chemistry

UAB
Universitat Autònoma
de Barcelona

Immobilization of ruthenium complexes on supports. Applications in catalysis

Joel Cejas Sánchez

Doctoral Thesis

PhD in Chemistry

Doctoral Advisors:

Prof. dr. hab. Karol Grela

Prof. dr. Rosa María Sebastián Pérez

Dr. hab. Anna Kajetanowicz

2024

University of Warsaw

Faculty of Chemistry

Immobilization of ruthenium complexes on supports. Applications in catalysis

Joel Cejas Sánchez

Doctoral Thesis
in the Field of Natural Sciences
in the Discipline of Chemical Sciences

Doctoral Advisors:
Prof. dr. hab. Karol Grela
Prof. dr. Rosa María Sebastián Pérez
Dr. hab. Anna Kajetanowicz

2024

Memòria presentada per aspirar al
Grau de Doctor per Joel Cejas Sánchez

Joel Cejas Sánchez

Vist i plau

Prof. dr. Rosa María Sebastián Pérez

Prof. dr. hab. Karol Grela

dr. hab. Anna Kajetanowicz, prof. UW

Oświadczenie kierującego pracą

Oświadczam, że niniejsza praca została przygotowana pod moim kierunkiem i stwierdzam, że spełnia ona warunki do przedstawienia jej w postępowaniu o nadanie stopnia doktora nauk chemicznych w dziedzinie nauk ścisłych i przyrodniczych.

Prof. dr. hab. Karol Grela

Data   Podpis kierującego pracą

Prof. dr. Rosa María Sebastián Pérez

Data   Podpis kierującego pracą

dr. hab. Anna Kajetanowicz, prof. UW

Data   Podpis kierującego pracą

Oświadczenie autora pracy

Świadom odpowiedzialności prawnej oświadczam, że niniejsza rozprawa doktorska została napisana przeze mnie samodzielnie i nie zawiera treści uzyskanych w sposób niezgodny z obowiązującymi przepisami.

Oświadczam również, że przedstawiona praca nie była wcześniej przedmiotem procedur związanych z uzyskaniem stopnia doktora w innej jednostce.

Oświadczam ponadto, że niniejsza wersja pracy jest identyczna z załączoną wersją elektroniczną.
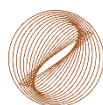
Data   Podpis autora pracą

Acknowledgements

I would like to extend my sincere thanks to the individuals mentioned below for their help and support during the course of this PhD project:

My supervisors, Prof. dr. hab. Karol Grela, Prof. dr. Rosa María Sebastián, and Dr. hab. Anna Kajetanowicz, for accepting me as their PhD student and giving me the great opportunity to pursue this dissertation. Thank you for the guidance, constant support, and critical awareness throughout the process of researching and writing this Thesis. Their expertise and mentorship have been crucial in shaping this work, and I am truly thankful for your commitment to my personal and academic growth.

Dr. Anne-Marie Caminade and Dr. Régis Laurent for their exceptional guidance and support during my stay in Toulouse. Their help significantly contributed to the success of this Thesis. I learned a lot and had a great time working with them in the labs. Thanks for all the valuable advice. I owe much of my success to their wisdom.

Dr. Olaf Hartmann and Jordan Díaz for the invaluable experience I gained during my time at Henkel. Thank you for their endless support, their hospitality, our insightful discussions, and for providing me with the opportunity to learn how the industry works as an insider.

Dr. Jordi Hernando for his consistent support throughout my time in the labs. For all the guidance, his endless patience, and the great atmosphere he creates within the group have made this journey much more enriching.

The CCIMC project and all the colleagues from the network, for creating a helpful and enjoyable experience full of knowledge. A special thanks to the PMT all the ESRs, Paweł, Joris, Irina, Zinnia, Sara, Wimonsiri, Anastasiia, Paven, Chantal, Deepthy, Max, Massimo, Aswin, and Agustín, for all the shared memories, struggles, and fun we had every place we met.

This PhD would not have been the same without all the "travel madness," where I had the chance to work and live in four different countries and to meet amazing people all the way. This is dedicated to all of you.

To the colleagues (and ex-colleagues) I had the opportunity to share a lab with, thank you for all the fruitful cooperation, the fun, great conversations, and the many drinks and memories together. Adri, Alba, Albert, Aleix, Amanda, Anastasiia, Arnau, Axel, Batten, Carolina, Cris, Dani, David, Ferran, Granados, Jaume, Kevin, Laura, Marc G., Marc V., Massimo and Ming from UAB; and Adam, Adrian, Agata, Anna, Błażej, Kasia, Kuba, Jannick, Louis, Łukasz G., Łukasz S., Magda, Maria,

Keywords

Ru-NHC complexes, Ru(p-cymene) complexes, Phosphorus dendrimers, Metal-Organic Frameworks, Immobilization, Supported catalysis, Olefin metathesis

Thesis Title in Polish

Immobilizacja kompleksów rutenu na nośnikach. Zastosowania w katalizie

Thesis Title in Catalan

Immobilització de complexos de ruteni en suports. Aplicacions en catàlisi

Thesis Title in Spanish

Inmovilización de complejos de rutenio en soportes. Aplicaciones en catálisis

Abstract

Immobilized catalysts play a key role in advancing modern and sustainable chemistry, by means of anchoring a catalyst onto supports to facilitate its recovery, recycling, and reuse. This approach offers several advantages, including the potential for enhanced catalyst activity, ease of handling and recovery through straightforward procedures, and the ability to reduce metal contamination in the final products. With the ultimate goal of obtaining novel supported ruthenium complexes for their application in catalytic reactions, this Thesis has focused on the development of poly-phosphorhydrazone-based (PPH) Janus dendrimers for grafting Ru-complexes and their applications in catalysis; and the preparation of novel Ru-NHC complexes and their immobilization on dendrimers and MOFs for olefin metathesis catalysis.

The development and synthesis optimization of PPH Janus dendrimers through a novel click-triazole alternative have been performed. This process included the selective modification of the dendrimer surface by incorporating PEG functionalities to induce solubility in water as well as the anchoring of Ru(p-cymene) complex. The resulting Janus dendrimer has been tested for the isomerization of allyl alcohols, and its catalytic performance has been compared to model monometallic and bimetallic complexes. The Ru@dendrimer showed good results in both THF and n-heptane/H$_2$O solvent mixtures, with particular interest in the latest case. Remarkably, a positive dendritic effect was observed for the biphasic system, where the dendrimeric catalyst showed a clear improvement in the performance when compared to the model analogues. Furthermore, the tests on the recyclability and reusability of the Ru@dendrimer demonstrated the possibility of using the system for up to three consecutive runs, displaying minimal ruthenium contamination in the final product.

Additionally, this Thesis has targeted the development of new ruthenium complexes for olefin metathesis catalysis. Two novel Ru-NHC complexes bearing 4-hydroxybenzyl groups in the NHC were successfully developed and tested in a model RCM reaction, showing good outcomes. Attempts to immobilize these Ru-NHC complexes on Janus dendrimers were made. However, due to unfavorable side reactions and a lack of reactivity, the focus shifted to incorporating these Ru-NHC complexes on MOF **(Al)MIL-101-NH$_2$**. The synthesis of the Ru@MOF system proved highly effective, with almost quantitative adsorption of the complex on the support and relatively low leaching. The resulting Ru@MOF was examined for the RCM of various substrates, demonstrating effective catalysis of this novel heterogeneous system, and providing proof-of-concept for the first reported case of catalyst immobilization through phenol/MOF interactions.

Abstract in Polish

Immobilizowane katalizatory odgrywają kluczową rolę w rozwoju nowoczesnej i równoważonej chemii, poprzez zakotwiczenie katalizatora na nośnikach w celu ułatwienia jego odzysku, recyklingu i ponownego użycia. Podejście to oferuje szereg korzyści, w tym potencjał zwiększonej aktywności katalizatora, łatwość użycia i odzyskiwania za pomocą prostych procedur oraz możliwość zmniejszenia zanieczyszczenia metalami w produktach końcowych. Mając na celu opracowanie nowych immobilizowanych kompleksów rutenu i ich zastosowanie w reakcjach katalitycznych, niniejsza rozprawa koncentruje się na opracowaniu dendrymerów Janus na bazie polifosforohydrazonu (PPH) do osadzania kompleksów Ru i ich zastosowania w katalizie; oraz na przygotowaniu nowych kompleksów Ru-NHC i ich immobilizacji na dendrymerach i MOF wykorzystywanych w reakcjach metatezy olefin.

Przeprowadzono optymalizację syntezy dendrymerów Janusa opartych na PPH poprzez nowatorską alternatywną reakcję klik z wykorzystaniem triazolu. Proces ten obejmował selektywną modyfikację powierzchni dendrymeru poprzez włączenie funkcjonalności PEG w celu zwiększenia rozpuszczalności w wodzie, a także zakotwiczenie kompleksów Ru(p-cymen). Powstały dendrymer Janusa został przetestowany pod kątem izomeryzacji alkoholi allilowych, a jego wydajność katalityczną porównano z modelowymi kompleksami mono- i bimetalicznymi. Ru@dendrymer wykazał dobre wyniki zarówno w THF, jak i mieszaninach rozpuszczalników n-heptan/H_2O, szczególnie interesujący był ostatni przypadek. Co ciekawe, pozytywny efekt dendrytyczny zaobserwowano dla układu dwufazowego, w którym katalizator osadzony na dendrymerze wykazał wyraźną poprawę wydajności w porównaniu z homogenicznymi analogami. Co więcej, testy dotyczące możliwości recyklingu i ponownego użycia Ru@dendrymer wykazały możliwość wykorzystania systemu do trzech kolejnych cykli, wykazując minimalne zanieczyszczenie rutenem w produkcie końcowym.

Dodatkowo, niniejsza rozprawa dotyczyła rozwoju kompleksów rutenu używanych w reakcjach metatezy olefin. Dwa nowe kompleksy Ru-NHC zawierające grupy hydroksybenzylowe w NHC zostały pomyślnie otrzymane i przetestowane w modelowej reakcji RCM, wykazując dobre wyniki. Podjęto próby osadzenia kompleksów Ru-NHC na dendrymerach Janusa. Jednak ze względu na niekorzystne reakcje uboczne i brak reaktywności, skupiono się na immobilizacji tych kompleksów na MOFie **(Al)MIL-101-NH₂**. Synteza katalizatora Ru@MOF okazała się wysoce skuteczna, z niemal ilościową adsorpcją kompleksu na nośniku i stosunkowo niskim wymywaniem katalizatora ze złoża. Powstały Ru@MOF został zbadany w reakcjach RCM różnych substratów, wykazując wysoką aktywność nowego heterogenicznego układu, co potwierdzało słuszność założenia, że immobilizacji katalizatora poprzez interakcje fenol/MOF jest możliwa.

Abstract in Catalan

La immobilització de catalitzadors juga un paper clau en l'avanç de la química moderna i sostenible, mitjançant l'ancoratge d'un catalitzador en suports per a facilitar la seva recuperació i reutilització. Aquesta metodologia ofereix diversos avantatges, incloent-hi el potencial per a millorar l'activitat del catalitzador, una major facilitat de manipulació i recuperació, i la capacitat de reduir la contaminació de metalls en els productes finals. Amb l'objectiu final de desenvolupar nous complexos de ruteni immobilitzats, aquesta Tesi s'ha centrat en el desenvolupament de dendrímers Janus basats en polifosforhidrazona (PPH) i MOFs com a suports per a l'ancoratge de complexos de ruteni, i les seves aplicacions en catàlisi per la metàtesi d'olefines i la isomerització d'alcohols al·lílics.

S'ha dut a terme el desenvolupament i l'optimització de la síntesi de dendrímers Janus PPH, a través d'una nova alternativa d'acoblament de dendrons a través d'una reacció clic-triazol. Aquest procés ha inclòs la modificació selectiva de la superfície del dendrímer mitjançant la incorporació de funcions PEG per a induir la solubilitat en aigua, així com l'ancoratge de complexos tipus Ru(p-cumè). El dendrímer Janus resultant ha estat utilitzat en catàlisi per a la isomerització d'alcohols al·lílics, i el seu rendiment s'ha comparat amb complexos monometàl·lics i bimetàl·lics model. El Ru@dendrímer ha mostrat bons resultats tant en THF com en la mescla H_2O/n-heptà. Cal destacar que s'ha observat un efecte dendrític positiu en el sistema bifàsic, on el dendrímer ha mostrat una millora clara en el rendiment en comparació amb els anàlegs model. A més, les proves de reciclatge i reutilització del Ru@dendrímer han demostrat la possibilitat d'utilitzar aquest sistema fins a tres cicles de manera consecutiva, mostrant una contaminació mínima de ruteni en el producte final.

Altrament, aquesta Tesi s'ha centrat també en el desenvolupament de complexos de ruteni com a catalitzadors de metàtesi d'olefines. S'han sintetitzat amb èxit dos nous complexos Ru-NHC amb grups fenòlics en el lligand NHC, i s'han provat en catàlisi per a una reacció model de RCM, tot mostrant bons resultats. S'han realitzat intents per a immobilitzar aquests complexos Ru-NHC en dendrímers Janus, desafortunadament sense èxit. No obstant això, la immobilització d'aquests complexos de ruteni també s'ha provat en un MOF **(Al)MIL-101-NH₂**. La síntesi d'un Ru@MOF ha resultat ser molt efectiva, amb una adsorció gairebé quantitativa i una desorció relativament baixa. El sistema Ru@MOF s'ha fet servir com a catalitzador per a la RCM de diversos substrats, demostrant una bona eficiència d'aquest sistema heterogeni, i proporcionant una prova de concepte per al primer exemple d'immobilització d'un catalitzador mitjançant interaccions fenol/MOF.

Abstract in Spanish

La inmovilización de catalizadores juega un papel clave en el avance de la química moderna y sostenible, mediante el anclaje de un catalizador en soportes para facilitar su recuperación y reutilización. Este enfoque ofrece varias ventajas, incluyendo el potencial para mejorar la actividad del catalizador, una mayor facilidad de manipulación y recuperación, y la capacidad de reducir la contaminación de metales en los productos finales. Con el objetivo final de desarrollar nuevos complejos de rutenio inmovilizados, esta Tesis se ha centrado en el desarrollo de dendrímeros Janus basados en polifosforhidrazona (PPH) y MOFs como soportes para el anclaje de complejos de rutenio, y su aplicación en catálisis en procesos de metátesis de olefinas y la isomerización de alcoholes alílicos.

Se ha llevado a cabo el desarrollo y la optimización de la síntesis de dendrímeros Janus PPH, a través de una nueva alternativa de ensamblaje de dendrones a través de una reacción clic-triazol. Este proceso ha incluido la modificación selectiva de la superficie del dendrímero mediante la incorporación de funciones PEG para inducir la solubilidad en agua, así como el anclaje de complejos tipo Ru(p-cumeno). El dendrímero Janus resultante ha sido probado en catálisis para la isomerización de alcoholes alílicos, y su rendimiento se ha comparado con complejos monometálicos y bimetálicos modelo. El Ru@dendrímero ha mostrado buenos resultados tanto en THF como en la mezcla H_2O/n-heptano. Cabe destacar que se ha observado un efecto dendrítico positivo en el sistema bifásico, donde el dendrímero ha mostrado una mejora clara en el rendimiento en comparación con los análogos modelo. Además, las pruebas de reciclaje y reutilización del Ru@dendrímero han demostrado la posibilidad de utilizar dicho sistema hasta en tres ciclos de forma consecutiva, mostrando una contaminación de rutenio mínima en el producto final.

Además, esta Tesis se ha centrado también en el desarrollo de complejos de rutenio como catalizadores de la metátesis de olefinas. Se han sintetizado con éxito dos nuevos complejos Ru-NHC con grupos fenólicos en el ligando NHC, y se han probado en catálisis para una reacción modelo de RCM, mostrando buenos resultados. Se han realizado intentos para inmovilizar estos complejos Ru-NHC en dendrímeros Janus, desafortunadamente sin éxito. Sin embargo, la inmovilización de dichos complejos de rutenio también se ha probado en un MOF **(Al)MIL-101-NH₂**. La síntesis del Ru@MOF ha resultado ser altamente efectiva, con una adsorción casi cuantitativa y una desorción relativamente baja. El sistema Ru@MOF se ha usado como catalizador para la RCM de varios sustratos, demostrando una buena eficiencia de este sistema heterogéneo, y proporcionando una prueba de concepto para el primer caso de inmovilización de un catalizador mediante interacciones fenol/MOF.

List of Publications

The present Thesis has led to the following publications:

[1] A water-soluble polyphosphorhydrazone Janus dendrimer built by "click" chemistry as support for Ru-complexes in catalysis
Cejas-Sánchez, J.; Caminade, A.-M.; Kajetanowicz, A.; Grela, K.; Sebastián, R.M. *Dalton Trans.* **December 2023**, Submitted.

[2] Strategies for the Preparation of Phosphorus Janus Dendrimers and Their Properties
Cejas-Sánchez, J.; Kajetanowicz, A.; Grela, K.; Caminade, A.-M.; Sebastián, R.M. *Molecules* **2023**, *28*, 5570-5588.

[3] Synthesis of Phenol-Tagged Ruthenium Alkylidene Olefin Metathesis Catalysts for Robust Immobilisation Inside Metal–Organic Framework Support
Nadirova, M.; Cejas-Sánchez, J.; Sebastián, R.M.; Wiszniewski, M.; Chmielewski, M.J.; Kajetanowicz, A.; Grela, K. *Catalysts* **2023**, *13*, 297-309.

Publications by the author not represented in this Thesis:

[4] Synthesis and Catalytic Properties of a Very Latent Selenium-Chelated Ruthenium Benzylidene Olefin Metathesis Catalyst
Monsigny, L.; Cejas-Sánchez J.; Piątkowski, J.; Kajetanowicz, A.; Grela, K. *Organometallics* **2021**, *40*, 3608–3616.

List of Conference contributions

[1] Cutting-Edge Homogeneous Catalysis 1 (CEHC-1)

4th – 6th May 2021; Laboratoire de Chimie de Coordination CNRS, Toulouse, France (online).

Poster presentation: "Immobilization of N-heterocyclic carbene ligands on Janus dendrimers. Catalysis in green solvents".

[2] Interdisciplinary Conference I – PhD Studies in Chemistry UW

10th – 13th October 2021; European Geological Education Center, Chęciny, Poland.

Flash presentation: "Immobilization of N-heterocyclic carbene ligands on Janus dendrimers. Catalysis in green solvents".

[3] 4th GDRI-HC3A Meeting. Heteroelements and Coordination Chemistry: From Concepts to Applications

20th – 21st January 2022; Universitat de Barcelona, Barcelona, Spain.

Poster presentation: "In the way to prepare Janus dendrimers surface modified with ruthenium-NHC complexes for olefin metathesis catalysis in sustainable solvents".

[4] Cutting-Edge Homogeneous Catalysis 2 (CEHC-2)

29th – 31st March 2022; University of Leipzig, Leipzig, Germany.

Poster presentation and flash presentation: "Modified dendrimers for olefin metathesis catalysis in green solvents".

[5] International School on Innovations in Homogeneous and Supported Homogeneous Catalysis (ISI-HSHC)

25th – 28th April 2023; University of Bucharest, Bucharest, Romania.

Poster presentation: Synthesis of phosphorus dendrimers for applications in green solvent catalysis".

Oral communication: "My Thesis in 180 seconds".

[6] Doctoral Workshop of the PhD programme in Chemistry UAB

29th – 30th June and 2nd July 2023; Universitat Autònoma de Barcelona, Bellaterra, Spain.

Poster presentation and oral communication: "Synthesis of phosphorus dendrimers for applications in green solvent catalysis".

Table of Contents

List of Abbreviations

ADMET	Acyclic diene metathesis polymerization
anh.	Anhydrous
API(s)	Active Pharmaceutical Ingredient(s)
BET	Brunauer, Emmett, and Teller
Boc	*Tert*-butyloxycarbonyl
br	Broad
c	Concentration
ca.	*Circa*
calcd.	Calculated
cat.	Catalytic
CM	Cross Metathesis
COD	Cyclooctadiene
Cp	Cyclopentadienyl
Cy	Cyclohexane, cyclohexyl
°	Degree
δ	Chemical Shift (in NMR spectroscopy)
d	Doublet
DCM	Dichloromethane
DEDAM	Diethyl diallylmalonate
DIPEA	*N,N*-Diisopropylethylamine
DIPP	2,6-Diisopropylphenyl
DMF	*N,N*-Dimethylformamide
DMSO	Dimethyl sulfoxide
DNA	Deoxyribonucleic acid
dd	Doublet of doublets
ddd	Doublet of doublets of doublets
dt	Doublet of triplets
e.g.	*exempli gratia*, for example
equiv.	Equivalent(s)
ESI	Electrospray ionization
Et al.	*Et alii*
G	Generation(s) – for dendrimer chemistry
g	Gram(s)
GC	Gas chromatography

Gru	Grubbs-type catalyst
h	Hour(s)
Hov	Hoveyda-type catalyst
HR-MS	High-resolution mass spectrometry
Hz	Hertz [cm^{-1}]
I / I'	First-generation (associated with Ru-complexes for OM)
ICP	Inductively coupled plasma
II / II'	Second generation (associated with Ru-complexes for OM)
IMes	1,3-Bis(2,4,6-trimethylphenyl)-imidazol-2-ylidene
Ind	Indenylidene-type complex
*i*Pr	Isopropyl
IPr	1,3-Bis(2,6-diisopropylphenyl)imidazol-2-ylidine
IR	Infrared
J	Coupling constant
L	Ligand
LiHMDS	Lithium bis(trimethylsilyl)amide
m	*meta*
m	Multiplet
MDM	Model dendrimer molecule
Mes	Mesityl
mg	Milligram(s)
mmol	Millimol(s)
MOF(s)	Metal-Organic Framework(s)
M.p.	Melting point
NHC(s)	N-heterocyclic carbene(s)
nm	Nanometer
NMR	Nuclear Magnetic Resonance
o	*orto*
OM	Olefin metathesis
OTs	*p*-Toluenesulfonate
p	*para*
PAMAM	Poly(amido)amine
PBzE	Poly(benzyl)ether
PEA	Poly(ether amide)
PEG	Polyethylene glycol
Ph	Phenyl

PPH	Polyphosphorhydrazone
PPh$_3$	Triphenylphosphine
PPI	Poly(propylamine)
ppm	Parts per million
PS-DVB	Poly(styrene-divinyl benzene)
PXRD	Powder X-Ray diffraction
q	Quartet
quin	Quintet
R	Substituent
RCM	Ring-closing metathesis
ROCM	Ring-opening cross metathesis
ROMP	Ring-opening metathesis polymerization
RT	Room temperature
s	Singlet
scCO$_2$	Supercritical carbon dioxide
sept	Septet
SIMes	1,3-Bis(2,4,6-trimethylphenyl)-imidazoline-2-ylidene
SIPr	1,3-Bis(2,6-diisopropylphenyl)imidazoline-2-ylidine
t	Triplet , time
TBAF	Tetrabutylammonium fluoride
TBDMS	*Tert*-butyldimethylsilyl
TBTU	*O*-(benzotriazol-1-yl)-1,1,3,3-tetramethyluronium tetrafluoroborate
*t*Bu	*Tert*-butyl
TFA	Trifluoroacetic acid
THF	Tetrahydrofuran
TLC	Thin layer chromatography
TMS	Trimethylsilane
TMSCl	Trimethylsilyl chloride
uNHC(s)	Unsymmetrical N-heterocyclic carbene(s)
UV-Vis	Ultraviolet-Visible

Goal

This PhD Thesis is part of the "Coordination Chemistry Inspires Molecular Catalysis" (CCIMC) project, a European Union-funded European Joint Doctorate network seeking for the implementation of cutting-edge molecular catalysis. The primary objective of this network is to push the boundaries of knowledge in coordination chemistry by introducing innovative ligand designs, exploring novel approaches to pre-catalyst development, and implementing catalytic processes. In the frame of CCIMC project, this work seeks to contribute to the broader goals of the network by conducting a study on the development of new catalytic systems through the immobilization of new-fashioned metal pre-catalysts within specific supports. The study of both homogeneous and heterogeneous systems is targeted in this Thesis, with the purpose to afford new methodologies to improve the efficiency of the selected catalytic processes.

Bearing the previous approach in mind, one of the key objectives of this dissertation is the development of phosphorus Janus dendrimers as innovative catalyst supports. These novel dendrimers are expected to bridge the gap between homogeneous and heterogeneous catalysis, leading to the synthesis of a system that would behave as a homogeneous catalyst but possessing the recoverability and reusability possibilities of a heterogeneous approach. Specifically, this project aims to immobilize Ru-NHC olefin metathesis pre-catalysts onto the structure of phosphorus Janus dendrimers for applications in environmentally friendly solvents such as water. To achieve this, novel ruthenium complexes with unsymmetrical NHC ligands are synthesized, incorporating functionalities that enable their coupling to phosphorus Janus dendrimers. Simultaneously, these Janus dendrimers are designed to incorporate polyoxyethylenated chains to enhance water solubility, along with specific functional groups enabling the immobilization of the desired ligand/metal pre-catalyst. The synthesis of phosphorus Janus dendrimers is pursued through dendron synthesis and coupling procedures, with the goal of establishing a comprehensive protocol for grafting dendrimeric halves. The prepared dendrimers will be assessed for their ability to immobilize ruthenium pre-catalysts, and the dendritic effect on the catalytic entity's activity and selectivity will be analyzed.

Furthermore, the versatility of both Ru-NHC complexes and phosphorus Janus dendrimers is set to be explored in parallel projects. In this context, the dendrimer capacity to graft alternative ruthenium complexes and their performance in environmentally friendly solvent catalysis will be evaluated. This evaluation will also aim to compare the catalytic performance —in terms of activity, efficiency, and recyclability of these systems— with single, non-immobilized versions of the same catalysts. Concurrently, the immobilization of Ru-NHC metathesis catalysts on heterogeneous supports (MOFs) is planned to assess their suitability for developing alternative approaches to catalytic system development.

Chapter I. Introduction

1. Dendrimers: Introduction and state of the art

The concept of dendrimers is widely recognized and established within the domains of chemistry and material science, owing to the extraordinary expansion of such compounds in the past decades associated with the exceptional properties and versatility of these arborescent structures with a perfectly controlled molecular structure in various fields.[1]

Etymologically, the concept "dendrimer" derives from the Greek words *dendron* (tree) and *meros* (parts), offering an appropriate description of these compounds. Dendrimers are hyperbranched, monodispersed, three-dimensional macromolecules that typically exhibit a spherical configuration.[1,2] Dendrimers are characterized by a controlled synthetic process, which allows precise manipulation of the shape, size, and molecular dimensions of the resultant dendrimeric structures, enabling the creation of highly structured polymers.[3] One of the most significant features of dendrimers is the presence of a high number of peripheral functional groups within their structure, due to the highly branched nature of such compounds. In particular, the synthesis of dendrimers is characterized by the so-called "generations" (to be named "**G**" in this Thesis), obtained at each branching point in the structure and, therefore, leading to the formation of a new dendritic layer.[1,4,5]

From a structural perspective, different components of a dendrimer can be distinguished (**Figure 1**).[6] Beginning with the central core (**Figure 1, purple**), referred to as generation zero (G_0). The core is a polyfunctionalized moiety composed of a specific number of functionalities serving as anchoring points for monomers. Dendrimer growth occurs in the form of generations at the branching points (**Figure 1, cyan**), facilitating the exponential expansion of the dendritic branches (**Figure 1, black**). In particular, at the end of each reaction cycle, dendrimers are characterized by an exponential multiplication of the terminal functionalities in the structure, derived from the bifurcations occurring at the branching points. The progressive increase in dendrimer generation leads to the development of highly branched and structured compounds, with a flexible internal space within the structure. It is worth noting that the internal cavities of dendrimers can find applications in diverse fields, such as encapsulating desired guest molecules for drug delivery purposes.

The surface of dendrimers (**Figure 1, navy blue**) unquestionably represents the most versatile region. Situated at the periphery of these macromolecules, the dendrimeric surface can be in general easily functionalized with a plethora of functional groups, accommodating a wide range of moieties for various applications.[7]

Surface
functionalities

Branching points

Polyfunctional
core

Branches

Internal
cavities
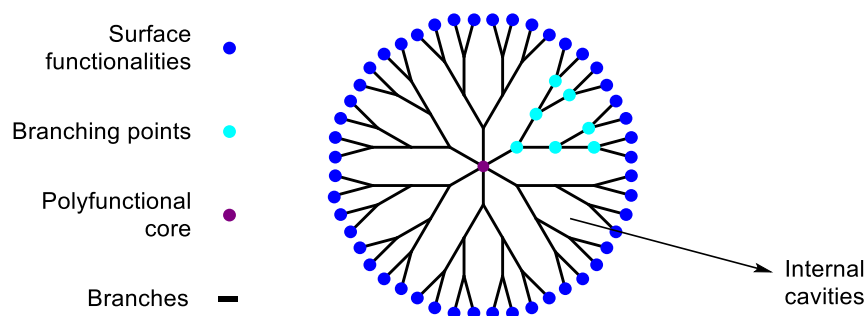
Figure 1. Schematic representation of a third-generation dendrimer and its main parts.

1.1.   Synthetic methodologies

Over the preceding decades, the synthesis of dendrimers has been subjected to diverse method-
ologies including the divergent method,[8] the convergent method,[9] the mixed synthetic ap-
proach,[10] the synthesis of onion-peel dendrimers[11] (yielding dendrimers with distinct chemical
compositions at each generation), and the preparation of dendrimers through an orthogonal syn-
thesis[12] (yielding dendrimers without undergoing classical deprotection and activation steps).
Among the various synthetic methodologies, two have emerged as preeminent and extensively
employed: the divergent method and the convergent method.

1.1.1. Synthesis of dendrimers *via* a divergent method

The divergent approach for dendrimer synthesis was first pioneered by the research groups of
Vögtle and Tomalia.[3,4] This method involves the stepwise construction of dendrimers from a cen-
tral core, where the core is sequentially reacted with monomers of interest to build the den-
drimer structure and periphery. The process relies on polyfunctional cores and AB_n-type mono-
mers (n = 2–6 as most common ones) containing reactive groups responsible for introducing
points of divergence at each coupling site, thereby creating new dendrimer generations. Subse-
quent surface modification allows for further coupling with additional AB_n monomers, enabling
the sequential repetition of activation and coupling steps to obtain higher generations.[13]
Scheme 1 depicts a representation of the divergent method through the repetition of these steps.
In 1978, Vögtle and co-workers introduced the first divergent approach to synthesize den-
drimers, named "cascade molecules".[4] This pioneering work laid the foundation for controlled
supramolecular chemistry. The approach involved starting with a primary diamine core and em-
ploying two sequential reactions—a Michael-type addition of the amine **1** to acrylonitrile (**2**) to
yield a derivative as in **3**, and a reduction of nitrile groups to primary amines—to produce the
polybranched amine **4** (**Scheme 2**).
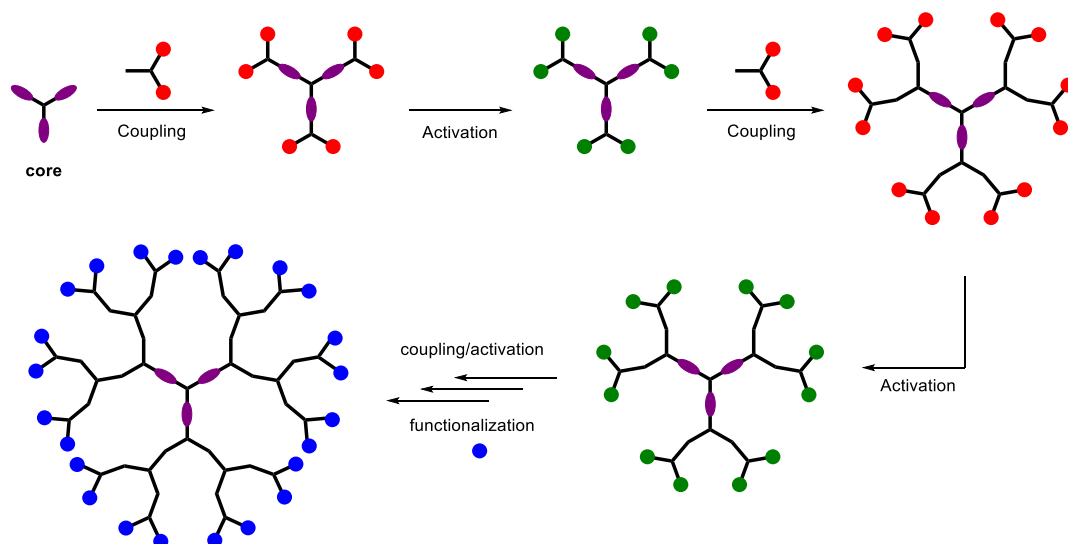
Scheme 1. Representation of the divergent method for the synthesis of dendrimers (up to the third generation) from a trifunctional core and incorporating AB_2 monomers.
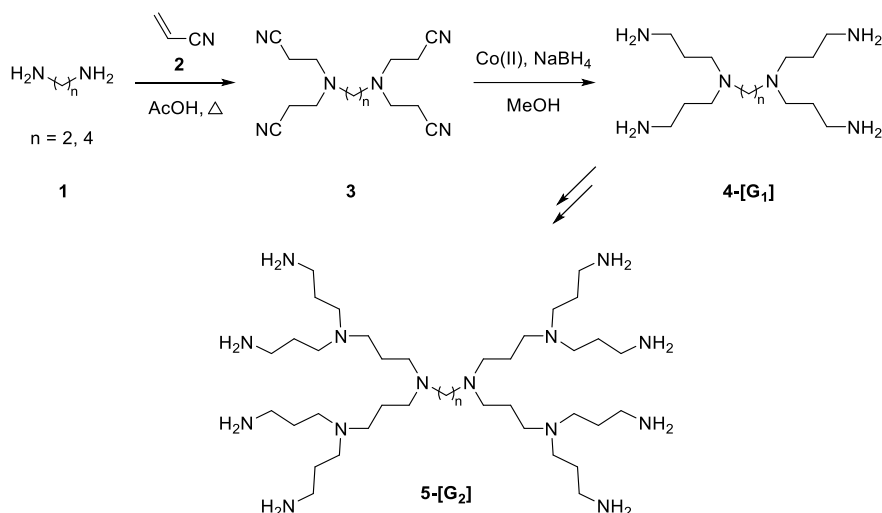
Scheme 2. First reported synthesis of dendrimers, by Vögtle and co-workers in 1978.[4]

Due to the intricacy of the synthesis, it was not until 1993 when E.M.M. De Brabander-Van Den Berg and Meijer optimized the dendrimer synthesis and elucidated their structures up to the fifth generation.[13] These dendrimers, known as poly(propylamine) (PPI) dendrimers, are now produced at an industrial scale[14,15] and are commercially available.[16]

Following the success of PPI dendrimers, Tomalia and colleagues presented a similar dendrimer synthetic approach in 1985,[3] but with the inclusion of two different monomeric units. Unlike PPI dendrimers, where only one type of monomer was used, this novel methodology employed two consecutive reactions: a Michael-type addition between diamine **6** with an methyl acrylate (**7**), followed by the formation of an amide from the terminal ester groups in **8** and diamine **6** (**Scheme 3**). The simplicity and atom economy of this method led to the development of poly(amido)amine dendrimers (PAMAM).[17] Tomalia's work on PAMAM dendrimers was reported up to the tenth generation and marked the first usage of the term "dendrimer" in their research. These

PAMAM dendrimers, often referred to as Starburst-PAMAM dendrimers, can also be found commercially available.[3,13,17]
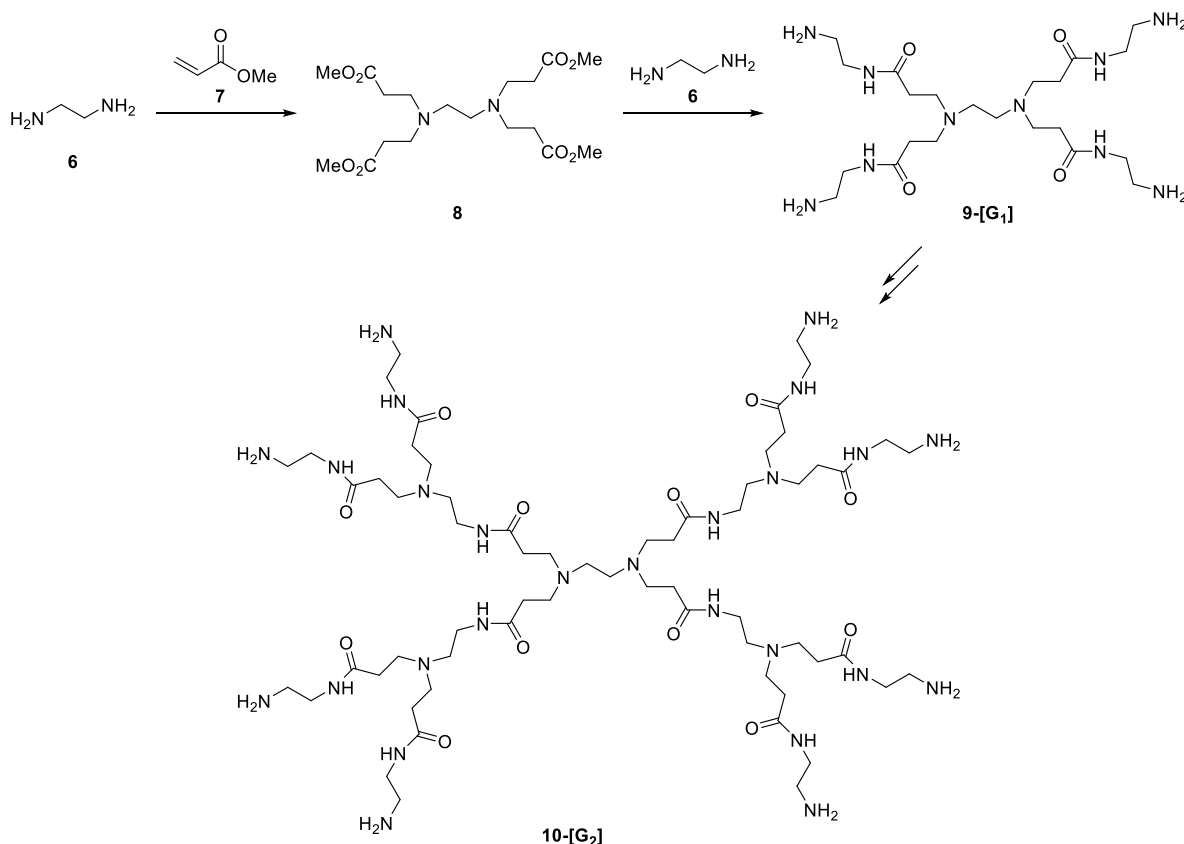
Scheme 3. Synthesis of a second-generation PAMAM dendrimer, as described by Tomalia in 1985.[3]

The divergent method employed in dendrimer synthesis presents notable advantages, such as its expeditious and straightforward approach, allowing for the production of dendrimers in substantial quantities and high generations.[3] However, this methodology has some limitations, giving rise to certain challenges. Based on the synthetic strategy for the preparation of dendrimers though this methodology, each step of the synthesis requires a high number of reactions happening at once (particularly noticeable at higher generations where hundreds of reactions might be happening for a single dendritic molecule). This fact could lead to the obtention of defects in the structure due to the possible lack of reactivity or full substitution of the dendrimer.[1,3,18] To overcome this limitation a substantial excess of reagents is required at each step, making the purification process arduous and possibly leading to the contamination of dendrimers.

1.1.2. Synthesis of dendrimers *via* a convergent method

The first synthesis of convergent dendrimers was documented in 1990 by Fréchet,[9] offering an alternative approach to overcome the limitations associated with divergent synthesis.

In this methodology, synthesis is commenced at the periphery and proceeds incrementally towards the core. The main concept sustaining this approach is based on the concept of "dendron", denoting dendrimeric wedge-shaped moieties that contain a core-level functionality which remains unchanged throughout the synthetic process.

Fréchet's synthetic strategy (depicted in **Scheme 4**) initiates with the preparation of dendrons by growing them iteratively up to the desired generation through the previously reported activation and coupling reactions, and its subsequent incorporation to the core. This approach allows the preparation of dendrons up to the desired level of branching. Ultimately, the last step involves the coupling of these dendrons to a polyfunctional core, yielding the final dendrimeric structure of the same generation as that of the dendrons.

It is worth to mention that the biggest challenge derived from this synthetic methodology is the coupling of higher generation dendrons to the core, due to steric hinderance. In this regard, dendrimers synthesized through this methodology have been reported in the literature of smaller generations than for the divergent approach (up to the fifth generation).
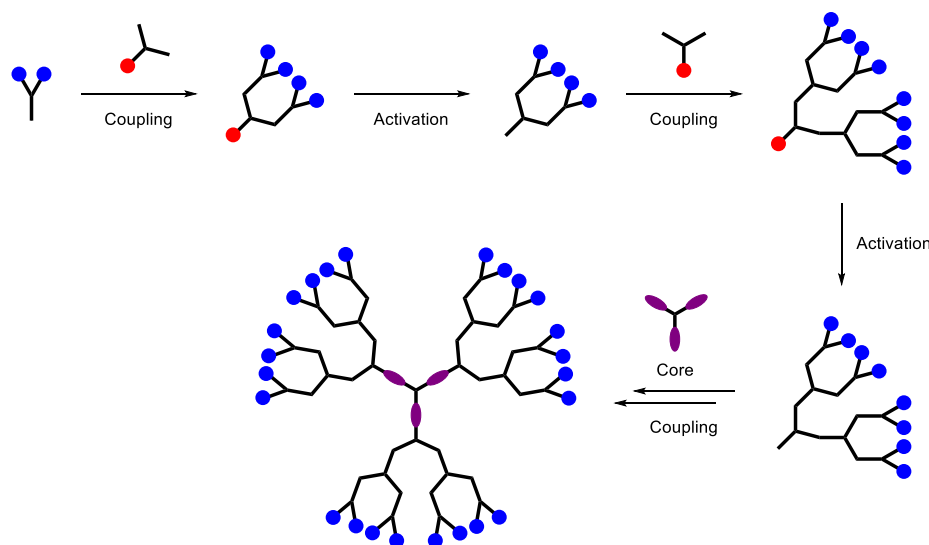
Scheme 4. Representation of the convergent method for the synthesis of dendrimers (up to the third generation).

The convergent synthesis outlined by Fréchet entailed an iterative sequence of two reactions, utilizing 3,5-dihydroxybenzyl alcohol as the sole monomer for constructing the dendrimer branches.[9] As illustrated in **Scheme 5**, the initial step involved a nucleophilic substitution reaction wherein a benzyl bromide **12** reacted with 3,5-dihydroxybenzyl alcohol (**11**) under basic conditions to build the surface of the final dendrimer. Subsequently, benzyl alcohol **13** at the core was transformed (activated) into benzyl bromide **14** using triphenylphosphine and carbon

tetrabromide, and later reacted again with **11**. By iteratively implementing these two stages, Fréchet accomplished the synthesis of poly(benzyl)ether (PBzE) dendrons up to the fifth generation. In the final step, after achieving the dendron of the desired generation, it was coupled to a poly-functionalized core (triphenolic compound **17**) to yield the intended dendrimer with the same generation as that of the dendrons.
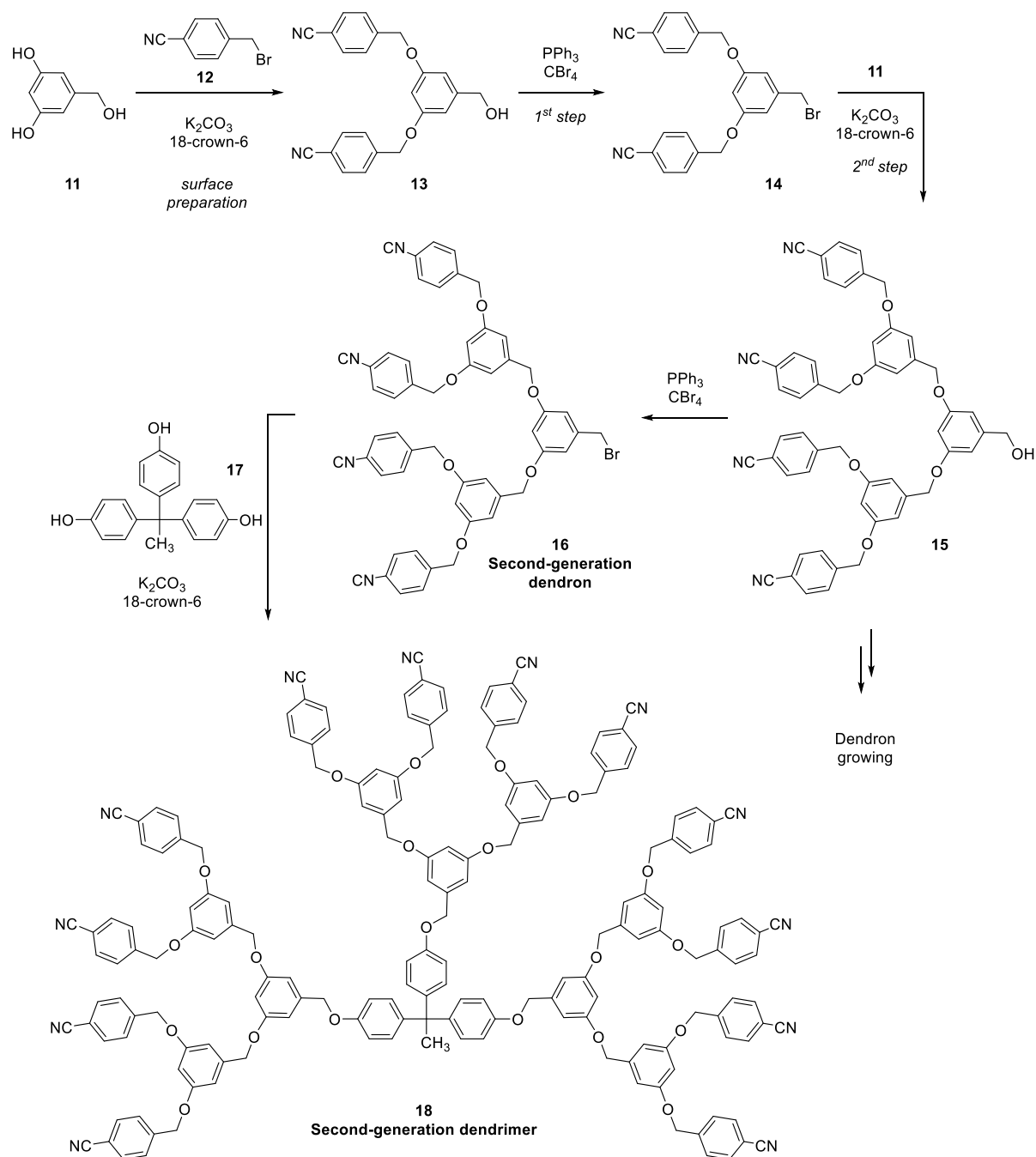
Scheme 5. Synthesis of a PBzE dendrimer, as described by Fréchet in 1990.[9]

The principal advantage of utilizing the convergent method in dendrimer preparation relies on the monodispersity exhibited by the final dendrimers. This stems from the significantly reduced occurrence of defects within the dendrimeric structure when this approach is employed. Additionally, the convergent method facilitates a straightforward protocol for developing asymmetric

dendrimers by the anchoring of different pre-formed dendrons to the core. Furthermore, the ease of production and characterization contributes substantially to the merits of this synthesis.[9,18] Notwithstanding these highly promising attributes, the convergent methodology does entail several drawbacks, being the steric hinderance the most important one. In this regard, the coupling of dendrons (particularly those of higher generations) to the core is highly limited due to the bulky nature of the dendrons and its reaction with relatively small cores.[19,20] This fact has led to the obtention of dendrimers typically of smaller generations for the convergent approach compared to the divergent method.

At a glance, the divergent method for dendrimer synthesis serves adeptly in yielding structures with elevated generations, albeit with the potential for statistical imperfections at the branches. On the contrary, the convergent method, while affording limited defect counts, contends with synthesis constraints due to steric hindrance during both dendron and dendrimer formation. Given these pros and cons, the most intricate dendrimeric architectures documented in the literature typically meld elements of the aforementioned methods. These synthetic approaches harmoniously integrate the foremost attributes of the divergent and convergent methodologies to give multidendritic structures.

1.2.   Families of dendrimers

Dendrimers exist in various types and incorporate a wide array of functionalities. They can be categorized into distinct families based on the diverse building blocks employed in their synthesis. Section §1.1 has already elucidated a selection of renowned dendrimer families. Specifically, the cascade structures pioneered by Vögtle,[4] also known as PPI dendrimers (depicted in **Scheme 2**), PAMAM structures (outlined in **Scheme 3**) and PBzE dendrimers (illustrated in **Scheme 5**),[17] have all been previously expounded upon.

Furthermore, a multitude of other dendrimer families have been documented over the years. In the same year that Tomalia introduced the concept of arborols, which paved the way for PAMAM dendrimers, Newkome and his colleagues presented a similar notion.[21] Their proposition involved tripling the number of terminal functions with each successive generation. This line of inquiry by Newkome culminated in the synthesis of a novel variant known as poly(ether amide) dendrimers (PEA).[22] Their methodology included three distinct stages for each dendrimer generation. Illustrated in **Scheme 6**, a polyol core **19** was reacted with acrylonitrile (**2**) in basic conditions to afford the alkyl ether derivative **20**. The terminal nitrile groups were then cleaved with MeOH/HCl and later treated using NaOH to yield carboxylic acid terminal groups, subsequently transformed into the acyl chloride **23** *via* reaction with $SOCl_2$. Lastly, an AB_3 unit **24** was coupled to the acyl chloride derivative, forming amide linkages, and introducing a fresh layer of terminal

ester groups that can be used for further synthetic cycles, ultimately facilitating the production of higher dendrimer generations. Moreover, PEA dendrimers described in **Scheme 6** serves as an example to show the synthesis of dendrimers through a non-conventional procedure, starting from a tetrafunctional core and incorporating AB_3 monomers.
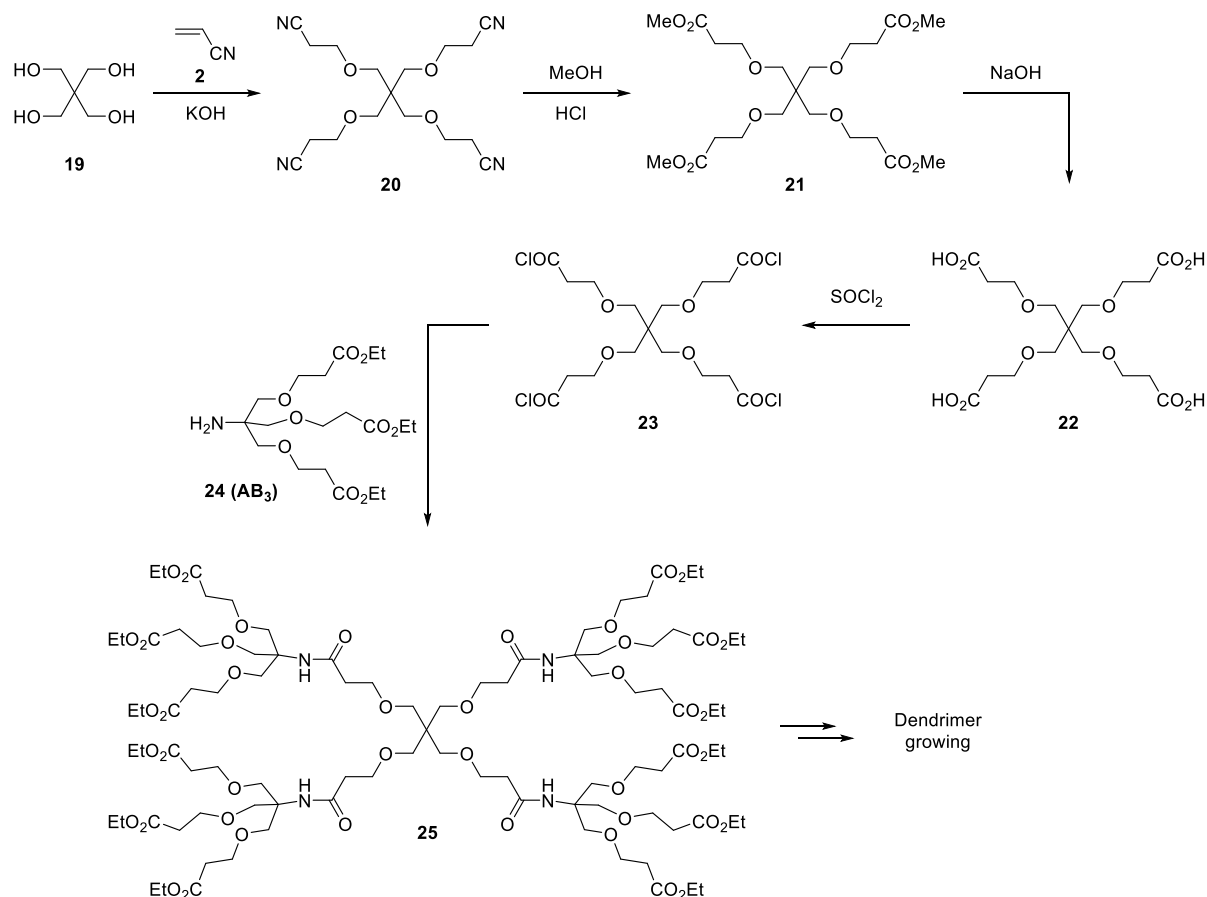
Scheme 6. Synthesis of PEA dendrimers, reported by Newkome and co-workers from tetrafunctionalized cores and AB_3 monomers.[22]

Numerous additional examples of dendrimeric families have been documented within the literature, including poly(ether) dendrimers,[23] poly(ester) dendrimers,[24,25] and dendrimers featuring heteroatoms at their branching points.[26] This latter classification holds particularly significant interest due to the wide spectrum of heteroatomic chemistry, which has stimulated its utilization in dendrimer synthesis.

The pioneering heteroatom-incorporating dendrimer was reported by Muzafarov and co-workers.[27] In their investigation, they detailed a two-step synthesis for a polysiloxane dendrimer, commencing with trichloromethylsilane as the core. As depicted in **Scheme 7**, the synthesis of polysiloxane dendrimers initiates with a nucleophilic substitution involving chlorosilyl groups from $SiMeCl_3$ (**26**) and the sodium salt of diethoxyhydroxymethylsilane (**27**), followed by a reaction with $SOCl_2$ involving the ethoxysilane groups to yield dendrimer **29** with Si–Cl bonds. By sequentially replicating these two stages, the authors reported the synthesis of polysiloxane dendrimers extending to the fourth generation.

Polysiloxane dendrimers laid the foundation for the development of more robust silicon-based dendrimers. Given the limited stability of polysiloxane dendrimers in aqueous environments, *van Leeuwen et al.* later introduced the synthesis of carbosilane dendrimers as a more enduring alternative to silicon-containing counterparts.[28,29] The methodology for carbosilane dendrimer synthesis, depicted in **Scheme 8**, yields compounds with commendable efficiency. The process involves the alkenylation of tetrachlorosilane (**31**) with a Grignard reagent, followed by a hydrosilylation reaction, culminating in the formation of the first-generation carbosilane dendrimer **33**. Due to their adaptability and resilience in aqueous conditions, numerous carbosilane dendrimers have found description in the literature, with variations in branch length, alkyl chain composition, Grignard reagent selection, and branching multiplicity.[29–31]
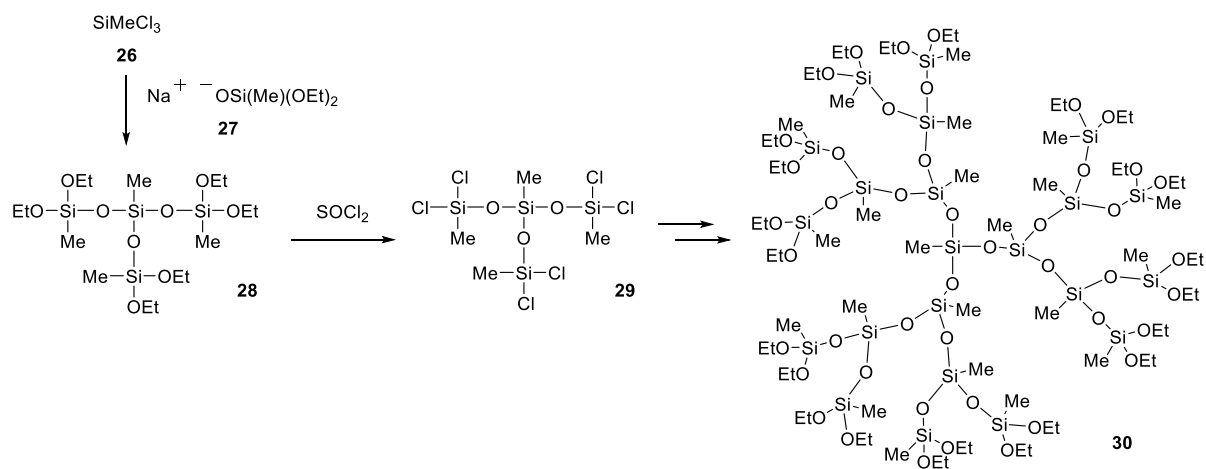
Scheme 7. Synthesis of a third-generation polysiloxane dendrimer.[27]
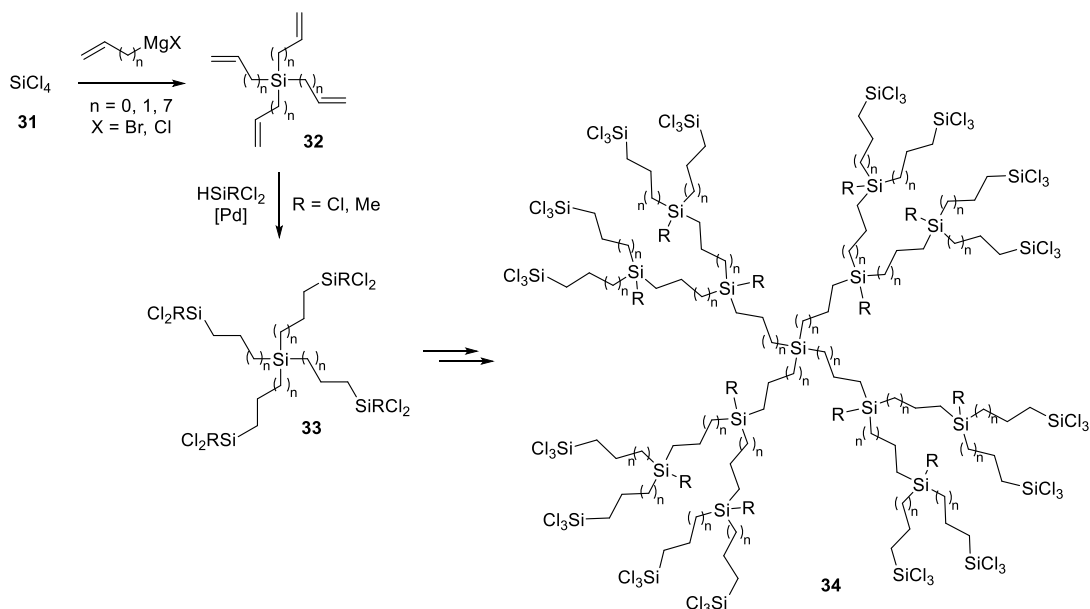
Scheme 8. Synthesis of a third-generation carbosilane dendrimer.[32]

In addition to silicon-based dendrimers, another highly significant class of heteroatom den-drimers is constituted by dendrimers incorporating phosphorus atoms, which particularly cap-tivate the focus within this Thesis.

1.3.   Phosphorus dendrimers

Phosphorus dendrimers are dendritic entities featuring at least one phosphorus atom at their branching points within their structure. The first example of phosphorus dendrimers emerged in 1990, as described by Engel and co-workers.[33] This reported structure relied on the inclusion of phosphonium salts at each branching point, resulting in a threefold multiplication of the ter-minal functions with each successive generation.

However, it was the class of phosphorus dendrimers described by Caminade, Majoral, and co-workers in 1994[34] that has garnered substantial attention due to its multifarious applications. These phosphorus dendrimers were produced through a two-step iterative process employing 4-hydroxybenzaldehyde under basic conditions, alongside N-methyldichlorothiophosphorhy-drazide as branching units.[35,36] A distinctive aspect of this neutral phosphorus dendrimer cate-gory is the quantitative nature of both growth processes, yielding solely NaCl/HCl and H_2O as by-products.[37]

Typically, these dendritic structures are synthesized utilizing two distinct core units: trifunc-tional thiophosphoryl chloride ($P(S)Cl_3$) and hexafunctional hexachlorocyclotriphosphazene ($N_3P_3Cl_6$). Following the previously mentioned methodology, dendrimers based on $P(S)Cl_3$ cores have been synthesized up to the tenth generation,[35,38] while those utilizing $N_3P_3Cl_6$ core extend to the eighth generation.[34] The synthesis of these phosphorus dendrimers follows the same pro-tocol for both core types. **Scheme 9** illustrates the synthesis using the previously mentioned hex-afunctionalized core. Initially, a nucleophilic substitution of P−Cl bonds by 4-hydroxybenzalde-hyde under basic conditions leads to the formation of G_0' dendrimers with aldehyde terminal functions. Subsequently, a condensation reaction between aldehydes and N-methyldichlorothio-phosphorhydrazide yields G_1 dendrimers, possessing $P(S)Cl_2$ groups on the surface and phos-phorhydrazone units as branches. Employing this approach, higher generations are attainable. These dendrimers, recognized as poly(phosphorhydrazone) dendrimers (PPH), shall be referred to as such throughout this manuscript.

Importantly, to enhance comprehension of dendrimers, a linear representation has been devised to simplify understanding of their architecture. **Scheme 9** also illustrates the linear representa-tion of G_0' and G_1 PPH dendrimers.
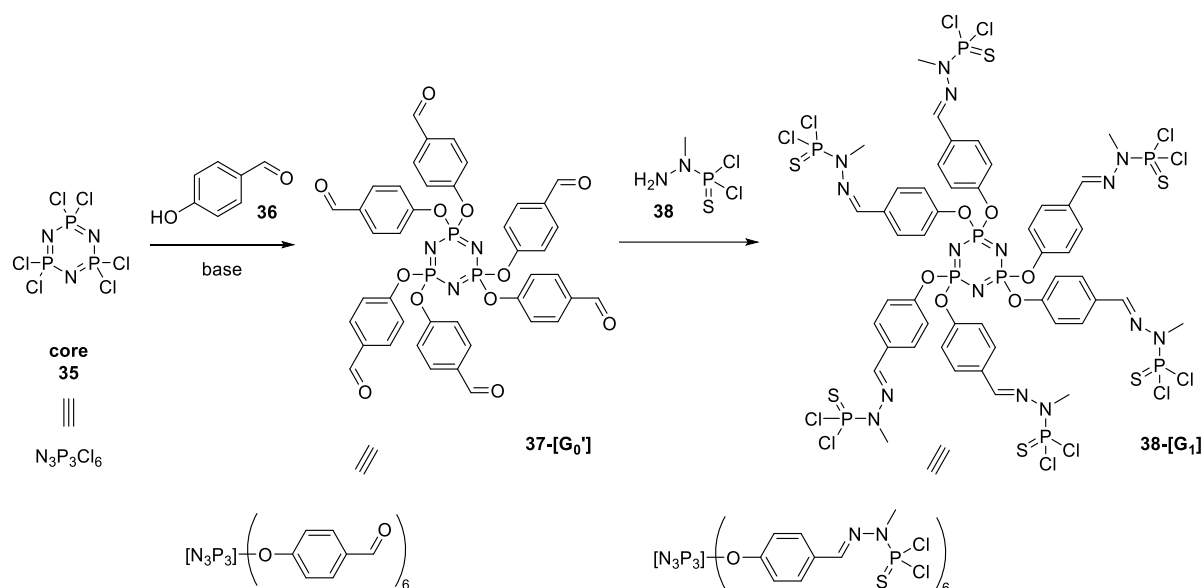
Scheme 9. Synthesis of a first-generation PPH dendrimer. Structures for the dendrimers are shown both in expanded and linear form.

With the advent of PPH dendrimers, Nuclear Magnetic Resonance (NMR) has emerged as a crucial tool for their characterization. Despite their macromolecular nature, the symmetrical properties of phosphorus dendrimers allow their interpretation amenable through $^{31}P\{^{1}H\}$ NMR. This technique proves especially valuable for monitoring dendrimer growth, as at least one phosphorus atom is present throughout every key parts the structure, at the core and at each generation (both in the branches and the periphery).[39]

Figure 2 displays the chemical shift of the phosphorus atom for each generation for a PPH dendrimer system based on $N_3P_3Cl_6$, and up to G_4. While the core $N_3P_3Cl_6$ signal consistently resides around ~8 ppm, the most notable chemical shift deviations are observed in the branch and periphery signals. Generally, when a new PPH dendrimer generation is formed, the $-P(S)Cl_2$ groups on the surface exhibit a chemical shift approximately at 63 ppm. This signal experiences an upfield shift to approximately ~62 ppm upon functionalization with 4-hydroxybenzaldehyde.[26,39] This straightforward chemical shift alteration during the PPH synthesis facilitates its efficient monitoring.
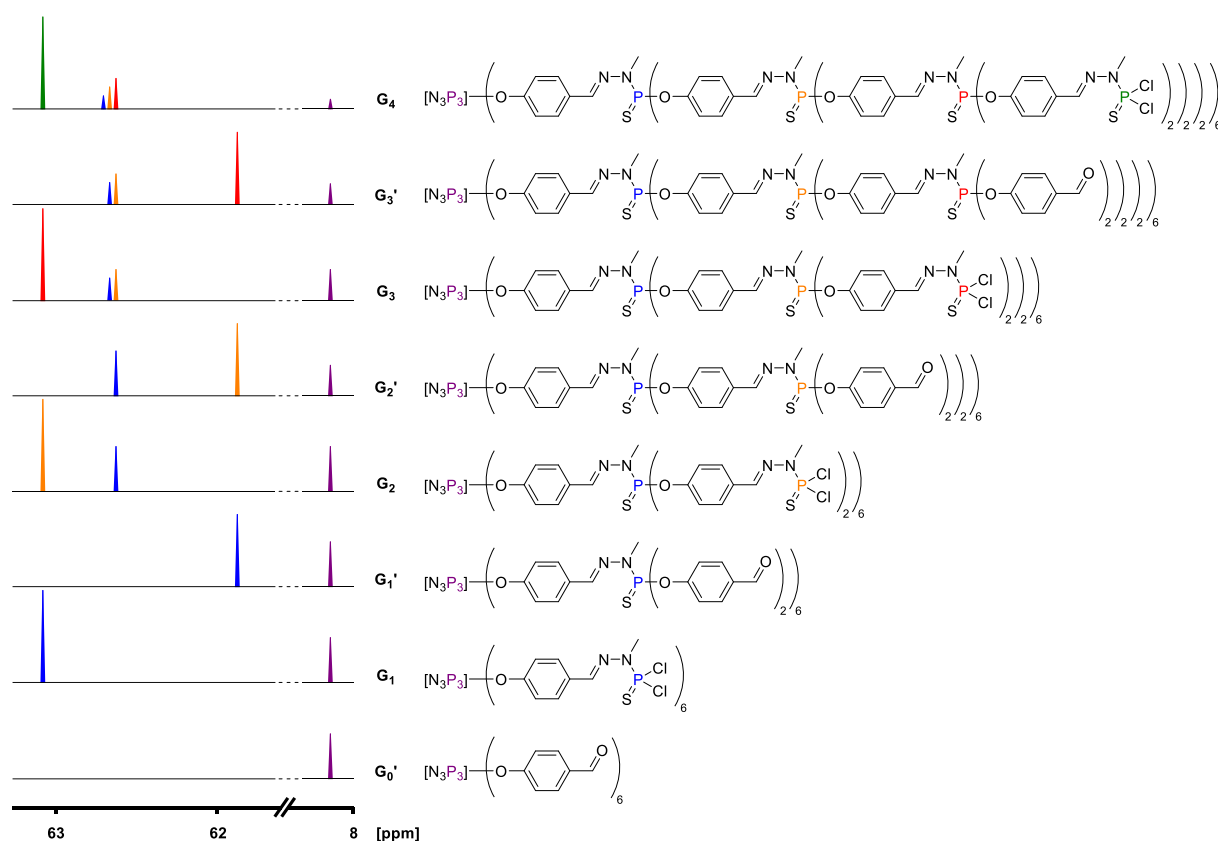
Figure 2. ³¹P{¹H} NMR spectra of PPH dendrimers up to the fourth generation. Adapted from ref. [39].

1.3.1. Applications of phosphorus dendrimers

The potential use of phosphorus dendrimers relies (beyond the structure of these compounds) mainly in the functionalities that are anchored in their structure. Applications for phosphorus dendrimers can be found by incorporating the desired functionality at the level of the core —and subsequently growing the dendrimers from it at the branches, but mostly by functionalizing the surface. In particular, the presence of both −P(S)Cl₂ and benzaldehyde groups at the surface of dendrimers has allowed the development of a rich diversity of reactions using mainly nucleophilic substitutions of the P−Cl bonds with phenols or amines, and condensation reactions.

PPH dendrimers are one of the most versatile dendrimers of all the previously described, as the applicability of such compounds is immense. Modified PPH dendrimers show very interesting and novel properties, that have led to their application in many fields such as catalysis,[40] biology[41] or medicine,[42,43] in a range of applications from anticancer tools,[44,45] therapeutic agents for infection prevention,[46] or antiinflammation agents.[47] Moreover, phosphorus dendrimer have also found its applications in material science, either incorporated inside the material during the creation or used to modify the surface of an existing material. Examples have been developed for their use in the elaboration of gels and hydrogels,[48] mesostructured materials,[49] chemical sensors and biosensors,[50,51] or for imaging.[52]

Despite the wide range of applicability of phosphorus dendrimers, and in light of the interest of this Thesis, the description of phosphorus dendrimers will be focused on the study of functionalized dendrimers for solubility modulation, and their use as supports in catalysis (*vide infra* section §1.5).

1.3.1.1. Modified phosphorus dendrimers for solubility modulation

The solubility of dendrimers has been shown in the literature to be generally very high in a wide range of solvents, even when working with high dendrimer generations and large molecular weights, and phosphorus dendrimers have been shown to have a high solubility in classical organic solvents (being THF, CH_2Cl_2, CH_3CN, Et_2O and $CHCl_3$ the most commonly used). In this context, the introduction of functional groups at the periphery of such compounds could modify or facilitate their solubility in special media such as water,[53] supercritical carbon dioxide[54,55] or ionic liquids.[56,57]

In particular, this Thesis aims to describe the surface modification of PPH dendrimers incorporating moieties to provide solubility in water. At a glance, the reactions performed on the surface of dendrimers to induce a water-solubility end up in the obtention of charged functional groups (ammonium salts,[53,58] carboxylic acid salts[59] or other salts like phosphonates and sulfonates), or neutral moieties such as PEG chains[60,61] or sugars.[62]

The first example of water-soluble PPH dendrimer was described by the group of Caminade and Majoral. In their innovative work,[59] a PPH dendrimer based on a trifunctional core and grown up to the G_1' (aldehyde terminal groups) was functionalized through a Horner-Wadsworth-Emmons reaction with a set of phosphonates derived from natural aminoacids. This reaction led to the obtention of a set carboxylic acid lithium salt terminated dendrimers (**Figure 3**, Prévôte *et al.* 1997). Similar methodologies to obtain carboxylates have been studied in the literature for the preparation of different water-soluble PPH dendrimers. In this regard, **Figure 3** shows two of the used approaches for the obtention of dendrimers terminated with carboxylic acid salts. In the first one, reported by Spartaro *et al.*,[62] a reaction of the terminal $-P(S)Cl_2$ with *tert*-butyl 4-hydroxybenzoate in basic conditions was followed by the generation of an acid-terminated dendrimer under acidic conditions, and the subsequent reaction between the acid groups from the dendrimer with carteolol, to afford the depicted carboxylic acid salt dendrimer.

On the other side, the example of Boggiano *et al*. in 2000[62] reported the synthesis of an acid-terminated dendrimer starting from the dendrimer aldehyde function through a Doebner-like reaction in the presence of $CH_2(CO_2H)_2$, pyridine and piperazine (**Figure 3**). This dendrimer, which does not exhibit solubility in water, was treated with either sodium hydroxide or with an amine (galactosylceramide in the mentioned case) to afford the desired carboxylic acid salt dendrimer, with the water-solubility property.
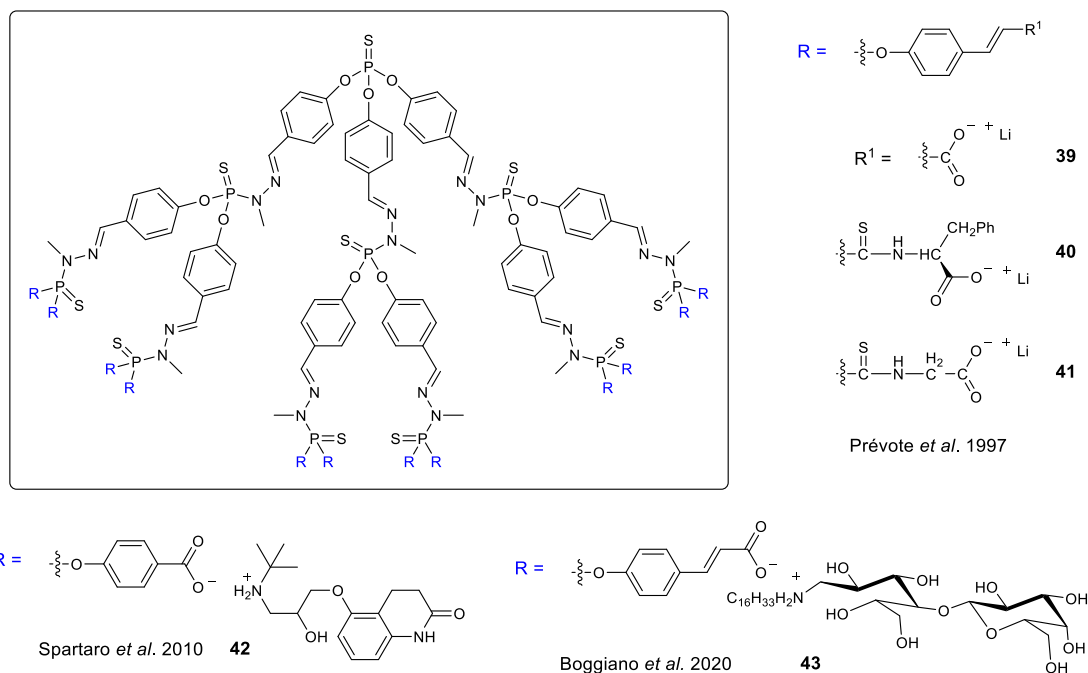
Figure 3. Water-soluble PPH dendrimers based on a trifunctional core bearing carboxylic acid salts as solubility modulation moieties.[59,62]

With the same final purpose of obtaining water-soluble PPH dendrimers, several other approaches have been reported in the literature. As shown in **Figure 4**, other moieties have also been incorporated into dendrimers to obtain structures with this solubility feature. All the examples reported are based on the same approaches of introducing a phenol derivative functionalized with the appropriate solubility modulation chains; or the reaction of dendrimers with amines and their further quaternarization. In this regard, the group of Caminade and Majoral has reported a great variety of systems by the incorporation of ammonium salts,[53,58] phosphonate salts,[63–65] or PEG-moieties[60,61] for the induction of the desired water solubility (**Figure 4**), and their applications in the fields of biology and biomedicine.
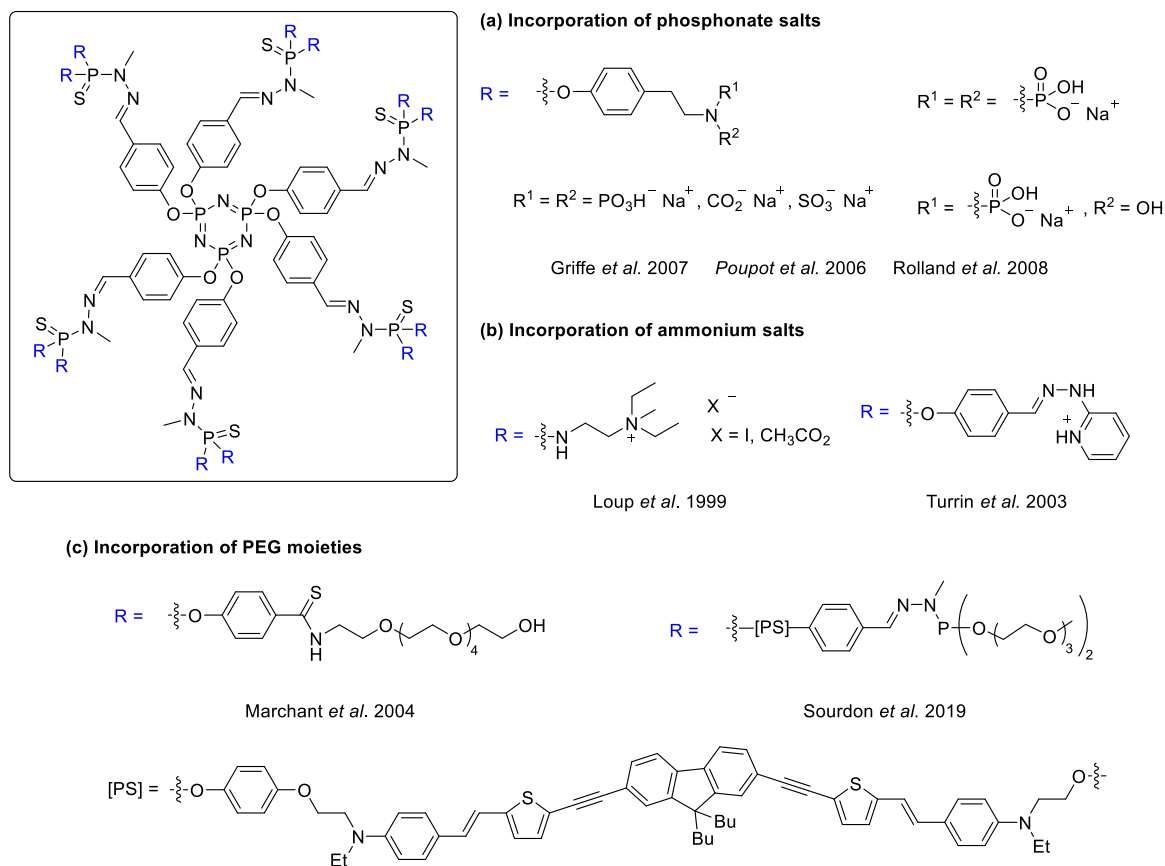
Figure 4. Water-soluble PPH dendrimers based on $N_3P_3Cl_6$ as a core and functionalized at the branches with: *(a)* different carboxylate, phosphonate and sulfonate salts;[64,65] *(b)* ammonium tags;[53,58] and *(c)* addition of PEG chains.[60,61]

Of interest, Sebastián *et al.* also contributed to the aforementioned solubility modulation of dendrimers.[66] As shown in **Figure 5**, the synthesis of *N,N*-disubstituted hydrazones as terminal groups for PPH dendrimers was studied, and the incorporation of carbohydrates, carboxylic acids or boronic acid derivatives through Schiff condensation reactions successfully performed for the obtention of water-soluble dendrimers.
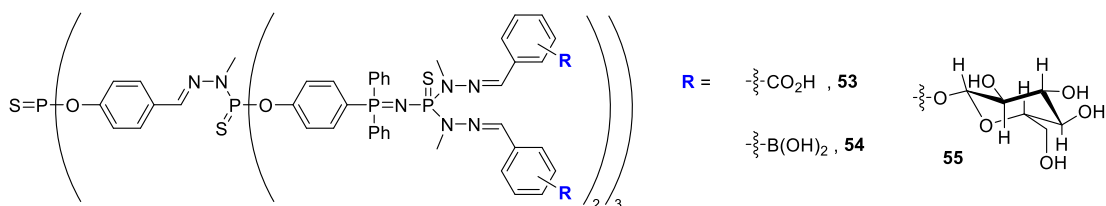
Figure 5. Synthesis of *N,N*-hydrazone terminated dendrimers decorated with carboxylic acids, boronic acids or carbohydrates for the obtention of water-soluble structures.[66]

1.4. Janus dendrimers

Dendrimers are a captivating subject of research due to their inherent adaptability. Nonetheless, the functionalization of dendrimer surfaces has mainly been confined to a uniform array of functional groups, consequently limiting their applicability to specific fields (as demonstrated in the preceding section). To surpass this limitation and to facilitate the incorporation of varied

terminal groups onto dendrimer surfaces, numerous methodologies have been developed. These approaches are based on the inclusion of multiple functional groups, allowing the creation of dendrimers that embody combined properties within a single molecule. One prevalent method involves grafting two distinct functions onto the surface, either in a stochastic[67,68] or precise manner. This last approach is achieved through sequential reactions that layer one functionality upon another in a stepwise synthetic process.[69]

Another intriguing strategy entails crafting dendrimers that feature multifunctional surfaces by merging two dendrons around a central core. This results in structures named Janus dendrimers.[70–72] This name is drawn from the Roman deity Janus, symbolizing transitions and dualities with its two opposing faces. Janus dendrimers are also known by various names in literature, such as surface block dendrimers or di-block dendrimers.[73,74]

Three primary methodologies have been developed for Janus dendrimer synthesis, as depicted in **Scheme 10**. These methodologies encompass the reaction of two dendrons, each possessing complementary functionalities, at the core level (Method A); the sequential interaction of a well-defined difunctional core with an initial dendron, followed by the attachment of a second dendron to the remaining core sites (Method B); or the divergent expansion of new branches from a focal point of a dendron (Method C).
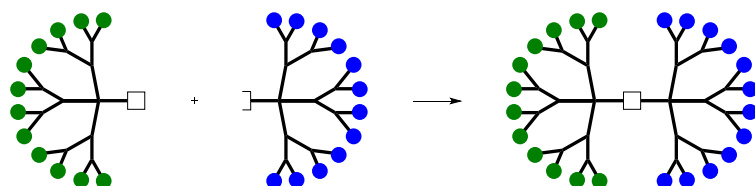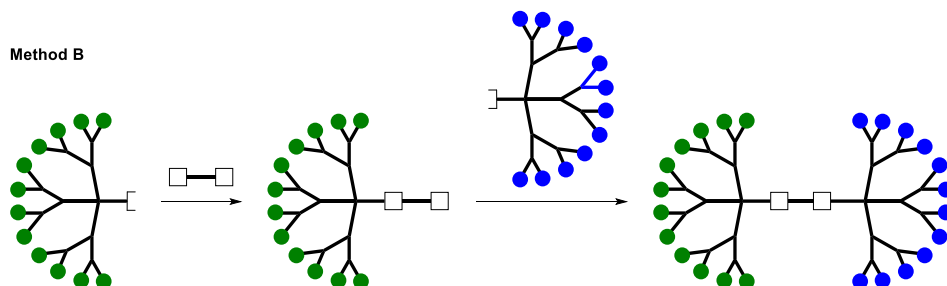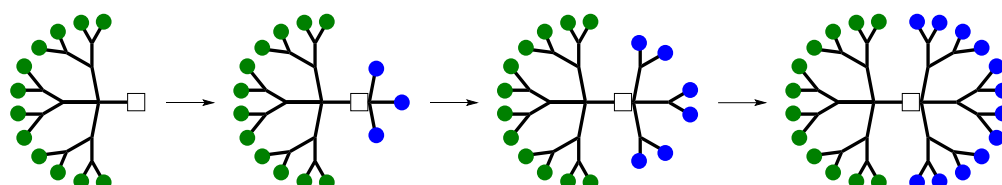
Scheme 10. Graphic representation of the three principal methodologies to obtain Janus dendrimers featuring dual functionalities on the surface. Reproduced from "Cejas-Sánchez, J.; Kajetanowicz, A.; Grela, K.; Caminade, A.-M.; Sebastián, R.M. *Molecules* **2023**, *28*, 5570-5588" under open access Creative Commons CC BY 4.0 license.

Janus dendrimers have captured significant attention ever since their initial depiction by *Fréchet et al.* in 1991.[75] Their pioneering work involved a convergent approach, joining two PBzE dendrons. One dendron, possessing a benzyl bromide group at the core, was linked to a polyphenolic trifunctional core through a monosubstitution reaction under alkaline conditions. The remaining phenol groups of the core subsequently reacted with a distinct benzyl bromide-functionalized dendron carrying different terminal functionalities, culminating in the synthesis of the Janus dendrimer (**Figure 6**).

Substitution reactions involving phenols and benzylic halides have been extensively utilized for PBzE Janus dendrimer synthesis, leading to structures exhibiting benzyl/carboxylate terminal groups or benzyl/nitrile functionalities.[76]
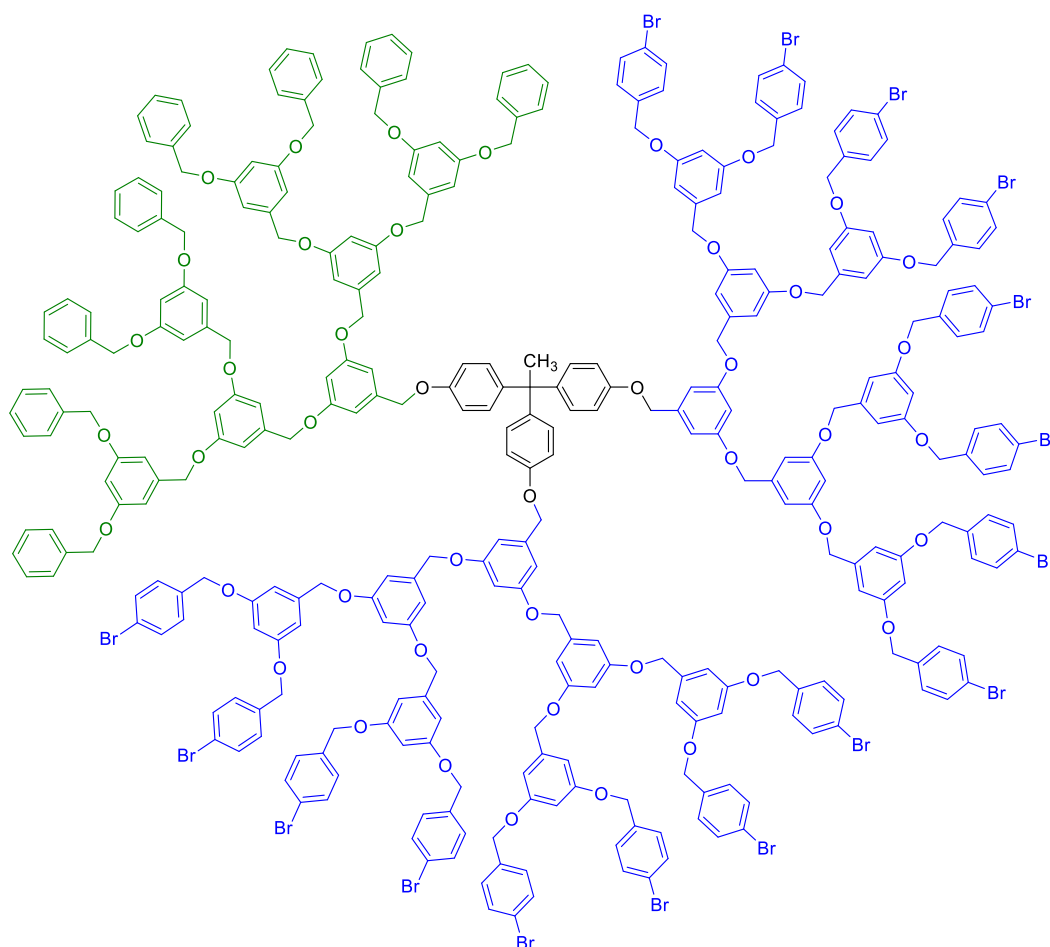
Figure 6. Third-generation PBzE Janus dendrimer with a polyphenol core and poly(benzyl ether) branches with two different terminal groups.[75]

Besides PBzE dendrimers, PAMAM structures have been utilized for the fabrication of Janus dendrimers. Aoi *et al.*[77] demonstrated this by attaching a dendron with a primary amine core and sugar chains as termini to a second PAMAM dendron decorated with phthaloyl groups on its surface and a carbamoyl chloride core, creating a urea linker through the reaction of the two cores (**Scheme 11**). These entities exhibit potential applications in supramolecular self-assembly, as well as in biology and biomedicine by connecting surface segments with proteins and DNA.
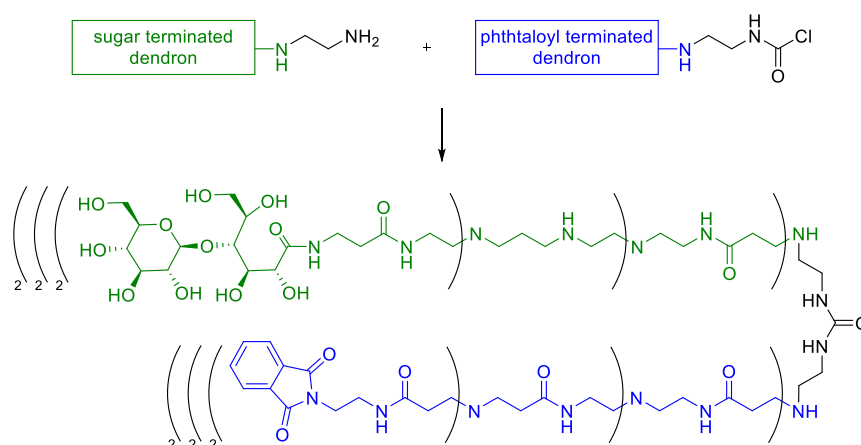
Scheme 11. Second generation PAMAM Janus dendrimer containing phthaloyl groups and sugar moieties in its structure.[77]

The above examples only provide a glimpse of the extensive literature encompassing Janus dendrimers. Investigation on the topic has resulted in a wide range of compounds and applications. For a comprehensive understanding of Janus dendrimer synthesis and properties, refer to the work of Caminade *et al*.[71] and Căta *et al*.[78]

1.4.1. Phosphorus Janus dendrimers

Although a familiar concept, Janus dendrimers incorporating phosphorus atoms at every branching point remain a relatively unexplored domain, holding significant potential across various fields. In this context, the utilization of Janus dendrimers remains constrained due to the limited number of systems documented in current literature. As we recently highlighted in a review on phosphorus-based Janus dendrimers, no more than ten research articles have been published, elucidating the utilization of such structures.[79]

The pioneering effort by the Caminade and Majoral group introduced the first Janus dendrimer with phosphorus atoms at every branching point.[80] The initial phosphorus-based Janus dendrimer was synthesized by combining two dendrons, each carrying complementary functionalities at the core level. Initially, PPH dendrons were created through a divergent method featuring a vinyl group at the core and diverse functional groups on the surface (**Scheme 12**). Firstly, AB$_2$ monomers bearing an azido group and two benzaldehyde moieties (**57**) were reacted with a phosphine modified with a vinyl group (**56**) through a Staudinger reaction. The obtained **G$_0$'** dendron was grown using classic PPH conditions until the desired generation, always bearing the unmodified vinyl group at the core. The obtained dendrons were functionalized in the surface with different phenol derivatives. Later, one functionalized dendron was subsequently transformed into an amine-core dendron *via* a reaction with a diamine **62**, allowing for subsequent linkage with another dendron (**Scheme 12**). This synthetic pathway facilitated the creation of Janus dendrimers by modification the core of a first dendron and the coupling of a second one

through a vinyl/amine coupling, following the *Method B* for the synthesis of Janus dendrimers (**Scheme 10**).

Employing the same methodology, the Caminade group has reported the synthesis of additional PPH-based Janus dendrimers utilizing the same amine/vinyl core linkage.[35,81]
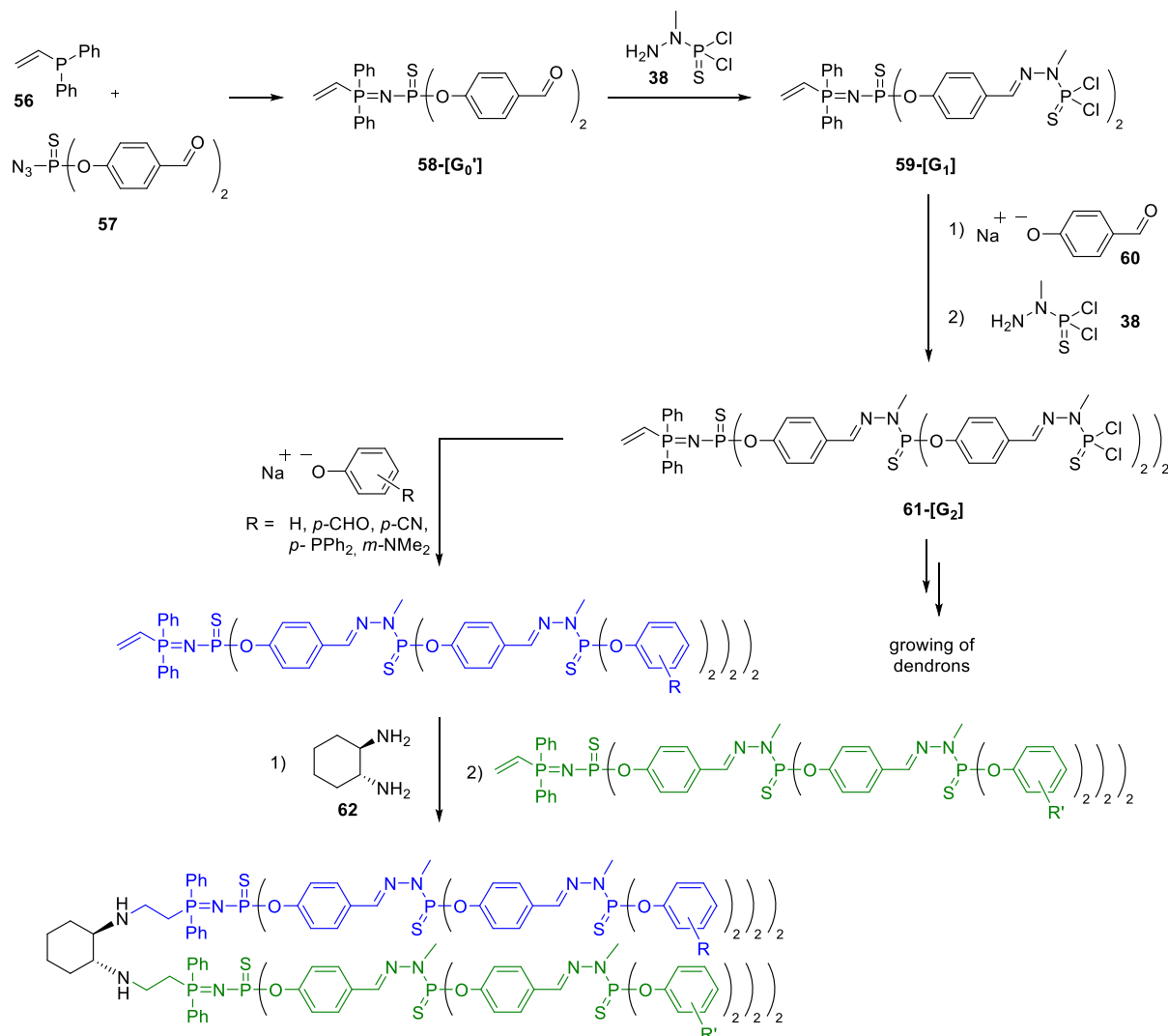
Scheme 12. First PPH Janus dendrimer reported in the literature, based on (1*R*,2*R*)-cyclohexane-1,2-diamine as a core.

In 2001, the group of Caminade and Majoral introduced an innovative approach for synthesizing core-core-built Janus dendrimers (**Scheme 13**).[82] This method involved the alkylation, substitution and subsequent desulfurization of a dendron **63** with a P=N—P(S) core to yield the cationic dendron **64**, followed by a Staudinger reaction with a desired second dendron **57**, as illustrated in **Scheme 13**. This coupling resulted in the formation of a novel (S)P—N=P(—N=P) core linkage as in dendrimer **65**.

Lastly, the obtained dendrimer **65** was modified to incorporate phosphane moieties in the surface. To achieve this, the aldehyde groups were reacted with an excess of methylhydrazine, followed by treatment with Ph$_2$PCH$_2$OH, leading to a dendrimer **68** with the desired phosphine

groups. The prepared dendrimer, containing a phosphine group on its surface, could be employed for metal complexation, such as palladium or iron, with potential applications in catalysis.

Scheme 13. Synthesis of a PPH Janus dendrimer through desulfurization and further Staudinger reaction at the core, bearing ammonium salts and phosphines in the structure.

In recent years, the advancement of phosphorus-containing dendrimers has led to the description of more intricate dendrimers with a distinct core function (AB$_5$) in the literature. The introduction of this type of compound raises concerns about the compatibility of the core function. It must be sufficiently reactive to allow for dendrimer synthesis processes and surface functionalization without disruption.[83] These compounds are synthesized using a divergent method. **Scheme 14** below illustrates the two distinct synthetic pathways employed to create AB$_5$ dendrons up to the first generation. The initial stage involves a penta-substitution of the core (N$_3$P$_3$Cl$_6$) with 4-hydroxybenzaldehyde, followed by the replacement of the final chlorine with a different functional group. In the subsequent step, a condensation reaction between the aldehyde groups and *N*-methyldichlorothiophosphorhydrazide is conducted to yield a first-generation AB$_5$ dendron known as G$_1$, possessing 10 surface chlorine atoms.[84] Interestingly, the synthesis of AB$_5$-like dendrons can also be achieved through the reverse procedure, where one chlorine from the core is initially substituted, and 4-hydroxybenzaldehyde is subsequently introduced to complete the core's full substitution.

Scheme 14. Representation of the two methodologies reported in the literature for the preparation of AB$_5$-type first-generation PPH dendrons.

Drawing from the previous synthetic approach, an illustrative example is found in the work of Martinez-Ferrero *et al*.,[85] where dendrons were synthesized as hybrid optical sensors affixed to mesoporous titania nanocomposites. An AB$_5$ dendron was crafted using N$_3$P$_3$Cl$_6$ in a two-step procedure: initially, the core underwent a reaction with one equivalent of 4-hydroxybenzaldehyde, leading to the monosubstitution of a single P–Cl bond; subsequently, the remaining five P–Cl bonds were reacted with maleimide-based phenolic chromophores. The successful substitution was confirmed via NMR and IR spectroscopy. The ^{1}H and ^{13}C NMR spectra revealed multiple signals owing to the asymmetric arrangement of dendron branches around the core. To further modify the dendron structure, the AB$_5$ core was then functionalized with H$_2$NN(Me)P(S)Cl$_2$. The terminal –P(S)Cl$_2$ group was adorned with diverse phosphonate groups known for their stability in forming complexes with metal oxides (**Scheme 15**). With the preparation of Janus dendrimers in mind, novel hybrid materials emerged by merging the fluorescent attributes of the maleimide derivative and anchoring this material onto a nanocrystalline mesoporous titania thin film. The principal characteristic of these materials is their potential utility as fluorescent probes.
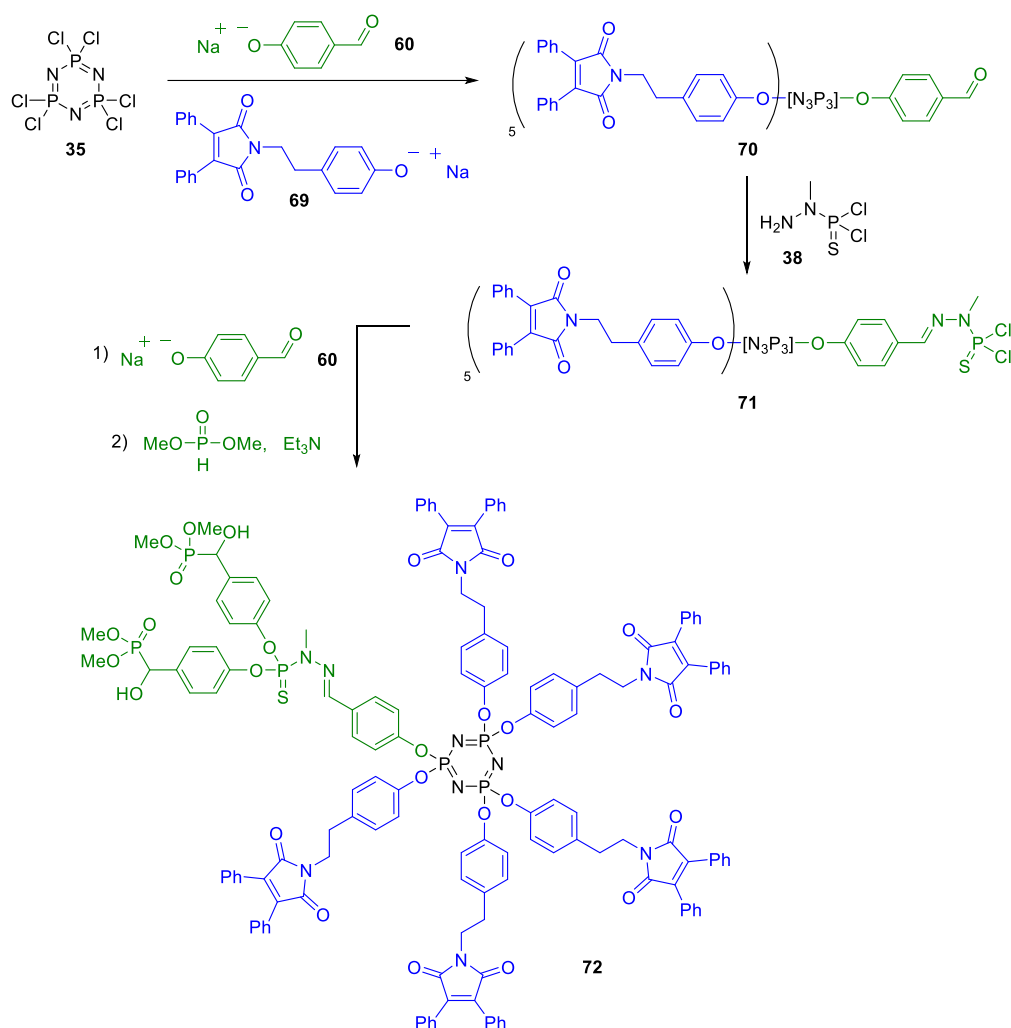
Scheme 15. Representation of the PPH dendron described by bearing five maleimide moieties and two phosphonate groups at the surface of the dendron, with application as fluorescent probes.[85]

Although AB$_5$ compounds have found wide applications in various fields such as biology, material science, and catalysis (for a comprehensive review, refer to Zibarov *et al.*[86]) most of the reported examples have focused on the development of dendrons for specific applications, rather than dendrimers.

In this context, the sole example of PPH Janus dendrimers based on the AB$_5$ system was reported by Fuchs *et al.* in 2005.[87] Employing the previously mentioned methodology, two dendrons were synthesized. One dendron comprised five amino groups protected with tert-butyloxycarbonyl (Boc) groups and a single carboxylic acid function; and the other contained five dansyl deriva-tives and one primary ammonium group (**Scheme 16**). Dansyl groups were chosen as the func-tional moiety for fluorescent labeling, as previously reported in dendritic fluorescent probes.

The synthesis of the Janus dendrimer followed an amide formation process. Initially, the carbox-ylic acid group of the first dendron was activated using TBTU (*O*-(benzotriazol-1-yl)-1,1,3,3-tet-ramethyluronium tetrafluoroborate) in the presence of DIPEA (*N,N'*-diisopropylethylamine). Subsequently, the activated dendron was reacted with the ammonium salt of the second dendron

under basic conditions to create an amide bond. Finally, the resulting Janus dendrimer was treated with an excess of trifluoroacetic acid in dichloromethane to remove the Boc protecting groups on the surface, leading to a dendrimer featuring dansyl groups on one side and ammonium tags on the other.

An alternative approach to creating Janus dendrimers with dansyl and ammonium tags involved using a hydrazone bond. This method was selected due to the anticipated higher stability of hydrazones compared to amines in condensation reactions. For this purpose, two new dendrons were synthesized: the first containing five Boc-protected primary amines and a hydrazide group, and the second containing five dansyl groups and one aldehyde group. Coupling the two AB$_5$ dendrons was achieved under basic conditions, yielding the desired Janus dendrimer connected by a hydrazone linker. The resulting Janus dendrimer underwent treatment with trifluoroacetic acid again to remove the surface Boc protecting groups (**Scheme 16**). Both synthesized Janus dendrimers were designed for applications in the fields of material science and biology, capitalizing on the presence of fluorescent dansyl groups, and ammonium tags that offer water solubility.
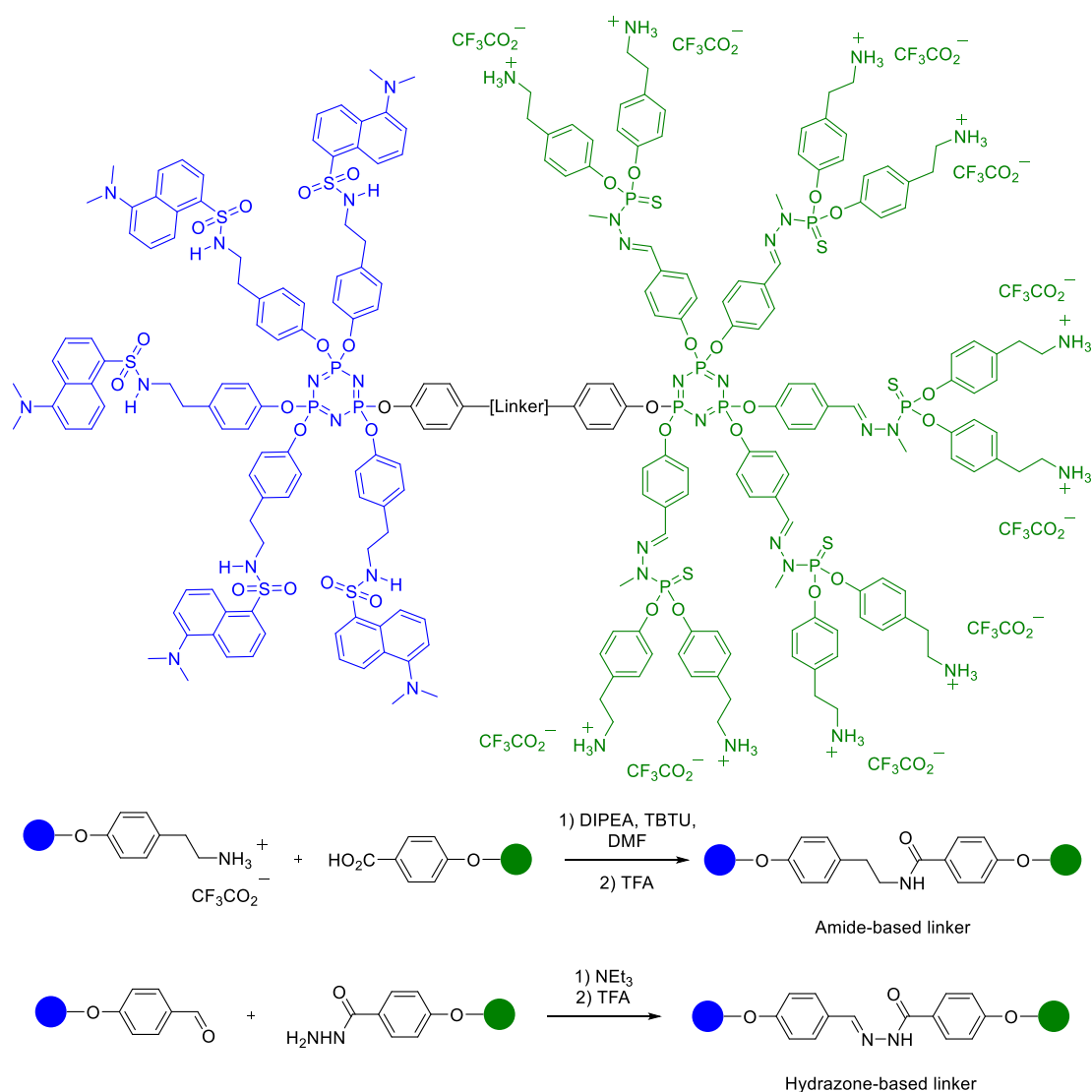
Scheme 16. Representation of two PPH Janus dendrimers built from a dendron bearing dansyl groups and a dendron bearing ammonium tags through either an amide or hydrazone linker.

Despite AB$_5$ compounds have been widely used in the literature in several fields such as biology, material science, or catalysis, most the examples reported are based on the development of dendrons for the desired applications, but not dendrimers. For a broader knowledge on the synthetic methodologies for the preparation of PPH Janus dendrimers and their properties, one can refer to our recently published review on the topic.[79]

1.5.   Dendrimers in catalysis

Among the various applications of dendrimers, catalysis stands out as one of the most important ones. Dendrimers present a significant opportunity to combine the advantages of both homogeneous and heterogeneous catalysis while maintaining well-defined and monodispersed structures.[88] Functionalized dendritic catalysts have been reported to be able to exhibit the same level of activity and selectivity as conventional homogeneous catalysts,[40] while allowing their recoverability and reusability from the reaction medium much more easily than conventional catalysts.[89] This ease of recoverability and reusability, added with the possibilities that dendrimers offer in terms of fine-tuning the catalysts (such as ligand design) serves to bridge the gap between homogeneous and heterogeneous catalysis using dendrimeric structures.

Dendrimeric structures can be tuned in terms of structure, size, shape, and solubility, and these properties make of dendrimers very promising candidates to host catalytic entities. In this regard, the catalyst can be placed in different parts of the dendrimer, such as the core,[90,91] at the branches,[92–94] at the periphery of such structures or within the dendrimeric cavities[95–97] (**Figure 7**).

Catalyst at the core   Catalyst at the branches   Catalyst at the periphery   Catalyst confined inside the dendrimer
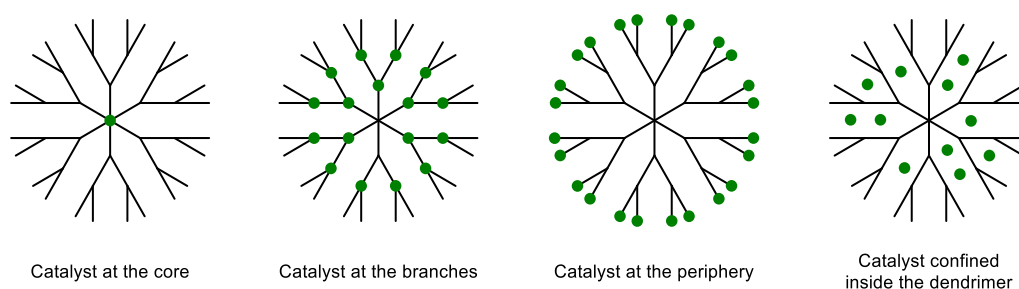
Figure 7. Schematic representation of different dendrimeric architectures containing catalytic moieties at different positions in the structure.

The development of unprecedented/different properties of catalyst@dendrimer systems compared to small catalyst analogues is known as "dendrimer effect". In particular, when a catalyst is placed at the periphery of a dendrimer, the modification that the final system has (in terms of the modification of the catalytic behavior, activity, reactivity or the possibility to reduce the metal leaching) can be attributed to the high local concentration of catalyst, leading to a modification of the catalytic activity (multivalent effect) due to cooperative effects or be the origin of the catalyst deactivation.[32,98] Moreover, it has been observed that the presence of a high local

concentration of catalyst can provide an unexpected behavior such as the increase/decrease of the efficiency or selectivity, the need of milder reaction conditions to perform the desired catalytic process. In a similar trend, another feature is the so-called "generation effect",[99,100] which is the higher modulation of the previously mentioned properties (in a positive or negative way) as higher the generation of the dendrimer is.

Aside from the possible modification of the catalytic behavior of catalyst@dendrimer systems, dendrimers possess another quality that makes them suitable candidates for catalysis: their ease of recovery and recyclability from reaction mixtures. Among all the possible techniques, the recovery of dendrimers (and catalyst@dendrimers) has been reported mainly based on filtration through membranes[101] or precipitation in co-solvent systems.[40] Of interest, one of the most used techniques for the isolation and reusability of dendrimeric catalysts is based on precipitation. Since the solubility of dendrimers relies mainly on the functional groups at the periphery of such compounds, the addition of apolar solvents (such as n-pentane or n-heptane) induces the precipitation of the catalyst@dendrimer system while the products are maintained in the solution.[89,102,103]

The first example on the use of dendrimers in catalysis reported by van Koten and co-workers in 1994, based on the grafting of diamino arylnickel compounds onto the surface of poly(silane) dendrimers (**Figure 8**).[32] Authors showed the synthesis of a G_1 dendrimer and compared its catalytic activity for the Kharasch addition of polyenolalkenes to olefins.

73-[**G$_0$**]-[SiMe$_2$-ArNiBr]$_4$ **74**-[**G$_1$**]-[SiMe$_2$ArNiBr]$_{12}$
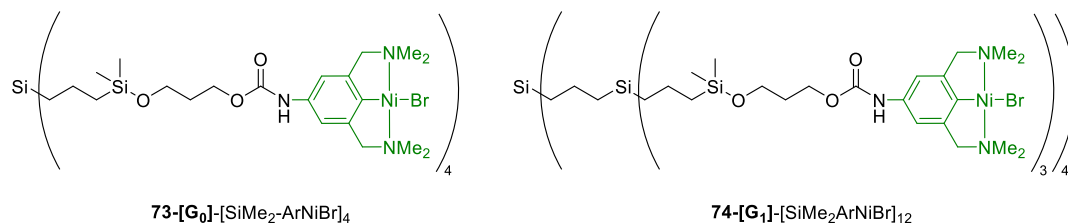
Figure 8. Representation of the first catalyst@dendrimer system, based on the immobilization of nickel (II) at the surface of a poly(silane) dendrimer.

Despite the work by van Koten resulted in a negative dendritic effect, as the conversion of the **G$_1$** Ni@dendrimer showed less conversion than the G_0 and the monomeric analogue, it settled the basis for the further implementation of dendrimers in catalysis. In this regard, extensive research has been performed in the topic yielding to the obtentions of catalyst@dendrimer systems, and **Scheme 17** depicts selected examples for the use of different families of dendrimer in catalysis, demonstrating the use of ─for example─ PPI and PEA dendrimers for applications in cross coupling reactions, or the use of PAMAM dendrimers for their utilization in hydrogenation reactions, just to cite few examples.[57,104,105]
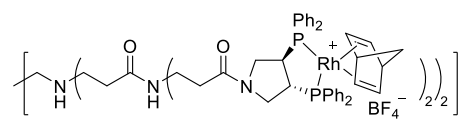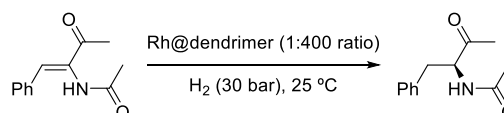
For practical purposes, this Thesis will be focused on the use of catalysts anchored on phosphorus-based dendrimers.
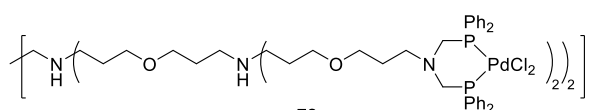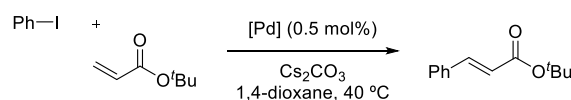
a) PPI-based dendrimer for Sonogashira couplings
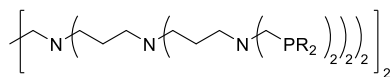
b) PAMAM-based dendrimer for hydrogenation reactions

R = - Cy, **75**
-^{t}Bu, **76**

77

c) PEA-based dendrimer for Heck couplings

78

Scheme 17. Selected examples of catalyst@dendrimer system for applications in catalysis.[57,104,105]

1.5.1. Catalytic systems with phosphorus (Janus) dendrimers

Due to the success on the implementation of dendrimers in catalysis, the applicability and development of such catalytic systems also was implemented in phosphorus dendrimers, mostly based on the efforts of Caminade, Majoral, and co-workers. In particular, the phosphorus-containing dendrimers described in the literature are mostly based on the previously mentioned PPH systems, synthesized either from a trifunctional core (P(S)Cl$_3$) or an hexafunctional core (N$_3$P$_3$Cl$_6$).

In the same trend as previously described, the incorporation of catalytic moieties within phosphorus dendrimers can be performed in different regions of the dendrimer (such as the core or the branches). Nonetheless, the most used approach for the obtention of catalyst@dendrimer systems with PPH macromolecules has been based on the incorporation of such catalysts at the periphery. Of interest, selected examples are described herewith.

For the case of hexafunctionalized core dendrimers, **Scheme 18a** shows the applicability of a palladium-catalyzed Suzuki coupling.[106] In particular, a PPH dendrimer bearing azabismethylenediphenylphosphine moieties at the periphery was synthesized for the reaction of 4-bromoaniline and phenylboronic acid using a 1 mol% of palladium acetate. The desired reaction occurred with the *in situ* complexation of the palladium complex under basic conditions to afford the desired product in moderate conversion after 5 h at 120 °C in a water/acetonitrile solvent mixture.
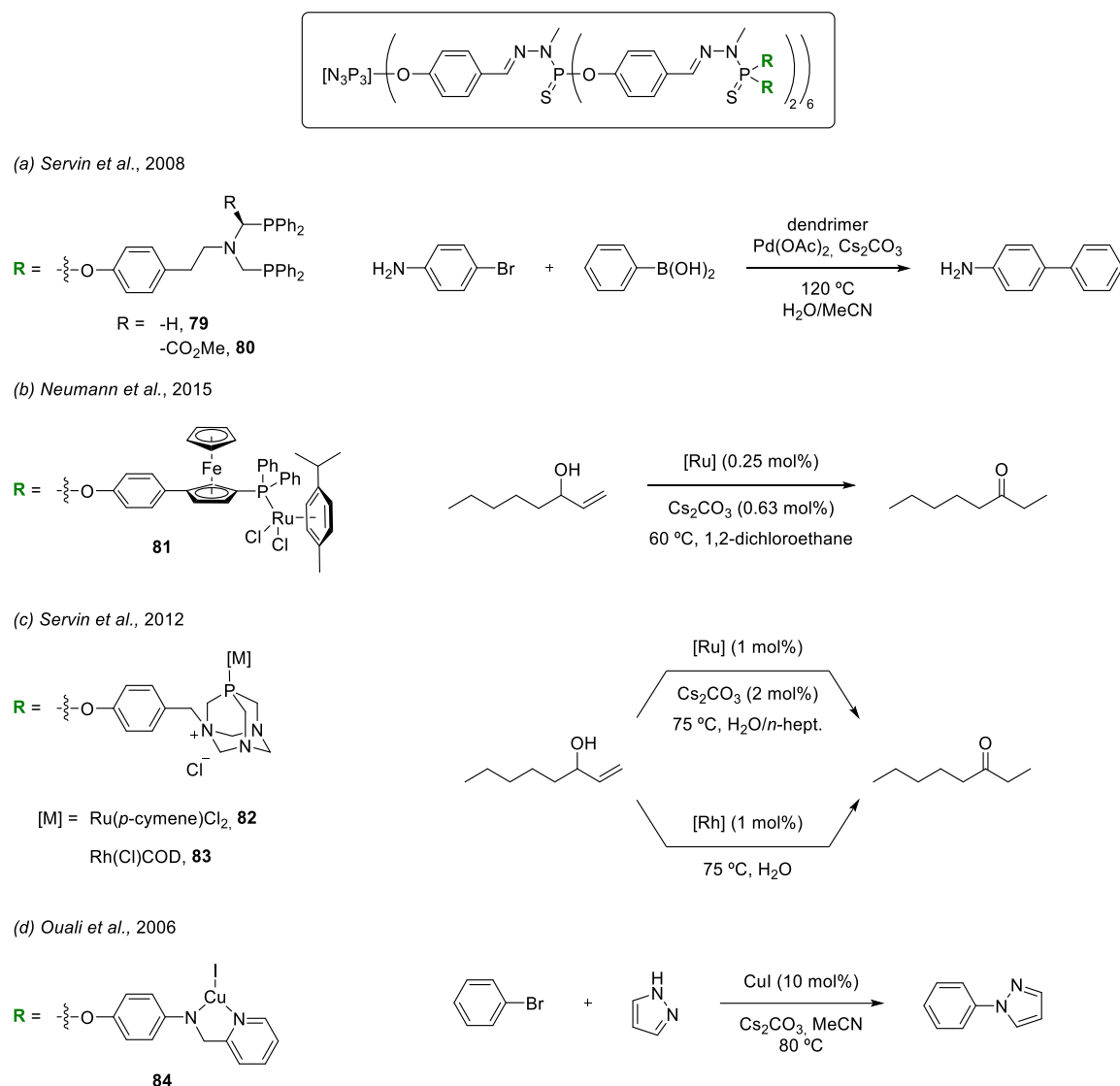
Another interesting example was reported by the groups of Caminade and Hey-Hawkins (**Scheme 18b**).[107] In their work, the synthesis of PPH dendrimers from **G$_1$** to **G$_3$** bearing a phosphine ruthenium complex at the surface linked through a ferrocene moiety was reported. The dendrimers prepared were employed for the isomerization of allyl alcohols with cesium

carbonate as co-catalyst, showing a positive dendritic effect for all the Ru@dendrimer systems. The particularity of these complexes was the redox-active ferrocene moiety. In this regard, authors reported the obtention of a redox-switchable Ru@dendrimer system, showing remarkable results for the first-generation dendrimer.
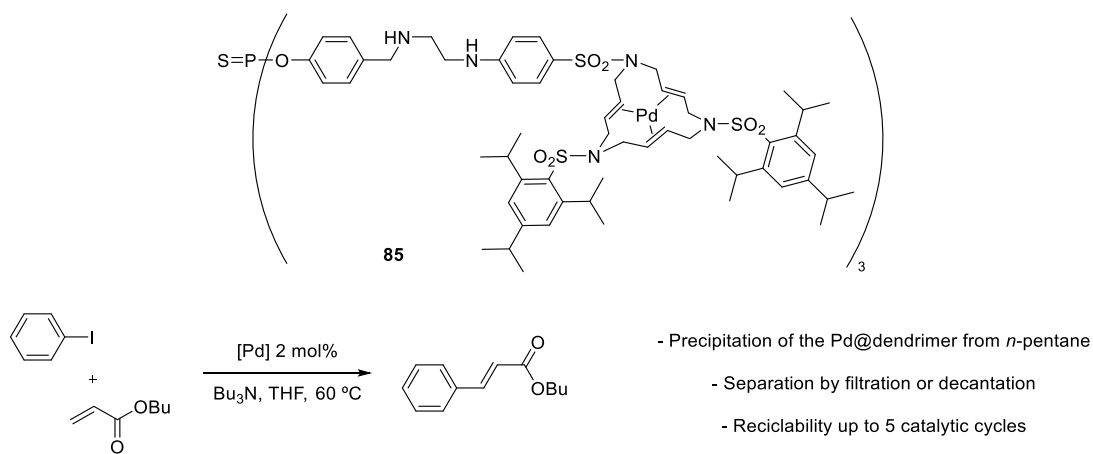
Continuing with the isomerization of allyl alcohols, Servin *et al.*[108] reported very interesting research on the use of metal@dendrimer systems in green solvent catalysis (**Scheme 18c**). A PPH dendrimer was reported bearing 1,3,5-triaza-7-phosphaadamantan-1-ium moiety, which provided at the same time solubility in water and an anchoring point for the grafting of a catalytic center. Of interest, $[Ru(p\text{-cymene})Cl_2]_2$ and RhCl(COD) were grafted at the surface of the dendrimer. A great positive dendritic effect was observed for the Ru@dendrimer system in the isomerization of 1-octen-3-ol to octan-3-one with an increase of more than a 30% conversion when comparing the monomeric and the G_3 complexes.

In addition to the previous examples, copper catalysts have been also employed for this purpose. **Scheme 18d** shows the work by *k et al.* for the use of a Cu@dendrimer system for arylation of aromatic amines.[109] In this regard, a PPH dendrimer bearing a pyridine imine functionality was obtained and CuI was complexed on its structure. It must be highlighted that the catalytic outcome showed a quantitative conversion when employing the Cu@dendrimer systems (up to the fourth generation) using Cs_2CO_3 as co-catalyst, while the monomeric copper complex did not afford any conversion.

Lastly, another example of a Ru@dendrimer system that is worth to be highlighted was the reported by the groups of Sebastián and Caminade (**Scheme 19**). In this regard, the synthesis of PPH dendrimers based on $P(S)Cl_3$ as a core was performed for its use in Heck reactions. Of interest, the grafting of 15-membered azamacrocyclic structures onto the surface of dendrimers was performed, followed by the complexation of Pd(0). The formation of dendrimers up to the third generation was reported. Of note, the small dendrimeric structures afforded discrete complexes when treated with Pd(0) sources, while the higher generations yielded also to the formation of palladium nanoparticles. Pd@dendrimers were used for the Heck reaction of iodobenzene and *n*-butylacrylate in basic conditions. The outcome of the catalytic tests showed not only excellent conversions, but a great recyclability and reusability up to 5 cycles of the dendritic catalyst by simple precipitation from *n*-pentane and subsequent filtration.

(a) Servin et al., 2008

R =   -H, **79**
      -CO$_2$Me, **80**

(b) Neumann et al., 2015

(c) Servin et al., 2012

[M] = Ru(*p*-cymene)Cl$_2$, **82**

       Rh(Cl)COD, **83**

(d) Ouali et al., 2006

Scheme 18. Examples of metal catalyst immobilized at the surface of PPH dendrimers based on an hexa-functionalized core, and their applications in catalysis.

- Precipitation of the Pd@dendrimer from *n*-pentane

  - Separation by filtration or decantation

  - Reciclability up to 5 catalytic cycles

Scheme 19. Pd@PPH dendrimer bearing a 15-member azamacrocyclic units at the surface of the structure, used for Heck cross-coupling reaction.

The examples shown above are intended to provide few examples of catalyst@dendrimer systems based on the most popular metals. In addition to these examples, many more dendrimeric systems have been developed for a huge range of applications. Of interest, dendrimeric systems for catalysis have been developed incorporating several other catalysts such as gold,[110] scandium,[111] or the use of organocatalysts,[112] to cite some examples. For deeper insights in the use of dendrimers in catalysis and excellent reviews, refer to the work of Caminade,[40] Majoral,[113] or Laurent.[114]

Despite the extensive work on PPH dendrimers in catalysis, there is, at the moment of writing of this Thesis, no example reported in the literature that shows the applicability of phosphorus Janus dendrimers in catalysis. In this regard, despite some promising candidates have been described, this Thesis aims to tackle the development of the first PPH Janus dendrimers with applicability in catalysis.

2. Olefin metathesis

2.1. State of the art and metathesis pre-catalysts

First discovered over half a century ago, olefin metathesis (OM) has evolved into one of the most significant reactions in modern synthetic chemistry, with applications spanning both organic chemistry laboratory and industrial scales, *inter alia* for manufacturing of crucial products such as polymers, fine chemicals, active pharmaceutical ingredients (APIs), but also with potential applications in biology and materials science. The fundamental idea behind olefin metathesis originates from the Greek word μετάθεσις, signifying a change in position, referring the reconfiguration of alkene fragments through the cleavage and regeneration of carbon-carbon double bonds (**Scheme 20**).[115]
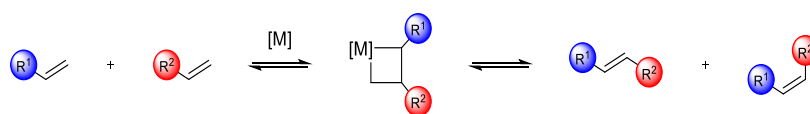
Scheme 20. General scheme of olefin metathesis.

The initial records of olefin metathesis were documented by Dupont's Petrochemical Department, where Eleuterio and co-workers achieved the production of a propylene-ethylene co-polymer in 1956.[116] They accomplished this by passing a propylene feed through an aluminum-supported molybdenum catalyst. In their findings, the resulting polymer seemed to have been crafted as though someone had taken a pair of scissors, unfolded cyclopentene, and then sewed it back together.

This discovery led in 1960 to the first example of OM for the norbornene polymerization catalyzed by WCl_6/$AlEt_2Cl$. Additionally, Banks and Bailey documented a phenomenon termed "olefin disproportionation" in 1964.[117] They observed the conversion of propene into ethylene and 2-butene using molybdenum- and tungstenhexacarbonyl on alumina.

Concurrently, in 1967, Calderon and his co-workers presented an explanation for the process of metathesis. They illustrated that one carbon of the double bond in one olefin exchanges all its attached constituents with another carbon from the second olefin, along with its attached constituents. This exchange occurred through a four-centered cyclobutane-metal intermediate.[118] Nonetheless, the exact structure and functioning of the catalyst remained undisclosed.

Drawing from the prior investigations, numerous endeavors were dedicated to uncovering the precise mechanism governing olefin metathesis. In this context, Pettit[119] and Grubbs[120] put forth their respective mechanistic theories, involving a tetramethylene intermediate and migration of substituents around a double bond, leading to a rearrangement into a metallocyclopentane intermediate. However, their proposals did not align with the experimental results.

It was only in 1971 that Chauvin and Hérisson made a breakthrough by identifying a metallacyclobutane species as the pivotal intermediate in the metathesis process.[121] The proposed

mechanism, depicted in **Scheme 21**, commences with a metal alkylidene species **I**, which coordinates with an olefin **II** to generate the aforementioned metallacyclobutane **III**. Subsequently, **III** undergoes a reverse [2+2] cycloaddition reaction, releasing ethylene and a metal-alkylidene species **IV**. This regenerated species **IV** can then re-enter the catalytic cycle, following the same pattern as the initial species **I**, coordinating with another olefin **V** forming a new metallacyclobutane **VI**, and furnishing the desired final olefin **VII**, regenerating **I** which could enter in a new catalytic cycle.

This proposed mechanism was reaffirmed by several other research groups. For instance, teams led by Schrock,[122,123] Grubbs,[124,125] and Katz[126,127] carried out extensive studies that culminated in the widespread acceptance of Chauvin's mechanism.

It is worth noting that this mechanism put forth by Chauvin is applicable across the entire spectrum of olefin metathesis reactions. Of particular significance, **Scheme 22** illustrates the principal variations in olefin metathesis reactions, encompassing the Ring-Closing Metathesis (RCM), Cross-Metathesis (CM), and Ring-Opening Metathesis Polymerization (ROMP), among others.

The progress of metathesis reactions, along with the identification of the first well-defined catalysts and the elucidation of the reaction mechanism, resulted in the Chemistry Nobel Prize being awarded upon Chauvin, Grubbs, and Schrock for their advancements in the metathesis technique within organic synthesis.[128–130]
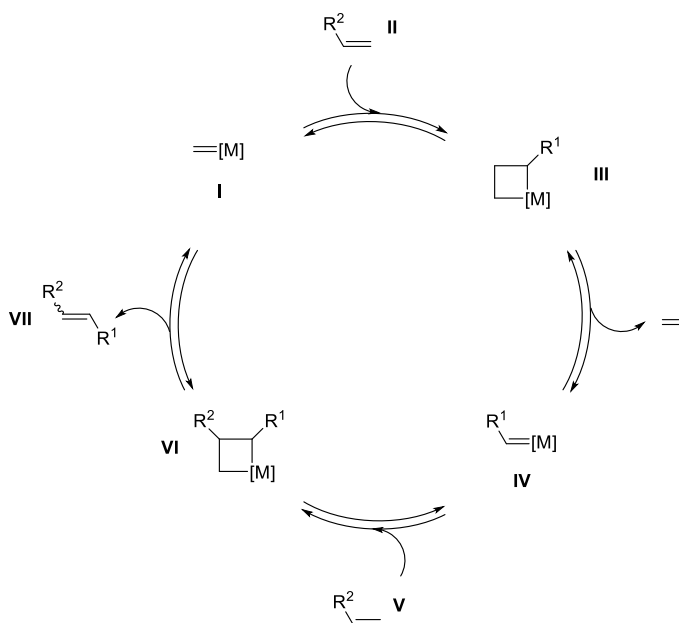
Scheme 21. Representation of Chauvin's proposed metathesis mechanism.
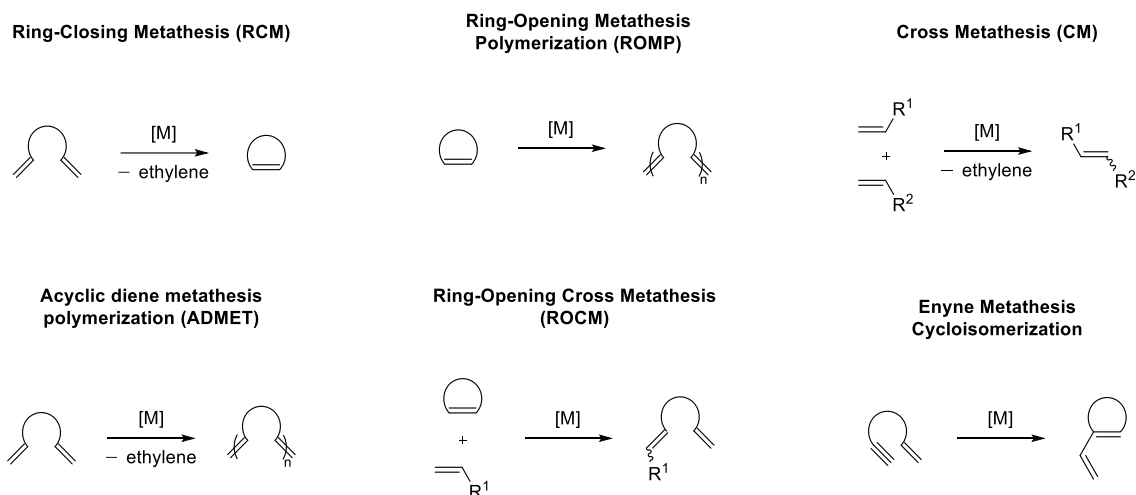
Scheme 22. Selected variations of olefin metathesis reaction.

Over the past few decades, there has been a growing interest in metal-alkylidene complexes, which eventually has led to the synthesis of numerous metathesis metal complexes. Within this context, metathesis catalysts have been extensively documented in literature. These complexes involve over ten different metals, such as rhenium,[131] niobium,[132] rhodium,[133] osmium,[134] iridium,[135] iron,[136] vanadium,[137] and notably the versatile ones crafted from tungsten, molybdenum, and ruthenium.

In 1980, Tebbe *et al.*[138] presented the synthesis of a titanium methylidene complex [$Cp_2Ti(=CH_2)(ClAlMe_2)$]. Grubbs subsequently demonstrated that this complex could act as a catalyst for olefin metathesis in the presence of pyridine, leading to the isolation of the initial metallacyclobutane and laying the foundation for identifying olefin metathesis intermediates.[139,140] Concurrently, Schrock and his team unveiled the first well-defined tantalum-alkylidene complex [$Ta(=CH-^tBu)Cl(PMe_3)(O^tBu)_2$] for olefin metathesis of *cis*-2-pentene.[141]

The inaugural well-defined tungsten-based catalysts were developed by Schrock[142,143] and Osborn during the 1980s. These metal-alkylidene complexes (depicted in **Figure 9**), necessitating the presence of a Lewis acid for activation, were eventually superseded by breakthroughs from Basset and his associates.[144] They reported the first tungsten catalysts that functioned without requiring such activation. Notably, this achievement marked a significant advancement in the field. Following this trajectory, the progression of metathesis catalysts motivated Schrock to create a molybdenum-based catalyst in the 1990s (**Figure 9**), offering a broad activity range and compatibility with diverse functional groups.[144]
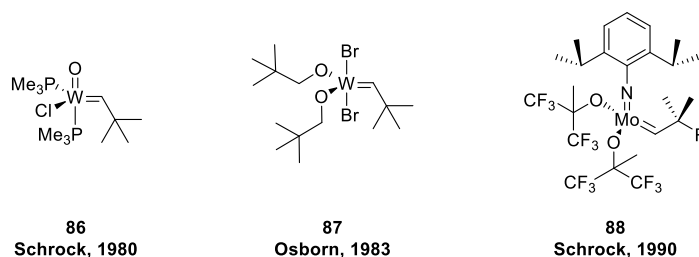
86
Schrock, 1980

87
Osborn, 1983

88
Schrock, 1990

Figure 9. First well-defined olefin metathesis catalysts.

Although the molybdenum and tungsten metathesis catalysts demonstrated remarkable reactivity and a high degree of adjustability, they also exhibited a significant drawback—sensitivity to both air and moisture.[145] This limitation prompted the exploration of an alternative avenue, especially for applications involving technical-grade solvents or polar substrates. Consequently, a new class of catalysts emerged to fill this gap: the air and water-stable ruthenium complexes.

2.2.   Ruthenium pre-catalysts for olefin metathesis

Among all transition metals, ruthenium is recognized as one of the most versatile and appealing choices for catalytic reactions, especially in the context of olefin metathesis.

The initial exploration of ruthenium-based olefin metathesis catalysts dates back to the 1960s. Drawing inspiration from Natta's work on cyclobutane polymerization using $RuCl_3$,[146] Grubbs documented the polymerization of norbornene derivatives in protic solvents. This was achieved using $RuCl_3 \cdot H_2O_x$ and $[Ru(H_2O)_6(OTs)_2]$, resulting in the formation of a ruthenium-alkylidene intermediate.[147]

This endeavor led to the creation of the first well-defined ruthenium-alkylidene complex by Grubbs in 1992 (**Figure 10**).[124] This complex played a main role in enabling Ring-Opening Polymerization (ROMP) and Ring-Closing Metathesis (RCM) reactions.

In 1995, Grubbs and his collaborators introduced faster-initiating ruthenium complexes $[Ru(=CHPh)Cl_2(PR_3)_2]$, renowned as the first-generation Grubbs Catalysts (**Gru-I**, **Figure 10**).[125] This groundbreaking achievement resulted in air-stable ruthenium complexes that exhibited compatibility with a wide array of functional groups. These complexes also demonstrated relatively high stability in air, making them highly versatile.

Similarly, in 1999, Hoveyda's team developed a novel recyclable ruthenium olefin metathesis catalyst.[148] This catalyst, known as Hoveyda first-generation catalyst (**Hov-I**), incorporated a benzylidene moiety with an *orto*-isopropoxy chelating group in its structure replacing one phosphine (**Figure 10**). Remarkably, this catalyst maintained its activity even after multiple uses, and showed an increased resistance to moisture and air, as well as improved thermal stability.

Concurrently in 1999, the Nolan group introduced a third type of ruthenium complex, incorporating an indenylidene moiety into the structure. This catalyst marked the advent of the indenylidene-type catalyst category (**Ind**, **Figure 10**).[149]

Collectively, the advancements made by Grubbs, Hoveyda, and Nolan culminated in the creation of the so-called first-generation metathesis complexes, as depicted in **Figure 10**. This significant progress triggered a surge in research groups dedicated to devising active olefin metathesis catalysts. Consequently, the number of novel complexes reported in the field experienced an exponential increase.
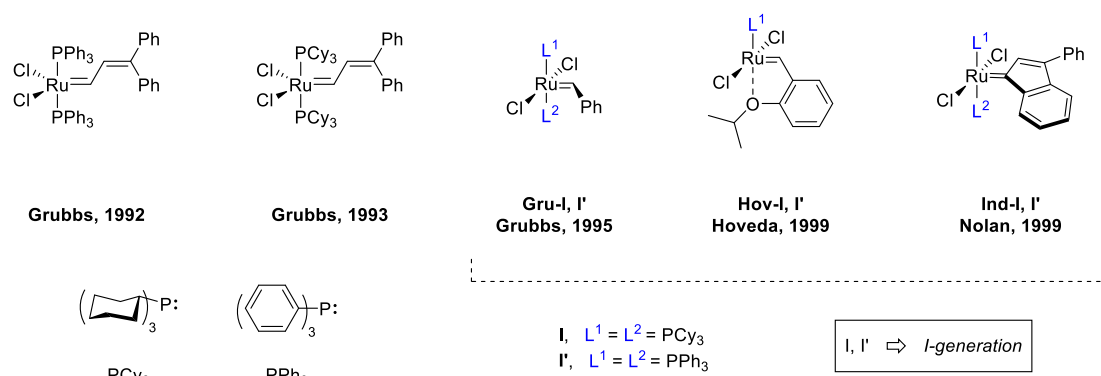
Figure 10. First well-defined ruthenium-alkylidene complexes, comprising the first discoveries by Grubbs and the so-called first-ruthenium complexes.

2.2.1. N-heterocyclic carbene (NHC) ligands

Carbenes exhibit robust Lewis base characteristics, acting as potent σ-donors yet weak π-acceptors. A key attribute of carbenes is their ability to form metal-carbon bonds that typically possess greater stability compared to metal-phosphine bonds. This feature contributes to the enhanced thermal endurance of the corresponding organometallic complexes. Furthermore, the electronic attributes and steric surroundings of heterocyclic carbenes can be readily adjusted by altering substituents on the carbene structure.[115] These traits enable precise tailoring of catalytic behavior and the resultant organometallic complexes.

In efforts to enhance the catalytic efficiency of **Gru-I**, Herrmann and co-workers explored the application of an N-heterocyclic carbene (NHC) ligand. Their approach led to the generation of bis(aminocarbene) complexes,[150] which exhibited a slight activity improvement over **Gru-I** in ROMP reactions.

The collective work of Hermann,[151,152] Nolan,[149] and Grubbs[153] yielded hindered NHC ligands such as 1,3-bis(2,4,6-trimethylphenyl)-imidazol-2-ylidene (**IMes**), 1,3-bis(2,4,6-trimethylphenyl)-imidazoline-2-ylidene (**SIMes**), and their corresponding diisopropylphenyl derivatives (**IPr** and **SIPr**). These ligands facilitated the formation of mixed phosphine/NHC complexes by replacing a single phosphine of **Gru-I** with the desired NHC.

The resulting Ru-NHC complexes proved substantially more effective than their bis(phosphine) counterpart (**Gru-I**) or bis(NHC) complexes (in scenarios where both phosphine groups were replaced by NHCs). As a result, the incorporation of NHCs into ruthenium complex structures for olefin metathesis marked a significant milestone in catalyst design.[154] It is worth noting that nowadays, ruthenium complexes featuring an NHC component are referred to as second-generation catalysts (e.g., **Gru-II**, **Hov-II**, or **Ind-II**, denoting second-generation complexes stemming from the contributions of Grubbs, Nolan, and Hoveyda, **Figure 11**).[153,155,156]

With the development of modern ruthenium complexes, Grela and co-workers described the synthesis of a novel **Hov-II**-based catalyst bearing a nitro group in the structure (**Gre-II**, **Figure 11**) that was shown to provide increased activity for metathesis reactions, allowing the use of lower reaction temperatures, a decrease of the catalyst loading and the obtention of products with a higher selectivity.[157,158]
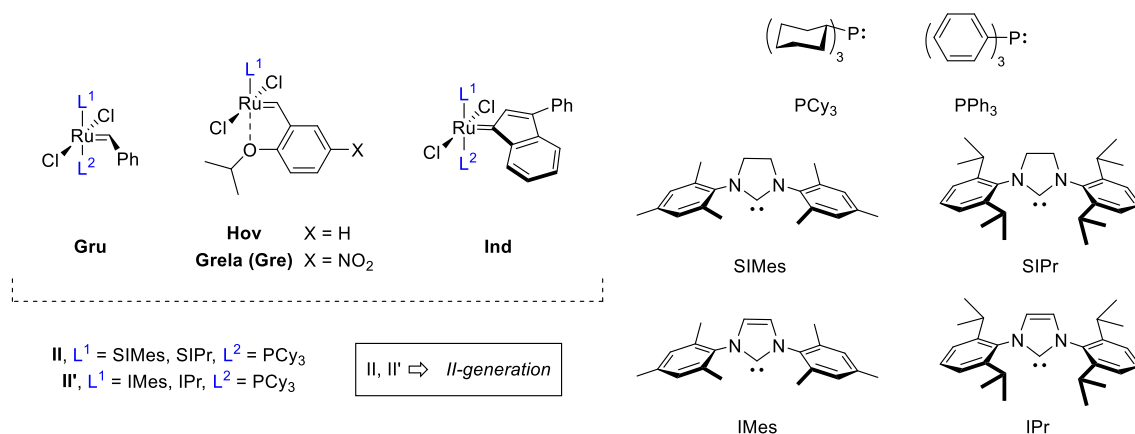
Figure 11. Examples of the so-called second-generation ruthenium complexes for olefin metathesis derived from the Grubbs-, Hoveyda- and indenylidene-type complexes.

While the utilization of ruthenium complexes featuring symmetrical NHCs is widely embraced within the metathesis community for general applications, yielding impressive results, there exist specific metathesis scenarios that have introduced more specialized catalysts. These specialized catalysts are based on what's known as unsymmetrical NHC ligands (uNHC).

One of the initial instances of ruthenium metathesis catalysts incorporating uNHC ligands was detailed by the Fürstner group in the 2000s.[159,160] They documented the synthesis of a series of Grubbs-type complexes with *N*-alkyl-*N'*-mesityl NHCs, wherein diverse modifications were implemented in the alkyl chain (**Figure 12a**). Further examples of uNHC ruthenium complexes, to cite a few instances, include those elucidated by Mol,[161] Blechert,[162] and Verpoort,[163] as depicted in **Figure 12b**. In this trend, our group has also contributed notably to this field by reporting a wide range of Ru-uNHC complexes, enhancing to broaden the library of uNHC-based complexes (**Figure 12c**).[164–166]

The scope of applications for uNHC-based ruthenium complexes extends beyond that of their symmetric counterparts. Several of the applications and attributes demonstrated by Ru-uNHC complexes are featured in the literature. These include a high level of latency, reduced proclivity for undesired olefin bond shifts along the aliphatic chain in terminal or internal olefins, and their efficacy in more challenging reactions. For a comprehensive exploration of this topic, I would recommend referring to the review published by our group in 2021.[167]
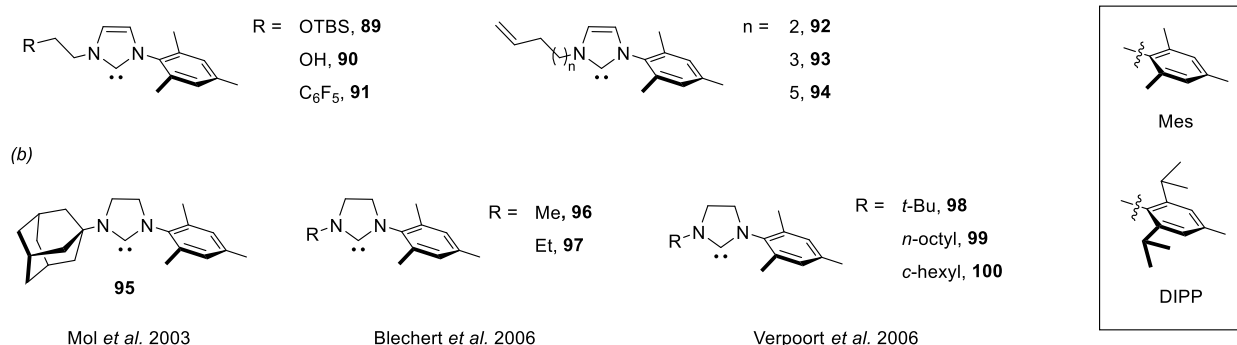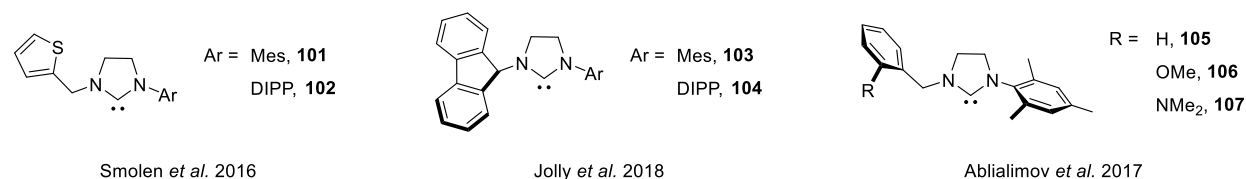
Figure 12. Selected uNHC ligands reported in the literature.

2.3.   Olefin metathesis in special media

Despite the enormous success and progress in the development of olefin metathesis catalysts, one of the most challenging topics to be addressed in the field is the sustainable performance of such transformations. This situation has led to a tremendous interest in the supported or tagged versions of olefin metathesis catalysts to allow the catalytic system to perform in special media, either to reduce the environmental impact of such transformations or to allow an easier removal of the catalyst from the products through simple purification methods.

One of the most easily accessible ways to minimize the environmental factor is the performance of such reactions in non-conventional, non-harmful solvents as reaction media. As many trans-formations in organic chemistry, OM is usually performed under anhydrous conditions and using chlorinated solvents. In this regard, many efforts have been focused on the development of OM in green organic solvents, or the use of aqueous media for the reactions. Among the different alternatives to reach the desired goal of using greener solvents, variations such as the use of or-ganic carbonates, poly(ethylene) glycol, the use of supercritical carbon dioxide ($scCO_2$), the use

of alternative green bio-based solvents for catalysis or solvent-free reactions have emerged as promising candidates.[115]

From all the different approaches to reach the desired goal, the use of water as reaction media has focused the main attention in this field, due to the inexpensive and environmentally friendly characteristics, as well as the potential applications that metathesis in water could provide, such as their use in biological and pharmaceutical synthesis.

Among all complexes described for OM, Ru-based are known for their tolerance and stability for aqueous processes and are the ones that will focus our attention. Despite the promising features, it has to be mentioned that water could lead to the formation of catalytically inactive Ru-hydride species —as isolated and reported by Fürstner,[160] Dinger and Mol,[168] and Cazin.[169]

Since the first reported examples of OM in water during the decade of 1990 using $RuCl_3 \cdot H_2O$ and $[Ru(H_2O)_6](OTs)_2$,[170,171] many research groups have garnered their attention on the development of such transformations.

The first approaches to the aqueous metathesis were performed by employing hydrophobic catalysts in water/co-solvent mixtures as reaction media. The group of Blechert reported the use of **Hov-II** modified catalysts bearing alkoxy- and cyano- groups in their structure,[172] while Raines and co-workers employed the use of conventional **Gru-II** and **Hov-II** complexes for the same purpose.[173] Both approaches were used for the RCM, CM and ROMP reactions employing protic $H_2O/MeOH$ emulsions, leading to moderate conversions. The catalytic outcome determined that the role of the hydrophobic effect played a major part on the catalytic activity.

Therefore, the use of aqueous metathesis substrates has been a topic of interest for the researchers aiming to perform olefin metathesis in water. Of interest, **Figure 13** displays a selection of water-soluble metathesis substrates.
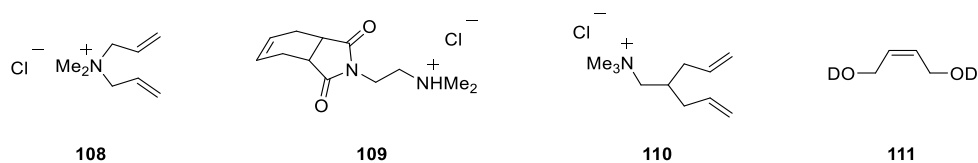

Figure 13. Selected water-soluble metathesis substrates.

The incorporation of amphiphilic moieties/molecules by Lipshutz and co-workers allowed the obtention of the first efficient metathesis in water.[174–176] In this regard, authors generalized the application of a three-component non-ionic surfactants to be used in a wide range of catalytic transformations, OM included.

Among all the described possibilities for metathesis in aqueous media the incorporation of ionic tags or PEG chains in the ligands structure of the catalyst has become the most powerful tool for this aim.

Mostly, water-soluble catalysts are obtained through derivatization of classical Grubbs- and Hov-eyda-type complexes. The introduction of PEG chains has been shown to be one of the alternative methodologies for the preparation of water-soluble, for example modifying the NHC moiety in the Ru-complex to incorporate these water-soluble chains. **Figure 14** intends to show some examples of the aforementioned class of complexes, based on the work of Hong and Grubbs[177] (**Ru1** and **Ru3**) and Kim *et al.*[178] (**Ru2**).
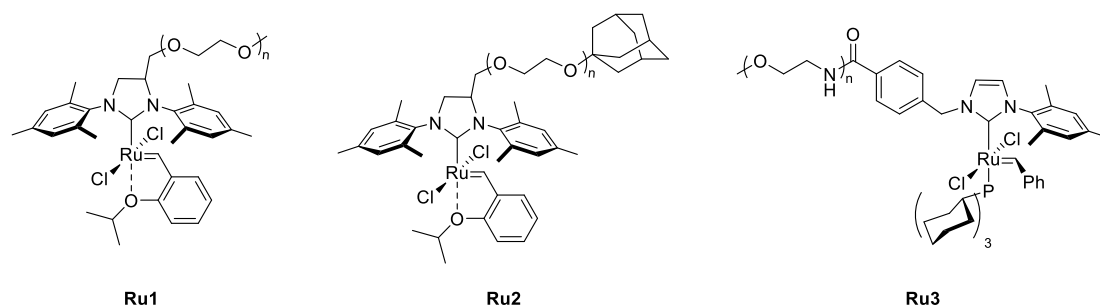
Figure 14. **Hov-II**- and **Gru-II**-based complexes bearing PEG chains in the structure for applications in aqueous olefin metathesis.

Another methodology employed for the obtention of water-soluble ruthenium complexes is the incorporation of cationic or anionic moieties within the catalyst structure through phosphine exchange. In this regard, phosphines containing ionic groups (such as ammonium salts or sulfonates, **Figure 15**) have been incorporated in **Gru-I**-type complexes to obtain water-soluble catalysts by Grubbs and co-workers as the main representatives of this chemistry.[179–181]
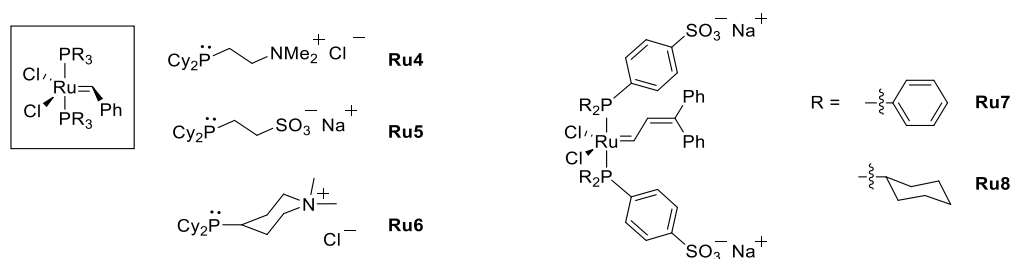
Figure 15. **Gru-I**-type complexes bearing ionic tags in their structure through modification of the phosphine ligands, for applications in aqueous olefin metathesis.

The compounds displayed in **Figure 15** showed a high water and methanol solubility, while being insoluble in organic solvents. Despite the promising structural adjustment, compounds **Ru4–Ru8** appeared to be highly air-sensitive decomposing in solution after 2 days. Ru-catalysts were tested in the ROMP and RCM reactions of water-soluble substrates, showing that the metathesis in water had a high dependency of the conversion on the substrate polarity. To overcome the limitations of the previous examples, the most successful methodology for aqueous metathesis developed up to now is the incorporation of ammonium tag modifications onto **Hov-II**-type complexes. In 1997, Grubbs and co-workers reported the synthesis of Ru-catalysts incorporating such ammonium tags to both modified NHC and 2-styreneisopropoxy moieties (as shown in **Scheme 23a**).

The introduction of ammonium moieties to the structure of Ru-complexes has been widely studied by Grela's group. Of interest, in 2006, Grela and co-workers reported the synthesis of a Ru-catalyst (**Ru14**) obtained *in situ* by treatment of **Ru13** with MeCl (**Scheme 23b**),[182] showing good performance in metathesis reactions carried out in H_2O/MeOH mixtures.
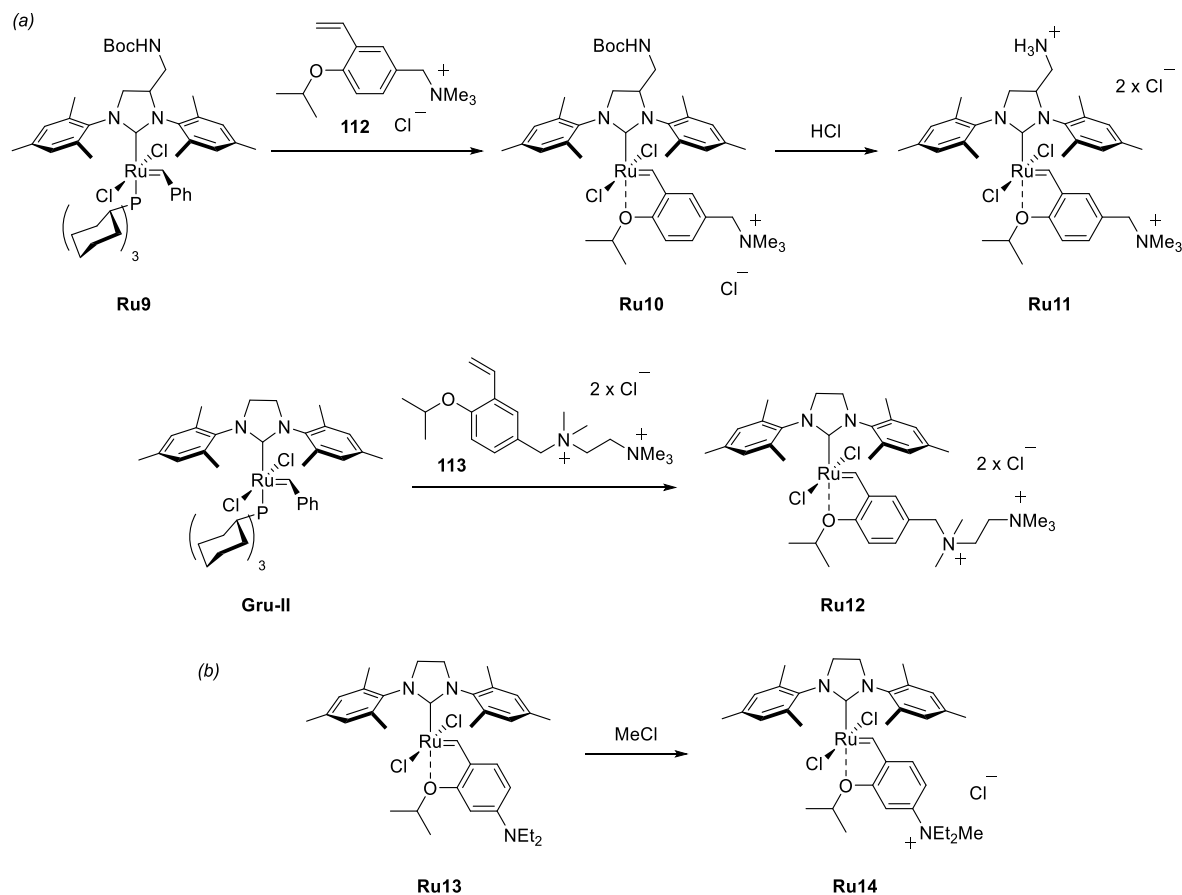
Scheme 23. Synthesis of **Hov-II**-based complexes bearing ammonium tags in the structure, developed by *(a)* Grubbs, and *(b)* Grela.

The same methodology employed by Grela was further studied in his group in collaboration with the company Apeiron Synthesis, applying *in situ* quaternarization of catalysts bearing amine groups to the corresponding ammonium salts (**Figure 16**).[183] Catalytic performance was tested in non-degassed D_2O under air showing conversions up to the 94% in CM and RCM reactions.
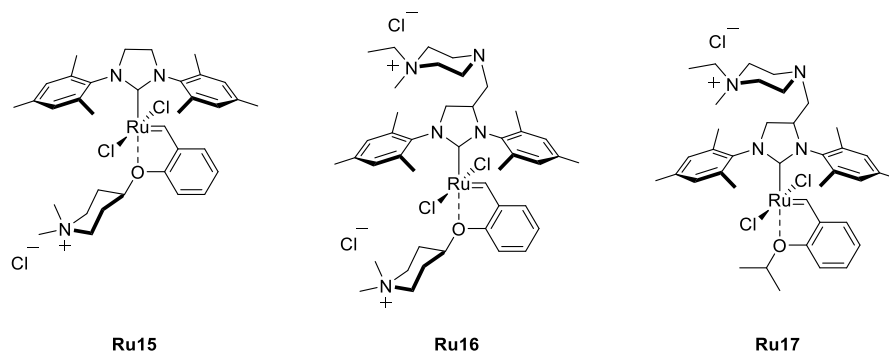
Figure 16. Ammonium-tagged Ru-catalysts synthesized by Grela and co-workers by *in situ* quaternarization of the amino groups.

Metathesis catalysts bearing quaternary ammonium groups provide an attractive alternative to classical ruthenium catalysts. These structures significantly improve the water solubility and facilitate the removal of ruthenium residues from reaction mixtures —simplifying the post-reaction treatments to get rid of the catalyst by precipitation of extractions.

In this context, the development of tagged versions of Ru-complexes provides a great alternative for the use of green solvents in metathesis. The examples shown above are only few of the many reported tagged-Ru-catalysts. For comprehensive reviews on the topic of olefin metathesis in water, refer to the work of Tomasek *et al.,*[184] and Sabatino *et al.*[185]

2.4.   Supported olefin metathesis catalysis

Metal complexes remaining after the olefin metathesis step may cause undesired side reactions such as product isomerization, polymerization, or degradation during work-up.[115] Therefore, the development of efficient and economical methods to remove ruthenium compounds present in the reaction mixture is crucial for the application of metathesis methodology in industry.[186] A number of efforts to remove the catalyst or the products of its decomposition by the addition of various scavengers such as peroxides, charcoal, silica gel, and other sorbents or by biphasic extraction have been carried out; however, none are universally applicable so far.[184,187,188]

An alternative to address the obtention of clean metathesis products is the preparation of ruthenium complexes immobilized on supports. This section aims to highlight some examples of the different methodologies employed to graft Ru-catalysts on supports, such as the immobilization through a phosphine exchange, alkylidene exchange, through the NHC ligand or *via* halogen exchange.[189] The implementation of such concepts requires the presence of remotely functionalized ligands within the metal coordination sphere. The first example of a supported ruthenium OM complex was reported by Grubbs and co-workers in 1995.[190] In their work, several phosphines were derivatized with a PS-DVB resin and later reacted with $Cl_2Ru=CH-CH=CPh_2$ to obtain the desired immobilized system (**Figure 17a**). The new Ru-catalyst was tested in the metathesis of *cis*-2-pentane and the ROMP of 2-norbornene showing a reduced activity compared to the parental complex. Based on that approach, Verpoort and co-workers reported in 2001 the grafting of **Gru-I** complexes on a phosphine-derivatized mesoporous silica.[191] Particularly, the silica support (P-MCM-41) was derivatized with $(EtO)_3SiCH_2CH_2PPh_2$ groups at the surface, for the later immobilization of the ruthenium precursor (**Figure 17b**). The obtained systems showed a large polydispersity which dramatically affected the conversions for the tested RCM reaction of DEDAM.

A similar approach was later used by Grubbs and co-workers in 2009.[192] In particular, they reported the covalent immobilization of a **Hov-II**-type complex on silica gel through the NHC moiety (**Figure 17c**), resulting in the obtention of a novel methodology that was shown to be a much

better approach than the previously used ones for such purpose (such as the immobilization through phosphine ligands or the alkylidene moiety).

A very efficient covalent immobilization through an exchange of anionic ligands was reported by Buchmeiser and co-workers who synthesized a series of monolith-supported catalysts (*e.g.* **Figure 17d**) which gave metathesis products with extremely low residual ruthenium.[193,194] In terms of immobilization of Ru-catalysts through the alkylidene moiety, Barret and co-workers described the use of a vinyl-modified support.[195] In their example, a poly(vinyl-styrene-co-divinylbenzene) was reacted in an alkylidene exchange reaction with **Gru-I** catalyst to obtain the desired supported complex. (**Figure 17e**).

Non-covalent links between the Ru-catalyst and the support have also been extensively tested. For example, Grela's group reported an activated catalyst deposited on Raschig glass (**Figure 17f**),[196,197] and Mauduit and co-workers showed the same immobilization employing a pyridinium-tagged complex deposited on modified silica gel.[198]

All the previously mentioned examples on the development of supported OM catalysts present their own positive aspects and drawbacks, as there is not nowadays an optimal methodology for the obtention of supported systems. For a deeper insight on the topic, excellent reviews have been published.[186,189,199–201]

Among all the supports for metathesis, there are two systems that we would like to draw particular attention to: Metal-Organic Frameworks (MOFs) and dendrimers.
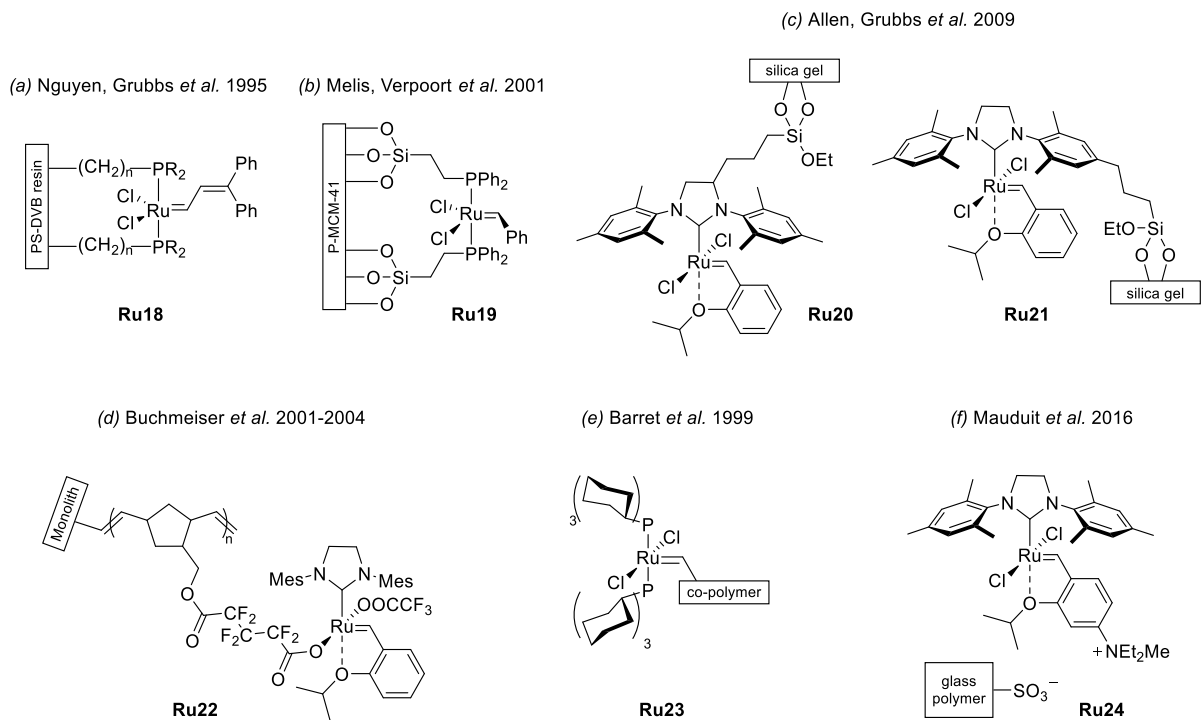
Figure 17. Selected examples of supported ruthenium complexes for OM.

2.4.1. MOFs as supports for olefin metathesis

Metal-organic frameworks (MOFs) are increasingly gaining recognition as highly auspicious materials for heterogeneous catalysis. Their crystalline, remarkably porous, and easily modifiable structures provide distinctive environments for the immobilization of catalytically active species.[202] Unlike certain conventional solid substrates, catalytic sites within MOFs are not merely affixed to their surface; rather, they are situated within defined nanoscopic voids within a crystalline framework. These voids in MOFs can be expansively designed to comfortably accommodate typical homogeneous catalysts and their corresponding substrates, thus avoiding notable transport challenges.[203,204] Contrarily, the spatial limitations imposed by the nanocavities of MOFs introduce novel approaches for regulating shape selectivity, regioselectivity, and enantioselectivity of the immobilized catalysts. In this aspect, MOFs exhibit parallels with crystalline mesoporous silicas and zeolites, yet outperform them due to their facile tunability, a characteristic attributable to their hybrid organic-inorganic composition.[205]

Indeed, by properly selecting linkers and clusters, the voids within MOFs can be sufficiently enlarged to encapsulate even the most intricate homogeneous catalysts and to facilitate unhindered diffusion of substrates and resultant products. Furthermore, these cavities can be tailored to specific requirements by appropriate functionalization of the MOFs' organic ligands and/or coordination of functional moieties onto the metal clusters.[204] Consequently, catalysts immobilized within MOFs not only profit from facile isolation and potential reusability but also experience spatial segregation within a defined and adjustable nano environment.

However, achieving robust immobilization of active olefin metathesis catalysts within MOFs presents challenges. These catalysts are unlikely to endure the typically harsh solvothermal conditions of MOF synthesis, prompting the development of diverse post-synthetic immobilization strategies. For instance, in 2016, Spekreijse *et al.* described the synthesis of a Ru@MOF through the confinement of a **Hov-II** complex within the MOF structure using a mechanochemical immobilization technique, involving grinding the catalyst and support together.[206] The resultant structure was evaluated in the RCM reaction of DEDAM, yielding an initial conversion rate of 98% and demonstrating reusability for up to eight cycles.

In the same year, Klemperer and co-workers reported the creation of a covalently immobilized system.[207] This involved utilizing an aldehyde-modified **Hov-II**-type complex **Ru25**, which subsequently reacted with an **IRMOF-74-III** featuring an amine group. This reaction established a covalently bonded system through an imine bond (as depicted in **Scheme 24**).
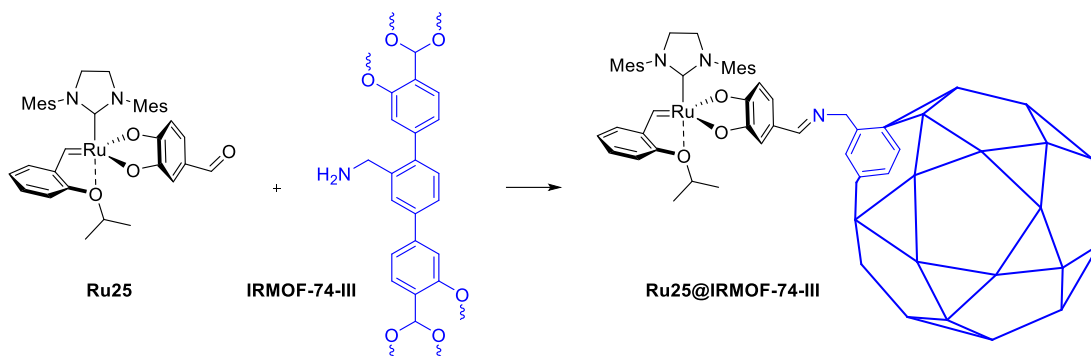
Scheme 24. Covalent immobilization of a **Hov-II**-type complex in the **IRMOF-74-III** structure through imine bond formation.

In addition to these examples, Ru@MOF systems have been obtained through non-covalent interactions, largely attributable to the extensive efforts undertaken by the Chmielewski and Grela research groups. A noteworthy case reported by Chmielewski and collaborators in 2016 involved employing **(Al)MIL-101-NH₂·HCl** to non-covalently immobilize a suite of ammonium-tagged Ru-catalysts based on **Hov-II**-type complexes (**Figure 18a**).[208] These Ru-catalysts were integrated within the MOF structure *via* impregnation, yielding solid heterogeneous catalysts by merely blending solutions containing the catalyst and the MOF. The resulting Ru@MOFs exhibited stability under batch and flow conditions, demonstrated high activity in metathesis reactions with turnover frequencies of up to 8900, and exhibited minimal Ru content in the RCM product (below 0.02 ppm).

Utilizing the same **(Al)MIL-101-NH₂·HCl** MOF, Grela and co-workers reported in 2020 the synthesis of two analogous Ru-benzylidene catalysts through Coulomb interactions, followed by an investigation into the initiation and propagation steps during the catalytic cycle.[209]

Another instance reported by Grela, Kajetanowicz, and collaborators involved immobilizing ammonium-bearing **Ru16** within a **(Cr)MIL-101-SO₃(Na 15-crown-5)** MOF *via* cation metathesis.[210] The resultant Ru@MOF exhibited stability across a broad range of solvents, including polar ones like isopropanol. Additionally, it demonstrated considerable potential for facile separation from reaction mixtures through simple filtration. Moreover, the metathesis of pharmaceutically relevant substrates gave impressive yields and impeccable selectivity (as illustrated in **Figure 18b**). Simultaneously, Chmielewski's group in 2019 detailed the immobilization of Ru-catalysts bearing amino groups onto the same MOF structure featuring a sulfonic acid group. Specifically, they employed an acid-base reaction to form a salt, which served as the immobilization methodology for achieving the desired Ru@MOF.[211]

(a)

(Al)MIL-101-NH₂

L =

Ru27

Ru28

Ru16

Ru29

Grela, Chmielewski et al., 2016

(b)

Ru16

Ru@(Cr)MIL-101-SO₃

Grela et al., 2019   *Chmielewski et al.*, 2019
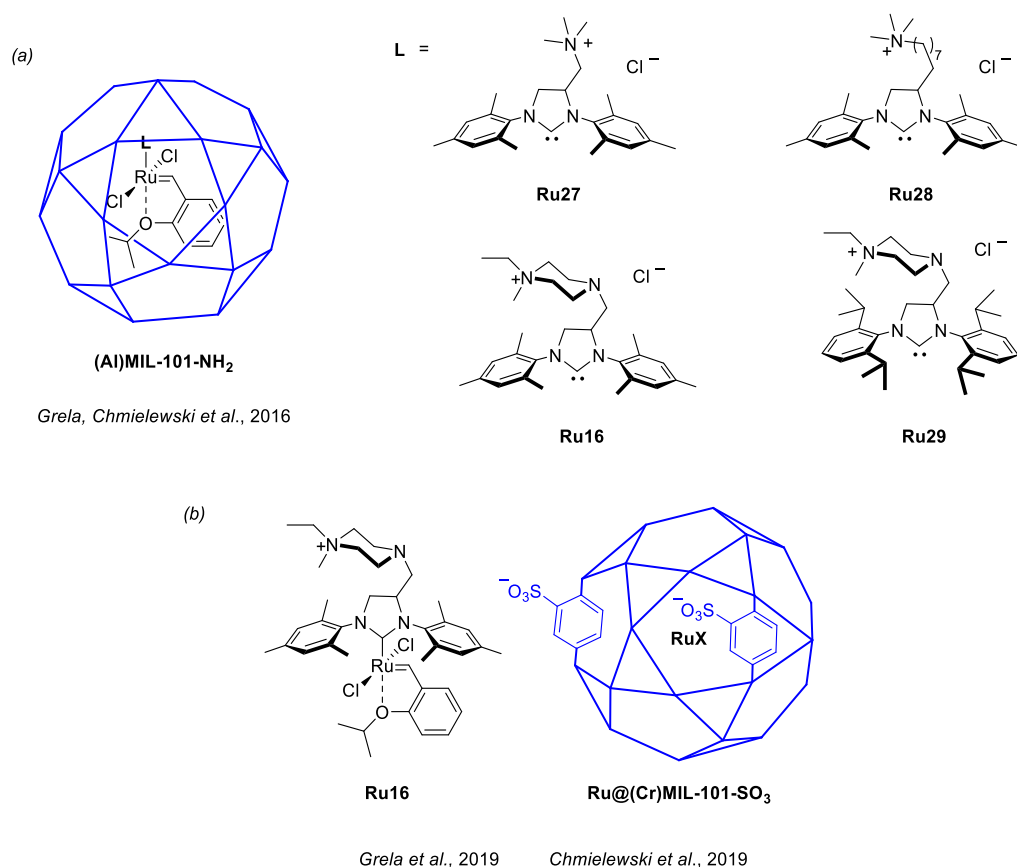
Figure 18. Representation of the non-covalently immobilized Ru@MOFs described by the groups of Grela and Chmielewski. Used MOFs: **(Al)MIL-101-NH₂** and **(Cr)MIL-101-SO₃Na**.

2.4.2. Dendrimers as supports for olefin metathesis

As previously described, dendrimers can be considered as a great alternative for the incorporation of various catalysts onto their structure. However, only few examples of the immobilization of the ruthenium OM complexes on the dendrimers have been reported.

In 2000, Hoveyda and co-workers presented the pioneering example of a Ru-dendrimer system for olefin metathesis.[148] Their study detailed the creation of silicon-based dendrimers that included **Hov-I** and **Hov-II** catalysts, marking a significant milestone in the field (**Figure 19a**). To construct the desired dendritic structures, they synthesized a silicon-core dendrimer with branches consisting of $(CH_2)_3$-$SiMe_2(CH_2)_3OC(O)(CH_2)_2$ linked to the benzylidene *orto*-isopropoxy ligand. This process resulted in dendrimer configurations adorned with four ruthenium complexes on the surface. The **Hov-I**-based dendrimer underwent testing in the RCM of *N,N*-diallyl-4-methylbenzenesulfonamide, utilizing 5 mol% of Ru-dendrimer. This led to a remarkable 99% conversion rate. Particularly noteworthy was their achievement of recovering and reusing the Ru-dendrimer catalyst. Following the first cycle, the catalyst was reclaimed with only a 13% loss of ruthenium. This system displayed activity for up to 6 cycles, achieving conversions as high as 87%, though with a corresponding loss of ruthenium content reaching 59%. The **Hov-II** variant of the Ru-dendrimer, in which the phosphine ligand was substituted with an IMes NHC,

exhibited even greater catalytic efficiency compared to the analogous **Hov-I**@dendrimer. This version experienced a mere 8% reduction in ruthenium content after the catalytic process. Moreover, due to its elevated polarity and molecular weight, it could be readily separated from reaction mixtures by filtration or precipitation techniques.

In the same year that Hoveyda introduced the first dendritic system for olefin metathesis, the van Koten's group achieved the synthesis of carbosilane dendritic compounds functionalized with 2-hydroxyalkylpyridyl groups. Following a transmetallation step, these compounds were transformed into the desired Ru-dendrimer systems (**Figure 19b**).[212] Testing these systems in the RCM of diethyl diallylmalonate (DEDAM) with just 1 mol% of ruthenium catalyst resulted in complete conversion within 0.5 hour of reaction time at 80 °C.

Finally, in 2014, Klein Gebbink's group reported the third instance of a Ru-dendrimer system for olefin metathesis (**Figure 19c**).[213] Their work centered on the synthesis of a carbosilane dendrimer that carried a terminal chlorohexyl chain. This chain served as a grafting point for the attachment of dendritic mesitylimidazolium ligands, subsequently reacting with the ruthenium precursor. Employing this approach, the authors successfully created Ru@carbosilane dendrimers containing **Gru-II'** and **Hov-II'**-type complexes. While these dendritic entities displayed acceptable conversion rates in the RCM of DEDAM, their performance was slightly inferior to that of commercially available complexes.

Therefore, dendrimer-supported Ru-catalysts could offer a great alternative for a greener approach to olefin metathesis catalysis. In this regard, Ru@dendrimer systems could perform the catalytic process in homogeneous phase due to their solubility attributes but allowing their recovery and recyclability through straightforward techniques.

(a) Garber, Hoveyda et al., 2000
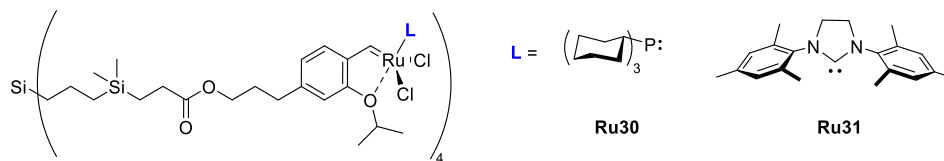
(b) Wijkens, van Koten et al., 2000
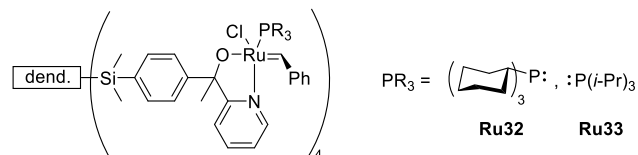
(c) Pijnenburg, Klein Gebbink et al., 2014
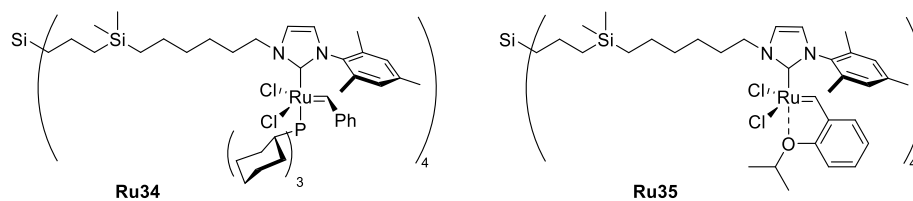
Figure 19. Reported Ru@dendrimer systems for olefin metathesis catalysis.

Chapter II. Objectives

In light of the information presented in the Introduction and recognizing the research areas that require further investigation in the literature, the focus of this Thesis was directed towards the synthesis of novel ruthenium complexes for their immobilization on supports such as dendrimers and MOFs, and to the study of the catalytic capacity and recovery of these complexes, with an emphasis on using sustainable solvents whenever possible.

Therefore, the following specific objectives were proposed:

[1] To synthesize an unprecedented PPH Janus dendrimer containing PEG chains on one side of the structure and functional groups capable of immobilizing Ru-complexes on the other side. The obtention of Janus dendrimers will involve synthesizing dendrimer wedges containing either azide or acetylene groups at the level of the core, selectively functionalizing the surface to incorporate the desired moieties, and coupling dendrons through click triazole chemistry.

[2] To develop novel NHC ligands containing phenolic moieties in their structure and their corresponding **Hov-II**-type complexes for olefin metathesis. Moreover, to evaluate the stability of the prepared complexes and their performance as homogeneous catalysts in model metathesis reactions.

[3] To investigate the ways of preparation of a Ru-NHC@Janus dendrimer system for olefin metathesis catalysis. Incorporate Ru-NHC complexes bearing a phenol group within the structure of a PPH Janus dendrimer, with the ultimate goal of conducting metathesis reactions in aqueous media. Also, to assess the feasibility of immobilization and analyze the dendritic effect on the catalytic entity's activity and selectivity.

[4] To examine the versatility of previously synthesized Ru-NHC complexes by immobilizing them on MOFs as a support. For that, to synthesize an **(Al)MIL-101-NH$_2$** MOF and test the viability of obtaining a heterogeneous Ru@MOF catalyst through phenol/MOF interactions. Besides, to evaluate the supported catalyst in terms of leaching and its activity in metathesis reactions.

[5] To assess the adaptability of the PPH Janus dendrimer for immobilizing alternative Ru-complexes. In this context, to perform the grafting of Ru(*p*-cymene) pre-catalysts on the dendrimer surface. Test the resulting Ru@dendrimer system for the isomerization reaction of allyl alcohols and analyze the dendritic effect of the final catalyst in comparison with model monometallic and bimetallic species.

Chapter III. Results and Discussion

1. Synthesis of modified PPH Janus dendrimers to favor the solubility in water

Since the introduction of PPH dendrimers by Caminade and Majoral in the 1990s, interest in and the development of such compounds has experienced tremendous growth in fields such as materials science, biology, medicine, and catalysis.[40,41,43,49,86] As mentioned in the introduction of this thesis, the utilization of PPH dendrimers can vary significantly depending on the selected functionality grafted onto these hyperbranched macromolecules. In this regard, the applicability of phosphorus dendrimers has traditionally been limited to a single field due to the homogeneous incorporation of a single type of moiety into the dendrimer structure, resulting in its well-known structural uniformity.

However, several methodologies have been reported to enhance the applicability of dendritic systems by introducing two or more functionalities within the structure, typically at the surface of dendrimers.[69] By employing such methodologies, a single dendritic entity can combine the properties of two types of functional groups.

Typically, polyfunctionalized dendrimers are synthesized using a stochastic approach, where the final structures are obtained without control over the number and location of the different functionalities within the dendritic structure (**Scheme 25**).[67,68] Although this methodology is the easiest way to obtain bifunctional dendrimers, the stochastic approach contradicts the concept of perfectly arranged, controlled, and reproducible structures derived from dendrimer synthesis.
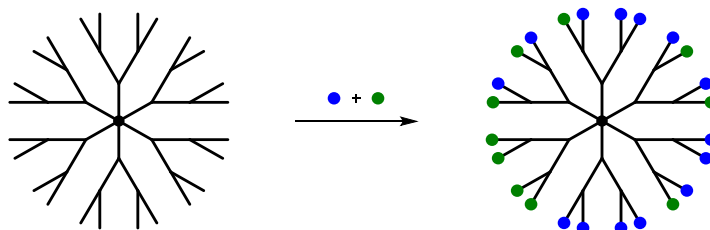
Scheme 25. Representation of an example of the stochastic synthesis of bifunctional dendrimers, obtaining a randomly substituted dendrimer.

To address the issues arising from stochastic synthesis, such as low reproducibility in different batches and the potential increase in impurities, various alternatives have been documented in the literature to mitigate these effects. These methodologies are typically based on grafting pre-existing bifunctional molecules onto the dendrimer structure or sequentially modifying the surface to incorporate the two desired functionalities.

In the first approach, as depicted in the example in **Scheme 26a**, the preparation of bifunctional molecules for incorporation into PPH dendrimers has been extensively investigated by the Caminade research group.[69] As illustrated in the example,[106] a L-tyrosine derivative **115** bearing a diphosphine group on the surface was synthesized and subsequently coupled to the dendrimer

structure, resulting in the desired bifunctional first-generation dendrimeric structure **116**. This obtained bifunctional dendrimer was later employed for catalyzing cross-coupling reactions following palladium complexation.

In the second approach, as shown in **Scheme 26b**, the synthesis of a bifunctional dendrimer was accomplished by substituting two amine derivatives directly on the surface of the dendrimer.[214] Notably, amine **117** was initially reacted under basic conditions to introduce it into half of the terminal P–Cl bonds (6.0 equiv.) to form compound **118**. Subsequently, **118** reacted with the second amine **119** to complete the substitution of the bifunctional dendrimer **120**.
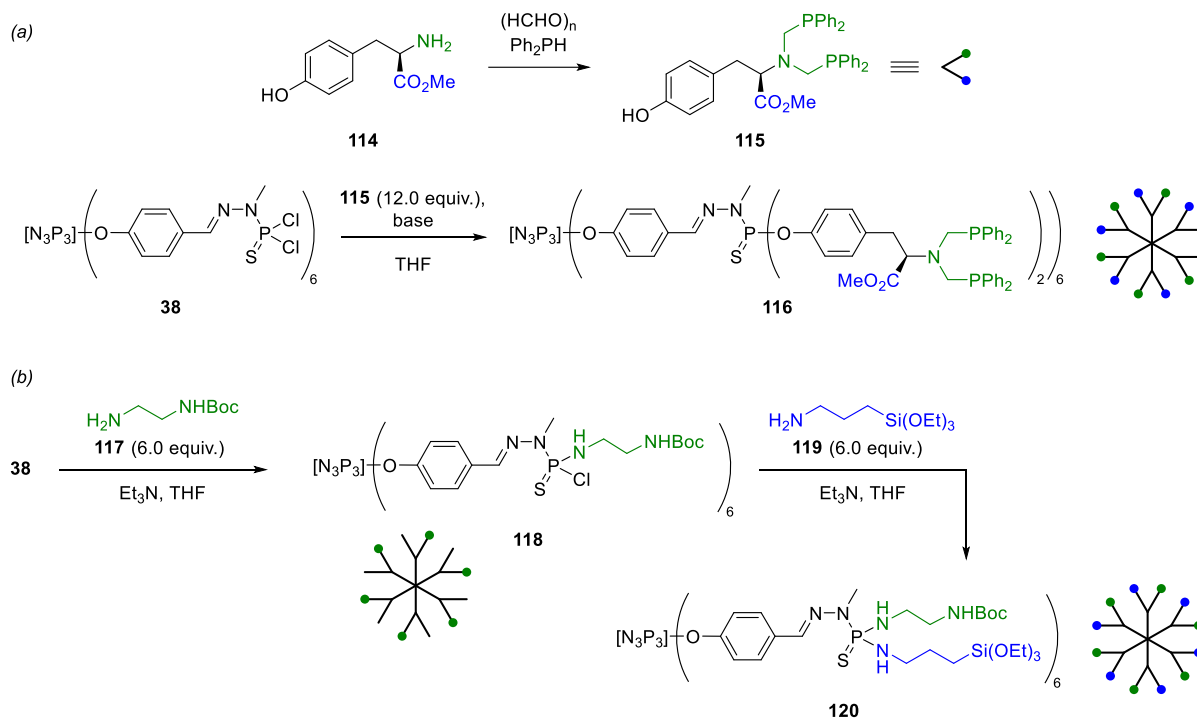
Scheme 26. *(a)* Synthesis of a bifunctional PPH dendrimer by reaction of a bifunctional phenol **115** with a first-generation PPH dendrimer **38**. *(b)* Synthesis of a bifunctional PPH dendrimer **120** by sequentially reacting two amino derivatives on the surface of **38**.

Despite the numerous examples found in the literature, primarily following the approach outlined in **Scheme 26a**, synthesizing this type of dendrimer remains a current challenge. Consequently, Janus dendrimers could offer a compelling alternative for producing bifunctional dendrimers.[71,79,215]

In this context, one of the objectives of this Thesis was to develop a PPH Janus dendrimer designed to impart dual properties of the final structure. Specifically, the Janus dendrimer envisioned was designed to possess solubility modulation chains on one half of the structure to induce hydrophilicity (such as PEG chains), and −P(S)Cl$_2$ groups on the other, for grafting the desired ligand/metal complex for applications in catalysis, particularly in environmentally friendly aqueous media (**Figure 20**).

Remarkably, although the synthesis of PPH Janus dendrimers with potential catalytic applications has been documented,[216,217] this Thesis aimed to achieve the first-ever reported functional

metal@dendrimer system for catalysis, particularly in water. Keeping this approach in mind, the synthesis of the water-soluble Janus dendrimer was pursued through a combined procedure using Methods *B* and *C* (Chapter I, section §1.4), employing the methodology of AB_5 dendrons and dendrimers previously reported by Caminade.[86]
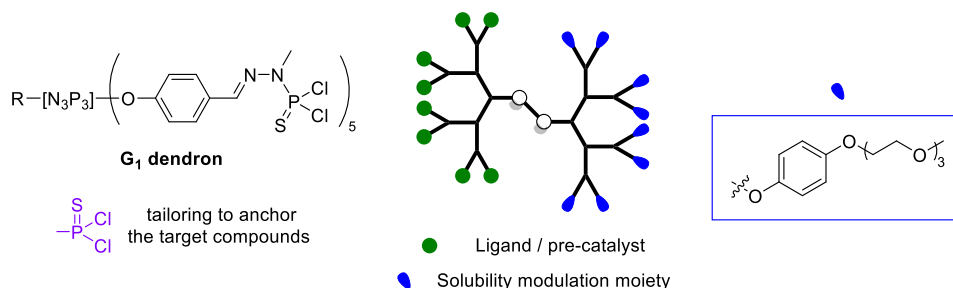
Figure 20. Schematic representation of the goal Janus dendrimer, bearing PEG chains to provide water solubility on one side (*right, blue*), and a grafting point for the incorporation of ligands/metal complexes (*left, green*) for its use in supported aqueous catalytic reactions.

As previously explained in the introduction, the obtention of Janus dendrimers through the coupling of dendrons can be accomplished by joining two dendritic wedges through complementary functions at the core level. Importantly, and in this regard, the development of phosphorus Janus dendrimers in this Thesis was planned to be carried out using a "click chemistry" approach.

The term "click chemistry" was initially coined by Sharpless in 2001 to describe straightforward, atom-economical reactions with a broad scope, high yields, and by-products that can be easily eliminated without requiring chromatographic techniques.[218] Therefore, "click chemistry" reactions can be viewed as a method for creating molecules by securely connecting two blocks, much like assembling Lego pieces. Many reactions meet the "click chemistry" criteria, but this thesis particularly focuses on one of the most prominent: the copper-catalyzed azide-alkyne cycloaddition for the selective formation of 1,2,3-triazoles.[219,220] This reaction has had a significant impact on contemporary organic synthesis, particularly in the realm of bioorthogonal synthesis. It is worth noting that the development and application of click chemistry in bioorthogonal synthesis led to the Nobel Prize in Chemistry being awarded to Carolyn Ruth Bertozzi, Morten Meldal, and Karl Barry Sharpless in 2022.

The azide-alkyne cycloaddition reactions were originally reported by Huisgen,[221] where the thermal formation of 1,2,3-triazoles through the 1,3-dipolar cycloaddition of an azide and an alkyne was achieved. In this process (see **Scheme 27**), a mixture of 1,4- and 1,5-cycloaddition products was obtained with excellent yields and a wide range of applicable reactions. While Huisgen's work laid the foundation, Sharpless[222] and Meldal[223] played a crucial role by introducing copper(I) as a catalyst for this transformation, enabling the selective formation of 1,4-substituted triazoles and coining the term "click chemistry."

(a)

(b)
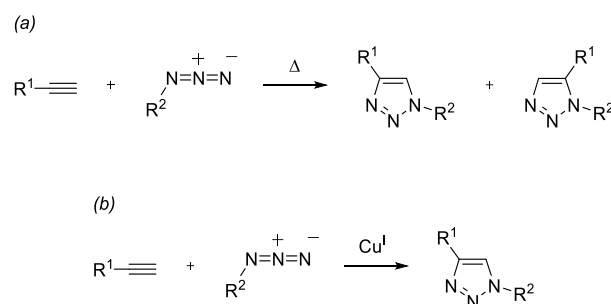
Scheme 27. *(a)* Representation of Huisgen's thermal 1,3-dipolar cycloaddition. *(b)* Representation of the copper-catalyzed azide-alkyne cycloaddition.

Hence, the synthesis of the desired phosphorus Janus dendrimer was approached by preparing AB$_5$-type PPH dendrons using N$_3$P$_3$Cl$_6$ as the core and a divergent methodology. These dendrons, each containing either an azide or an acetylene moiety at the core level, would be coupled through the previously mentioned copper-catalyzed azide-alkyne cycloaddition.

1.1. Synthesis of PPH dendrons bearing azide and alkyne groups at the core

The synthesis of dendrons commenced with the preparation of the desired azide and acetylene derivatives, which were developed as phenol derivatives due to the well-documented reactivity of phenols with PPH dendrimers.

The initial synthesis is focused on creating 4-(2-azidoethyl)phenol **123**, a two-step process starting from 4-(2-hydroxyethyl)phenol (**121**) (**Scheme 28**) and based on the previously reported procedures.[224,225] Firstly, a nucleophilic substitution was carried out by reacting **121** in hydrobromic acid at 85 °C for 15 hours, resulting in the formation of the bromo derivative **122**. This compound, obtained as a white solid, was isolated with a 90% yield through liquid-liquid extractions. Secondly, compound **122** was subjected to a second substitution reaction with sodium azide in dimethylformamide (DMF) at 45 °C for 4 hours. The product was purified as well through liquid-liquid extractions, yielding the desired product **123** as a yellow oil with a 74% yield.

The verification of the desired product was confirmed through NMR and IR spectroscopy. The most crucial aspect in characterizing the obtained product **123** relied on IR spectroscopy. Azide-containing compounds exhibit a distinctive sharp N=N=N stretching band at approximately 2100 cm^{-1}. In line with this, **Figure 21** displays the IR spectrum of compound **123**, clearly demonstrating the aforementioned stretching band at 2090 cm^{-1}.
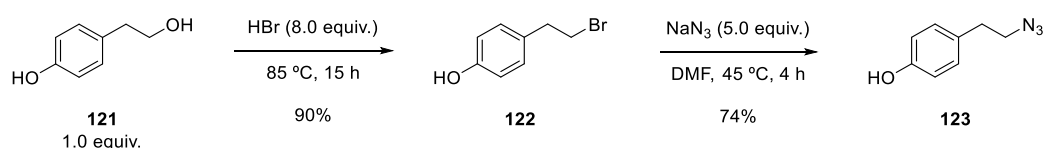
Scheme 28. Synthesis of 4-(2-azidoethyl)phenol **123** in two steps from 4-(2-hydroxyethyl)phenol (**121**).
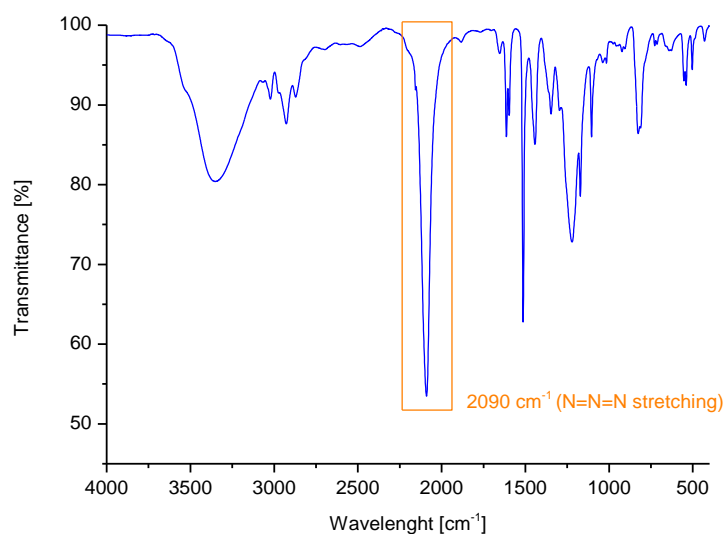
Figure 21. FT-IR spectrum of 4-(2-azidoethyl)phenol **123.**

Concurrently, the synthesis of 4-(prop-2-yn-1-yloxy)phenol (**126**) was undertaken, as outlined in **Scheme 29**. Its preparation involved a two-step reaction starting from hydroquinone, as previously reported in the literature.[226] Firstly, hydroquinone (**124**) was treated with an excess of K_2CO_3 in acetone and stirred for 30 minutes at room temperature. Subsequently, propargyl bromide (**125**) was added dropwise in a slight excess, and the mixture was stirred for 20 hours under acetone reflux conditions. The desired product was separated from the di-substituted product and the remaining hydroquinone using column chromatography, resulting in the desired product as a dark yellow oil in a 52% yield.
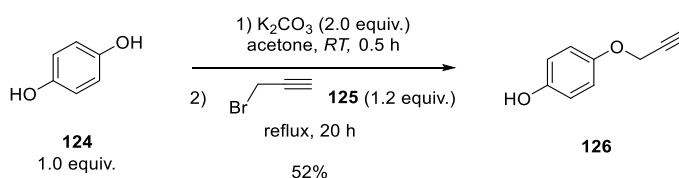
Scheme 29. Synthesis of 4-(prop-2-yn-1-yloxy)phenol **126** from hydroquinone (**124**).

Having successfully obtained the two desired azido and acetylenic phenol derivatives, the next step in synthesizing the dendrons was to introduce **123** and **126** to the hexafunctionalized dendrimer core ($N_3P_3Cl_6$) to create the **G_0'** dendrons. Specifically, the methodology explored for dendron synthesis aimed at preparing AB_5-type dendrons, wherein one functionality at the core level would differ from the remaining five. In the context of the dendritic systems of interest, this meant that the substitution of the core was carried out in such a way that five functionalities were employed for dendrimer growth (and thus reacting the core with 4-hydroxybenzaldehyde), while the sixth functionality was the azide or acetylene derivative (compounds **123** and **126**).

To achieve a fully substituted $N_3P_3Cl_6$ core, the initial reaction involved the selective penta-substitution of $N_3P_3Cl_6$ by reacting the core with 5.1 equivalents of 4-hydroxybenzaldehyde under

basic conditions in THF at 0 °C (**Scheme 30**) This reaction led to the formation of the desired AB$_5$-core **127** in 38% yield after purification *via* column chromatography. The primary characterization of **127** was conducted by analyzing the ^{31}P{^{1}H} NMR spectrum (**Figure 22**), where the product's characteristic signals were observed, including two doublets at 5.6 ppm and 4.8 ppm and a doublet of doublets at 20.7 ppm ($^2J_{P,P}$ = 88.2 Hz, 84.2 Hz).

Of note, when referring to generations in the context of PPH dendrimers, G_1 refers to a full generation (first, in this example) with terminal −P(S)Cl$_2$ groups, while G_0' refers to a so-called half generation bearing aldehyde groups on the surface.
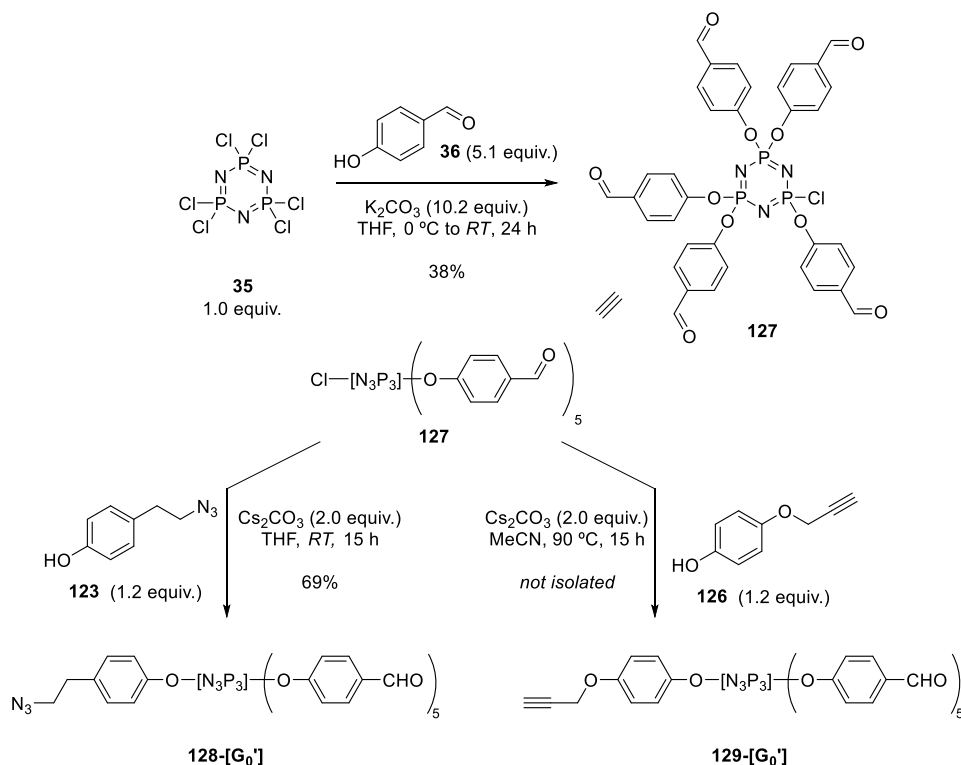
Scheme 30. Synthetic methodology for the obtention of AB$_5$ core **127**, and first attempts for the preparation of G_0' dendrons **128** and **129**.
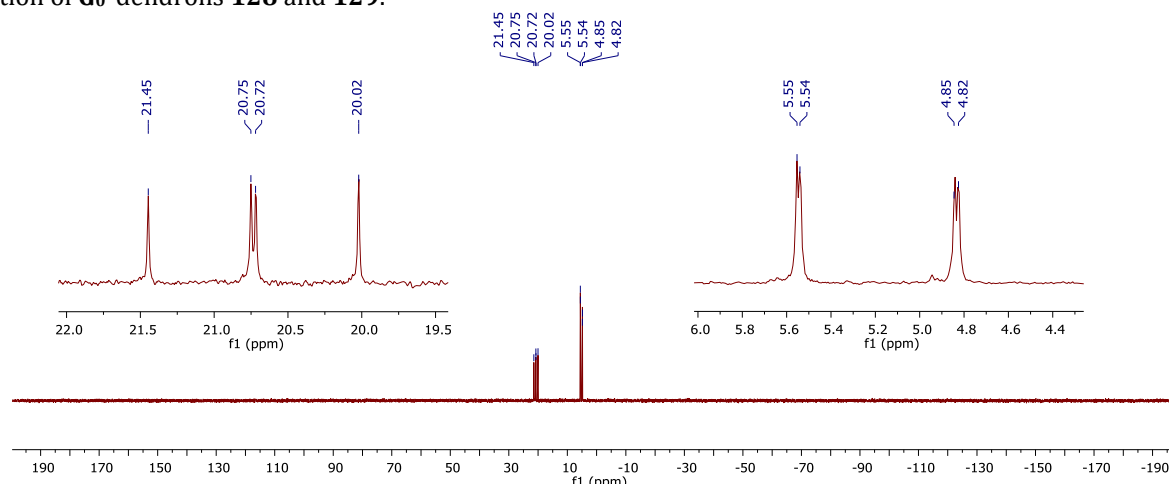
Figure 22. ^{31}P{^{1}H} NMR spectrum of AB$_5$ core **127**, recorded in CDCl$_3$ (162 MHz) at room temperature.

The obtained AB_5 core **127** was subsequently subjected to reactions with the modified phenols of interest to produce the so-called G_0' dendrons, each containing either the azide or acetylene group at the core. The reaction conditions used are detailed in **Scheme 30**.

First, the reaction to incorporate the azide derivative **123** was carried out under basic conditions at room temperature with a slight excess of **123**. The desired product was obtained in 69% yield after purification *via* column chromatography. The resulting new product, **128-[G$_0$']**, was characterized, and its synthesis was confirmed by the appearance of a new singlet at 7.4 ppm in the $^{31}P\{^1H\}$ NMR spectrum,corresponding to the full substitution of the core.

However, obtaining the acetylene derivative **129-[G$_0$']** proved to be more challenging than anticipated. Various reaction conditions were explored, including different solvents (THF, MeCN), reaction temperatures (from room temperature to 90 °C), and purification techniques (filtration, precipitation, or column chromatography). Unfortunately, in all attempts, the desired product could not be isolated in pure form, resulting in the formation of degradation products observable in the $^{31}P\{^1H\}$ NMR spectrum, as well as in ^1H and $^{13}C\{^1H\}$ NMR.

The inability to isolate **129-[G$_0$']** led to the development of a second approach to obtain the desired G_0' dendrons. This alternative method involved the introduction of the azide/acetylene derivative initially, followed by the subsequent penta-substitution with 4-hydroxybenzaldehyde in a second step. **Scheme 31** outlines the experimental procedure for obtaining the desired **128-[G$_0$']** and **129-[G$_0$']** dendrons through this alternative pathway.

The new approach began with the incorporation of the azide/acetylene phenol derivatives into the $N_3P_3Cl_6$ core. For instance, azide derivative **123** was reacted in a limited amount (0.5 equiv.) with $N_3P_3Cl_6$ under basic conditions by slow addition and stirring for 12 hours. This reaction was designed with a defect of **123** to maximize the formation of the mono-substituted product **130** while minimizing unwanted poly-substitution. The progress of the reaction was monitored using $^{31}P\{^1H\}$ NMR, showing the emergence of characteristic signals for a mono-substituted $N_3P_3Cl_6$ core, including a doublet at 22.4 ppm and a triplet at 12.3 ppm.

Similarly, the formation of the mono-substituted acetylene **131** was achieved by slightly modifying the previous procedure. In this case, compound **126** was reacted in limited quantity (0.5 equiv.) under reflux conditions for 20 hours. $^{31}P\{^1H\}$ NMR spectroscopy exhibited the same trend in the formation of characteristic signals for the desired compound.[227]
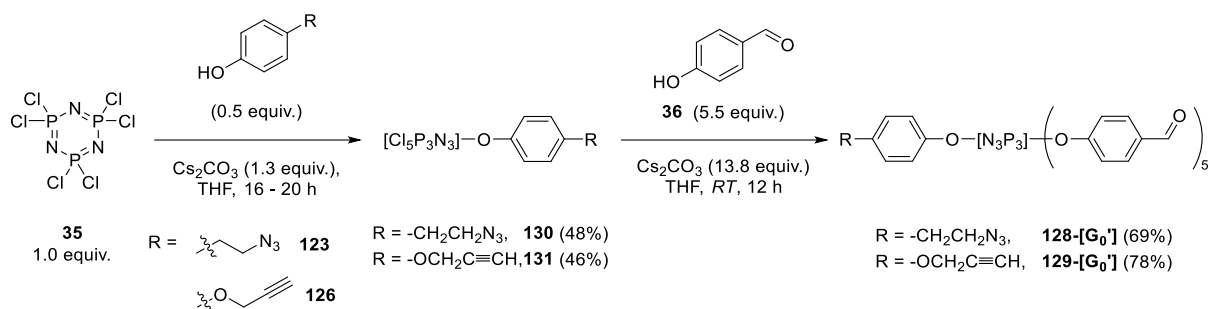
Scheme 31. Synthesis of **G₀'** dendrons containing one azide and one acetylene groups explored in this Thesis.

After successfully synthesizing the desired mono-substituted cores, the next step involved completing the core substitution with 4-hydroxybenzaldehyde. The reaction was carried out similarly for both compounds **128** and **129**, by adding an excess of 4-hydroxybenzaldehyde (5.5 equiv.) under basic conditions. The desired **G₀'** dendrons were obtained in moderate yields after column chromatography. Unlike the first attempt described in **Scheme 30**, $^{31}P\{^1H\}$ NMR spectroscopy confirmed the isolation of pure products.

Another critical tool for confirming the proper formation of the desired **G₀'** dendrons was ^1H NMR spectroscopy. In particular, the most important signals to look for were those corresponding to the aldehyde groups, which were present in the five aldehyde functionalities in the structure. Due to the nature of the $N_3P_3Cl_6$ molecule in terms of its symmetry, the introduction of different substituents (as in the case for AB_5 systems) induces a distortion of the symmetry. As a result of this asymmetry, it was observed that the ^1H NMR spectra of the **G₀'** dendrons exhibited the presence of two singlets in the aldehyde region in a 3:2 ratio. As an example, **Figure 23** illustrates the aldehyde region (^1H NMR spectrum) of **128-[G₀']**.

It's worth noting that the Caminade research group has also reported the synthesis of similar AB_5-type compounds, where the signals for the terminal five characteristic functionalities were shown in a 2:2:1 ratio instead of a 3:2 ratio.[86]
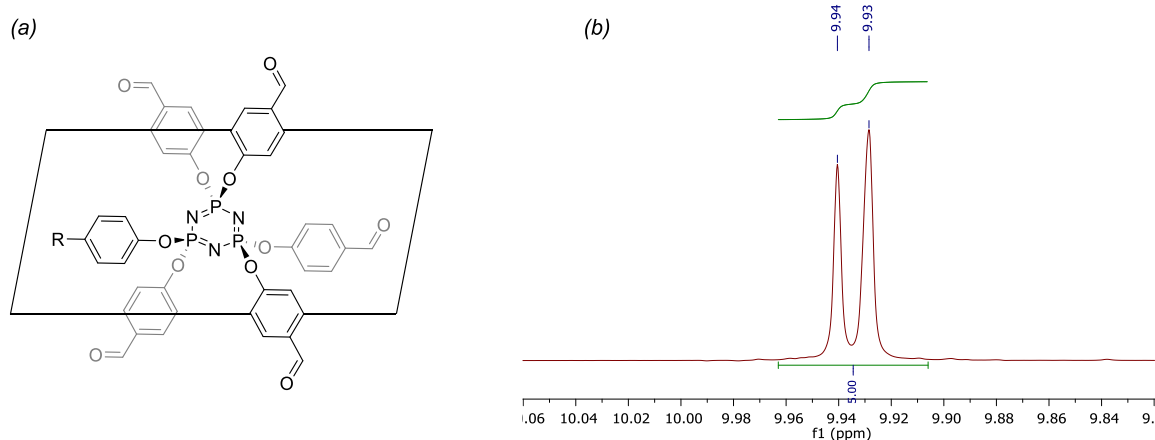
Figure 23. *(a)* Representation of the spatial arrangement of a **G₀'** dendron based on an AB_5-type core; and *(b)* ^1H NMR spectrum for the aldehyde region of **128-[G₀']** showing the two aldehyde peaks in the structure, recorded in CDCl₃ (162 MHz) at room temperature.

Having successfully obtained the G_0' dendrons, the subsequent steps involved growing these dendrons to higher generations. As described in the standard synthesis of PPH dendrimers, dendron growth follows a specific methodology: first, incorporating *N*-methyldichlorothiophosphorhydrazide to reach the full generation, followed by coupling with 4-hydroxybenzaldehyde to continue growth.

Therefore, the synthesis of *N*-methyldichlorothiophosphorhydrazide as a building block was carried out using previously reported methodologies (**Scheme 32**).[36] Specifically, methylhydrazine (**66**) was slowly added dropwise over 8 hours to a cold solution (−61 °C) of thiophosphoryl chloride in dry CHCl$_3$, and then stirred overnight. This reaction resulted in the formation of the desired mono-substituted compound **38** with a 91% conversion. Of interest, the product was stored as a CHCl$_3$ solution of c = 0.30 mmol·L^{-1} at −30 °C until needed for further reactions.
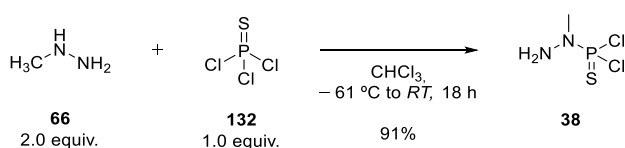
Scheme 32. Synthesis of *N*-methyldichlorothiophosphorhydrazide (**38**).

At this stage, dendron growth was carried out using the same methodology, by reacting the G_0' dendrons with an excess of compound **38** at 0 °C in a THF/CHCl$_3$ mixture, and in the presence of anhydrous Na$_2$SO$_4$ to capture the water generated during the aldehyde/hydrazine condensation reaction. **Scheme 33** outlines the synthetic approach to obtain G_1 dendrons.

The progress of the reaction was monitored using NMR spectroscopy. ^{31}P{^{1}H} NMR demonstrated the formation of a new set of signals at around ∼62 ppm, corresponding to the terminal $-\underline{P}(S)Cl_2$ groups, similar to standard symmetric PPH dendrimers. The main difference observed in the dendron systems lies in the structural asymmetry. Notably, **133-[G$_1$]** exhibited the presence of two overlapping singlets (at 62.4 ppm) in a 3:2 intensity ratio, corresponding to the newly formed surface phosphorus $-P(S)Cl_2$ groups. Similarly, **134-[G$_1$]** displayed the same pattern but with the observation of three singlets in a 2:2:1 relative intensity ratio (at 62.4 ppm, 62.5 ppm, and 62.6 ppm). **Figure 24** illustrates the ^{31}P{^{1}H} NMR spectra of **133-[G$_1$]** and **134-[G$_1$]**, with the newly formed P(S)Cl$_2$ groups highlighted.

Additionally, ^{1}H NMR revealed the characteristic trend, with the disappearance of the aldehyde signals from the G_0' dendrons and the appearance of imine signals in the aromatic region (∼8.0 – 8.5 ppm).
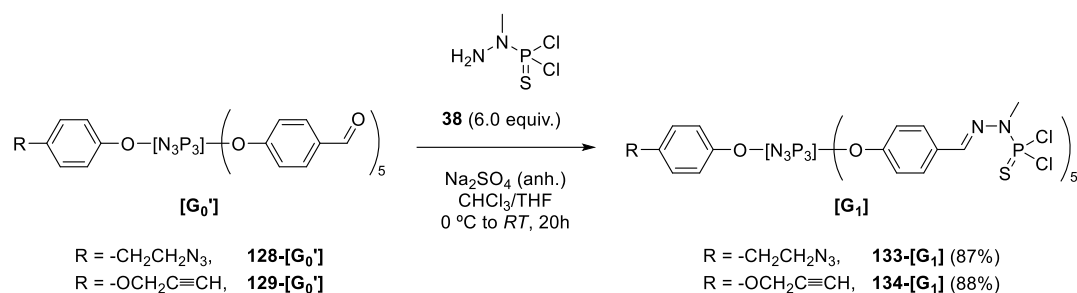
Scheme 33. Synthesis of first-generation dendrons containing azide (**133-[G₁]**) and acetylene groups (**134-[G₁]**) at the core.
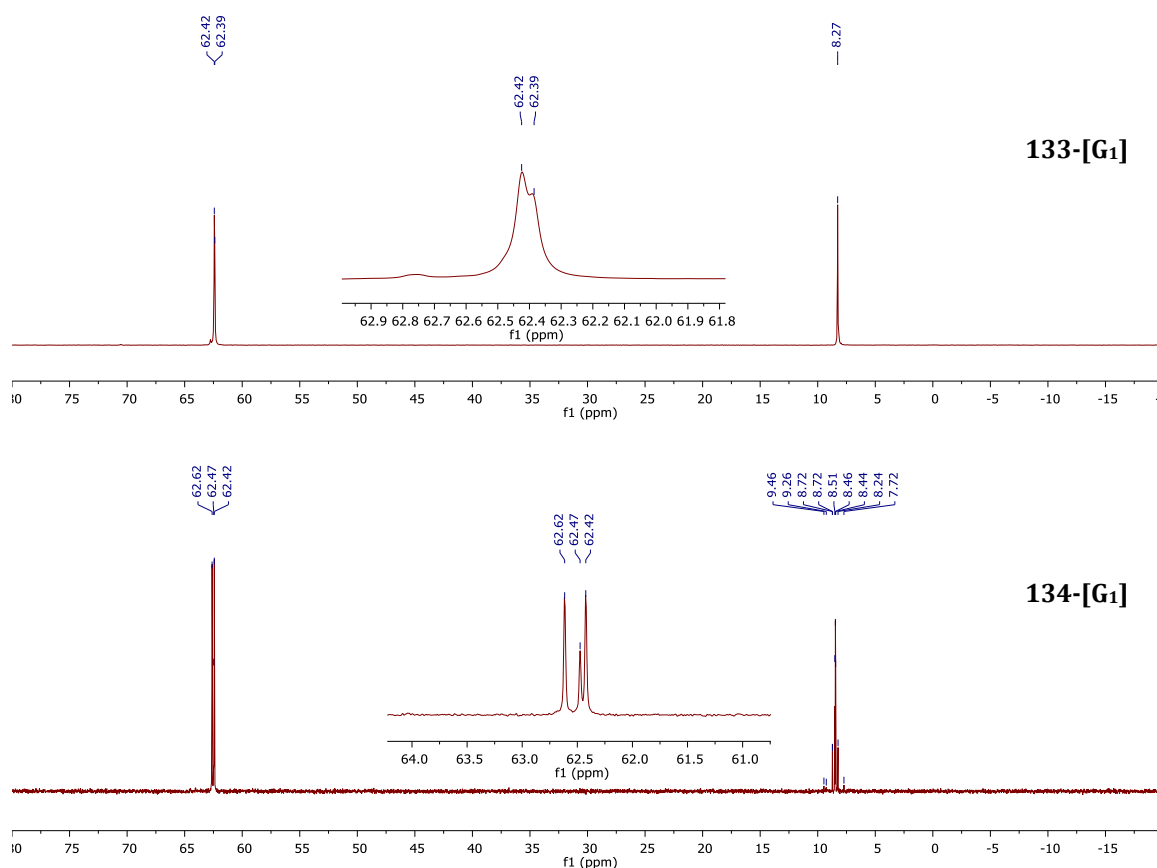
Figure 24. ^{31}P{^{1}H} NMR spectra of the first generation dendrons containing azide (**133-[G₁]**, *top*) and acetylene (**134-[G₁]**, *bottom*) groups at the level of the core, recorded in CDCl₃ (162 MHz) at room temperature.

After synthesizing the desired first-generation dendrons, the next step was to evaluate the feasibility of dendron growth, by testing its growing to the second generation. **Scheme 34** illustrates the synthetic pathway that was tested, involving the same substitution and condensation steps as previously executed.

In the initial step, **133-[G₁]** (bearing terminal −P(S)Cl₂ groups) was subjected to a reaction with an excess of 4-hydroxybenzaldehyde (11.0 equiv.) under basic conditions and in THF as the solvent. This aimed to replace every surface P−Cl bond, resulting in the successful production of **135-[G₁']** with excellent yields.

In the subsequent step, the aldehyde terminal groups in the obtained dendron **135** were once again subjected to the condensation reaction with *N*-methyldichlorothiophosphorhydrazide

(**38**), similarly to the one illustrated in the previous Scheme **33**. This led to the formation of 10 new hydrazone groups at the dendrimer surface, yielding the second-generation azide dendron **136-[G$_2$]**, which at this point possessed twenty P–Cl bonds.

As previously established, ^{31}P{^{1}H} NMR played a pivotal role in monitoring and characterizing the newly formed generations. To illustrate the shifts in phosphorus signals between the newly formed dendrons and those obtained earlier, **Figure 25** displays the spectra of the azide compounds, ranging from the initial mono-substituted core to the second generation. Upon closer examination, the formation of the **G$_1$'** dendron is evident through the shift of the terminal phosphorus atom, transitioning from two singlets at approximately ~62 ppm to two singlets at 60.4 ppm and 60.5 ppm.

Furthermore, the emergence of the second-generation azide dendron **136-[G$_2$]** can also be confirmed through ^{31}P{^{1}H} NMR. In this context, dendron **136-[G$_2$]** exhibited both a downfield shift of the phosphorus signal from the first branching point to 62 ppm and the appearance of a new set of signals corresponding to the newly generated –P(S)Cl$_2$ groups from the second generation (62.8 ppm and 62.9 ppm, **Figure 25**).

With these results in hand, the ability to synthesize new dendrons with various functionalities at the core level and extend their growth up to the second generation has been demonstrated. Keeping these findings in mind, subsequent efforts were directed towards incorporating the desired solubility-modulating chain to impart water-solubility and form water-soluble dendrimers.
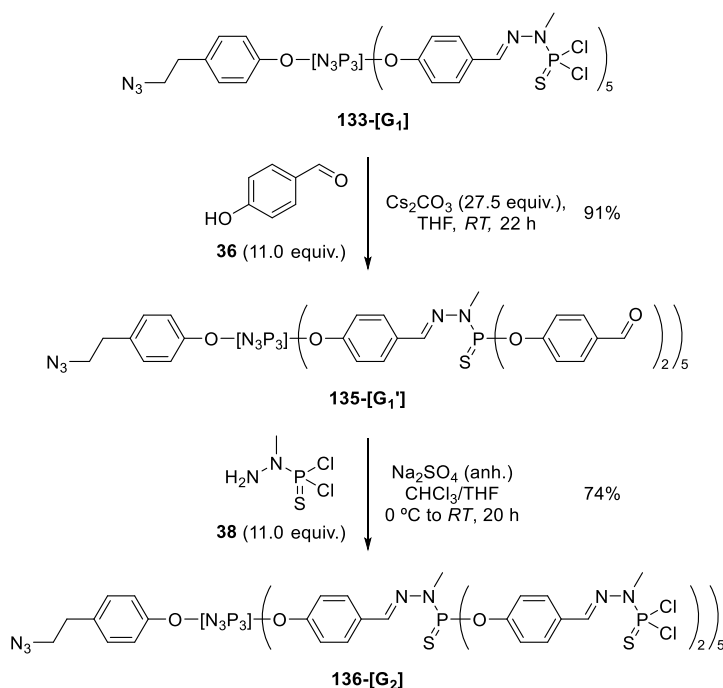
Scheme 34. Synthesis of the second-generation azide dendron **136-[G$_2$]** from **133-[G$_1$]**.
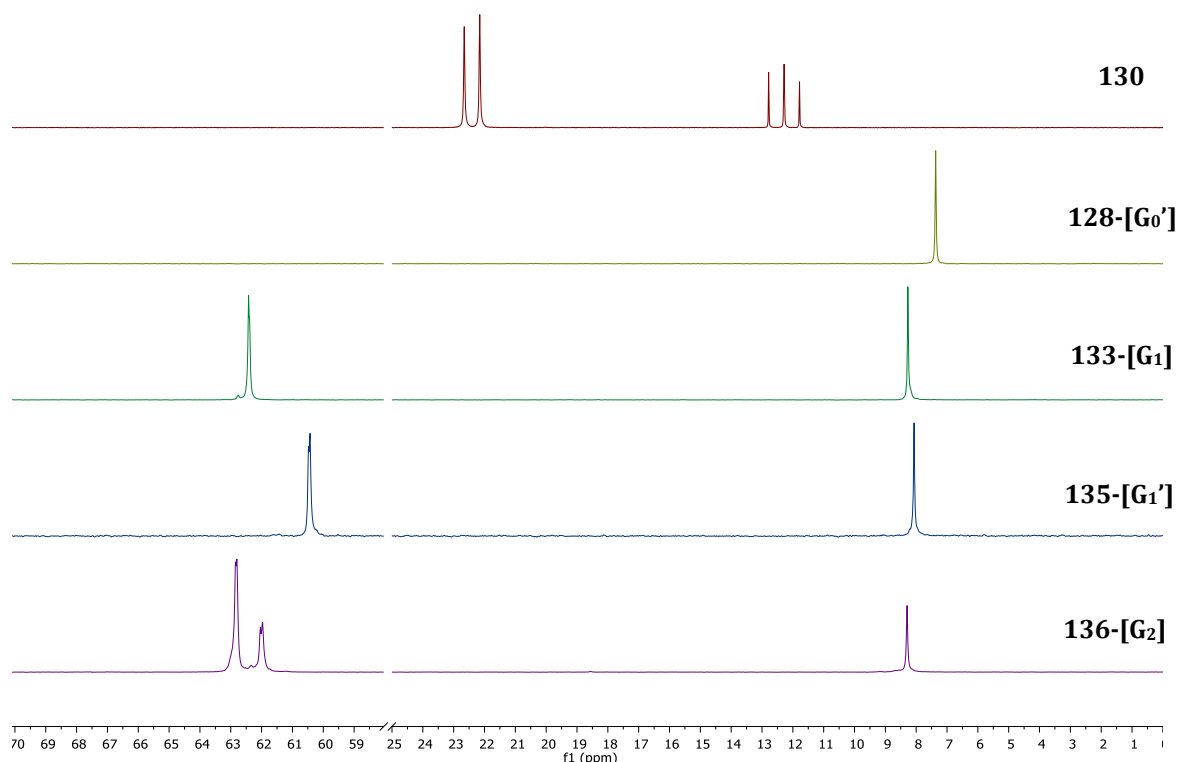
Figure 25. Evolution of the ^{31}P{^{1}H} NMR spectroscopy of the azide dendrons, ranging from the monosubstituted core **130** to the second-generation dendron **136-[G₂]**. Spectra were recorded in CDCl₃ (162 MHz) at room temperature.

1.2.   Surface modification of 133-[G₁]

The development of water-soluble dendrons by introducing PEG chains on one side of the dendrimeric structure was the next targeted objective. Specifically, the incorporation of a PEG-3 phenol derivative into one of the dendrons structure. To achieve this goal, the synthesis of a phenol modified with a PEG chain was envisioned, as outlined in **Scheme 35a**.

To begin, 2-(2-(2-methoxyethoxy)ethoxy)ethan-1-ol (**137**) was first derivatized to convert the primary alcohol into a mesylate group, making it a more suitable leaving group.[61] Subsequently, compound **139** was reacted with hydroquinone (**124**) to perform a mono-substitution reaction, resulting in the desired phenol **140** after purification by liquid-liquid extractions.[61] The desired phenolic derivative was obtained as a dark yellow oil in 39% yield over two steps. With the desired phenolic structure **140** successfully synthesized, its incorporation into the first-generation azide dendron **133-[G₁]** was attempted, as depicted in **Scheme 35b**. In this process, a THF solution of **140** was cooled down to 0 °C and stirred in the presence of Cs₂CO₃ for two hours. Then, **133-[G₁]** was added to the mixture and the reaction was further stirred for 22 hours at room temperature.
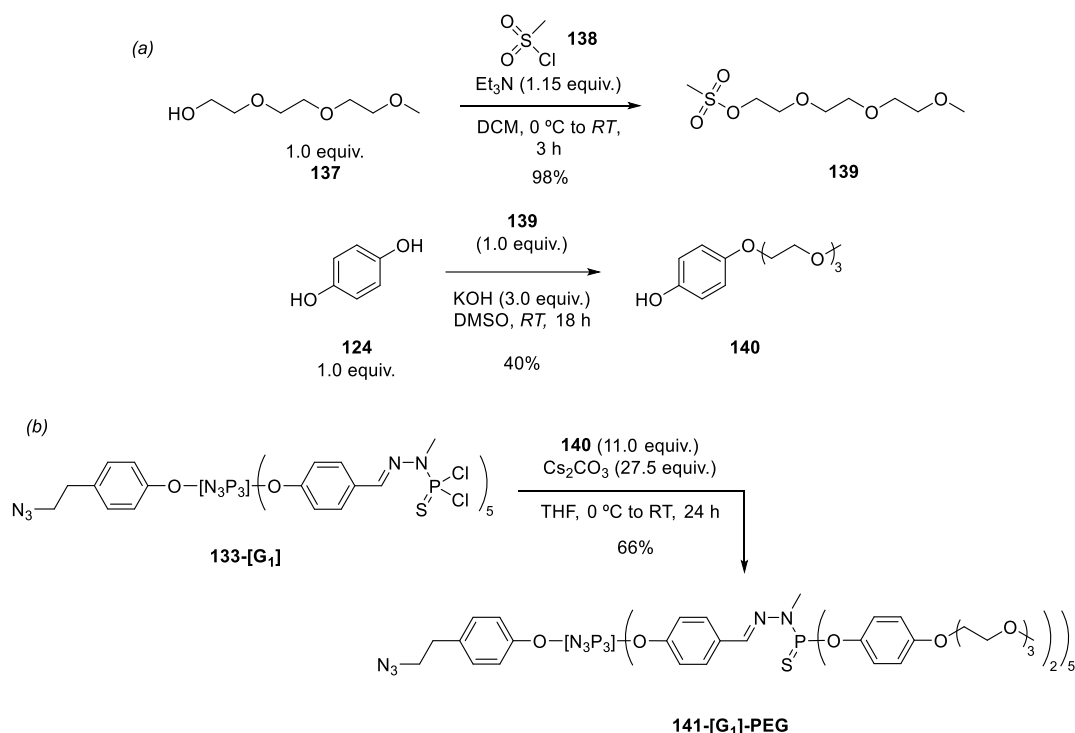
Scheme 35. *(a)* Synthesis of PEG$_3$-tagged phenol **140**; and *(b)* incorporation of **140** to the first-generation azide dendron to afford **141-[G₁]-PEG**.

The reaction progress was monitored using ^{31}P{^{1}H} NMR. Notably, the substitution of the chlorides in P−Cl surface bonds with PEG-tagged phenolic moiety (**140**) caused a downfield shift of the phosphorus NMR signal (to ~64.5 ppm). Despite the substituted −P(S)(OPh)$_2$ groups typically experience an upfield shift to approximately 60 – 62 ppm, the obtained results are in accordance with the results obtained by Caminade's group, where the incorporation of similar PEG chains have induced a downfield shift to ~64 ppm.[61] In line with this observation, **141-[G₁]-PEG** exhibited a similar downfield shift, resulting in two singlets at 64.5 ppm and 64.6 ppm (see **Figure 26**).
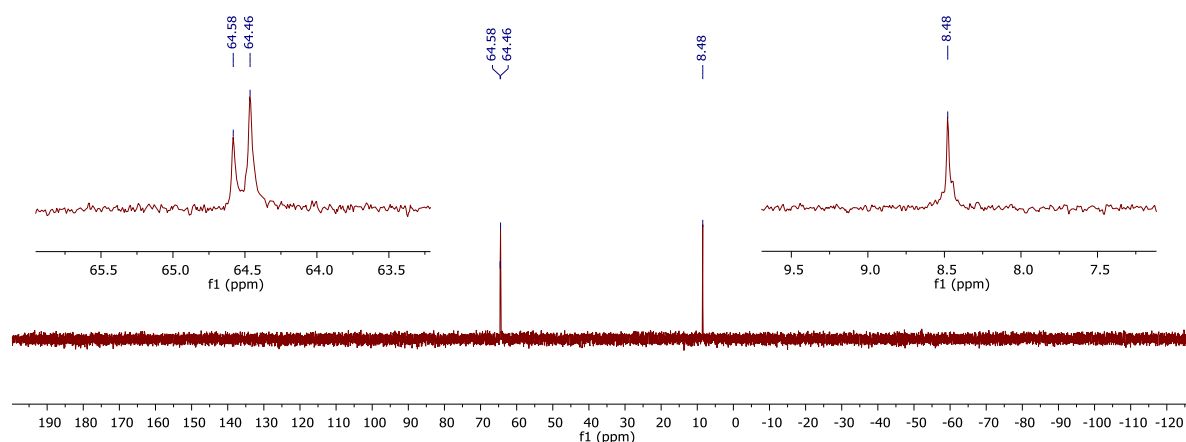
Figure 26. ^{31}P{^{1}H} NMR spectra of the first-generation azide dendron substituted with **140** at the periphery (**141-[G₁]-PEG**), recorded in CDCl$_3$ (162 MHz) at room temperature.

1.3.   Coupling of dendrons for the obtention of Janus dendrimers

Following the successful preparation of a first-generation PEG-substituted azide dendron (**141-[G$_1$]-PEG**), the next step in achieving the objective was to obtain a first-generation Janus dendrimer, featuring PEG chains on one side and terminated with $-P(S)Cl_2$ groups on the other side. The main purpose for the development of such structures was to afford a dendrimer bearing functional groups on its surface which could be modified for the later introduction of the desired ligands/metal pre-catalysts, for the final application of such system in catalysis.

To achieve this desired Janus dendrimer, a copper-catalyzed "click reaction" was pursued involving the coupling of **129-[G$_0$']** with the azide-containing dendron **141-[G$_1$]-PEG** to create a hybrid **G$_1$G$_0$′** dendrimer (**142-[G$_0$'][G$_1$]-PEG**) with PEG chains on one side and aldehyde groups on the other (**Scheme 36**). This reaction was inspired by the approach of Caminade and Majoral to dendrimer synthesis *via* a click triazole reaction.[228] Specifically, dendrons containing azide and acetylene groups were reacted in the presence of a base, catalyzed by CuI. To achieve this, stoichiometric amounts of dendrons **129-[G$_0$']** and **141-[G$_1$]-PEG** were combined with two equivalents of *N*,*N*-diisopropylethylamine (DIPEA) and 15 mol% CuI in THF, and the reaction was carried out at 45 °C for an extended period. The desired hybrid **G$_0$′G$_1$** Janus dendrimer **142** was obtained as a yellow solid in 66% yield after 30 hours of reaction.

The progress of the reaction was monitored using NMR and IR spectroscopy. Unlike for the previously discussed preparation and functionalization of dendrons, $^{31}P\{^1H\}$ NMR was not suitable for this specific reaction since no modifications to the phosphorus signals were expected. Instead, ^1H NMR and IR spectroscopy were the primary monitoring techniques. In particular, ^1H NMR was used to observe the disappearance of the acetylenic proton signal from the alkyne-containing dendron **129-[G$_0$']** (formerly a triplet at 2.56 ppm), the appearance of a singlet at 5.01 ppm from the methylenic protons in **142-[G$_0$'][G$_1$]-PEG** (formerly a doublet at 4.65 ppm), and the obtention of a singlet from the triazole unit around *ca.* 8 ppm.

Furthermore, the progress of the reaction was conveniently monitored through IR spectroscopy. Specifically, by tracking the disappearance of the N=N=N stretching band at 2095 cm^{-1} from the azide dendron **141-[G$_1$]-PEG**. **Figure 27** illustrates the evolution of the IR spectrum, clearly depicting the vanishing of the aforementioned band, signifying the successful progression of the desired reaction.
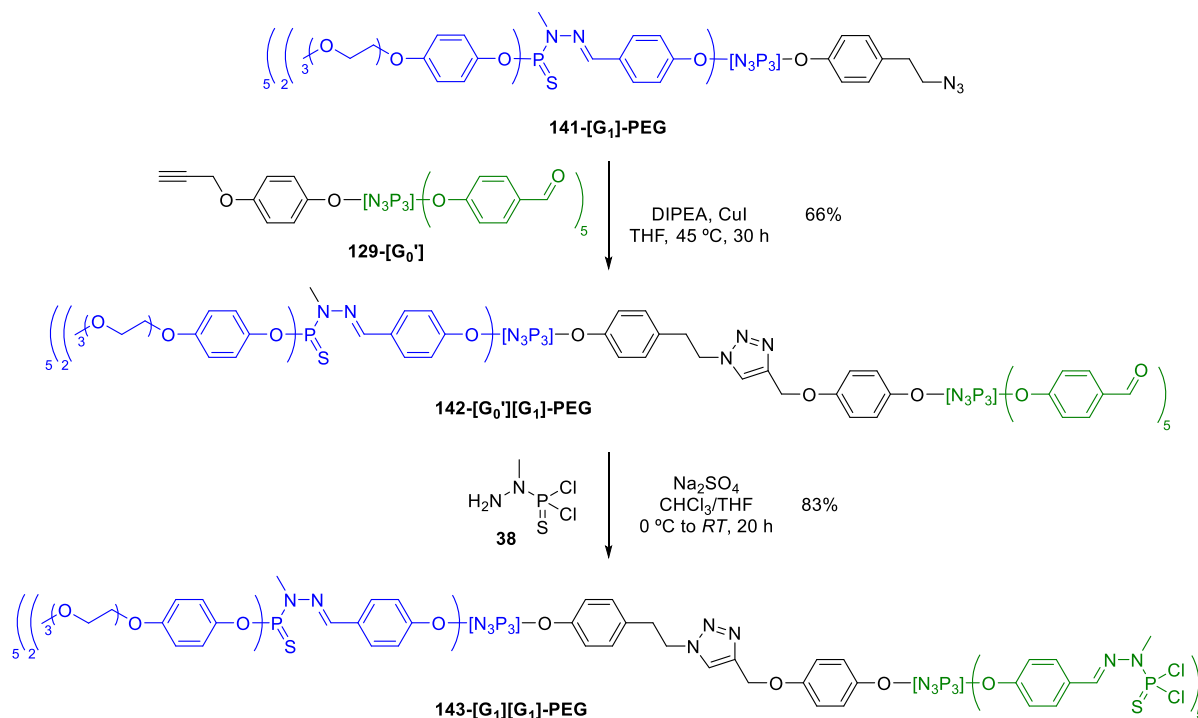
Scheme 36. Synthesis of a first-first-generation dendrimer containing PEG chains on one side and terminal P(S)Cl$_2$ groups on the other side (**143-[G$_1$][G$_1$]-PEG**) in two steps from dendrons **141-[G$_1$]-PEG** and **129-[G$_0$']**.
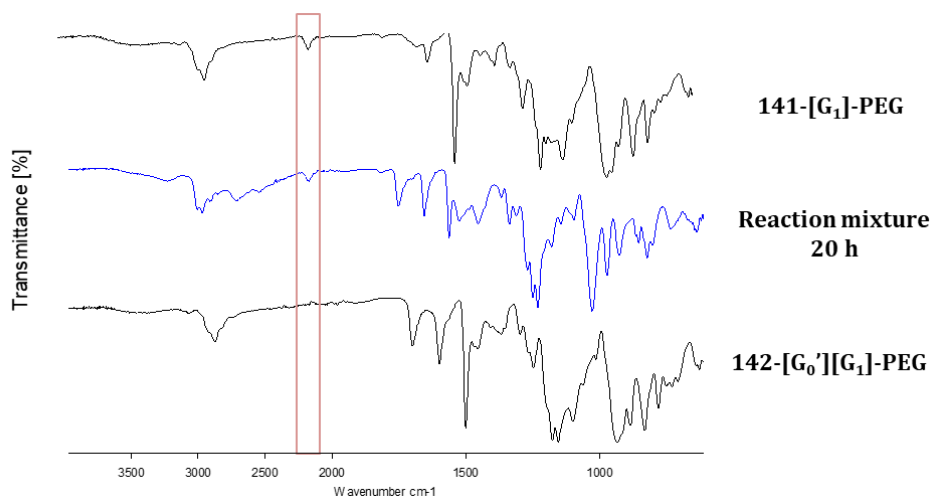
Figure 27. FT-IR spectra of **141-[G$_1$]-PEG** dendron (*top, black*), reaction mixture after 20 h (*middle, blue*), and final dendrimer **142-[G$_0$'][G$_1$]-PEG** after 30 h(*bottom, black*) obtained from "click" triazole reaction.

The final step to obtain the desired first-generation Janus dendrimer involved extending the aldehyde functionalities of the hybrid **142-[G$_0$'][G$_1$]-PEG** dendrimer to the full generation, resulting in the terminal −P(S)Cl$_2$ groups (**143-[G$_1$][G$_1$]-PEG**). This step followed the well-established reaction conditions for growing PPH dendrimers. It entailed the reaction of the hybrid dendrimer **142-[G$_0$'][G$_1$]-PEG** with *N*-methyldichlorothiophosphorhydrazide in the presence of anhydrous Na$_2$SO$_4$. The reaction took place in a THF/CHCl$_3$ mixture with a gradual addition of H$_2$NN(Me)P(S)Cl$_2$ at 0 °C, followed by stirring at room temperature for 20 hours. The progress of the reaction was monitored using ^{31}P{^{1}H} NMR spectroscopy.

Of interest, **Figure 28** displays the ^{31}P{^{1}H} NMR spectra of both **142-[G$_0$'][G$_1$]-PEG** and **143-[G$_1$][G$_1$]-PEG**. Notably, the extension to the full first-generation dendrimer resulted in the acquisition of the same ^{31}P{^{1}H} NMR pattern as observed in the previous structure. This pattern incorporated the newly generated phosphorus signals from the dendrimer surface, manifested as two singlets at 62.5 ppm and 62.7 ppm.
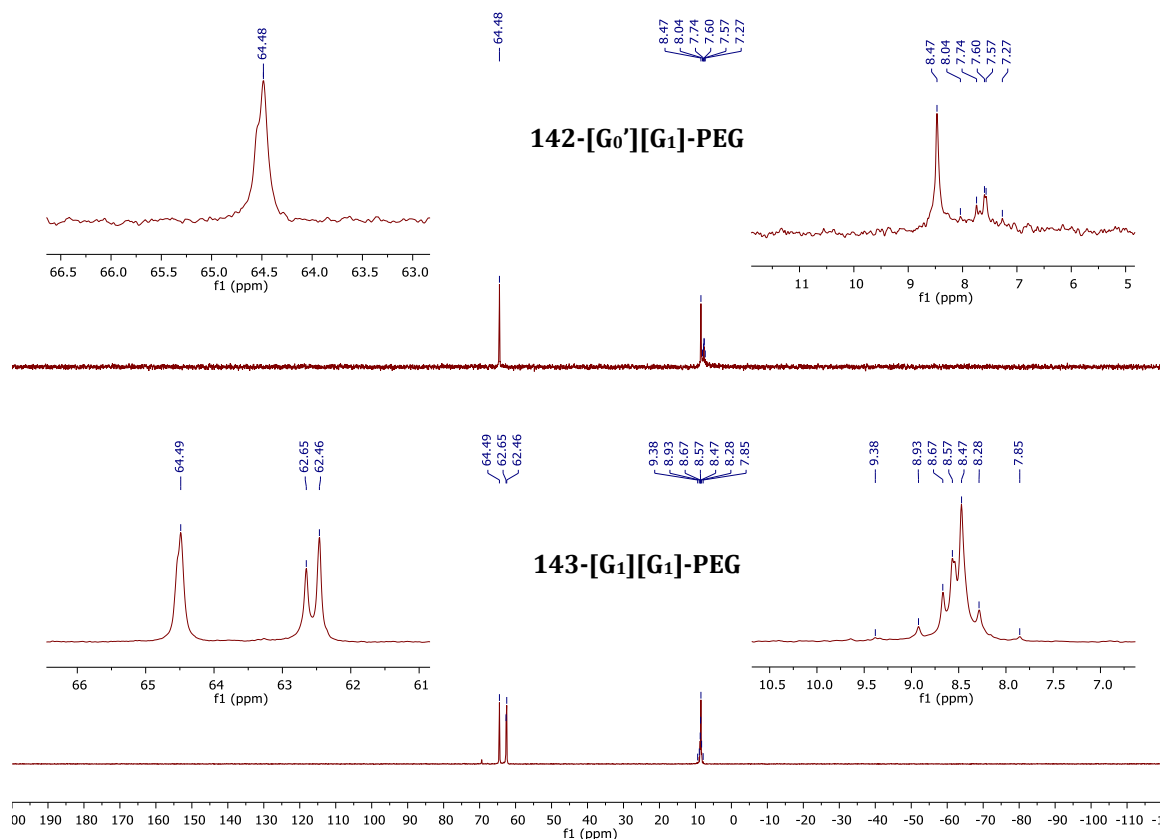
Figure 28. ^{31}P{^{1}H} NMR spectra of the first-generation Janus dendrimer **143-[G$_1$][G$_1$]-PEG**, and the hybrid Janus dendrimer **142-[G$_0$'][G$_1$]-PEG**, recorded in CDCl$_3$ (162 MHz) at room temperature.

In summary, the targeted PPH Janus dendrimer, bearing PEG chains on one side and −P(S)Cl$_2$ groups on another, has been successfully synthesized. This structure not only features PEG chains expected to promote water solubility but also provides anchoring points through the −P(S)Cl$_2$ groups. Consequently, we have demonstrated the synthesis of a PPH Janus dendrimer through a novel linkage of two dendrons *via* the formation of a 1,2,3-triazole. Moreover, the synthesized dendrimer could serve as a versatile platform for further potential incorporation of desired functionalities. Notably, **143-[G$_1$][G$_1$]-PEG** could be employed as an innovative support for integrating a wide range of ligands or metal pre-catalysts. This holds promise for achieving tailored final properties, particularly in catalytic applications in aqueous environments, thanks to the presence of PEG chains and adaptable phosphorus functional groups.

2. Synthesis of Ru-NHC complexes for olefin metathesis catalysis

The significance and relevance of olefin metathesis catalysts are closely linked to the development of N-heterocyclic carbene (NHC) ligands. This is primarily due to the increased stability of Ru-NHC complexes in comparison to their phosphine counterparts.[115,165] Additionally, the ease of adjusting the electronic and steric properties of Ru-NHC complexes by modifying substituents within their structure further underscores their importance.

Consequently, a wide range of NHC ligands have been developed in the literature, with most of them featuring symmetrical substituents in their structure. However, it's worth noting that while unsymmetrical NHCs (uNHCs) generally exhibit lower activity compared to their symmetrical counterparts, they hold promise as an attractive alternative for applications in non-conventional metathesis processes.[160] In this context, this thesis focuses on the development of novel uNHC ligands and their corresponding **Hov-II**-type complexes. Of particular interest is the creation of Ru-NHC complexes that feature functional groups suitable for attachment to various supports. This includes investigating their incorporation onto dendritic supports or metal-organic frameworks (MOFs).

The selection of appropriate functional groups for the uNHCs is a critical aspect of this endeavor. To achieve the desired objective, this section aims to outline the synthesis of uNHCs. These uNHCs will incorporate a mesityl group on one side and a phenolic group on the other. Furthermore, the research will explore how the presence of uNHCs influences the reactivity of Ru-NHC complexes. Additionally, the impact of temperature and solvent on olefin metathesis catalysis will be investigated to assess the suitability of these novel complexes for metathesis catalysis.

2.1. Synthesis of uNHCs bearing a phenolic arm in the structure

As previously mentioned, this Thesis aimed to synthesize uNHC ligands incorporating a phenolic substituent. The choice of phenol groups for integration into the structure of ruthenium complexes is based on the extensive chemistry of PPH dendrimers, which are known to interact with a wide variety of phenolic substituents. Additionally, complexes containing phenolic groups are expected to be readily deprotonated to generate phenolate structures. This, in turn, could lead to the formation of anionic complexes, making them suitable for grafting onto alternative supports such as MOFs.

The first uNHC investigated for the preparation of Ru-complexes containing phenolic moieties was based on the synthesis of 3-(4-hydroxybenzyl)-1-mesityl-4,5-dihydro-1*H*-imidazol-3-ium chloride (**149**), starting from commercially available 4-hydroxybenzaldehyde as the phenolic component. The synthesis of the desired imidazolium salt **149** was proposed to occur in four steps, following the procedures previously reported by Grela's group (**Scheme 37**).[229]

The synthesis commenced with mesitylamine (**144**), which underwent a substitution reaction with 2-bromoethan-1-amine derivative (**145**) under toluene reflux conditions following previously reported methodologies.[230] This reaction yielded *N*-mesitylethane-1,2-diamine (**146**), which was subsequently purified by column chromatography, resulting in the desired diamine in 71% yield. The next step involved the incorporation of 4-hydroxybenzaldehyde into diamine **146** *via* a condensation reaction. Formic acid served as a catalyst, while anhydrous Na_2SO_4 was used to capture the water generated during the reaction. This process led to the formation of imine **147**, which was then reduced *in situ* with $NaBH_4$, resulting in the production of substituted diamine **148** as a dark orange oil in 75% yield. Finally, cyclization of compound **148** was achieved using triethyl orthoformate (TEOF) and NH_4Cl under microwave irradiation conditions by modifying similar reported procedures,[231] ultimately yielding the desired imidazolium salt **149** in a good yield (83%).
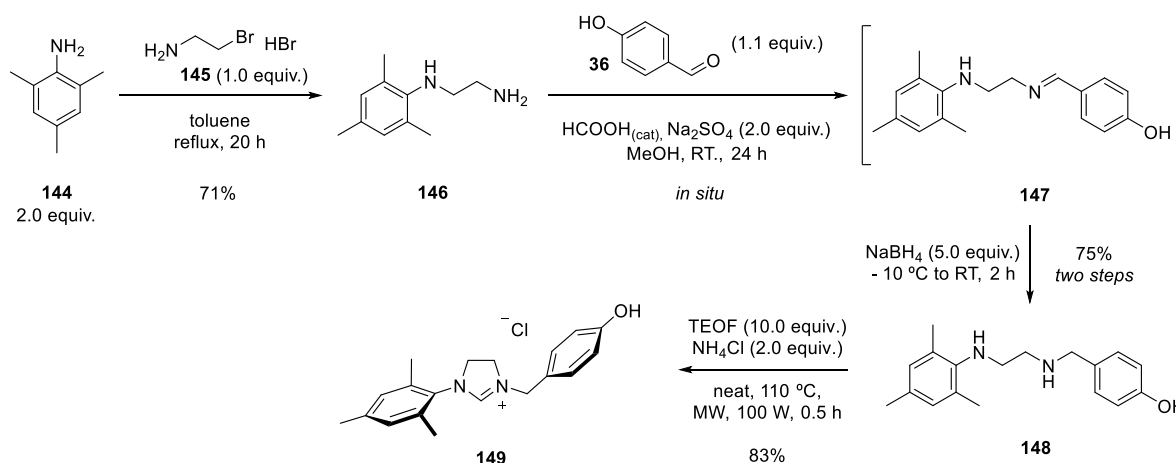
Scheme 37. Synthesis of the unsymmetrical NHC ligand precursor **149**, bearing a phenolic arm in the structure.

Simultaneously, an analogous unsaturated version of NHC precursor **149** was synthesized. The synthetic approach for acquiring 3-(4-hydroxybenzyl)-1-mesityl-1*H*-imidazol-3-ium chloride (**153**) is outlined in **Scheme 38**.

The synthesis began with the preparation of the *N*-mesityl-1*H*-imidazole (**152**) building block from mesitylamine (**144**) in a multi-step one-pot reaction.[232] This reaction involved glyoxal, formaldehyde, ammonium chloride, and phosphoric acid, resulting in the desired product in 38% yield after crystallization from a mixture of DCM and *n*-pentane.

In parallel, 4-(iodomethyl)phenol (**151**) was synthesized in two steps starting from 4-hydroxybenzaldehyde. First, the aldehyde **36** was reduced to the corresponding benzylic alcohol **150** using classical conditions with $NaBH_4$ in MeOH.[233] Then, in a second step, the alcohol group was transformed into the desired iodo-derivative **151** by reacting it with NaI in the presence of trimethylsilyl chloride (TMSCl). It is noteworthy that the synthesis of **151** could lead to the formation of the elimination product, liberating HI, and thus, the product had to be stored in the

fridge to prevent its decomposition. Overall, 4-(iodomethyl)phenol (**151**) was obtained in 49% overall yield over these two steps.

At this stage, the synthesis of the desired uNHC precursor was carried out. This involved the reaction of arylimidazole **152** with 4-(iodomethyl)phenol **151** through a simple alkylation reaction under microwave irradiation. The reaction yielded the desired imidazolium salt **153** as a pale-yellow solid with an excellent yield. The product was obtained through simple filtration and subsequent washings with toluene and diethyl ether.
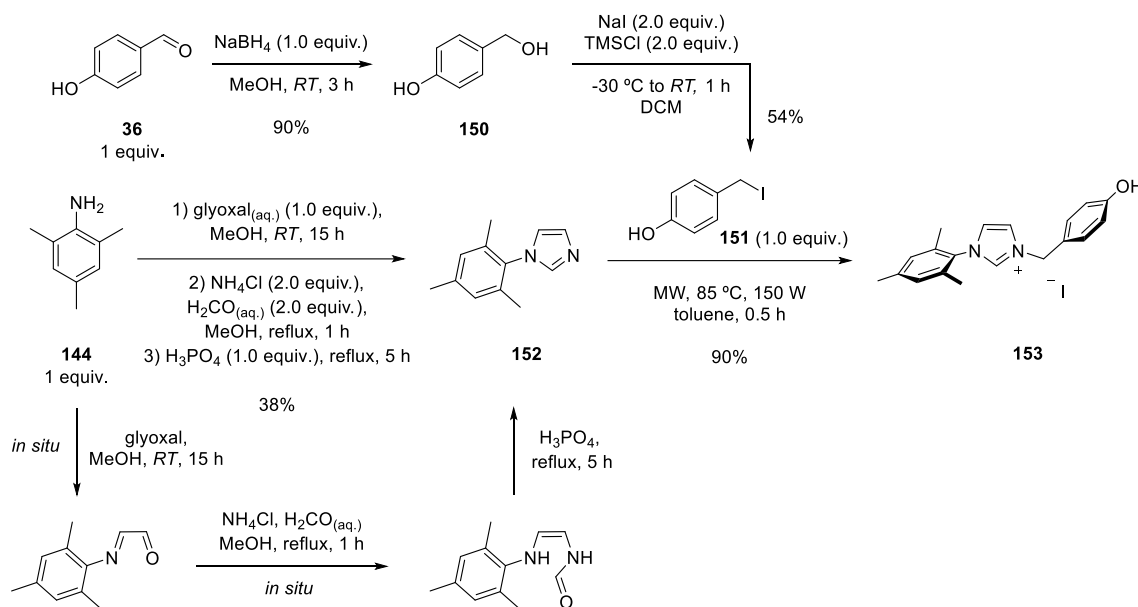
Scheme 38. Synthesis of 3-(4-hydroxybenzyl)-1-mesityl-1*H*-imidazol-3-ium iodide **153**.

2.2. Synthesis of Hov-II-type complexes bearing uNHC ligands

Following the synthesis of the two novel unsymmetrical NHC ligand precursors, the preparation of corresponding Ru-complexes based on **Hov-II** precursors was undertaken. The synthetic methodology employed to create these desired compounds was based on procedures previously reported by Grela's group.[229] However, certain reaction parameters were slightly modified to suit the current synthesis (**Scheme 39**).

To initiate the process, salts **149** and **153** were subjected to vacuum drying for 2 hours to remove any moisture content. Subsequently, they were suspended in toluene. Lithium bis(trimethylsilyl)amide (LiHMDS) was added to each suspension, and the resulting reaction mixtures were stirred at room temperature for 1 hour to facilitate the generation of the carbenic species. It is worth noting that a substantial excess of base (3.2 equiv.) was necessary in the reaction mixtures containing the NHC precursors to ensure the formation of the carbenes while also deprotonating the phenolic OH group. Additionally, THF was added into the solutions to aid in creating a homogeneous mixture of the carbene within the toluene/THF solution. It was crucial to achieve a homogeneous carbene solution before adding the ruthenium precursor.

Once homogeneous solutions were obtained, **Hov-I** ruthenium precursor and CuCl were intro-duced into the reaction mixture. The mixture was then stirred at room temperature until the de-sired product was formed (product formation checked by TLC on silica, *n*-hexane and EtOAc 1:1). Importantly, the desired **Hov-II**-phenolic complexes were obtained by exchanging the phosphine ligands from **Hov-I** with the synthesized uNHCs. The addition of CuCl to the reaction mixture served as a phosphine scavenger.

Finally, the reaction was quenched by adding HCl in dioxane, which regenerated the OH group from the phenol. The resulting products were isolated by column chromatography, , crystallized from a mixture of DCM and MeOH (ratio), yielding the desired **Ru36** and **Ru38** complexes in moderate yields.
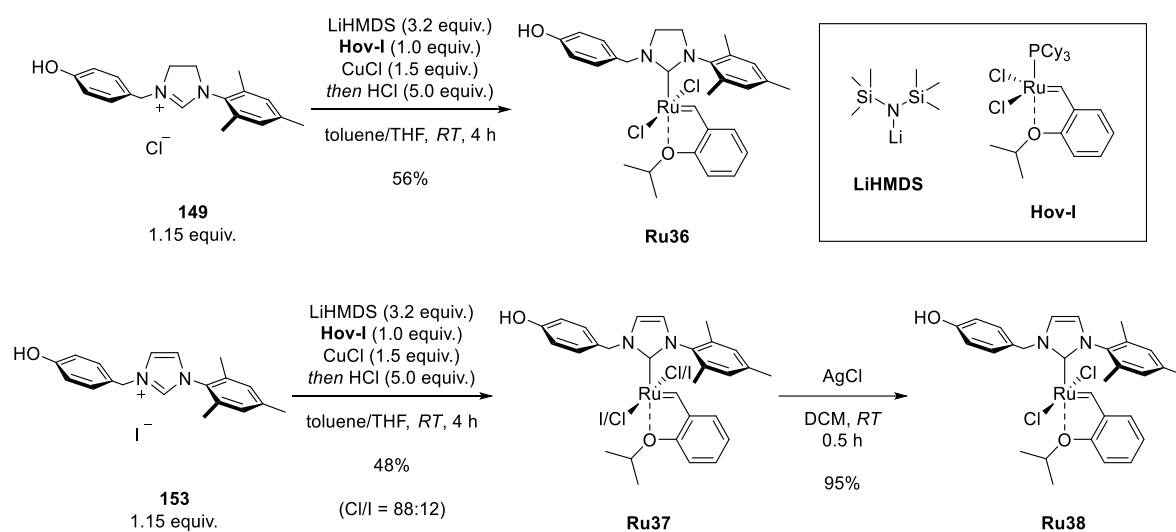
Scheme 39. Synthesis of **Hov-II**-based complexes **Ru36** and **Ru38** bearing uNHCs with a phenolic moiety.

NMR spectroscopy played a crucial role in assessing the conversion of the reaction, being ¹H NMR the most valuable tool for this purpose. **Figure 29** presents the ¹H NMR spectra of the resulting ruthenium complexes (**Ru36** and **Ru38**) and the precursor **Hov-I** (for the benzylidene region). Specifically, the ruthenium precursor **Hov-I** exhibited a distinctive doublet at 17.44 ppm, which was shifted in the case of **Ru36** and **Ru38**, displaying benzylidene protons within the range of 16.38 ppm to 16.22 ppm, consistent with the typical values for Hoveyda-type complexes.

Moreover, ³¹P{¹H} NMR proved to be a valuable tool for monitoring the reaction, especially in terms of tracking the disappearance of the phosphorus signal originating from **Hov-I** at 59.2 ppm. This provided additional confirmation of the progress of the reaction towards the de-sired products.
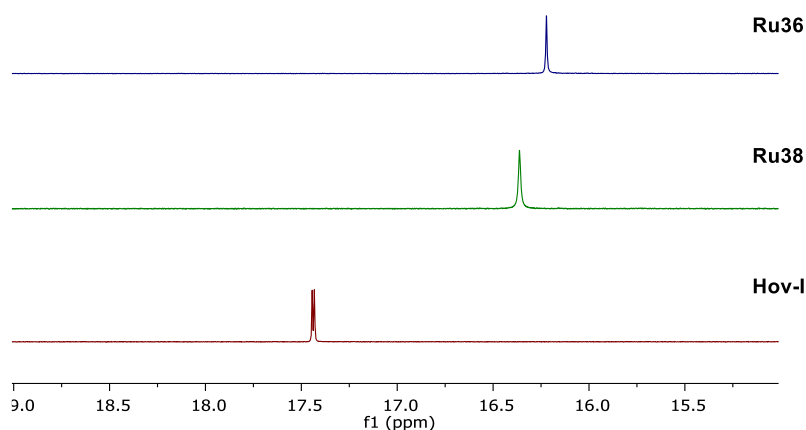
Figure 29. ^{1}H NMR spectra for the benzylidene proton of **Hov-I** ruthenium complex, and the synthesized **Ru36** and **Ru38**. NMR spectra were recorded in DCM-d_2 (400 MHz) at room temperature.

Interestingly, during the synthesis of the unsaturated complex **Ru38**, an unexpected observation was made. It was found that the chloride (Cl$^-$) ions at the ruthenium coordination center were replaced by the more labile iodide (I$^-$) ions from the imidazolium salt **153**. This resulted in a phenomenon known as "scrambling",[234] leading to the formation of an undefined mixture of complexes, namely [Ru]Cl$_2$ and [Ru](Cl/I)$_2$, collectively referred to as **Ru37**. To address this issue, **Ru37** (the mixture of [Ru](Cl/I)$_2$ complexes) underwent a treatment with AgCl in DCM for 0.5 hours. Subsequently, the mixture was centrifuged and filtered through Celite®. Following these steps, the desired [Ru]Cl$_2$ complex, **Ru38**, was obtained after crystallization as a green powder.

This scrambling phenomenon during the synthesis was detected by ^{1}H NMR spectroscopy, as evidenced by the emergence of a secondary benzylidene peak at 15.76 ppm (see **Figure 30**). Importantly, this additional peak disappeared after the treatment with silver chloride, confirming the successful isolation of **Ru38**.
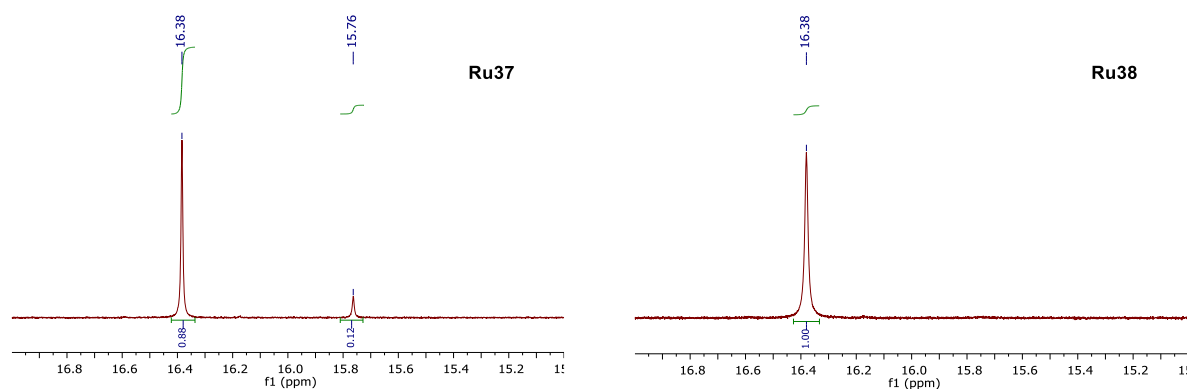
Figure 30. ^{1}H NMR spectra for the benzylidene region of **Ru37** (*left*) and **Ru38** (*right*), recorded in DCM-d_2 (162 MHz) at room temperature.

2.3.   Stability studies of Ru36 and Ru38

Following the synthesis and characterization of the phenolic complexes **Ru36** and **Ru38** (**Figure 31**), the next step was to investigate the stability of these complexes in solution. Thermal stability experiments were conducted to provide valuable insight into the complexes' reactivity and potential applications.
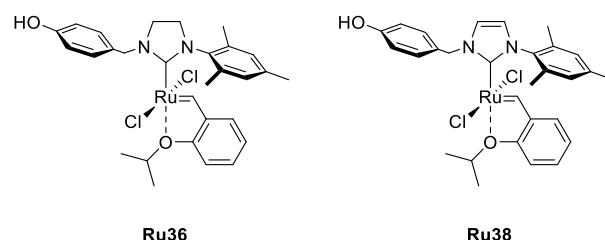
Figure 31. Structures of the synthesized Ru-complexes containing an uNHC with a phenolic arm.

The stability experiments involved dissolving the respective ruthenium complex (10.8 μmol) in 0.5 mL of DCM-d_2 in an NMR tube under an argon atmosphere. Additionally, 1,3,5-trimethoxybenzene (1.0 equiv.) was added as an internal standard, dissolved in 0.2 mL of DCM-d_2. The resulting solutions were allowed to stabilize at 30 °C, and ^{1}H NMR spectra were recorded at room temperature at specific time intervals to monitor the decomposition of the complexes. The decomposition was determined by analyzing the decrease in the intensity of benzylidene signals in the ^{1}H NMR spectra relative to the aromatic protons signal at 6.08 ppm from the internal standard.

Figure 32 presents the results obtained from the thermal stability analyses conducted over a period of 10 days. Both synthesized complexes, **Ru36** and **Ru38**, exhibited high stability in DCM-d_2, with decomposition rates of 6% and 4%, respectively. Comparing these results to previously reported catalysts featuring structurally related unsymmetrical NHCs, it is evident that the electron-donating OH group in the *N*-benzyl moiety effectively stabilized the ruthenium center against decomposition, leading to the obtention of two novel complexes with a high stability in solution.

Notably, stability analyses were also attempted at 50 °C in toluene-d_8. Unfortunately, maintaining the concentration of the mixture proved to be challenging, and the formation of a precipitate was observed after one day of experiment, rendering further analysis impossible.
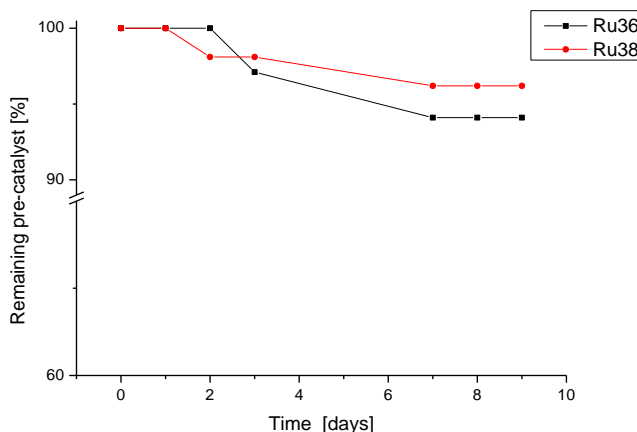
Figure 32. Results of the stability experiments for **Ru36** and **Ru38** in DCM-d_2 at room temperature.

2.4. Catalytic performance of Ru36 and Ru38

Following the synthesis and stability assessments of **Ru36** and **Ru38**, the activity and reaction profiles of these "phenolic" complexes were examined in the context of the ring-closing metathesis (RCM) reaction of the model substrate diethyl diallylmalonate (DEDAM, **S1**). The impact of structural modifications of the unsymmetrical NHC motif was evaluated, as illustrated in **Scheme 40**. For the experiments, malonate **S1** was dissolved in either DCM or toluene at a concentration of $C_{[\mathbf{S1}]}$ = 0.5 M. Subsequently, 1 mol% of catalyst (either **Ru36** or **Ru38**) was added to the reaction mixture. The progress of the reaction was monitored using gas chromatography (GC) to determine the time-dependent conversion of **S1**. Dodecane served as an internal standard in the analysis.
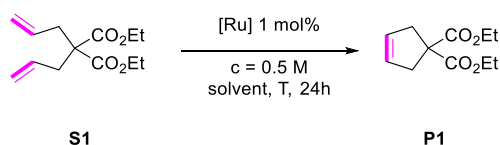
Scheme 40. Standard reaction conditions used for the RCM of DEDAM (**S1**).

The results of the catalytic evaluation are presented in **Table 1** and **Figure 33**. Initial tests were conducted at room temperature in DCM (**Table 1**, **Entries 1 and 4**). In these tests, both catalysts exhibited relatively moderate conversion after 24 hours of reaction. Specifically, **Ru36** achieved a conversion rate of only 49%, while the unsaturated **Ru38** showed an increase to 79%. This outcome was consistent with the behavior expected from this uNHC catalyst family, where lower temperatures typically lead to lower conversions.[229]

To address this issue, RCM of **S1** catalyzed by **Ru36** and with the addition of 1.0 equivalent of B(OEt)$_3$ was attempted, where B(OEt)$_3$ played a role of a Lewis acid that could coordinate with the OH moiety and potentially activate the catalytic system (**Table 1, Entry 2**). However, the results were not particularly encouraging, with the conversion after 24 hours increasing only up to 56%.

Subsequently, similar tests were conducted for the RCM of **S1** in toluene at 50 °C (**Table 1, Entries 3 and 5**). This time, both catalysts displayed satisfactory results, achieving full conversion of **S1** after 24 hours of reaction. Interestingly, the same trend observed in the room temperature experiments was maintained, with **Ru38** displaying higher activity than its saturated counterpart **Ru36**. Additionally, by analyzing the time/conversion plots for the RCM of **S1**, it became evident that the initiation rate of **Ru38** was consistently faster than that of **Ru36**. The improved performance of **Ru38** over **Ru36** can be attributed to the stability based on the electronic properties of the NHC ligands themselves.

Table 1. Outcome of the RCM of **S1** under various conditions (solvent, temperature, and addition of a Lewis acid) for **Ru36** and **Ru38**.

Entry	[Ru]	Solvent	Additive	Temperature [°C]	Conversion [%][a]
1		DCM	—	*RT*	49
2	**Ru36**	DCM	B(OEt)$_3$	*RT*	56
3		Toluene	—	50	>99
4	**Ru38**	DCM	—	*RT*	79
5		Toluene	—	50	>99

[a] Conversion assessed by GC using dodecane as an internal standard
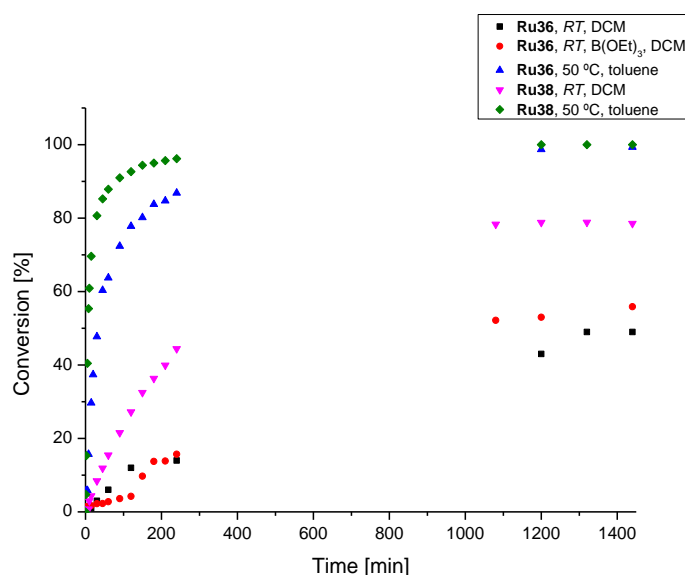
Figure 33. Time/conversion plot of the RCM of **S1** (0.1 M) catalyzed by **Ru36** and **Ru38** (1 mol%) in DCM at room temperature and in toluene at 50 °C. Conversion determined by GC.

In summary, this section has encompassed several key aspects of research. It began with the synthesis of two innovative unsymmetrical NHC-based ruthenium complexes, followed by the assessment of their stability in solution over time. Additionally, the catalytic activity of these complexes in the (RCM) reaction of DEDAM was evaluated.

The distinctive feature of the Ru-complexes synthesized is the incorporation of a 4-hydroxybenzyl moiety in the NHCs. Furthermore, the generation of complexes terminating with a phenolic

OH group opens up possibilities for novel applications. These complexes could potentially be immobilized on various supports, leading to the development of heterogenized Ru@support systems. Such systems could exhibit unprecedented and unique properties, making them valuable in various catalytic processes and applications.

3. Attempts on the immobilization of Ru-NHC complexes on Janus dendrimers

After synthesizing ruthenium complexes with a phenolic arm (**Ru36** and **Ru38**) and considering the development of PPH Janus dendrimers containing surface PEG chains for promoting solubility in water, the focus of this section was to explore the potential creation of a Ru@Janus dendrimer system. This system would combine the integration of chains for solubility modulation (such as PEG groups) on one side, along with the incorporation of metal pre-catalysts on the other. In this regard, the goal was to obtain the first phosphorus Janus dendrimer applicable in olefin metathesis catalysis, specifically in aqueous media.

It has been extensively studied that PPH dendrimers can be functionalized on their surface with various phenolic derivatives. Therefore, the targeted approach was to couple the "phenolic" complexes synthesized in section §2.2 onto the obtained PEG-modified PPH Janus dendrimer. This would result in the first example of phosphorus dendrimers for metathesis catalysis.

To analyze and optimize the reaction conditions for coupling the Ru-NHC complexes and dendrimers, the initial steps were carried out using a model dendrimer molecule, denoted as MDM **155**.

MDM was chosen for its structure, which contains a $-P(S)Cl_2$ group that mimics the surface of typical PPH dendrimers. This characteristic makes MDM an excellent candidate to fine-tune the reaction conditions for the desired coupling. The synthesis of MDM **155** followed the procedure reported by *Franc et al.*,[235] employing conventional conditions for dendrimer systems (**Scheme 41**). Specifically, benzaldehyde was subjected to a condensation reaction with *N*-methyldichlorothiophosphorhydrazide (**38**) involving the aldehyde and amino groups, resulting in the formation of **155** as a white solid in 90% yield. The successful formation of **155** was confirmed by $^{31}P\{^{1}H\}$ NMR, wherein the characteristic singlet at 63.4 ppm was observed, in contrast to the signal at 70.2 ppm corresponding to the starting material **38**.
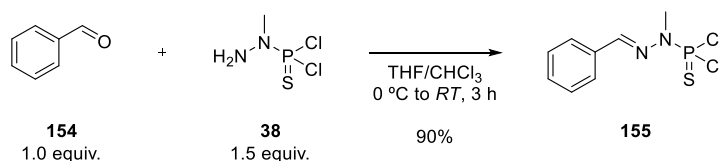
Scheme 41. Synthesis of the model dendrimer molecule **155**.

In line with the extensive research conducted by the group of Caminade and Majoral, it has been established that MDM **155** can be tailored similarly to dendrimers. Notably, **155** can undergo

reactions with phenols or amines for the substitution of the two chlorides in P−Cl bonds present on its surface.[235]

To confirm the successful substitution of the two mentioned bonds, $^{31}P\{^1H\}$ NMR spectroscopy plays a pivotal role in assessing the formation of the expected products. This is achieved by observing characteristic peaks in the NMR spectra, which are indicative of the degree of substitution of **155.** In the context of the substitution of **155** with a derivatized phenol, two distinct species are of particular importance (**Scheme 42**). First, the substitution of one P−Cl bond to form a mono-substituted derivative is characterized by a downfield shift, leading to a signal in the range of 68 – 70 ppm. Second, the completion of the substitution is characterized by an upfield shift, resulting in chemical shifts in the range of 60 – 62 ppm. This well-defined substitution pattern is the instrument for monitoring the reactions involving **155**, enabling the precise determination of reaction progress and product formation.
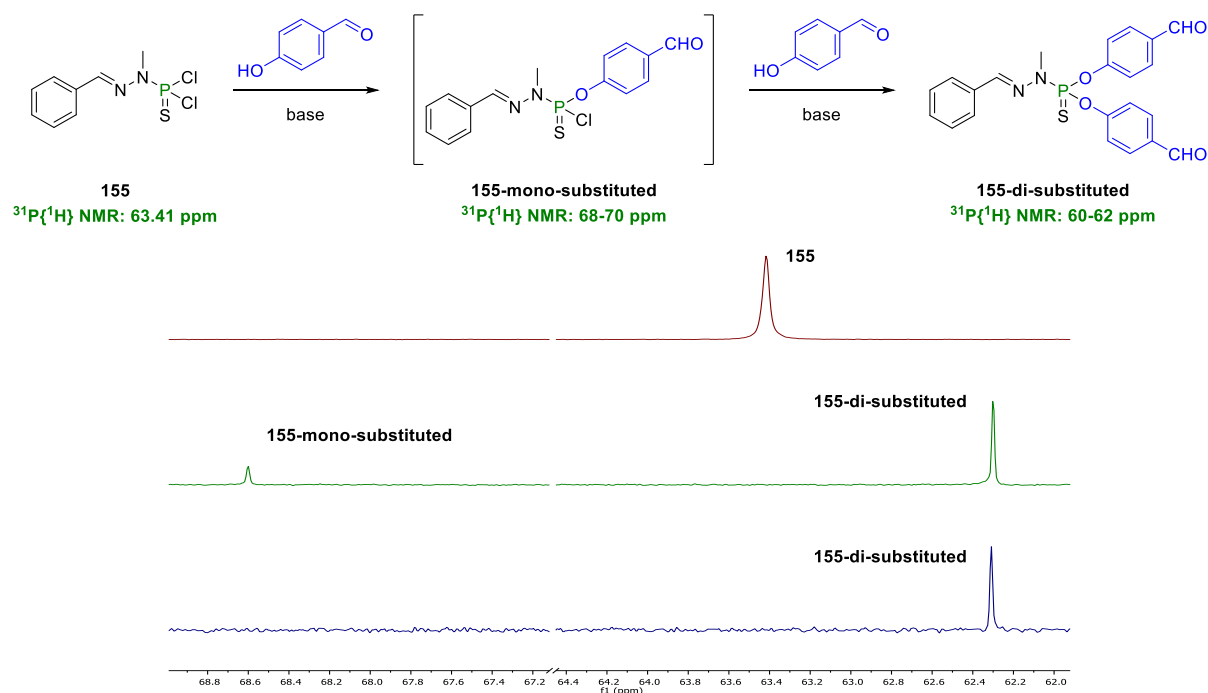
Scheme 42. Classical substitution pattern in **155** with phenol derivatives, and the corresponding $^{31}P\{^1H\}$ NMR shifts (recorded at room temperature in CDCl$_3$, 162 MHz) for the model reaction with 4-hydroxybenzaldehyde.

The initial attempt to obtain a Ru-NHC@**155** complex involved employing the conventional substitution conditions commonly used for the synthesis of dendrons and dendrimers (illustrated in **Scheme 43**).

In this process, model **155** was dissolved in dry THF, and Cs$_2$CO$_3$ and **Ru36** (in a slight excess) were added. The reaction mixture was stirred at room temperature, and the progression of the reaction was monitored using NMR spectroscopy. Specifically, the monitoring of the reaction relied on observing changes in the following key signals: *(i)* the benzylidene proton signal in ^1H NMR: this signal is crucial for tracking the reaction because the substitution occurring at the

NHC moiety is expected to alter the signal arising from the benzylidene proton from the original Ru-complex (~16.3 ppm); *(ii)* the *N*-C$\underline{H}_3$ group signal (doublet) of **155** in ^{1}H NMR at 3.5 ppm: the characteristic doublet exhibited by **155** in ^{1}H NMR, arising from the H−P coupling ($^3J_{\text{H-P}}$ = 14.0 Hz), is influenced by the substitution of the surface P−Cl bonds. Specifically, mono-substitution of **155** results in a characteristic doublet of doublet multiplicity, while full substitute alters this signal back to a doublet; and *(iii)* the phosphorus signal in ^{31}P{^{1}H} NMR: as explained earlier in **Scheme 42**, a noticeable shift in the phosphorus signal is anticipated to occur during the reaction process.
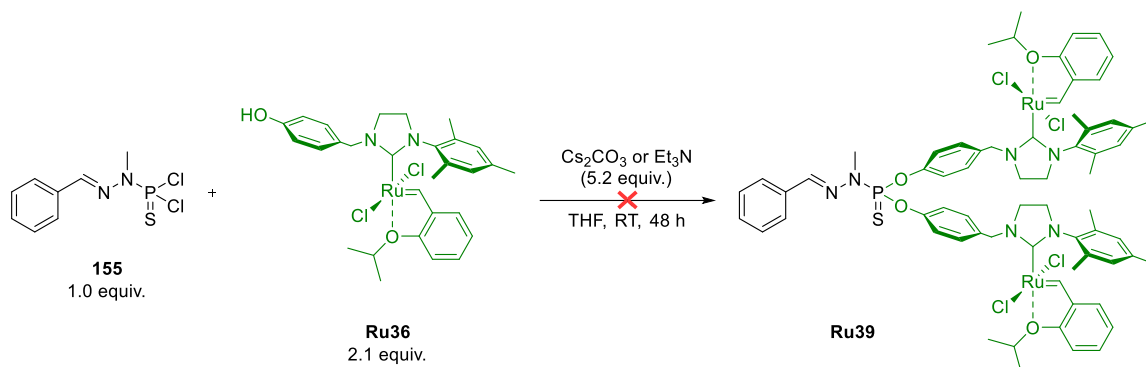
Scheme 43. Reaction conditions for the attempt on the synthesis of **Ru39**.

Based on the previous knowledge, the reaction progress was routinely monitored, and **Figure 34** presents the ^{1}H and ^{31}P{^{1}H} NMR spectra for selected regions at specific time intervals.

After 3 hours of reaction, the monitoring revealed the presence of two singlets in the benzylidene region of ^{1}H NMR at 16.25 and 16.30 ppm. Interestingly, these two peaks were slightly downfield shifted compared to the starting **Ru36** peak (at 16.22 ppm), suggesting that the reaction had initiated the substitution of **155**. This was further corroborated by the detection of two doublets at approximately 3.50 ppm in the ^{1}H NMR, consistent with the substitution of one P−Cl in **155** by the Ru-complex. Additionally, ^{31}P{^{1}H} NMR confirmed the suspected substitution by showing a signal at ~68.5 ppm, indicating the formation of a monosubstituted species.

After 24 hours of reaction, ^{31}P{^{1}H} NMR indicated the formation of a signal at 62.2 ppm, which was consistent with the production of a disubstituted product. To confirm the potential formation of this product, ^{1}H NMR was analyzed. Analysis revealed changes in the intensity of signals in the benzylidene region, with a signal at 16.26 ppm and traces of a signal at 16.30 ppm. These results aligned with the progress of the reaction.

Unfortunately, the reaction ultimately failed as the 48-hour time point showed the complete disappearance of benzylidene signals in ^{1}H NMR. Instead, a singlet at 10.50 ppm and a doublet at 9.92 ppm were detected, which were attributed to decomposition products. Moreover, ^{31}P{^{1}H} NMR exhibited the formation of a signal at *ca.* 50 ppm, which did not correspond to the expected products.
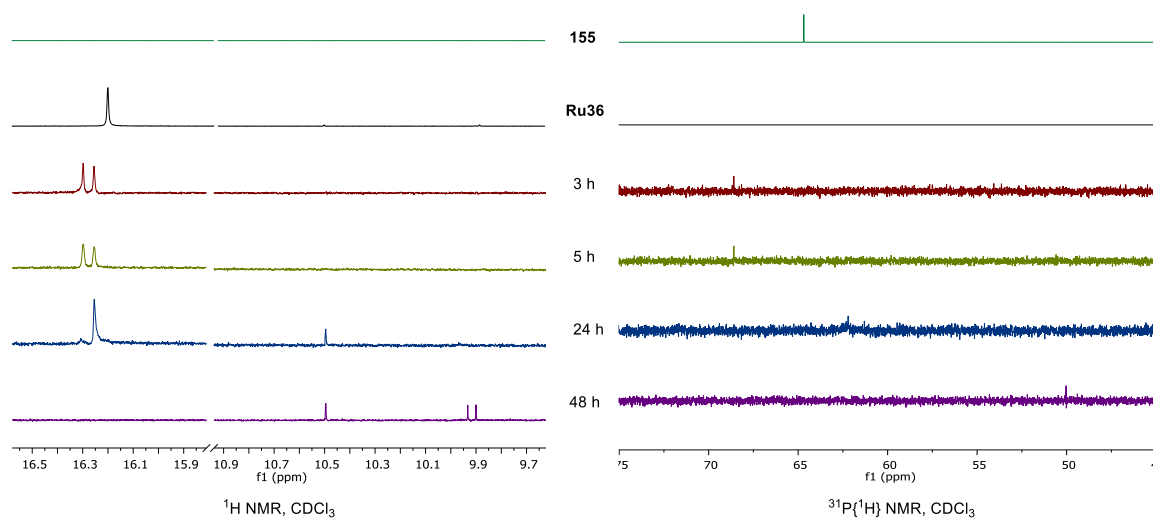
Figure 34. ^1H and $^{31}P\{^1H\}$ NMR spectra of the starting materials **155** and **Ru36**; and the monitoring of the attempt to synthesize **Ru39**. NMR spectra were recorded at room temperature in CDCl$_3$ (400 MHz and 162 MHz, for ^1H and $^{31}P\{^1H\}$ NMR respectively).

Despite the failed attempt to synthesize the Ru@dendrimer structure in the previous experiment, the promising results prompted further investigation into the influence of the base in the reaction. For this purpose, the same reaction as in **Scheme 43** was performed with Et$_3$N under the same conditions. Unfortunately, once again, the formation of decomposition products was observed. Given the preliminary results and considering research conducted by Fogg's group regarding the bimolecular decomposition of olefin metathesis catalysts when they are in close proximity,[236,237] it was hypothesized that the di-substitution of **155** to **Ru39** might have occurred, followed by rapid decomposition to form dimeric ruthenium species.

To address this issue, the second approach to obtain a Ru@dendrimer structure focused on the asymmetric substitution of **155**. The goal was to incorporate one Ru-complex unit into **155**, resulting in a mono-substituted species **156**, and then react it with a nucleophilic agent to complete the substitution (**Scheme 44**). Model dendrimer **155** was reacted under basic conditions with 1.0 equivalent of **Ru36** to obtain the corresponding mono-substituted species **156**. Subsequently, several nucleophilic agents (**157–159**, known to react with dendrimeric structures) were tested for their ability to react with **156** and complete the substitution.

The formation of intermediate **156** was confirmed by NMR spectroscopy, specifically by the shift of the phosphorus peak in $^{31}P\{^1H\}$ NMR to 68.5 ppm. Following the formation of **156**, attempts to introduce the previously mentioned nucleophilic species to produce the fully substituted model dendrimer were made. Unfortunately, despite using various compounds as potential nucleophilic agents (such as phenol, isopropylamine, or 2-methoxyethan-1-amine), none of the attempts resulted in successful formation of the desired Ru@model dendrimer molecules. Analysis of the reaction mixtures indicated that the introduction of such nucleophilic species to

form disubstituted compounds was not achieved, and the attempts to isolate any Ru@model dendrimer molecules led to compound degradation.
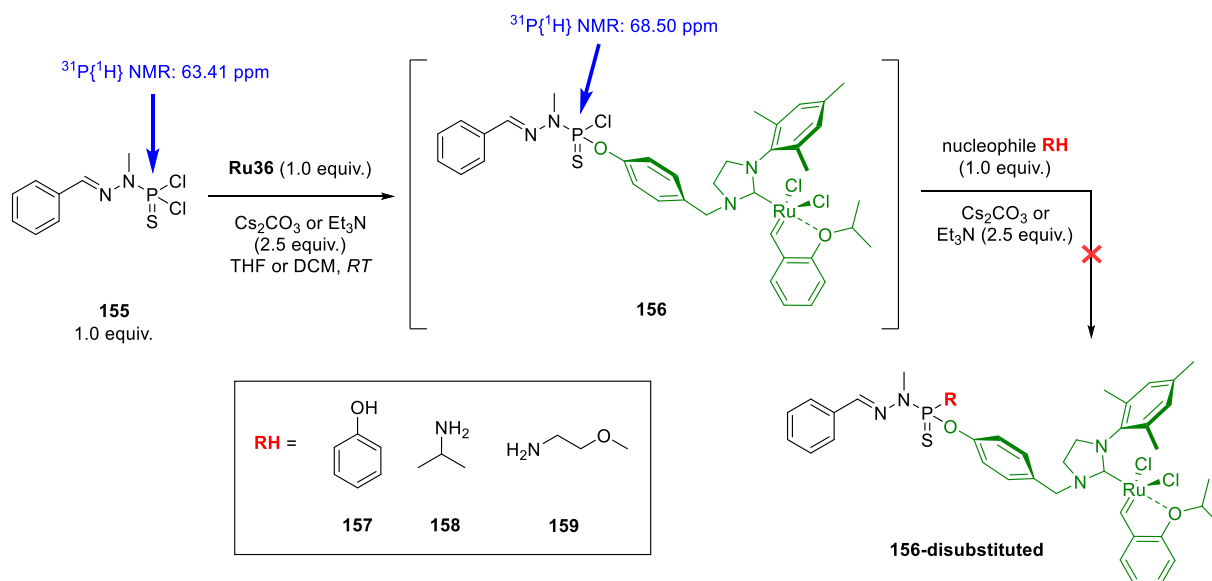
Scheme 44. Synthetic approaches attempted for the preparation of asymmetrically substituted model dendrimer **156** with one unit of **Ru36**. $^{31}P\{^1H\}$ NMR were recorded at room temperature in CDCl$_3$ (162 MHz).

The final attempt to prepare Ru@dendrimer structures was inspired by a recent development described by Grela's group.[238] In this approach (**Scheme 45**), Ru-NHC complexes were synthesized through the derivatization of **Ru40**, which already contained a primary alcohol tag in the NHC backbone. The authors reported the successful synthesis of various Ru-NHC complexes using an acylation reaction with the primary alcohol tag. They achieved this by reacting **Ru40** with a specific acyl chloride of interest under basic conditions, resulting in the desired complexes. These reactions were completed in relatively short reaction times, ranging from a few minutes up to 1 hour, and provided yields between 61 – 98% (**Scheme 45**).

This approach allowed for the efficient preparation of Ru-NHC complexes with tailored functionalities, which could potentially be used for subsequent coupling reactions with dendritic structures, such as dendrimers or dendronized polymers.
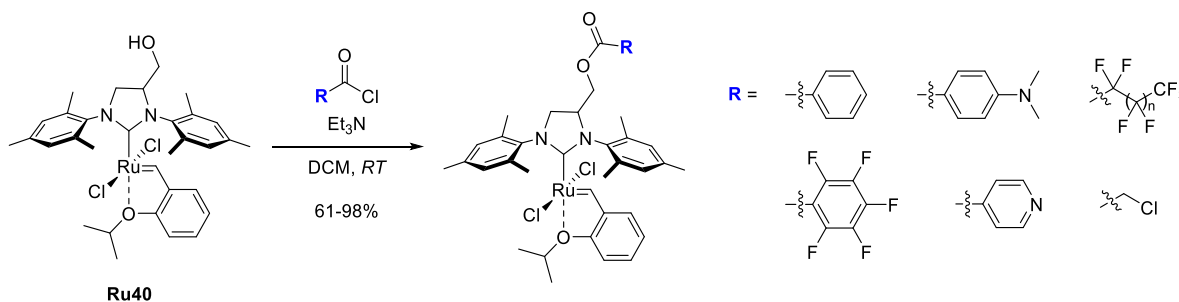
Scheme 45. Synthesis of Ru-NHC complexes *via* acylation reaction from **Ru40** reported by *Monsigny et al.*[238]

The synthesis of Ru@dendrimer systems through the described methodology involved the reaction of the phenolic Ru-complexes with an acid-terminated model dendrimer. This acid-terminated model dendrimer, denoted as **162**, was synthesized in two steps from **155** (**Scheme 46**). In the first step, **155** was subjected to a substitution reaction under basic conditions with an excess of *tert*-butyl 4-hydroxybenzoate. This reaction resulted in the formation of the ester derivative **161** in moderate yield. In the second step, the ester derivative **161** was treated with trifluoroacetic acid in DCM overnight. This treatment led to the hydrolysis of the ester group, resulting in the formation of the diacid compound **162**.

The formation of **162** was monitored using various analytical techniques. Initially, **155** exhibited in $^{31}P\{^1H\}$ NMR a phosphorus signal at 63.4 ppm, which shifted to 61.2 ppm in the ester derivative **161** and further to 61.1 ppm in the acid compound **162**. Additionally, IR spectroscopy was used to monitor the reaction by observing the shift in the C=O stretching band, which indicated the transformation from the ester (1711 cm^{-1}) to the acid functionality (1787 cm^{-1}).
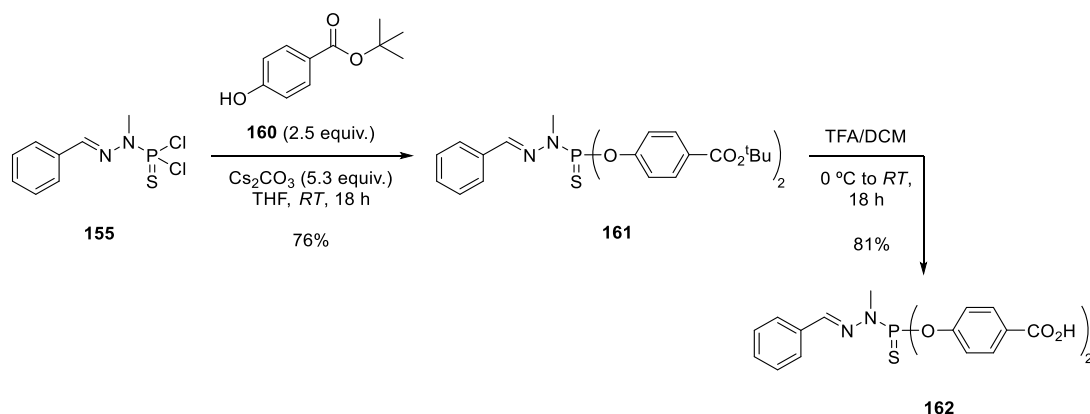
Scheme 46. Synthesis of acid-terminated model dendrimer **162** in two steps from **155**.

To assess the applicability of such acylation protocol for the preparation of Ru@dendrimer with a phenolic Ru-complex, the synthesis of **Ru41** was undertaken. This involved the reaction of **Ru38** with 4-methoxybenzoyl chloride (**163**), as outlined in **Scheme 47**. In the first step, **Ru38** was treated with Et$_3$N in DCM at −20 °C to generate the phenolate derivative. Subsequently, this phenolate was reacted with 4-methoxybenzoyl chloride (**163**) to form the desired ester linkage. The resulting novel ruthenium complex, **Ru41**, was obtained as an orange powder in 85% yield. The successful synthesis of **Ru41** indicated that the acylation of **Ru38**-type complexes with suitable acyl chlorides was feasible within this system, which was a crucial step toward the goal of preparing Ru@dendrimer systems.
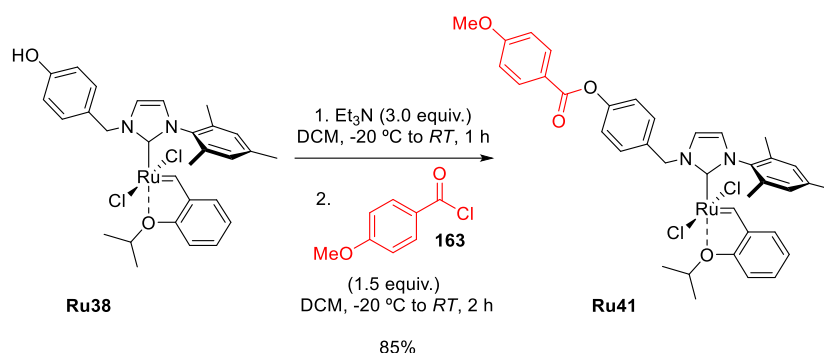
Scheme 47. Synthesis of **Ru41** *via* acylation of **Ru38** with 4-methoxybenzoyl chloride (**163**).

Therefore, the synthesis of Ru-NHC@model dendrimer **Ru42** was attempted by combining the approaches developed for the acid-terminated model dendrimer **162** and the acylation reaction of the "phenolic" ruthenium complexes. The process is outlined in **Scheme 48**.

First, acid-terminated model dendrimer **162** was subjected to oxalyl chloride in DCM at −20 °C to generate the acyl chloride derivative **164**. The formation of **164** was confirmed by NMR spectroscopy, which showed an upfield shift of the phosphorus signal in ^{31}P{^{1}H} NMR from 61.07 ppm to 59.90 ppm, along with the disappearance of the carboxylic acid proton signal in ^{1}H NMR.

Subsequently, the acyl chloride **164** solution generated *in situ* was slowly added to a DCM solution of **Ru38**, previously treated with an excess of triethylamine for 1 h. The reaction mixture was stirred for a period ranging from 1 to 16 hours, and its progress was monitored using NMR spectroscopy. The NMR results indicated the presence of two phosphorus species, as evidenced by two singlets at 60.88 ppm and 61.24 ppm, which was consistent with the formation of the desired product as well as a second phosphorus-containing species —either hydrolysis derivatives or decomposition products. However, no successful means of purification led to the isolation of the desired product.

The synthesis of Ru-NHC@model dendrimer **Ru42** represented a challenging endeavor, with complications arising during the purification process. Further optimization and investigation may be required to successfully obtain the desired product.
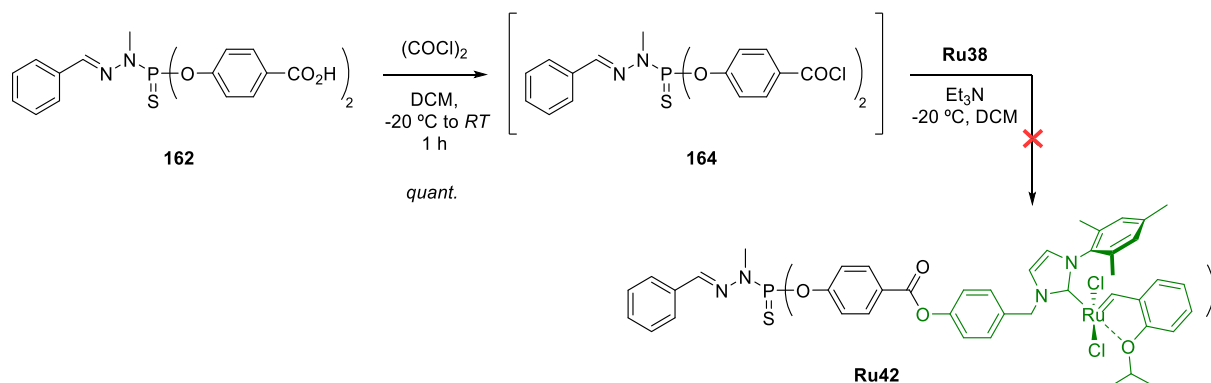
Scheme 48. Attempt on the synthesis of **Ru42** *via* acylation reaction from **162** and **Ru38**.

In summary and much of our regret, despite all the efforts performed for the immobilization of Ru-NHC complexes at the surface of dendrimers (in this case a model dendrimer compound), none of the attempted methodologies have been proved to be effective for the formation of the desired Ru@dendrimer system.

4. Synthesis of a heterogeneous Ru@MOF system for olefin metathesis

The next objective of this Thesis was to demonstrate the versatility of the previously synthesized Ru-NHC complexes with a phenolic arm by immobilizing these structures on MOFs. Specifically, the aim was to leverage the interactions between the ruthenium complexes with a phenolic moiety and the coordinatively unsaturated sites in an aluminum-based MOF known as **(Al)MIL-101-NH₂**.

Prior research had successfully immobilized ruthenium complexes with ammonium tags within MOF structures.[209] Similarly, other functional groups with donor properties and Lewis acidic centers, such as pyridines or carboxylates, had been successfully grafted onto MOFs.[239–246] However, due to the basic donor behavior of amines and carboxylates, which can deactivate transition metal complexes, it was hypothesized that phenolic tags could serve as an alternative for immobilizing ruthenium complexes on MOF supports. Additionally, when coordinated to unsaturated metal sites, the phenolic OH groups would become more acidic and amenable to deprotonation, resulting in the formation of phenolate structures and facilitating the creation of anionic ligands.

The grafting of phenols onto MOFs had seen limited exploration in the literature, with only one previous example reported by *Zhu et al.* in 2018.[247] In that case, the approach focused on charge-assisted immobilization, ultimately aiming to create a robust and stable Ru@MOF system that could serve as a reliable heterogeneous catalyst.

4.1. Synthesis of (Al)MIL-101-NH₂ MOF and sorption/desorption experiments

In the pursuit of immobilizing the phenolic Ru-NHC complexes on MOFs, the **(Al)MIL-101-NH₂** MOF was chosen as the most promising material for the immobilization experiments, based on the size and stability of the previously prepared ruthenium complexes.

The synthesis of the **(Al)MIL-101-NH₂** MOF (as shown in **Scheme 49**) began by creating a homogeneous solution of AlCl₃·6H₂O in DMF, followed by its reaction with 2-aminoterephthalic acid **165** in a pressure-sealed tube at high temperature for 72 hours. After filtration and washing of the resulting solid, the MOF was deformylated and purified through further filtration and washings, resulting in the desired product. The final **(Al)MIL-101-NH₂** MOF **166** had good purity but contained approximately 18 – 19% MeOH. Nonetheless, the structure of **166** was confirmed using Powder X-ray diffraction (PXRD).

This solid support consisted of supertetrahedral units formed by rigid terephthalate ligands and $AlCl_3$ octahedral clusters. The MOF **166** featured two types of quasi-spherical mesoporous cages, and the presence of coordinatively unsaturated metal sites in its structure made it suitable for use as a mild Lewis acid, which could potentially facilitate the functionalization of active catalytic species.
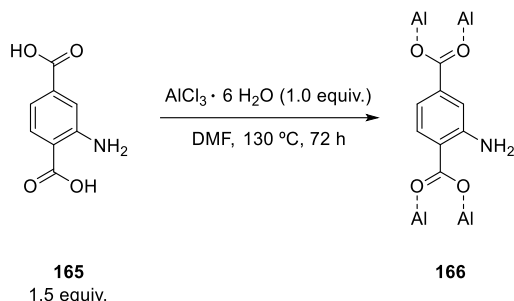
Scheme 49. Synthetic methodology for the preparation of (Al)MIL-101-NH$_2$ MOF.

Following the synthesis of the **(Al)MIL-101-NH₂** MOF, the next step was to attempt the immobilization of the metathesis pre-catalyst. In this case, **Ru38** was chosen for immobilization due to its demonstrated higher activity for metathesis (*vide supra*).

For this purpose, a 1.0 mM solution of **Ru38** (at a loading of 10% w/w) was prepared in either DCM or toluene. Subsequently, MOF **166** (12 mg) was added to the solution, and the resulting mixture was stirred at room temperature for one hour. Following this, the suspension was centrifuged, and the supernatant was carefully removed. Of interest, the proposed mode of immobilization of **Ru38** on the **(Al)MIL-101-NH₂** is illustrated in **Figure 35**.
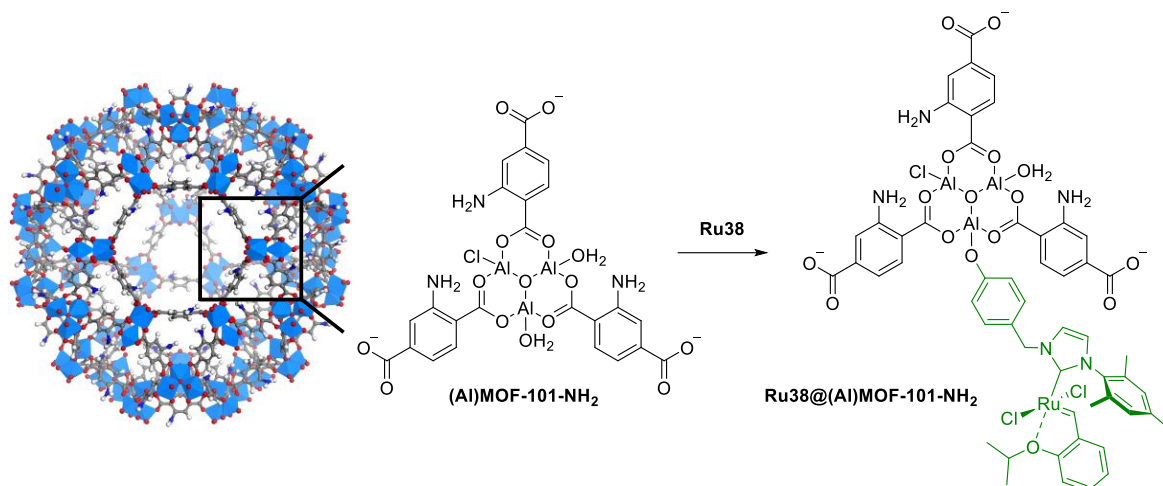
Figure 35. Representation of the proposed mode for the immobilization of **Ru38** on **(Al)MIL-101-NH₂**.

The analysis of the supernatant by UV-Vis spectroscopy was crucial to determine the concentration of the catalyst in the supernatant and, consequently, the amount of catalyst immobilized within the MOF structure (see Experimental Section for details). To accurately determine the amount of catalyst in the supernatant, solutions of known **Ru38** concentration were prepared, and their UV-Vis spectra were recorded. This allowed for the calculation of the

molar absorption coefficients (**Figure 36**), and therefore determine the concentration of catalyst in the supernatant upon immobilization through interpolation on the linear regression. The analyses showed that almost quantitative sorption was achieved, with 99.2% and 99.4% of the catalyst being absorbed into the MOF for the DCM and toluene approaches, respectively (**Table 2**).

With the successful immobilization of **Ru38** confirmed, the next step was to conduct desorption experiments to test for ruthenium leaching and assess the robustness of the immobilized catalyst. Since the catalyst was immobilized inside the MOF voids through non-covalent reversible interactions, desorption experiments provided valuable information regarding the leaching of ruthenium. To perform these experiments, dried **Ru38@(Al)MIL-101-NH₂** was suspended in toluene and placed in a G4 filtering funnel under a stream of argon. The suspension was slowly filtered and washed with toluene and DCM. The collected supernatants were then analyzed by UV-Vis spectroscopy to determine the quantity of leached ruthenium complex. Remarkably, the results showed low leaching of the absorbed catalyst from the **(Al)MIL-101-NH₂**, with less than 10% of the Ru-complex in total being desorbed.
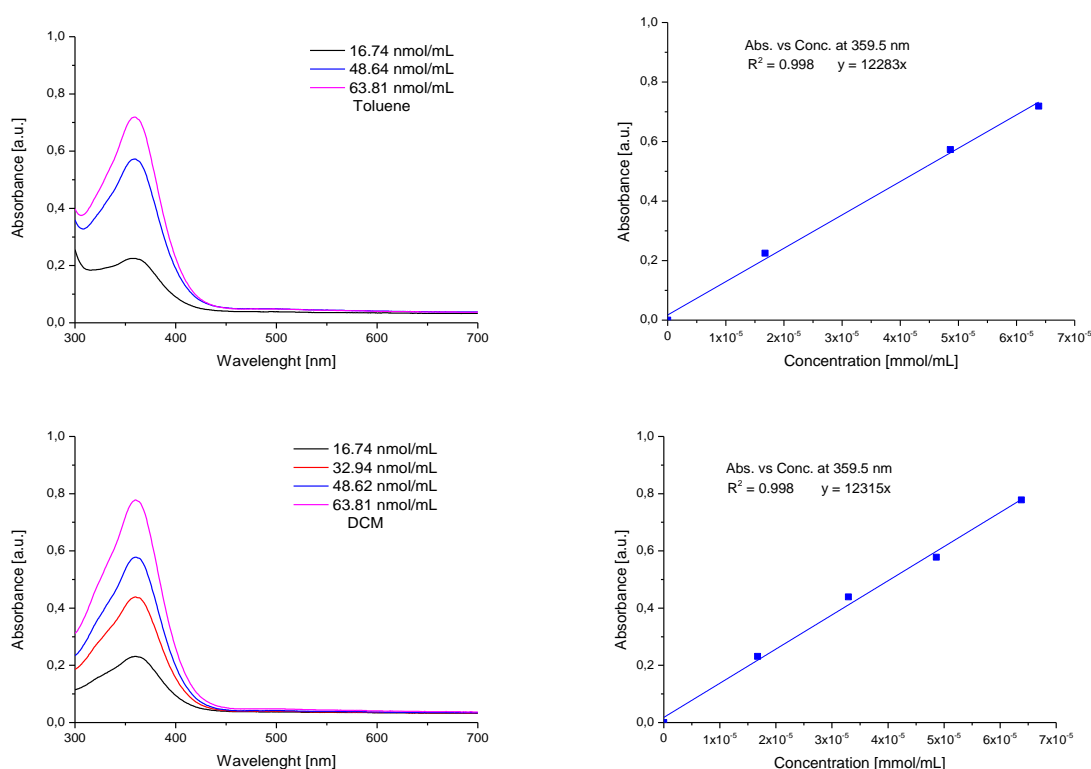
Figure 36. UV-Vis spectra of catalyst **Ru38** in toluene (*top*) and DCM (*bottom*) and determination of their molar absorption coefficients ε by linear regression.

Table 2. Results of the adsorption experiments of **Ru38** from DCM and toluene solutions based on the absorbance of the supernatant.

Catalyst	Solvent	Absorbance of the supernatant at 359.5 nm	Catalyst adsorbed from solution [%][a]
Ru38	DCM	0.071	99.2
	Toluene	0.049	99.4

[a] Determined by interpolation based on the absorbance value from UV-Vis measurement of the supernatant.

The crystallinity and porosity of the **Ru38@(Al)MIL-101-NH$_2$** were also evaluated. In terms of crystallinity, PXRD analysis was performed (**Figure 37**), which demonstrated that the crystallinity of **Ru38@(Al)MIL-101-NH$_2$** (**Figure 37b**) was maintained after catalyst immobilization compared to the PXRD of the starting MOF (**Figure 37a**). Regarding porosity, it was assessed in terms of the BET (Brunauer, Emmett, and Teller) surface area. The results showed a significant reduction in surface area, dropping from 1753 m^2/g for **(Al)MIL-101-NH$_2$ 166** (**Figure 38a**) to 564 m^2/g for **Ru38@(Al)MIL-101-NH$_2$** (**Figure 38b**), consistent with the incorporation of the ruthenium complex within the MOF structure.
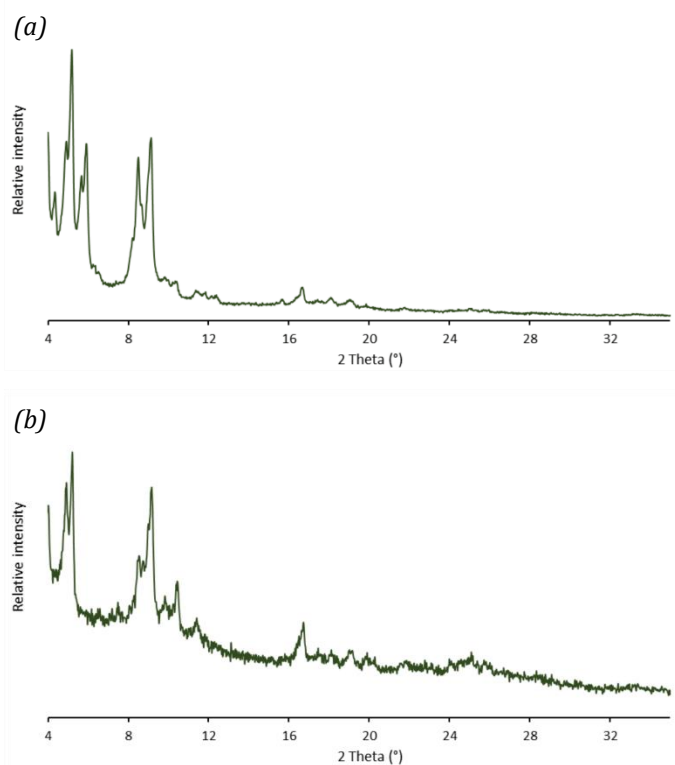
Figure 37. (*a*) PXRD pattern of pattern of **(Al)MIL-101-NH$_2$** MOF. (*b*) PXRD pattern of pattern of **Ru38@(Al)MIL-101-NH$_2$**.
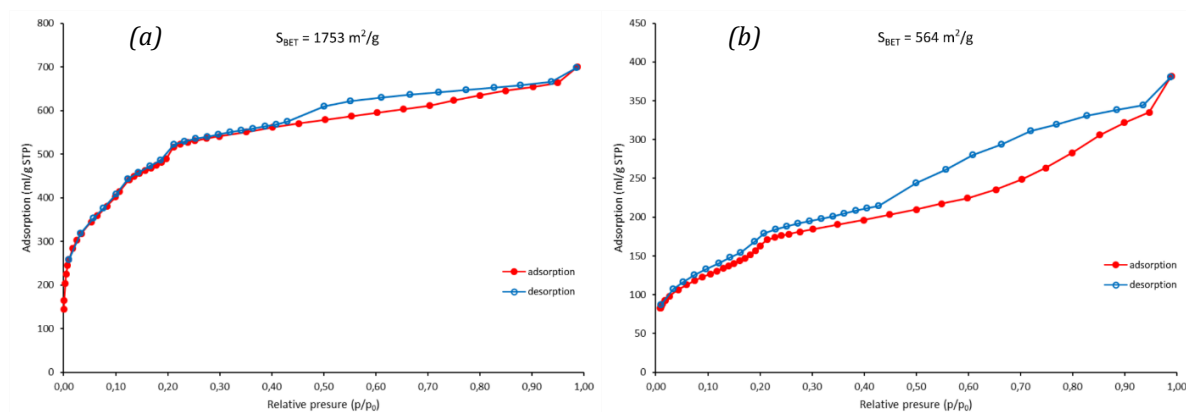
Figure 38. N$_2$ adsorption/desorption isotherm of: (*a*) **(Al)MIL-101-NH$_2$**; and (*b*) **Ru38@(Al)MIL-101-NH$_2$**. Points in the range p/p$_0$ = 0.0005−0.21 were used to calculate BET surface area.

4.2.   Catalytic studies for Ru38@(Al)MIL-101-NH$_2$ in metathesis

Having successfully immobilized **Ru38** within the structure of **(Al)MIL-101-NH$_2$** and conducting sorption and leaching experiments, the next step was to test the activity of the newly obtained heterogeneous catalyst in metathesis. Toluene was chosen as the solvent for the reaction based on the leaching experiments, which showed that toluene led to low desorption of the catalyst. **Ru38@(Al)MIL-101-NH$_2$** was then tested for the RCM of the model molecule DEDAM using 1 mol% of the heterogenized catalyst in toluene at 80 °C (**Scheme 50**).
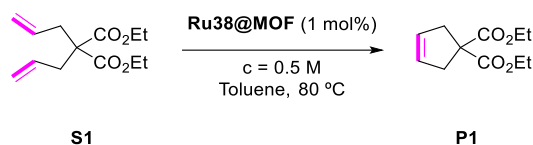
Scheme 50. Standard reaction conditions used for the RCM of DEDAM (**S1**) employing **Ru38@(Al)MIL-101-NH$_2$**.

The use of **Ru38@(Al)MIL-101-NH$_2$** for the RCM of **S1** proved to be less effective than expected. In this regard, as shown in **Table 3, Entry 4**, the conversion after 24 hours of the reaction time was only 54% under these conditions. Furthermore, it was observed that the conversion of **S1** did not significantly improve after 3 hours of the reaction, as 53% conversion had already been achieved (**Table 3, Entry 3**). When comparing the catalytic activity of **Ru38@(Al)MIL-101-NH$_2$** with its homogeneous counterpart **Ru38** under the same conditions (**Table 3, Entry 1**), it was evident that **Ru38** led to complete conversion after 24 hours of reaction and 95% conversion after just 3 hours.

In an attempt to address the poor performance of **Ru38@(Al)MIL-101-NH$_2$** in the RCM, the same metathesis reaction was conducted with an increased catalyst loading of 2 mol% (**Table 3, Entry 6**). Interestingly, this increase in loading did not result in a higher conversion, yielding only a 51% conversion after 24 hours of reaction.

Table 3. Results of the RCM of DEDAM (**S1**) with **Ru38** (homogeneous) and **Ru38@(Al)MIL-101-NH₂** (heterogeneous) complexes in toluene.
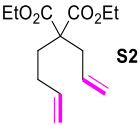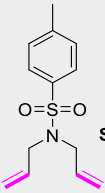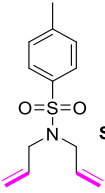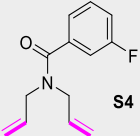
Entry	[Ru]	Loading [mol%]	Time [h]	Conversion [%][a]
1	Ru38	1.0	3	95
2			24	>99
3	Ru38@(Al)MIL-101-NH₂	1.0	3	53
4			24	54
5		2.0	3	50
6			24	51

[a] Conversion was determined by GC using tetradecane as internal standard

In addition to the previous catalytic examples, the novel **Ru38@(Al)MIL-101-NH₂** was tested with a variety of metathesis substrates, using a 1 mol% catalyst loading and the previously mentioned reaction conditions (toluene, 80 °C, 24 hours of reaction). Catalyst and metathesis substrates were suspended in toluene and stirred at 80 °C. An aliquot of the supernatant was collected at specific time intervals, filtered, and quenched to determine the conversions by GC analysis. The results of the catalytic experiments are presented in **Table 4**, indicating conversions ranging from 30% to 91% after 24 hours. Interestingly, the RCM of DATA (**S3**) exhibited an excellent conversion of 65% after 3 hours and a final conversion of 91% after 24 hours (**Table 4, Entry 2**). Conversely, the metathesis of substrates **S2** and **S4** showed relatively poor performance, with conversions in the range of 30% within 24 hours of reaction (**Table 4, Entries 1 and 4, *in suspension***).

To attempt an enhancement of the previous metathesis results in terms of performance, the heterogeneous catalyst was treated with dry HCl in Et₂O after the adsorption of **Ru38**, following the methodology reported by Chołuj *et al.*[211] As shown in **Table 4, Entry 3**, the metathesis outcome exhibited a much faster initial conversion, reaching 78% after 15 minutes of reaction, though this unfortunately did not increase after 24 hours.

Table 4. Results of the RCM reaction of selected dienes **S2**-**S4** using **Ru38@(Al)MIL-101-NH₂** complex (1 mol%) in toluene at 80 °C.

Entry	[Ru]@MOF	Substrate	Conversion [%][a]		
			At split	In filtrate (24 h)	In suspension (24 h)
1	Ru38@(Al)MIL-101-NH₂	EtO₂C CO₂Et **S2**	26 (3 h)	26	31
2	Ru38@(Al)MIL-101-NH₂	O=S=O N **S3**	65 (3 h)	65	91[b]
3	Ru38@(Al)MIL-101-NH₂·HCl	O=S=O N **S3**	78 (0.25 h)	78	78
4	Ru38@(Al)MIL-101-NH₂	O F N **S4**	13 (3 h)	14	30

[a] Conversion was determined by GC using tetradecane as internal standard.
[b] Isolated yield for the compound is 79 %.

In summary, the Ru-complex containing a phenolic arm, **Ru38**, was effectively immobilized within the structure of **(Al)MIL-101-NH₂** MOF. Desorption analysis demonstrated that the porous framework of **(Al)MIL-101-NH₂** provided a suitable nanoenvironment for the non-covalent immobilization of **Ru38**. Furthermore, the immobilization of ruthenium complexes within the coordinatively unsaturated Lewis acid centers of the MOF exhibited strong binding, as evidenced by leaching studies that showed negligible desorption in toluene and DCM.

Although the catalytic activity of heterogeneous **Ru38@(Al)MIL-101-NH₂** was found to be lower than its homogeneous counterpart **Ru38** in solution, the system proved capable of catalyzing the tested metathesis reactions. This demonstrates the feasibility of immobilizing ruthenium complexes on MOFs through the implementation of an interaction with a phenol, serving as a proof-of-concept for this approach.

5. Synthesis of a Ru(*p*-cymene)@Janus dendrimer system for its use in catalysis

Continuing with the applications of supported ruthenium complexes in catalysis, the last part of this Thesis was dedicated to preparing a metal@dendrimer system for catalytic applications in water-based systems.

As previously mentioned in the introduction, phosphorus dendrimers have been widely employed in catalysis by incorporating various metal complexes into their structures. Despite numerous examples in the literature demonstrating the use of PPH dendrimers in catalysis, both in traditional organic solvents and water, this section aims to describe the synthesis of the first-ever reported PPH Janus dendrimer for the use in catalysis. In particular, the targeted systems are based on the dendrimers described in section §1.3, which have been synthesized to include PEG moieties on one side (to provide water solubility) and $-P(S)Cl_2$ moieties on the other side (to serve as anchoring points for the desired functionality). These dendrimers have been prepared and are ready to be used for the intended applications. **Figure 39** illustrates the previously synthesized PPH first-generation Janus dendrimer.
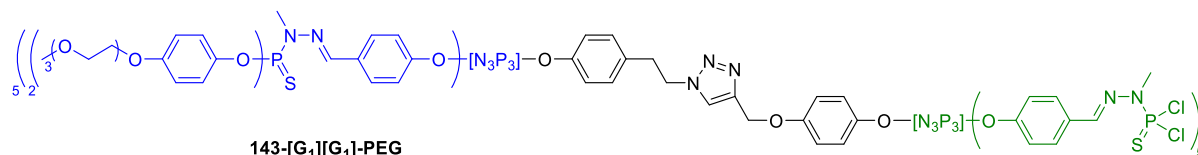
143-[G₁][G₁]-PEG

Figure 39. Structure of the first-generation PPH Janus dendrimer **143-[G₁][G₁]-PEG** synthesized in this Thesis.

Based on the previous knowledge, the idea of preparing a novel Ru@dendrimer system was conceived. In this regard, research was conducted to identify a suitable catalytic entity for anchoring on the surface of dendrimers. The selected methodology is illustrated in **Scheme 51**. Specifically, the synthesis of the Ru@dendrimer system was pursued by introducing a phosphine moiety onto the dendrimers surface and subsequently incorporating a commercially available ruthenium complex ([Ru(*p*-cymene)Cl₂]₂). This approach was chosen based on prior research conducted by the Caminade's group, where they reported the synthesis of phosphine-terminated dendrimers and the grafting of metal complexes onto their structures.[248,249]

PEG functionalized surface
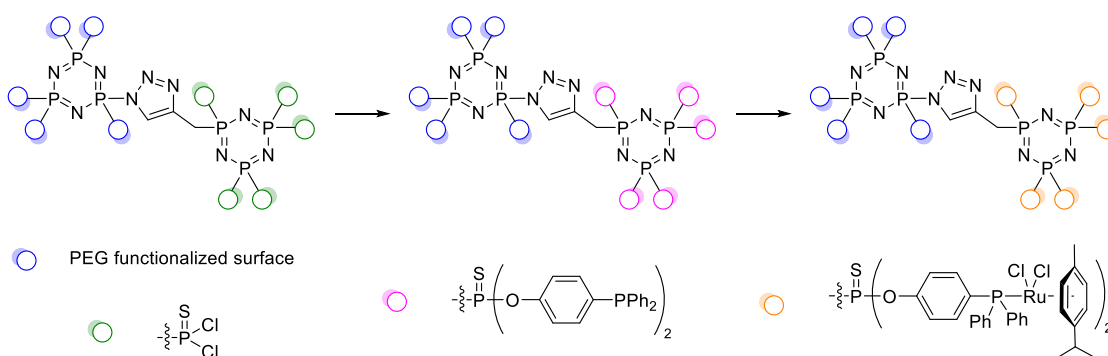
Scheme 51. Strategy for the preparation of the desired Ru@dendrimer system for applications in catalysis in water.

Considering all this information, the synthesis of the Ru@dendrimer system commenced with the preparation of the phosphine ligand for its introduction onto the dendrimers surface. Specifically, the synthesis of 4-(diphenylphosphoryl)phenol **170** was chosen as the suitable candidate, due to the presence of both a phenol group —which serves as a grafting point for the reaction with **143-[G₁][G₁]-PEG**— and the phosphine itself, which would be used for the complexation of the ruthenium catalyst. **Scheme 52** illustrates the synthetic methodology employed for the synthesis of phosphine **170**.

The synthesis started with the introduction of a silyl-protecting group to 4-bromophenol **167**, reacting it under basic conditions with *tert*-butyldimethylsilyl chloride (TBDMSCl) in DCM to yield the desired protected derivative **168** in 98% yield. Subsequently, **168** was converted to phosphine **169** in a two-step lithiation and phosphination reaction. In the first step, **168** was dissolved in dry and degassed THF and cooled to −78 °C, and *n*-butyl lithium was later added dropwise to the mixture. Chlorodiphenylphosphine was then added to the lithiated mixture to give the desired compound **169** as a white solid after work-up in excellent yield. Finally, the desired phenol phosphine **170** was obtained by deprotecting **169** using tetrabutylammonium fluoride. The desired product was obtained with an overall yield of 84% in three steps by employing previously reported methodologies.[250]

Characterization of the product was performed using NMR, revealing the formation of the desired phosphine with a $^{31}P\{^{1}H\}$ NMR signal at −7.0 ppm, consistent with previously reported syntheses.
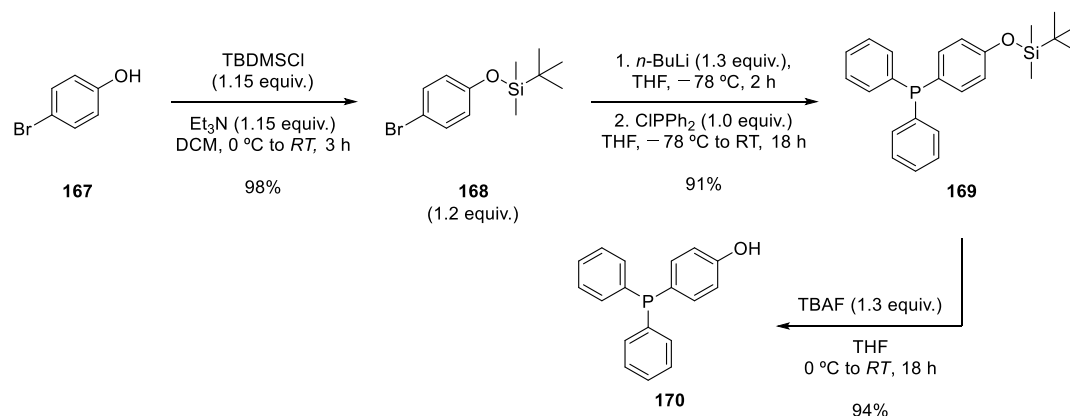
Scheme 52. Synthesis of 4-(diphenylphosphoryl)phenol **170** in three steps from 4-bromophenol **167**.

After successfully synthesizing phosphine **170**, the next step involved its introduction to the first-generation Janus dendrimer **143-[G₁][G₁]-PEG**. To prepare the desired phosphine-terminated dendrimer, standard reaction conditions for the introduction of phenol derivatives to −P(S)Cl₂-terminated dendrimers were employed. Specifically, **143-[G₁][G₁]-PEG** was dissolved in THF, and phosphine **170** was added under basic Cs_2CO_3 conditions (as shown in **Scheme 53**).
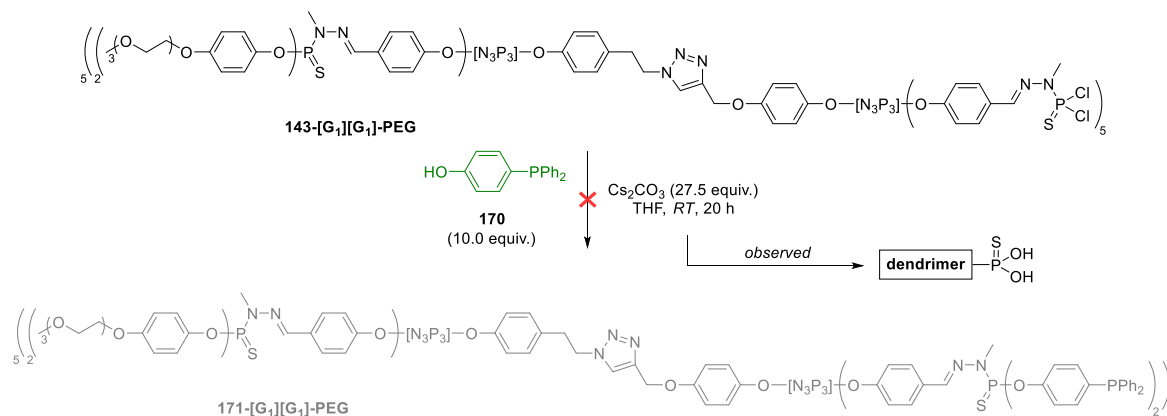
Scheme 53. First attempt on the synthesis of the phosphine-terminated Janus dendrimer **171**.

Unfortunately, despite the seemingly straightforward nature of the reaction, the monitoring of the reaction *via* $^{31}P\{^{1}H\}$ NMR (**Figure 40**, *blue*) revealed the presence of an unexpected phosphorus species. While the formation of the desired **171-[G$_1$][G$_1$]-PEG** dendrimer was confirmed by the upfield shift of the terminal phosphorus signals from 62.5 ppm to 61.0−61.5 ppm and the shift of the phosphine **170** signal from −7.0 ppm to −6.5 ppm, a new phosphorus species was detected at 42.5 ppm.

The appearance of a phosphorus species at 42.5 ppm was consistent with the hydrolysis of the terminal −P(S)Cl$_2$ groups present in the initial **143-[G$_1$][G$_1$]-PEG**. The hypothesis for the formation of this side-product was based on the large tendency of PEG moieties to trap water molecules forming hydrogen bonds.[251] Considering this, and given that the reaction occurred under basic conditions, it was suggested that despite water molecules reacted more slowly with the base than the phenol phosphine **170**, the higher nucleophilicity of the hydroxyl (OH$^-$) group compared to the phenolate form of **170** lead to the formation of a mixture of the hydrolyzed product and the desired substitution product.
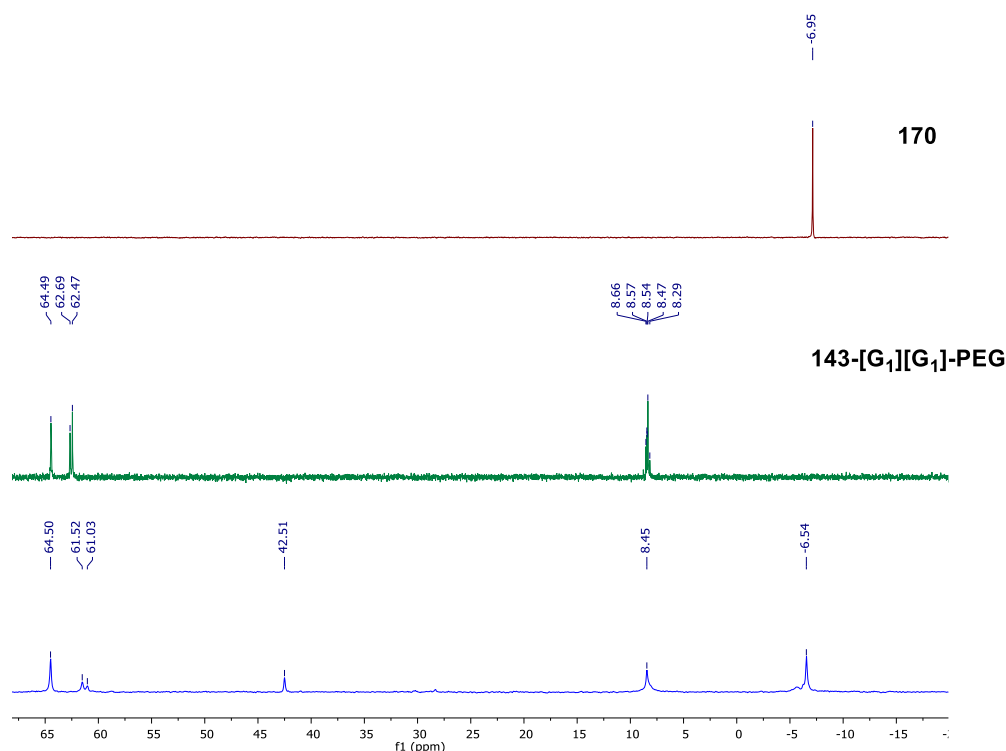
Figure 40. $^{31}P\{^1H\}$ NMR spectra of (4-hydroxyphenyl)diphenylphosphine **170** (*top, red*), **143-[G$_1$][G$_1$]-PEG** dendrimer (*middle, green*); and crude mixture obtained from the attempt to prepare phosphine-terminated dendrimer **171-[G$_1$][G$_1$]-PEG** (*blue, bottom*), recorded in CDCl$_3$ (162 MHz) at room temperature.

To attempt to overcome the issue encountered during the synthesis, a relatively simple alternative was tested. Specifically, the addition of a drying agent to the initial dendrimer solution before introducing the base and phosphine **170** could potentially lead to the successful production of the desired product by effectively capturing the water present within the dendrimer structure. To evaluate this approach, two model reactions were conducted, as illustrated in **Scheme 54**. In the first model reaction (**Scheme 54a**), a solution of model dendrimer molecule **155** was prepared in THF along with Na$_2$SO$_4$ as drying agent. Subsequently, Cs$_2$CO$_3$ and two equivalents of water were added, and the mixture was allowed to stir for 24 hours. After one day of reaction, the $^{31}P\{^1H\}$ NMR analysis revealed that hydrolysis had not occurred, demonstrating a sharp singlet at 63.4 ppm, corresponding to the starting **155**.

In parallel, the same reaction was tested in **Scheme 54b**, this time incorporating 2.5 equivalents of 4-hydroxybenzaldehyde. After 24 hours of reaction, NMR analysis indicated the formation of the desired substitution product, without evidence of the hydrolysis side-product.
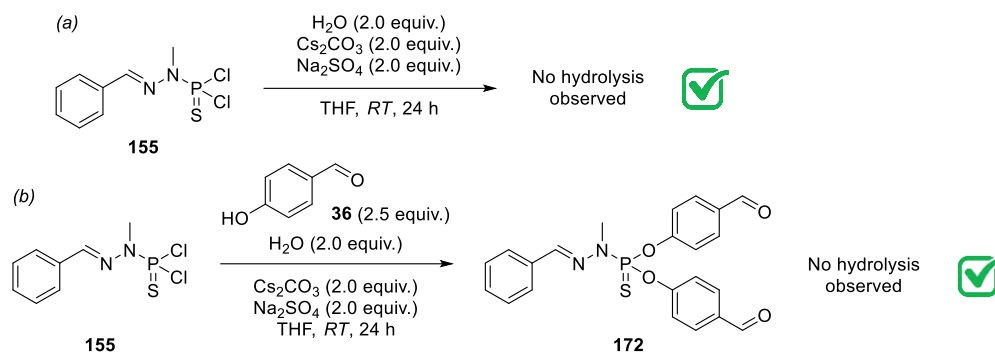
Scheme 54. Test reactions performed to analyze the effect of Na_2SO_4 as drying agent to prevent the hydrolysis of **155**.

Based on the promising results observed regarding the use of Na_2SO_4 as a drying agent for the substitution reaction in the model dendrimer **155**, this approach was employed for the synthesis of the desired phosphine-terminated **171-[G₁][G₁]-PEG**. In this context, the procedure involved dissolving **143-[G₁][G₁]-PEG** in a THF suspension containing Na_2SO_4 and stirring for 1 hour before adding phosphine **170** and Cs_2CO_3 (as outlined in **Scheme 55**).
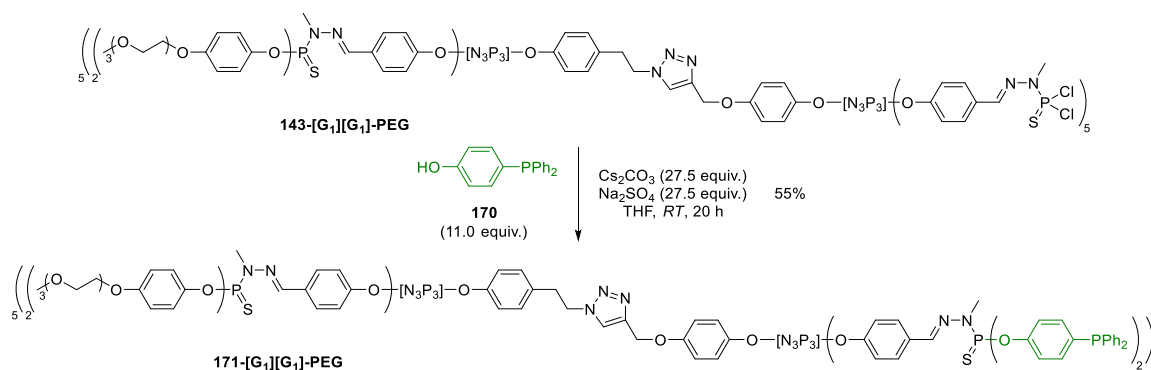
Scheme 55. Synthesis of the phosphine-terminated Janus dendrimer **171** from **143-[G₁][G₁]-PEG**.

The reaction progress was once more monitored by $^{31}P\{^1H\}$ NMR (**Figure 41**). In the crude mixture, the appearance of two singlets at approximately 61.3 ppm was observed, consistent with the substitution of the terminal chlorides of $-P(S)Cl_2$ group from **143-[G₁][G₁]-PEG** with the corresponding $-P(S)(OR)_2$ groups, which typically resonate around 62.5 ppm. In a similar trend, the grafting of 4-(diphenylphosphoryl)phenol onto the dendrimer was confirmed by the emergence of a singlet at −6.5 ppm, slightly shifted compared to the parent phenol phosphine **170** (δ_{170} = −7.0 ppm).

Furthermore, the formation of the hydrolyzed dendrimer (previously detected in $^{31}P\{^1H\}$ NMR by the presence of a signal at 42.5 ppm) was not observed, affirming the successful substitution of the first-generation Janus dendrimer with the desired phosphine derivative.
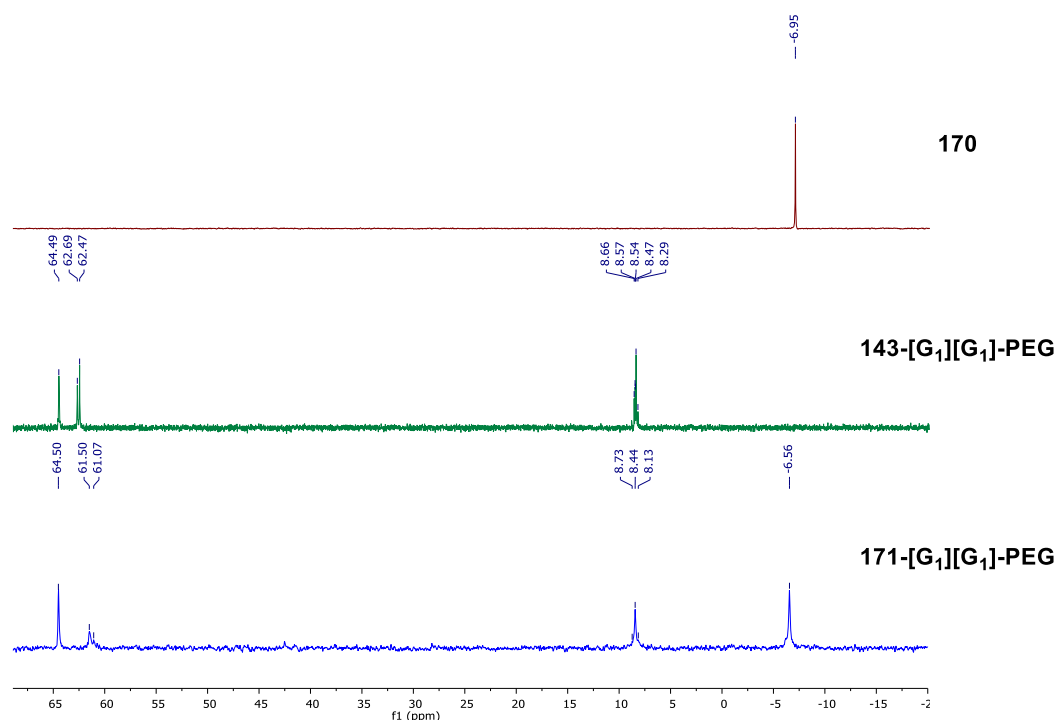
Figure 41. ^{31}P{^{1}H} NMR spectra of phosphine **170** (*top, red*), **143-[G$_1$][G$_1$]-PEG** dendrimer (*middle, green*); and the novel phosphine-terminated dendrimer **171-[G$_1$][G$_1$]-PEG** (*blue, bottom*), recorded in CDCl$_3$ (162 MHz) at room temperature.

Lastly, the desired Ru@dendrimer system was obtained by grafting a Ru-complex onto the surface of the newly synthesized phosphine-terminated dendrimer **171-[G$_1$][G$_1$]-PEG**. To accomplish this, commercially available [Ru(*p*-cymene)Cl$_2$]$_2$ was anchored to the dendrimer **171** through the complexation ability of the terminal phosphines. As illustrated in **Scheme 56**, five equivalents of [Ru(*p*-cymene)Cl$_2$]$_2$ were reacted with one equivalent of dendrimer **171-[G$_1$][G$_1$]-PEG** in THF at room temperature, following a similar procedure as previously reported in the literature by Caminade.[248] The reaction proceeded smoothly, yielding the expected **173-Ru@[G$_1$][G$_1$]-PEG** as an orange solid in good yield, by simple precipitation and further purification by washings.

The newly formed Ru@dendrimer product was characterized by ^{31}P{^{1}H} NMR, which revealed a significant deshielding effect upon complexation, shifting from −6.6 ppm to 24.0 ppm, and the formation of a doublet with a coupling constant of $^1J_{\text{P-Ru}}$ = 37.2 Hz.

Additionally, the newly prepared Ru@dendrimer system was characterized by ^{1}H and ^{13}C{^{1}H} NMR, IR, and elemental analysis, confirming the successful synthesis of this novel immobilized structure. Furthermore, one of the crucial techniques used for analysis was the inductively coupled plasma (ICP) analysis, which was carried out to assess the ruthenium content in the Janus dendrimer. The analysis demonstrated that the supported **173-Ru@[G$_1$][G$_1$]-PEG** contained a Ru content of 9.1%, aligning with the calculated theoretical value.
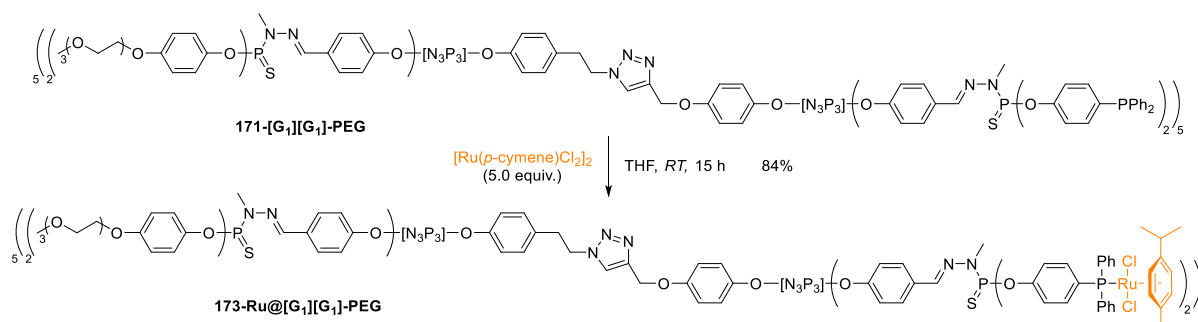
Scheme 56. Synthesis of **173-Ru@[G₁][G₁]-PEG** Janus dendrimer, bearing PEG moieties on one side and Ru(*p*-cymene) complexes on the other.

In summary, a novel immobilized system has been successfully prepared by grafting Ru(*p*-cymene) complexes on a phosphorus Janus dendrimer. This dendrimer contained PEG chains for water-solubility modulation and Ru(*p*-cymene) complexes for potential applications in catalysis. To the best of our knowledge, this work described the first-ever PPH Janus dendrimer for the possible use in catalysis. Nevertheless, to confirm its utility, the **173-Ru@[G₁][G₁]-PEG** Janus dendrimer needed to be tested in model reactions, such as the targeted isomerization of allyl alcohols (*vide infra*).

5.1. Synthesis of analogous monometallic and bimetallic Ru(*p*-cymene) complexes

As mentioned in the introduction of this Thesis, dendrimers can exhibit various effects when applied in catalysis. These effects include the potential for a modification of catalytic activity mainly due to the high local concentration of catalysts in dendrimeric entities, an effect derived from the anchoring, possible modifications by electronic effects, and the feasibility of easier catalyst recyclability and reusability in dendrimeric systems.[40,252]

Evaluating these parameters is essential to assess the performance of the catalyst@dendrimer system.

To properly assess the performance of the previously described immobilized ruthenium complex **173-Ru@[G₁][G₁]-PEG**, it was necessary to synthesize simpler analogous Ru-complexes for comparison purposes. Therefore, the next objective was to synthesize Ru(*p*-cymene)-based monometallic and bimetallic species with structures that would emulate the catalytic environment to that of the dendrimeric **173-Ru@[G₁][G₁]**. **Figure 42** illustrates the targeted compounds for synthesis, namely **Ru43** and **Ru44**.
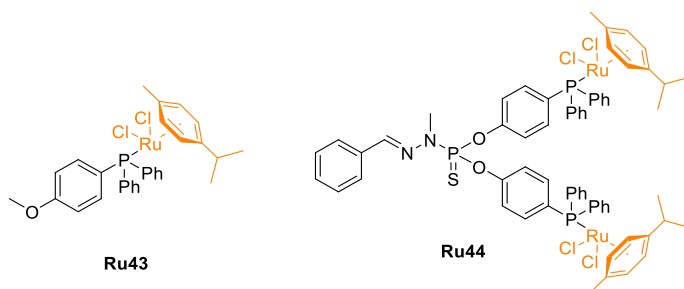
Figure 42. Targeted monometallic (**Ru43**) and bimetallic (**Ru44**) Ru-complexes synthesized for the comparison of their catalytic performance with dendrimer **173-Ru@[G₁][G₁]-PEG**.

Regarding the monometallic **Ru43**, this novel complex was synthesized in two steps, starting from 4-bromoanisole (**174**, **Scheme 57**). In the first step, 4-(diphenylphosphoryl)anisole (**175**) was synthesized by lithiation and further phosphination of **174**, resulting in the formation of a white solid in 80% yield.[253] The formation of the desired product was monitored using NMR spectroscopy, with the most characteristic signal being a singlet at −7.0 ppm in the $^{31}P\{^{1}H\}$ NMR spectrum.

Subsequently, in a second step, the complexation of [Ru(*p*-cymene)Cl₂]₂ was carried out based on the coordination ability of phosphine **175**. To achieve this, **175** was dissolved in THF, and the ruthenium precursor was added to the reaction mixture. After 1 hour of reaction, a precipitate formed, which was then filtered and washed with *n*-hexane, ultimately yielding the desired **Ru43** in excellent yield as an orange powder. The novel ruthenium complex was fully characterized by NMR spectroscopy, IR, HRMS, and elemental analysis to ascertain the formation of the desired structure.
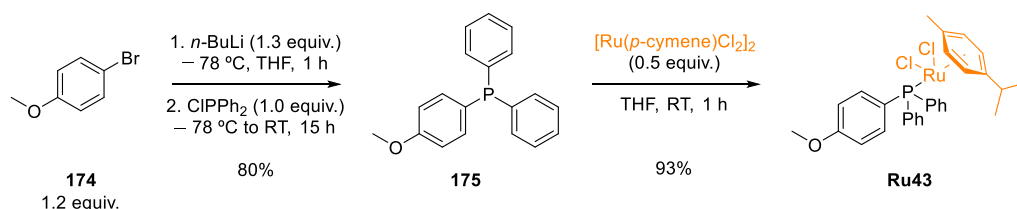
Scheme 57. Synthesis of **Ru43** from 4-bromoanisole (**174**).

Simultaneously, the synthesis of a bimetallic species, **Ru44**, was planned. To create a bimetallic species that would be chemically similar to the Ru@dendrimer **173**, the use of the model dendrimer molecule **155** was considered (**Scheme 58** outlines the synthetic protocol developed).

In a first step, the model dendrimer was derivatized with a slight excess of 4-(diphenylphosphoryl)phenol (**170**) under basic Cs₂CO₃ conditions at room temperature. This resulted in the substitution of the P−Cl bonds in **155** with **170**, leading to the formation of the phosphine-modified model dendrimer **176** in 67% yield. The progress of the reaction was monitored using $^{31}P\{^{1}H\}$ NMR spectroscopy. **Figure 43** displays the $^{31}P\{^{1}H\}$ NMR spectra of the

product and starting materials. The shift of the two reference signals of the starting materials indicated the substitution reaction in the P−Cl bonds of **155** taking place . Specifically, the phosphorus atom signal from **155** (δ_{155} = 63.4 ppm) shifted to 61.5 ppm upon substitution with the phenol phosphine **170**, confirming the disubstitution pattern. Additionally, the phosphorus atom signal from **170** also experienced a change due to the substitution, showing a slight downfield shift from −7.0 ppm to −6.4 ppm in the final product. These two new shifts observed in the ^{31}P{^{1}H} NMR were consistent with previously obtained similar systems.

The final step to obtain **Ru44** involved complexing [Ru(p-cymene)Cl$_2$]$_2$, employing the same reaction conditions previously reported for the synthesis of **Ru43**. Phosphine **176** was dissolved in THF, and [Ru(p-cymene)Cl$_2$]$_2$ was added to the reaction mixture. After the reaction was completed, the mixture was filtered through a silica pad, washed with EtOAc and concentrated under reduced pressure to give the desired bimetallic **Ru44** in 88% yield. Full characterization of **Ru44** was performed similarly to the monometallic species.
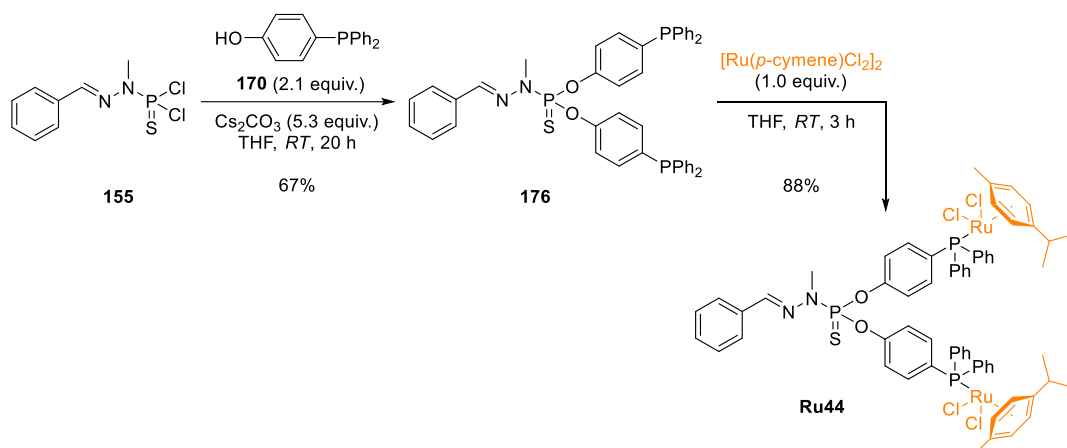
Scheme 58. Synthesis of bimetallic ruthenium complex **Ru44** from model dendrimer molecule **155**.
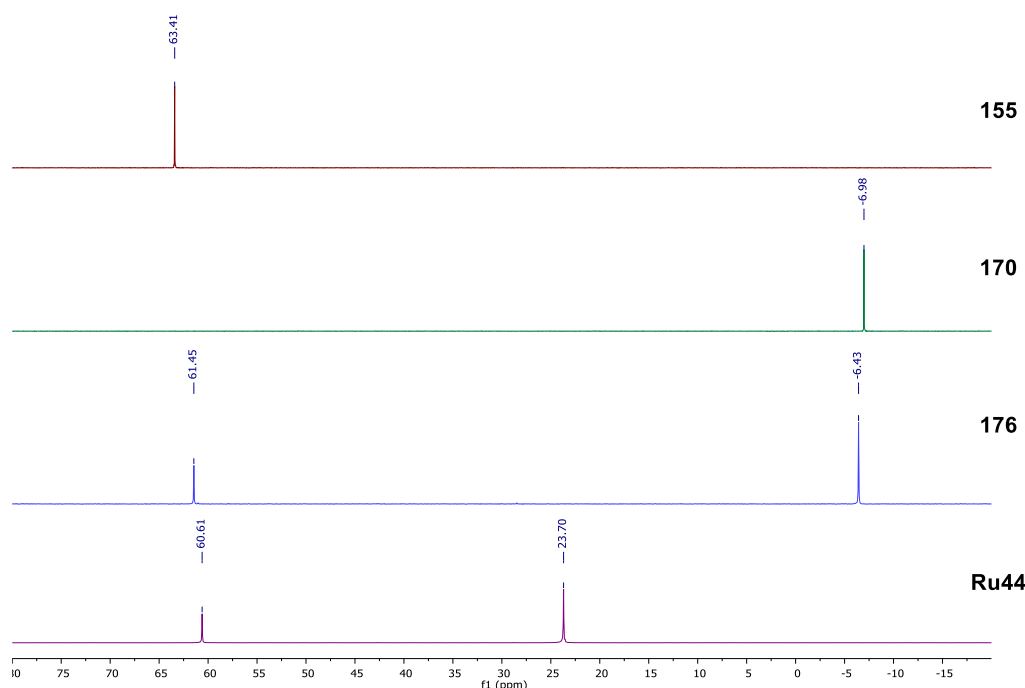
Figure 43. $^{31}P\{^{1}H\}$ NMR spectra of model dendrimer molecule **155** (*red*), 4-(diphenylphosphoryl)phenol **170** (*green*); phosphine modified model dendrimer **176** (*blue*), and **Ru44** (*purple*), recorded in CDCl$_3$ (162 MHz) at room temperature.

5.2. Catalytic studies for the isomerization of 1-octen-3-ol

Having successfully synthesized a Ru@Janus dendrimer system **173** containing Ru(*p*-cymene) complexes within its structure, along with analogous monometallic and bimetallic species **Ru43** and **Ru44**, the next step was to evaluate the catalytic activity of these three prepared complexes. Ru(*p*-cymene)-type complexes are well-documented in the literature for their applications as catalysts in various processes including the isomerization of allyl alcohols and the hydration of acetylenes, among others.[249] For this project, the isomerization of allyl alcohols was chosen as the target reaction to assess the performance of the prepared complexes. This reaction typically involves the conversion of allyl alcohols into ketones or aldehydes through a two-step process that combines oxidation and reduction, in a reaction carried out in a one-pot manner using organometallic complexes and Cs$_2$CO$_3$ as a co-catalyst.[254] In this context, the specific reaction chosen for evaluating the Ru(*p*-cymene) complexes is illustrated in **Scheme 59**. The reaction was tested with a 1 mol% loading of [Ru] and twice as much loading of the co-catalyst for the isomerization of 1-octen-3-ol to 3-octanone.
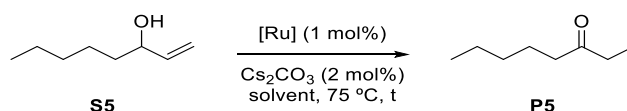
Scheme 59. Standard reaction conditions used for the isomerization of 1-octen-3-ol (**S5**).

The initial catalytic tests for the novel Ru-complexes were conducted to evaluate their activity under conventional organic solvent conditions. In these experiments, substrate **S5** was dissolved

in a THF solution containing Cs_2CO_3 prior to adding the catalyst. **Table 5** presents the results obtained from these tests.

As anticipated, all three Ru-complexes achieved full conversion within the reported time frames in the literature.[249,254] Specifically, the monometallic **Ru43** achieved complete conversion after 3 hours of the reaction time. Notably, both the bimetallic **Ru44** and the dendrimeric structure **173-Ru@[G1][G1]-PEG** yielded **P5** in half the reaction time. This result was highly encouraging as it indicated that the proximity of ruthenium centers could potentially lead to a cooperative effect, enhancing the reaction's efficiency.

Table 5. Results of the isomerization of allyl alcohol **S5** catalyzed by **173-Ru@[G1][G1]-PEG** dendrimer, as well as monometallic and bimetallic **Ru43** and **Ru44** complexes (1 mol% of [Ru]) in THF at 75 °C.

Entry	Catalyst	Solvent	Time of full conversion
1	**Ru43** – monometallic		3 h
2	**Ru44** – bimetallic	THF	90 min
3	**173-Ru@[G1][G1]-PEG**		90 min

[a] Conversion was determined by GC using 1,3,5-trimetoxybenzene as internal standard

Following the promising results under organic solvent conditions, the focus shifted to the primary objective of this section: utilizing water as the solvent for the catalytic process. Initially, a test was conducted by replicating the reaction conditions used in the previous example, but with a change in the solvent from THF to water. Unfortunately, after 24 hours of reaction, no conversion was observed for the three novel Ru-catalysts. Further investigation into the solubility of substrates and reagents led to the hypothesis that the limited solubility of **S5** and the internal standard in water was the primary constraint for aqueous catalysis.

To address this limitation, the use of a biphasic system was considered. Specifically, an *n*-heptane/water mixture (1:1) was chosen as the solvent system, considering the presence of both hydrophobic and hydrophilic components within the dendrimeric Ru-complex. The selection of this biphasic system was based on previously reported procedures by the group of Caminade.[249] Importantly, the presence of an *n*-heptane/water mixture resulted in the formation of a biphasic system where: (*i*) substrate **S5**, product **P5**, and the internal standard resided in the organic *n*-heptane phase; and (*ii*) cesium carbonate and the Ru@dendrimer **173** remained in the water phase.

Catalytic tests were conducted once again, following the previously established reaction conditions, which included a 2 mol% loading of base as a co-catalyst, a reaction temperature of 75 °C, and the use of the biphasic solvent system. Aliquots were sampled at specific time intervals, and conversion was determined by GC (**Table 6**). The catalytic results revealed that both the monometallic **Ru43** and bimetallic **Ru44** systems yielded no isomerization product after 24 hours of reaction. Intriguingly, when the **173-Ru@[G1][G1]-PEG** catalyst was employed, full conversion was achieved after 24 hours of reaction.

Table 6. Results of the isomerization of allyl alcohol **S5** catalyzed by **173-Ru@[G$_1$][G$_1$]-PEG** dendrimer, as well as monometallic and bimetallic **Ru43** and **Ru44** complexes (1 mol% of [Ru]) in n-heptane/water biphasic mixture at 75 °C.

Entry	Catalyst	Solvent	Conversion after 24 h [%][a]
1	**Ru43** – monometallic	n-heptane/water (1:1)	traces
2	**Ru44** – bimetallic		traces
3	**173-Ru@[G$_1$][G$_1$]-PEG**		>99

[a] Conversion was determined by GC using 1,3,5-trimetoxybenzene as internal standard

The obtained results were highly positive in terms of the activity of the Ru@dendrimer system. Notably, despite longer reaction times than in THF, a positive dendritic effect was observed for the isomerization of **S5** in both organic solvent and biphasic mixtures. Particularly intriguing was the use of the biphasic system, where only **173-Ru@[G$_1$][G$_1$]-PEG** exhibited catalytic activity for the desired reaction.

Encouraged by the successful isomerization of allyl alcohols in the presence of the dendrimeric complex **173**, the recyclability of the dendrimeric system was investigated. In this context, a catalytic test was conducted in the biphasic solvent conditions, and the reaction was allowed to proceed for 24 hours. After 24 h, the reaction was stopped, and the organic phase was separated from the aqueous phase. Analysis by GC confirmed the full conversion of **S5** to 3-octanone (**P5**) in the recovered organic phase. Subsequently, a fresh mixture of **S5** and 1,3,5-trimethoxybenzene in n-heptane was added to the remaining water phase containing the Ru@dendrimer catalyst **173**. Repetition of this procedure resulted in the attainment of full conversion of **S5** for up to three consecutive runs (**Figure 44**). Moreover, the possibility of metal leaching was also investigated. For this purpose, the model isomerization reaction using **173-Ru@[G$_1$][G$_1$]-PEG** was repeated, and the organic phase was separated from the aqueous layer. Analysis of Ru content in the organic phase by ICP revealed no significant leaching, even after full conversion to **P5**. ICP results indicated the presence of less than 0.1% Ru contamination in the sample, confirming the excellent stability of the catalyst.
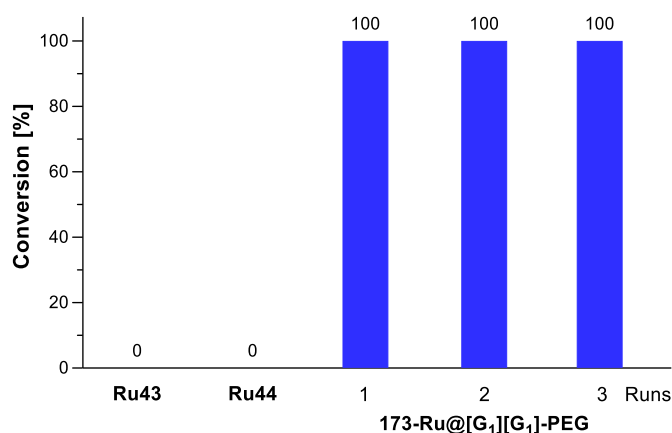
Figure 44. Conversion obtained for the isomerization of allyl alcohol **S5** catalyzed by **173-Ru@[G$_1$][G$_1$]-PEG** dendrimer, as well as monometallic and bimetallic **Ru43** and **Ru44** complexes (1 mol% of [Ru]) in a *n*-heptane/water biphasic mixture at 75 °C; and recyclability experiments performed with **173-Ru@[G$_1$][G$_1$]-PEG** for three consecutive runs.

In summary, the first-ever PPH Janus dendrimer with potential applications in catalysis has been reported. Specifically, **173-Ru@[G$_1$][G$_1$]-PEG** was synthesized, featuring PEG chains on one side of the structure and Ru(*p*-cymene) derivatives on the other side, making it a highly promising material for use in catalysis.

The applicability of the Ru@dendrimer **173** in catalysis was tested for the isomerization of 1-octen-3-ol in both THF and biphasic *n*-heptane/water mixtures, demonstrating a positive dendritic effect in both scenarios. Notably, in the biphasic solvent system, only the dendrimeric complex **173-Ru@[G$_1$][G$_1$]-PEG** exhibited activity for the targeted reaction, while monometallic and bimetallic **Ru43** and **Ru44** showed no conversion of **S5** (after 24 h). Furthermore, the recyclability and reusability of the dendrimeric system were assessed, revealing full conversion of **S5** for up to three consecutive runs, with minimal metal contamination in the final product (<0.1%). These findings highlight the potential of dendrimeric catalysts in catalytic applications, particularly for reactions in aqueous or biphasic systems, and underscore the stability and effectiveness of the developed Ru@dendrimer complex.

Chapter IV. Summary and Conclusions

The primary aim of this research has been to advance the field of catalysis by developing novel supported ruthenium complexes. This Thesis has centered on two key objectives: the preparation of PPH Janus dendrimers to facilitate the grafting of Ru-complexes on their surfaces for catalytic applications, and the synthesis of innovative Ru-NHC complexes for olefin metathesis, followed by the immobilization attempts onto dendrimers and MOFs.

The initial part of this Thesis was dedicated to the synthesis of innovative PPH Janus dendrimers. These dendrimers were designed to incorporate water-soluble PEG moieties on one side while featuring functional groups for ligand/metal pre-catalyst integration on the opposite side. To achieve this, phosphorus dendrimers were crafted employing two distinct dendron structures. Each dendron bore either an acetylene or azide group at the core level to enable subsequent coupling. These dendrimers were grown up to the second generation. The desired Janus dendrimer was then created through click chemistry, which facilitated the fusion of the two targeted dendrons by forming a 1,2,3-triazole. The resultant PPH Janus dendrimer, named **143-[G$_1$][G$_1$]-PEG** (**Figure 45**), served as a platform for immobilizing the desired ligand/metal pre-catalyst.
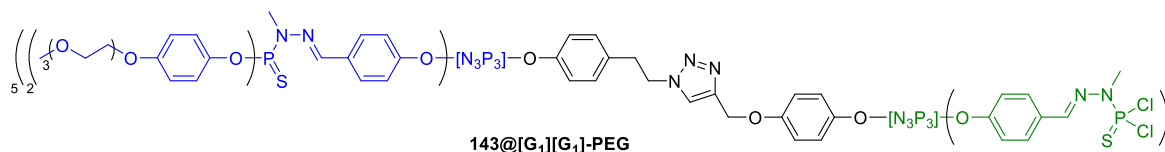
Figure 45. First-first-generation PPH Janus dendrimer described in this Thesis.

Concurrently, we conducted the synthesis of novel Ru-NHC complexes that incorporated phenolic moieties within their structures. This involved obtaining two novel ligands, which were subsequently successfully integrated to prepare **Hov-II**-type complexes, denoted as **Ru36** and **Ru38** (**Figure 46**). These two Ru-complexes were subjected to testing in the RCM of the model substrate diethyl diallylmalonate. Under room temperature conditions in DCM, the complexes exhibited moderate conversions. However, they achieved full conversion when the reaction was conducted in toluene at 50 °C over a 24-hour period. Notably, in all cases, the unsaturated **Ru38** outperformed its counterpart. Furthermore, we conducted stability studies of these complexes in a DCM-d_2 solution, revealing their excellent stability over time at room temperature. After 10 days, only a minimal decomposition of 6% was observed for **Ru36**, and a 4% for **Ru38**.
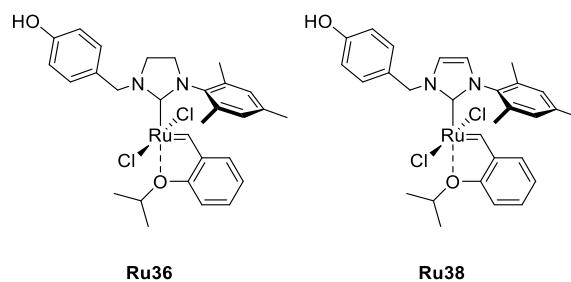
Figure 46. Ru-NHC complexes bearing a phenolic handler explored in this Thesis.

Subsequently, we embarked on the challenging task of immobilizing the newly synthesized Ru-NHC complexes onto a dendrimeric support. Initially, we attempted this by employing a model dendrimer molecule, denoted as **155**. We explored various methodologies in our quest to create Ru@dendrimer systems. Unfortunately, despite our best efforts, we were unable to achieve the desired outcome. This was primarily due to the formation of degradation products or the lack of reactivity, presenting significant obstacles to our objectives.

In addition to the previously unsuccessful project, we also attempted to immobilize the Ru-NHC complexes onto MOFs as heterogeneous supports, and explored the immobilization of alternative ruthenium complexes onto dendrimeric supports. In terms of the immobilization of Ru-NHC on MOFs, we selected the more active **Ru38** complex as the candidate for immobilization. Of interest, **Ru38** was successfully incorporated into the structure of MOF **(Al)MIL-101-NH₂** (**Figure 47**), with nearly quantitative adsorption of the Ru-complex on the MOF confirmed. Desorption studies indicated that the MOF structure chosen was suitable for effective immobilization, displaying less than 10% of leaching. The resulting heterogeneous **Ru38@(Al)MIL-101-NH₂** was tested for the RCM of various substrates, unfortunately yielding to lower conversions than the homogeneous analogue. Nonetheless, the novel immobilized system showed promise in terms of minimal metal leaching. Despite the catalytic outcome, **Ru38@(Al)MIL-101-NH₂** was proven effective in catalyzing the tested reactions, establishing a proof-of-concept for the first reported case of catalyst immobilization relying on phenol/MOF interactions.
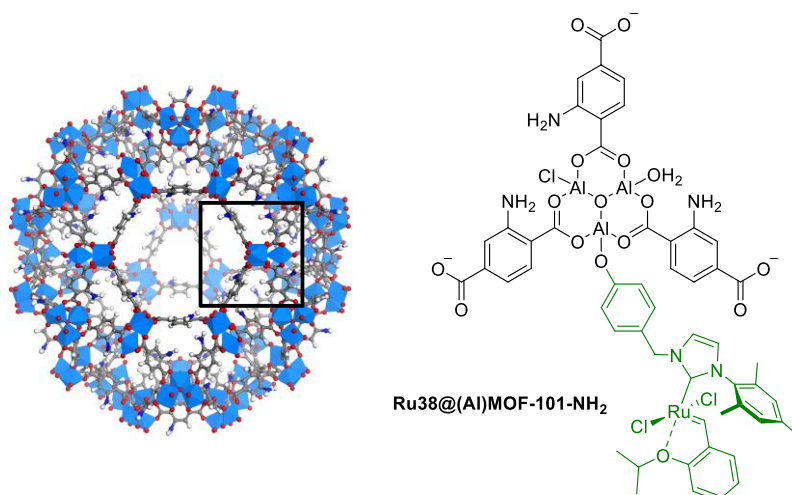
Figure 47. Immobilization of **Ru38** within the structure of **(Al)MIL-101-NH₂** explored in this Thesis.

In parallel, the Janus dendrimer **143-[G₁][G₁]-PEG** was tested in terms of immobilization by the incorporation of [Ru(p-cymene)Cl₂]₂ complex. Despite facing challenges such as the formation of hydrolyzed or oxidized products, we successfully introduced a phenol phosphine on the surface of the dendrimer. Subsequently, we accomplished the immobilization of the ruthenium pre-catalyst by coordination through the phosphine-terminated dendrimer. This effort resulted in the creation of an unprecedented dendritic structure, **173-Ru@[G₁][G₁]-PEG** (**Figure 48**), featuring ten PEG chains on one side of the molecule and ten Ru-complexes on the other. We subjected this novel immobilized Ru-system to evaluation for its catalytic activity in the isomerization of 1-octen-3-ol to 3-octanone. To assess its performance, we compared it with that of two small novel Ru-complexes, **Ru43** and **Ru44**, which were designed and synthesized to mimic the active catalytic moieties as in the dendrimer (**Figure 48**).
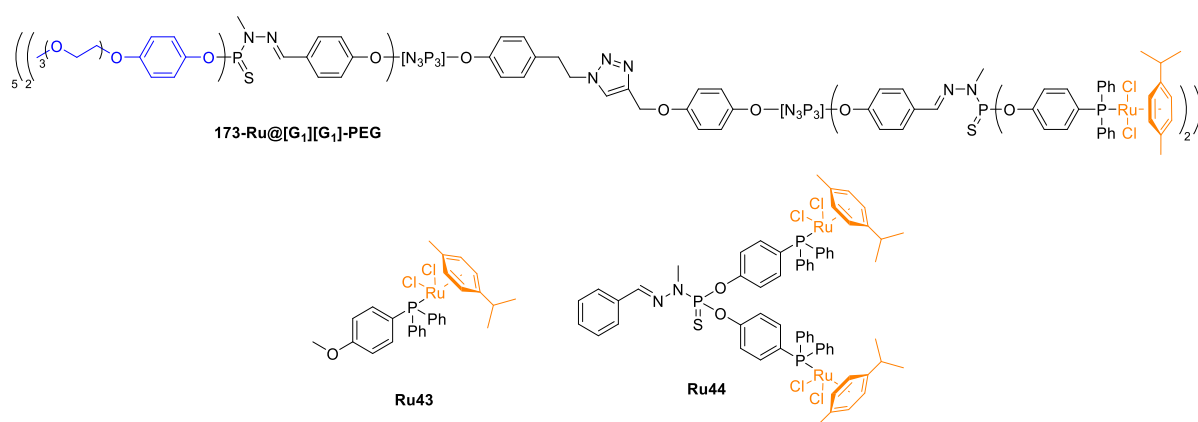
Figure 48. [Ru(p-cymene)Cl₂]₂ derivatives explored in this Thesis for the isomerization of allyl alcohols.

Catalytic tests conducted in THF as solvents yielded excellent results for all three Ru systems, with full conversions achieved within 3 hours for **Ru43** and even faster, within 1.5 hours, for the bimetallic **Ru44** and the Ru@dendrimer **173**. We also explored catalysis in biphasic water/n-heptane systems, where a notable positive dendritic effect was observed. Specifically, only **173-Ru@[G₁][G₁]-PEG** achieved full conversion in the biphasic conditions after 24 hours of reaction, while **Ru43** and **Ru44** did not produce the isomerization product in this chosen solvent system. Furthermore, we tested the recyclability of **173-Ru@[G₁][G₁]-PEG** and found that it could be recycled and reused for up to three consecutive runs, with ruthenium contamination in the final product amounting to less than 0.1%. Through this approach, we have developed an innovative methodology for obtaining PPH Janus dendrimers by coupling azide and acetylene dendrons through click chemistry. Furthermore, in light of the catalytic performance of **173-Ru@[G₁][G₁]-PEG**, we have demonstrated that this Janus dendrimer is well-suited for the tested application, resulting in enhanced catalytic performance and the creation of a recyclable system with minimal leaching into the final product.

In summary, although one of the targeted objectives of this thesis—immobilization of Ru-NHC complexes on Janus dendrimers—was not achieved, the development of two unprecedented Ru-supported systems for catalysis has been unveiled. Specifically, the **Ru38@MOF** system has been developed, demonstrating that **(Al)MIL-101-NH$_2$** offers a favorable environment for the non-covalent immobilization of a phenol-tagged ruthenium catalyst. Additionally, the preparation of a novel Ru(*p*-cymene)@dendrimer catalyst has been achieved, marking the first-ever reported example of a PPH Janus dendrimer with tested applications in catalysis.

Chapter V. Experimental Section

Materials and methods

Commercial reagents were used as received unless stated otherwise. All reactions were carried out under an inert atmosphere of either argon or nitrogen using standard Schlenk line technique unless stated otherwise. Molecular sieves (3 Å or 4 Å) were activated at 300 °C for a minimum of 12 h. Dry, oxygen-free solvents (THF, toluene, CH_2Cl_2) were obtained from a solvent purification system (Innovative technology PureSolv-MD-2 or SPS MBraun) and directly stored under 4 Å. Other solvents (Et_2O, *n*-pentane, acetonitrile) were distilled and degassed by freeze-pump-thaw technique before use. The addition of dry solvents or reagents was carried out using nitrogen/argon flushed syringes.

Stock solutions of catalysts were prepared in dry and degassed toluene, THF or CH_2Cl_2 under an inert atmosphere of argon using standard Schlenk techniques.

SnatchCat metal scavenger (1,4-bis(2-isocyanopropyl)piperazine) was used as a solution in dichloromethane (C = 10 mg/mL) to quench metathesis reactions.

Analytical thin layer chromatography (TLC) was performed on Merck silica gel 60 F_{254} precoated aluminum sheets (0.20 mm thickness) that were visualized by observation under UV light (254 nm or 365 nm).

Flash column chromatography was performed using silica gel 60 (230-400 mesh) purchased from Merck.

^{1}H NMR spectra were recorded at room temperature on Agilent Mercury spectrometers (400 MHz) and Bruker Ascend spectrometers (300 MHz, 400 MHz). Chemical shifts (δ) are reported in parts per million (ppm) downfield from trimethylsilane (TMS) and referred to residual solvent peak: $CDCl_3$ (δ_H = 7.26 ppm), DCM-d_2 (δ_H = 5.32 ppm), THF-d_8 (δ_H = 3.58 ppm), toluene-d_8 (δ_H = 2.09 ppm), MeOH-d_4 (δ_H = 3.31 ppm) or DMSO-d_6 (δ_H = 2.50 ppm). The following abbreviations are used to indicate the multiplicity signal: s (singlet), d (doublet), t (triplet), q (quartet), quin (quintet), sept (septet), dd (doublet of doublets), dt (doublet of triplets), ddd (doublet of doublets), br s (broad singlet), m (multiplet), 2 x s (two singlets), 2 x d (two doublets). The spectra were processed using MestReNova software.

^{13}C NMR spectra were recorded at room temperature. Chemical shifts are reported in parts per million downfield from TMS signal and referred to residual peak solvent: $CDCl_3$ (δ_C = 77.2 ppm), DCM-d_2 (δ_C = 54.0 ppm), THF-d_8 (δ_C = 67.6 ppm), toluene-d_8 (δ_C = 20.4 ppm), MeOH-d_4 (δ_C = 49.0 ppm) or DMSO-d_6 (δ_C = 39.5 ppm). Otherwise stated, the multiplicity refers to ^{1}H decoupled spectra. The spectra were processed using MestReNova software.

^{31}P NMR spectra were recorded at room temperature in CDCl$_3$. Chemical shifts are reported in parts per million relative to H$_3$PO$_4$ 85% aqueous solution (δ_P = 0.00 ppm) as an external standard. The spectra were processed using MestReNova software.

IR spectra were recorded with (*i*) a Bruker Tensor 27 spectrometer fitted with a universal Attenuated Total Reflectance (ATR) Golden Gate module; (*ii*) on a Perkin-Elmer Spectrum one FTIR spectrometer. Substances were applied as a film, solid, or solution. The obtained data were processed with the software Omni32, and plotted with the software OriginPro 8.6. Wavenumbers are given in cm^{-1}.

Melting points (M.p.) were recorded using a Kofler Reichert apparatus, and are uncorrected.

GC chromatograms were recorded: (*i*) using a PerkinElmer Clarus 580 model; as capillary column, an IntertCap 5MS-Sil column was employed with helium as carrier gas; (*ii*) using an Agilent Technologies Network GC System 6850; as capillary column, an HP-5MS column was employed with helium as carrier gas. GC conversions were determined based on the ratio of an internal standard (trimethoxybenzene, mesitylene or dodecane) and the starting material.

High-resolution mass spectra (HR-MS) were carried out at the Polish Academy of Science, Institute of Organic Chemistry in an AutoSpec Premier spectrometer; or by the Servicio de Espectrometría de Masas at the Universidad de Zaragoza in a Bruker Esquire 3000+ spectrometer. Electrospray ionization (ESI) or Atmospheric-pressure chemical ionization (APCI).

Ultraviolet-visible (UV-Vis) spectra were recorded using a Thermo Scientific Evolution 300 UV-Vis spectrometer with a VISIONPro 4.5.0 software. The obtained data were plotted with the software OriginPro 8.6.

Elemental Analyses were carried out at the Sevei d'Anàlisi Química de l'Universitat Autònoma de Barcelona in a Thermo Scientific Flash 2000 analyzer; or at the Polish Academy of Science, Institute of Organic Chemistry in an Elementar UNIcube automatic analyzer.

Inductively coupled plasma (ICP-OES) was measured at the Servei d'Anàlisi Química de l'Universitat Autònoma de Barcelona in an ICP-OES Agilent 5900 spectrometer by measuring the samples after digestion with HNO$_3$ and HCl in a microwave oven.

The **nitrogen adsorption isotherms** were measured in liquid nitrogen (77 K) using a Quantachrome Autosorb-IQ_MP sorption analyzer. Before the measurements, all the samples were dried for at least 24 h under vacuum at room temperature. The specific surface areas were calculated according to the Brunauer-Emmet-Teller (BET) method.

Powder X-ray diffraction (PXRD) patterns were recorded on a Bruker D8 Discover X-ray diffractometer (CuKα radiation), with a parallel beam formed by a Goebel mirror equipped with a VANTEC 1 position-sensitive detector. All measurements were performed in an aluminum holder.

Chemical Structures were drawn with CambridgeSoft ChemDraw® Professional (Version 18.1) for Windows®.

1. Synthesis of polyphosphorhydrazone dendrons

1.1. Synthesis of 4-(2-bromoethylphenol) 122
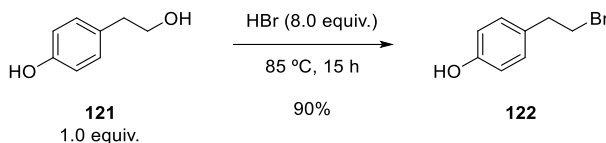
In a round-bottom flask equipped with a magnetic stirring bar, under nitrogen atmosphere, 4-(2-hydroxyethyl)phenol (**121**) (3.00 g, 27.1 mmol, 1.0 equiv.) and hydrobromic acid (20 mL, 173 mmol, 8.0 equiv.) were added, and the mixture was stirred at 85 °C for 15 h. Next, the mixture was allowed to cool down to room temperature, diluted with water (70 mL), and extracted with CH_2Cl_2 (3 x 100 mL). The organic phases were collected, dried over anhydrous Na_2SO_4, filtered, and the volatiles were removed under reduced pressure. The desired product was obtained as a colorless solid (3.97 g, 19.7 mmol, 91% yield).
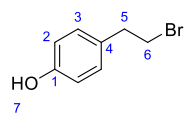
M.p.: 88 – 89 °C.

^{1}H NMR (400 MHz, CDCl$_3$) δ (ppm): 7.08 (d, $^3J_{H,H}$ = 8.6 Hz, 2H, H3), 6.79 (d, $^3J_{H,H}$ = 8.6 Hz, 2H, H2), 4.74 (s, 1H, H7), 3.53 (t, $^3J_{H,H}$ = 7.6 Hz, 2H, H6), 3.09 (t, $^3J_{H,H}$ = 7.6 Hz, 2H, H5).

^{13}C{^{1}H} NMR (101 MHz, CDCl$_3$) δ (ppm): 154.4 (C1), 131.2 (C4), 129.9 (C3), 115.4 (C2), 38.5 (C5), 33.4 (C6).

IR (ATR) ν (cm^{-1}): 3180, 3020, 2962. 1647, 1610, 1508, 1442, 1365, 1230, 1207, 833, 777.

NMR spectra are in accordance with previously reported syntheses.[224]

1.2. Synthesis of 4-(2-azidoethyl)phenol 123
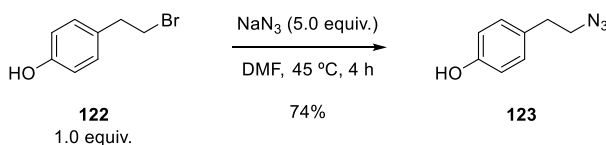
In a round-bottom flask equipped with a magnetic stirring bar, under nitrogen atmosphere, 4-(bromoethyl)phenol (**122**) (2.00 g, 9.94 mmol, 1.0 equiv.) and NaN$_3$ (3.23 g, 49.7 mmol, 5.0 equiv.) were dissolved in anhydrous DMF (20 mL), and heated up at 45 °C for 4 h. Upon reaction completion, the mixture was let to cool down to room temperature, diluted with water (150 mL), and the product was extracted with DCM (3 x 100 mL). The organic layers were collected, dried over anhydrous Na_2SO_4, filtered, and the volatiles were removed under reduced pressure. The residue was dissolved in Et$_2$O (100 mL), washed with hydrochloric acid (2.5%, 100 mL) and brine (3 x 100 mL). The organic layer was collected, dried over anhydrous Na_2SO_4, filtered, and the volatiles were removed. The desired product was obtained as a yellow oil (1.20 g, 7.35 mmol, 74% yield).
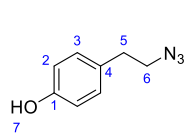
¹H NMR (400 MHz, CDCl₃) δ (ppm): 7.10 (d, $^3J_{H,H}$ = 8.6 Hz, 2H, H3), 6.83 (d, $^3J_{H,H}$ = 8.6 Hz, 2H, H2), 3.48 (t, $^3J_{H,H}$ = 7.2 Hz, 2H, H6), 2.85 (t, $^3J_{H,H}$ = 7.2 Hz, 2H, H5).

¹³C{¹H} NMR (101 MHz, CDCl₃) δ (ppm): 154.0 (C1), 130.0 (C4), 129.8 (C3), 115.4 (C2), 52.4 (C6), 34.2 (C5).

IR (ATR) v (cm⁻¹): 3352, 2927, 2869, 2090, 1613, 1597, 1513, 1443, 1222, 1172, 1105, 827.

NMR spectra are in accordance with previously reported syntheses.[225]

1.3.   Synthesis of 4-(prop-2-yn-yloxy)phenol 126
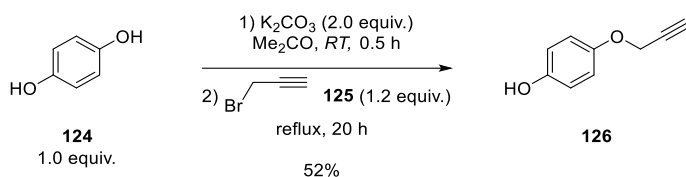
In a round-bottom flask equipped with a magnetic stirring bar, under nitrogen atmosphere, hydroquinone (**124**)(2.00 g, 18.1 mmol, 1.0 equiv.) and potassium carbonate (5.02 g, 36.3 mmol, 2.0 equiv.) were dissolved in acetone (50 mL), and the resulting mixture was stirred for 0.5 h at room temperature. Later, propargyl bromide (**125**) (3.18 g, 2.4 mL, 28.1 mmol, 1.2 equiv.) was added dropwise, and the mixture was stirred at reflux for 20 h. The evolution of the reaction was followed by TLC. Upon reaction completion, the mixture was allowed to cool down to room temperature, the remaining salts were filtered off, and the volatiles were removed under reduced pressure. The crude product was purified by column chromatography on silica (petroleum ether/EtOAc 20:1), yielding the desired compound as a yellow oil (1.39 g, 9.39 mmol, 52% yield).
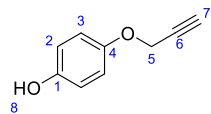
¹H NMR (400 MHz, CDCl₃) δ (ppm): 6.88 (d, $^3J_{H,H}$ =9.0 Hz, 2H, H2), 6.78 (d, $^3J_{H,H}$ =9.0 Hz, 2H, H3), 4.84 (s, 1H, H8) 4.63 (d, $^4J_{H,H}$ =2.4 Hz, 2H, H5), 2.50 (t, $^4J_{H,H}$ = 2.4 Hz, 1H, H7).

¹³C{¹H} NMR (161 MHz, CDCl₃) δ (ppm): 151.7 (C1), 150.2 (C4), 116.4 (C2), 116.0 (C3), 78.8 (C6), 75.3 (C7), 56.7 (C5).

NMR spectra are in accordance with previously reported syntheses.[226]

1.4. Synthesis of *N*-methyldichlorothiophosphorhydrazide 38
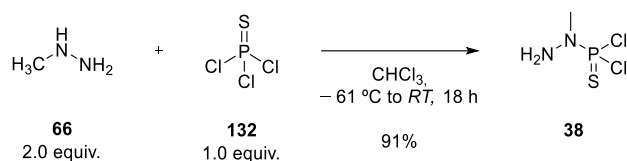
To a solution of tiophosphoryl chloride (**132**) (2.99 g, 5.0 mL, 49.3 mmol, 1.0 equiv.) in 100 mL of dry chloroform, a solution of methylhydrazine (**66**) (4.54 g, 5.2 mL, 98.6 mmol, 2.0 equiv.) in dry chloroform (20 mL) was slowly added dropwise at −61 °C. After the complete addition, the mixture was allowed to warm up to room temperature and stirred vigorously overnight. The reaction evolution was followed by $^{31}P\{^1H\}$ NMR. The crude reaction mixture was then filtered with a cannula, and the obtained $CHCl_3$ solution was stocked in the freezer. The concentration of the resulting solution was calculated with the NMR spectrum by integrating the characteristic proton peaks (c = 0.30 mol·L^{-1}, 44.9 mmol, 91% conversion).

^1H NMR (400 MHz, CDCl$_3$) δ (ppm): 4.21 (br s, 2H, H2), 3.21 (d, $^3J_{H,P}$ = 15.6 Hz, 3H, H1).

$^{13}C\{^1H\}$ NMR (101 MHz, CDCl$_3$) δ (ppm): 40.7 (d, $^2J_{C,P}$ = 14.4 Hz, C1).
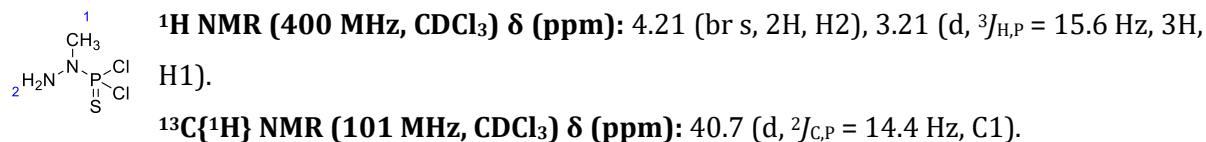
$^{31}P\{^1H\}$ NMR (162 MHz, CDCl$_3$) δ (ppm): 70.3.

NMR spectra are in accordance with previously reported syntheses.[36]

1.5. Synthesis of AB₅ core 127
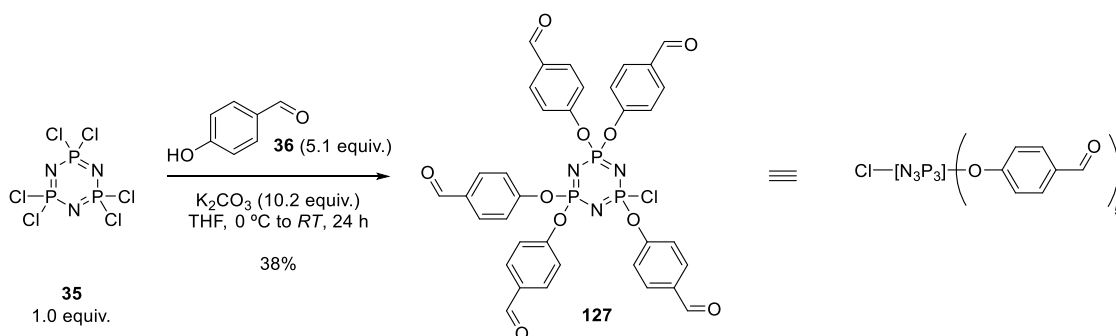
In a round-bottom Schlenk flask equipped with a magnetic stirring bar, under nitrogen atmosphere, hexachlorocyclotriphosphazene (**35**) (3.00 g, 8.63 mmol, 1.0 equiv.) and potassium carbonate (28.1 g, 86.3 mmol, 10.2 equiv.) were suspended in dry THF (25 mL) and cooled down to 0 °C. A solution of 4-hydroxybenzaldehyde (**36**) (5.37 g, 44.0 mmol, 5.1 equiv.) in THF (25 mL) was later added dropwise. Upon complete addition, the mixture was let to warm up to room temperature while stirring overnight. The salts formed were removed by filtration, and the volatiles were removed under reduced pressure. The residue was purified by column chromatography on silica (*n*-hexane/EtOAc 8:2 to 6:4). The desired product was obtained as a colorless crystalline solid upon recrystallization at −30 °C (2.59 g, 3.33 mmol, 38% yield).

M.p.: 93 – 94 °C

^{1}H NMR (300 MHz, CDCl$_3$) δ (ppm): 10.00 – 9.92 (3 x s, 5H, H5), 7.85 – 7.74 (m, 10H, H3), 7.25 – 7.17 (m, 10H, H2).

^{13}C{^{1}H} NMR (75 MHz, CDCl$_3$) δ (ppm): 190.6 (2 x s, C5), 154.5 (m, C1), 134.2 (2 x s, C4), 131.6 (s, C3), 121.7 (m, C2).

^{31}P{^{1}H} NMR (121 MHZ, CDCl$_3$) δ (ppm): 5.2 (2 x d, $^2J_{P,P}$ = 88.8 Hz, 84.2 Hz), 20.7 (dd, $^2J_{P,P}$ = 88.2 Hz, 84.2 Hz).

IR (ATR) ν (cm^{-1}): 2359, 1699, 1587, 1585, 1499, 1203, 1172, 1151, 941, 831.

NMR spectra are in accordance with previously reported syntheses.[255]
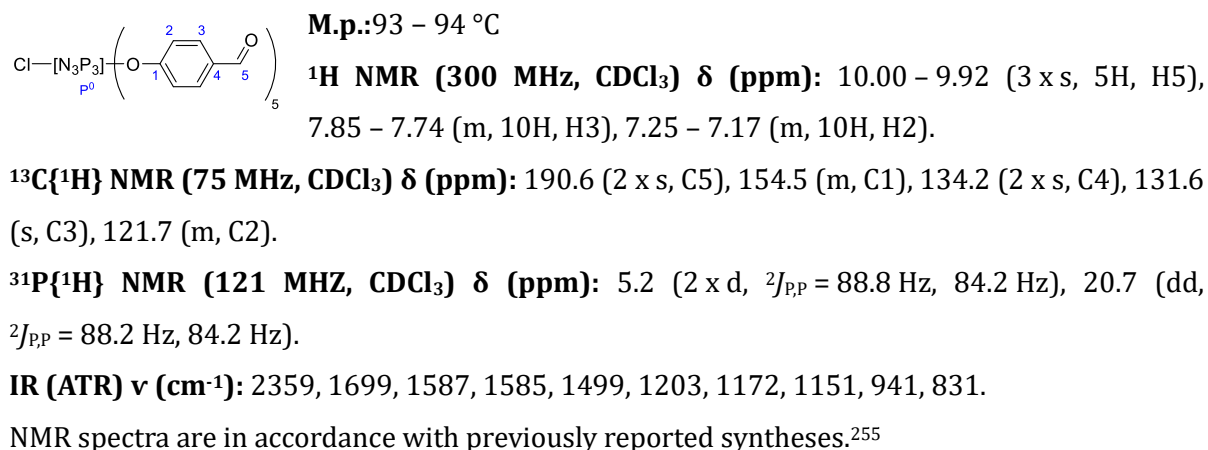
1.6. Synthesis of 2-(4-(2-azidoethyl)phenoxy)-2,4,4,6,6-pentachlorotriazatri-phosphazene 130
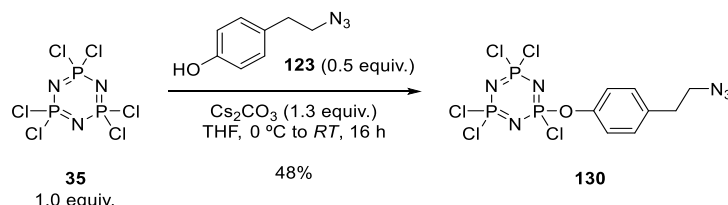
In a round bottom Schlenk equipped with a magnetic stirring bar, under nitrogen atmosphere, hexachlorocyclotriphosphazene (**35**) (3.00 g, 8.58 mmol, 1.0 equiv.) and dry cesium carbonate (2.80 g, 11.2 mmol, 1.3 equiv.) were suspended in anhydrous THF (100 mL). Next, the mixture was cooled down to 0 °C, 4-(2-azidoethyl)phenol (**123**) (700 mg, 4.29 mmol, 0.5 equiv.) in anhydrous THF (20 mL) was added dropwise, and the reaction was allowed to warm up to room temperature while stirring for 16 hours. Upon completion, the mixture was filtered, the volatiles were removed, and the crude product was purified by column chromatography on silica (*n*-hexane/EtOAc 9:1 to 1:1) yielding the desired product as a pale-yellow oil (0.93 g, 1.96 mmol, 48% yield).

^{1}H NMR (400 MHz, CDCl$_3$) δ (ppm): 7.30 – 7.19 (m, 4H, H2, H3), 3.51 (t, $^3J_{H,H}$ = 7.1 Hz, 2H, H6), 2.90 (t, $^3J_{H,H}$ = 7.1 Hz, 2H, H5).
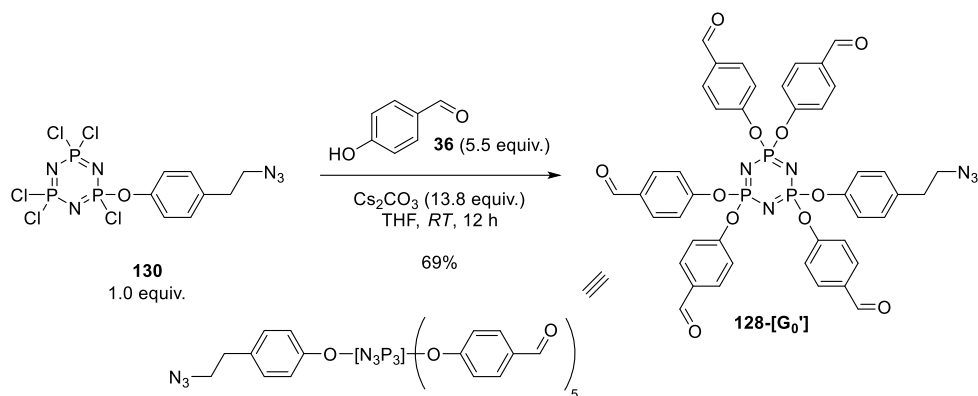
^{13}C{^{1}H} NMR (101 MHz, CDCl$_3$) δ (ppm): 148.2 (d, $^2J_{C,P}$ = 10.3 Hz, C1), 136.9 (d, $^5J_{C,P}$ = 2.9 Hz, C4), 130.3 (d, $^3J_{C,P}$ = 2.3 Hz, C2), 121.5 (d, $^4J_{C,P}$ = 5.3 Hz, C3), 52.3 (d, $^7J_{C,P}$ = 1.7 Hz, C6), 34.7 (d, $^6J_{C,P}$ = 0.8 Hz, C5).

^{31}P{^{1}H} NMR (162 MHz, CDCl$_3$) δ (ppm): 22.4 (d, $^2J_{P,P}$ = 60.9 Hz), 12.3 (t, $^2J_{P,P}$ = 60.9 Hz).

IR (ATR) ν (cm^{-1}): 2928, 2870, 2093, 1504, 1196, 1177, 1153, 976.

Elemental analysis (%) calcd. for C$_8$H$_8$Cl$_5$N$_6$OP$_3$: C 20.26; H 1.70; N 17.72; found: C 20.26; H 1.74; N 17.33.

1.7. Synthesis of azide dendron 128-[G₀']

In a round bottom Schlenk flask equipped with a magnetic stirring bar, under nitrogen atmosphere, 2-(4-(2-azidoethyl)phenoxy)-2,4,4,6,6-pentachlorotriazatriphosphazene (**130**) (0.52 g, 1.10 mmol, 1.0 equiv.), 4-hydroxybenzaldehyde (**36**) (0.74 g, 6.03 mmol, 5.5 equiv.), and dry cesium carbonate (4.91 g, 15.1 mmol, 13.8 equiv.) were suspended in anhydrous THF (100 mL), and the mixture was stirred at room temperature for 12 h. Upon reaction completion, the mixture was filtered, and the volatiles were removed. The crude product was washed with THF/methanol and purified by column chromatography on silica (*n*-hexane/EtOAc 8:2 to 1:1). The desired product was obtained as a yellow oil (0.68 g, 0.76 mmol, 69% yield).

¹H NMR (400 MHz, CDCl₃) δ (ppm): 9.91 (2 x s, 5H, H11), 7.71 (d, $^3J_{H,H}$ = 8.5 Hz, 10H, H9), 7.17 – 7.07 (m, 10H, H8), 7.05 (d, $^3J_{H,H}$ = 8.6 Hz, 2H, H3), 6.92 (d, $^3J_{H,H}$ = 8.6 Hz, 2H, H2), 3.47 (t, $^3J_{H,H}$ = 6.9 Hz, 2H, H6), 2.82 (t, $^3J_{H,H}$ = 6.9 Hz, 2H, H5).

¹³C{¹H} NMR (101 MHz, CDCl₃) δ (ppm): 190.5 (3 x s, C11), 154.8 (2 x d, $^2J_{C,P}$ = 5.0 Hz, C7), 148.8 (2 x d, $^2J_{C,P}$ = 5.2 Hz, C1), 135.8 (C4), 133.7 (3 x s, C10), 131.4 (2 x s, C9), 130.0 (C3), 121.3 (m, C8), 120.8 (2 x d, $^3J_{C,P}$ = 3.3 Hz ,C2), 52.2 (C6), 34.6 (C5).

³¹P{¹H} NMR (162 MHz, CDCl₃) δ (ppm): 7.4 (s, P⁰).

IR (ATR) ṽ (cm⁻¹): 3068, 2827, 2737, 2097, 1697, 1595, 1501, 1420, 1389, 1267, 1202, 1173, 1148, 1101, 937, 881, 829, 727, 704.

1.8.   Synthesis of azide dendron 133-[G₁]

128-[G₀']
1.0 equiv.

133-[G₁]
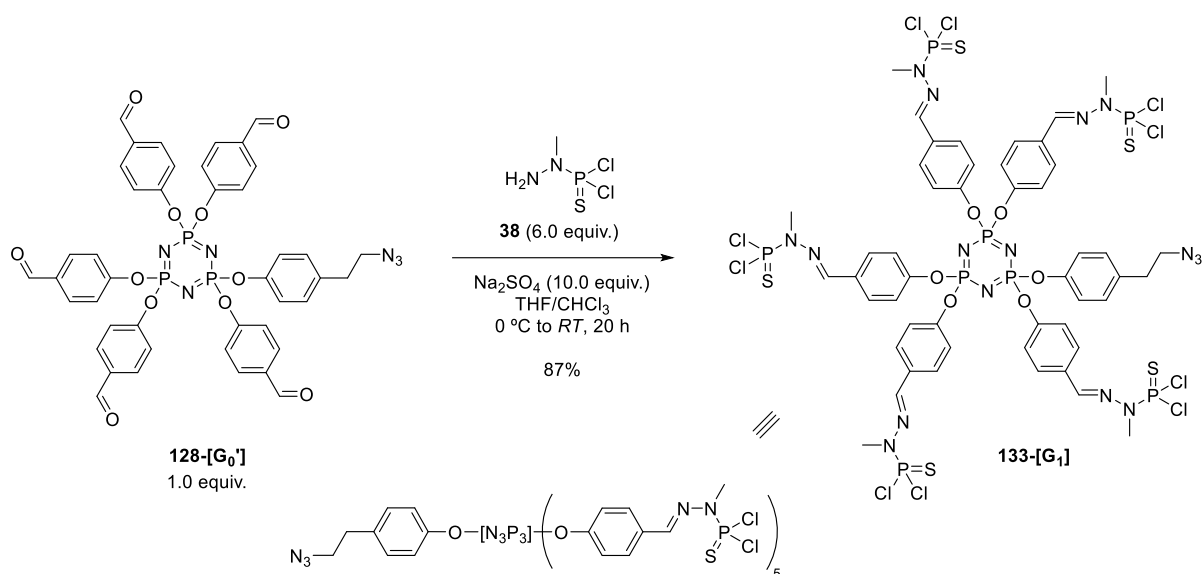
In a Schlenk flask equipped with a magnetic stirring bar, under nitrogen atmosphere, **128-[G₀']** dendron (0.30 g, 0.332 mmol, 1.0 equiv.) and anhydrous Na_2SO_4 (0.47 g, 3.32 mmol, 10.0 equiv.) were suspended in anhydrous THF (5 mL). Next, *N*-methyldichlorothiophosphorhydrazide (**38**) (6.7 mL, 1.99 mmol, 6.0 equiv., c = 0.30 mol·L⁻¹ in CHCl₃) was added dropwise at 0 °C. Upon complete addition, the mixture was allowed to warm up to room temperature while stirring overnight. The mixture was filtered, and the filtrate was concentrated to 3 mL. The product was precipitated from *n*-pentane, the supernatant removed, and the product washed with *n*-pentane/Et₂O (4:1) twice. The volatiles were removed under reduced pressure, and the product was dried to provide a colorless solid (0.49 g, 0.29 mmol, 87% yield).
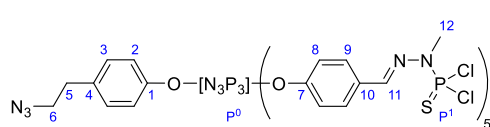
M.p.: 96 – 97 °C.

¹H NMR (400 MHz, CDCl₃) δ (ppm): 7.67 – 7.54 (m, 15H, H11, H9), 7.09 – 6.97 (m, 12H, H8, H3), 6.93 (d, $^3J_{H,H}$ = 8.2 Hz, 2H, H2), 3.53 – 3.41 (m, 17H, H12, H6), 2.83 (d, $^3J_{H,H}$ = 7.1 Hz, 2H, H5).

¹³C{¹H} NMR (101 MHz, CDCl₃) δ (ppm): 151.9 (2 x d, $^2J_{C,P}$ = 5.0 Hz, C7), 149.3 (2 x d, $^2J_{C,P}$ = 5.2 Hz, C1), 140.8 (2 x d, $^3J_{C,P}$ = 5.0 Hz, C11), 135.3 (C4), 131.4 (C10), 130.0 (C9), 128.8 (C3), 121.5 (m, C8), 121.2 (2 x d, $^3J_{C,P}$ = 3.1 Hz, C2), 52.4 (C6), 34.8 (C5), 32.1 (2 x d, $^3J_{C,P}$ = 12.8 Hz, C12).

³¹P{¹H} NMR (162 MHz, CDCl₃) δ (ppm): 62.4 (s, P¹), 62.4 (s, P¹), 8.3 (s, P⁰).

IR (ATR) ν (cm⁻¹): 2929, 2866, 2094, 1601, 1504, 1462, 1267, 1235, 1184, 1175, 1159, 1132, 937, 875, 837, 748, 687.

1.9. Synthesis of azide dendron 135-[G₁']
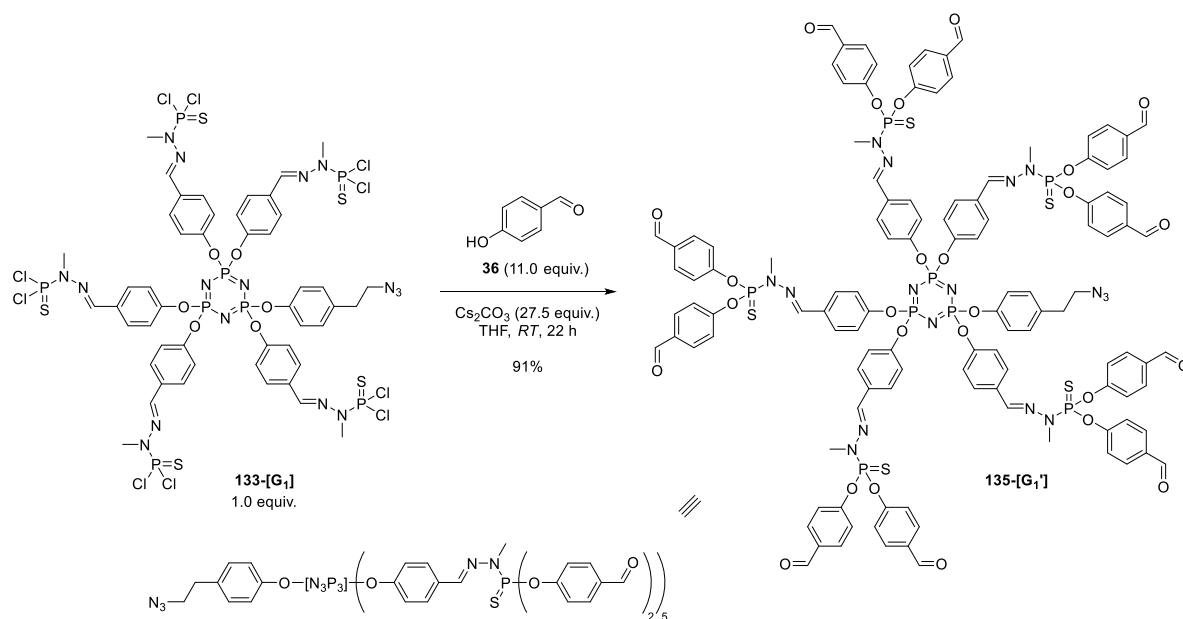
In a Schlenk flask equipped with a magnetic stirring bar, under nitrogen atmosphere, **133-[G₁]** azide (0.25 g, 0.15 mmol, 1.0 equiv.), cesium carbonate (1.29 g, 3.95 mmol, 27.5 equiv.), and 4-hydroxybenzaldehyde (**36**) (0.20 g, 1.61 mmol, 11.0 equiv.) were suspended in dry THF (15 mL), and the mixture was stirred at room temperature overnight. Upon reaction completion (assessed by $^1H\{^{31}P\}$ NMR), the salts were filtered off by cannula filtration, and the crude was concentrated to 5 mL. The product was precipitated from *n*-pentane, the supernatant was removed, and the product washed with *n*-pentane/Et₂O (4:1) twice. The volatiles were removed and the product dried obtaining a colorless solid (0.34 g, 0.13 mmol, 91% yield).
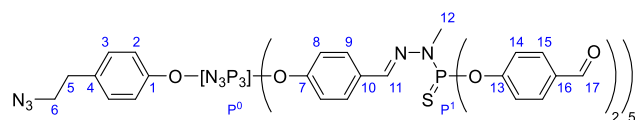
M.p.: 113 – 116 °C.

^1H NMR (400 MHz, CDCl₃) δ (ppm): 9.95 – 9.88 (3 x s, 10H, H17), 7.87 – 7.77 (m, 20H, H15), 7.66 – 7.53 (m, 15H, H9, H11), 7.40 – 7.29 (m, 22H, H3, H14), 7.09 – 6.96 (m, 10H, H8), 6.89 (d, $^3J_{H,H}$ = 8.5 Hz, 2H, H2), 3.41 – 3.29 (m, 17H, H6, H12), 2.73 (t, $^3J_{H,H}$ = 6.9 Hz, 2H, H5).

$^{13}C\{^1H\}$ NMR (101 MHz, CDCl₃) δ (ppm): 190.7 (2 x s, C17), 155.1 (2 x d, $^2J_{C,P}$ = 7.6, 3.6 Hz, C13), 151.6 (d, $^2J_{C,P}$ = 1.8 Hz, C7), 142.9 (C1), 139.5 (2 x d, $^3J_{C,P}$ = 4.2 Hz, C11), 133.8 (C4), 133.8 (C16), 131.9 – 131.5 (m, C10), 131.4 (C15), 129.9 (C9), 128.3 (C3), 122.0 – 121.9 (C14), 121.6 –121.3 (m, C8), 121.0 (C2), 52.1 (C6), 34.5 (C5), 32.9 (d, $^3J_{C,P}$ = 12.8 Hz, C12).

$^{31}P\{^1H\}$ NMR (162 MHz, CDCl₃) δ (ppm): 60.5 (s, P¹), 60.4 (s, P¹), 8.1 (s, P⁰).

1.10. Synthesis of azide dendron 136-[G$_2$]
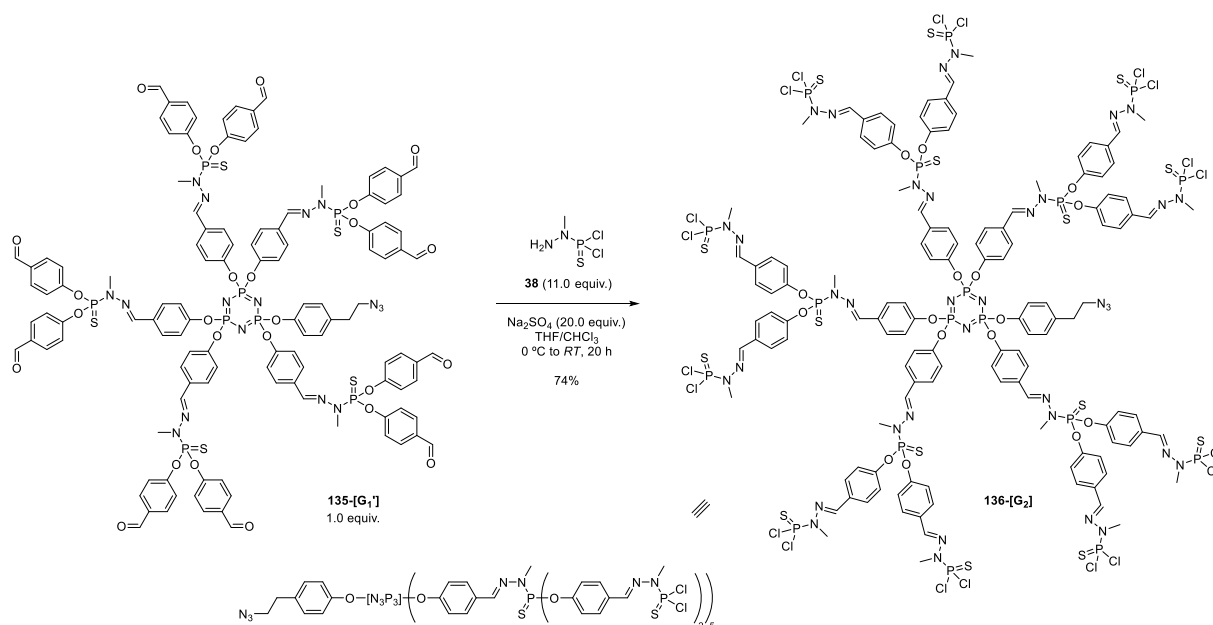
In a Schlenk flask equipped with a magnetic stirring bar, under nitrogen atmosphere, **135-[G$_1$']** dendron (0.15 g, 0.06 mmol, 1.0 equiv.) and anhydrous Na$_2$SO$_4$ (0.17 g, 1.17 mmol, 20.0 equiv.) were suspended in anhydrous THF (5 mL). Next, *N*-methyldichlorothiophosphor-hydrazide (**38**) (2.1 mL, 0.64 mmol, 11.0 equiv., c = 0.30 mol·L^{-1} in CHCl$_3$) was added dropwise at 0 °C. Upon complete addition, the mixture was allowed to warm up to room temperature while stirring overnight (assessed by ^{31}P{^{1}H} NMR). The salts were filtered off by cannula filtration, and the crude was concentrated to 3 mL. The product was precipitated from *n*-pentane, the supernatant removed, and the product washed with *n*-pentane/Et$_2$O (4:1) twice. The volatiles were removed and the product dried obtaining a colorless solid (0.18 g, 0.43 mmol, 74% yield).
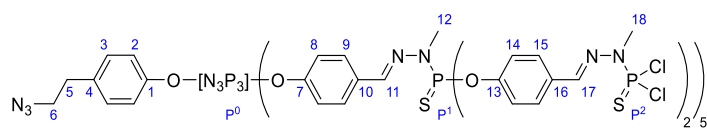
M.p.: 143 – 145 °C.

^{1}H NMR (400 MHz, CDCl$_3$) δ (ppm): 7.71 – 7.55 (m, 47H, H3, H9, H11, H15, H17), 7.26 – 7.19 (m, 20H, H14), 7.05 – 6.97 (m, 10H, H8), 6.92 (d, $^3J_{H,H}$ = 8.4 Hz, 2H, H2), 3.49 – 3.39 (m, 30H, H18), 3.37 – 3.22 (m, 17H, H6, H12), 2.72 (t, $^3J_{H,H}$ = 7.0 Hz, 2H, H5).

^{13}C{^{1}H} NMR (101 MHz, CDCl$_3$) δ (ppm): 151.9 (2 x d, $^2J_{C,P}$ = 6.9 Hz), 151.7 – 151.4 (m, C7), 145.4 (m, C1), 140.7 (2 x s, C17), 139.1 (2 x s, C11) 135.3 (C4), 132.1 (2 x s, C10), 131.7 (C16), 130.0 (C9), 128.9 (C15), 122.4 – 121.8 (m, C14), 121.6 – 121.4 (m, C8), 121-.2 (C2), 52.3 (C6), 34.3 (C5), 33.2 (d, $^2J_{C,P}$ = 12.5 Hz, C12), 32.0 (d, $^2J_{C,P}$ = 13.2 Hz, C18).

^{31}P{^{1}H} NMR (162 MHz, CDCl$_3$) δ (ppm): 62.9 (s, P^2), 62.8 (s, P^2), 62.0 (s, P^1), 62.0 (s, P^1), 8.3 (s, P^0).

IR (ATR) ν (cm⁻¹): 2930, 2099, 1603, 1504, 1465, 1408, 1268, 1237, 1191, 1160, 1136, 914, 885, 837, 780, 691.

Elemental analysis (%) calcd. for $C_{128}H_{128}Cl_{20}N_{36}O_{16}P_{18}S_{15}$: C 36.83; H 3.09; N 12.08; S 11.52; Found: C 37.63; H 3.38; N 11.30; S 10.93.

1.11. Synthesis of 2-(4-(4-(pro-2-yn-yloxy)phenoxy)-2,4,4,6,6-pentachlorotriaza-triphosphazene 131
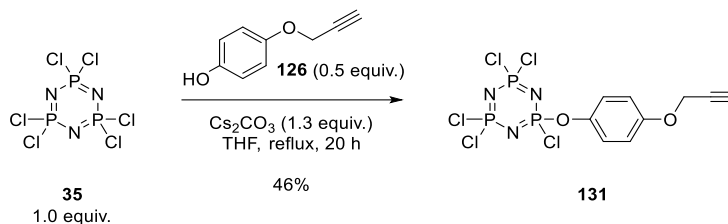
In a round bottom Schlenk flask equipped with a magnetic stirring bar, under nitrogen atmosphere, hexachlorocyclotriphosphazene (**35**) (1.28 g, 3.68 mmol, 1.0 equiv.), dry cesium carbonate (0.68 g, 4.60 mmol, 1.3 equiv.), and 4-(prop-2-yn-yloxy)phenol (**126**) (0.6 g, 1.84 mmol, 0.5 equiv.) were suspended in anhydrous THF (100 mL), and the mixture was stirred at reflux for 20 h. Upon reaction completion (followed by $^{31}P\{^1H\}$ NMR), the salts were filtered off by cannula filtration, the volatiles removed, and the crude purified by column chromatography on silica (*n*-hexane/EtOAc 8:2 to 1:1) affording the desired product as a colorless oil (0.77 g, 1.68 mmol, 46% yield).

¹H NMR (400 MHz, CDCl₃) δ (ppm): 7.21 (dd, $^3J_{H,H}$ = 9.1 Hz, $^5J_{H,P}$ = 2.2 Hz, 2H, H2), 6.99 (dd, $^3J_{H,H}$ = 9.1 Hz, $^4J_{H,P}$ = 0.8 Hz, 2H, H3), 4.69 (d, $^4J_{H,H}$ = 2.4 Hz, 2H, H5), 2.53 (t, $^4J_{H,H}$ = 2.4 Hz, 1H, H7).
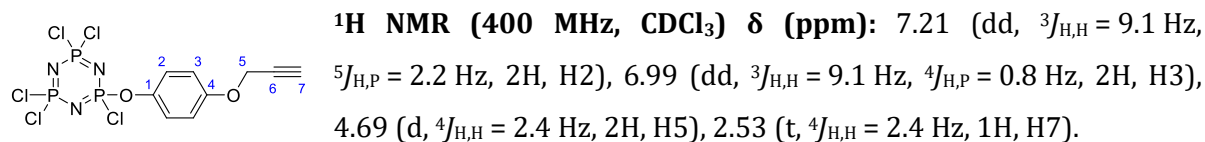
¹³C{¹H} NMR (101 MHz, CDCl₃) δ (ppm): 156.0 (d, $^5J_{C,P}$ = 2.7 Hz, C4), 143.5 (d, $^2J_{C,P}$ = 10.3 Hz, C1), 122.4 (d, $^3J_{C,P}$ = 5.0 Hz, C2), 116.1 (d, $^4J_{C,P}$ = 2.3 Hz, C3), 78.2 (C6), 76.1 (C7), 56.4 (C5).

³¹P{¹H} NMR (162 MHz, CDCl₃) δ (ppm): 22.4 (d, $^2J_{P,P}$ = 59.2 Hz), 13.1 (d, $^2J_{P,P}$ = 59.2 Hz).

IR (ATR) ν (cm⁻¹): 3000, 2024, 1594, 1500, 1455, 1194, 1157, 1027, 978, 870, 830, 770.

NMR spectra are in accordance with previously reported syntheses.[227]

1.12. Synthesis of acetylene dendron 129-[G₀']
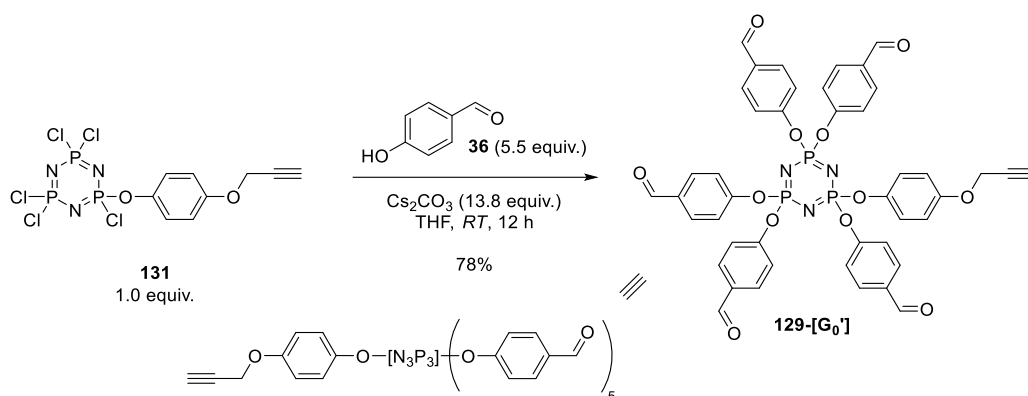
In a round bottom Schlenk flask equipped with a magnetic stirring bar, under nitrogen atmosphere, 2-(4-(4-(pro-2-yn-yloxy)phenoxy)-2,4,4,6,6-pentachlorotriazatriphosphazene (**131**) (0.35 g, 0.76 mmol, 1.0 equiv.), 4-hydroxybenzaldehyde (**36**) (0.51 g, 4.19 mmol, 5.5 equiv.) and dry cesium carbonate (3.41 g, 10.5 mmol, 13.8 equiv.) were suspended in dry THF (100 mL), and the mixture was stirred at room temperature for 12 h. Upon reaction completion, the mixture was filtered, and the volatiles were removed. The crude was dissolved in DCM (50 mL) and washed with a saturated solution of Na_2CO_3 (3 x 50 mL). The organic phase was taken, dried over anhydrous Na_2SO_4, filtered, and the volatiles were removed *in vacuo*. The product was precipitated from *n*-pentane to obtain the desired product as a colorless solid (0.52 g, 0.59 mmol, 78% yield).
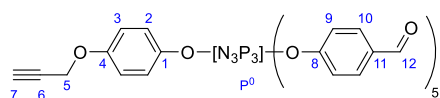
M.p.: 66 – 68 °C.

¹H NMR (400 MHz, CDCl₃) δ (ppm): 9.93 (2 x s, 5H, H12), 7.77 – 7.69 (m, 10H, H10), 7.16 (d, $^3J_{H,H}$ = 8.5 Hz, 6H, H9), 7.06 (d, $^3J_{H,H}$ = 8.5 Hz, 4H, H9), 6.93 – 6.86 (m, 2H, H2), 6.80 – 6.73 (m, 2H, H3), 4.65 (d, $^3J_{H,H}$ = 2.4 Hz, 2H, H5), 2.56 (t, $^3J_{H,H}$ = 2.4 Hz, 1H, H7).

¹³C{¹H} NMR (101 MHz, CDCl₃) δ (ppm): 190.71 – 190.45 (m, C12), 155.6 – 154.6 (m, C4, C8), 144.1 (d, $^2J_{C,P}$ = 6.4 Hz, C1), 134.0 – 133.6 (m, C11), 131.5 (d, $^4J_{C,P}$ = 2.3 Hz, C10), 121.8 (d, $^3J_{C,P}$ = 3.9 Hz, C2), 121.5 – 121.3 (m, C9), 115.9 (C3), 78.4 (C6), 76.2 (C7), 56.3 (C5).

³¹P{¹H} NMR (162 MHz, CDCl₃) δ (ppm): 8.7 −6.9 (m. P⁰).

IR (ATR) ν (cm⁻¹): 3268, 2924, 2851, 2737, 1770, 1697, 1596, 1499, 1421, 1388, 1298, 1266, 1194, 1171, 1149, 1101, 1013, 939, 882, 828, 725, 705.

1.13. Synthesis of acetylene dendron 134-[G₁]
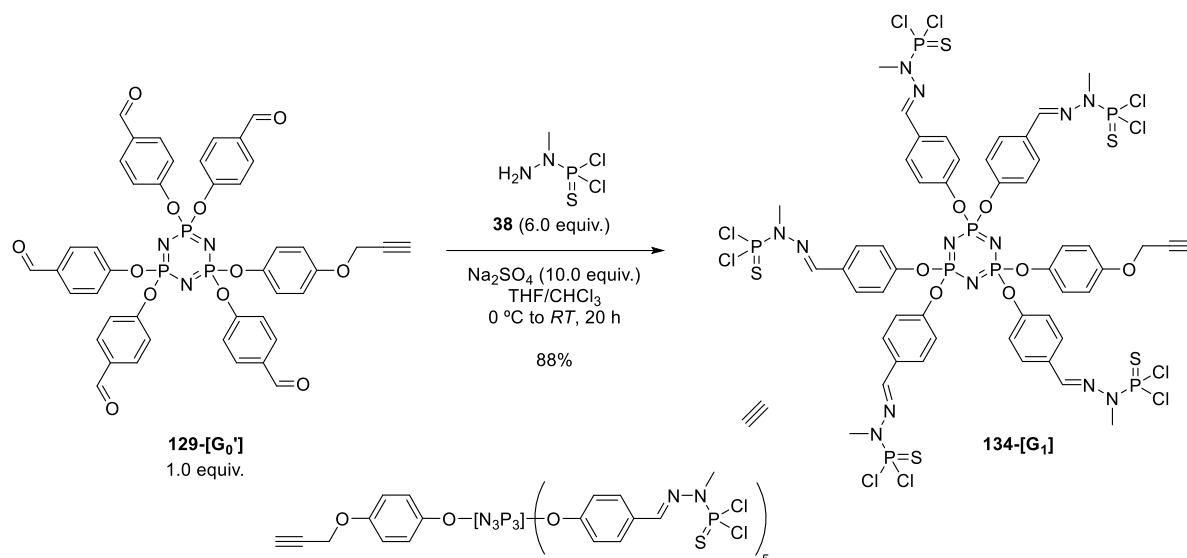
In a Schlenk flask equipped with a magnetic stirring bar, under nitrogen atmosphere, **129-[G₀']** dendron (0.42 g, 0.47 mmol, 1.0 equiv.) and anhydrous Na_2SO_4 (0.67 g, 4.73 mmol, 10.0 equiv.) were suspended in dry THF (5 mL). Next, *N*-methyldichlorothiophosphorhydrazide (9.8 mL, 2.84 mmol, 6.0 equiv., c = 0.30 mol·L⁻¹ in $CHCl_3$) was added dropwise at 0 °C. Upon complete addition, the mixture was allowed to warm up to room temperature while stirring overnight (reaction evolution was followed by $^1H\{^{31}P\}$ NMR). The mixture was filtered by cannula filtration, and the filtrate concentrated to 3 mL. The product was precipitated from *n*-pentane, the supernatant removed, and the product washed with *n*-pentane/Et₂O (4:1) twice. The volatiles were removed and the product dried under reduced pressure obtaining a colorless solid (704 mg, 0.416 mmol, 88% yield).
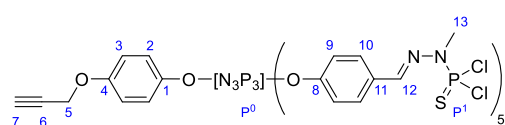
M.p.: 88 – 91 °C.

^{1}H NMR (400 MHz, CDCl₃) δ (ppm): 7.66 (2 x d, $^4J_{H,P}$ = 2.1 Hz, 5H, H12), 7.61 (2 x d, $^3J_{H,H}$ = 8.8 Hz, 10H, H10), 7.07 (d, $^3J_{H,H}$ = 8.6 Hz, 6H, H9), 7.00 (d, $^3J_{H,H}$ = 8.6 Hz, 4H, H9), 6.90 (d, $^3J_{H,H}$ = 9.0 Hz, 2H, H2), 6.77 (d, $^3J_{H,H}$ = 9.0 Hz, 2H, H3), 4.63 (d, $^4J_{H,H}$ = 2.4 Hz, 2H, H5), 3.51 (2 x d, $^3J_{H,P}$ = 13.9 Hz, 15H, H13), 2.52 (t, $^3J_{H,H}$ = 2.4 Hz, 1H, H7).

^{13}C{^{1}H} NMR (101 MHz, CDCl3) δ (ppm): 154.9 (C4), 152.3 – 151.4 (m, C8), 140.9 (C1), 140.7 (C12), 131.4 (2 x s, C11), 128.8 (C10), 122.0 (d, $^3J_{C,P}$ = 3.1 Hz, C2), 121.5 (2 x s, C9), 115.8 (C3), 78.5 (C6), 76.0 (C7), 56.4 (C5), 32.2 (d, $^2J_{C,P}$ = 13.1 Hz, C13).

^{31}P{^{1}H} NMR (162 MHz, CDCl₃) δ (ppm): 62.6 (s, P¹), 62.5 (s, P¹), 62,4 (s, P¹), 9.5 −7.7 (m, P⁰)

IR (ATR) ν (cm⁻¹): 2932, 1601, 1500, 1194, 1174, 1160, 1133, 939, 880, 835, 779, 745, 688, 527, 495

1.14. Surface modification of 133-[G₁]

1.14.1.   Synthesis of 2-(2-(2-methoxyethoxy)ethoxy)ethyl methanesulfonate 139
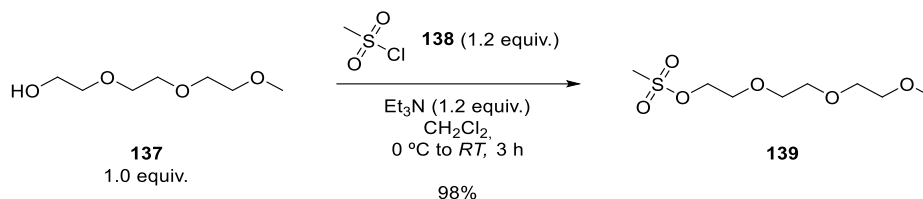
In a Schlenk flask equipped with a magnetic stirring bar, 2-(2-(2-methoxyethoxy)ethoxy)ethan-1-ol (**137**) (2.00 g, 12.2 mmol, 1.0 equiv.) was dried in vacuo at 130 °C for 3 h. Next, under nitrogen atmosphere, dry DCM (30 mL) and triethylamine (1.60 g, 2.2 mL, 15.8 mmol, 1.2 equiv.) were added, and the solution was cooled down to 0 °C. Methanesulfonyl chloride (**138**) (1.81 g, 15.8 mmol, 1.2 equiv.) in 20 mL of dry DCM was added dropwise, the mixture was stirred for 0.5 h at 0 °C, and for additional 3 h at room temperature. Upon reaction completion, the precipitate formed was filtered off, and the resulting solution washed with water (3 x 50 mL). The organic phase was dried over anhydrous Na_2SO_4, filtered, and the volatiles were removed under reduced pressure to give the desired product as a yellow oil (2.89 g, 11.9 mmol, 98% yield).

¹H NMR (300 MHz, CDCl₃) δ (ppm): 4.37 – 4.28 (m, 2H, H2), 3.76 – 3.68 (m, 2H, H4), 3.68 – 3.53 (m, 6H, H3, H5, H6), 3.53 – 3.45 (m, 2H, H7), 3.32 (s, 3H, H8), 3.02 (s, 3H, H1).
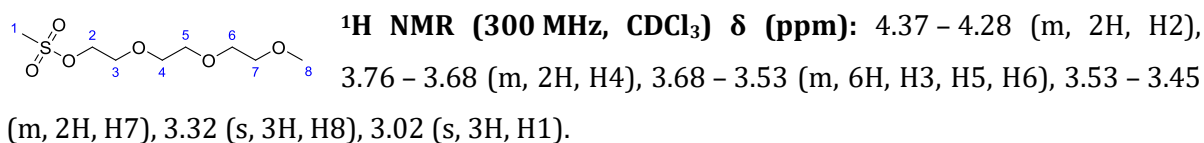
¹³C{¹H} NMR (75 MHz, CDCl₃) δ (ppm): 71.8 (C7), 70.5 (C4, C5), 70.4 (C6), 69.4 (C3), 68.9 (C2), 58.9 (C8), 37.5 (C1).

NMR spectra are in accordance with previously reported syntheses.[61]

1.14.2.   Synthesis of 4-(2-(2-(2-methoxyethoxy)ethoxy)ethoxy)phenol 140
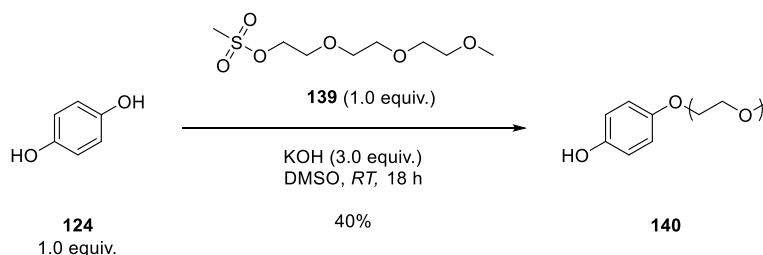
In a Schlenk flask equipped with a magnetic stirring bar, under nitrogen atmosphere, hydroquinone (**124**) (3.00 g, 27.2 mmol, 1.0 equiv.), 2-(2-(2-methoxyethoxy)ethoxy)ethyl methanesulfonate (**139**) (6.60 g, 27.2 mmol, 1.0 equiv.) and potassium hydroxide (4.59 g, 81.7 mmol, 3.0 equiv.) were dissolved in DMSO (25 mL), and the mixture was stirred at room temperature for 18 h. Next, water (25 mL) was added, and the resulting mixture was extracted

with Et_2O (3 x 30 mL). The aqueous layer was acidified with HCl and extracted with $CHCl_3$ (3 x 30 mL). The combined organic layers were washed with water (3 x100 mL), dried over anhydrous Na_2SO_4, filtered, and the volatiles were removed under reduced pressure. The desired product was obtained as a dark yellow oil (2.81 g, 11.0 mmol, 40% yield).
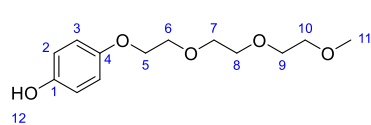
^{1}H NMR (400 MHz, DCM-d_2) δ (ppm): 6.80 – 6.70 (m, 4H, H2, H3), 5.27 (s, 1H, H12), 4.04 – 3.97 (m, 2H, H5), 3.80 – 3.73 (m, 2H, H7), 3.69 – 3.64 (m, 2H, H6), 3.64 – 3.58 (m, 4H, H8, H9), 3.55 – 3.48 (m, 2H, H10), 3.34 (s, 3H, H11).

^{13}C{^{1}H} NMR (101 MHz, DCM-d_2) δ (ppm): 152.7 (C4), 151.1 (C1), 116.5 (C2), 116.0 (C3), 72.2 (C10), 71.0 (C8), 70.9 (C7), 70.7 (C9), 70.2 (C6), 68.4 (C5), 59.0 (C11).

NMR spectra are in accordance with previously reported syntheses.[61]

1.14.3. Synthesis of azide dendron 141-[G$_1$]-PEG
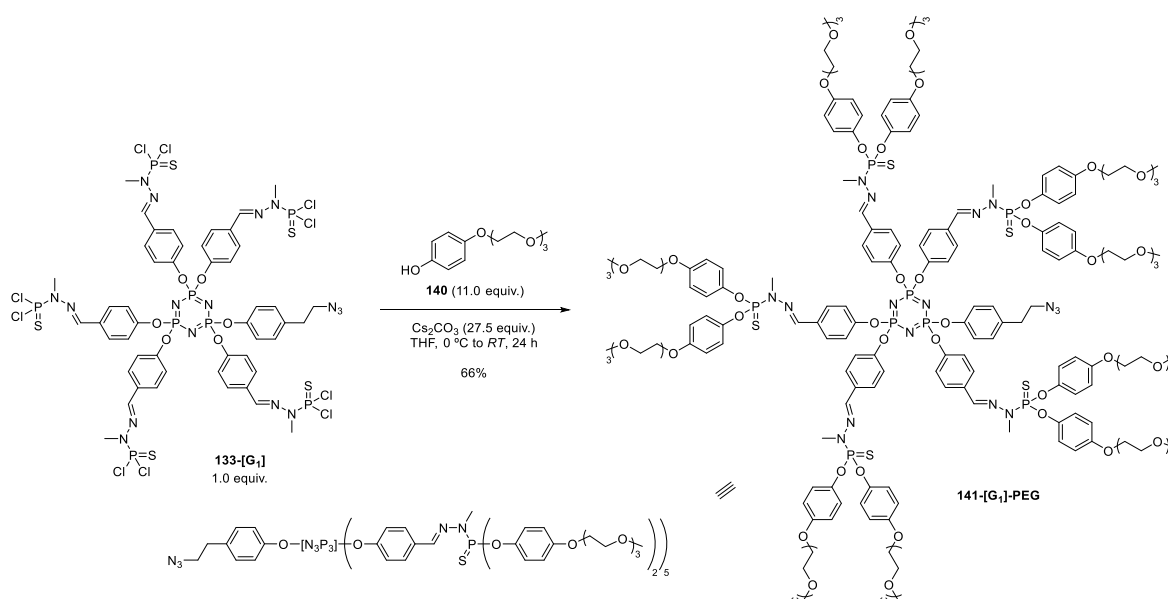
In a Schlenk flask equipped with a magnetic stirring bar, under nitrogen atmosphere, 4-(2-(2-(2-methoxyethoxy)ethoxy)ethoxy)phenol (**140**) (0.50 g, 1.93 mmol, 11.0 equiv.) and cesium carbonate (1.57 g, 4.83 mmol, 27.5 equiv.) were dissolved in dry THF (20 mL), and the mixture was stirred at 0 °C for 2 h. A solution of **133-[G$_1$]** dendron (0.30 g, 0.18 mmol, 1.0 equiv.) in THF (20 mL) was added dropwise at 0 °C. Upon complete addition, the mixture was let to warm up to room temperature while stirring overnight. THF was then evaporated, the residue was dissolved in DCM, and the mixture was centrifuged. The salts were filtered off, the product concentrated to 5 mL, and precipitated in a *n*-pentane/Et$_2$O (4:1) mixture thrice. The desired product was obtained as a pale-red oil (0.45 g, 0.12 mmol, 66% yield).
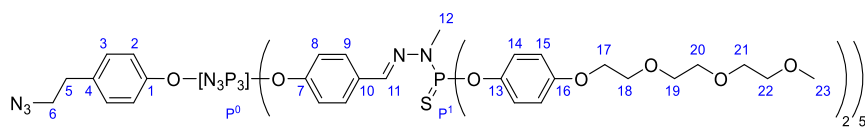
¹H NMR (CDCl₃, 400 MHz) δ (ppm): 7.64 – 7.55 (m, 15H, H9, H11), 7.11 – 6.95 (m, 34H, H2, H3, H8, H15), 6.84 – 6.73 (m, 20H, H14), 4.04 – 3.99 (m, 20H, H17), 3.82 – 3.75 (m, 20H, H19), 3.72 – 3.67 (m, 20H, H18), 3.66 – 3.61 (m, 40H, H20, H21), 3.54 – 3.50 (m, 20H, H22), 3.35 (2 x s, 30H, H23), 3.31 – 3.18 (m, 17H, H6, H12), 2.73 (t, $^3J_{H,H}$ = 6.9 Hz, 2H, H5).

¹³C{¹H} NMR (CDCl₃, 101 MHz) δ (ppm): 156.3 – 156.1 (m, C13), 151.4 – 151.1 (m, C7), 148.2 (C1), 144.2 (d, $^3J_{C,P}$ = 7.1 Hz, C11), 138.6 – 138.2 (m, C16), 135.3 (C4), 132.5 – 132.0 (m, C10), 129.9 (C9), 128.5 (d, $^4J_{C,P}$ = 5.6 Hz, C3), 122.3 – 122.2 (m, C14), 121.5 – 121.2 (m, C8), 121.2 – 121.0 (m, C2), 115.2 (C15), 71.9 (C22), 70.8 (C19), 70.7 (C20), 70.6 (C21), 69.7 (C18), 67.8 (C17), 59.0 (C23), 52.2 (C6), 34.5 (C5), 33.1 (d, $^2J_{C,P}$ = 11.8 Hz, C12).

³¹P{¹H} NMR (CDCl₃, 162 MHz) δ (ppm): 64. 6 (s, P¹), 64.5 (s, P¹), 8.5 (s, P⁰).

IR (ATR) ν (cm⁻¹): 2871, 2095, 1602, 1500, 1454, 1352, 1247, 1179, 932, 833, 779.

2. Synthesis of polyphosphorhydrazone Janus dendrimers

2.1. Synthesis of 142-[G$_0$'][G$_1$]-PEG
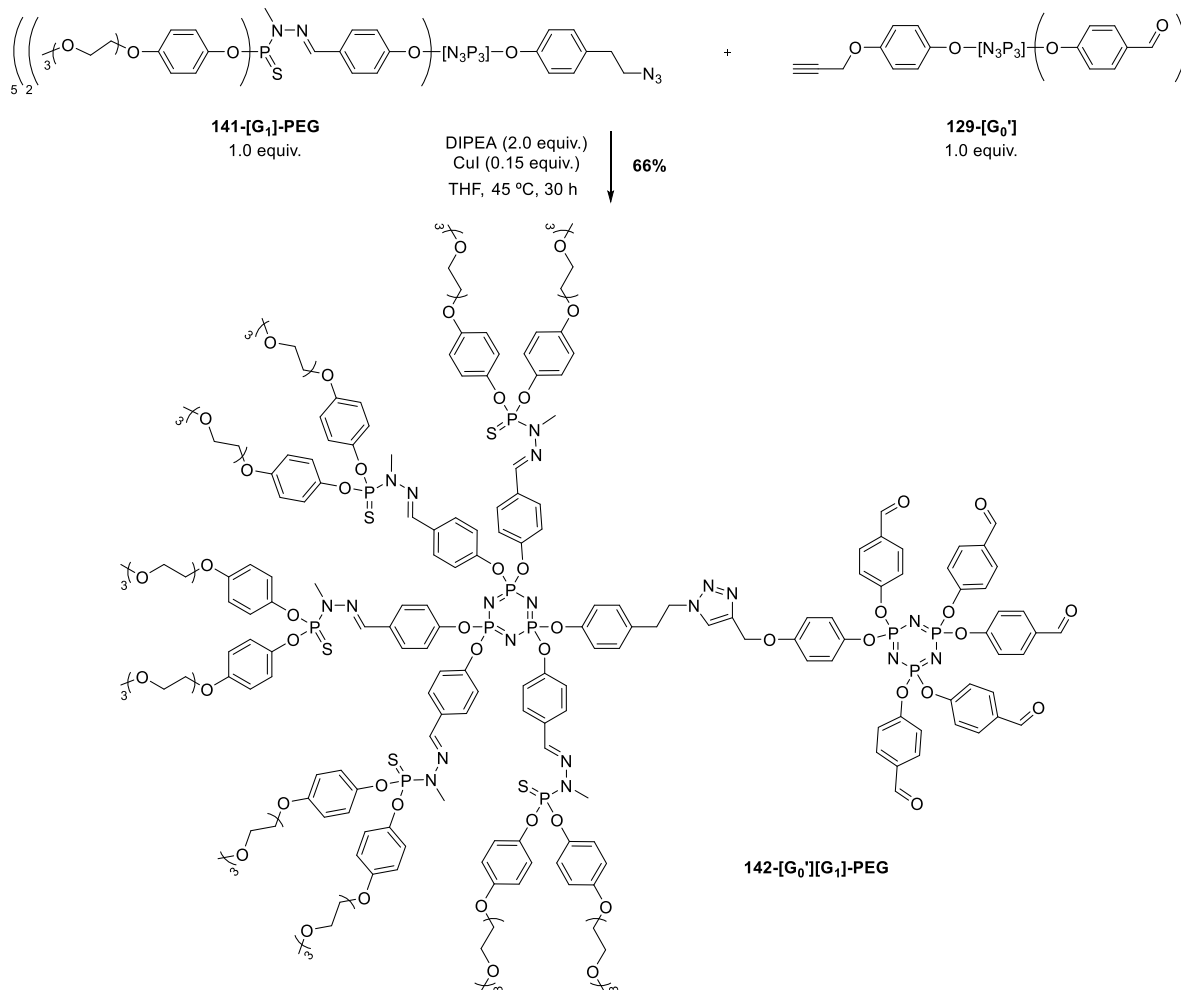
In a Schlenk flask equipped with a magnetic stirring bar, under nitrogen atmosphere, **129-[G$_0$']** dendron (0.50 g, 0.13 mmol, 1.0 equiv.) and **141-[G$_1$]-PEG** dendron (0.11 g, 0.13 mmol, 1.0 equiv.) were dissolved in dry, degassed THF (20 mL). DIPEA (45 μL, 0.26 mmol., 2.0 equiv.) and CuI (3.66 mg, 0.02 mmol, 0.15 equiv.) were added, and the mixture was heated at 45 °C for 30 h. The reaction evolution was followed by NMR and IR. Upon reaction completion, the mixture was filtered through Celite®, diluted with NH$_4$Cl (sat. solution, 30 mL), and the product extracted with THF (3 x 30 mL). The combined organic layers were collected, dried over anhydrous Na$_2$SO$_4$, filtered, and the solution was concentrated to 5 mL. The crude was precipitated in *n*-pentane (100 mL) twice, the volatiles removed and the product dried *in vacuo*. The desired product was obtained as a pale-yellow solid (0.41 g, 0.09 mmol, 66% yield).

M.p.: 76 –79 °C.
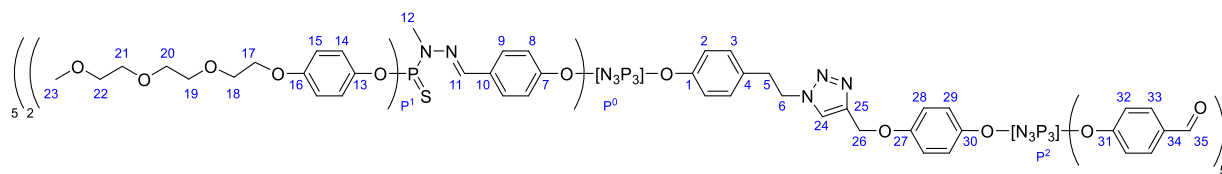
¹H NMR (CDCl₃, 400 MHz) δ (ppm): 9.94 – 9.87 (m, 5H, H35), 7.75 – 7.65 (m, 10H, H33), 7.64 – 7.54 (m, 16H, H9, H11, H24), 7.15 (d, $^3J_{H,H}$ = 8.6 Hz, 6H, H32), 7.11 – 6.94 (m, 40H, H2, H3, H8, H15, H28, H32), 6.82 – 6.73 (m, 22H, H14, H29), 5.01 (s, 2H, H26), 4.39 (t, $^3J_{H,H}$ = 7.5 Hz, 2H, H5), 4.07 – 3.97 (m, 20H, H17), 3.82 – 3.75 (m, 20H, H19), 3.71 – 3.58 (m, 60H, H18, H20, H21), 3.55 – 3.48 (m, 20H, H22), 3.34 (s, 30H, H23), 3.30 – 3.18 (m, 17H, H6, H12).

¹³C{¹H} NMR (CDCl₃, 101 MHz) δ (ppm): 190.7 – 190.3 (3 x s, C35), 156.2 (d, $^2J_{C,P}$ = 2.4 Hz, C13), 154.9 (d, $^2J_{C,P}$ = 6.1 Hz, C7), 154.6 (d, $^2J_{C,P}$ = 7.6 Hz, C31), 151.2 (C27), 149.4 (C1), 144.2 (d, $^3J_{C,P}$ = 7.0 Hz, C11), 143.2 (C25), 138.7 – 138.2 (m, C16), 135.4 (C4), 133.7 (C24), 133.6 (d, $^2J_{C,P}$ = 4.2 Hz, C30), 132.3 (C34), 131.7 – 131.0 (m, C10, C33), 129.8 (C9), 128.2 (d, $^4J_{C,P}$ = 5.6 Hz, C3), 122.2 (d, $^4J_{C,P}$ = 4.2 Hz, C15), 121.8 – 121.6 (m, C29, C32), 121.4 – 121.0 (m, C2, C8), 115.5 (C28), 115.2 (C14), 77.3 (C26), 71.9 (C22), 70.8 (C19), 70.6 (C20), 70.5 (C21), 69.7 (C18), 67.7 (C17), 59.0 (C23), 51.3 (C6), 35.7 (C5), 33.1 (d, $^2J_{C,P}$ = 11.9 Hz, C12).

³¹P{¹H} NMR (CDCl₃, 162 MHz) δ (ppm): 64.7 (2 x s, P¹), 8.5 (s, P⁰), 8.0 –7.3 (m, P²).

IR (ATR) ν (cm⁻¹): 2872, 1699, 1598, 1499, 1367, 1247, 1154, 1100, 932, 885, 831, 780.

2.2. Synthesis of 143-[G₁][G₁]-PEG

142-[G₀'][G₁]-PEG
1.0 equiv.

38 (6.0 equiv.)

Na₂SO₄ (10.0 equiv.)

THF/CHCl₃
0 °C to *RT*, 22 h   83%

143-[G₁][G₁]-PEG
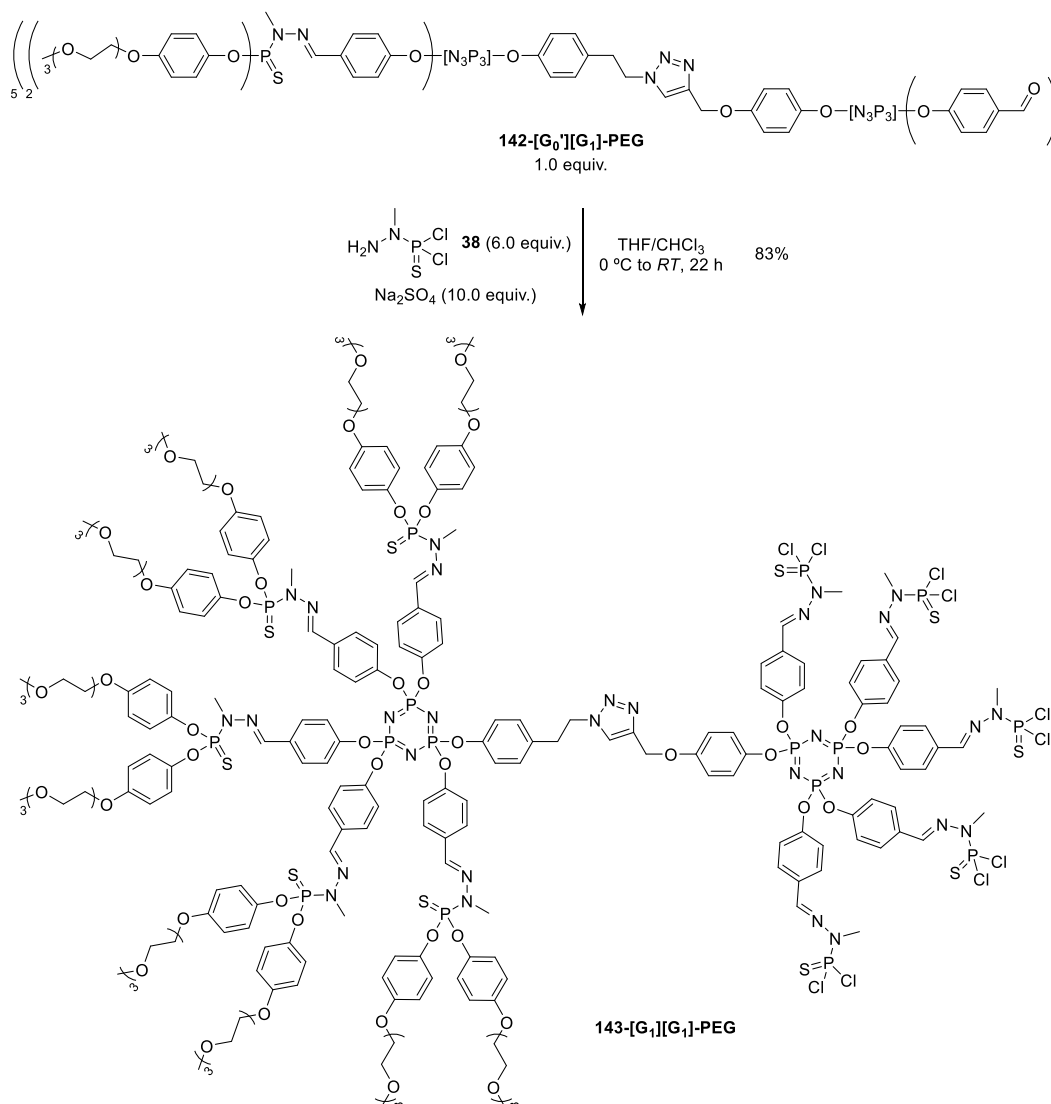
In a Schlenk flask equipped with a magnetic stirring bar, under nitrogen atmosphere, **142-[G₀'][G₁]-PEG** dendrimer (0.45 g, 0.09 mmol, 1.0 equiv.) and anhydrous Na₂SO₄ (0.13 g, 0.94 mmol, 10.0 equiv.) were suspended in dry THF (5 mL), and the mixture was cooled down to 0 °C. Next, *N*-methyldichlorothiophosphorhydrazide **38** (1.9 mL, 0.56 mmol, 6.0 equiv., c = 0.30 mol·L⁻¹ in CHCl₃) was added dropwise at 0 °C. Upon complete addition, the mixture was allowed to warm up to room temperature while stirring overnight (reaction evolution was followed by ³¹P{¹H} NMR). The mixture was filtered by cannula filtration, and the filtrate concentrated to 3 mL. The product was precipitated from *n*-pentane, the supernatant removed, and the product washed with *n*-pentane/Et₂O (4:1) twice. The volatiles were removed and the product dried obtaining a colorless solid (0.44 g, 0.078 mmol, 83% yield).
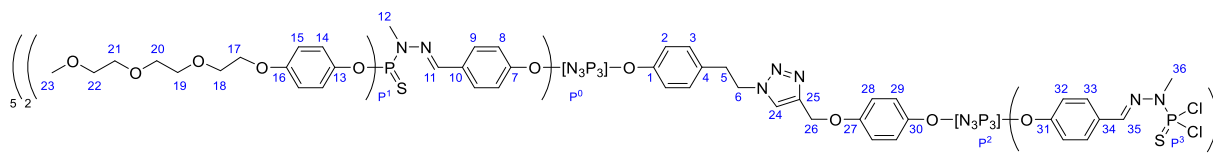
M.p.: 56 – 60 °C.

¹H NMR (400 MHz, CDCl₃) δ (ppm): 7.66 – 7.52 (m, 26H, H9, H11, H33, H35), 7.09 – 6.90 (m, 33H, H2, H3, H9, H15, H24), 6.86 – 6.68 (m, 40H, H8, H14, H28, H29, H32), 4.95 (s, 2H, H26), 4.42 – 4.34 (m, 2H, H5), 4.06 –°3.98 (m, 20H, H17), 3.83 – 3.75 (m, 20H, H19), 3.70 – 3.59 (m, 60H, H18, H20, H21), 3.55 – 3.48 (m, 20H, H22), 3.34 (2 x s, 30H, H23), 3.29 – 3.19 (m, 32H, H6, H12, H36).

¹³C{¹H} NMR (101 MHz, CDCl₃) δ (ppm): 156.4 – 156.3 (m, C13), 151.5 – 151.2 (m, C7, C31), 144.4 – 144.1 (m, C11, C35), 138.7 – 138.5 (C16), 132.4 (2 x s, C34), 131.5 –131.2 (m, C10), 128.8 – 128.7 (2 x s, C9), 128.5 – 128.2 (C33), 122.4 (d, $^4J_{C,P}$ = 4.2 Hz, C15), 122.1 – 122.0 (C8), 121.6 – 121.3 (m, C32), 115.4 (C14), 77.3 (C26), 72.1 (C22) 70.9 (C19), 70.8 (C20), 70.7 (C21), 69.8 (C18), 67.9 (C17), 59.2 (C23), 33.4 – 33.0 (m, C36), 32.3 – 32.0 (2 x d, $^2J_{C,P}$ = 13.1 Hz, 12.5 Hz, C12). Carbon signals corresponding to the cores and triazole linker were not detected due to the low concentration and the poor solubility of the compound in deuterated solvents.

³¹P{¹H} NMR (162 MHz, CDCl₃) δ (ppm): 64.5 (s, P³), 62.7 (s, P¹), 62.5 (s, P¹), 9.5 –7.8 (m, P⁰, P²).

IR (ATR) ν (cm⁻¹): 2874, 1605, 1501, 1461, 1367, 1247, 1179, 1161, 935, 888, 834, 781.

3. Synthesis of unsymmetrical NHC ligands

3.1. Synthesis of *N*-mesitylethylenediamine 146
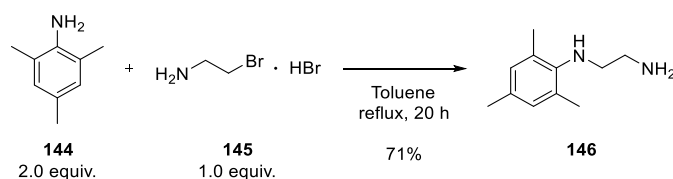
In a round bottom flask equipped with a magnetic stirring bar, under argon atmosphere, mesitylamine (**144**) (3.02 g, 3.5 mL, 24.4 mmol, 2.0 equiv.), 2-bromoethylamine hydrobromide (**145**) (2.58 g, 12.2 mmol, 1.0 equiv.), and dry toluene (30 mL) were added, and the mixture was stirred at reflux for 20 hours. After the reaction completion, the mixture was allowed to cool down to room temperature, 2M KOH (30 mL) was added, and the mixture vigorously stirred for 10 minutes. The aqueous layer was then extracted with dichloromethane, (100 mL) washed with brine (2x100 mL), dried over MgSO₄, filtered, and the volatiles were removed under reduced pressure. The resulting oil was purified by column chromatography on silica (*n*-hex/EtOAc 9:1 to 8:2) affording the product as a colorless oil (1.54 g, 8.66 mmol, 71% yield).
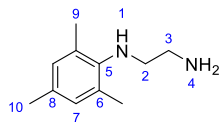
^{1}H NMR (400 MHz, CDCl$_3$) δ (ppm): 6.87 (s, 2H, H7), 3.03 – 2.95 (m, 2H, H2), 2.92 – 2.85 (m, 2H, H3), 2.33 (s, 6H, H9), 2.29 (s, 3H, H10), 2.03 (br s, 3H; H1, H2).

^{13}C{^{1}H} NMR (101 MHz, CD$_3$OD) δ (ppm): 143.7 (C5), 131.1 (C8), 129.7 (C7), 129.5 (C6), 51.3 (C2), 42.6 (C3), 20.7 (C10), 18.4 (C9).

NMR spectra are in accordance with previously reported syntheses.[230]

3.2. Synthesis of 4-(((2-(mesitylamino)ethyl)amino)methyl)phenol 148
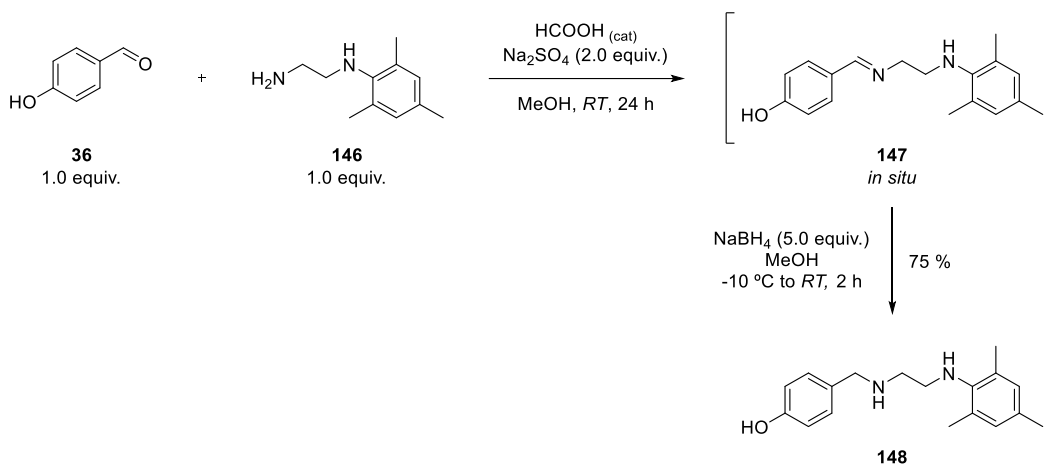
In a round bottom flask equipped with a magnetic stirring bar, 4-hydroxybenzaldehyde (**36**) (1.03 g, 8.4 mmol, 1 equiv.) was dissolved in MeOH (40 mL). Then, 2 drops of formic acid, *N*-mesitylethane-1,2-diamine (**146**) (1.50 g, 8.4 mmol, 1 equiv.), and Na$_2$SO$_4$ (2.40 g, 16.8 mmol, 2.0 equiv.) were added. The reaction mixture was stirred at room temperature for 24 hours (TLC control, EtOAc/*n*-hexane 1:1). After the reaction time was completed, the desiccant was filtered off and washed with CH$_2$Cl$_2$ (3 x 10 mL). The organic layers were combined and concentrated under reduced pressure. The product of condensation was obtained as an orange oil and used in the next step without purification.

In a round bottom flask equipped with a magnetic stirring bar, the obtained imine **147** was dissolved in MeOH (40 mL). The mixture was cooled down to −10 °C, and NaBH$_4$ (1.62 g, 42.1 mmol, 5.0 equiv.) was added portion-wise to the cooled mixture. After the completion of the addition, the resulting mixture was allowed to warm up to room temperature while stirred for 2 hours (TLC control, 40% EtOAc/*n*-hexane), then, extracted with CH$_2$Cl$_2$ (3 x 50 mL). The combined organic fractions were collected, dried over anhydrous Na$_2$SO$_4$. Then, the desiccant was filtered off, and the volatiles were removed under reduced pressure affording a dark orange oil (1.80 g, 75%). The product was used for the next step without further purification.
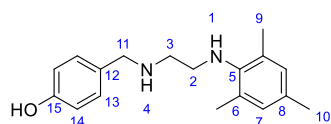
¹H NMR (400 MHz, CDCl₃) δ (ppm): 7.09 (d, $^3J_{H,H}$ = 8.5 Hz, 2H, H13), 6.82 (s, 2H, H7), 6.62(d, $^3J_{H,H}$ = 8.5 Hz, 2H, H14), 3.74 (s, 2H, H11), 3.09 (dd, $^3J_{H,H}$ = 6.6, 4.7 Hz, 2H, H2), 2.89 (dd, $^3J_{H,H}$ = 6.6, 4.7 Hz, 2H, H3), 2.26 (s, 6H, H9), 2.23 (s, 3H, H10).

¹³C{¹H} NMR(101 MHz, CDCl₃) δ (ppm): 156.0 (C15), 143.1 (C5), 131.9 (C8), 130.3 (C12), 130.1 (C13), 129.8 (C7), 129.6 (C6), 115.9 (C14), 53.3 (C2), 49.3 (C2), 47.9 (C3), 20.7 (C10), 18.5 (C9).

3.3. Synthesis of 1-(4-hydroxybenzyl)-3-mesityl-4,5-dihydro-1*H*-imidazol-3-ium chloride 149
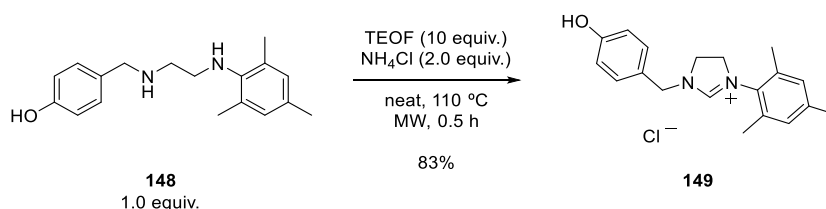
In a microwave tube equipped with a magnetic stirring bar, under argon atmosphere, 4-(((2-(mesitylamino)ethyl)amino)methyl)phenol (**148**) (1.50 g, 5.27 mmol, 1.0 equiv.), triethyl orthoformate (7.98 g, 9.0 mL, 52.7 mmol, 10 equiv.), and NH₄Cl (560 mg, 10.5 mmol, 2.0 equiv.) were mixed, and the mixture was heated up at 110 °C under 100 W of microwave irradiation for 0.5 h. Upon reaction completion, the formed precipitate was filtered, washed with cold toluene and cold diethyl ether affording the desired product as a yellow solid (1.30 g, 4.40 mmol, 83% yield).
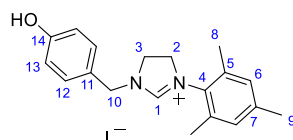
¹H NMR (400 MHz, CD₃OD) δ (ppm): 8.75 (s, 1H, H1), 7.29 (d, $^3J_{H,H}$ = 8.5 Hz, 2H, H12), 7.02 (s, 2H, H6), 6.87 (d, $^3J_{H,H}$ = 8.5 Hz, 2H, H13), 4.73 (s, 2H, H10), 4.20 – 4.05 (m, 4H, H2, H3), 2.29 (s, 9H, H8, H9).

¹³C{¹H} NMR (101 MHz, CD₃OD) δ (ppm): 158.6 (C14), 158.1 (C1), 140.2 (C4), 135.4 (C7), 130.9 (C12), 130.0 (C6), 129.4 (C5), 123.4 (C11), 115.6 (C13), 51.3 (C3), 50.7 (C2), 47.8 (C10), 19.7 (C9), 16.3 (C8).

IR (ATR) ν (cm⁻¹): 3088, 3006, 2802, 1659, 1637, 1618, 1596, 1515, 1497, 1457, 1449, 1361, 1287, 1263, 1235, 1213, 1136, 851, 701.

HRMS (ESI TOF *m/z*) calculated for C₁₉H₂₃N₂O [M-I]⁺ : 295.1810, Found: 295.1814.

3.4.   Synthesis of 4-(hydroxymethyl)phenol 150
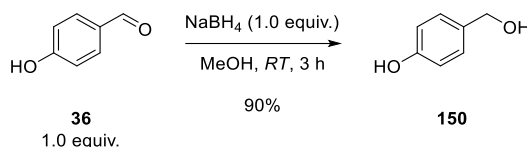
In a round bottom flask opened at air, 4-hydroxybenzaldehyde (**36**) (5.00 g, 40.1 mmol, 1.0 equiv.) was dissolved in MeOH (50 mL) at room temperature. When the solution turned to transparent, NaBH$_4$ (1.60 g, 40.1 mmol, 1.0 equiv.) was added portion-wise. The resulting mixture was stirred for additional 3 h at room temperature (TLC control, 30% EtOAc/n-hexane). After the reaction time was completed, the mixture was extracted with EtOAc (3 x 30 mL). The combined organic layers were dried over anhydrous MgSO$_4$ and the volatiles removed under reduced pressure. The product was obtained as a colorless powder and used without further purification (4.50 g, 36.2 mmol, 90% yield).
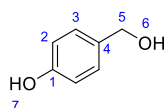
^{1}H NMR (400 MHz, DMSO-d_6) δ (ppm): 9.21 (m, 1H, H7), 7.12 – 7.09 (m, 2H, H3), 6.70 (dd, $^3J_{H,H}$ = 8.5 Hz, $^4J_{H,H}$ = 2.5 Hz, 2H, H2), 4.94 – 4.91 (m, 1H, H6), 4.36 (dd, $^4J_{H,H}$ = 5.5 Hz, $^3J_{H,H}$ = 2.5 Hz, 2H, H5).

^{13}C{^{1}H} NMR (101 MHz DMSO-d_6) δ (ppm): 156.2 (C1), 132.8 (C4), 128.1 (C3), 114.8 (C2), 62.8 (C5).

NMR spectra are in accordance with previously reported syntheses.[233]

3.5.   Synthesis of 4-(iodomethyl)phenol 151
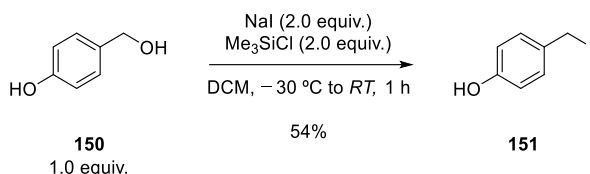
In a round-bottom flask equipped with a magnetic stirring bar, under argon atmosphere, 4-hydroxybenzyl alcohol (**150**) (1.50 g, 12.1 mmol, 1.0 equiv.) and NaI (3.66 g, 24.2 mmol, 2.0 equiv.) were suspended in dry dichloromethane (20 mL). The reaction mixture was cooled down to −30 °C and TMSCl (2.65 g, 3.1 mL, 24.2 mmol, 2.0 equiv.) was added dropwise avoiding the fuming. After the completion of addition, the reaction was allowed to warm up to room temperature while stirring. Upon reaction completion, brine (20 mL) was added, and the mixture was vigorously stirred for 20 minutes. Then, the organic phase was extracted with DCM (3 x 30 mL), dried over anhydrous MgSO$_4$, and the volatiles were removed under reduced pressure to provide the product as a dark orange solid (1.52 g, 6.49 mmol, 54% yield)
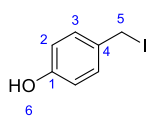
¹H NMR (400 MHz, DMSO-d_6) δ (ppm): 7.27 (d, $^3J_{H,H}$ = 8.7 Hz, 2H, H3), 6.75 (d, $^3J_{H,H}$ = 8.7 Hz, 2H, H2), 4.82 (s, 1H, H6), 4.46 (s, 2H, H5).

¹³C{¹H} NMR (101 MHz DMSO-d_6) δ (ppm): 155.1 (C1), 131.6 (C4), 130.3 (C3), 115.7 (C2), 6.36 (C5).

NMR spectra are in accordance with previously reported syntheses.[256]

3.6.   Synthesis of 1-mesityl-1*H*-imidazole 152
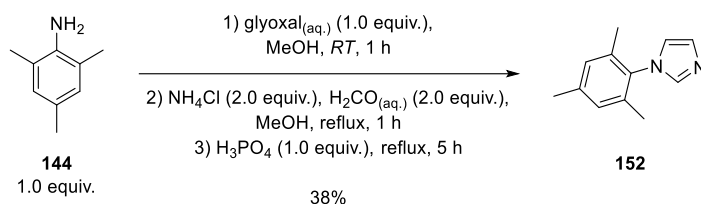
In a round bottom flask, mesitylamine (**144**) (5.0 mL, 34.9 mmol, 1.0 equiv.) was dissolved in methanol (75 mL) with glyoxal solution (40% in water, 4.0 mL, 34.9 mmol, 1.0 equiv.) and stirred at room temperature until a solid was formed (1 h). After that time, ammonium chloride (2.0 mL, 69.8 mmol, 2.0 equiv.) and formaldehyde (37% solution, 5.2 mL, 69.8 mmol, 2.0 equiv.) were added. The reaction mixture was diluted with MeOH (75 mL) and refluxed for 1 h. After that time, phosphoric acid (2.4 mL, 34.9 mmol, 1.0 equiv.) was added and the mixture stirred at reflux for 5 h (until reaction completion, followed by TLC). Next, the solvent was removed, the residue poured in ice, and neutralized with KOH until a pH of 9. The mixture was extracted with diethyl ether, dried over MgSO₄, filtered, and the volatiles were removed under reduced pressure. The product was achieved as a colorless solid after recrystallization from DCM/pentane (2.45 g, 13.2 mmol, 38% yield).
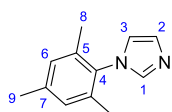
¹H NMR (400 MHz, CDCl₃) δ (ppm): 7.43 (s, 1H, H3), 7.23 (s, 1H, H2), 6.97 (s, 2H, H6), 6.89 (s, 1H, H1), 2.33 (s, 3H, H9), 1.98 (s, 6H, H8).

¹³C{¹H} NMR (101 MHz, CDCl₃) δ (ppm): 138.8 (C1), 137.5 (C4), 135.4 (C7), 133.3 (C6), 129.5 (C5), 129.0 (C2), 120.0 (C3), 21.0 (C9), 17.3 (C8).

NMR spectra are in accordance with previously reported syntheses.[232]

3.7. Synthesis of 1-(4-hydroxybenzyl)-3-mesityl-1*H*-imidazol-3-ium iodide 153
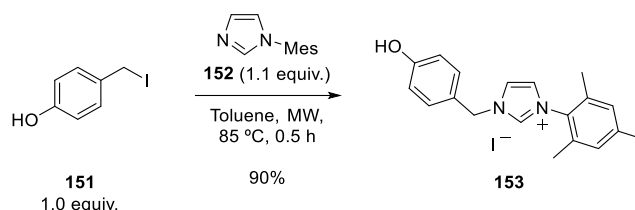
In a microwave tube equipped with a magnetic stirring bar, under argon atmosphere, 1-mesityl-1*H*-imidazole (**152**) (0.32 g, 1.73 mmol, 1.1 equiv.) and 4-(iodomethyl)phenol (**151**) (0.37 g, 1.58 mmol, 1.0 equiv.) were suspended in dry toluene (20 mL), and the mixture was heated up at 85 °C under 150 W of microwave irradiation for 0.5 h. Upon the reaction completion, the formed precipitate was filtered, washed with cold toluene and cold diethyl ether affording the desired product as a yellow solid (0.59 g, 1.41 mmol, 90% yield).
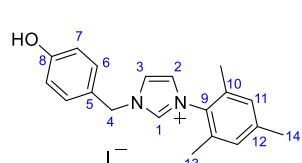
^{1}H NMR (400 MHz, CH$_3$OD) δ (ppm): 9.26 (s, 1H, H1), 7.84 (m, 1H, H3), 7.69 (m, 1H, H2), 7.33 (d, $^3J_{H,H}$ = 8.6 Hz, 2H, H6), 7.12 (s, 2H, H11), 6.85 (d, $^3J_{H,H}$ = 8.6 Hz, 2H, H7), 5.43 (s, 2H, H4), 2.35 (s, 3H, H14), 2.04 (s, 6H, H13).

^{13}C{^{1}H} NMR (161 MHz, CH$_3$OD) δ (ppm): 158.5 (C8), 141.2 (C1), 134.3 (C9), 131.1 (C12), 129.8 (C10), 129.3 (C11), 128.8 (C5), 124.3 (C6), 124.2 (C3), 122.8 (C2), 115.8 (C7), 52.9 (C4), 19.7 (C14), 15.8 (C13).

IR (ATR) ν (cm^{-1}): 3153, 2962, 1747, 1610, 1592, 1529, 1513, 1483, 1441, 1418, 1347, 1258, 1211, 1191, 1170, 1151, 1099, 1061, 859, 822, 787, 745, 690, 583, 546.

HRMS (ESI TOF *m/z*) calculated for C$_{19}$H$_{21}$N$_2$O [M-I]$^+$: 293.1654, Found: 293.1657.

4. Synthesis of Ru-NHC complexes

4.1. Synthesis of Ru36
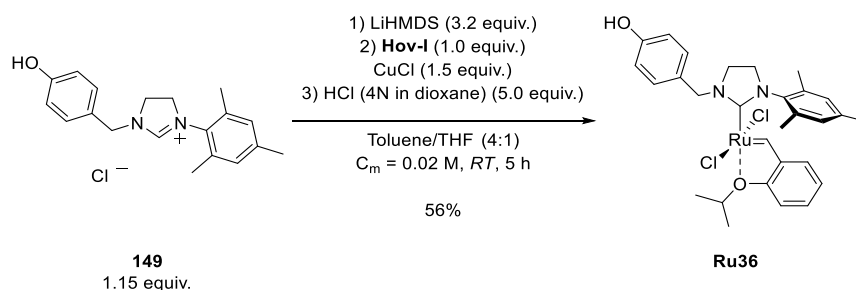
In an oven-dried 50 mL Schlenk flask equipped with a magnetic stirring bar, under argon atmosphere, 1-(4-hydroxybenzyl)-3-mesityl-4,5-dihydro-1*H*-imidazol-3-ium chloride (**149**) (0.10 g, 0.30 mmol, 1.15 equiv.) was suspended in dry toluene (12 mL). To the resulting suspension LiHDMS (0.11 g, 0.66 mmol, 3.2 equiv.) was added and the mixture was stirred for 1 hour at room temperature in an atmosphere of argon. To this suspension, dry THF (3 mL) was

added, and the reaction was stirred until the solution became clear and homogeneous. To this solution, **Hov-I** was added (0.16 g, 0.26 mmol, 1.0 equiv.). The resulting solution was stirred at room temperature for 2 hours (the reaction was monitored by TLC, *n*-hexane/EtOAc 1:1). After the complete disappearance of **Hov-I** on TLC, CuCl (39.4 mg, 0.39 mmol, 1.5 equiv.) was added to the reaction and stirred for additional 30 min followed by dropwise addition of 4N HCl in dioxane (0.12 mL, 1.31 mmol). The reaction mixture was stirred for another 30 min, transferred to a round bottom flask and volatiles were evaporated to dryness. The crude mixture was purified by column chromatography (*n*-hexane/EtOAc 8:2 to 1:1). The desired product was crystallized from the mixture of DCM/MeOH (3:1) to give a fine dark green powder (72.0 mg, 0.12 mmol, 56% yield).
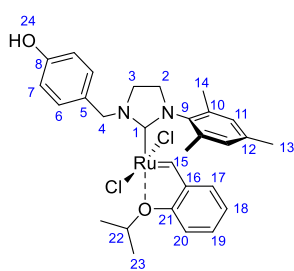
1H NMR (400 MHz, DCM-*d*₂) δ (ppm): 16.22 (s, 1H, H15), 7.67 − 7.54 (m, 3H, H6, H19), 7.11 (s, 2H, H11), 7.04 − 6.95 (m, 3H, H7, H17), 6.90 (d, $^3J_{H,H}$ = 7.8 Hz, 2H, H16, H18), 5.55 (s, 1H, H24), 5.53 (s, 2H, H4), 5.18 (sept, $^3J_{H,H}$ = 6.1 Hz, 1H, H22), 3.92 (t, $^3J_{H,H}$ = 10.0 Hz, 2H, H2), 3.64 (d, $^3J_{H,H}$ = 10.0 Hz, 2H, H3), 2.48 (s, 3H, H13), 2.24 (s, 6H, H14), 1.71 (d, $^3J_{H,H}$ = 6.1 Hz, 6H, H23).

13C{1H} NMR (101 MHz, DCM-*d*₂) δ (ppm): 155.7 (C8), 152.2 (C21), 143.8 (C9), 138.9 (C16), 138.0 (C12), 137.7 (C10), 135.2 (C5) 130.6 (C19), 129.5 (C11), 129.4 (C6), 122.5 (C20), 122.1 (C18), 115.3 (C17), 112.9 (C7), 75.2 (C22), 47.7 (C4), 21.7 (C23), 20.9 (C13), 17.7 (C14).

4.2.   Synthesis of Ru38
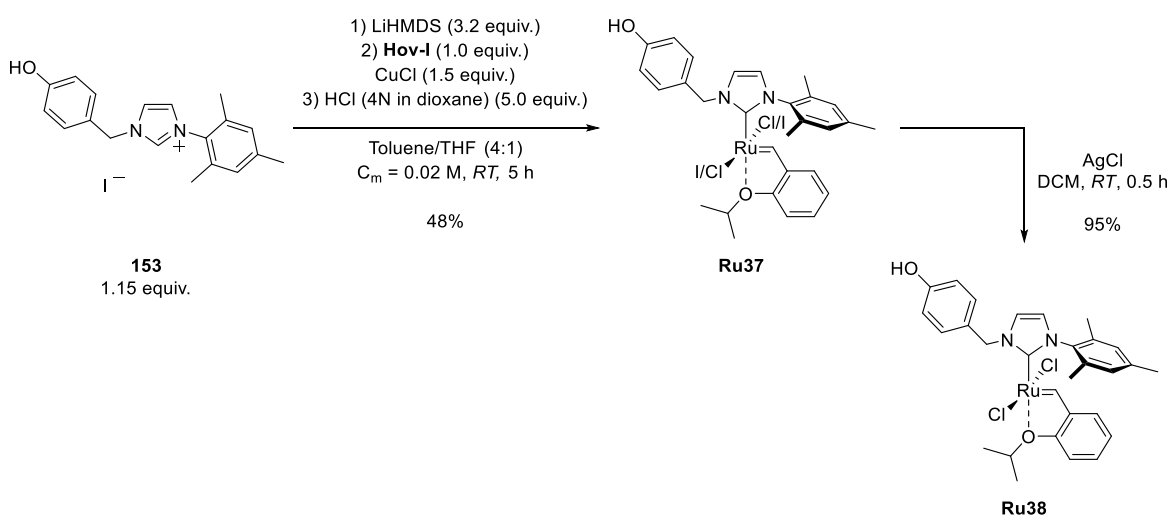
In an oven-dried Schlenk flask equipped with a magnetic stirring bar, under argon atmosphere, 1-(4-hydroxybenzyl)-3-mesityl-1*H*-imidazol-3-ium   iodide   (**153**)   (0.10 g,   0.24 mmol, 1.15 equiv.) was suspended in dry toluene (12 mL). To the resulting suspension, LiHDMS (0.11 g, 0.66 mmol, 3.2 equiv.) was added and the mixture was stirred for 1 hour at room temperature in an atmosphere of argon. To this suspension, dry THF (3 mL) was added, and the reaction was

stirred until the solution became clear and homogeneous. To this solution, **Hov-I** was added (0.12 g, 0.21 mmol, 1.0 equiv.). The resulting solution was stirred at room temperature for 2 hours (the reaction was monitored by TLC, *n*-hexane/EtOAc 1:1). After the complete disappearance of **Hov-I** on TLC, CuCl (31 mg, 0.31 mmol, 1.5 equiv.) was added to the reaction mixture and stirred for an additional 30 min. followed by dropwise addition of 4N HCl in dioxane (0.26 mL, 1.03 mmol). The reaction mixture was stirred for another 30 min, transferred to a round bottom flask and volatiles were removed to dryness. The crude mixture was purified by column chromatography (*n*-hexane/EtOAc 8:2 to 1:1). The desired product was crystallized from the mixture of DCM/MeOH (3:1) to give a fine dark green powder (60 mg, 0.10 mmol, 48% yield). The ratio of Cl/I at the ruthenium coordination center was established based on integration of benzylidene signals by ^{1}H NMR as 88:12.

An oven-dried vial was charged with AgCl (1.1 equiv. per iodide) and Ru-complex (30 mg). The vial was evacuated, and three times flushed with argon, dry DCM (1 mL) was added, and the resulting mixture was stirred for 30 minutes at room temperature. The resulting solution was centrifuged, filtered through Celite® pad and washed with MeOH (20 mL). Solvents were evaporated and the residue was crystallized from the mixture of DCM/MeOH and dried under vacuum overnight to provide pure product as a fine dark green powder (26.8 mg, 0.004 mmol, 95% yield).
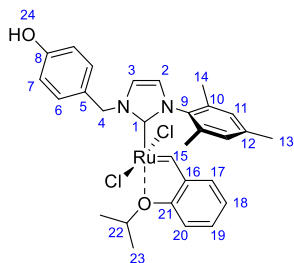
^{1}H NMR (400 MHz, DCM-d_2) δ (ppm): 16.38 (s, 1H, H15), 7.58 (ddd, $^3J_{H,H}$ = 8.4, 7.2 Hz, $^4J_{H,H}$ = 1.9 Hz, 1H, H19), 7.52 (d, $^3J_{H,H}$ = 8.5 Hz, 2H, H6), 7.15 (m, 2H, H11), 7.08 – 6.99 (m, 3H, H17, H18, H20), 6.91 (m, 3H, H2, H7), 6.86 (d, $^3J_{H,H}$ = 2.1 Hz, 1H, H3), 6.07 (s, 2H, H4), 5.44 (s, 1H, H24), 5.19 (sept, $^3J_{H,H}$ = 6.2 Hz, 1H, H22), 2.52 (s, 3H, H13), 2.02 (s, 6H, H14), 1.75 (d, $^3J_{H,H}$ = 6.1 Hz, 6H, H23).

^{13}C{^{1}H} NMR (101 MHz, DCM-d_2) δ (ppm): 287.5 (C15), 172.3 (C1), 156.2 (C8), 152.4 (C21), 144.1 (C9), 139.8 (C16), 137.2 (C12), 137.2 (C10), 131.1 (C5), 129.1 (C3), 129.0 (C19), 127.9 (C11), 124.4 (C6), 122.6 (C20), 121.7 (C18), 121.2 (C17), 115.6 (C2), 112.9 (C7), 75.3 (C22), 54.8 (C4), 21.8 (C23), 21.0 (C13), 17.6 (C14).

Elemental analysis: calculated for $C_{29}H_{32}Cl_2N_2O_2Ru$: C 56.86; H 5.27; N 4.57; Found C 56.59; H 5.48; N 4.34.

4.3.   Synthesis of Ru41
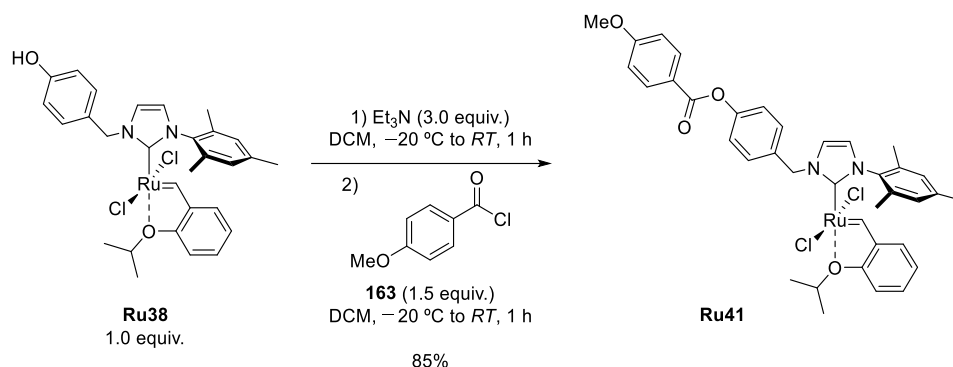
In a Schlenk flask equipped with a magnetic stirring bar, under nitrogen atmosphere, **Ru38** (50 mg, 0.08 mmol, 1.0 equiv.) was dissolved to dry CH_2Cl_2 (5 mL), and the mixture was cooled down to −20 °C. Triethylamine (0.03 mL, 0.244 mmol, 3.0 equiv.) was added and the mixture was stirred for 1 h in an atmosphere of nitrogen. 4-methoxybenzoyl chloride (**153**) (20.9 mg, 0.12 mmol, 1.5 equiv.) was added to the resulting mixture and stirred for an additional hour while warming up to room temperature (the reaction was monitored by TLC, *n*-hexane/EtOAc 1:1). The crude mixture was purified by column chromatography (*n*-hexane/EtOAc 8:2 to 1:1). The desired product was crystallized from the mixture of DCM/MeOH (3:1) to give a fine dark orange powder (52 mg, 0.07 mmol, 85% yield).
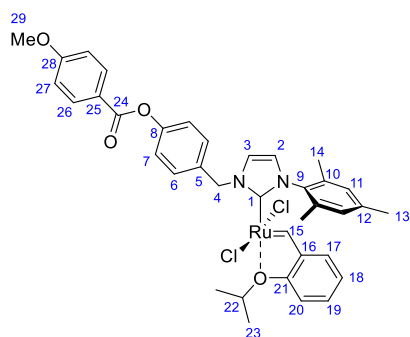
^{1}H NMR (400 MHz, DCM-d_2) δ (ppm): 16.44 (s, 1H, H15), 8.18 (d, $^3J_{H,H}$ = 8.9 Hz, 2H, H26), 7.73 (d, $^3J_{H,H}$ = 8.5 Hz, 2H, H6), 7.52 (ddd, $^3J_{H,H}$ = 8.7, 7.2 Hz, $^4J_{H,H}$ = 1.8 Hz, 1H, H19), 7.31 (d, $^3J_{H,H}$ = 8.5 Hz, 2H, H7), 7.13 (s, 2H, H11), 7.06 – 6.94 (m, 5H, H17, H18, H20, H27), 6.91 (d, $^3J_{H,H}$ = 2.1 Hz, 1H, H2), 6.83 (d, $^3J_{H,H}$ = 2.1 Hz, 1H, H3), 6.20 (s, 2H, H4), 5.21 (sept, $^3J_{H,H}$ = 6.1 Hz, 1H, H22), 3.91 (s, 3H, H29), 2.52 (s, 3H, H13), 2.07 (s, 6H, H14), 1.81 (d, $^3J_{H,H}$ = 6.1 Hz, 6H, H23).

^{13}C{^{1}H} NMR (101 MHz, DCM-d_2) δ (ppm): 173.4 (C1), 164.9 (C24), 164.2 (C28), 152.9 (C8), 151.6 (C21), 144.4 (C9), 139.8 (C16), 137.5 (C12), 137.4 (C10), 133.2 (C26), 132.5 (C5), 131.1 (C25), 129.4 (C19), 129.2 (C3), 124.6 (C11), 122.7 (C6), 122.6 (C20), 122.3 (C18), 121.8 (C17), 121.6 (C2), 114.1 (C27), 113.1 (C7), 75.4 (C22), 55.7 (C29), 55.1 (C4), 22.2 (C23), 21.4 (C13), 18.2 (C14).

IR (ATR) ν (cm^{-1}): 2919, 2365, 2164, 1730, 1604, 1511, 1379, 1255, 1201, 1164, 1067, 1021, 778, 631.

HRMS (ESI TOF *m/z*) calculated for $C_{37}H_{39}N_2O_4Ru$ [M-Cl$_2$]$^+$: 677.1948; Found: 677.1960.

4.4. Stability studies of Ru36 and Ru38

In an NMR tube under argon atmosphere, a corresponding ruthenium complex (10.8 μmol, 1.0 equiv.) dissolved in CD_2Cl_2 (0.5 mL) and 1,3,5-trimethoxybenzene (1.82 mg, 10.8 μmol, 1.0 equiv.) dissolved in DCM-d_2 (0.2 mL) were mixed and let stabilize at 30 °C. NMR was recorded at room temperature at selected time to establish the decomposition of the complexes.

The same protocol was followed to establish the decomposition of obtained ruthenium complexes **Ru36** and **Ru38** in toluene-d_8. However, after 24 hours, the formation of a precipitate in the samples at 50 °C was observed which made it impossible to record reliable NMR spectra and finish the experiment in toluene-d_8.

Table 7. Results of the stability tests of **Ru36** and **Ru38** performed in DCM-d_2 at room temperature over 10 days.
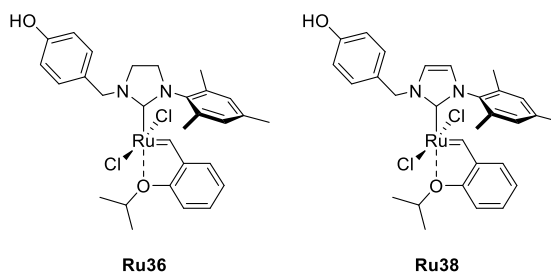
Ru36		Ru38	
Time [Days]	**Remained complex [%]**	**Time [Days]**	**Remained complex [%]**
0	100	**0**	100
1	100	**1**	100
2	100	**2**	98.1
3	97.1	**3**	98.1
7	94.1	**7**	96.2
8	94.1	**8**	96.2
9	94.1	**9**	96.2

4.5. Ring-Closing Metathesis of DEDAM

To the solution of diethyl diallylmalonate (38.7 mg, 0.16 mmol, 1.0 equiv.) and mesitylene (19.0 mg 0.16 mmol, 1.0 equiv., used as an internal standard) in a dry solvent (DCM or toluene, 9.5 mL) 1 mol% of a corresponding ruthenium complex (**Ru36**, **Ru38**, **Ru41**) was added in one portion in argon flow. The resulting mixture was stirred under given conditions for 24 hours. Aliquots (0.5 mL) were taken at selected times and quenched with SnatchCat (4.4 equiv. vs Ru). The conversion of the substrate was determined by GC.

Table 8. Results of the RCM of DEDAM (**S1**) catalyzed by **Ru36**, **Ru38** and **Ru41** (1 mol%) in various temperature and solvent conditions.
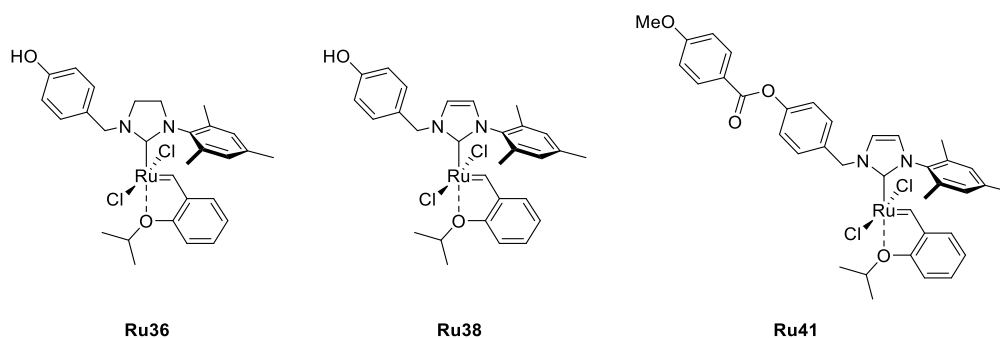
[Ru]	Conditions	Time [h]	Conversion [%][a]
Ru36	DCM, *RT*	3	15
		24	49
	B(OEt)$_3$ (1 mol%), DCM, *RT*	3	16
		24	56
	Toluene, 50 °C	3	84
		24	>99
Ru38	DCM, *RT*	3	36
		24	79
	Toluene, 50 °C	3	95
		24	>99
Ru41	DCM, *RT*	3	18
		24	49
	Toluene, 50 °C	3	97
		24	>99

[a] Conversion assessed by GC using dodecane or 1,3,5-trimethoxybenzene as internal standard

5.   Synthesis of a Ru@MOF system for olefin metathesis catalysis

5.1.   Synthesis of (Al)MIL-101-NH₂

165
1.5 equiv.

166
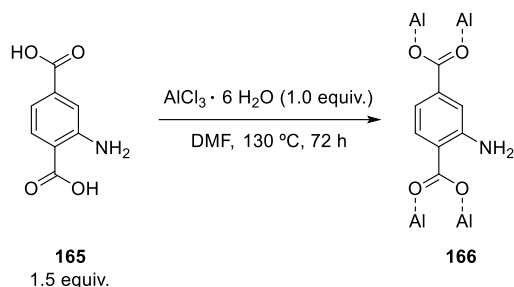
Aluminum trichloride hexahydrate (1.53 g, 6.34 mmol, 1.0 equiv.) and a magnetic stir bar were placed in a 150 mL pressure tube followed by DMF (120 mL) and stirred overnight at room temperature until homogenous solution formed. 2-aminoterephthalic acid (**165**) (1.68 g, 9.27 mmol, 1.46 equiv.) was later added, and after its dissolution, the magnetic stir bar was removed, and the pressure tube was sealed and placed in a preheated oven at 130 °C for 70 hours. Over this period, a yellow precipitate formed, which was filtered off on a filter funnel (G4) under reduced pressure and washed with DMF (50 mL), acetone (50 mL) and methanol (50 mL). The synthesized MOF was partially formylated, so the crude material was suspended in methanol (60 mL) and placed in an autoclave at 120 °C for 20 hours, according to the deformylation methodology.[257] After cooling down, the solid was collected by filtration (G4), washed with methanol (200 mL) and dried under vacuum ($4 \cdot 10^{-2}$ mbar, room temperature, 24 hours) to yield 1.58 g of a pure product, containing however *ca.* 18-19% MeOH (w/w).

(Al)MIL-101-NH₂ was synthesized using a modified procedure developed by Gascon *et. al.*[208,258]

5.2.   Sorption experiments

Solutions of precisely known concentrations of catalysts **Ru38** were prepared, and their UV-Vis spectra measured in both toluene and DCM. Molar absorption coefficients were determined by linear regression, by plotting the absorbance value at the maximum of absorbance (359.5 nm) *vs* concentration (*vide supra* Chapter III, Section §4.1).

5.2.1.   Sorption of Ru38 to (Al)MIL-101-NH₂

1.00 mM solutions of catalyst **Ru38** in DCM and toluene were prepared. To a 4 mL vial with a screw cap a sample of (Al)MIL-101-NH₂ **166** was weighed (10.0 mg), and 1.00 mM solution of the complex in a given solvent was added (2.0 mL, 2.0 µmol). The resulting suspension was stirred at room temperature for 1 h. Then, the reaction mixture was centrifuged, the supernatant was removed off through a syringe filter (PTFE, 0.2 µm) and the solid residue was dried under vacuum (at least 2 h in 8 µbar) at room temperature.

The supernatant was analyzed by UV-Vis spectroscopy (**Figure 49**) to determine the amount of non-adsorbed catalyst by interpolation from the maximum absorbance at 359.5 nm in the previously prepared linear regression, and therefore calculating the amount of adsorbed catalyst.

Table 9. Results of the sorption experiments of **Ru38** on MOF **166** in toluene and DCM.

Catalyst / Solvent	Absorbance of the supernatant at 359.5 nm	Catalyst adsorbed from solution [%]
Ru38 / DCM	0.071	99.2
Ru38 / Toluene	0.049	99.4
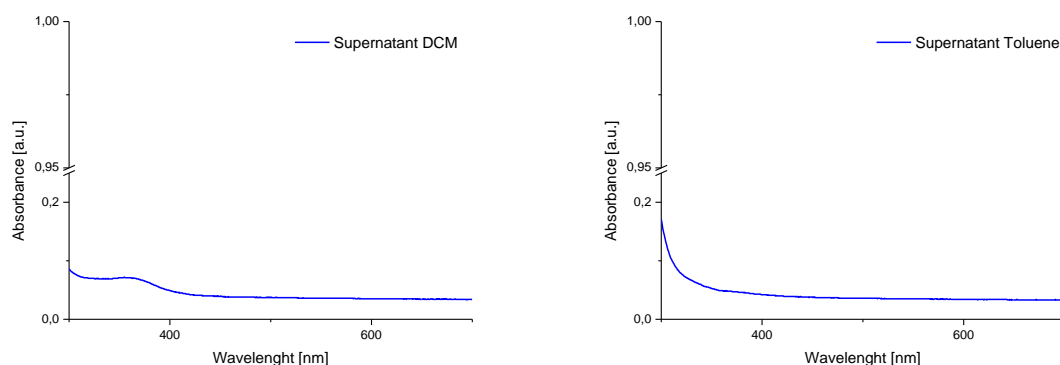
Figure 49. UV-Vis spectra of the supernatants after adsorption of **Ru38** on **Al(MIL)-101-NH₂** in DCM (*left*) and toluene (*right*).

5.3.   Desorption experiments

Ru38@(Al)MIL-101-NH$_2$ complex was suspended in 3 mL of toluene with short sonication and placed in a G4 filtering funnel with a side argon inlet. The rest of toluene (up to 20 mL) followed by DCM (20 mL) were slowly passed through the sample and were collected in vials. The experiment was conducted in argon flow.

The concentration of catalysts in each extract was analyzed by UV-Vis spectroscopy in batches of 4 mL (five UV-Vis analyses per solvent), and the leaching calculated as previously reported[208] by interpolation of the maximum of absorbance to the linear regression, determining a final leaching of a 9.2%. **Figure 50** displays the evolution of the leaching compared to the flow of solvent.
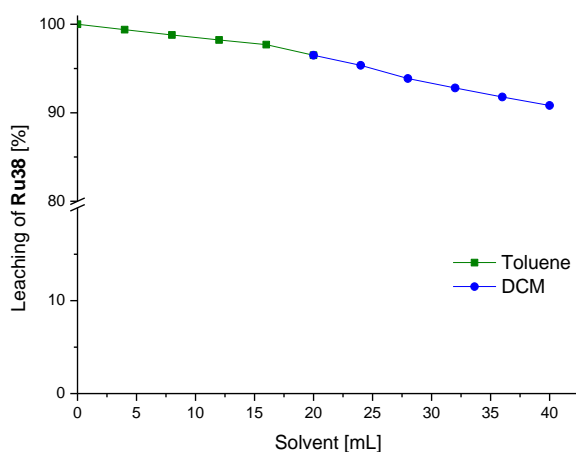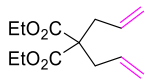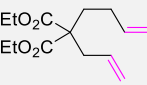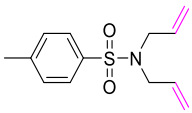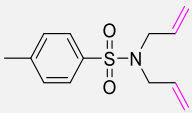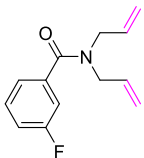
Figure 50. Desorption of **Ru38** from **Al(MIL)-101-NH₂** by washings with toluene and DCM.

5.4. Activity of Ru38@(Al)MIL-101-NH₂ in Ring-Opening Metathesis
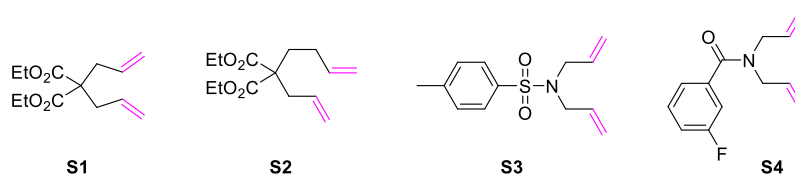
A 4 mL vial with a septum cap was charged with a magnetic stirring bar, **Ru38@MOF** (1 mol% of [Ru] *vs*. a substrate **S1-S4**), toluene (2 mL) and a corresponding substrate (0.95 mmol). The suspension was stirred for 3 h in a vial with perforated septum at 80 °C (0.4 mm needle was stuck in the septum, to release ethylene). After this time the vial was taken from the stirring plate and 1 mL of the supernatant was withdrawn and filtered through a syringe filter. 0.1 mL of the filtrate was added to a vial containing 10 mg of Apeiron SnatchCat™ to quench the reaction, whereas the remaining 0.9 mL was added to another vial with septum cap to perform split test. After 24 h, both heterogeneous and homogeneous reaction were quenched with 0.1 mL of 1M SnatchCat™ solution in DCM and subjected to GC analysis to determine the conversion of the substrate.[208,258] The product of the RCM reaction of DATA was isolated by column chromatography (*n*-hexane/EtOAc 8:2 to 1:1).

Table 10. Results of the RCM reaction of selected dienes **S2-S4** catalyzed by **Ru38@(Al)MIl-101-NH₂** complex (1 mol%) in toluene at 80 °C.

[Ru]@MOF	Substrate	Conversion [%]		
		At split	In filtrate (24 h)	In suspension (24 h)
Ru38@(Al)MIL-101-NH₂	EtO₂C / EtO₂C	52 (3 h)	53	53
Ru38@(Al)MIL-101-NH₂	EtO₂C / EtO₂C	26 (3 h)	26	31
Ru38@(Al)MIL-101-NH₂		65 (3 h)	65	91*
Ru38@(Al)MIL-101-NH₂·HCl		78 (0.25 h)	78	78
Ru38@(Al)MIL-101-NH₂		13 (3 h)	14	30

* Isolated yield for the compound is 79 %

6. Synthesis of dimeric structures for the immobilization attempts of Ru-NHC complexes on dendrimers

6.1. Synthesis of (2-benzylidene-1-methylhydrazineyl)phosphonothioic dichloride 155
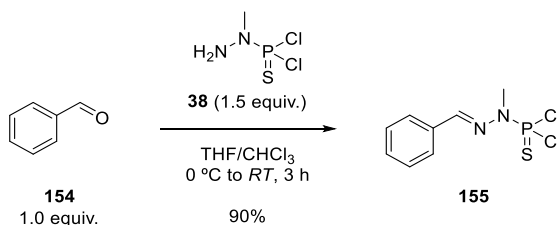
In a Schlenk flask equipped with a magnetic stirring bar, under nitrogen atmosphere, a solution of *N*-methyldichlorothiophosphorhydrazide (**38**) (c = 0.30 mol·L^{-1} in chloroform, 49.0 mL, 14.7 mmol, 1.5 equiv.) was placed, and the solution was cooled down to 0 °C. A solution of benzaldehyde (**154**) (1.0 mL, 9.80 mmol, 1.0 equiv.) in dry THF (10 mL) was then added dropwise with vigorous stirring. Upon complete addition, the mixture was let to warm up to room temperature while stirring for 3 h. Reaction evolution was followed by ^{31}P{^{1}H} NMR. Upon reaction completion, volatiles were removed under reduced pressure, and the crude was filtered through a silica pad (*n*-pentane/DCM 9:1) to remove the excess of phosphorhydrazine. The fraction containing the product was collected, the volatiles were removed under reduced pressure, and the product was obtained as a colorless powder (2.39 g, 8.96 mmol, 90% yield).
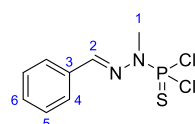
M.p.: 61 − 62 °C.

^{1}H NMR (400 MHz, CDCl$_3$) δ (ppm): 7.79-7.69 (m, 3H, H2, H4), 7.47-7.37 (m, 3H, H5, H6), 3.51 (d, $^3J_{H,P}$ = 14.0 Hz, 3H, H1).

^{13}C{^{1}H} NMR (101 MHz, CDCl$_3$) δ (ppm): 141.9 (d, $^3J_{C,P}$ = 18.7 Hz, C2), 134.1 (d, $^4J_{C,P}$ = 1.6 Hz, C3), 130.2 (C6), 128.8 (C4), 127.4 (C5), 31.8 (d, $^2J_{C,P}$ = 13.4 Hz, C1).

^{31}P{^{1}H} NMR (162 MHz, CDCl$_3$) δ (ppm): 63.4.

IR (ATR) ν (cm^{-1}): 2358, 1737, 1440, 1369, 1238, 1138, 954, 946, 771, 752, 689.

NMR spectra are in accordance with previously reported syntheses.[235]

6.2. Synthesis of di-*tert*-butyl 4,4'-(((2-benzylidene-1-methylhydrazineyl)-phosphorthioyl)bis(oxy))-dibenzoate 161
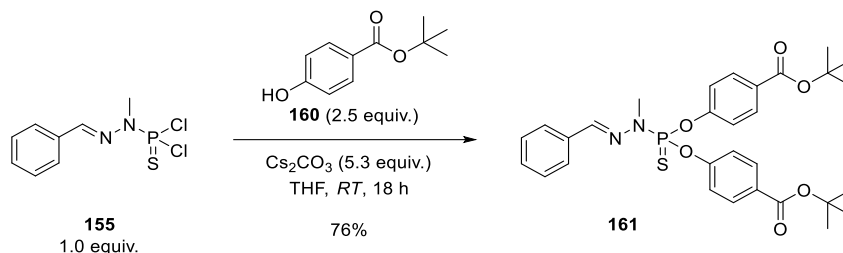
In a Schlenk flask equipped with a magnetic stirring bar, under nitrogen atmosphere, (2-benzylidene-1-methylhydrazineyl)phosphonothioic dichloride (**155**) (0.65 g, 2.43 mmol, 1.0 equiv.), dry cesium carbonate (4.16 g, 12.8 mmol, 5.3 equiv.), and *tert*-butyl-4-hydroxybenzoate (**160**) (1.18 g, 6.08 mmol, 2.5 equiv.) were dissolved in dry THF (20 mL), and the mixture was stirred at room temperature for 18 h. The reaction evolution was followed by $^{31}P\{^1H\}$ NMR. Upon reaction completion, the salts were filtered off, and the mixture was purified by column chromatography (*n*-hexane/EtOAc 9:1 to 1:1) affording the desired product as a colorless solid (1.08 g, 1.85 mmol, 76% yield).
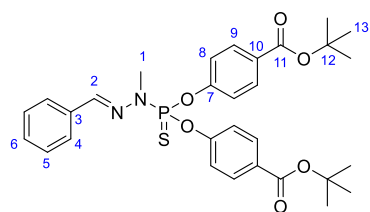
M.p.: 128 – 129 °C.

^{1}H NMR (400 MHz, CDCl$_3$) δ (ppm): 7.96 (d, $^3J_{H,H}$ = 8.4 Hz, 4H, H9), 7.72 – 7.62 (m, 3H, H2, H4), 7.45 – 7.35 (m, 3H, H3, H5, H6), 7.31 – 7.24 (m, 4H, H8), 3.37 (d, $^3J_{H,P}$ = 10.8 Hz, 3H, H1), 1.57 (s, 18H, H13).

^{13}C$\{^1$H$\}$ NMR (101 MHz, CDCl$_3$) δ (ppm): 164.9 (C11), 153.9 (d, $^2J_{C,P}$ = 7.2 Hz, C7), 140.3 (d, $^2J_{C,P}$ = 13.7 Hz, C2), 134.6 (C3), 131.2 (d, $^4J_{C,P}$ = 1.5 Hz, C9), 129.7 (C6), 129.3 (d, $^5J_{C,P}$ = 1.9 Hz, C4), 128.8 (C5), 127.1 (C10), 121.2 (d, $^3J_{C,P}$ = 4.9 Hz, C8), 81.2 (C12), 33.0 (d, $^2J_{C,P}$ = 13.5 Hz, C1), 28.2 (C13).

^{31}P$\{^1$H$\}$ NMR (162 MHz, CDCl$_3$) δ (ppm): 61.2.

IR (ATR) ν (cm^{-1}): 2976, 1711, 1598, 1499, 1410, 1367, 1289, 1250, 1194, 1153, 1116, 1094, 916, 764.

HRMS (ESI TOF *m/z*) calcd. for C$_{30}$H$_{35}$N$_2$NaO$_6$PS [M+Na]$^+$: 605.1847; Found: 605.1827.

Elemental analysis (%) calcd. for C$_{30}$H$_{35}$N$_2$O$_6$PS: C 61.84; H 6.06; N 4.81; S 5.50; Found: C 61.98, H 6.17, N 4.54, S 5.23.

6.3. Synthesis of 4,4'-(((2-benzylidene-1-methylhydrazineyl)phosphorothioyl)-bis(oxy))dibenzoic acid 162

161
1.0 equiv.

TFA/CH$_2$Cl$_2$

0 ºC to *RT*, 18 h

81%

162
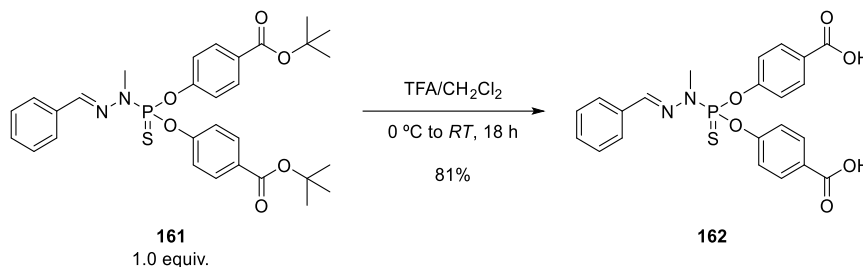
In a Schlenk flask equipped with a magnetic stirring bar, di-*tert*-butyl 4,4'-(((2-benzylidene-1-methylhydrazineyl)phosphorothioyl)bis(oxy))-dibenzoate (**161**) (0.30 g, 0.515 mmol, 1.0 equiv.) was dissolved in CH$_2$Cl$_2$ (2.5 mL), and the mixture cooled down to 0 °C. Later, trifluoroacetic acid (2.6 mL, 2.57 mmol, 1.0 M, 5.0 equiv.) was added dropwise, and the mixture was let to warm up to room temperature while stirring for 18 h. Upon reaction completion, the volatiles were removed under reduced pressure, and the product was washed with EtOAc(2 x 5 mL) affording a colorless solid (0.20 g, 0.418 mmol, 81% yield).
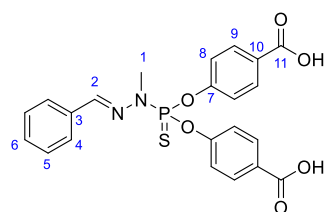
M.p.: 156 – 158 °C.

^{1}H NMR (300 MHz, DMSO-*d$_6$*) δ (ppm): 8.03 – 7.94 (m, 5H, H9, H2), 7.70 – 7.62 (m, 2H, H4), 7.46 – 7.37 (m, 3H, H5, H6), 7.33 (dd, $^3J_{H,H}$ = 8.6 Hz, $^4J_{H,P}$ = 1.5 Hz, 4H, H8), 3.40 (d, $^3J_{H,P}$ = 11.1 Hz, 3H, H1).

^{13}C{^{1}H} NMR (75 MHz, DMSO-*d$_6$*) δ (ppm): 166.5 (C11), 153.5 (d, $^2J_{C,P}$ = 7.0 Hz, C7), 142.1 (d, $^3J_{C,P}$ = 14.4 Hz, C2), 134.5 (C3), 131.4 (C9), 129.6 (C6), 128.8 (C5), 128.1 (d, $^5J_{C,P}$ = 1.7 Hz, C4), 126.9 (C10), 121.0 (d, $^3J_{C,P}$ = 5.1 Hz, C8), 32.9 (d, $^2J_{C,P}$ = 12.3 Hz, C1).

^{31}P{^{1}H} NMR (121 MHz, DMSO-*d$_6$*) δ (ppm): 61.1

IR (ATR) ν (cm^{-1}): 2932, 2658, 2537, 1787, 1686, 1600, 1502, 1421, 1289, 1197, 1154, 955, 913, 768.

HRMS (ESI TOF *m/z*) calcd. for C$_{22}$H$_{19}$N$_2$NaO$_6$PS [M+Na]$^+$: 493.0594; Found: 493.0576.

Elemental analysis (%) calcd. for C$_{22}$H$_{19}$N$_2$O$_6$PS: C 56.17; H 4.07; N 5.95; S 6.81; Found: C 56.63; H 4.82; N 4,67; S 5.40.

7. Synthesis of [Ru(*p*-cymene)Cl₂]₂-based complexes

7.1.   Synthesis of a Ru@Janus dendrimer system

7.1.1. Synthesis of (4-bromophenoxy)(tert-butyl)dimethylsilane 168
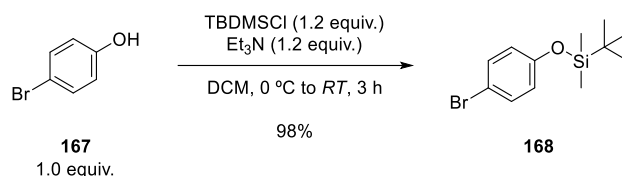
In a Schlenk flask equipped with a magnetic stirring bar, under nitrogen atmosphere, 4-bromophenol (**167**) (1.00 g, 5.78 mmol, 1.0 equiv.) and triethylamine (1.0 mL, 6.65 mmol, 1.2 equiv.) were dissolved in dry CH_2Cl_2 (20 mL) and the mixture was cooled down to 0 °C. *tert*-butylchlorodimethylsilane (1.2 mL, 6.65 mmol, 1.15 equiv.) was added dropwise with vigorous stirring, and the mixture was allowed to warm up to room temperature for 3 h. Upon reaction completion, brine (20 mL) was added. The product was extracted with CH_2Cl_2 (3 x 20 mL) and washed with water (3 x 30 mL). The combined organic layers were collected, dried over anhydrous Na_2SO_4, filtered, and the volatiles removed under reduced pressure. The desired product was purified by running through a silica pad (*n*-hexane 100%) affording the desired product as a colorless oil (1.63 g, 5.67 mmol, 98% yield).

¹H NMR (400 MHz, CDCl₃) δ (ppm): 7.32 (d, $^3J_{H,H}$ = 8.9 Hz, 2H, H3), 6.72 (d, $^3J_{H,H}$ = 8.9 Hz, 2H, H2, 0.97 (s, 9H, H7), 0.18 (s, 6H, H5).

¹³C{¹H} NMR (101 MHz, CDCl₃) δ (ppm): 154.9 (C1), 132.3 (C3), 121.9 (C2), 113.6 (C4), 25.63 (C7), 18.2 (C6), −4.48 (C5).
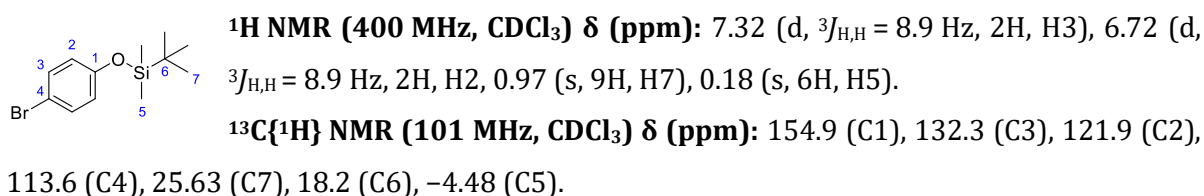
NMR spectra are in accordance with previously reported syntheses.[250]

7.1.2. Synthesis of (4-((*tert*-butyldimethylsilyl)oxy)phenyl)diphenylphosphane 169
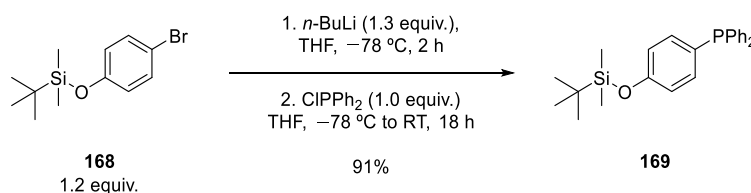
In a Schlenk flask equipped with a magnetic stirring bar, under nitrogen atmosphere, (4-bromophenoxy)(*tert*-butyl)dimethylsilane (**168**) (0.83 g, 2.88 mmol, 1.2 equiv.) was dissolved in dry and degassed THF (15 mL), and the mixture was cooled down to −78 °C. Next, *n*-BuLi (2.0 mL, 3.12 mmol, 1.6 M in *n*-hexane, 1.3 equiv.) was added and the mixture was stirred for 2 h. Chlorodiphenylphosphine (0.4 mL, 2.40 mmol, 1.0 equiv.) was added dropwise, the mixture was stirred at −78 °C for 0.5 h, and then let to warm up to room temperature while stirring for 18 h.

Upon reaction completion, the volatiles were removed under reduced pressure and the product was purified by running through a short silica pad (*n*-hexane 100%). The desired product was obtained as a colorless solid (0.86 g, 2.19 mmol, 91% yield).
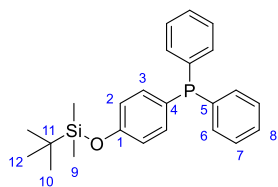
^{1}H NMR (300 MHz, CDCl$_3$) δ (ppm): 7.37 – 7.15 (m, 12H, H3, H6, H7, H8), 6.82 (d, $^3J_{H,H}$ = 8.6, 2H, H2), 0.98 (s, 9H, H12), 0.20 (s, 6H, H9).

^{13}C{^{1}H} NMR (75 MHz, CDCl$_3$) δ (ppm): 156.8 (C1), 138.1 (d, $^1J_{C,P}$ = 10.7 Hz, C5), 135.6 (d, $^2J_{C,P}$ = 21.0 Hz, C3), 133.6 (d, $^2J_{C,P}$ = 19.2 Hz, C6),129.3 (C8), 128.6 (C7), 128.5 (d, $^1J_{C,P}$ = 6.8 Hz, C4), 120.5 (d, $^3J_{C,P}$ = 8.1 Hz, C2), 25.8 (C12), 18.3 (C11), −4.3 (C10).

^{31}P{^{1}H} NMR (121 MHz, CDCl$_3$) δ (ppm): −6.9.

NMR spectra are in accordance with previously reported syntheses.[250]

7.1.3. Synthesis of 4-(diphenylphosphoryl)phenol 170
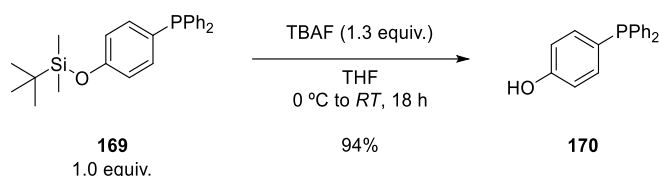
In a Schlenk flask equipped with a magnetic stirring bar, under nitrogen atmosphere, (4-((*tert*-butyldimethylsilyl)oxy)phenyl)diphenylphosphane (**169**) (0.60 g, 1.53 mmol, 1.0 equiv.) was dissolved in dry and degassed THF (15 mL), and the mixture was cooled down to 0 ℃. Next, tetrabutylammonium fluoride (TBAF) (2.0 mL, 1.99 mmol, 1 M in THF, 1.3 equiv.) was added dropwise. The reaction was let to warm up to room temperature while stirring for 18 h. Upon reaction completion, the crude mixture was concentrated to 5 mL, dissolved in Et$_2$O (20 mL), and washed with aqueous solution of NH$_4$Cl (3 x 20 mL) and water (3 x 20 mL). The combined organic layers were collected, dried over anhydrous Na$_2$SO$_4$, filtered, and the product was purified by column chromatography on silica (*n*-hexane/Et$_2$O 4:1) to give a colorless powder (0.40 g, 1.43 mmol, 94% yield).
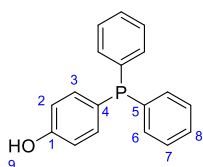
M.p.: 106 – 108 °C.

^{1}H NMR (300 MHz, CDCl$_3$) δ (ppm): 7.29 – 7.12 (m, 12H, H3, H6, H7, H8), 6.74 (d, $^3J_{H,H}$ = 8.2, 2H, H2), 4.91 (s, 1H, H9).

^{13}C{^{1}H} NMR (75 MHz, CDCl$_3$) δ (ppm): 156.5 (C1), 137.9 (d, $^1J_{C,P}$ = 10.3 Hz, C5), 136.0 (d, $^2J_{C,P}$ = 21.0 Hz, C3), 133.6 (d, $^2J_{C,P}$ = 19.1 Hz, C6), 128.7 (C8), 128.6 (d, $^3J_{C,P}$ = 6.8 Hz, C7), 128.0 (d, $^1J_{C,P}$ = 8.1 Hz, C4), 115.9 (d, $^3J_{C,P}$ = 8.1 Hz, C2).

^{31}P{^{1}H} NMR (121 MHz, CDCl$_3$) δ (ppm): −7.0.

NMR spectra are in accordance with previously reported syntheses.[250]

7.1.4. Synthesis of 171-[G₁][G₁]-PEG

143-[G₁][G₁]-PEG
1.0 equiv.

HO———PPh₂
170
(11.0 equiv.)

Cs₂CO₃ (27.5 equiv.)
Na₂SO₄ (27.5 equiv.) 55%
THF, *RT*, 20 h

171-[G₁][G₁]-PEG
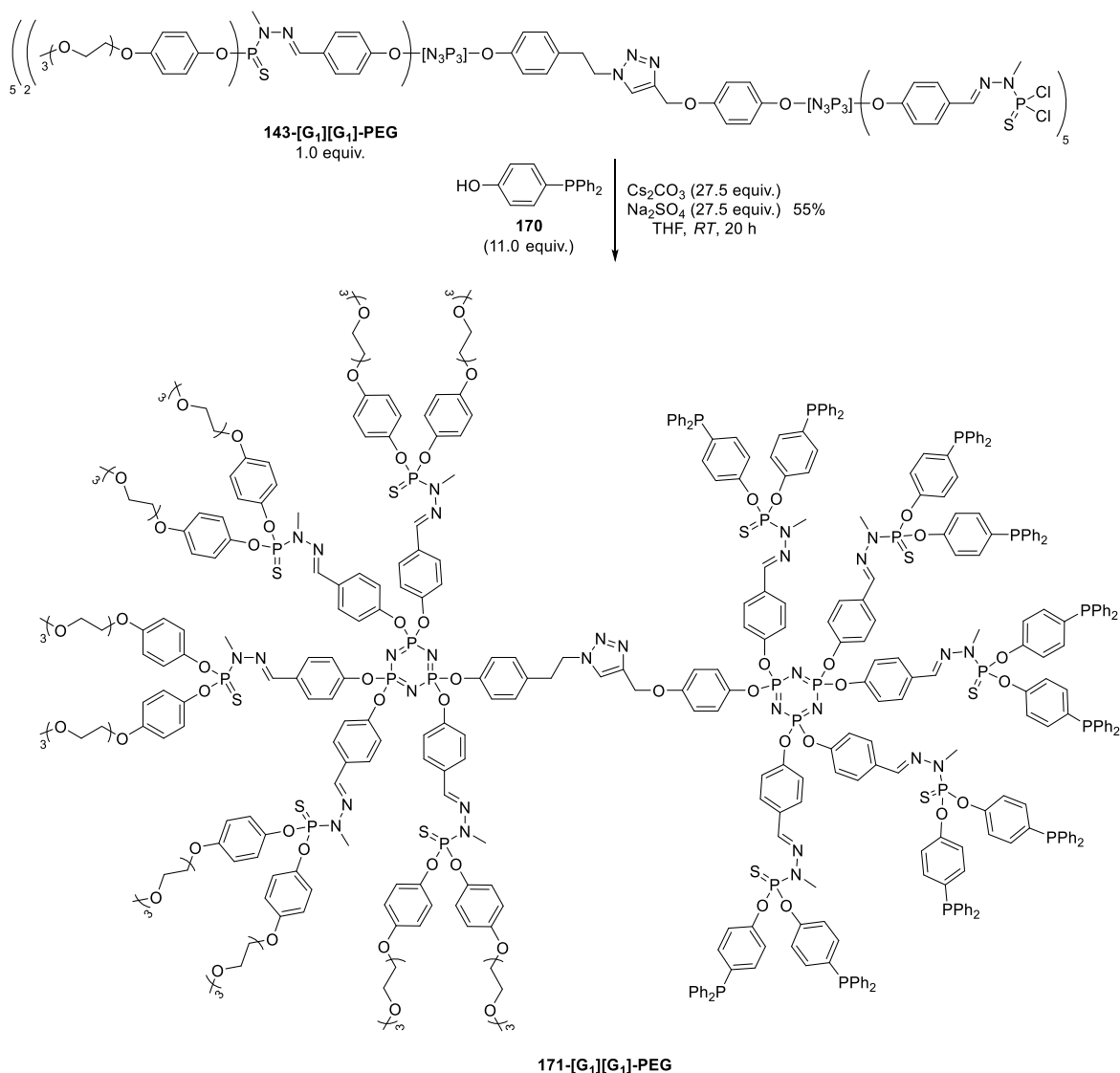
In a Schlenk flask equipped with a magnetic stirring bar, under nitrogen atmosphere, **143-[G₁][G₁]-PEG** dendrimer (93.0 mg, 0.017 mmol, 1.0 equiv.), 4-(diphenylphosphoryl)phenol (**170**) (50.9 mg, 0.183 mmol, 11.0 equiv.), dry cesium carbonate (0.15 g, 0.457 mmol, 27.5 equiv.), and anhydrous Na₂SO₄ (64.9 mg, 0.458 mmol, 27.5 equiv.) were suspended in dry and degassed THF (30 mL), and the mixture was stirred at room temperature overnight. Upon reaction completion (assessed by ^{31}P{^{1}H} NMR), the salts were filtered off by cannula filtration, and the crude was concentrated to 5 mL. The product was precipitated from *n*-pentane, the supernatant was removed, and the product washed with *n*-pentane/Et₂O (4:1) thrice. The volatiles were removed and the product was dried obtaining a colorless powder (73.2 mg, 0.091 mmol, 55% yield).
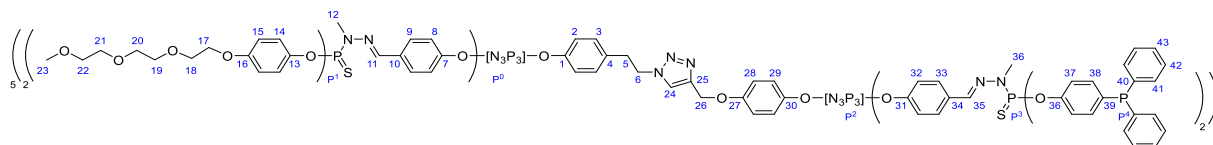
M.p.: 78 – 81 °C.

^{1}H NMR (400 MHz, CDCl$_3$) δ (ppm): 7.65 – 7.52 (m, 26H), 7.50 – 7.41 (m, 15H), 7.27 – 7.09 (m, 118H), 7.07 – 7.01 (m, 24H), 6.97 – 6.88 (m, 16H), 6.78 – 6.73 (m, 20H, H37), 4.88 (s, 2H, H26), 4.32 (m 2H, H5), 4.03 – 3.96 (m, 20H, H17), 3.81 – 3.73 (m, 20H, H19), 3.70 – 3.56 (m, 60H, H18, H20, H21), 3.55 – 3.46 (m, 20H, H19), 3.36 – 3.30 (m, 30H, H23), 3.29 – 3.17 (m, 32H, H6, H12, H36). The signal of one secondary carbon was not detected due to overlapping.

^{13}C{^{1}H} NMR (101 MHz, CDCl$_3$) δ (ppm): 157.0 (C13), 156.4 (C31), 137.0 (d, $^1J_{C,P}$ = 10.7 Hz, C40), 135.2 (2 x d, $^2J_{C,P}$ = 20.5 Hz, C38), 133.8 (2 x d, $^2J_{C,P}$ = 19.7 Hz, C41), 129.0 (C43), 128.8 (d, $^3J_{C,P}$ = 7.1 Hz, C42), 128.3 (m, C39), 122.7 – 122.2 (m, C15), 121.8 – 121.3 (m, C32), 115.5 – 115.3 (m, C37), 72.1 (C22) 70.9 (C19), 70.8 (C20), 70.7 (C21), 69.8 (C18), 67.9 (C17), 59.2 (C23). Only the signals from the dendrimer branches can be detected due to the low concentration and poor solubility of the compound in deuterated solvents.

^{31}P{^{1}H} NMR (162 MHz, CDCl$_3$) δ (ppm): 64.5 (s, P^1), 61.5 (s, P^3), 61.1 (s, P^3), 8.7 –8.1 (m, P^0, P^2), −6.6 (s, P^4).

IR (ATR) ν (cm^{-1}): 2872, 1586, 1500, 1434, 1247, 1160, 1095, 913, 832, 781, 742, 695.

7.1.5. Synthesis of 173-Ru@[G₁][G₁]-PEG

171-[G₁][G₁]-PEG
1.0 equiv.

[Ru(*p*-cymene)Cl₂]₂
(5.0 equiv.)   THF, *RT*, 15 h   84%

173-Ru@[G₁][G₁]-PEG
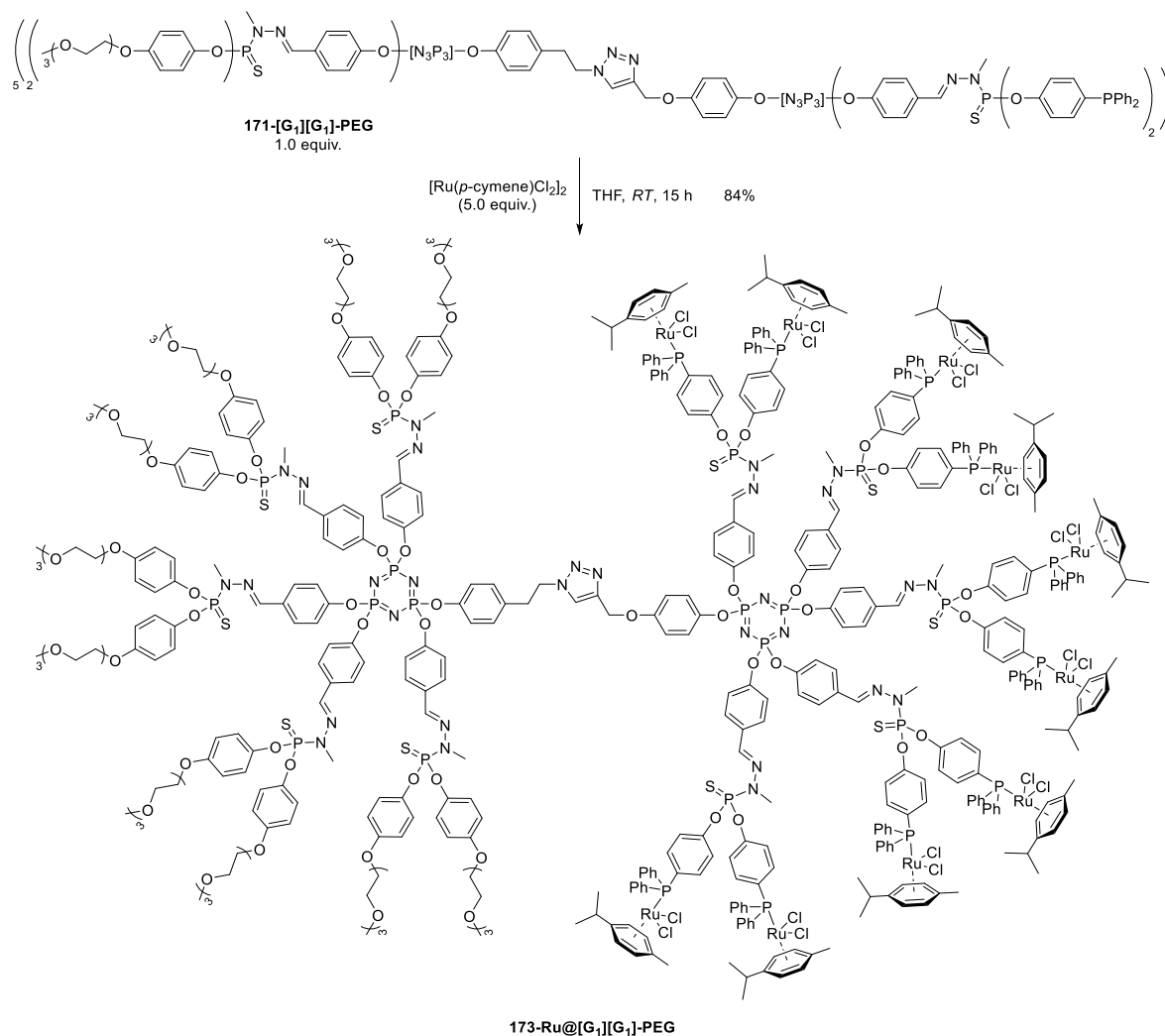
In a Schlenk flask equipped with a magnetic stirring bar, under nitrogen atmosphere, **171-[G₁][G₁]-PEG** dendrimer (63.3 mg, 0.008 mmol, 1.0 equiv.) and Ru[(*p*-cymene)Cl₂]₂ (24.2 mg, 0.034 mmol, 5.0 equiv.) were dissolved in dry THF (10 mL), and the mixture was stirred at room temperature overnight. The evolution of the reaction was monitored by ³¹P{¹H} NMR. Upon reaction completion, the solution was concentrated to 5 mL and the product was precipitated from *n*-pentane. The product was washed thrice with *n*-pentane/CH₂Cl₂ (4:1) to give a dark orange solid (73.2 mg, 0.007 mmol, 84% yield).
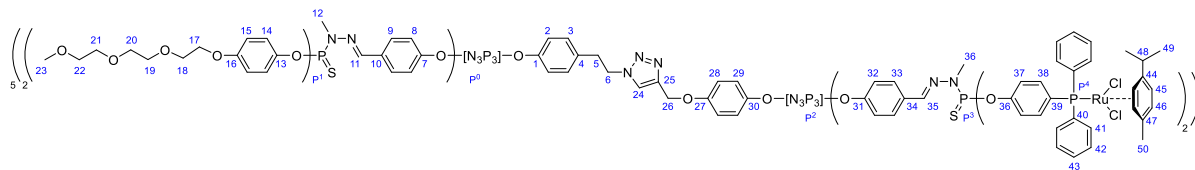
M.p.: 113 –117 °C.

¹H NMR (400 MHz, CDCl₃) δ (ppm): 7.88 – 7.64 (m, 41H), 7.40 – 7.26 (m, 118H), 7.12 – 6.99 (m, 42H), 6.85 – 6.70 (m, 20H), 5.20 (d, $^3J_{H,H}$ = 6.0 Hz, 20H, H45), 4.96 (d, $^3J_{H,H}$ = 6.0 Hz, 20H, H46),

4.09 – 3.93 (m, 20H, H17), 3.83 – 3.72 (m, 20H, H19), 3.72 – 3.56 (m, 60H, H18, H20, H21), 3.56 – 3.47 (m, 20H, H19), 3.34 (s, 30H, H23), 3.28 – 3.16 (m, 32H, H6, H12, H36), 2.33 – 2.18 (m, 10H, H48), 1.85 (s, 30H, H50), 1.11 (d, $^3J_{H,H}$ = 7.0 Hz, 60H, H15).

^{13}C{^{1}H} NMR (101 MHz, CDCl$_3$) δ (ppm): 134.3 (d, $^2J_{C,P}$ = 9.2 Hz, C41), 130.2 (C43), 128.0 (d, $^3J_{C,P}$ = 9.8 Hz, C42), 122.4 (C15), 115.4 (C37), 96.2 (C47), 87.3 (C45), 72.1 (C22) 70.9 (C19), 70.8 (C20), 70.7 (C21), 69.8 (C18), 67.9 (C17), 59.2 (C23), 29.9 (C48), 22.1 (C49), 17.9 (C50). Only the signals from the dendrimer branches can be detected due to the low concentration and poor solubility of the compound in deuterated solvents.

^{31}P{^{1}H} NMR (162 MHz, CDCl$_3$) δ (ppm): 64.6 (s, P^1), 61.0 (br s, P^3), 24.0 (d, $^1J_{P,Ru}$ = 37.2 Hz, P^4), 9.0 – 7.7 (m, P^0, P^2).

IR (ATR) ν (cm^{-1}): 2922, 1768, 1587, 1499, 1435, 1247, 1161, 1093, 1030, 941, 835, 796, 695.

Elemental analysis (%) calcd. for C$_{507}$H$_{565}$Cl$_{20}$N$_{29}$O$_{73}$P$_{26}$Ru$_{10}$S$_{10}$: C 54.97; H 5.14; N 2.67; S 2.89; Found: C 54.37; H 5.50; N 2.69; S 2.24.

ICP-OES (%) calc. for C$_{507}$H$_{565}$Cl$_{20}$N$_{29}$O$_{73}$P$_{26}$Ru$_{10}$S$_{10}$: Ru 9.12; Found: Ru 9.1.

7.2. Synthesis of monometallic and bimetallic Ru(*p*-cymene) derivatives

7.2.1. Synthesis of diphenyl(4-methoxyphenyl)phosphine 175
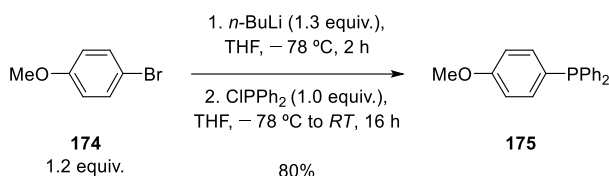
In a Schlenk flask equipped with a magnetic stirring bar, under nitrogen atmosphere, 4-bromoanisole (**174**) (0.78 g, 4.15 mmol, 1.2 equiv.) was dissolved in dry and degassed THF (25 mL), and the mixture was cooled down to −78 °C. Next, *n*-BuLi (2.8 mL, 4.49 mmol, 1.6 M in *n*-hexane,1.3 equiv.) was added and the mixture stirred for 0.5 h. Chlorodiphenylphosphine (0.62 mL, 3.46 mmol, 1.0 equiv.) was added dropwise and the mixture stirred at −78 °C for 0.5 h, and then let to warm up to room temperature while stirring overnight. Upon reaction completion, the volatiles were removed under reduced pressure and the product was purified by column chromatography (*n*-hexane 100%). The fractions containing the product were collected and the volatiles removed *in vacuo* to afford a colorless powder (0.81 g, 2.77 mmol, 80% yield).
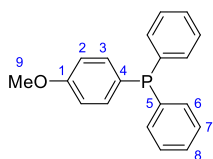
M.p.: 64 – 65 °C.

^{1}H NMR (300 MHz, CDCl$_3$) δ (ppm): 7.44 – 7.33 (m, 12H, H3, H6, H7, H8), 6.97 (dd, $^3J_{H,H}$ = 8.9 Hz, $^4J_{H,P}$ = 0.9 Hz, 2H, H2), 3.85 (s, 3H, H9).

^{13}C{^{1}H} NMR (75 MHz, CDCl$_3$) δ (ppm): 160.5 (C1), 138.0 (d, $^1J_{C,P}$ = 10.7 Hz, C5), 135.7 (d, $^2J_{C,P}$ = 21.5 Hz, C3), 133.5 (d, $^3J_{C,P}$ = 19.2 Hz, C6), 128.5 (C8), 128.4 (C7), 127.7 (d, $^1J_{C,P}$ = 8.2 Hz, C4), 114.3 (d, $^3J_{C,P}$ = 8.1 Hz, C2), 55.2 (C9).

^{31}P{^{1}H} **NMR (121 MHz, CDCl$_3$) δ (ppm):** −7.0.

NMR spectra are in accordance with previously reported syntheses.[253]

7.2.2. Synthesis of Ru43
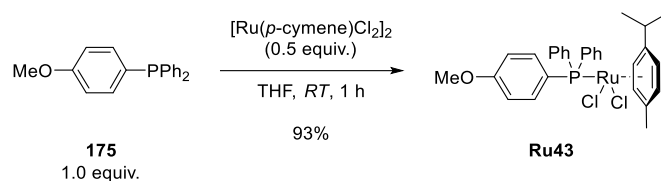
In a Schlenk flask equipped with a magnetic stirring bar, under nitrogen atmosphere, diphenyl(4-methoxyphenyl)phosphine (**175**) (0.29 g, 0.98 mmol, 1.0 equiv.) and Ru[(*p*-cymene)Cl$_2$]$_2$ (0.30 g, 0.49 mmol, 0.5 equiv.) were dissolved in dry THF (10 mL), and the mixture stirred at room temperature until the formation of a precipitate (1 h). The supernatant was removed by cannula filtration, and the residue washed with *n*-hexane (10 mL) twice. The desired product was obtained as an orange powder (0.27 g, 0.46 mmol, 93% yield).
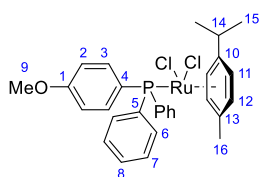
M.p. > 230 °C.

^{1}H NMR (300 MHz, CDCl$_3$) δ (ppm): 7.87 – 7.71 (m, 6H), 7.43 – 7.30 (m, 6H), 6.86 (dd, $^3J_{H,H}$ = 7.3 Hz, $^4J_{H,P}$ = 1.8 Hz 2H, H2), 5.20 (d, $^3J_{H,H}$ = 6.0 Hz, 2H, H11), 4.97 (d, $^3J_{H,H}$ = 5.6 Hz, 2H, H12), 3.80 (s, 3H, H9), 2.86 (sept, $^3J_{H,H}$ = 6.9 Hz, 1H, H14), 1.86 (s, 3H, H16), 1.10 (d, $^3J_{H,H}$ = 6.9 Hz, 6H, H15).

^{13}C{^{1}H} NMR (75 MHz, CDCl$_3$) δ (ppm): 161.2 (d, $^4J_{C,P}$ = 2.3 Hz, C1), 136.5 (d, $^2J_{C,P}$ = 11.1 Hz, C3), 134.7 (d, $^1J_{C,P}$ = 45.8 Hz, C5),134.2 (d, $^2J_{C,P}$ = 9.3 Hz, C6), 130.2 (d, $^4J_{C,P}$ = 2.6 Hz, C8), 128.1 (d, $^3J_{C,P}$ = 9.9 Hz, C7), 123.9 (d, $^1J_{C,P}$ = 50.5 Hz, C4), 113.7 (d, $^3J_{C,P}$ = 11.0 Hz, C2), 111.2 (d, $^3J_{C,P}$ = 3.5 Hz, C10), 96.0 (C13), 89.1 (d, $^4J_{C,P}$ = 3.2 Hz, C12), 87.3 (d, $^4J_{C,P}$ = 5.6 Hz, C11), 55.4 (C9), 30.4 (C14), 22.0 (C15), 17.9 (C16).

^{31}P{^{1}H} NMR (121 MHz, CDCl$_3$) δ (ppm): 23.2.

IR (ATR) ν (cm^{-1}): 3051, 2972, 1735, 1593, 1568, 1497, 1479, 1460, 1434, 1380, 1305, 1288, 1254, 1181, 1161, 1092, 1060, 1020, 829, 801, 755, 697.

HRMS (ESI TOF *m/z*) calcd. for C$_{29}$H$_{31}$ClOPRu [M-Cl]$^+$: 563.0917; Found: 563.0846.

Elemental analysis (%) calcd. for C$_{29}$H$_{31}$Cl$_2$OPRu: C: 58.20; H 5.22; Found: C 58.65; H 5.05.

7.2.3. Synthesis of *O,O*-bis(4-(diphenylphosphanyl)phenyl)(2-benzylidene-1-me-thylhydrazineyl)phosphonothioate 176
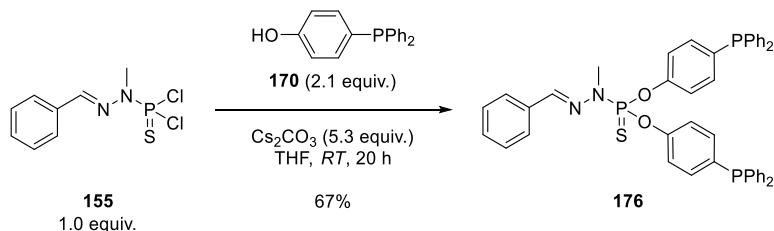
In a Schlenk flask equipped with a magnetic stirring bar, under nitrogen atmosphere, (2-benzylidene-1-methylhydrazineyl)phosphonothioic dichloride (**155**) (0.20 g, 0.749 mmol, 1.0 equiv.), 4-(diphenylphosphoryl)phenol (**170**) (0.44 g, 1.57 mmol, 2.1 equiv.), and cesium carbonate (1.28 g, 3.93 mmol, 5.3 equiv.) were suspended in dry and degassed THF (20 mL), and the mixture was stirred at room temperature overnight. Upon reaction completion (followed by $^{31}P\{^1H\}$ NMR), the salts were filtered off with cannula, the volatiles removed under reduced pressure, and the product purified by column chromatography on silica (*n*-hexane/EtOAc 8:2 to 1:1). The fractions containing the product were collected and dried *in vacuo* affording a colorless powder (0.38 g, 0.50 mmol, 67% yield).
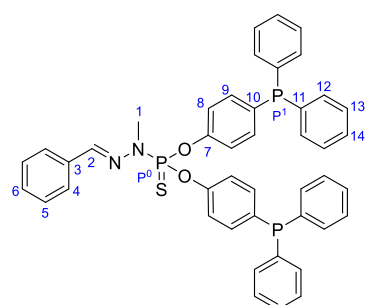
^{1}H NMR (400 MHz, CDCl$_3$) δ (ppm): 7.80 – 7.70 (m, 3H, H2, H4), 7.49 – 7.27 (m, 30H, H5, H6, H10, H11, H14, H15), 3.47 (d, $^3J_{H,P}$ = 10.7 Hz, 3H, H1).

^{13}C{^{1}H} NMR (101 MHz, CDCl$_3$) δ (ppm): 151.4 (d, $^2J_{C,P}$ = 7.5 Hz, C7), 140.0 (d, $^3J_{C,P}$ = 13.7 Hz, C11), 137.2 (d, $^1J_{C,P}$ = 10.7 Hz, C12), 135.2 (dd, $J_{C,P}$ = 20.4, 1.5 Hz, C9), 134.9 (C2), 134.1 (d, $^4J_{C,P}$ = 2.2 Hz, C14), 133.8 (dd, $^1J_{C,P}$ = 19.6, 1.7 Hz, C10), 129.7 (C3), 129.0 (C6), 128.9 (C4), 128.7 (d, $^3J_{C,P}$ = 6.9 Hz, C13), 127.2 (C5), 121.7 (dd, $^3J_{C,P}$ = 7.3, 4.9 Hz, C8), 33.1 (d, $^2J_{C,P}$ = 13.3 Hz, C1).

^{31}P{^{1}H} NMR (162 MHz, CDCl$_3$) δ (ppm): 61.5 (P^0), −6.4 (P^1).

7.2.4. Synthesis of Ru44
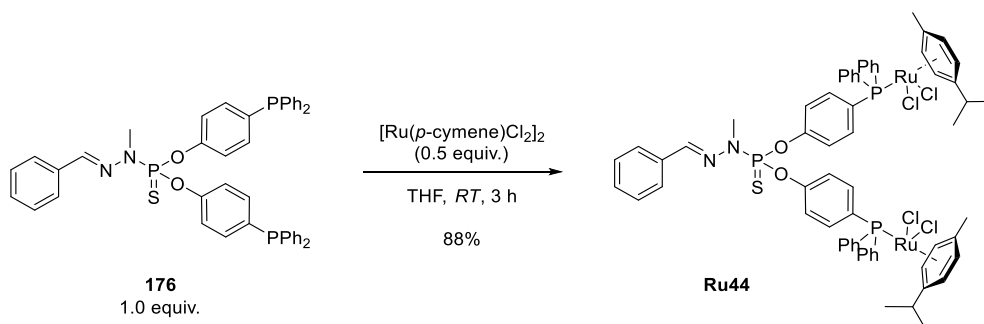
In a Schlenk flask equipped with a magnetic stirring bar, under nitrogen atmosphere, *O,O*-bis(4-(diphenylphosphanyl)phenyl)(2-benzylidene-1-methylhydrazineyl)phosphonothioate **(176)** (0.17 g, 0.22 mmol, 1.0 equiv.) and [Ru(*p*-cymene)Cl$_2$]$_2$ (68.1 mg, 0.11 mmol, 0.5 equiv.) were added to dry and degassed THF (10 mL), and the mixture was stirred at room temperature for 3 h. Upon reaction completion (followed by ^{31}P{^{1}H} NMR), the volatiles were removed under reduced pressure and the crude was purified by column chromatography on silica (EtOAc 100%), affording the desired product as a dark orange powder (0.27 g, 0.20 mmol, 88% yield).
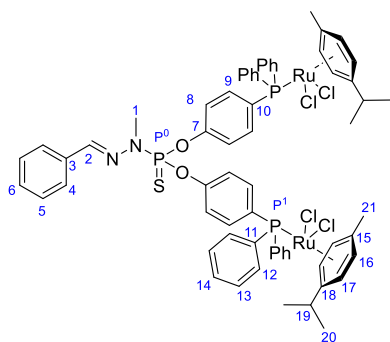
M.p.: 119 – 121 °C.

^{1}H NMR (400 MHz, CDCl$_3$) δ (ppm): 7.81 – 7.73 (m, 12H), 7.66 – 7.59 (m, 3H), 7.41 – 7.30 (m, 15H), 7.17 (d, $^3J_{H,H}$ = 8.6 Hz, 4H, H8), 5.17 (d, $^3J_{H,H}$ = 5.2 Hz, 4H, H17), 4.96 (d, $^3J_{H,H}$ = 5.2 Hz, 4H, H16), 3.34 (d, $^2J_{H,P}$ = 10.7 Hz, 3H, H1), 2.80 (sept, $^3J_{H,H}$ = 6.9 Hz, 2H, H19), 1.82 (s, 6H, H21), 1.07 (d, $^3J_{H,H}$ = 6.9 Hz, 12H, H20).

^{13}C{^{1}H} NMR (101 MHz, CDCl$_3$) δ (ppm): 152.2 (dd, $^2J_{C,P}$ = 7.3 Hz, $^4J_{C,P}$ = 2.5 Hz, C7), 140.3 (d, $^1J_{C,P}$ = 14.1 Hz, C11), 135.9 (d, $^2J_{C,P}$ = 10.3 Hz, C12), 134.6 (s, C2) 134.3 (d, $^2J_{C,P}$ = 9.5 Hz, C9), 133.9 (C14), 1335 (C3), 130.4 (C6), 130.0 (C4), 128.8 (C13), 128.1 (d, $^1J_{C,P}$ = 9.7 Hz, C10), 127.1 (C5), 120.78 (dd, $^3J_{C,P}$ = 10.8, 5.0 Hz, C8), 111.2 (d, $J_{C,P}$ = 3.3 Hz, C18), 96.1 (C15), 89.1 (m, C16), 87.2 (d, $J_{C,P}$ = 5.5 Hz, C17), 53.5 (C1), 30.3 (C19), 21.9 (C20), 17.8 (C21).

^{31}P{^{1}H} NMR (162 MHz, CDCl$_3$) δ (ppm): 60.6 (P^0), 23.7 (P^1).

IR (ATR) v (cm^{-1}): 3653, 3051, 2961, 1588, 1485, 1436,1377, 1205, 1166, 1093, 1019, 912, 840, 795, 770, 695.

HRMS (ESI TOF m/z) calcd. for C$_{64}$H$_{65}$Cl$_4$N$_2$NaO$_2$P$_3$Ru$_2$S [M+Na]$^+$: 1385.0821; Found: 1385.0717.

Elemental analysis (%) calcd. for C$_{64}$H$_{65}$Cl$_4$N$_2$O$_2$P$_3$Ru$_2$S: C 56.39; H 4.81; N 2.06; S 2.05; Found: C 56.04; H 4.61; N 1.59; S 1.89.

7.3. Activity of [Ru(*p*-cymene)Cl₂]₂ derivatives in the isomerization of 1-octen-3-ol to 3-octanone
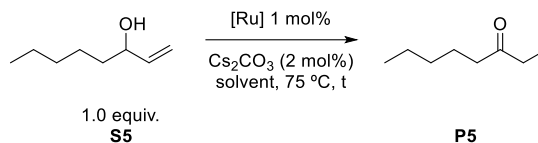
To a solution of 1-octen-3-ol (0.2 mL, 1.29 mmol, 1.0 equiv.), Cs₂CO₃ (8.44 mg, 0.026 mmol, 2 mol%) and 1,3,5-trimethoxybenzene (108 mg, 0.640 mmol, 0.5 equiv., used as an internal standard) in an appropriate solvent (THF or *n*-heptane/water 1:1 mixture, 6 mL) heated up at 75 °C, 1 mol% of "ruthenium"(0.013 mmol) was added in one portion in a nitrogen flow.

The resulting mixture was vigorously stirred under given conditions and the selected solvent for 24 h. Aliquots (0.5 mL) were taken at selected times and the conversion of the substrate was determined by GC.

Table 11. Time (in hours) for the isomerization of 1-octen-3-ol to 3-octanone to reach full conversion under the given conditions.

Entry	[Ru]	Solvent	Time to full conversion [h][a]
1	**Ru43** – monometallic		3
2	**Ru44** – bimetallic	THF	1.5
3	**173-Ru@[G₁][G₁]-PEG**		1.5
4	**Ru43** – monometallic		—
5	**Ru44** – bimetallic	*n*-heptane/water	—
6	**173-Ru@[G₁][G₁]-PEG**		24

[a] Conversion was determined by GC using 1,3,5-trimethoxybenzene as internal standard

For the recyclability tests, reaction was performed for 24 h. Upon reaction time, stirring was stopped observing the formation of two layers. The organic layer was recovered and analyzed by GC to assess conversion. Then, fresh *n*-heptane (3.0 mL) and 1-octen-3-ol (0.2 mL, 1.29 mmol, 1.0 equiv.) were added to the remaining aqueous phase.

References

[1]   Caminade, A.-M.; Turrin, C.-O.; Laurent, R.; Ouali, A.; Delavaux-Nicot, B. *Dendrimers: Towards Catalytic, Material and Biomedical Uses*, 1st ed.; John Wiley & Sons Ltd., 2011.

[2]   Wu, L. P.; Ficker, M.; Christensen, J. B.; Trohopoulos, P. N.; Moghimi, S. M. Dendrimers in Medicine: Therapeutic Concepts and Pharmaceutical Challenges. *Bioconjug. Chem.,* **2015**, *26*, 1198–1211.

[3]   Tomalia, D. A.; Baker, H.; Dewald, J.; Hall, M.; Kallos, G.; Martin, S.; Roeck, J.; Ryder, J.; Smith, P. A New Class of Polymers: Starburst-Dendritic. *Polym. J.,* **1985**, *17*, 117–132.

[4]   Buhleier, E.; Wehner, W.; Vötgle, F. "Cascade"- and "Nonskid-Chain-like" Syntheses of Molecular Cavity Topologies. *Synthesis* **1978**, *2*, 155–158.

[5]   Vötgle, F.; Weber, E. Octopus Molecules. *Angew. Chem. Int. Ed.,* **1974**, *13*, 814-816.

[6]   Abbasi, E.; Aval, S. F.; Akbarzadeh, A.; Milani, M.; Nasrabadi, H. T.; Woo Joo, S.; Hanifehpour, Y.; Nejati-Koshki, K.; Pashaei-Asl, R. Dendrimers: Synthesis, Applications, and Properties. *Nanoscale Res. Lett.,* **2014**, *9*, 247–257.

[7]   Bondareva, J. *Sulfonimide-Based Dendrimers: Synthesis and Application for Surface Functionalization*. PhD Thesis. Skolkovo Institute of Science and Technology, Moscow, 2020.

[8]   Feuerbacher, N.; Vötgle, F. Iterative Synthesis in Organic Chemistry. In *Dendrimers. Topics in Current Chemistry*; Springer: Berlin, Ed.; Heidelberg, 1998; pp 1–18.

[9]   Hawker, C.; Fréchet, J. M. J. A New Convergent Approach to Monodisperse Dendritic Macromolecules. *J. Chem. Soc. Chem. Commun.,* **1990**, *15*, 1010–1013.

[10] Kawaguchi, T.; Moore, J. S.; Walker, K. L.; Wilkins, C. L. Double Exponential Dendrimer Growth. *J. Am. Chem. Soc.,* **1995**, *117*, 2159–2165.

[11] Sharma, R.; Naresh, K.; Chabre, Y. M.; Rej, R.; Saadeh, N. K.; Roy, R. "Onion peel" dendrimers: a straightforward synthetic approach towards highly diversified architectures. *Polym. Chem.,* **2014**, *5*, 4321–4331.

[12] Barany, G.; Merrifield, R. B. A New Amino Protecting Group Removable by Reduction. Chemistry of the Dithiasuccinoyl (Dts) Function. *J. Am. Chem. Soc.,* **1997**, *99*, 7363–7365.

[13] Tomalia, D. A. Starburst Dendrimers - Nanoscopic Supermolecules According To Dendritic Rules And Principles. *Macromol. Symp.,* **1996**, *255*, 243–255.

[14] de Brabander-van den Berg, E. M. M.; Meijer, E. W. Poly(Propylenimine) Dendrimers: Large-Scale Synthesis via Heterogeneously Catalyzed Hydrogenation. *Angew. Chem. Int. Ed.,* **1993**, *32*, 1308–1311.

[15] de Brabander-van den Berg, E. M. M.; Nijenhuis, A.; Mure, M.; Keulen, J.; Reintjens, R.; Vandenbooren, F.; Bosnian, B.; De Raat, R.; Frijns, T.; Wal, S. v.D.; Castelijns, M.; Put, J.; Meijer, E. W. Large-Scale Production of Polypropylenimine Dendrimers. *Macromol. Symp.,* **1994**, *77*, 51–62.

[16] Zhao, C.; Wang, Y.; Su, Y.; Zhang, H.; Ding, L.; Yan, X.; Zhao, D.; Shao, N.; Ye, X.; Cheng, Y. Inclusion Complexes of Isoflavones with Two Commercially Available Dendrimers: Solubility, Stability, Structures, Release Behaviors, Cytotoxicity, and Anti-Oxidant Activities. *Int. J. Pharm.,* **2011**, *421*, 301–309.

[17] Tomalia, D. A.; Naylor, A. M.; Goddard, William, A. Starburst Dendrimers: Molecular-Level Control of Size, Shape, Surface Chemistry, Topology, and Flexibility from Atoms to Macroscopic Matter. *Angew. Chem. Int. Ed.,* **1990**, *29*, 138–175.

[18] Gupta, V.; Nayak, S. K. Dendrimers: A Review on Synthetic Approaches. *J. Appl. Pharm. Sci.,* **2015**, *5*, 117–122.

[19] Carnahan, M. A.; Grinstaff, M. W. Synthesis and Characterization of Polyether-Ester Dendrimers from Glycerol and Lactic Acid. *J. Am. Chem. Soc.,* **2001**, *123*, 2905–2906.

[20] Carnahan, M. A.; Grinstaff, M. W. Synthesis and Characterization of Poly(Glycerol-Succinic Acid) Dendrimers. *Macromolecules* **2001**, *34*, 7648–7655.

[21] Newkome, G. R.; Yao, Z.; Baker, G. R.; Gupta, V. K. Cascade Molecules: A New Approach to Micelles. A [27]-Arborol. *J. Org. Chem.,* **1984**, *50*, 2003–2004.

[22] Newkome, G. R.; Lin, X. Symmetrical, Four-Directional, Poly(Ether-Amide) Cascade Polymers. *Macromolecules* **1991**, *24*, 1443–1444.

[23] Padias, A. B.; Hall, H. K. Starburst Polyether Dendrimers. *J. Org. Chem.,* **1987**, *52*, 5305–5312.

[24] Hawker, C. J.; Lee, R. One-Step Synthesis of Hyperbranched Dendritic Polyesters. *J. Am. Chem. Soc.,* **1991**, *133*, 4583–4588.

[25] Ihre, H.; Hult, A.; So, E. Synthesis, Characterization, and ^{1}H NMR Self-Diffusion Studies of Dendritic Aliphatic Polyesters Based on 2,2-Bis(Hydroxymethyl)Propionic Acid and 1,1,1-Tris(Hydroxyphenyl)Ethane. *J. Am. Chem. Soc.,* **1996**, *15*, 6388–6395.

[26] Majoral, J.-P.; Caminade, A.-M. Dendrimers Containing Heteroatoms (Si, P, B, Ge, or Bi). *Chem. Rev.,* **1999**, *99*, 845–880.

[27] Rebrov, E. A.; Muzafarov, A. M.; Papkov, V. S.; Zhadanov, A. A. Space-Network Polyorganosiloxanes. *Doklady Akademii Nauk SSSR* **1989**, *309*, 376–380.

[28] van der Made, A. W. Van Der; Piet, W. Silane Dendrimers. *J. Chem. Soc., Chem. Commun.,* **1992**, *19*, 1400–1401.

[29] van der Made, A. W.; van Leeuwen, P. W. N. M.; de Wilde, J. C.; Brandes, R. A. C. Dendrimeric Silanes. *Adv. Mater.,* **1993**, *5*, 466–468.

[30] Zhou, L.-L.; Hoovers, J. Synthesis of Novel Carbosilane Dendritic Macromolecules. *Macromolecules* **1993**, *26*, 963–968.

[31] Bonds, S.; Seyferth, D.; Son, D. Y.; Rheingold, A. L.; Ostrander, R. L. Synthesis of an Organosilicon Dendrimer Containing 324 Si-H Bonds. *Organometallics* **1994**, *13*, 2682–2690.

[32] Knapen, J. W. J.; van der Made, A. W.; de Wilde, J. C.; van Leeuwen, P. W. N. M.; Wijkens, P.; Grove, D. M.; van Koten, G. Homogeneous Catalysts Based on Silane Dendrimers Functionalized with Arylnickel(II) Complexes. *Nature* **1994**, *372*, 659–663.

[33] Rengan, K.; Engel, R. Phosphonium Cascade Molecules. *J. Chem. Soc., Chem. Commun.,* **1990**, 1084–1085.

[34] Launay, N.; Caminade, A.-M.; Majoral, J.-P. Synthesis of Bowl-Shaped Dendrimers from Generation 1 to Generation 8. *J. Organomet. Chem.,* **1997**, *529*, 1589–1592.

[35] Launay, N.; Caminade, A.-M.; Majoral, J.-P. Synthesis and Reactivity of Unusual Phosphorus Dendrimers. A Useful Divergent Growth Approach Up to the Seventh Generation. *J. Am. Chem. Soc.,* **1995**, *117*, 3282–3283.

[36] Larré, C.; Bressolles, D.; Turrin, C.-O.; Donnadieu, B.; Caminade, A.-M.; Majoral, J.-P. Chemistry within Megamolecules: Regiospecific Functionalization after Construction of Phosphorus Dendrimers. *J. Am. Chem. Soc.,* **1998**, *120*, 13070–13082.

[37] Launay, N.; Caminade, A.-M.; Lahana, R.; Majoral, J.-P. A General Synthetic Strategy for Neutral Phosphorus-Containing Dendrimers. *Angew. Chem. Int. Ed.,* **1994**, *33*, 1589–1592.

[38] Slany, M.; Bardají, M.; Casanove, M.-J.; Caminade, A.-M.; Majoral, J.-P.; Chaudret, B. Dendrimer Surface Chemistry. Facile Route to Polyphosphines and Their Gold Complexes. *J. Am. Chem. Soc.,* **1995**, *8*, 9764–9765.

[39] Caminade, A.-M.; Laurent, R.; Turrin, C.-O.; Rebout, C.; Delavaux-Nicot, B.; Ouali, A.; Zablocka, M.; Majoral, J.-P. Phosphorus Dendrimers as Viewed by ^{31}P NMR Spectroscopy; Synthesis and Characterization. *C. R. Chim.,* **2010**, *13*, 1006–1027.

[40] Caminade, A.-M.; Laurent, R. Homogeneous Catalysis with Phosphorus Dendrimer Complexes. *Coord. Chem. Rev.,* **2019**, *389*, 59–72.

[41] Majoral, J.-P.; Caminade, A.-M. Biological Properties of Phosphorus Dendrimers. *New J. Chem.,* **2010**, *34*, 1512–1524.

[42] Mignani, S.; Shi, X.; Ceña, V.; Shcharbin, D.; Bryszewska, M.; Majoral, J.-P. In Vivo Therapeutic Applications of Phosphorus Dendrimers : State of the Art. *Drug Discov. Today* **2021**, *26*, 677–689.

[43] Caminade, A.-M. Phosphorus Dendrimers for Nanomedicine. *Chem. Commun.,* **2017**, *53*, 9830–9838.

[44] Batteries, S.; Bhattacharya, P.; Lu, D.; Tang, Z.; Tran, N. Q.; Nguyen, C. K.; Nguyen, T. P. Dendrimer Applications for Cancer Therapies Dendrimer Applications for Cancer Therapies. *J. Phys. Conf. Ser.,* **2021**, 1948–1957.

[45] Brahmi, N. El; Mignani, S. M.; Caron, J.; Kazzouli, S. El; Bousmina, M. M.; Caminade, A.-M.; Cresteil, T.; Majoral, J.-P. Investigations on Dendrimer Space Reveal Solid and Liquid Tumor Growth-Inhibition by Original Phosphorus-Based Dendrimers and the Corresponding Monomers and Dendrons with Ethacrynic Acid Motifs. *Nanoscale* **2015**, 3915–3922.

[46] Rolland, O.; Turrin, C.-O.; Caminade, A.-M.; Majoral, J.-P. Dendrimers and Nanomedicine: Multivalency in Action. *New J. Chem.,* **2009**, *33*, 1809–1824.

[47] Poupot, M.; Ouali, A.; Caminade, A.-M. The Key Role of the Scaffold on the Efficiency of Dendrimer Nanodrugs. *Nat. Commun.,* **2015**, *6*, 7722–7733.

[48] Apartsin, E.; Caminade, A.-M. Single-Component Physical Hydrogels of Dendritic Molecules. *J. Compos. Sci.,* **2023**, *7*, 26–45.

[49] Caminade, A.-M.; Majoral, J.-P. Phosphorus Dendrimers for the Controlled Elaboration of Organic–Inorganic Materials. *J. Mater. Chem.,* **2005**, *15*, 3643–3649.

[50] Leclaire, J.; Dagiral, R.; Fery-Forgues, S.; Coppel, Y.; Donnadieu, B.; Caminade, A.-M.; Majoral, J.-P. Octasubstituted Metal-Free Phthalocyanine as Core of Phosphorus Dendrimers: A Probe for the Properties of the Internal Structure. *J. Am. Chem. Soc.,* **2005**, *127*, 15762–15770.

[51] Vidal, L.; Aissa, A. Ben; Salabert, J.; Jara, J. J.; Vallribera, A.; Pividori, M. I., Sebastián, R. M. Biotinylated Phosphorus Dendrimers as Control Line in Nucleic Acid Lateral Flow Tests. *Biomacromolecules* **2020**, *21*, 1315–1323.

[52] Lloveras, V.; Vidal-Gancedo, J. Polyphosphorhydrazone-Based Radical Dendrimers. *Molecules* **2021**, *26*, 1230–1239.

[53] Loup, C.; Zanta, M.; Caminade, A.-M.; Majoral, J.-P. Preparation of Water-Soluble Cationic Phosphorus-Containing Dendrimers. *Chem. Eur. J.,* **1999**, *5*, 3644–3650.

[54] Goetheer, E. L. V.; Baars, M.; van den Broeke, L. J. P.; Meijer, E. W.; Keurentjes, J. T. F. Functionalized Poly(Propylene Imine) Dendrimers as Novel Phase Transfer Catalysts in Supercritical Carbon Dioxide. *Ind. Eng. Chem. Res.,* **2000**, *39*, 4634–4540.

[55] Rodríguez, L. I.; Rossell, O.; Seco, M.; Orejon, A.; Masdeu-Bulto, A. M. Palladocarbosilane Dendrimers as Catalysts for the Asymmetric Hydrovinylation of Styrene in Supercritical Carbon Dioxide. *J. Organomet. Chem.,* **2008**, *693*, 1857–1860.

[56] Ou, G. N.; Xu, L.; He, B. Y.; Yuan, Y. Z. Enhanced Stability of Charged Dendrimer-Encapsulated Pd Nanoparticles in Ionic Liquids. *Chem. Commun.,* **2008**, 4210–4212.

[57] Kassube, J. K.; Gade, L. H. Immobilisation of the Pyrphos Ligand on Soluble Hyperbranched Supports and Use in Rhodium-Catalysed Hydrogenation in Ionic Liquids. *Adv. Synth. Catal.,* **2009**, *351*, 739–749.

[58] Turrin, C.-O.; Maraval, V.; Leclaire, J.; Dantras, E.; Lacabanne, C.; Caminade, A.-M.; Majoral, J.-P. Surface, Core, and Structure Modifications of Phosphorus-Containing Dendrimers. Influence on the Thermal Stability. *Tetrahedron* **2003**, *59*, 3965–3973.

[59] Prévôte, D.; Le Roy-Gourvennec, S.; Caminade, A.-M.; Masson, S.; Majoral, J.-P. Application of the Horner-Wadsworth-Emmons Reaction to the Functionalization of Dendrimers: Synthesis of Amino Acid Terminated Dendrimers. *Synthesis* **1997**, *10*, 1199–1207.

[60] Marchand, P.; Griffe, L.; Caminade, A.-M.; Majoral, J.-P.; Destarac, M. Thioacylation Reactions for the Surface Functionalization of Phosphorus-Containing Dendrimers. *Org. Lett.,* **2004**, *6*, 1309–1312.

[61] Sourdon, A.; Gary-Bobo, M.; Maynadier, M.; Garcia, M.; Majoral, J.-P.; Caminade, A.-M.; Mongin, O.; Blanchard-Desce, M. Dendrimeric Nanoparticles for Two-Photon Photodynamic Therapy and Imaging: Synthesis, Photophysical Properties, Innocuousness in Daylight and Cytotoxicity under Two-Photon Irradiation in the NIR. *Chem. Eur. J.,* **2019**, *25*, 3637–3649.

[62] Soler-Illia, G. J. de A. A.; Rozes, L.; Boggiano, M. K.; Sanchez, C.; Turrin, C.-O.; Caminade, A.-M.; Majoral, J.-P. New Mesotextured Hybrid Materials Made from Assemblies of Dendrimers and Titanium(IV)-OX-Organo Clusters. *Eur. J. Med. Chem.,* **2000**, *45*, 326–334.

[63] Griffe, L.; Poupot, M.; Marchand, P.; Maraval, A.; Turrin, C.-O.; Rolland, O.; Métivier, P.; Bacquet, G.; Fournié, J.-J.; Caminade, A.-M.; Poupot, R.; Majoral, J.-P. Multiplication of Human Natural Killer Cells by Nanosized Phosphonate-Capped Dendrimers. *Angew. Chem.*

Int. Ed., **2007**, *119*, 2575–2578.

[64] Poupot, M.; Griffe, L.; Marchand, P.; Maraval, A.; Rolland, O.; Martinet, L.; Caminade, A.-M.; Fournie, J.; Majoral, J.-P.; Poupot, R. Design of Phosphorylated Dendritic Architectures to Promote Human Monocyte Activation. *FASEB J.* **2006**, *20*, 2339–2351.

[65] Rolland, O.; Griffe, L.; Poupot, M.; Maraval, A.; Ouali, A.; Coppel, Y.; Fournié, J. J.; Bacquet, G.; Turrin, C. O.; Caminade, A.-M.; Majoral, J.-P.; Poupot, R. Tailored Control and Optimisation of the Number of Phosphonic Acid Termini on Phosphorus-Containing Dendrimers for the Ex-Vivo Activation of Human Monocytes. *Chem. Eur. J.,* **2008**, *14*, 4836–4850.

[66] Sebastián, R. M.; Magro, G.; Caminade, A.-M.; Majoral, J.-P. Dendrimers with *N,N*-Disubstituted Hydrazines as End Groups, Useful Precursors for the Synthesis of Water-Soluble Dendrimers Capped with Carbohydrate, Carboxylic or Boronic Acid Derivatives. *Tetrahedron* **2000**, *56*, 6269–6277.

[67] Mullen, D. G.; Borgmeier, E. L.; Desai, A. M.; van Dongen, M. A.; Barash, M.; Cheng, X.; Baker, J. R.; Banaszak Holl, M. M. Isolation and Characterization of Dendrimers with Precise Numbers of Functional Groups. *Chem. Eur. J.,* **2010**, *16*, 10675–10678.

[68] Thomas, T. P.; Haung, B.; Choi, S. K.; Slipe, J. E.; Kotlyar, A.; Desai, A. M.; Zong, H.; Gam, J.; Joice, M.; Baker, J. R. Polyvalent Dendrimer-Methotrexate as a Folate Receptor-Targeted Cancer Therapeutic. *Mol. Pharm.,* **2012**, *9*, 2669–2676.

[69] Petriccone, M.; Laurent, R.; Turrin, C.-O.; Sebastián, R. M.; Caminade, A.-M. Specific Bifunctionalization on the Surface of Phosphorus Dendrimers Syntheses and Properties. *Organics* **2022**, *3*, 240–261.

[70] Najafi, F.; Salami-Kalajahi, M.; Roghani-Mamaqani, H. Janus-Type Dendrimers: Synthesis, Properties, and Applications. *J. Mol. Liq.,* **2022**, *347*, 118396-118417.

[71] Caminade, A.-M.; Laurent, R.; Delavaux-Nicot, B.; Majoral, J.-P. "Janus" Dendrimers: Syntheses and Properties. *New J. Chem.,* **2012**, *36*, 217–226.

[72] de Gennes, P.-G. Nanoparticles and Dendrimers: Hopes and Illusions. *Croat. Chem. Acta* **1998**, *71*, 833–836.

[73] Yanagimoto, Y.; Takaguchi, Y.; Tuboi, S. Novel Synthesis of Surface-Block Dendrimer Using [4+4] Photocycloaddition of Anthryl Dendrons. *Polym. J.,* **2006**, *38*, 1230–1236.

[74] Nierengarten, J. F.; Eckert, J. F.; Rio, Y.; Del Pilar Carrion, M.; Gallani, J. L.; Guillon, D. Amphiphilic Diblock Dendrimers: Synthesis and Incorporation in Langmuir and Langmuir-Blodgett Films. *J. Am. Chem. Soc.,* **2001**, *123*, 9743–9748.

[75] Wooley, K. L.; Hawker, C. J.; Fréchet, J. M. J. Polymers with Controlled Molecular Architecture: Control of Surface Functionality in the Synthesis of Dendritic Hyperbranched Macromolecules Using the Convergent Approach. *J. Chem. Soc. Perkin Trans. 1* **1991**, *5*, 1059–1076.

[76] Hawker, C. J.; Wooley, K. L.; Fréchet, J. M. J. Unimolecular Micelles and Globular Amphiphiles: Dendritic Macromolecules as Novel Recyclable Solubilization Agents. *J. Chem. Soc. Perkin Trans. 1* **1993**, *12*, 1287–1297.

[77] Aoi, K.; Itoh, K.; Okada, M. Divergent/Convergent Joint Approach with a Half-Protected Initiator Core To Synthesize Surface-Block Dendrimers. *Macromolecules* **1997**, *30*, 8072–8074.

[78] Căta, A.; Ienaşcu, I. M. C.; Ştefănuţ, M. N.; Roşu, D.; Pop, O. R. Properties and Bioapplications of Amphiphilic Janus Dendrimers: A Review. *Pharmaceutics* **2023**, *15,* 589-618.

[79] Cejas-Sánchez, J.; Kajetanowicz, A.; Grela, K.; Caminade, A.; Sebastián, R. M. Strategies for the Preparation of Phosphorus Janus Dendrimers and Their Properties. *Molecules* **2023**, *28*, 5570–5588.

[80] Maraval, V.; Laurent, R.; Donnadieu, B.; Mauzac, M.; Caminade, A.-M.; Majoral, J.-P. Rapid Synthesis of Phosphorus-Containing Dendrimers with Controlled Molecular Architectures: First Example of Surface-Block, Layer-Block, and Segment-Block Dendrimers Issued from the Same Dendron. *J. Am. Chem. Soc.,* **2000**, *122*, 2499–2511.

[81] Galliot, C.; Prévoté, D.; Caminade, A.-M.; Majoral, J.-P. Polyaminophosphines Containing Dendrimers. Syntheses and Characterizations. *J. Am. Chem. Soc.,* **1995**, *117*, 5470–5476.

[82] Maraval, V.; Sebastián, R. M.; Ben, F.; Laurent, R.; Caminade, A.-M.; Majoral, J.-P. Varying Topology of Dendrimers - A New Approach toward the Synthesis of Di-Block Dendrimers. *Eur. J. Inorg. Chem.,* **2001**, *7*, 1681–1691.

[83] Caminade, A.-M.; Hameau, A.; Majoral, J.-P. The Specific Functionalization of Cyclotriphosphazene for the Synthesis of Smart Dendrimers. *Dalton Trans.,* **2016**, *46*, 1810–1822.

[84] Maraval, V.; Caminade, A. M.; Majoral, J. P.; Blais, J. C. Dendrimer Design: How to Circumvent the Dilemma of a Reduction of Steps or an Increase of Function Multiplicity? *Angew. Chem. Int. Ed.,* **2003**, *42*, 1822–1826.

[85] Martínez-Ferrero, E.; Franc, G.; Mazères, S.; Turrin, C.-O.; Boissière, C.; Caminade, A.-M.; Majoral, J.-P.; Sanchez, C. Optical Properties of Hybrid Dendritic-Mesoporous Titania Nanocomposite Films. *Chem. Eur. J.,* **2008**, *14*, 7658–7669.

[86] Zibarov, A.; Oukhrib, A.; Catot, J. A.; Turrin, C.-O.; Caminade, A.-M. AB$_5$ Derivatives of Cyclotriphosphazene for the Synthesis of Dendrons and Their Applications. *Molecules* **2021**, *26*, 1–24.

[87] Fuchs, S.; Otto, H.; Jehle, S.; Henklein, P.; Schlüter, A. D. Fluorescent Dendrimers with a Peptide Cathepsin B Cleavage Site for Drug Delivery Applications. *Chem. Commun.,* **2005**, *1*, 1830–1832.

[88] Reek, J. N. H.; Arévalo, S.; van Heerbeek, R.; Kamer, P. C. J.; van Leeuwen, P. W. N. M. Dendrimers in Catalysis. *Adv. Catal.,* **2006**, *49*, 71–151.

[89] van Heerbeek, R.; Kamer, P. C. J.; van Leeuwen, P. W. N. M.; Reek, J. N. H. Dendrimers as Support for Recoverable Catalysts and Reagents. *Chem. Rev.,* **2002**, *102*, 3717–3756.

[90] Yamamoto, K.; Kawana, Y.; Tsuji, M.; Hayashi, M.; Imaoka, T. Additive-Free Synthesis of Poly(Phenylene Oxide): Aerobic Oxidative Polymerization in a Base-Condensed Dendrimer Capsule. *J. Am. Chem. Soc.,* **2007**, *129*, 9256–9257.

[91] Wang, Z.; Deng, G.; Li, Y.; He, Y.; Tang, W.; Fan, Q. Enantioselective Hydrogenation of Quinolines Catalyzed by Ir(BINAP)-Cored Dendrimers: Dramatic Enhancement of Catalytic Activity. *Org. Lett.,* **2007**, *9*, 1243–1246.

[92] Ooe, L.; Murata, M.; Mizugani, T.; Ebitani, K.; Kaneda, K. Supramolecular Catalysts by Encapsulating Palladium Complexes within Dendrimers. *J. Am. Chem. Soc.,* **2004**, *126*, 1604–1605.

[93] van de Coevering, R.; Alfers, A. P.; Meeldijk, J. D.; Martinez-Viviente, E.; Pregosin, P. S.; Klein Gebbink, R. J. M.; van Koten, G. Ionic Core–Shell Dendrimers with an Octanionic Core as Noncovalent Supports for Homogeneous Catalysis. *J. Am. Chem. Soc.,* **2006**, *128*, 12700–12712.

[94] Miedaner, A.; Curtis, C. J.; Barkley, R. M.; DuBois, D. L. Electrochemical Reduction of CO$_2$ Catalyzed by Small Organophosphine Dendrimers Containing Palladium. *Inorg. Chem.,* **1994**, *33*, 5482–6490.

[95] Zhao, M.; Crooks, R. M. Homogeneous Hydrogenation Catalysis with Monodisperse, Dendrimer-Encapsulated Pd and Pt Nanoparticles. *Angew. Chem. Int. Ed.,* **1999**, *38*, 364–366.

[96] Imaoka, T.; Kitazawa, H.; Chun, W.-J.; Omura, S.; Albrecht, K.; Yamamoto, K. Magic Number Pt13 and Misshapen Pt12 Clusters: Which One Is the Better Catalyst? *J. Am. Chem. Soc.,* **2013**, *135*, 13089–13095.

[97] Liu, X.; Gregurec, D.; Irigoyen, J.; Mantinez, A.; Moya, S.; Ciganda, R.; Hermange, P.; Ruiz, J.; Astruc, D. Precise Localization of Metal Nanoparticles in Dendrimer Nanosnakes or Inner Periphery and Consequences in Catalysis. *Nature Commun.* **2016**, *7*, 13152–13160.

[98] Helms, B.; Fréchet, J. M. J. The Dendrimer Effect in Homogeneous Catalysis. *Adv. Synth. Catal.,* **2006**, *348*, 1125–1148.

[99] Ávila-Salas, F.; Gonza, R. I.; Ríos, P. L.; Araya-Durán, I.; Camarada, M. B. Effect of the Generation of PAMAM Dendrimers on the Stabilization of Gold Nanoparticles. *J. Chem. Inf. Model.,* **2020**, *60*, 2966–2876.

[100] Kaufman, E. A.; Tarallo, R.; Falanga, A.; Galdiero, S.; Weck, M. Generation Effect of Newkome Dendrimers on Cellular Uptake. *Polymer* **2017**, *113*, 67–73.

[101] Nemanashi, M.; Meijboom, R. "Cat in a Bag" Recycling of Dendrimer Encapsulated Au Nanoparticles by Use of Dialysis Membrane Bag in the Reduction of 4-Nitrophenol: Proof of Heterogeneous Catalysis. *Catal. Commun.,* **2016**, *83*, 53–57.

[102] Kragl, U.; Dreisbach, C. Continuous Asymmetric Synthesis in a Membrane Reactor. *Angew. Chem. Int. Ed.,* **1996**, *35*, 642–644.

[103] Dijkstra, H. P.; van Blink, G. P. M.; van Koten, G. The Use of Ultra- and Nanofiltration Techniques in Homogeneous Catalyst Recycling. *Acc. Chem. Res.,* **2002**, *35*, 798–810.

[104] Heuzé, K.; Méry, D.; Gauss, D.; Astruc, D. Copper-Free, Recoverable Dendritic Pd Catalysts for the Sonogashira Reaction. *Chem. Commun.,* **2003**, 2274–2275.

[105] Jayamurugan, G.; Jayaraman, N. Increased Efficacies of an Individual Catalytic Site in Clustered Multivalent Dendritic Catalysts. *Adv. Synth. Catal.,* **2009**, *351*, 2379–2390.

[106] Servin, P.; Laurent, R.; Romerosa, A.; Peruzzini, M.; Majoral, J.-P.; Caminade, A.-M. Synthesis of Dendrimers Terminated by Bis(Diphenylphosphinomethyl)Amino Ligands and Use of Their Palladium Complexes for Catalyzing C–C Cross-Coupling Reactions. *Organometallics* **2008**, *27*, 2066–2073.

[107] Neumann, P.; Dib, H.; Caminade, A.-M.; Hey-Hawkins, E. Redox Control of a Dendritic Ferrocenyl-Based Homogeneous Catalyst. *Angew. Chem. Int. Ed.,* **2015**, *54*, 311–314.

[108] Servin, P.; Laurent, R.; Dib, H.; Gonsalvi, L.; Peruzzini, M.; Majoral, J.-P.; Caminade, A.-M. Number of Terminal Groups versus Generation of the Dendrimer, Which Criteria Influence the Catalytic Properties? *Tetrahedron Lett.,* **2012**, *53*, 3876–3879.

[109] Ouali, A.; Laurent, R.; Caminade, A.-M.; Majoral, J.-P.; Taillefer, M. Enhanced Catalytic Properties of Copper in *O-* and *N*-Arylation and Vinylation Reactions, Using Phosphorus Dendrimers as Ligands. *J. Am. Chem. Soc.,* **2006**, *128*, 15990–15991.

[110] Mignani, S. M.; El Brahami, N.; El Kazzouli, S.; Laurent, R.; Ladeira, S.; Caminade, A.-M.; Pedziwiatr-Werbicka, E.; Szewczyk, E. M.; Bryszewska, M.; Bousmina, M. M.; Cresteil, T.; Majoral, J.-P. Original Multivalent Gold(III) and Dual Gold(III)–Copper(II) Conjugated Phosphorus Dendrimers as Potent Antitumoral and Antimicrobial Agents. *Mol. Pharm.* **2017**, *14*, 4087–4097.

[111] Perrier, A.; Keller, M.; Caminade, A.-M.; Majoral, J.-P.; Ouali, A. Efficient and Recyclable Rare Earth-Based Catalysts for Friedel–Crafts Acylations under Microwave Heating: Dendrimers Show the Way. *Green Chem.,* **2013**, *15*, 2075–2080.

[112] Rull, J.; Casals, M.; Sebastián, R. M.; Vallribera, A.; Majoral, J.-P.; Caminade, A.-M. (+)-Cinchonine-Decorated Dendrimers as Recoverable Organocatalysts. *ChemCatChem* **2015**, *7*, 2698–2704.

[113] Majoral, J.-P.; Zablocka, M.; Caminade, A.-M.; Balczewski, P.; Shi, X.; Mignani, S. Interactions Gold/Phosphorus Dendrimers. Versatile Ways to Hybrid Organic–Metallic Macromolecules. *Coord. Chem. Rev.,* **2018**, *358*, 80–91.

[114] Laurent, R.; Servin, P.; Ouali, A.; Keller, M.; Travers, L.; Majoral, J.-P.; Caminade, A.-M. Phosphorus Dendrimers: Efficient Tools for "Greener" Catalyst Design. *Phosphorus, Sulfur, and Silicon* **2010**, *186*, 869–877.

[115] Grela, K. *Olefin Metathesis: Theory and Practice*; Grela, K., Ed.; Wiley: Hobboken, 2014.

[116] Eleuterio, H. S. German Patent 1072811, **1960**.

[117] Banks, R. L.; Bailey, G. C. Olefin Disproportionation. A New Catalytic Process. *Ind. Eng. Chem. Prod. Res. Dev.,* **1964**, *3*, 170–173.

[118] Calderon, N.; Yu Chen, H.; Scott, K. W. Olefin Metathesis-A Novel Reaction for Skeletal Transformations of Unsaturated Hydrocarbons. *Tetrahedron Lett.,* **1967**, *8*, 3327–3329.

[119] Lewandos, G. S.; Pettit, R. Mechanism of the Metal-Catalyzed Disproportionation of Olefins. *J. Am. Chem. Soc.,* **1971**, *93*, 7087–7088.

[120] Grubbs, R. H.; Brunk, T. K. Possible Intermediate in the Tungsten-Catalyzed Olefin Metathesis Reaction. *J. Am. Chem. Soc.,* **1972**, *94*, 2538–2540.

[121] Hérisson, J.-L.; Chauvin, Y. Catalyse de Transformation Des Oléfines Par Les Complexes Du Tungstène. II. Télomérisation des Oléfines Cycliques en Présence d'Oléfines Acycliques. *Makromol. Chem.* **1971**, *141*, 161–176.

[122] Schrock, R. R. Alkylcarbene Complex of Tantalum by Intramolecular α-Hydrogen Abstraction. *J. Am. Chem. Soc.,* **1974**, *96*, 6796–6797.

[123] Schrock, R. R. Catalysis by Transition Metals: Metal-Carbon Double and Triple Bonds. *Science* **1983**, *219*, 13–18.

[124] Nguyen, S. T.; Johnson, L. K.; Grubbs, R. H.; Ziller, J. W. Ring-Opening Metathesis Polymerization (ROMP) of Norbornene by a Group VIII Carbene Complex in Protic Media. *J. Am. Chem. Soc.,* **1992**, *114*, 3974–3975.

[125] Schwab, P.; France, M. B.; Ziller, J. W.; Grubbs, R. H. A Series of Well-Defined Metathesis Catalysts–Synthesis of [RuCl$_2$(=CHR′)(PR$_3$)$_2$] and Its Reactions. *Angew. Chem. Int. Ed.,* **1995**, *34*, 2039–2041.

[126] Katz, T. J.; Lee, S. J. Initiation of Acetylene Polymerization by Metal Carbenes. *J. Am. Chem. Soc.,* **1980**, *102*, 422–425.

[127] Katz, T. J. The Olefin Metathesis Reaction. In *Advances in Organometallic Chemistry*; Stone, F. G. A., Grubbs, R. H., Eds.; Academic Press, 1977; pp 283–317.

[128] Chauvin, Y. Olefin Metathesis: The Early Days (Nobel Lecture). *Angew. Chem. Int. Ed.,* **2006**, *45*, 3740–3747.

[129] Schrock, R. R. Multiple Metal–Carbon Bonds for Catalytic Metathesis Reactions (Nobel Lecture). *Angew. Chem. Int. Ed.,* **2006**, *45*, 3748–3759.

[130] Grubbs, R. H. Olefin-Metathesis Catalysts for the Preparation of Molecules and Materials (Nobel Lecture). *Angew. Chem. Int. Ed.,* **2006**, *45*, 3760–3765.

[131] Chabanas, M.; Baudouin, A.; Copéret, C.; Basset, J.-M. A Highly Active Well-Defined Rhenium Heterogeneous Catalyst for Olefin Metathesis Prepared via Surface Organometallic Chemistry. *J. Am. Chem. Soc.,* **2001**, *123*, 2062–2063.

[132] Rocklage, S. M.; Fellmann, J. D.; Rupprecht, G. A.; Messere, L. W.; Schrock, R. R. Multiple Metal-Carbon Bonds. 19. How Niobium and Tantalum Complexes of the Type M(CHCMe$_3$)(PR$_3$)$_2$Cl$_3$ Can Be Modified to Give Olefin Metathesis Catalysts. *J. Am. Chem. Soc.,* **1981**, *103*, 1440–1447.

[133] Marciniec, B.; Maciejewski, H.; Rzejak, L. Metathesis of Silicon Containing Olefins: II. Synthesis of 1,2-Bis(Silyl)Ethenes by Metathesis of Vinylsilanes. *J. Organomet. Chem.,* **1989**, *3*, 273–279.

[134] Hafner, A.; Mühlebach, A.; van der Schaff, P. One-Component Catalysts for Thermal and Photoinduced Ring Opening Metathesis Polymerization. *Angew. Chem. Int. Ed.,* **1997**, *36*, 2121–2124.

[135] France, M. B.; Feldman, J.; Grubbs, R. H. An Iridium-Based Catalyst System for Metathesis/Isomerization of Acyclic Olefins, Including Methyl Oleate. *J. Chem. Soc., Chem. Commun.,* **1994**, *11*, 1307–1308.

[136] Grau, B. W.; Neuhauser, A.; Aghazada, S.; Meyer, K.; Tsogoeva, S. B. Iron-Catalyzed Olefin Metathesis: Recent Theoretical and Experimental Advances. *Chem. Eur. J.,* **2022**, *28*, 1–17.

[137] Nomura, K.; Atsumi, T.; Fujiki, M.; Yamada, J. Efficient Ring-Opening Metathesis Polymerization of Norbornene by Vanadium-Alkylidenes Generated in Situ from V(NAr)Cl$_2$(L) (L: Ketimide, Aryloxo). *J. Mol. Catal. A Chem.,* **2007**, *275*, 1–8.

[138] Tebbe, F. N.; Parshall, G. W.; Reddy, G. S. Olefin Homologation with Titanium Methylene Compounds. *J. Am. Chem. Soc.,* **1978**, *100*, 3611–3613.

[139] Howard, T. R.; Lee, J. B.; Grubbs, R. H. Titanium Metallacarbene-Metallacyclobutane Reactions: Stepwise Metathesis. *J. Am. Chem. Soc.,* **1980**, *102*, 6876–6878.

[140] Anslyn, E. V.; Grubbs, R. H. Mechanism of Titanocene Metallacyclobutane Cleavage and the Nature of the Reactive Intermediate. *J. Am. Chem. Soc.,* **1987**, *109*, 4880–4890.

[141] Schrock, R. R.; Rocklage, S.; Wengrovius, J.; Rupprecht, G.; Fellmann, J. Preparation and Characterization of Active Niobium, Tantalum and Tungsten Metathesis Catalysts. *J. Mol. Catal.,* **1980**, *8*, 73–83.

[142] Wengrovius, J.; Schrock, R. R.; Churchill, M. R.; Missert, J. R.; Youngs, W. J. Multiple Metal-Carbon Bonds. 16. Tungsten-Oxo Alkylidene Complexes as Olefins Metathesis Catalysts and the Crystal Structure of W(O)(CHCMe$_3$(PEt$_3$)Cl$_2$. *J. Am. Chem. Soc.,* **1980**, *102*, 4513–4516.

[143] Kress, J.; Wesolek, M.; Osborn, John, A. Tungsten (IV) Carbenes for the Metathesis of Olefins. Direct Observation and Identification of the Chain Carrying Carbene Complexes in a Highly Active Catalyst System. *J. Chem. Soc., Chem. Commun.,* **1982**, 514–516.

[144] Barrett, A. G. M.; Baugh, S. P. D.; Braddock, D. C.; Flack, K.; Gibson, V. C.; Giles, M. R.; Marshall, E. L.; Procopiou, P. A.; White, Andrew, J. P.; Williams, D. J. Rapid Entry into Mono-, Bi-, and Tricyclic β-Lactam Arrays via Alkene Metathesis. *J. Org. Chem.,* **1998**, *63*, 7893–7907.

[145] Armstrong, S. K. Ring Closing Diene Metathesis in Organic Synthesis. *J. Chem. Soc. Perkin Trans. 1* **1998**, 371–388.

[146] Natta, G.; Dall'asta, G.; Porri, L. Polymerization of Cyclobutene and of 3-Methylcyclobutene by RuCl$_3$ in Polar Protic Solvents. *Die Makromol. Chemie* **1965**, *81*, 253–257.

[147] France, M. B.; Grubbs, R. H.; McGrath, D. V.; Paciello, R. A. Chain Transfer during the Aqueous Ring-Opening Metathesis Polymerization of 7-Oxanorbornene Derivatives. *Macromolecules* **1993**, *26*, 4742–4747.

[148] Garber, S. B.; Kingsbury, J. S.; Gray, B. L.; Hoveyda, A. H. Efficient and Recyclable Monomeric and Dendritic Ru-Based Metathesis Catalysts. *J. Am. Chem. Soc.,* **2000**, *122*, 8168–8179.

[149] Huang, J.; Stevens, E. D.; Nolan, S. P.; Petersen, J. L. Olefin Metathesis-Active Ruthenium Complexes Bearing a Nucleophilic Carbene Ligand. *J. Am. Chem. Soc.,* **1999**, *121*, 2674–2678.

[150] Weskamp, T.; Schattenmann, W. C.; Spiegler, M.; Herrmann, W. A. A Novel Class of Ruthenium Catalysts for Olefin Metathesis. *Angew. Chem. Int. Ed.,* **1998**, *37*, 2490–2493.

[151] Weskamp, T.; Böhm, V. P. W.; Herrmann, W. A. N-Heterocyclic Carbenes: State of the Art in Transition-Metal-Complex Synthesis. *J. Organomet. Chem.,* **2000**, *600*, 12–22.

[152] Ackermann, L.; Fürstner, A.; Weskamp, T.; Kohl, F. J.; Herrmann, W. A. Ruthenium carbene complexes with imidazolin-2-ylidene ligands allow the formation of tetrasubstituted cycloalkenes by RCM. *Tetrahedron Lett.,* **1999**, *40*, 4787–4790.

[153] Scholl, M.; Trnka, T. M.; Morgan, J. P.; Grubbs, R. H. Increased Ring Closing Metathesis Activity of Ruthenium-Based Olefin Metathesis Catalysts Coordinated with Imidazolin-2-Ylidene Ligands. *Tetrahedron Lett.,* **1999**, *40*, 2247–2250.

[154] Díez-González, S. N-Heterocyclic Carbenes: From Laboratory Curiosities to Efficient Synthetic Tools; Díez-González, S., Ed.; Royal Society of Chemistry, 2011.

[155] Kingsbury, J. S.; Harrity, J. P. A.; Bonitatebus, P. J.; Hoveyda, A. H. A Recyclable Ru-Based Metathesis Catalyst. *J. Am. Chem. Soc.,* **1999**, *121*, 791–799.

[156] Love, J. A.; Sandford, M. S.; Day, M. W.; Grubbs, R. H. Synthesis, Structure, and Activity of Enhanced Initiators for Olefin Metathesis. *J. Am. Chem. Soc.,* **2003**, *125*, 10103–10109.

[157] Michrowska, A.; Bujok, R.; Harutyunyan, S.; Sashuk, V.; Dolgonos, G.; Grela, K. Nitro-Substituted Hoveyda–Grubbs Ruthenium Carbenes: Enhancement of Catalyst Activity through Electronic Activation. *J. Am. Chem. Soc.,* **2004**, *126*, 9318–9325.

[158] Grela, K.; Harutyunyan, S.; Michrowska, A. A Highly Efficient Ruthenium Catalyst for Metathesis Reactions. *Angew. Chem. Int. Ed.,* **2002**, *41*, 4038–4040.

[159] Prühs, S.; Lehmann, C. W.; Fürstner, A. Preparation, Reactivity, and Structural Peculiarities of Hydroxyalkyl-Functionalized "Second-Generation" Ruthenium Carbene Complexes. *Organometallics* **2004**, *23*, 280–287.

[160] Fürstner, A.; Ackermann, L.; Gabor, B.; Goddard, R.; Lehmann, C. W.; Mynott, R.; Stelzer, F.; Thiel, O. R. Comparative Investigation of Ruthenium-Based Metathesis Catalysts Bearing N-Heterocyclic Carbene (NHC) Ligands. *Chem. Eur. J.,* **2001**, *7*, 3236–3253.

[161] Dinger, M. B.; Nieczypor, P.; Mol, J. B. Adamantyl-Substituted N-Heterocyclic Carbene Ligands in Second-Generation Grubbs-Type Metathesis Catalysts. *Organometallics* **2003**, *22*, 5291–5296.

[162] Vehlow, K.; Maechling, S.; Blechert, S. Ruthenium Metathesis Catalysts with Saturated Unsymmetrical N-Heterocyclic Carbene Ligands. *Organometallics* **2006**, *25*, 25–28.

[163] Ledoux, N.; Allaert, B.; Pattyn, S.; Mierde, H. V.; Vercaemst, C.; Verpoort, F. *N,N'*-Dialkyl- and *N*-Alkyl-*N*-Mesityl-Substituted *N*-Heterocyclic Carbenes as Ligands in Grubbs Catalysts. *Chem. Eur. J.,* **2006**, *12*, 4654–4661.

[164] Jolly, P. I.; Marczyk, A.; Małecki, P.; Ablialimov, O.; Trzybisńki, D.; Wozńiak, K.; Osella, S.; Trzaskowski, B. Azoliniums, Adducts, NHCs and Azomethine Ylides: Divergence in Wanzlick Equilibrium and Olefin Metathesis Catalyst Formation. *Chem. Eur. J.,* **2018**, *24*,

4785–4789.

[165] Ablialimov, O.; Kedziorek, M.; Malinska, M.; Woźniak, K.; Grela, K. Synthesis, Structure, and Catalytic Activity of New Ruthenium(II) Indenylidene Complexes Bearing Unsymmetrical N-Heterocyclic Carbenes. *Organometallics* **2014**, *33*, 2160–2171.

[166] Smoleń, M.; Kosńik, W.; Loska, R.; Gajda, R.; Malińska, M.; Woźniak, K.; Grela, K. Synthesis and Catalytic Activity of Ruthenium Indenylidene Complexes Bearing Unsymmetrical NHC Containing a Heteroaromatic Moiety. *RSC Adv.,* **2016**, *6*, 77013–77019.

[167] Monsigny, L.; Kajetanowicz, A.; Grela, K. Ruthenium Complexes Featuring Unsymmetrical N-Heterocyclic Carbene Ligands–Useful Olefin Metathesis Catalysts for Special Tasks. *Chem. Rec.,* **2021**, *21*, 3648–3661.

[168] Dinger, M. B.; Mol, J. C. Degradation of the First-Generation Grubbs Metathesis Catalyst with Primary Alcohols, Water, and Oxygen. Formation and Catalytic Activity of Ruthenium(II) Monocarbonyl Species. *Organometallics* **2003**, *22*, 1089–1095.

[169] Guidone, S.; Songis, O.; Nahra, F.; Cazin, C. S. J. Conducting Olefin Metathesis Reactions in Air: Breaking the Paradigm. *ACS Catal.,* **2015**, *5*, 2697–2701.

[170] Mühlebach, A.; Meunier, B.; Bühler, N.; Karlen, T.; Ludi, A. Ring Opening Metathesis Polymerization of Bicyclo [2.2.1] Hept-2-Ene (2-Norbornene) and Exo,Exo-5,6-Bis (Methoxycarbonyl)-7-Oxabicyclo [2.2.1]Hept-2-Ene Using Ru(II) and Ru(III) Complexes: Polymerization Kinetics and Ruthenium Content in Polymers. *J. Mol. Catal.,* **2001**, *90*, 143–156.

[171] Feast, W. J.; Harrisson, D. B. Poly(2,5-(3,4-Bis(Methoxymethyl)Furanylene)Vinyl-ene)s Prepared by Aqueous Ring Opening Metathesis Polymerisation. *Polym. Bull.,* **1991**, *25*, 343–350.

[172] Connon, S. J.; Rivard, M.; Zaja, M.; Blechert, S. Practical Olefin Metathesis in Protic Media under an Air Atmosphere. *Adv. Synth. Catal.,* **2003**, *245*, 572–575.

[173] Binder, J. B.; Blank, J. J.; Raines, R. T. Olefin Metathesis in Homogeneous Aqueous Media Catalyzed by Conventional Ruthenium Catalysts. *Org. Lett.,* **2007**, *9*, 4885–4888.

[174] Lipshutz, B.; Taft, B. R. Heck Couplings at Room Temperature in Nanometer Aqueous Micelles. *Org. Lett.,* **2008**, *10*, 1329–1332.

[175] Lipshutz, B.; Ghorai, S.; Aguinaldo, G. T. Ring-Closing Metathesis at Room Temperature within Nanometer Micelles Using Water as the Only Solvent. *Adv. Synth. Catal.,* **2008**, *350*, 953–958.

[176] Lipshutz, B.; Petersen, T. B.; Abela, A. R. Room-Temperature Suzuki–Miyaura Couplings in Water Facilitated by Nonionic Amphiphiles. *Org. Lett.,* **2008**, *10*, 1333–1336.

[177] Hong, S. H.; Grubbs, R. H. Highly Active Water-Soluble Olefin Metathesis Catalyst. *J. Am. Chem. Soc.,* **2006**, *128*, 3508–3509.

[178] Kim, C.; Ondrusek, B. A.; Chung, H. Removable Water-Soluble Olefin Metathesis Catalyst via Host–Guest Interaction. *Org. Lett.,* **2018**, *20*, 736–739.

[179] Mohr, B.; Lynn, D. M.; Grubbs, R. H. Synthesis of Water-Soluble, Aliphatic Phosphines and Their Application to Well-Defined Ruthenium Olefin Metathesis Catalysts. *Organometallics* **1996**, *15*, 4317–4325.

[180] Lynn, D. M.; Mohr, B.; Grubbs, R. H. Living Ring-Opening Metathesis Polymerization in Water. *J. Am. Chem. Soc.,* **1998**, *120*, 1627–1628.

[181] Kirkland, T. A.; Lynn, D. M.; Grubbs, R. H. Ring-Closing Metathesis in Methanol and Water. *J. Org. Chem.,* **1998**, *63*, 9904–9909.

[182] Michrowska, A.; Gulajski, L.; Kaczmarska, Z.; Mennecke, K.; Kirschning, A.; Grela, K. A Green Catalyst for Green Chemistry: Synthesis and Application of an Olefin Metathesis Catalyst Bearing a Quaternary Ammonium Group. *Green Chem.,* **2006**, *8*, 685–688.

[183] Skowerski, K.; Szczepaniak, G.; Wierzbicka, C.; Gułajski, L.; Bieniek, M.; Grela, K. Highly Active Catalysts for Olefin Metathesis in Water. *Catal. Sci. Technol.,* **2012**, *2*, 2424–2427.

[184] Tomasek, J.; Schatz, J. Olefin Metathesis in Aqueous Media. *Green Chem.,* **2013**, *15*, 2317–2338.

[185] Sabatino, V.; Ward, T. R. Aqueous Olefin Metathesis: Recent Developments and Applications. *Beilstein J. Org. Chem.,* **2019**, *15*, 445–468.

[186] Barteczko, N.; Grymel, M.; Chrobok, A. Heterogeneous Catalysts for Olefin Metathesis.

Catal. Commun., **2023**, *177,* 106662-106681.

[187] Clavier, H.; Grela, K.; Kirschning, A.; Mauduit, M.; Nolan, S. P. Sustainable Concepts in Olefin Metathesis. *Angew. Chem. Int. Ed.,* **2007**, *46*, 6786–6801.

[188] Wheeler, P.; Phillips, J. H.; Pederson, R. L. Scalable Methods for the Removal of Ruthenium Impurities from Metathesis Reaction Mixtures. *Org. Process Res. Dev.,* **2016**, *20*, 1182–1190.

[189] Buchmeiser, M. R. Design and Synthesis of Supported Catalysts on a Molecular Base. *Catal. Today* **2005**, *105*, 612–617.

[190] Nguyen, S. T.; Grubbs, R. H. The Syntheses and Activities of Polystyrene-Supported Olefin Metathesis Catalysts Based on Cl₂(PR₃)₂Ru=CH–CH=CPh₂. *J. Organomet. Chem.,* **1995**, *497*, 195–200.

[191] Melis, K.; de Vos, D.; Jacobs, P.; Verpoort, F. ROMP and RCM Catalysed by (R₃P)₂Cl₂Ru=CHPh Immobilised on a Mesoporous Support. *J. Mol. Catal. A Chem.,* **2001**, *169*, 47–56.

[192] Allen, D. P.; van Wingerden, M.; Grubbs, R. H. Well-Defined Silica-Supported Olefin Metathesis Catalysts. *Org. Lett.* **2009**, *11*, 1261–1264.

[193] Krause, J. O.; Lubbad, S. H.; Nuyken, O.; Buchmeiser, M. R. Heterogenization of a Modified Grubbs–Hoveyda Catalyst on a ROMP-Derived Monolithic Support. *Macromol. Commun.,* **2003**, *24*, 875–878.

[194] Yang, L.; Mayr, M.; Wurst, K.; Buchmeiser, M. R. Novel Metathesis Catalysts Based on Ruthenium 1,3-Dimesityl-3,4,5,6-Tetrahydropyrimidin-2-Ylidenes: Synthesis, Structure, Immobilization, and Catalytic Activity. *Chem. Eur. J.,* **2004**, *10*, 5761–5770.

[195] Barrett, A. G. M.; Cramp, S. M.; Roberts, R. S. ROMP-Spheres: A Novel High-Loading Polymer Support Using Cross Metathesis between Vinyl Polystyrene and Norbornene Derivatives. *Org. Lett.,* **1999**, *1*, 1083–1086.

[196] Michrowska, A.; Mennecke, K.; Kunz, U.; Kirschning, A.; Grela, K. A New Concept for the Noncovalent Binding of a Ruthenium-Based Olefin Metathesis Catalyst to Polymeric Phases: Preparation of a Catalyst on Raschig Rings. *J. Am. Chem. Soc.,* **2006**, *128*, 13261–13267.

[197] Kirschning, A.; Harmrolfs, K.; Mennecke, K.; Messinger, J.; Schön, U.; Grela, K. Homo- and Heterogeneous Ru-Based Metathesis Catalysts in Cross-Metathesis of 15-Allylestrone—towards 17β-Hydroxysteroid Dehydrogenase Type 1 Inhibitors. *Tetrahedron Lett.,* **2008**, *49*, 3019–3022.

[198] Borré, E.; Rouen, M.; Laurent, I.; Magrez, M.; Caijo, F.; Crévisy, C.; Solodenko, W.; Toupet, L.; Frankfurter, R.; Vogt, C.; Kirschning, A.; Mauduit, M. A Fast-Initiating Ionically Tagged Ruthenium Complex: A Robust Supported Pre-Catalyst for Batch-Process and Continuous-Flow Olefin Metathesis. *Chem. Eur. J.,* **2012**, *18*, 16369–16382.

[199] Buchmeiser, M. R. Polymer-Supported Well-Defined Metathesis Catalysts. *Chem. Rev.,* **2009**, *109*, 303–321.

[200] Buchmeiser, M. R. Recent Advances in the Synthesis of Supported Metathesis Catalysts. *New J. Chem.,* **2004**, *28*, 549–557.

[201] Skowerski, K.; Białecki, J.; Czarnocki, S. J.; Żukowska, K.; Grela, K. Effective Immobilisation of a Metathesis Catalyst Bearing an Ammonium-Tagged NHC Ligand on Various Solid Supports. *Beilstein J. Org. Chem.,* **2016**, *12*, 5–15.

[202] Yang, D.; Gates, B. C. Catalysis by Metal Organic Frameworks: Perspective and Suggestions for Future Research. *ACS Catal.,* **2019**, *9*, 1779–1798.

[203] Wei, Y.-S.; Zhang, M.; Zou, R.; Xu, Q. Metal–Organic Framework-Based Catalysts with Single Metal Sites. *Chem. Rev.,* **2020**, *120*, 12089–12174.

[204] Bavykina, A.; Kolobov, N.; Khan, I. S.; Bau, J. A.; Ramirez, A.; Gascon, J. Metal–Organic Frameworks in Heterogeneous Catalysis: Recent Progress, New Trends, and Future Perspectives. *Chem. Rev.,* **2020**, *120*, 8468–8535.

[205] Rogge, S. M. J.; Bavykina, A.; Hajek, J.; Garcia, H.; Olivos-Suarez, A. I.; Sepúlveda-Escribano, A.; Vimont, A.; Clet, G.; Bazin, P.; Kapteijn, F.; Daturi, M.; Ramos-Fernandez, E. V.; LLambrés i Xamena, F. X.; van Speybroeck, V.; Gascon, J. Metal–Organic and Covalent Organic Frameworks as Single-Site Catalysts. *Chem. Soc. Rev.,* **2017**, *46*, 3134–3184.

[206] Spekreijse, J.; Öhrström, L.; Sanders, J. P. M.; Bitter, J. H.; Scott, E. L. Mechanochemical Immobilisation of Metathesis Catalysts in a Metal–Organic Framework. *Chem. Eur. J.,* **2016**, *22*, 15437–15443.

[207] Yuan, J.; Fracaroli, A. M.; Klemperer, W. G. Convergent Synthesis of a Metal–Organic Framework Supported Olefin Metathesis Catalyst. *Organometallics* **2016**, *35*, 2149–2155.

[208] Chołuj, A.; Zieliński, A.; Grela, K.; Chmielewski, M. J. Metathesis@MOF: Simple and Robust Immobilization of Olefin Metathesis Catalysts inside (Al)MIL-101-NH$_2$. *ACS Catal.,* **2016**, *6*, 6343–6349.

[209] Chołuj, A.; Nogaś, W.; Patrzałek, M.; Krzesiński, P.; Chmielewski, M. J.; Kajetanowicz, A.; Grela, K. Preparation of Ruthenium Olefin Metathesis Catalysts Immobilized on MOF, SBA-15, and 13X for Probing Heterogeneous Boomerang Effect. *Catalysts* **2020**, *10*, 438–456.

[210] Chołuj, A.; Krzesiński, P.; Ruszczyńska, A.; Bulska, E.; Kajetanowicz, A.; Grela, K. Noncovalent Immobilization of Cationic Ruthenium Complex in a Metal–Organic Framework by Ion Exchange Leading to a Heterogeneous Olefin Metathesis Catalyst for Use in Green Solvents. *Organometallics* **2019**, *38*, 3397–3405.

[211] Chołuj, A.; Karczykowski, R.; Chmielewski, M. J. Simple and Robust Immobilization of a Ruthenium Olefin Metathesis Catalyst Inside MOFs by Acid-Base Reaction. *Organometallics* **2019**, *38*, 3392–3396.

[212] Wijkens, P.; Jastrzebski, J. T. B. H.; van der Schaff, P. A.; Kolly, R.; Hafner, A.; van Koten, G. Synthesis of Periphery-Functionalized Dendritic Molecules Using Polylithiated Dendrimers as Starting Material. *Org. Lett.,* **2000**, *2*, 1621–1624.

[213] Pijnenburg, N. J. M.; Tomás-Mendivil, E.; Maryland, K. E.; Kleijn, H.; Lutz, M.; Spek, A. . L.; van Koten, G.; Klein Gebbink, R. J. M. Monomeric and Dendritic Second Generation Grubbs- and Hoveyda–Grubbs-Type Catalysts for Olefin Metathesis. *Inorganica Chim. Acta* **2014**, *409*, 163–173.

[214] Riegert, D.; Bareille, L.; Laurent, R.; Majoral, J.-P.; Caminade, A.-M.; Chaumonnot, A. Silica Functionalized by Bifunctional Dendrimers: Hybrid Nanomaterials for Trapping CO$_2$. *Eur. J. Inorg. Chem.,* **2016**, *2016*, 3103–3110.

[215] Caminade, A.-M.; Majoral, J.-P. Bifunctional Phosphorus Dendrimers and Their Properties. *Molecules* **2016**, *21*, 538-562.

[216] Maraval, V.; Laurent, R.; Merino, S.; Caminade, A.-M.; Majoral, J.-P. Michael-Type Addition of Amines to the Vinyl Core of Dendrons - Application to the Synthesis of Multidendritic Systems. *Eur. J. Org. Chem.,* **2000**, *21*, 3555–3568.

[217] Gottis, S.; Rodriguez, L. I.; Laurent, R.; Angurell, I.; Seco, M.; Rossell, O.; Majoral, J.-P.; Caminade, A.-M. Janus Carbosilane/Phosphorhydrazone Dendrimers Synthesized by the 'Click' Staudinger Reaction. *Tetrahedron Lett.,* **2013**, *54*, 6864–6867.

[218] Kolb, H. C.; Finn, M. G.; Sharpless, K. B. Click Chemistry: Diverse Chemical Function from a Few Good Reactions. *Angew. Che. Int. Ed.,* **2001**, *40*, 2004–2021.

[219] Liang, L.; Astruc, D. The Copper(I)-Catalyzed Alkyne-Azide Cycloaddition (CuAAC) "Click" Reaction and Its Applications. An Overview. *Coord. Chem. Rev.,* **2011**, *255*, 2933–2945.

[220] Kolb, H. C.; Sharpless, K. B. The Growing Impact of Click Chemistry on Drug Discovery. *Drug Discov. Today* **2003**, *8*, 1128–1137.

[221] Huisgen, R. Centenary Lecture: 1,3-Dipolar Cycloadditions. *Proc. Chem. Soc.,* **1961**, 357–396.

[222] Rostovtsev, V. V.; Gree, L. G.; Fokin, V. V.; Sharpless, K. B. A Stepwise Huisgen Cycloaddition Process: Copper(I)-Catalyzed Regioselective "Ligation" of Azides and Terminal Alkynes. *Angew. Chem. Int. Ed.,* **2002**, *51*, 2596–2599.

[223] Tornøe, C. W.; Christensen, C.; Meldal, M. Peptidotriazoles on Solid Phase: [1,2,3]-Triazoles by Regiospecific Copper(I)-Catalyzed 1,3-Dipolar Cycloadditions of Terminal Alkynes to Azides. *J. Org. Chem.,* **2002**, *67*, 3057–3064.

[224] Spicer, C. D.; Pujari-Palmer, M.; Autefage, H.; Insley, G.; Procter, P.; Engqvist, H.; Stevens, M. M. Synthesis of Phospho-Amino Acid Analogues as Tissue Adhesive Cement Additives. *ACS Cent. Sci.,* **2020**, *6*, 226–231.

[225] Makarem, A.; Klika, K. D.; Litau, G.; Remde, Y.; Kopka, K. HBED-NN: A Bifunctional Chelator for Constructing Radiopharmaceuticals. *J. Org. Chem.,* **2019**, *84*, 7501–7508.

[226] Jiang, Y. Q.; Wu, K.; Zhang, Q.; Li, K. Q.; Li, Y. Y.; Xin, P. Y.; Zhang, W. W.; Guo, H. M. A Dual-Responsive Hyperbranched Supramolecular Polymer Constructed by Cooperative Host-Guest Recognition and Hydrogen-Bond Interactions. *Chem. Commun.,* **2018**, *54*, 13821–13824.

[227] Abbassi, L.; Chabre, Y. M.; Naresh, K.; Arnold, A. A.; André, S.; Josserand, J.; Gabius, H.-J.; Roy, R. Multifaceted Glycodendrimers With Programmable Bioactivity Through Convergent, Divergent, and Accelerated Approaches Using Polyfunctional Cyclotriphosphazenes. *Polym. Chem.,* **2015**, *6*, 7666–7683.

[228] Cavero, E.; Zablocka, M.; Caminade, A.-M.; Majoral, J.-P. Design of Bisphosphonate-Terminated Dendrimers. *Eur. J. Org. Chem.,* **2010**, *14*, 2759–2767.

[229] Małecki, P.; Gajda, K.; Gajda, R.; Woźniak, K.; Trzaskowski, B.; Kajetanowicz, A.; Grela, K. Hoveyda–Grubbs-Type Precatalysts with Unsymmetrical N-Heterocyclic Carbenes as Effective Catalysts in Olefin Metathesis. *Organometallics* **2017**, *36*, 2153–2166.

[230] Marshall, C.; Ward, M. F.; Skakle, J. M. S. Steric Variations between the Synthesis of a Stable Chiral C_2-Symmetric Diimidazolidinylidene and an Electron-Rich Tetraazafulvalene. *Synthesis* **2006**, *6*, 1040–1044.

[231] Aljuhani, A.; El-Sayed, W. S.; Sahu, P. K.; Rezki, N.; Aouad, M. R.; Salghi, R.; Messali, M. Microwave-Assisted Synthesis of Novel Imidazolium, Pyridinium and Pyridazinium-Based Ionic Liquids and/or Salts and Prediction of Physico-Chemical Properties for Their Toxicity and Antibacterial Activity. *J. Mol. Liq.,* **2018**, *249*, 747–753.

[232] Liu, J.; Chen, J.; Zhao, J.; Zhao, Y.; Li, L.; Zhang, H. A Modified Procedure for the Synthesis of 1-Arylimidazoles. *Synthesis* **2003**, *17*, 2661–2666.

[233] Kamaya, Y.; Fukaya, Y.; Suzuki, K. Acute Toxicity of Benzoic Acids to the Crustacean Daphnia Magna. *Chemosphere* **2005**, *59*, 255–261.

[234] Patrzałek, M.; Piątkowski, J.; Kajetanowicz, A.; Grela, K. Anion Metathesis in Facile Preparation of Olefin Metathesis Catalysts Bearing a Quaternary Ammonium Chloride Tag. *Synlett* **2019**, *30*, 1981–1987.

[235] Franc, G.; Badetti, E.; Duhayon, C.; Coppel, Y.; Turrin, C.-O.; Majoral, J.-P.; Sebastián, R. M.; Caminade, A.-M. An Efficient Synthesis Combining Phosphorus Dendrimers and 15-Membered Triolefinic Azamacrocycles: Towards the Stabilization of Platinum Nanoparticles. *New J. Chem.,* **2010**, *34*, 547–555.

[236] Nascimento, D. L.; Foscato, M.; Occhipinti, G.; Jensen, V. R.; Fogg, D. E. Bimolecular Coupling in Olefin Metathesis: Correlating Structure and Decomposition for Leading and Emerging Ruthenium–Carbene Catalysts. *J. Am. Chem. Soc.,* **2021**, *143*, 11072–11079.

[237] Bailey, G. A.; Foscato, M.; Higman, C. S.; Day, C. S.; Jensen, V. R.; Fogg, D. E. Bimolecular Coupling as a Vector for Decomposition of Fast-Initiating Olefin Metathesis Catalysts. *J. Am. Chem. Soc.,* **2018**, *140*, 6931–6944.

[238] Monsigny, L.; Czarnocki, S. J.; Sienkiewicz, M.; Kopcha, W.; Frankfurter, R.; Vogt, C.; Solodenko, W.; Kajetanowicz, A.; Kirschning, A.; Grela, K. Ruthenium Complex Bearing a Hydroxy Group Functionalised N-Heterocyclic Carbene Ligand – A Universal Platform for Synthesis of Tagged and Immobilised Catalysts for Olefin Metathesis. *Eur. J. Org. Chem.* **2021**, *46*, 6424–6434.

[239] Arnanz, A.; Pintado-Sierra, M.; Corma, A.; Iglesias, M.; Sánchez, F. Bifunctional Metal Organic Framework Catalysts for Multistep Reactions: MOF-Cu(BTC)-[Pd] Catalyst for One-Pot Heteroannulation of Acetylenic Compounds. *Adv. Synth. Catal.,* **2012**, *354*, 1347–1355.

[240] Sivan, S. E.; Oh, K.-R.; Yoon, J.-W.; Yoo, C.; Hwang, Y. K. Immobilization of a Trimeric Ruthenium Cluster in Mesoporous Chromium Terephthalate and Its Catalytic Application. *Dalton Trans.,* **2022**, *51*, 13189–13194.

[241] Berijani, K.; Morsali, A.; Hupp, J. T. An Effective Strategy for Creating Asymmetric MOFs for Chirality Induction: A Chiral Zr-Based MOF for Enantioselective Epoxidation. *Catal. Sci. Technol.,* **2019**, *9*, 3388–3397.

[242] Rimoldi, M.; Nakamura, A.; Vermeulen, N. A.; Henkelis, J. J.; Blackburn, A. K.; Hupp, J. T.; Stoddart, J. F.; Farha, O. K. A Metal–Organic Framework Immobilised Iridium Pincer Complex. *Chem. Sci.,* **2016**, *7*, 4980–4984.

[243] Baek, J.; Rungtaweevoranit, B.; Pei, X.; Park, M.; Fakra, S. C.; Liu, Y. S.; Matheu, R.; Alshmimri, S. A.; Alshehri, S.; Trickett, C. A.; Somorjai, G. A.; Yaghi, O. M. Bioinspired Metal-Organic Framework Catalysts for Selective Methane Oxidation to Methanol. *J. Am. Chem. Soc.,* **2018**, *140*, 18208–18216.

[244] Choi, S.; Jung, W. J.; Park, K.; Kim, S. Y.; Baeg, J. O.; Kim, C. H.; Son, H. J.; Pac, C.; Kang, S. O. Rapid Exciton Migration and Amplified Funneling Effects of Multi-Porphyrin Arrays in a Re(I)/Porphyrinic MOF Hybrid for Photocatalytic CO_2 Reduction. *ACS Appl. Mater. Interfaces* **2021**, *13*, 2710–2722.

[245] Wu, P.; He, C.; Wang, J.; Peng, X.; Li, X.; An, Y.; Duan, C. Photoactive Chiral Metal-Organic Frameworks for Light-Driven Asymmetric α-Alkylation of Aldehydes. *J. Am. Chem. Soc.,* **2012**, *134*, 14991–14999.

[246] Madrahimov, S. T.; Gallagher, J. R.; Zhang, G.; Meinhart, Z.; Garibay, S. J.; Delferro, M.; Miller, J. T.; Farha, O. K.; Hupp, J. T.; Nguyen, S. T. Gas-Phase Dimerization of Ethylene under Mild Conditions Catalyzed by MOF Materials Containing (Bpy)NiII Complexes. *ACS Catal.,* **2015**, *5*, 6713–6718.

[247] Zhu, W.; Xiang, G.; Shang, J.; Guo, J.; Motevalli, B.; Durfee, P.; Agola, J. O.; Coker, E. N.; Brinker, C. J. Versatile Surface Functionalization of Metal–Organic Frameworks through Direct Metal Coordination with a Phenolic Lipid Enables Diverse Applications. *Adv. Funct. Mater.,* **2018**, *28*, 1705274-1705286.

[248] Angurell, I.; Turrin, C.-O.; Laurent, R.; Maraval, V.; Servin, P.; Rossell, O.; Seco, M.; Caminade, A.-M.; Majoral, J.-P. Decorating Step-by-Step and Independently the Surface and the Core of Dendrons. *J. Organomet. Chem.,* **2007**, *692*, 1928–1939.

[249] Servin, P.; Laurent, R.; Gonsalvi, L.; Tristany, M.; Peruzzini, M.; Majoral, J.-P.; Caminade, A.-M. Grafting of Water-Soluble Phosphines to Dendrimers and Their Use in Catalysis: Positive Dendritic Effects in Aqueous Media. *Dalton Trans.,* **2009**, 4432–4434.

[250] Biancalana, L.; Batchelor, L. K.; De Palo, A.; Zacchini, S.; Pampaloni, G.; Dyson, P. J.; Marchetti, F. A General Strategy to Add Diversity to Ruthenium Arene Complexes with Bioactive Organic Compounds: Via a Coordinated (4-Hydroxyphenyl)Diphenylphosphine Ligand. *Dalton Trans.,* **2017**, *46*, 12001–12004.

[251] Leung, H.-W. Polyethylene Glycol. In *Encyclopedia of Toxicology*; Philip Wexler, Ed.; Academic Press, 2014; pp 1043–1044.

[252] Caminade, A.-M.; Maraval, V.; Laurent, R.; Turrin, C.-O.; Sutra, P.; Leclaire, J.; Griffe, L.; Marchand, P.; Baudoin-Dehoux, C.; Rebout, C.; Majoral, J.-P. Phosphorus Dendrimers: From Synthesis to Applications. *C. R. Chim.,* **2003**, *6*, 791–801.

[253] Bergbreiter, D. E.; Yang, Y. C. Variable-Temperature NMR Studies of Soluble Polymer-Supported Phosphine-Silver Complexes. *J. Org. Chem.,* **2010**, *75*, 873–878.

[254] Bäckvall, J.-E.; Andreasson, U. Ruthenium-Catalyzed Isomerization of Allylic Alcohols to Saturated Ketones. *Tetrahedron Lett.,* **1993**, *34*, 5459–5462.

[255] Franc, G.; Mazères, S.; Turrin, C.-O.; Vendier, L.; Duhayon, C.; Caminade, A.-M.; Majoral, J.-P. Synthesis and Properties of Dendrimers Possessing the Same Fluorophore(s) Located Either Peripherally or off-Center. *J. Org. Chem.,* **2007**, *72*, 8707–8715.

[256] Ho, T. -L; Olah, G. A. Cleavage of Esters and Ethers with Iodotrimethylsilane. *Angew. Chem. Int. Ed.,* **1976**, *15*, 774–775.

[257] Zwoliński, K. M.; Nowak, P.; Chmielewski, M. J. Towards Multifunctional MOFs-Transforming a Side Reaction into a Post-Synthetic Protection/Deprotection Method. *Chem. Commun.,* **2015**, *51*, 10030–10033.

[258] Serra-Crespo, P.; Ramos-Fernandez, E. V.; Gascon, J.; Kapteijn, F. Synthesis and Characterization of an Amino Functionalized MIL-101(Al): Separation and Catalytic Properties. *Chem. Mater.,* **2011**, *23*, 2565–2572.

Chapter VI. Annex: Spectra and analyses of selected compounds

1. Synthesis of polyphosphorhydrazone dendrons

1.1. 4-(2-bromoethylphenol) 122
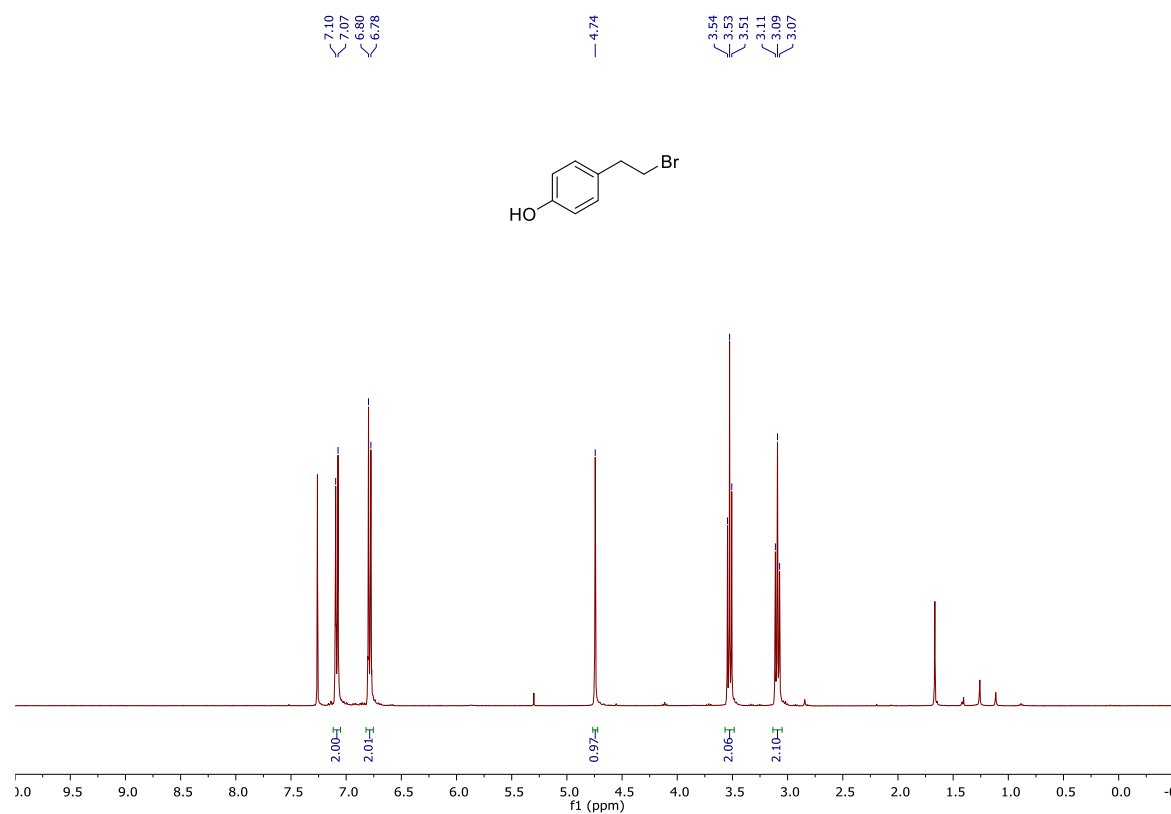
Figure S1.^{1}H NMR spectrum of 4-(2-bromoethylphenol) **122** in CDCl$_3$ recorded at room temperature (400 MHz).
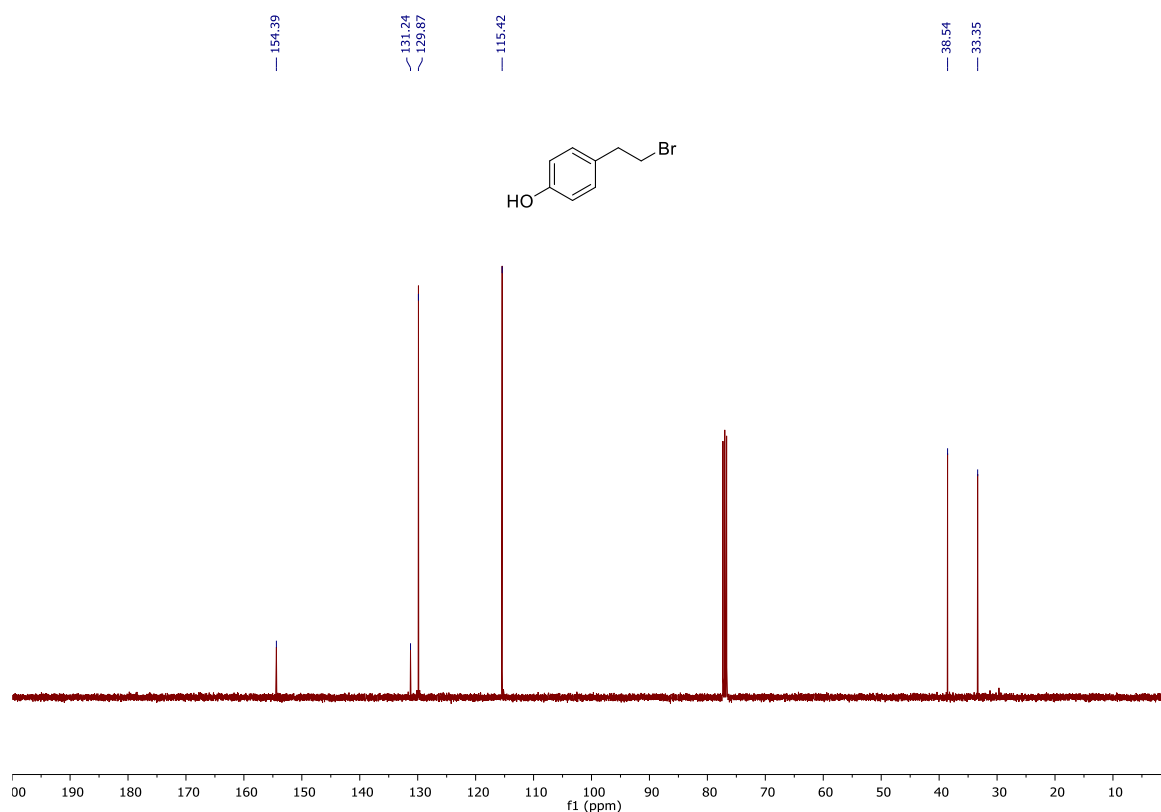
Figure S2. $^{13}C\{^1H\}$ NMR spectrum of 4-(2-bromoethylphenol) **122** in CDCl$_3$ recorded at room temperature (101 MHz).
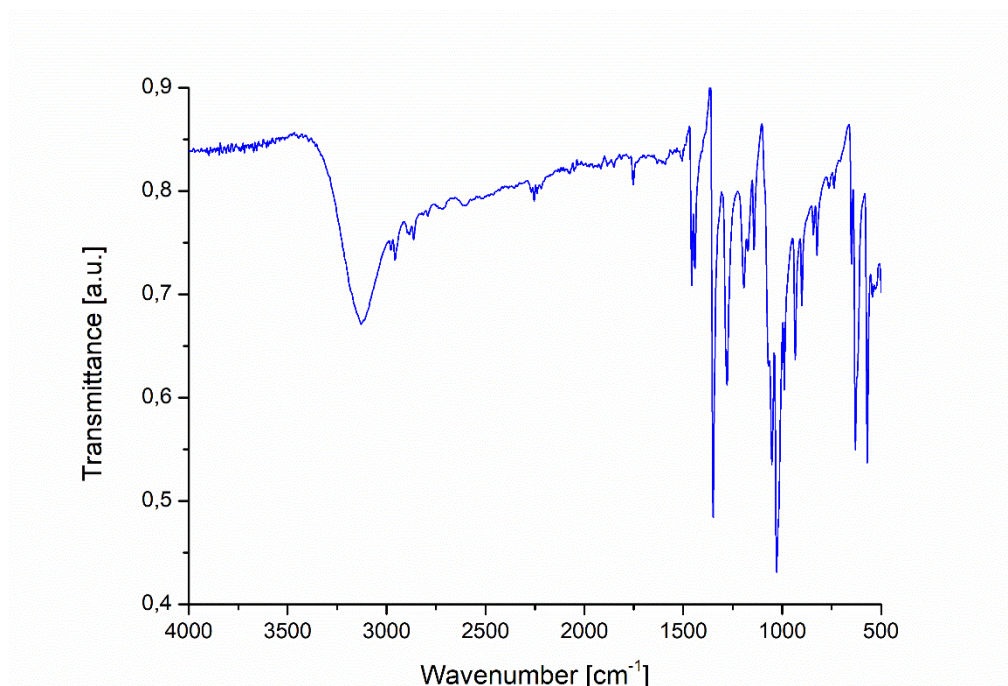
Figure S3. FT-IR spectrum of 4-(2-bromoethylphenol) **122**.

1.2.   4-(2-azidoethyl)phenol 123
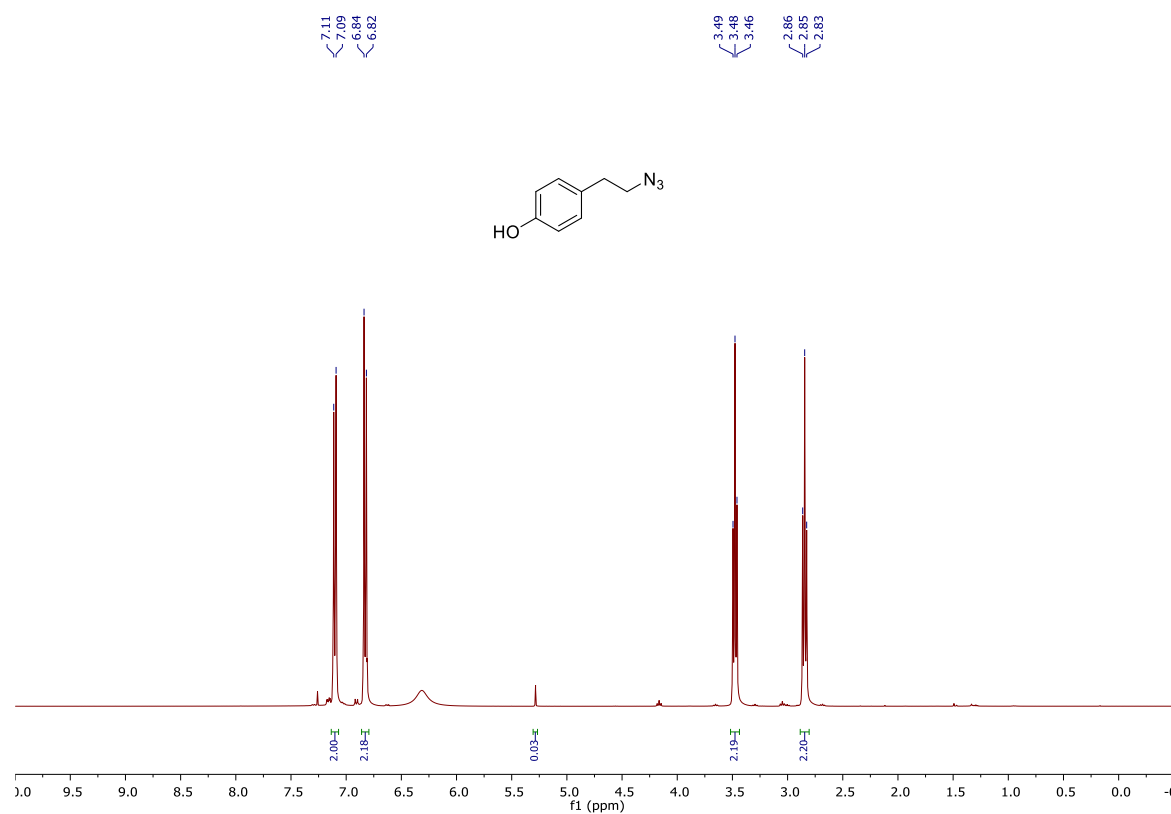
Figure S4. ¹H NMR spectrum of 4-(2-azidoethylphenol) **123** in CDCl₃ recorded at room temperature (400 MHz).
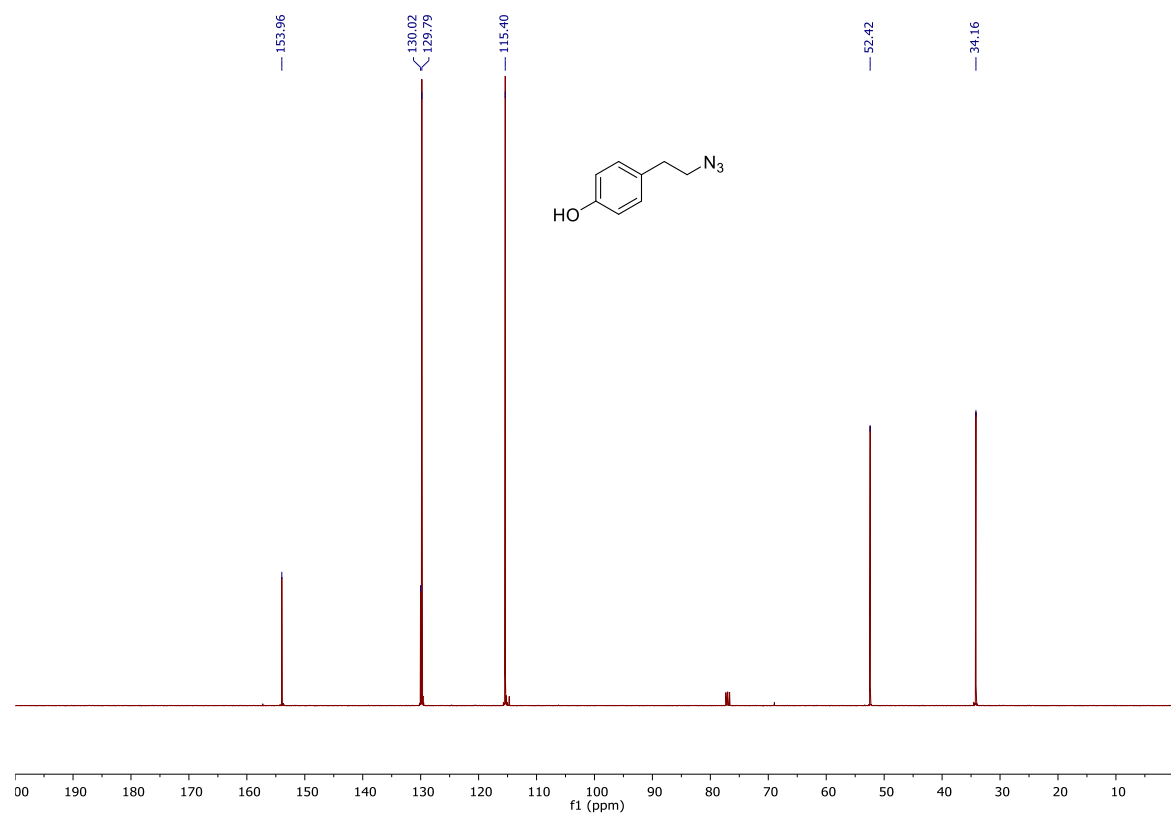
Figure S5. ¹³C{¹H} NMR spectrum of 4-(2-azidoethylphenol) **123** in CDCl₃ recorded at room temperature (101 MHz).
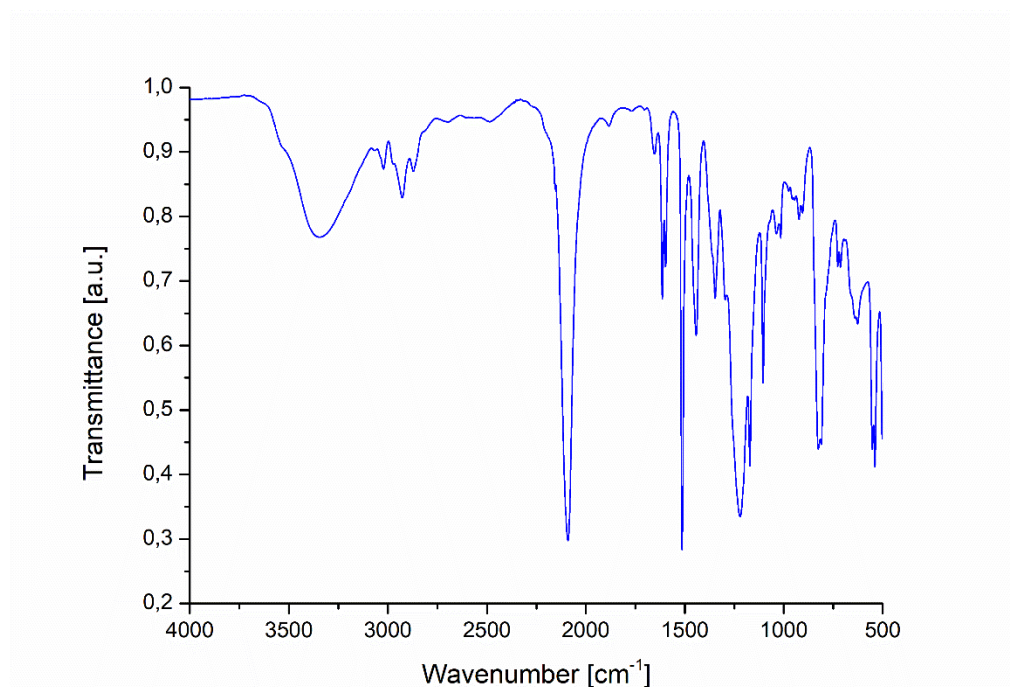
Figure S6. FT-IR spectrum of 4-(2-azidoethylphenol) **123**.

1.3. 4-(prop-2-yn-yloxy)phenol 126
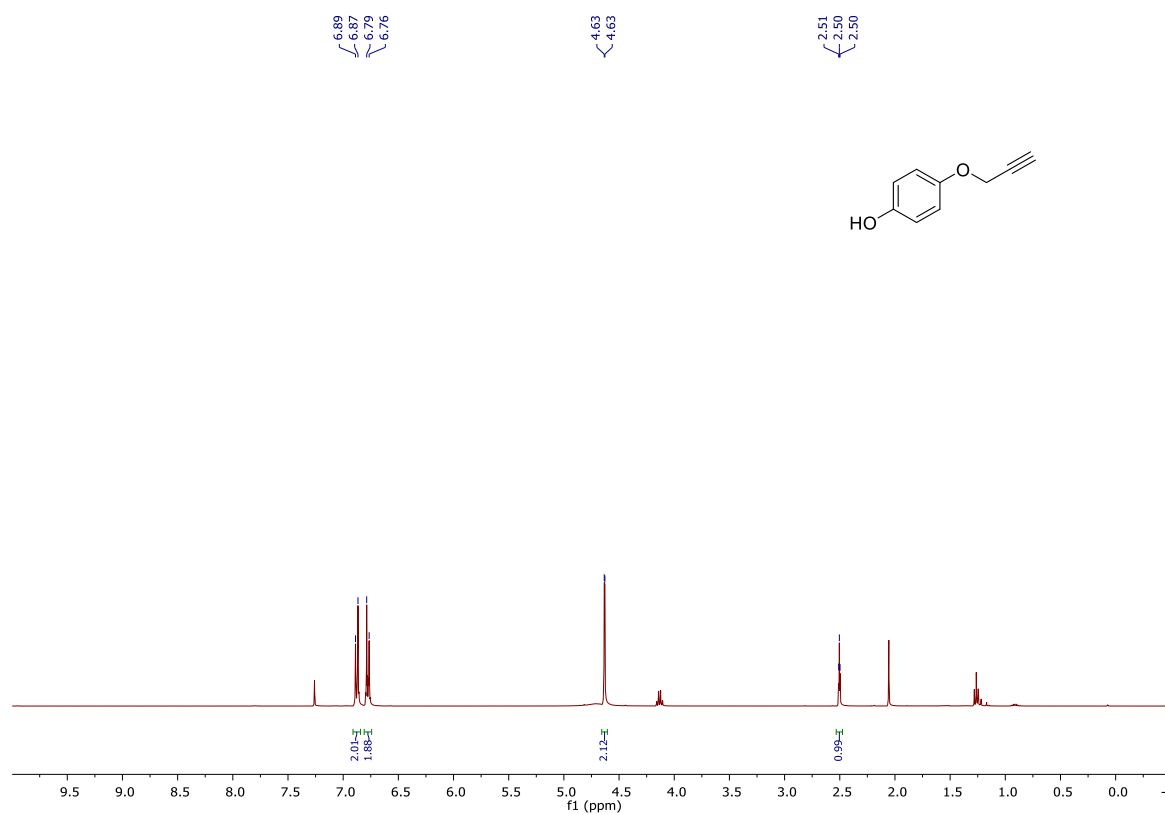
Figure S7. ¹H NMR spectrum of 4-(prop-2-yn-yloxy)phenol **126** in CDCl₃ recorded at room temperature (400 MHz).
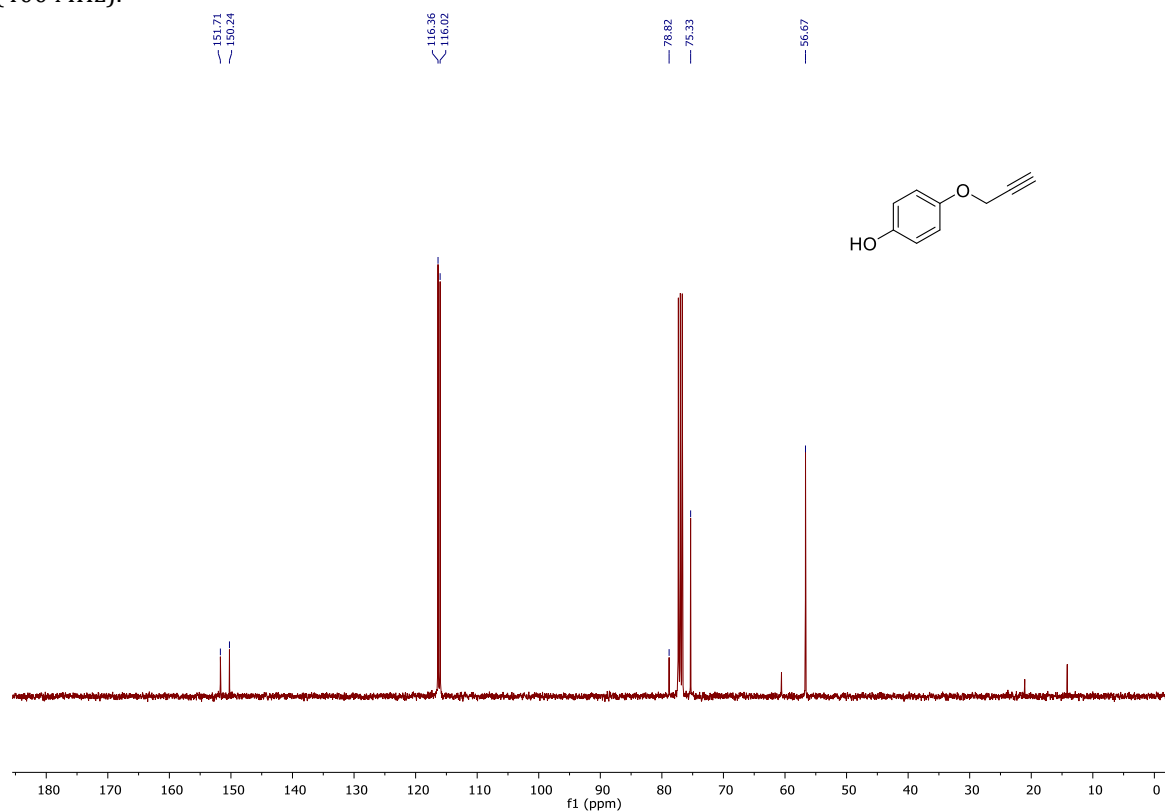
Figure S8. ¹³C{¹H} NMR spectrum of 4-(prop-2-yn-yloxy)phenol **126** in CDCl₃ recorded at room temperature (101 MHz).

1.4. *N*-methyldichlorothiophosphorhydrazide 38
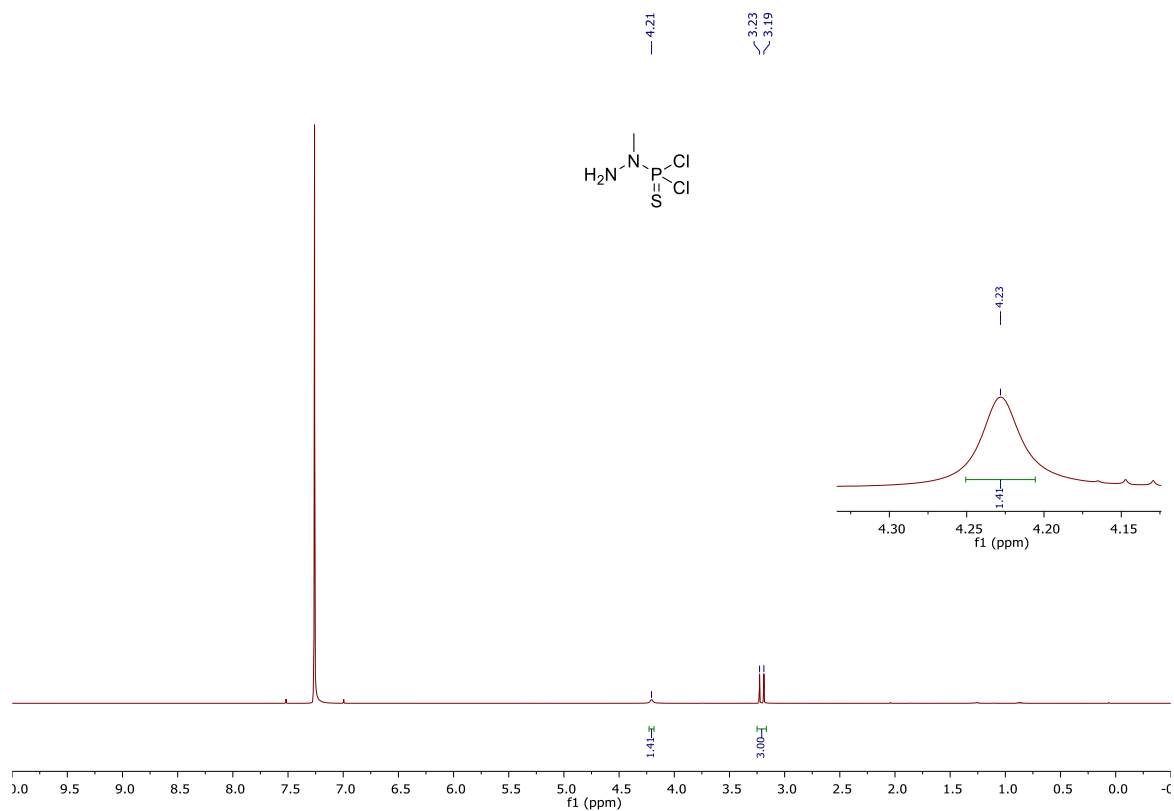
Figure S9. ^{1}H NMR spectrum of *N*-methyldichlorothiophosphorhydrazide **38** in CDCl$_3$ recorded at room temperature (400 MHz).
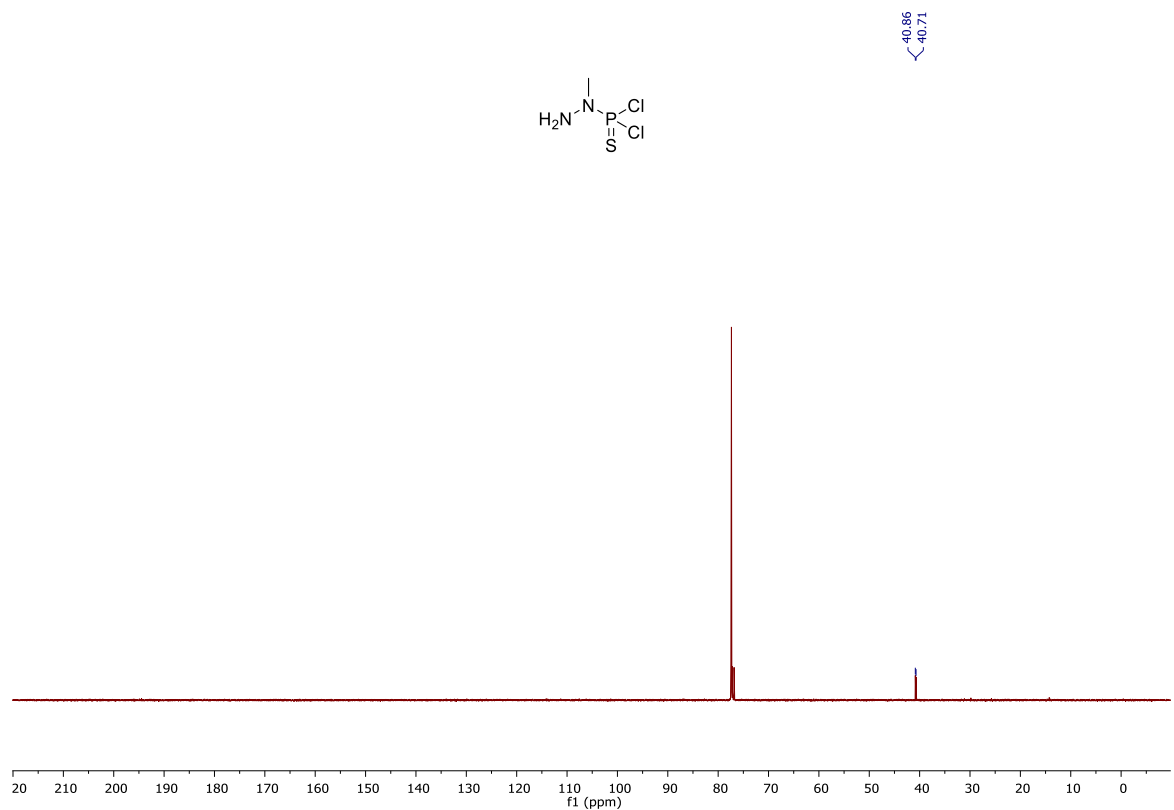
Figure S10. ^{13}C{^{1}H} NMR spectrum of *N*-methyldichlorothiophosphorhydrazide **38** in CDCl$_3$ recorded at room temperature (101 MHz).
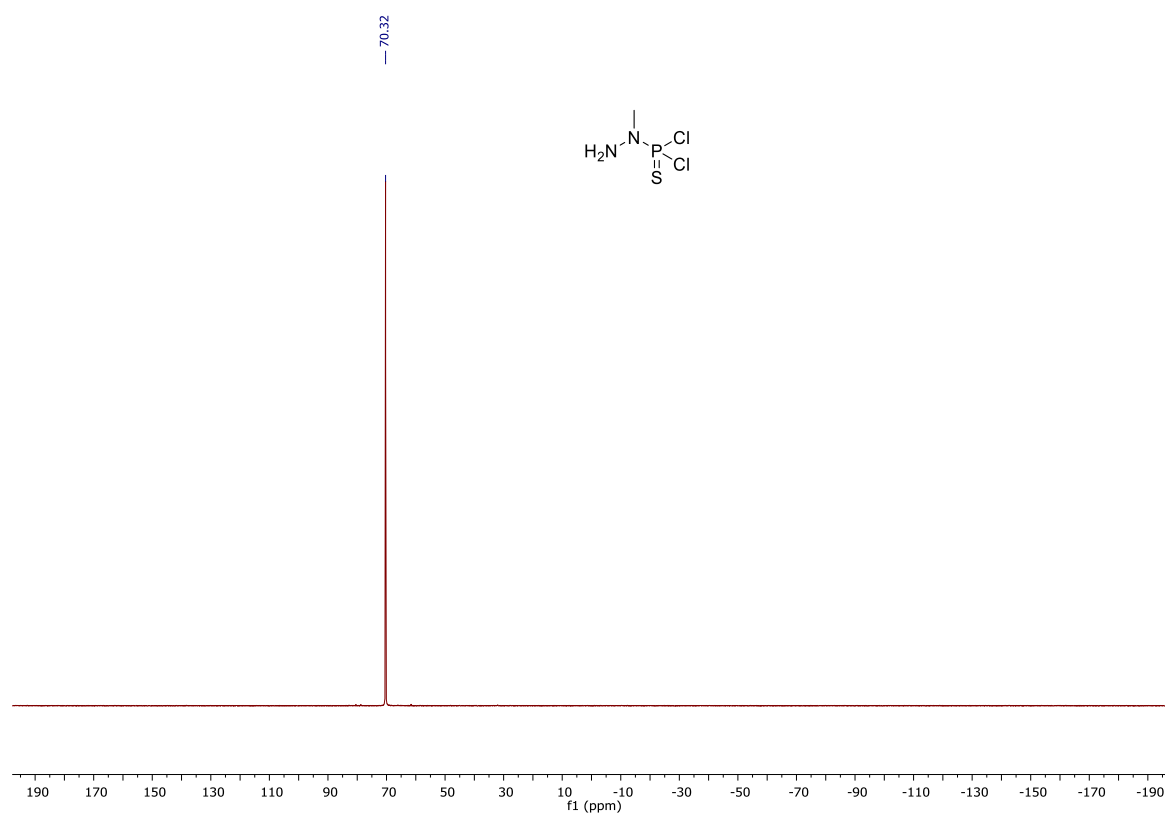
Figure S11. ^{31}P{^{1}H} NMR spectrum of *N*-methyldichlorothiophosphorhydrazide **38** in CDCl$_3$ recorded at room temperature (162 MHz).

1.5.   AB₅ core 127
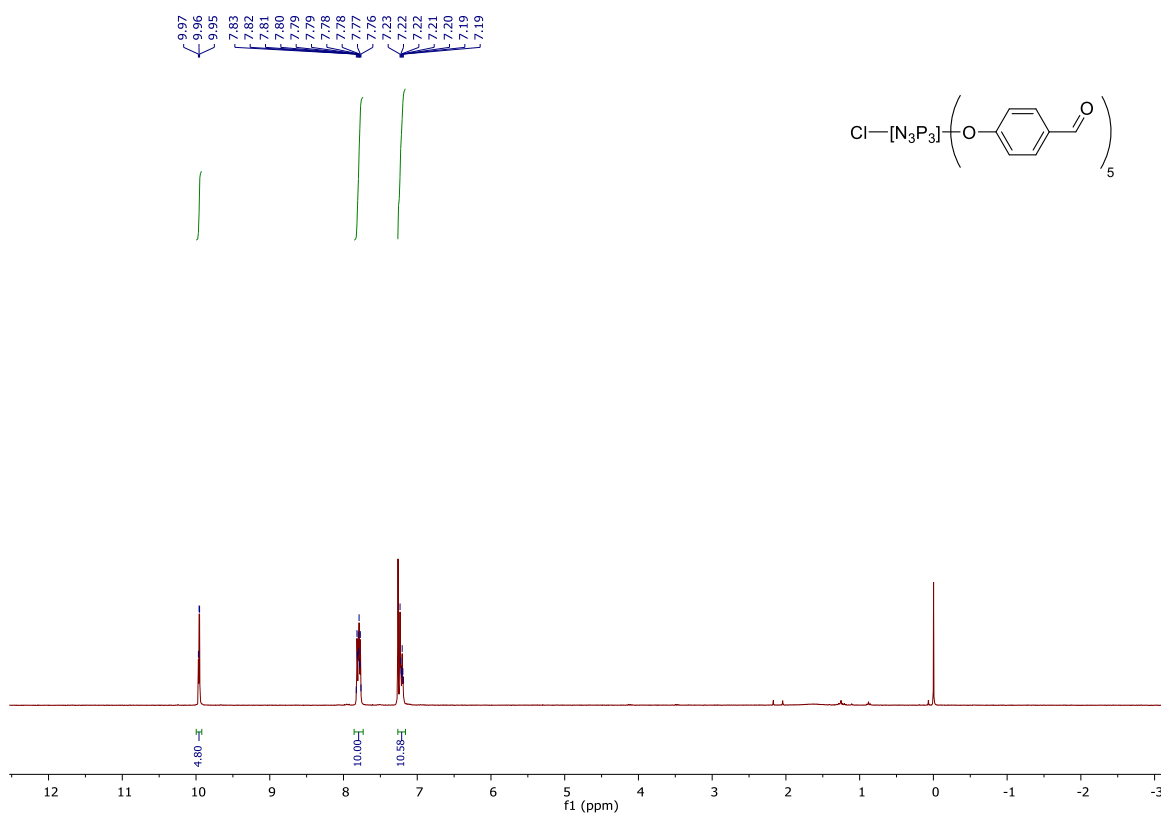
Figure S12. ¹H NMR spectrum of AB₅ core **127** in CDCl₃ recorded at room temperature (400 MHz).
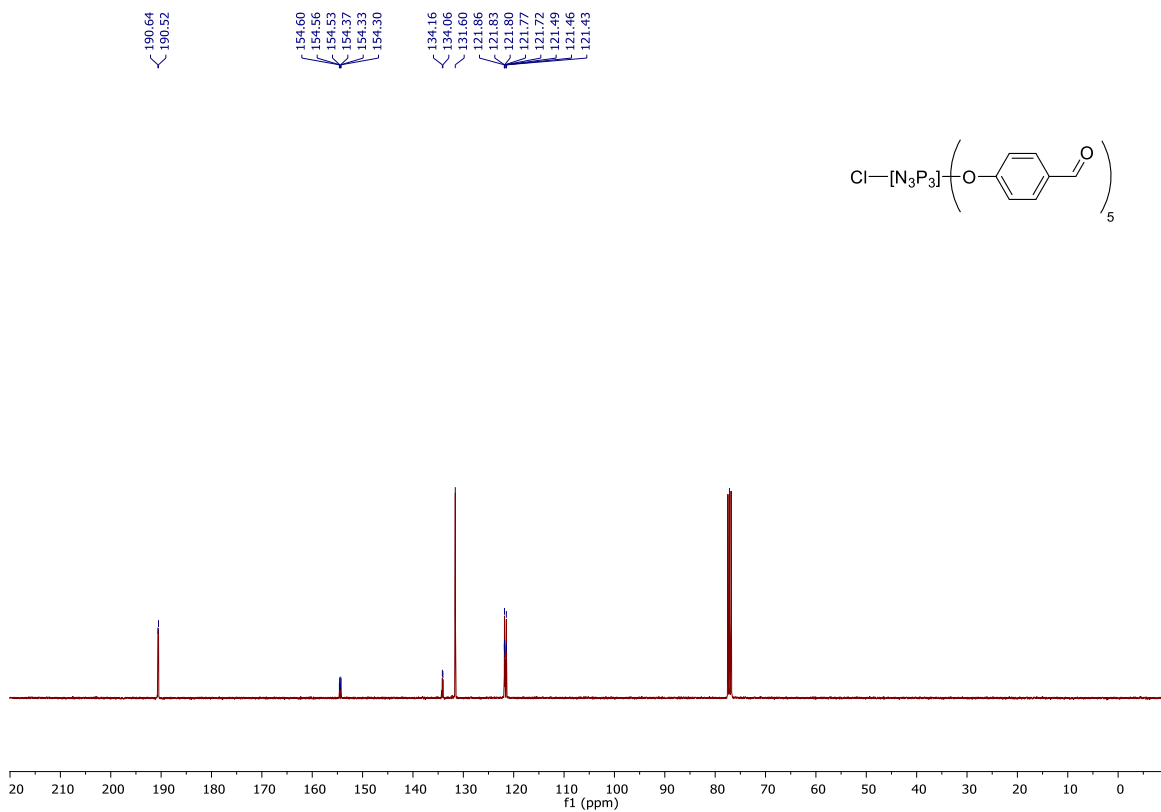
**Figure S13**. ¹³C{¹H} NMR spectrum of AB₅ core **127** in CDCl₃ recorded at room temperature (101 MHz).
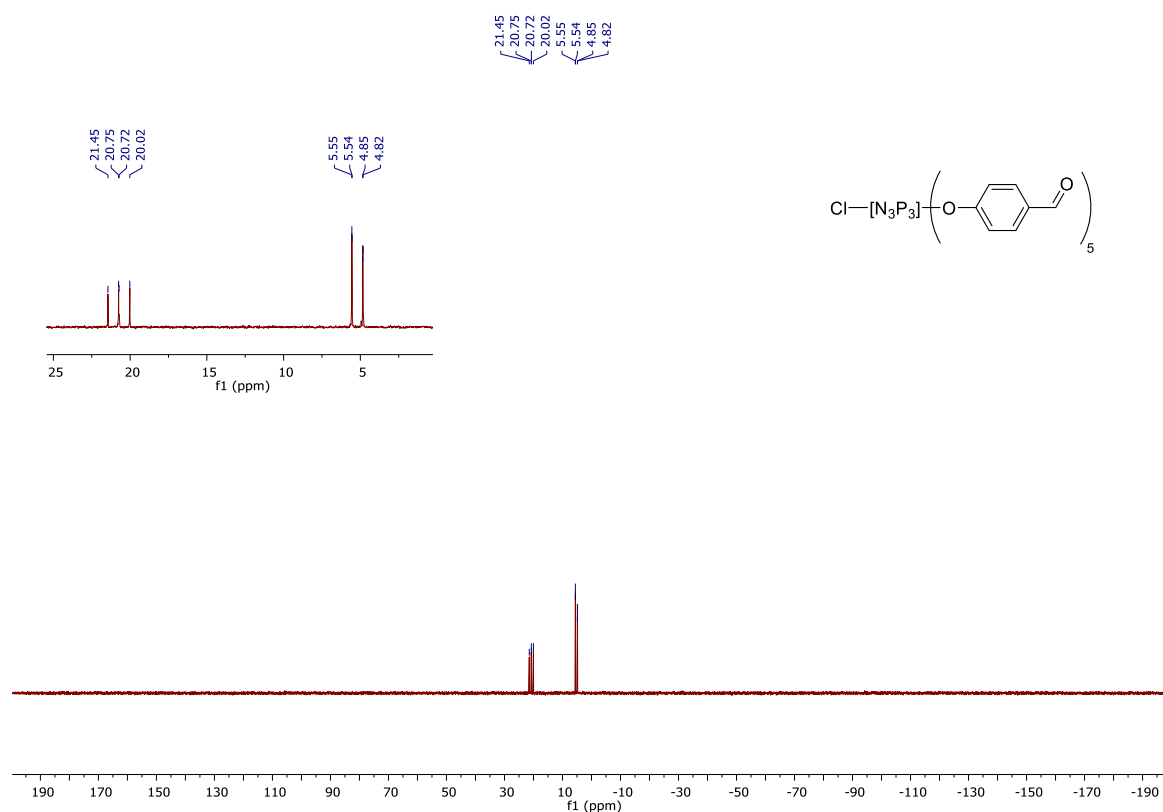
Figure S14. ^{31}P{^{1}H} NMR spectrum of compound AB$_5$ core **127** in CDCl$_3$ recorded at room temperature (162 MHz).
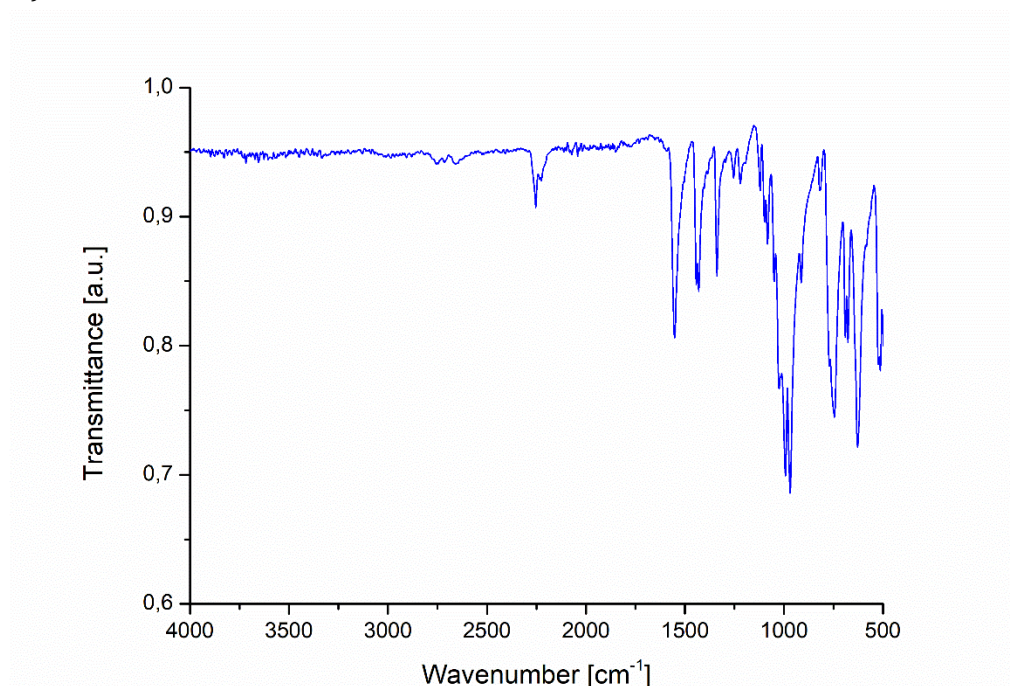
Figure S15. FT-IR spectrum of AB$_5$ core **127**.

1.6.   2-(4-(2-azidoethyl)phenoxy)-2,4,4,6,6-pentachlorotriazatriphosphazene 130
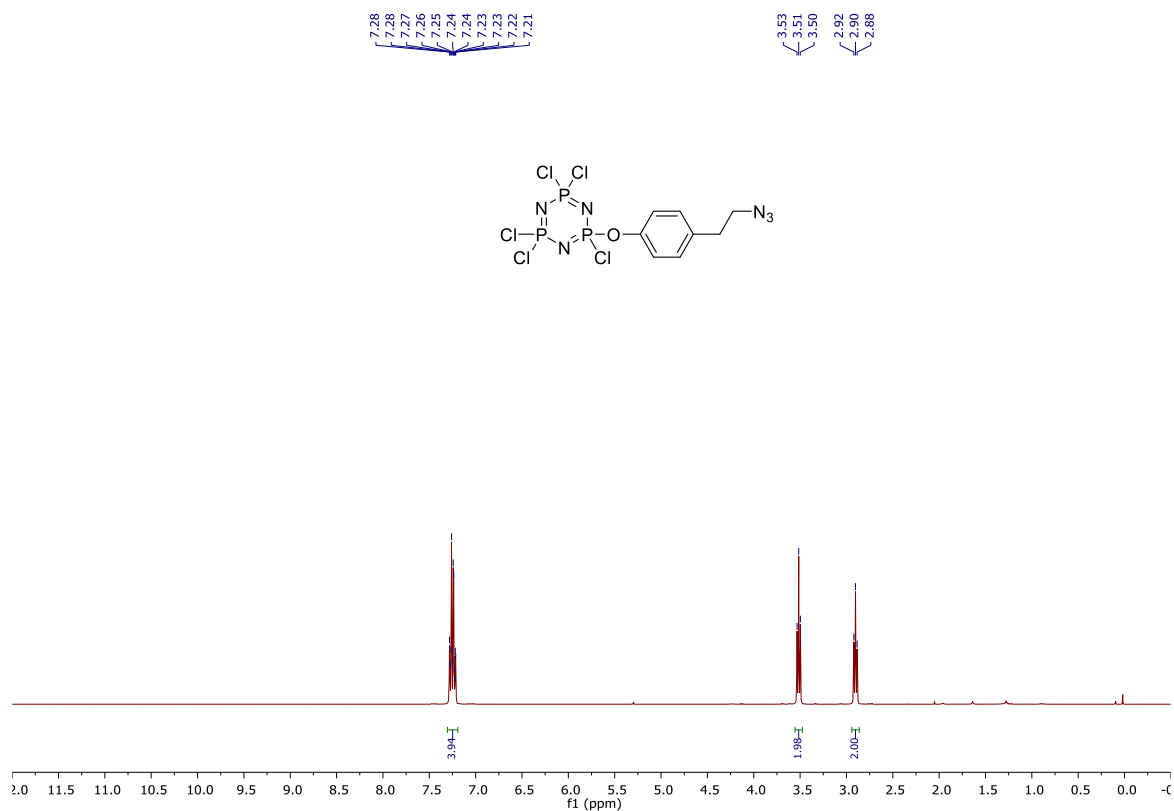
Figure S16. [1H] NMR spectrum of 2-(4-(2-azidoethyl)phenoxy)-2,4,4,6,6-pentachlorotriazatriphosphazene **130** in CDCl$_3$ recorded at room temperature (400 MHz).
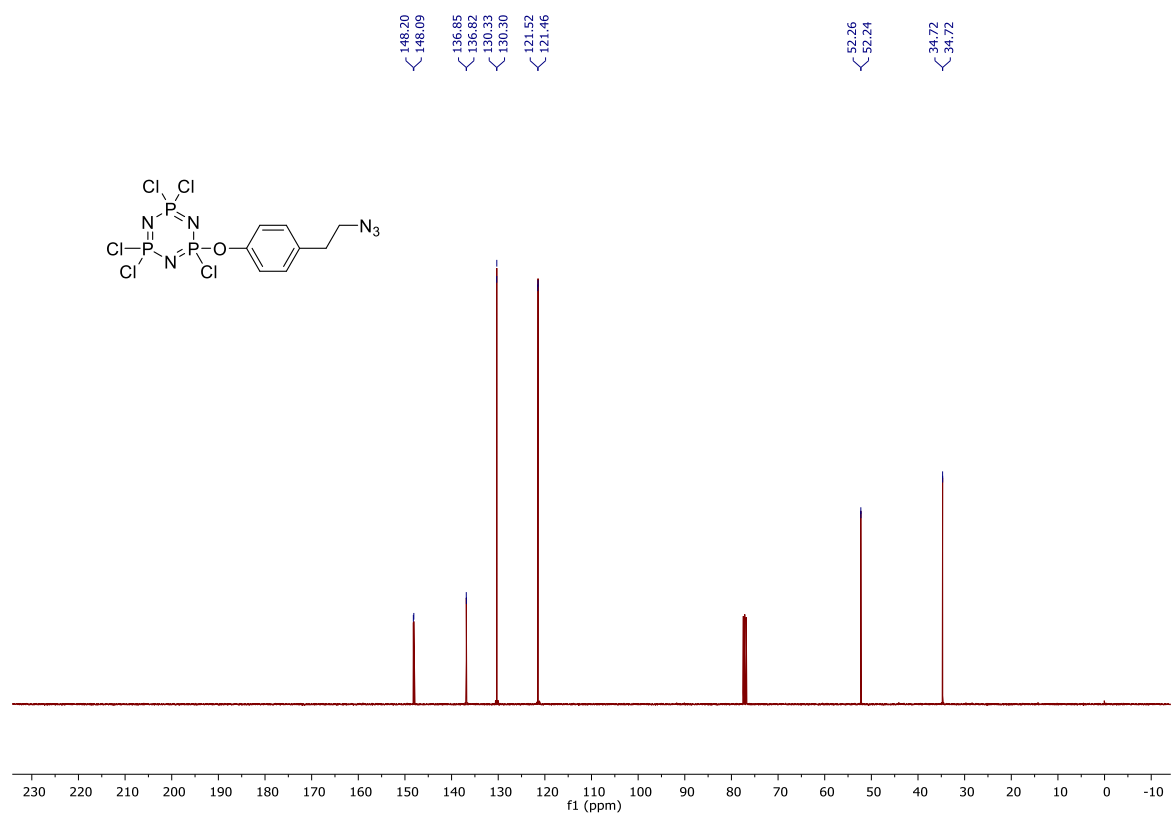
Figure S17. [13C{1H}] NMR spectrum of 2-(4-(2-azidoethyl)phenoxy)-2,4,4,6,6-pentachlorotriazatriphos-phazene **130** in CDCl$_3$ recorded at room temperature (101 MHz).
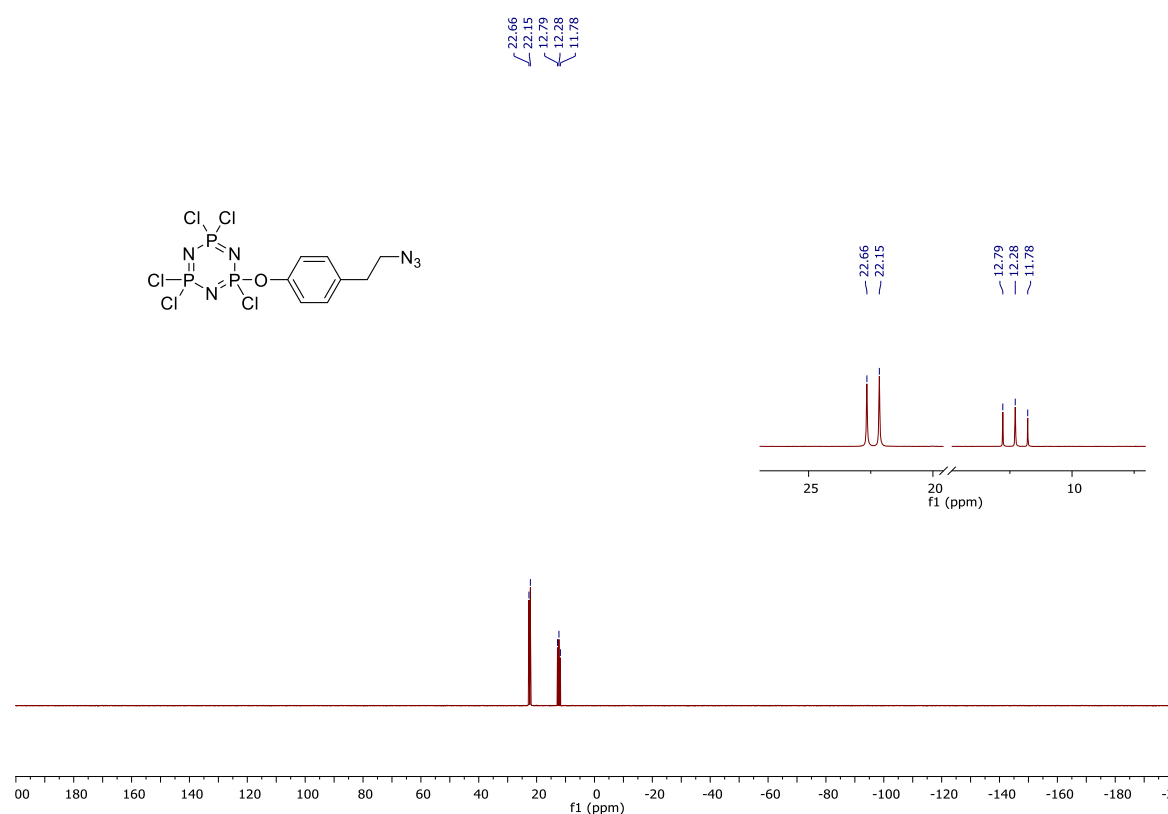
Figure S18. ^{31}P{^{1}H} NMR spectrum of 2-(4-(2-azidoethyl)phenoxy)-2,4,4,6,6-pentachlorotriazatriphosphazene **130** in CDCl$_3$ recorded at room temperature (162 MHz).
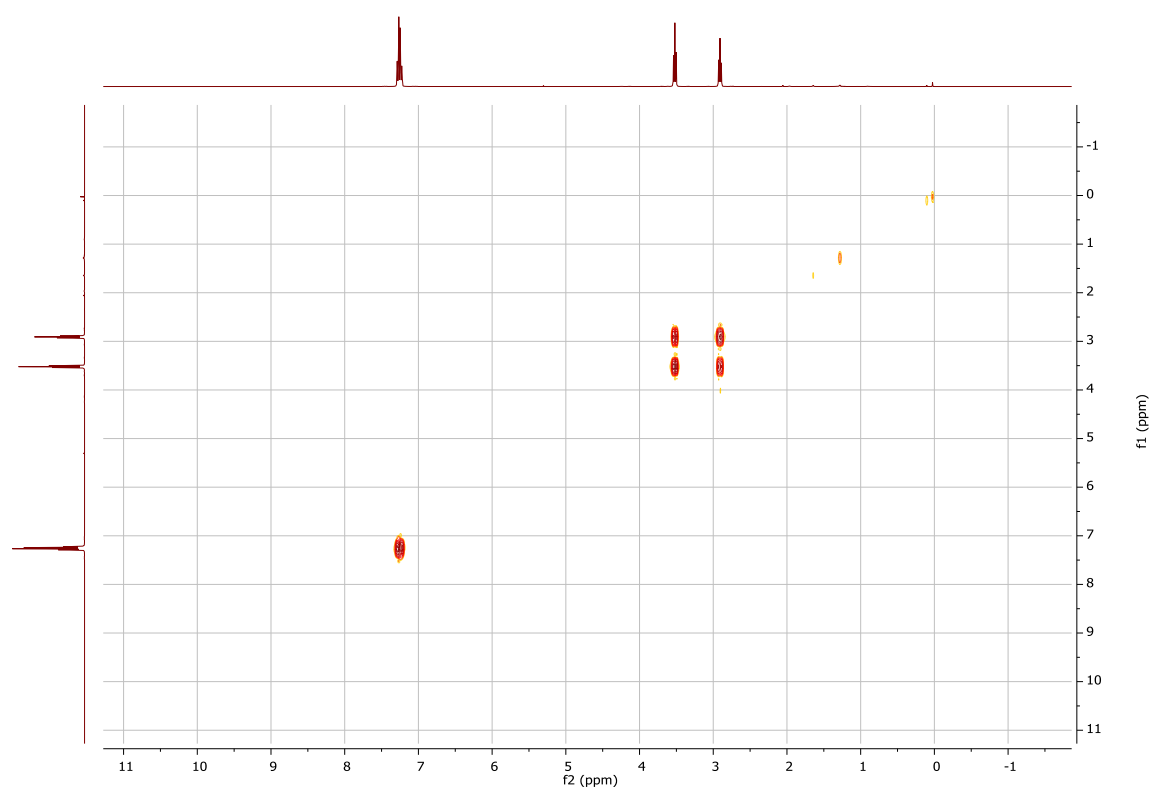
Figure S19. ^{1}H-^{1}H COSY spectrum of 2-(4-(2-azidoethyl)phenoxy)-2,4,4,6,6-pentachlorotriazatriphosphazene **130** in CDCl$_3$ recorded at room temperature (400 MHz).
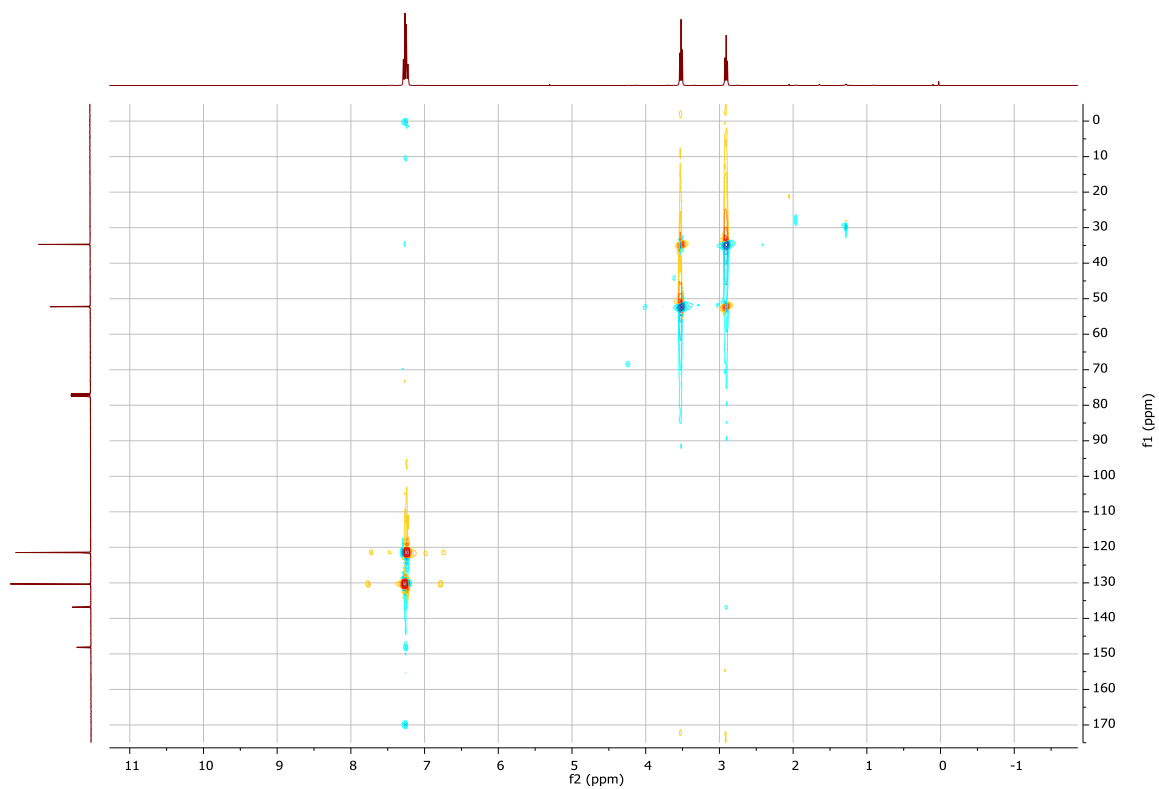
Figure S20. ¹H-¹³C{¹H} HSQC spectrum of 2-(4-(2-azidoethyl)phenoxy)-2,4,4,6,6-pentachlorotriazatri-phosphazene **130** in CDCl₃ recorded at room temperature (400 MHz, 101 MHz).
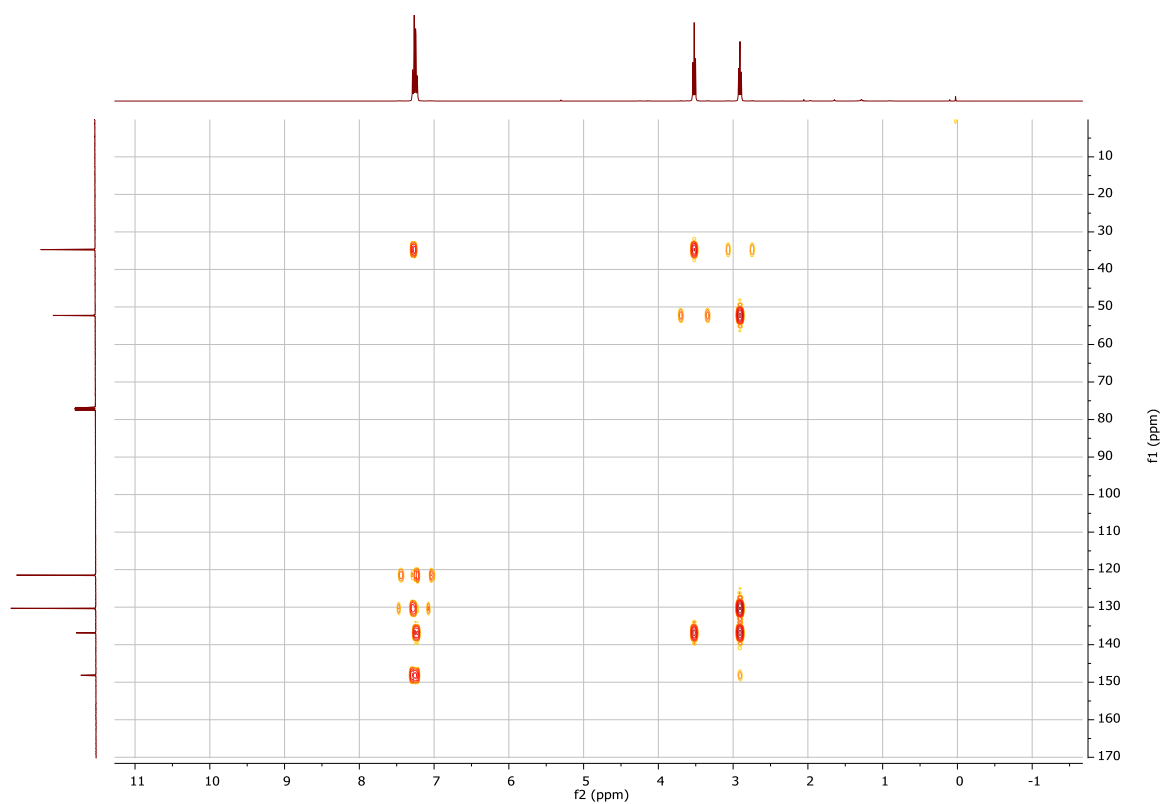
Figure S21. ¹H-¹³C{¹H} HMBC spectrum of 2-(4-(2-azidoethyl)phenoxy)-2,4,4,6,6-pentachlorotriazatri-phosphazene **130** in CDCl₃ recorded at room temperature (400 MHz, 101 MHz).
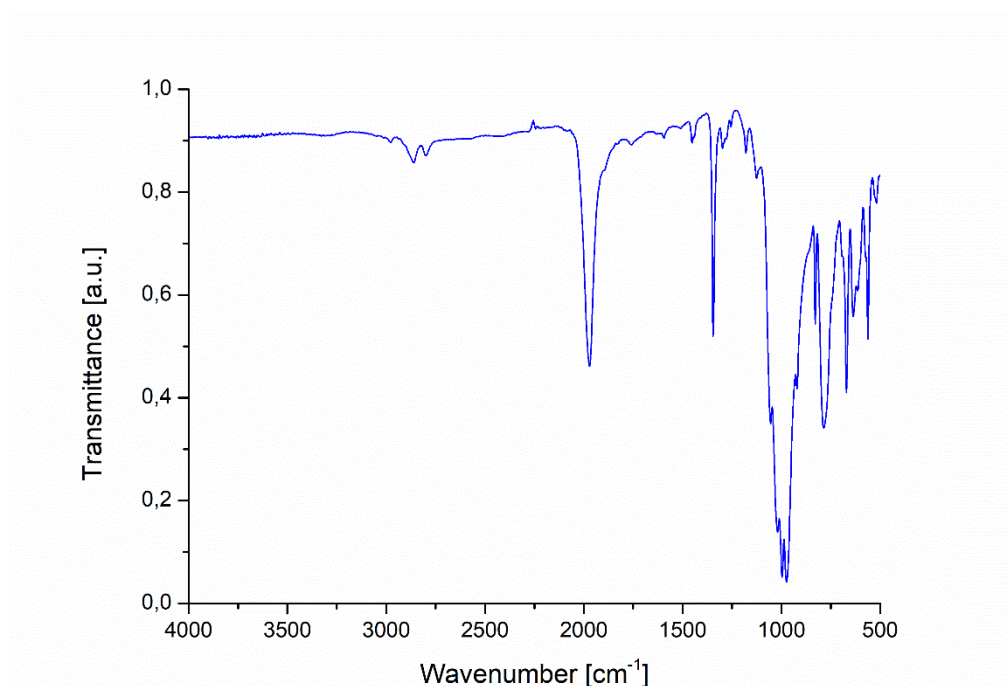
Figure S22. FT-IR spectrum of 2-(4-(2-azidoethyl)phenoxy)-2,4,4,6,6-pentachlorotriazatriphosphazene **130**.

Codi SAQ	Ref. mostra	%C	%H	%N	%S
23AE038/004	JCS2-AB1-azide	20,26	1,74	17,33	<0.1

Figure S23. Elemental analysis of 2-(4-(2-azidoethyl)phenoxy)-2,4,4,6,6-pentachlorotriazatri-phophazene **130**.

1.7.   Azide dendron 128-[G₀']

Figure S24. ¹H NMR spectrum of **128-[G₀']** in CDCl₃ recorded at room temperature (400 MHz).
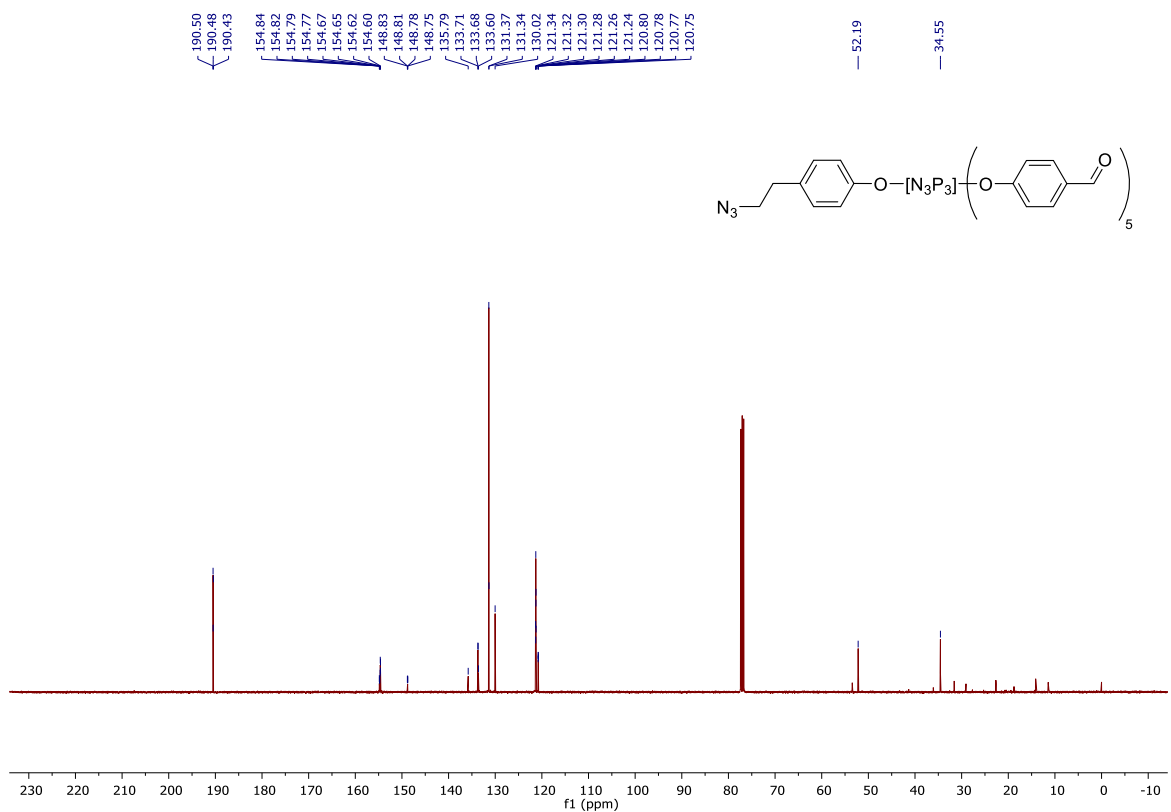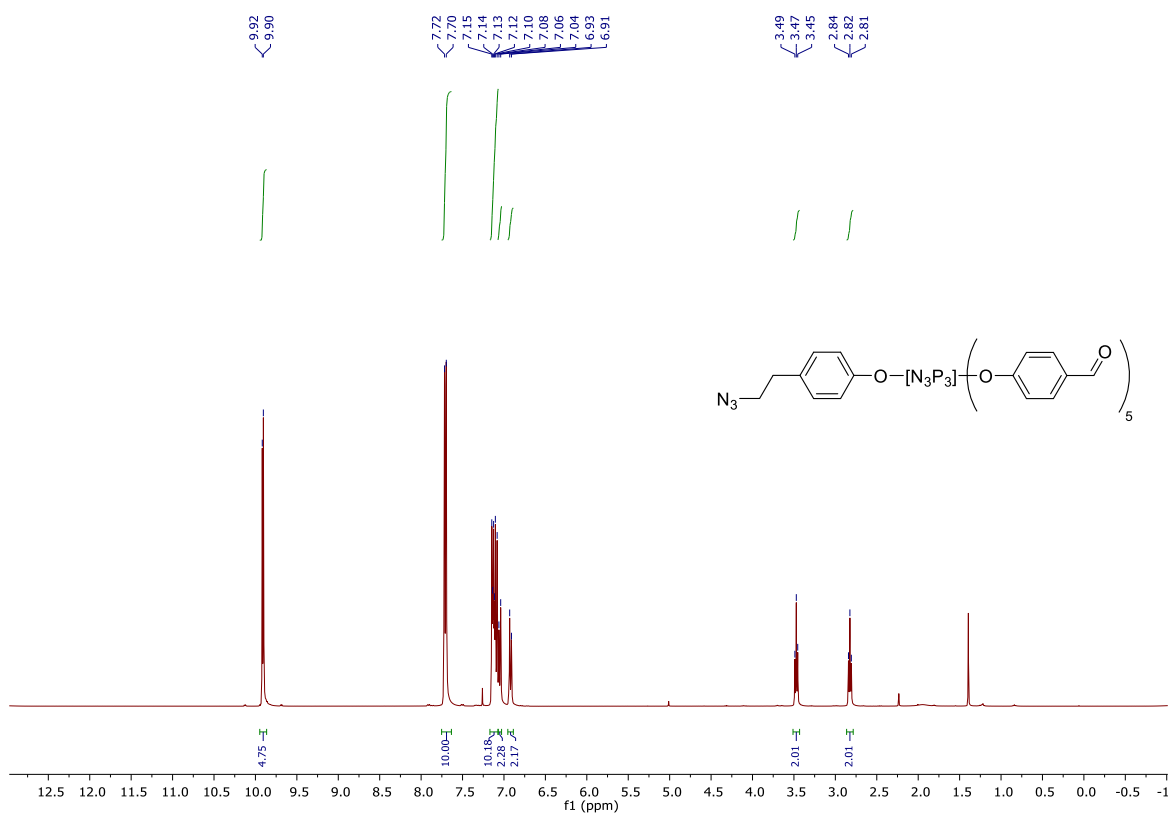
Figure S25. ¹³C{¹H} NMR spectrum of **128-[G₀']** azide dendron in CDCl₃ recorded at room temperature (101 MHz).
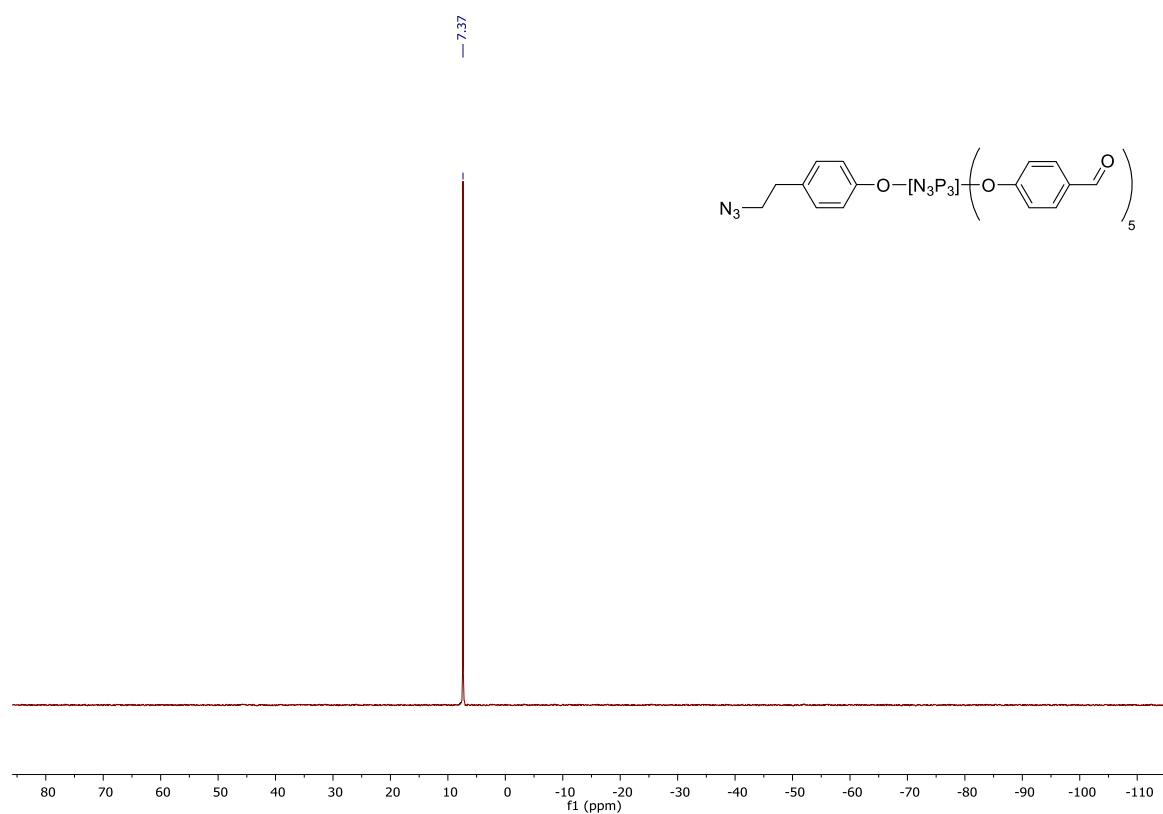
Figure S26. $^{31}P\{^1H\}$ NMR spectrum of **128-[G$_0$']** azide dendron in CDCl$_3$ recorded at room temperature (162 MHz).
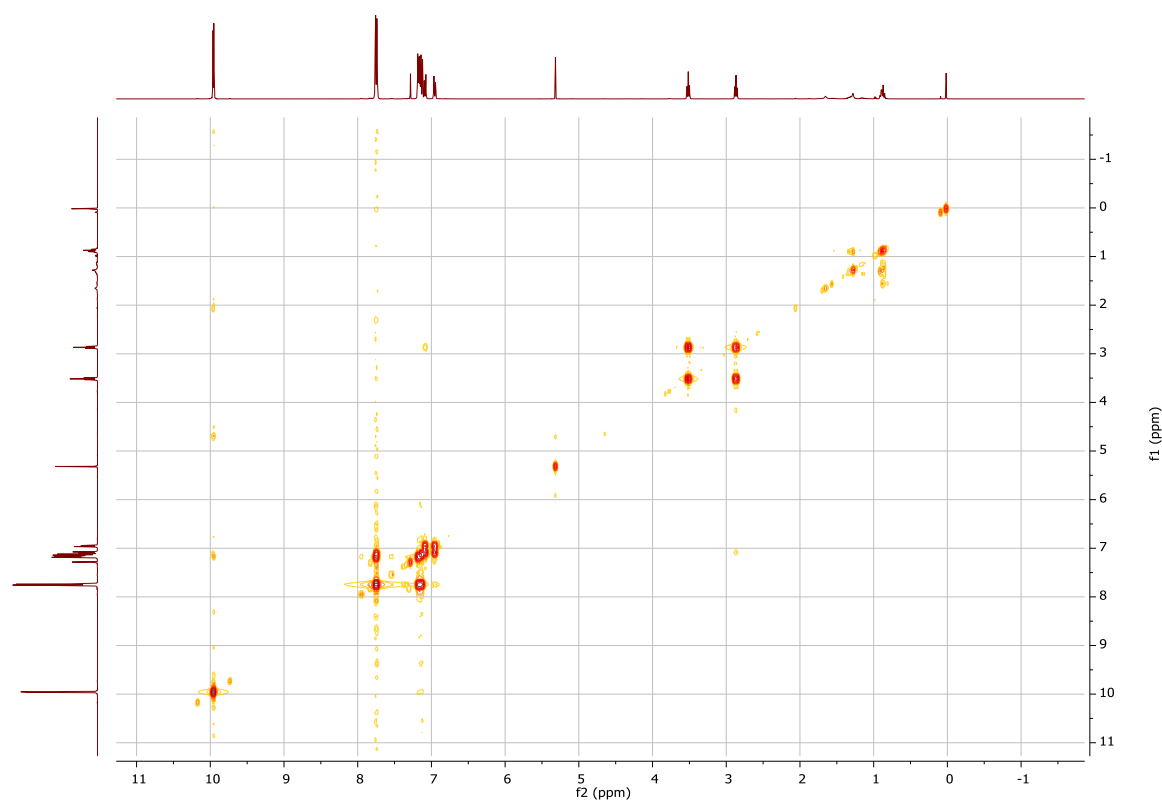
Figure S27. ^{1}H-^{1}H COSY spectrum of **128-[G$_0$']** azide dendron in CDCl$_3$ recorded at room temperature (400 MHz).
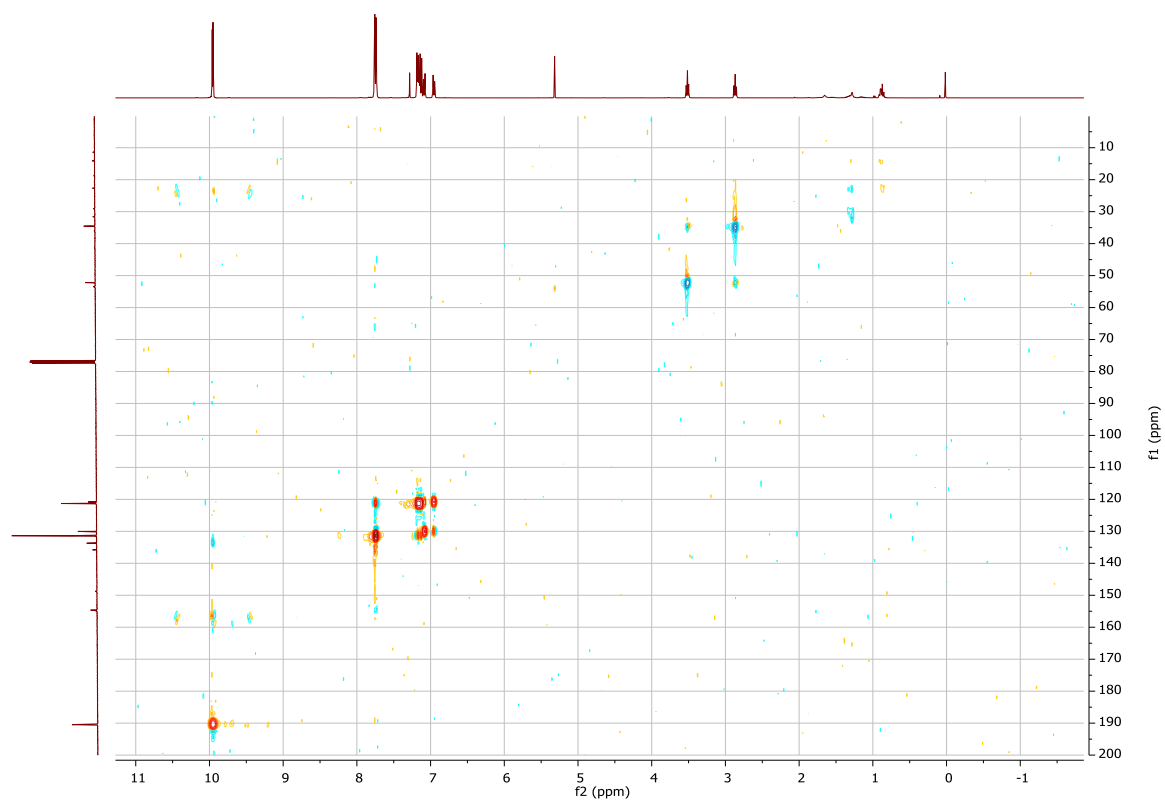
Figure S28. ^{1}H-^{13}C{^{1}H} HSQC spectrum **128-[G$_0$']** azide dendron in CDCl$_3$ recorded at room temperature (400 MHz, 101 MHz).
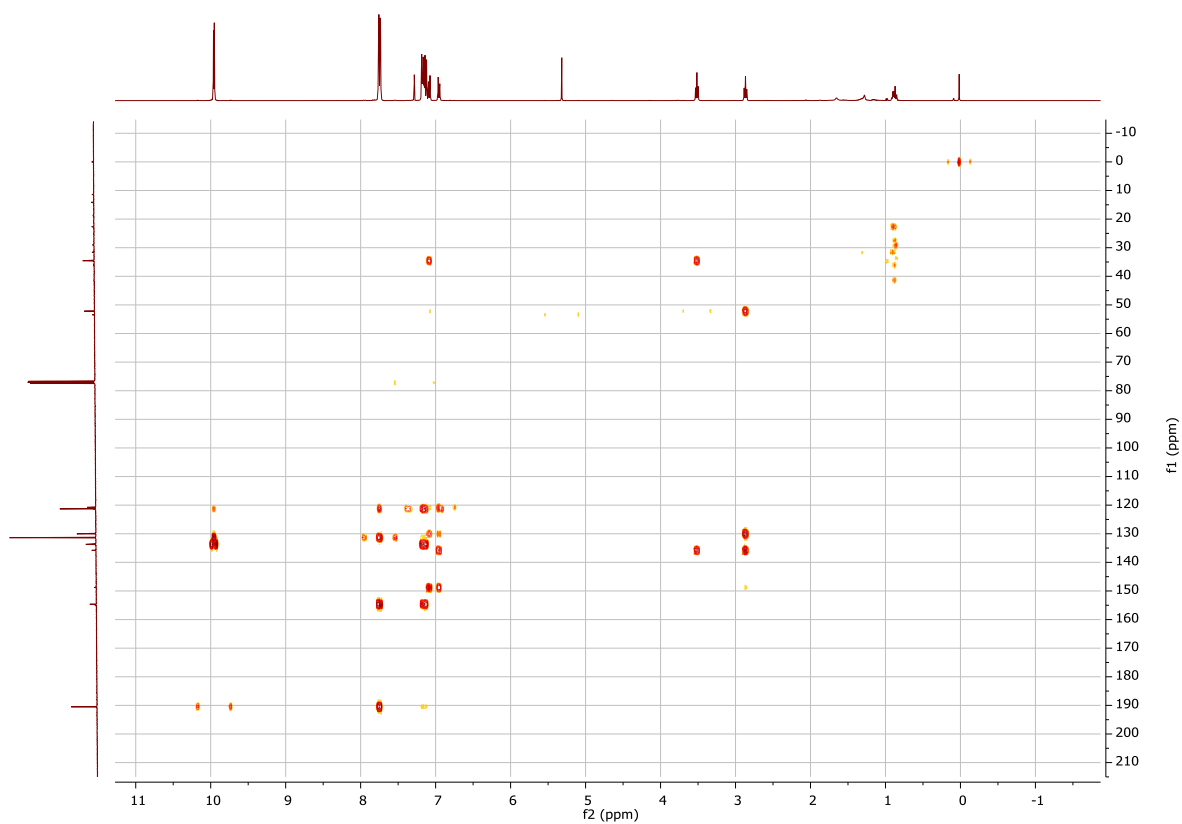
Figure S29. ^{1}H-^{13}C{^{1}H} HSQC spectrum **128-[G$_0$']** azide dendron in CDCl$_3$ recorded at room temperature (400 MHz, 101 MHz).
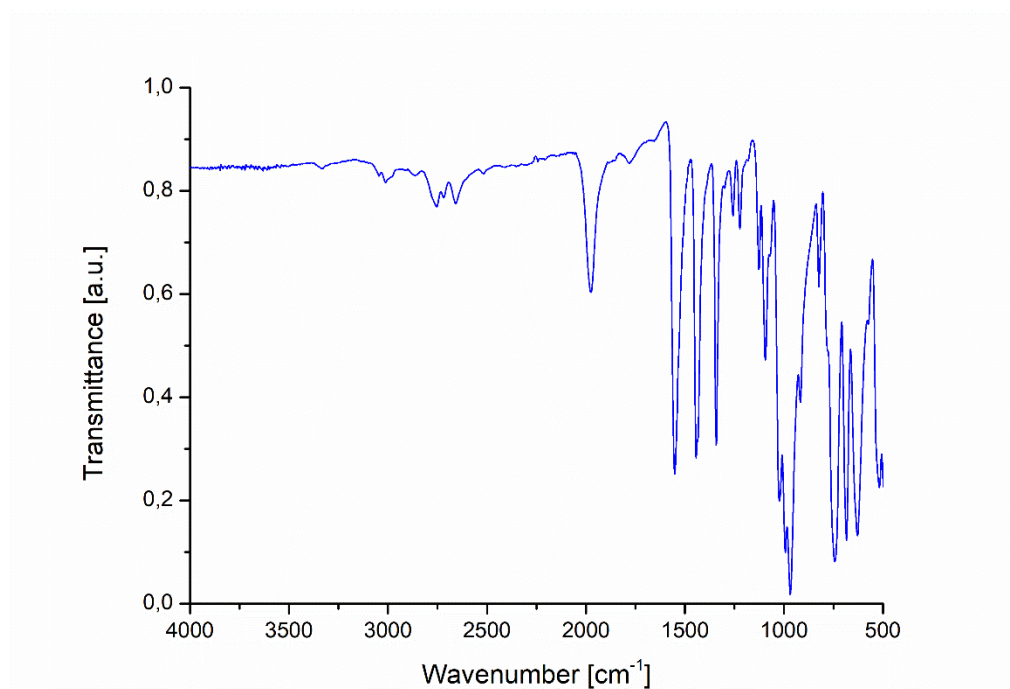
Figure S30. FT-IR spectrum of **128-[G₀']**.

1.8.   Azide dendron 133-[G₁]

Figure S31. ¹H NMR spectrum of **133-[G₁]** in CDCl₃ recorded at room temperature (400 MHz).

Figure S32. ¹³C{¹H} NMR spectrum of **133-[G₁]** in CDCl₃ recorded at room temperature (101 MHz).
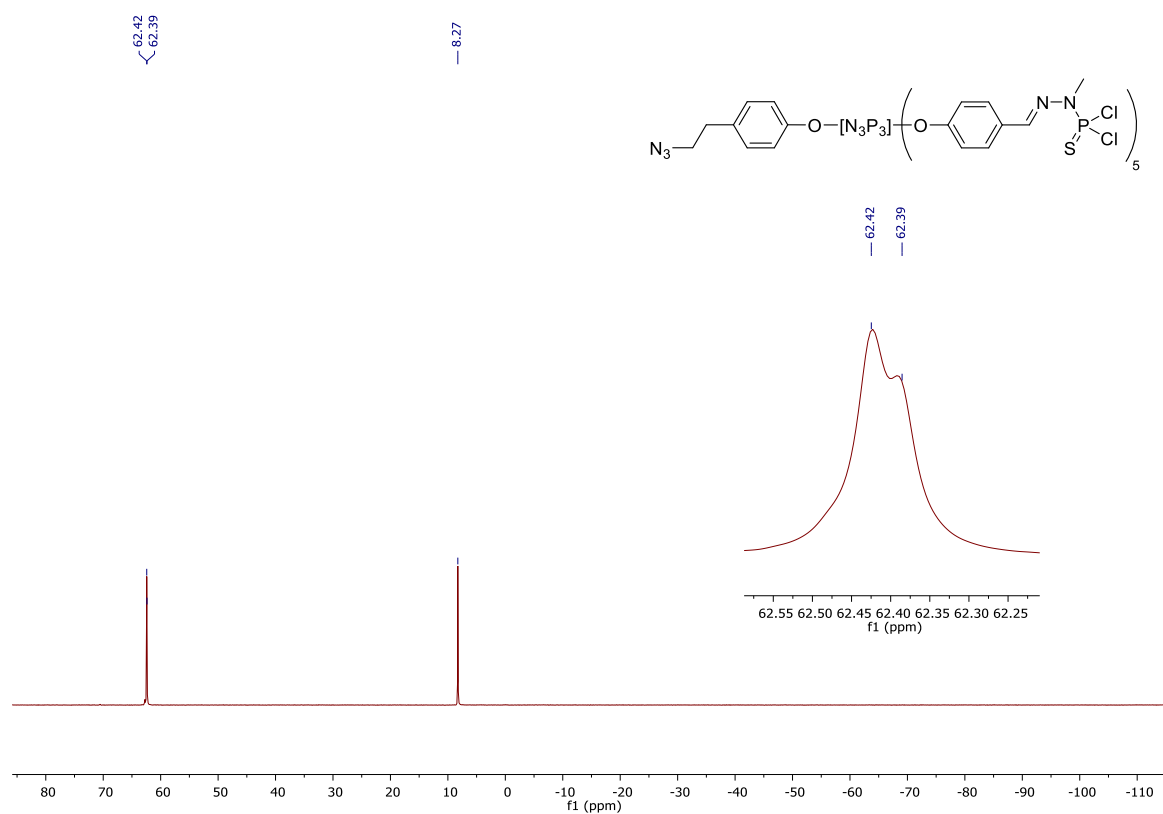
Figure S33. $^{31}P\{^1H\}$ NMR spectrum of **133-[G₁]** in CDCl₃ recorded at room temperature (162 MHz).
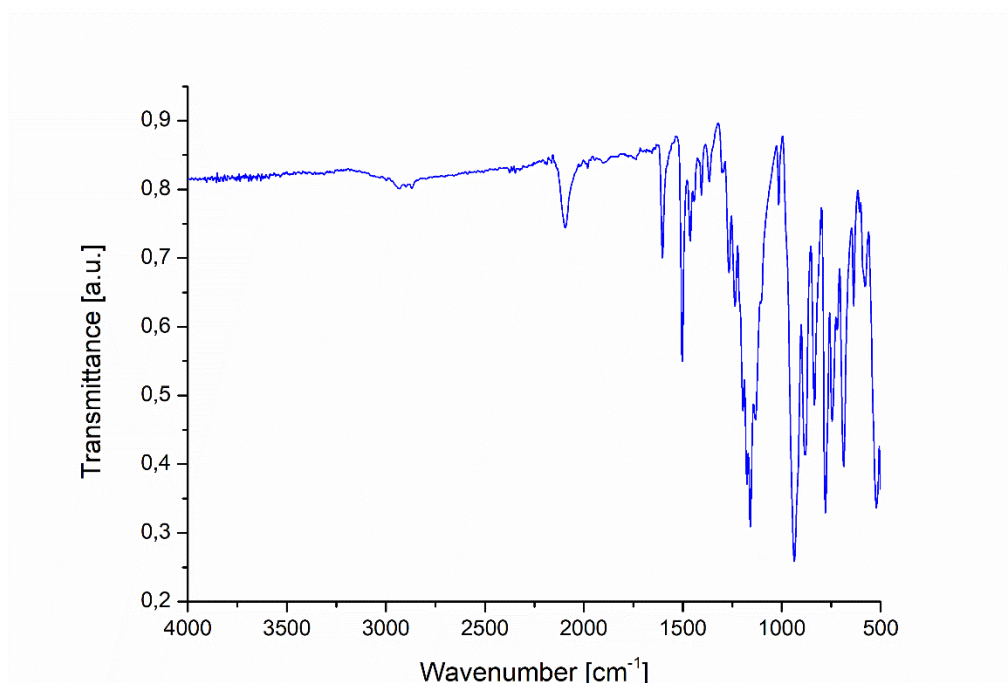
Figure S34. FT-IR spectrum of **133-[G₁]**.

1.9.   Azide dendron 135-[G$_1$′]

Figure S35. ^{1}H NMR spectrum of **135-[G$_1$′]** in CDCl$_3$ recorded at room temperature (400 MHz).

Figure S36. ^{13}C{^{1}H} NMR spectrum of **135-[G$_1$′]** in CDCl$_3$ recorded at room temperature (101 MHz).
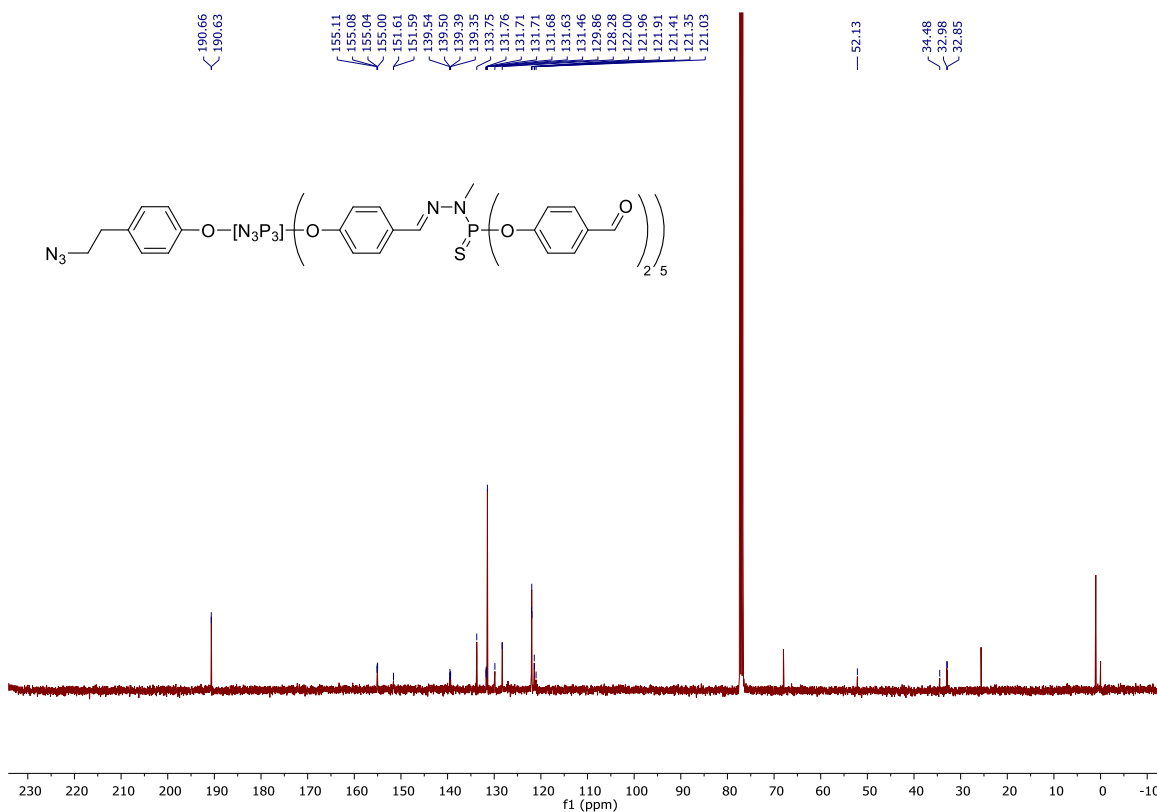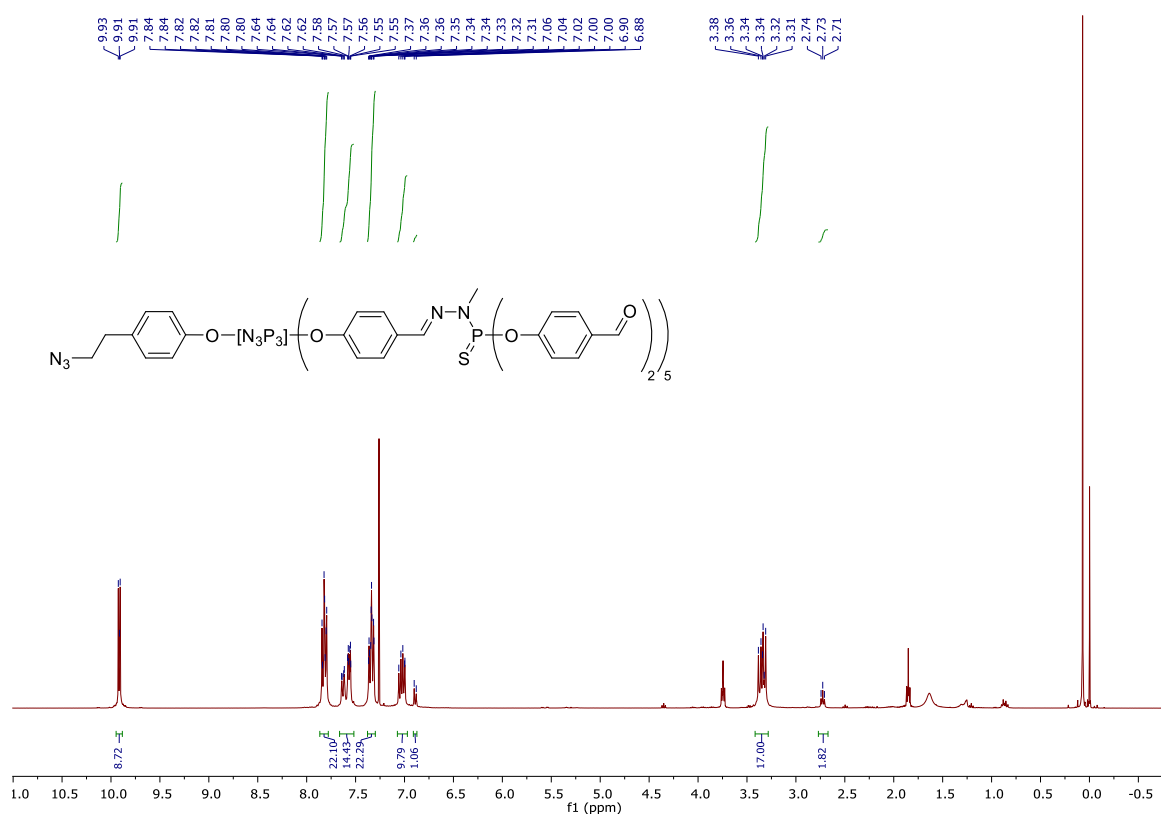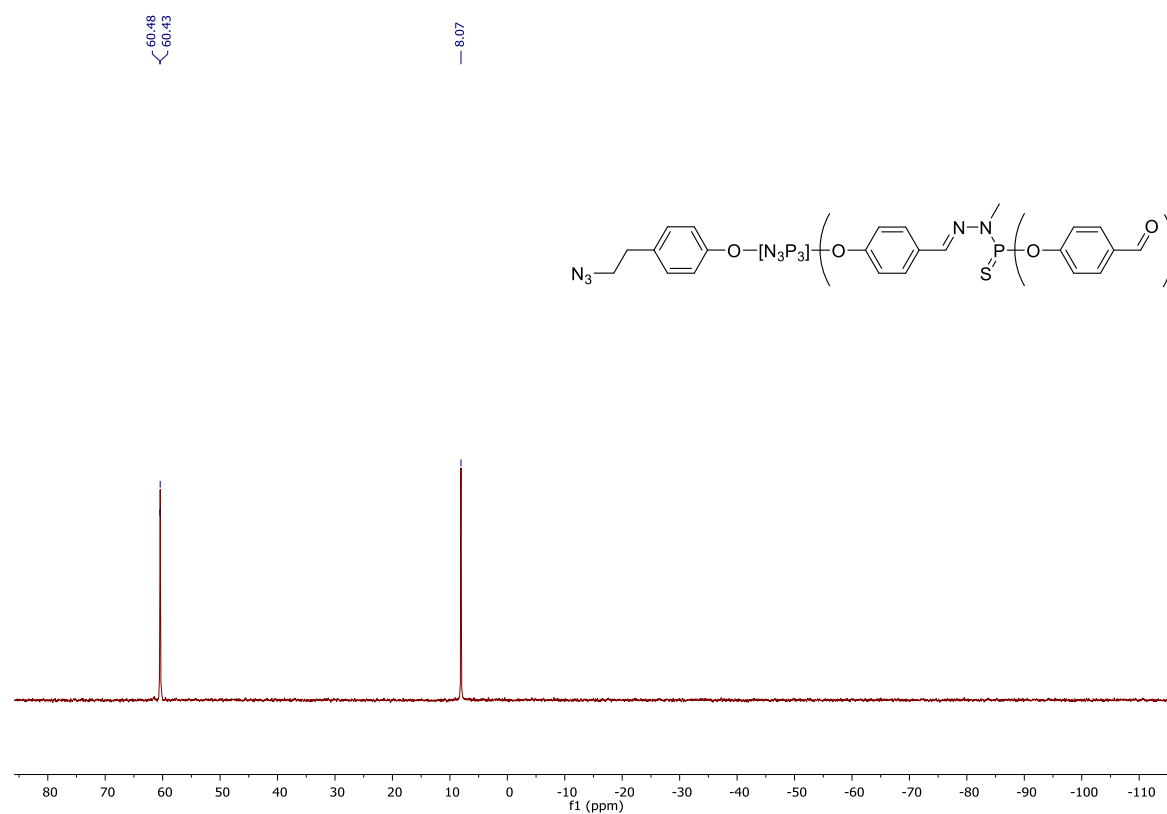
Figure S37. $^{31}P\{^1H\}$ NMR spectrum of **135-[G₁′]** in CDCl₃ recorded at room temperature (162 MHz).
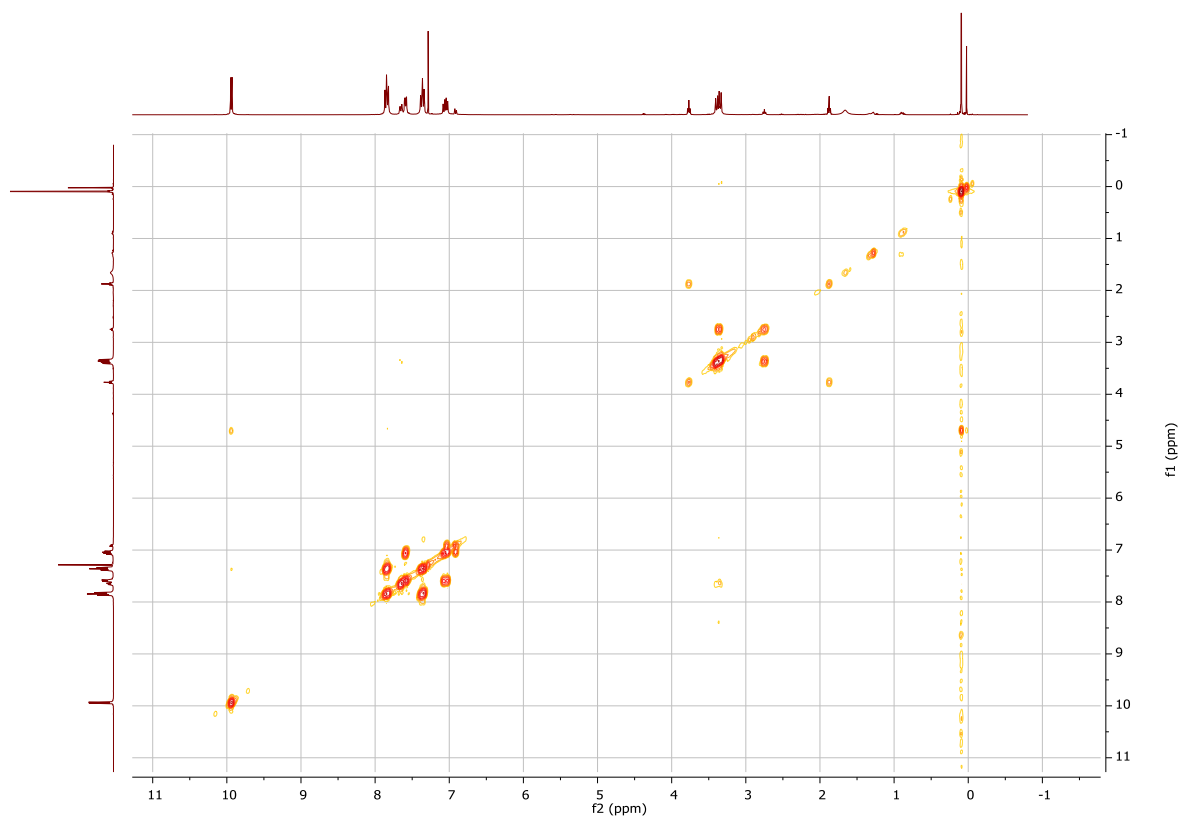
Figure S38. ^1H-^1H COSY spectrum of **135-[G₁′]** (400 MHz).
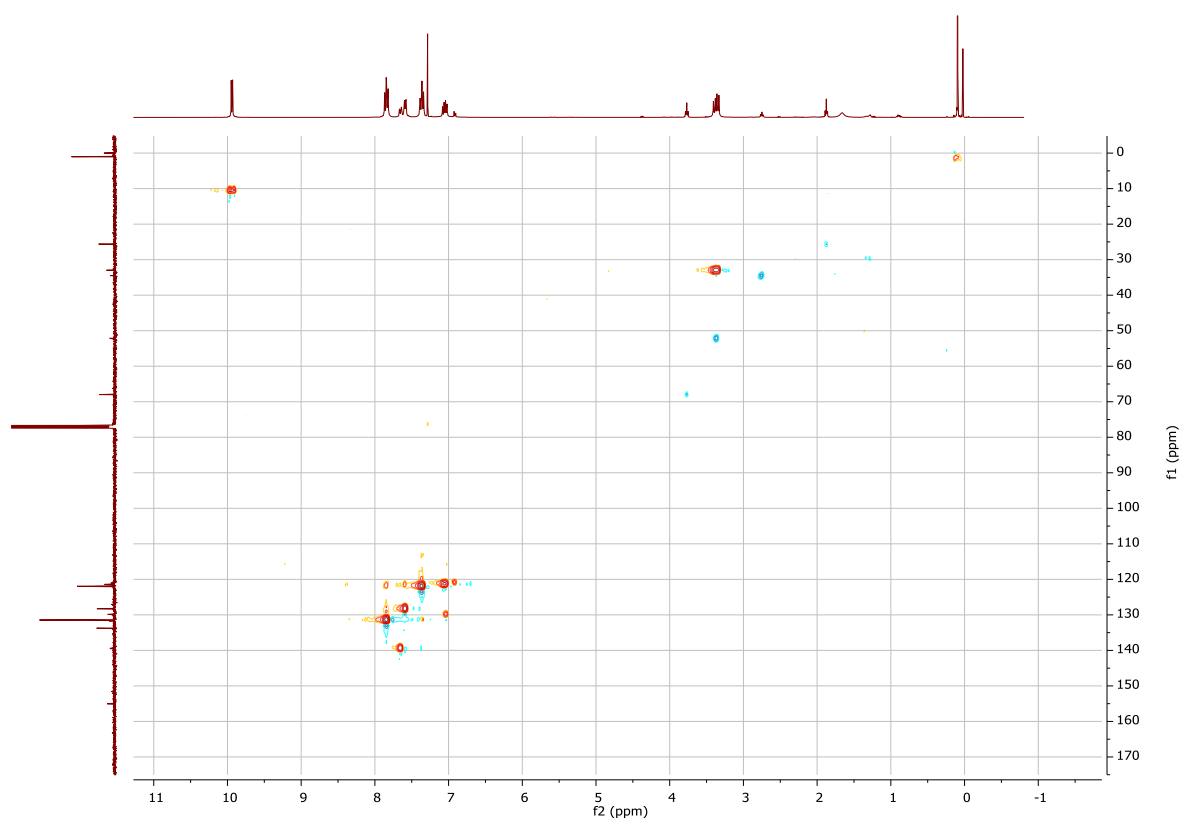
Figure S39. ^1H-$^{13}C\{^1H\}$ HSQC spectrum **135-[G$_1$']** azide dendron in CDCl$_3$ recorded at room temperature (400 MHz, 101 MHz).
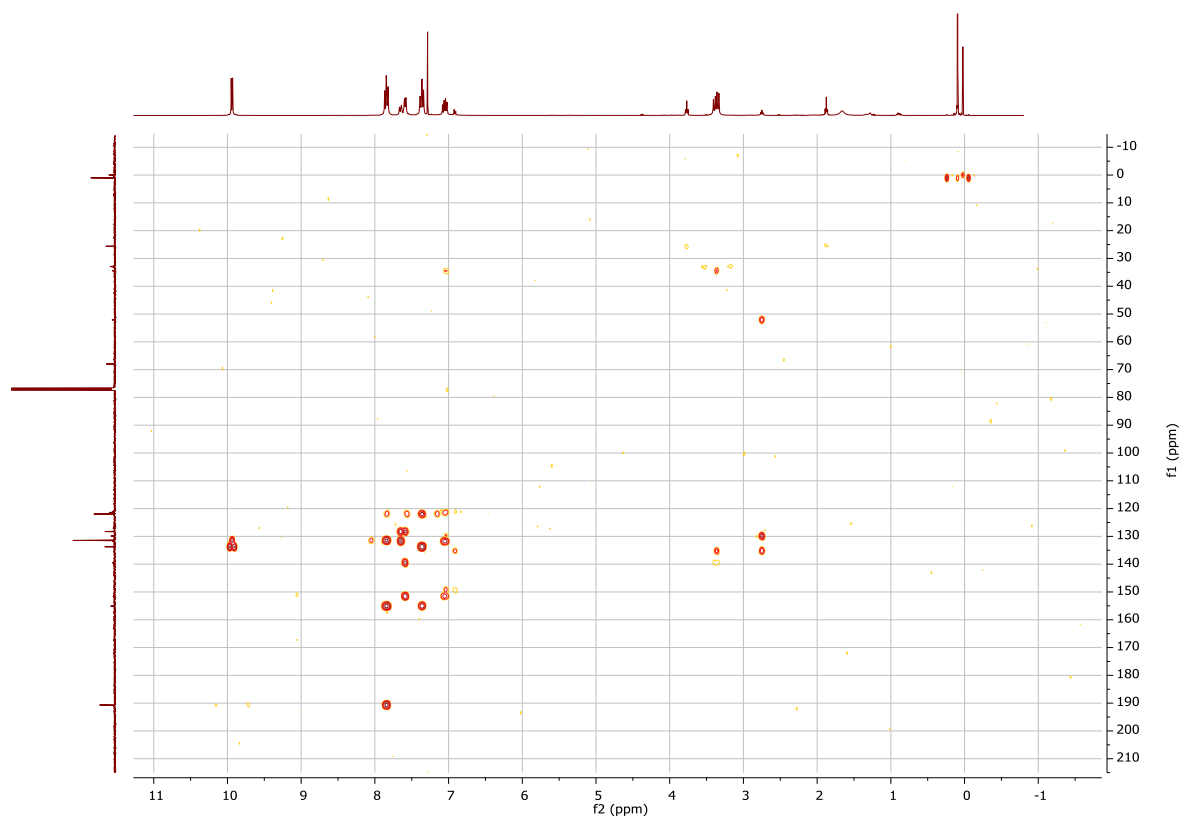
Figure S40. ^1H-$^{13}C\{^1H\}$ HMBC spectrum **135-[G$_1$']** azide dendron in CDCl$_3$ recorded at room temperature (400 MHz, 101 MHz).

1.10. Azide dendron 136-[G₂]
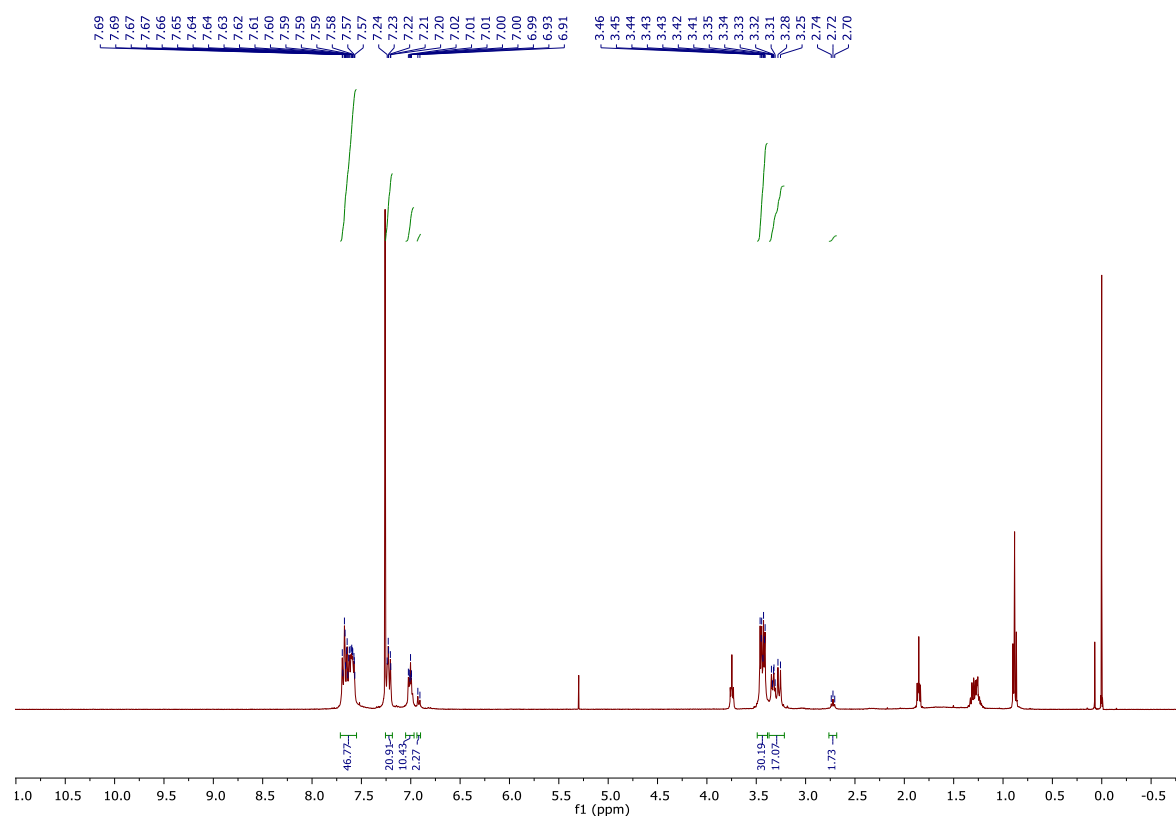
Figure S41. ¹H NMR spectrum of **136-[G₂]** in CDCl₃ recorded at room temperature (400 MHz).
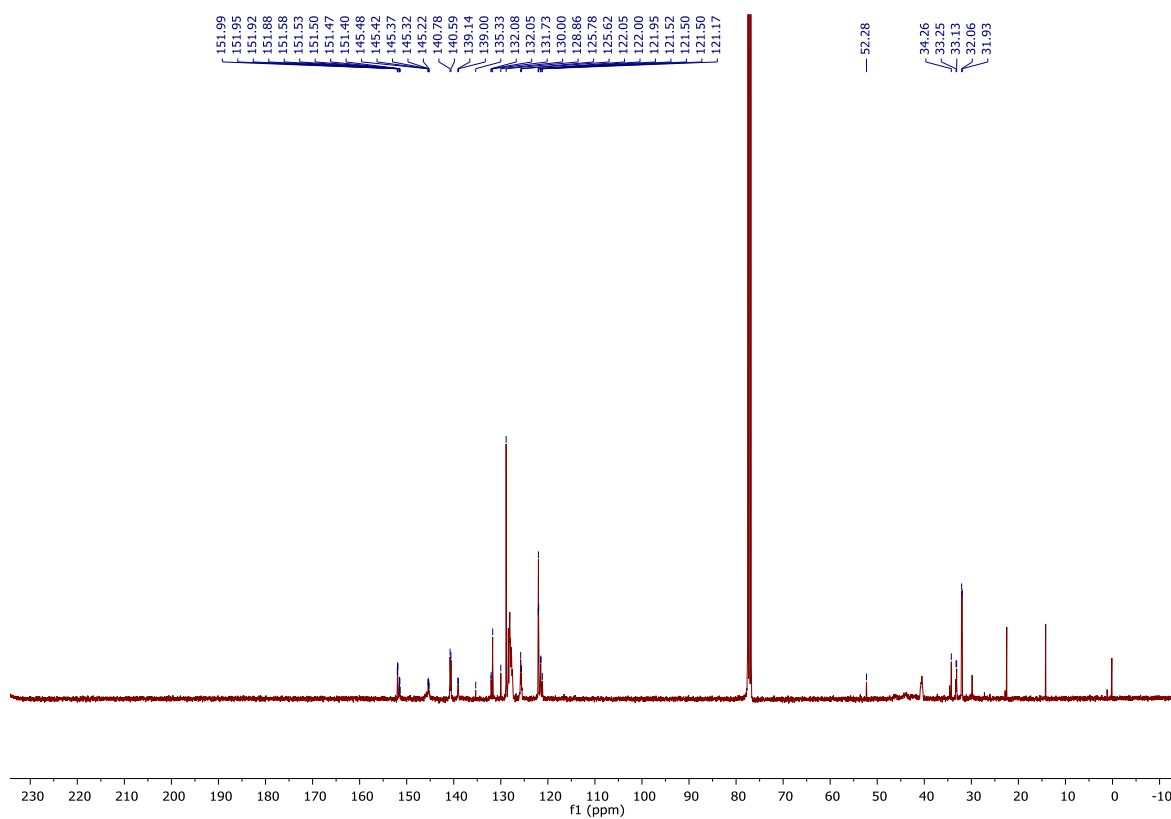
Figure S42. ¹³C{¹H} NMR spectrum of **136-[G₂]** in CDCl₃ recorded at room temperature (101 MHz).
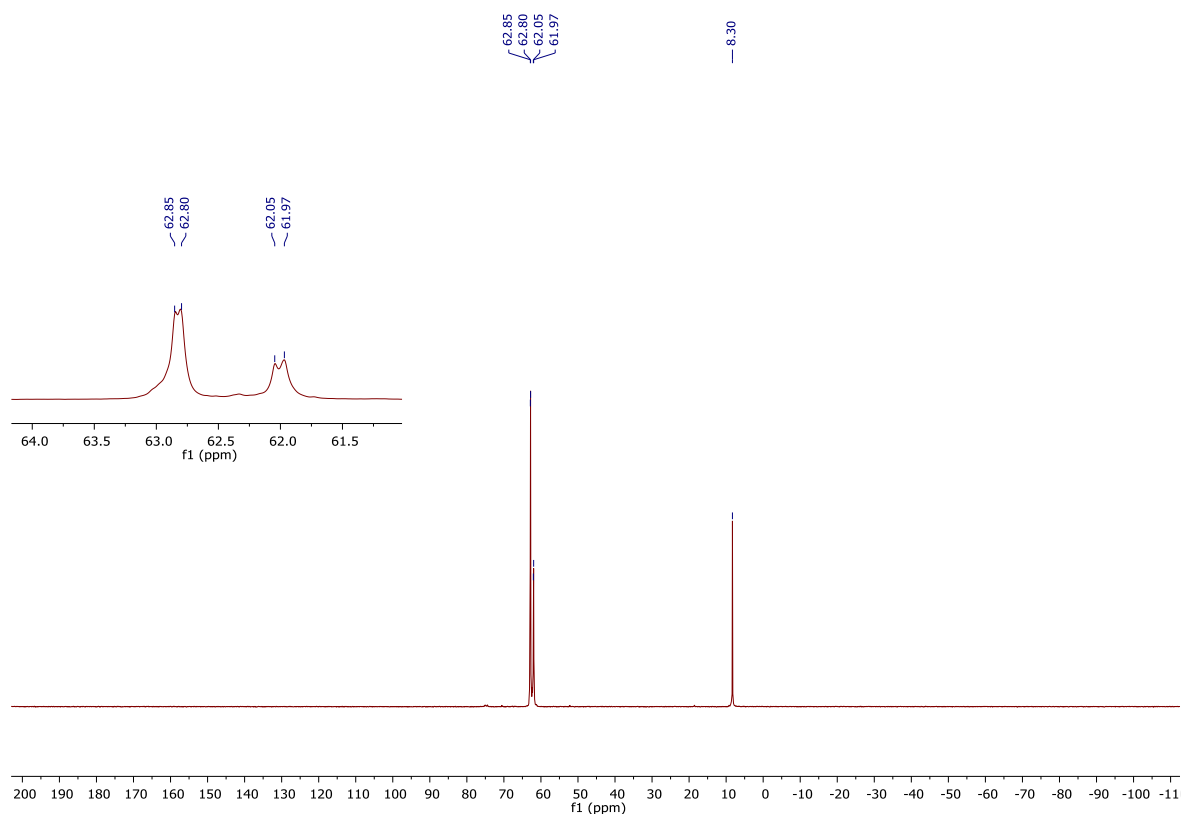
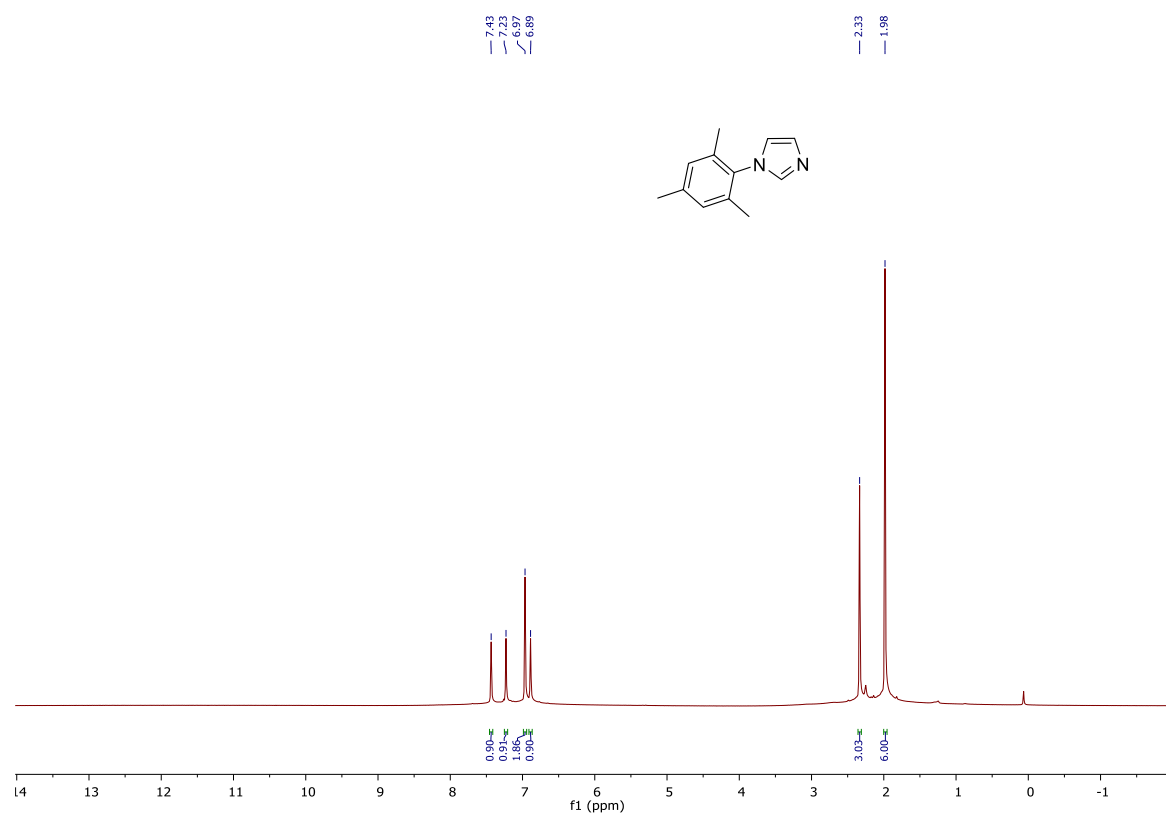**Figure S43**. ³¹P{¹H} NMR spectrum of **136-[G₂]** in CDCl₃ recorded at room temperature (162 MHz).
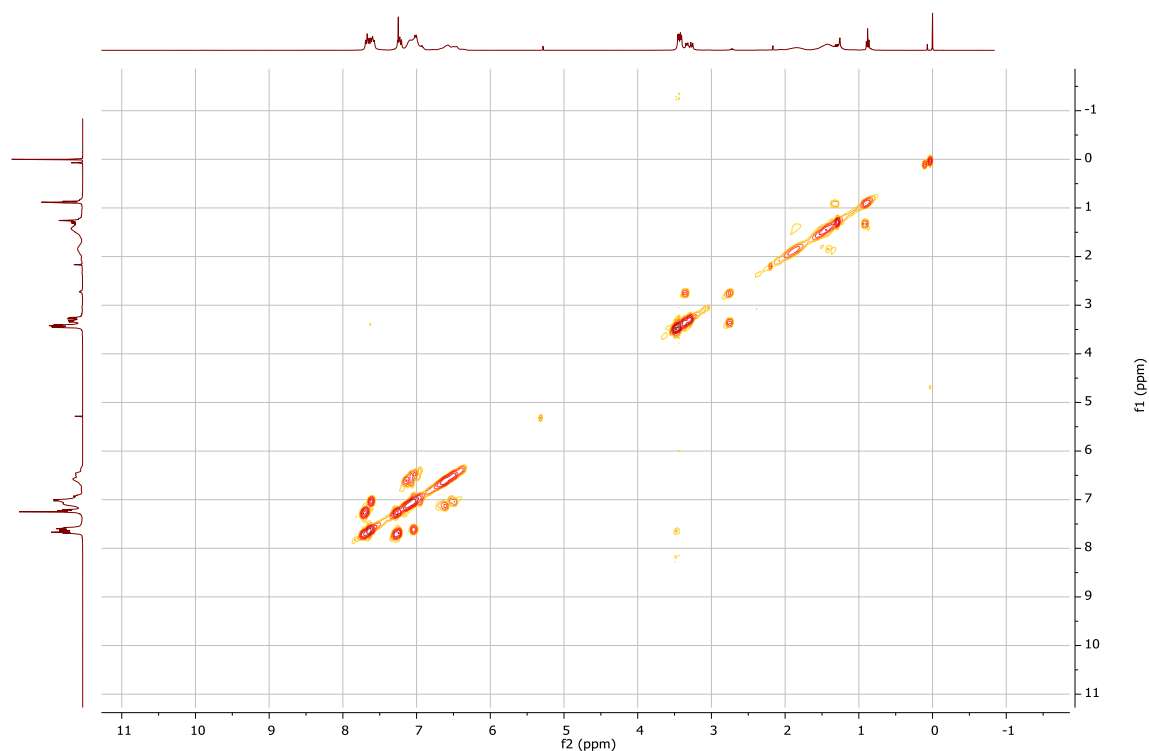
Figure S44. ¹H-¹H COSY spectrum of **136-[G₂]** in CDCl₃ recorded at room temperature (400 MHz).
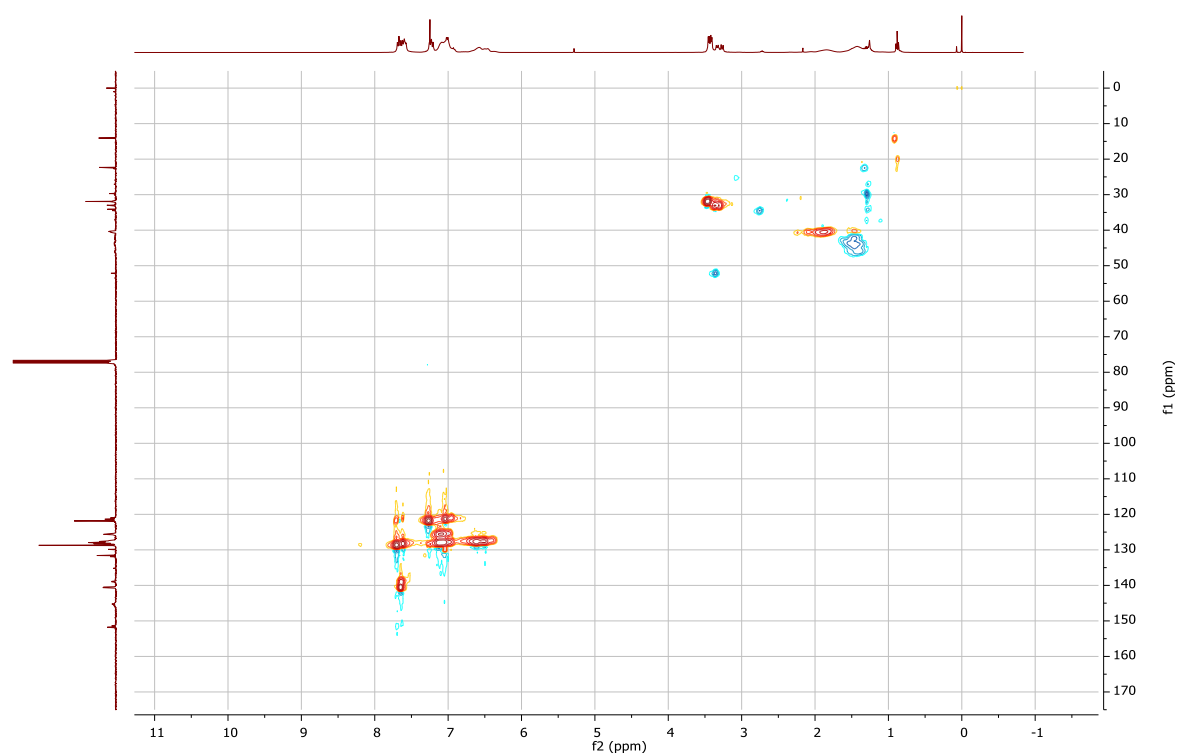
Figure S45. ^{1}H-^{13}C{^{1}H} HSQC spectrum **136-[G$_2$]** azide dendron in CDCl$_3$ recorded at room temperature (400 MHz, 101 MHz).
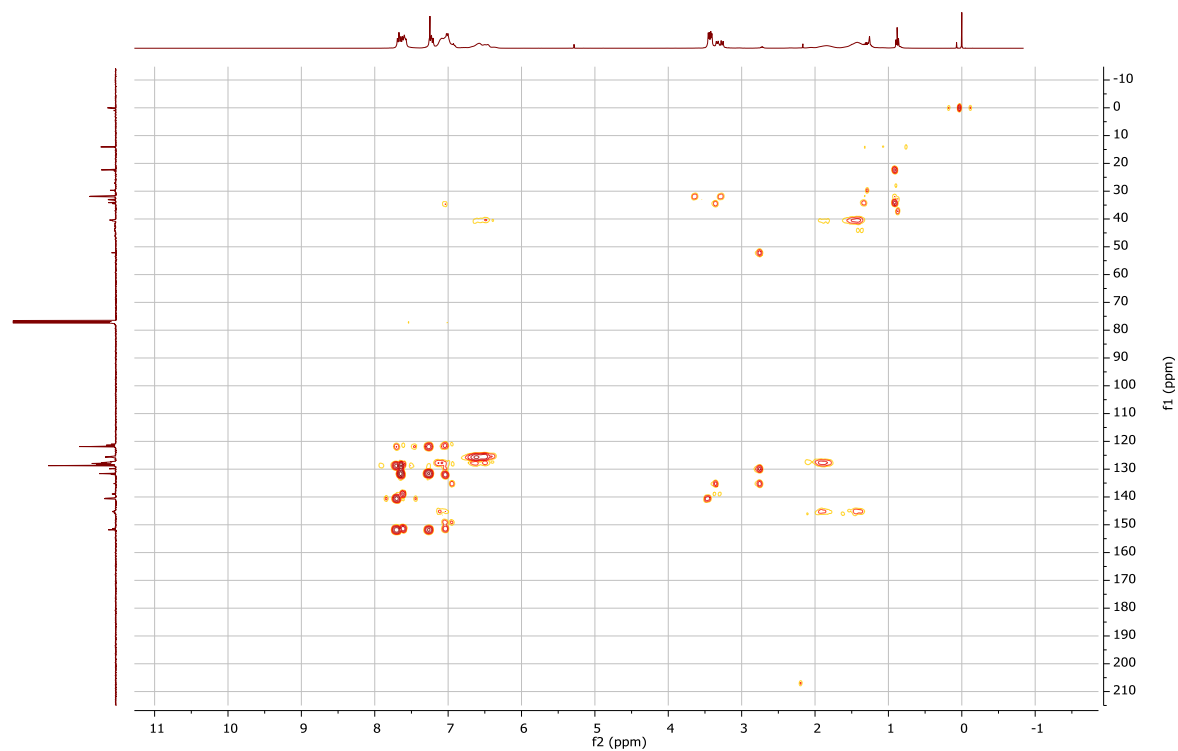
Figure S46. ^{1}H-^{13}C{^{1}H} HMBC spectrum **136-[G$_2$]** azide dendron in CDCl$_3$ recorded at room temperature (400 MHz, 101 MHz).
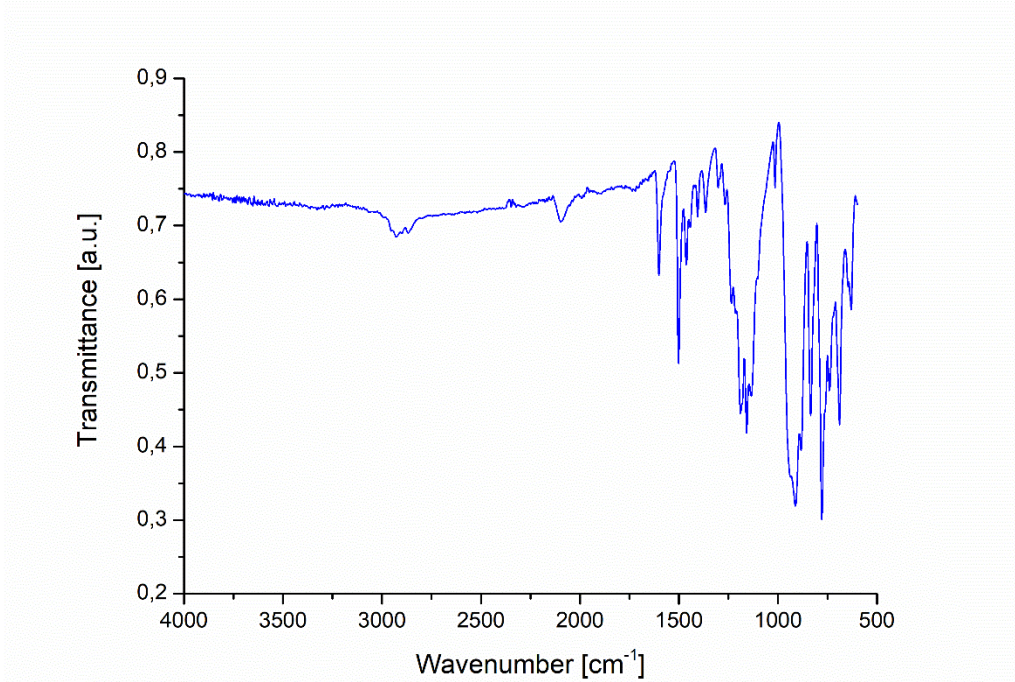
Figure S47. FT-IR spectrum of **136-[G₂]**.

Codi SAQ	Ref. mostra	%C	%H	%N	%S
23AE038/008	G2-azide	37,63	3,38	11,30	10,93

Figure S48. Elemental Analysis of **136-[G₂]**.

1.11. 2-(4-(4-(pro-2-yn-yloxy)phenoxy)-2,4,4,6,6-pentachlorotriazatriphos-phazene 131
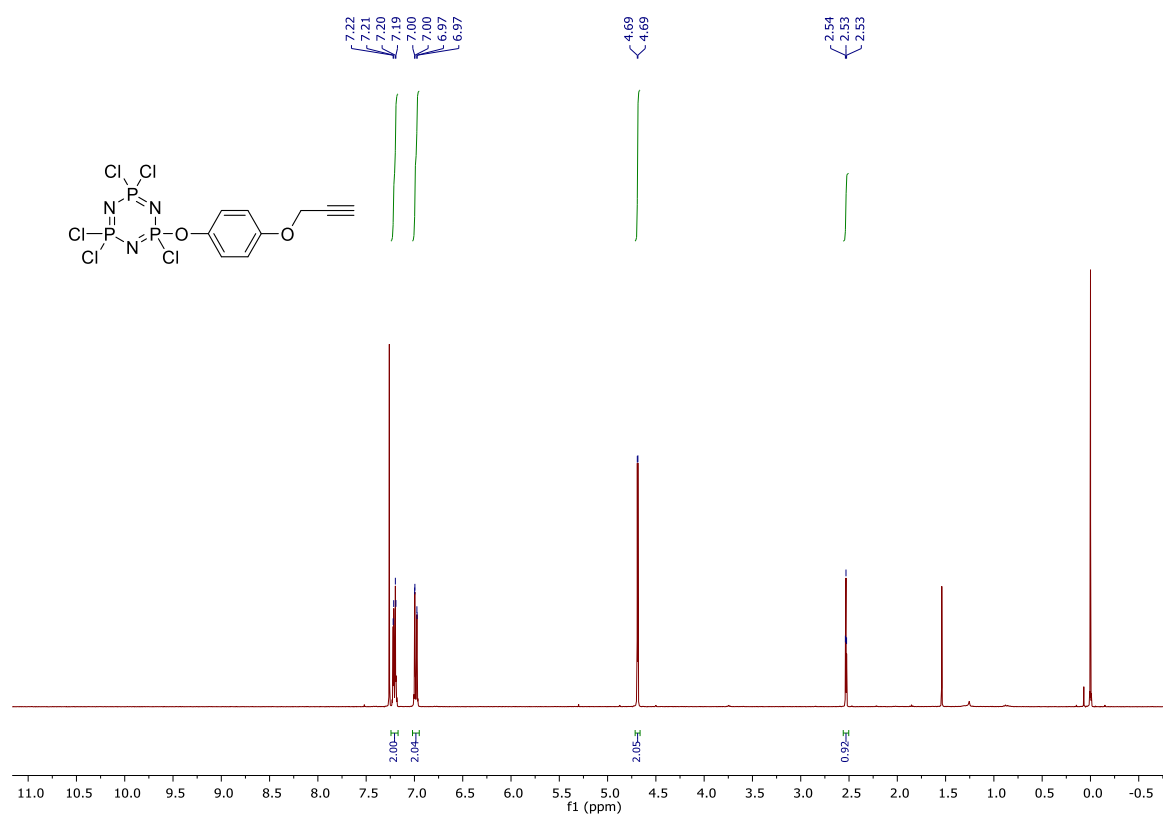
Figure S49. ^{1}H NMR spectrum of 2-(4-(4-(pro-2-yn-yloxy)phenoxy)-2,4,4,6,6-pentachlorotriazatriphos-phazene **131** in CDCl$_3$ recorded at room temperature (400 MHz).
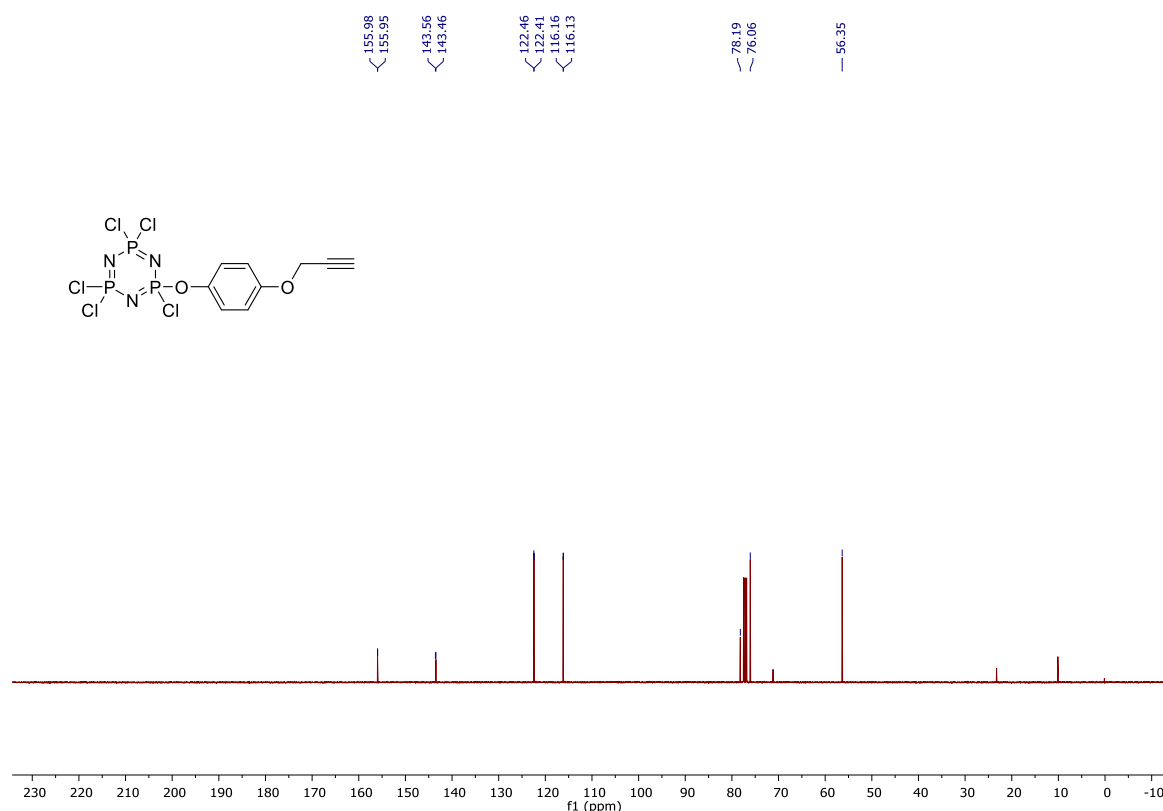
Figure S50. ^{13}C{^{1}H} NMR spectrum of 2-(4-(4-(pro-2-yn-yloxy)phenoxy)-2,4,4,6,6-pentachlorotriazatri-phosphazene **131** in CDCl$_3$ recorded at room temperature (101 MHz).
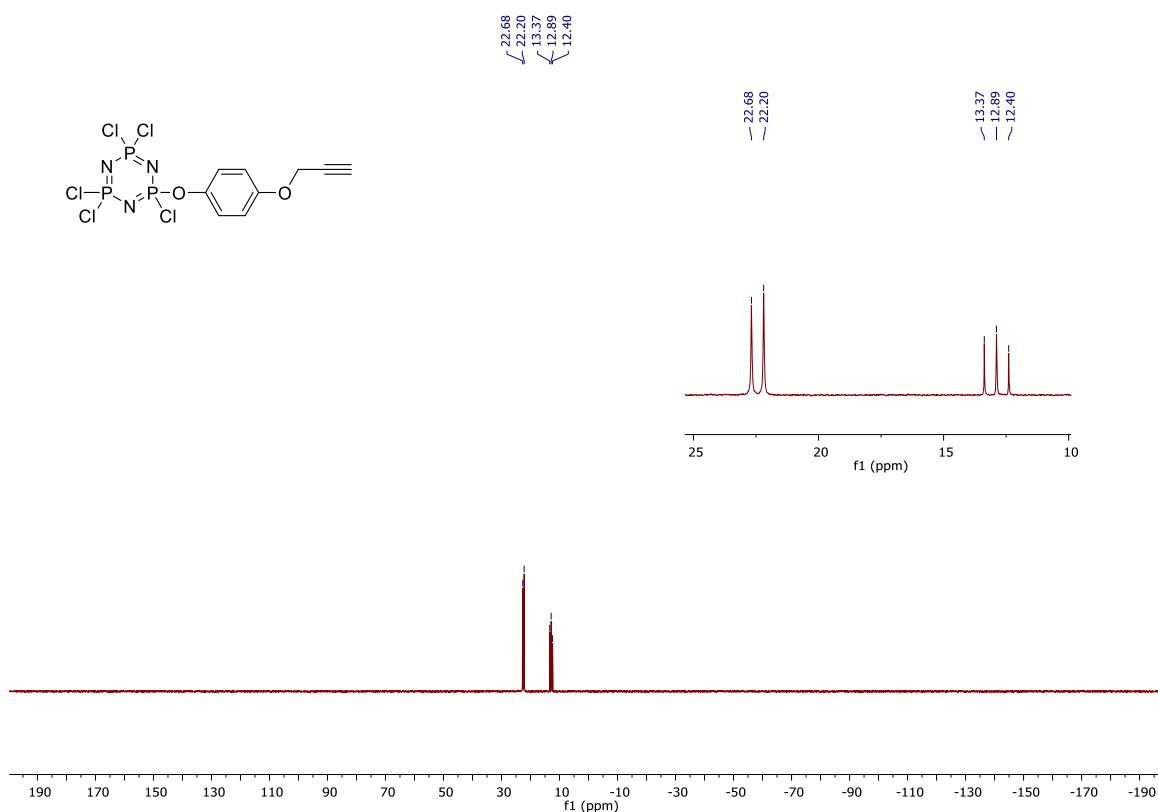
Figure S51. ³¹P{¹H} NMR spectrum of 2-(4-(4-(pro-2-yn-yloxy)phenoxy)-2,4,4,6,6-pentachlorotriazatri-phosphazene **131** in CDCl₃ recorded at room temperature (162 MHz).
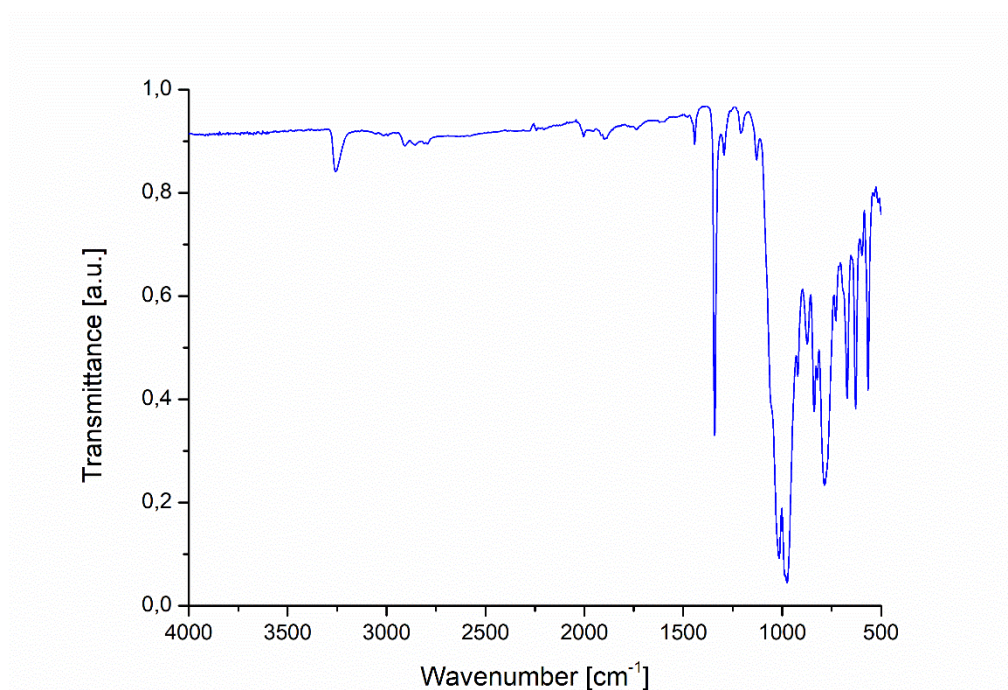
Figure S52. FT-IR spectrum of 2-(4-(4-(pro-2-yn-yloxy)phenoxy)-2,4,4,6,6-pentachlorotriazatriphos-phazene **131**.

1.12. Acetylene dendron 129-[G₀']
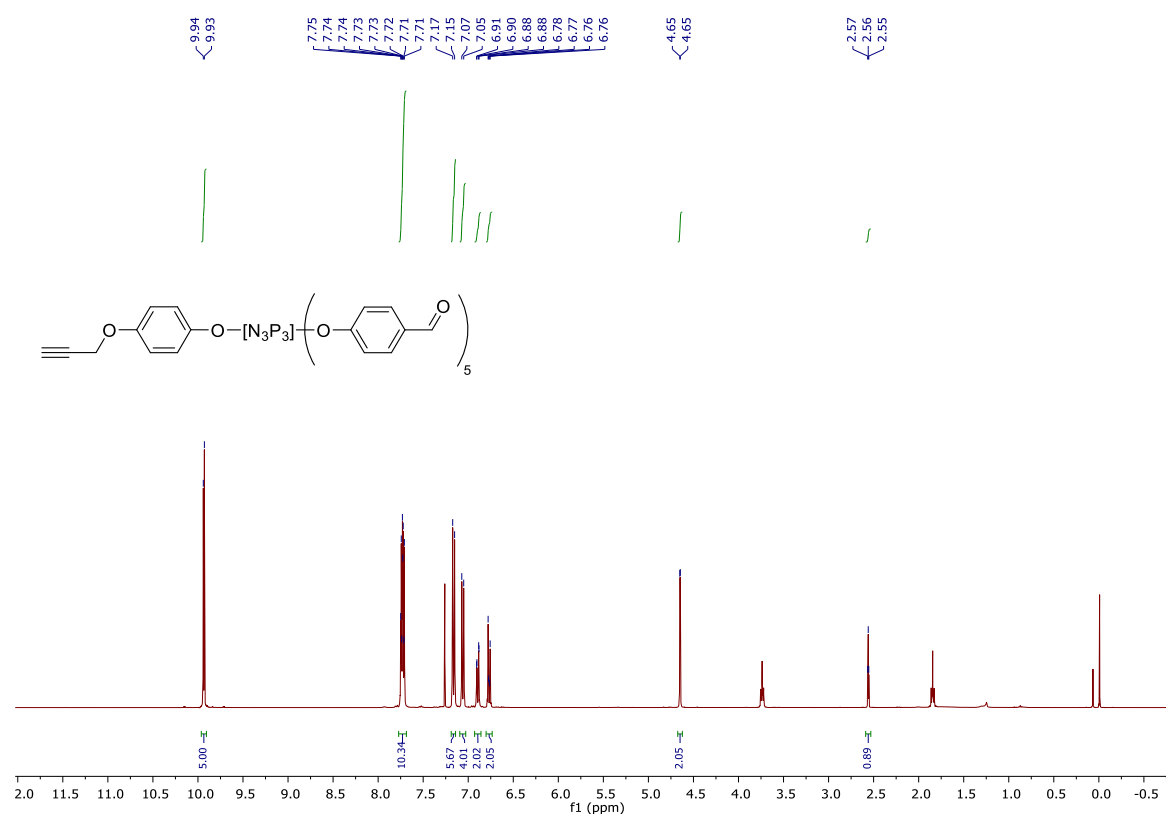
Figure S53. ^{1}H NMR spectrum of **129-[G₀']** in CDCl₃ recorded at room temperature (400 MHz).
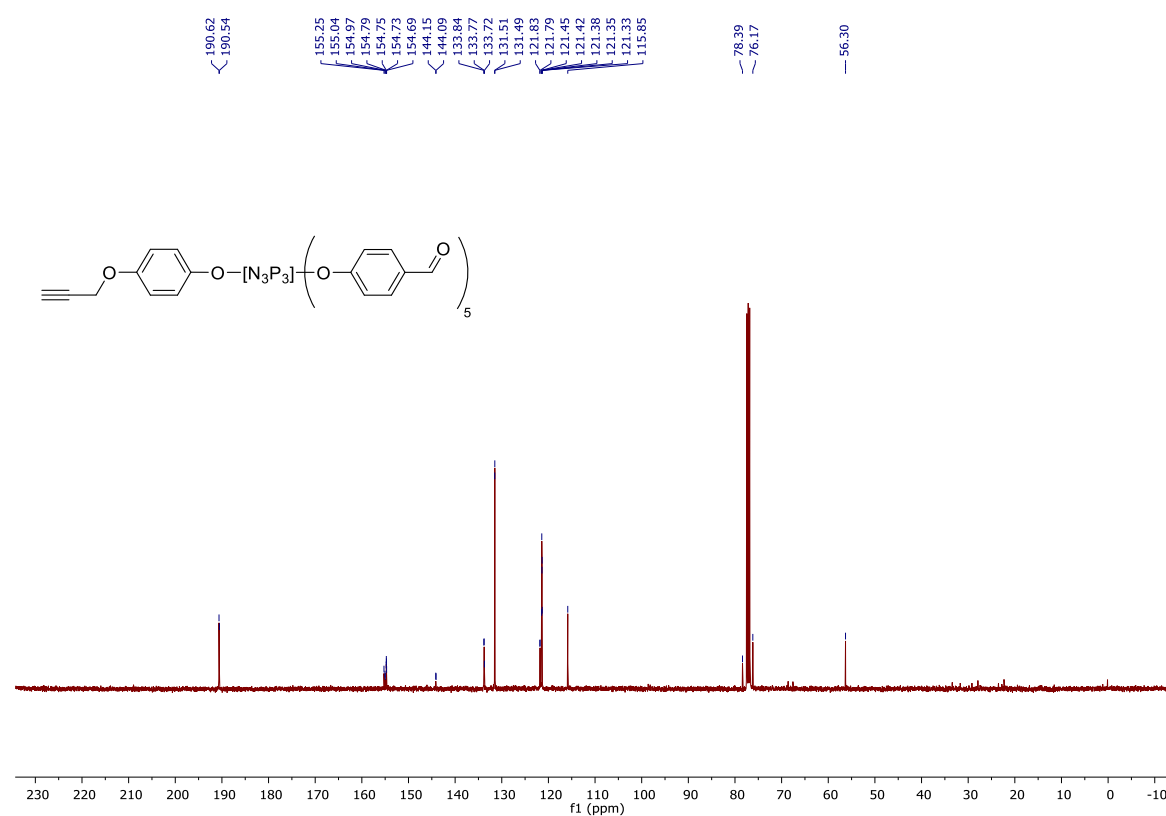
Figure S54. ^{13}C{^{1}H} NMR spectrum of **129-[G₀']** in CDCl₃ recorded at room temperature (101 MHz).
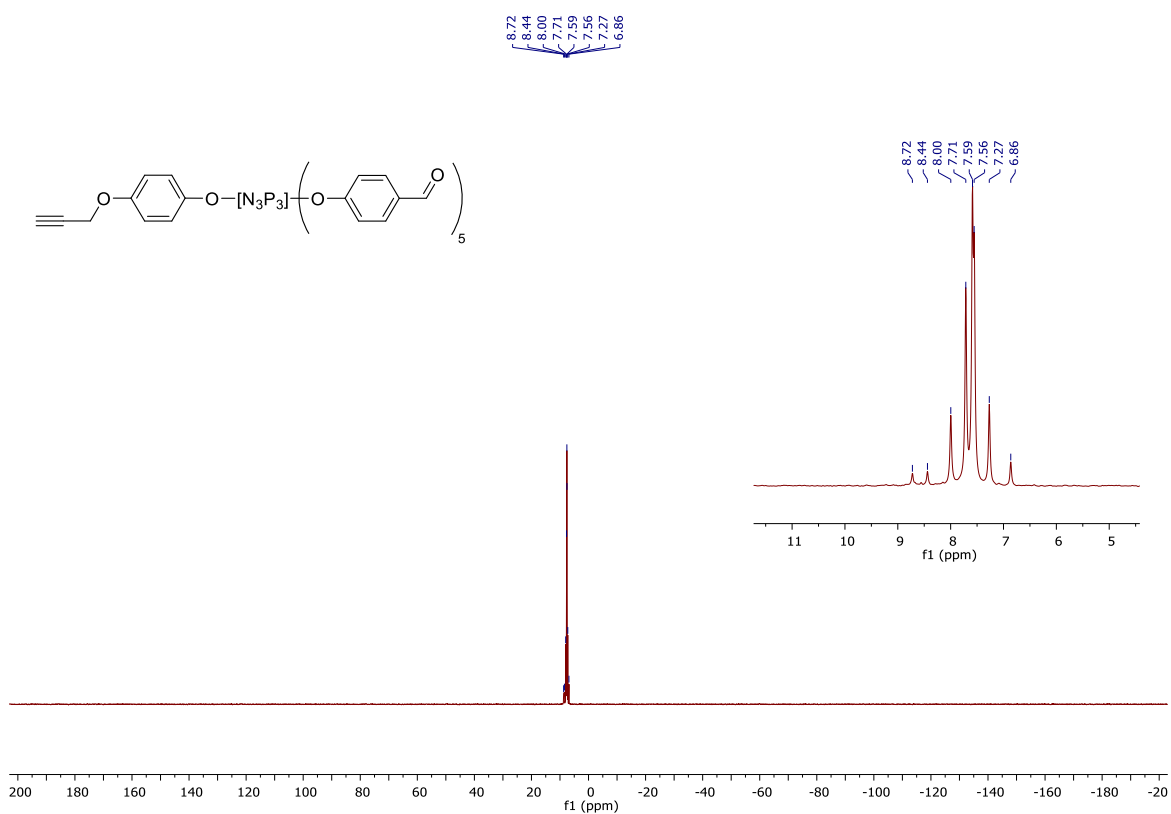
Figure S55. $^{31}P\{^1H\}$ NMR spectrum of **129-[G$_0$']** in CDCl$_3$ recorded at room temperature (162 MHz).
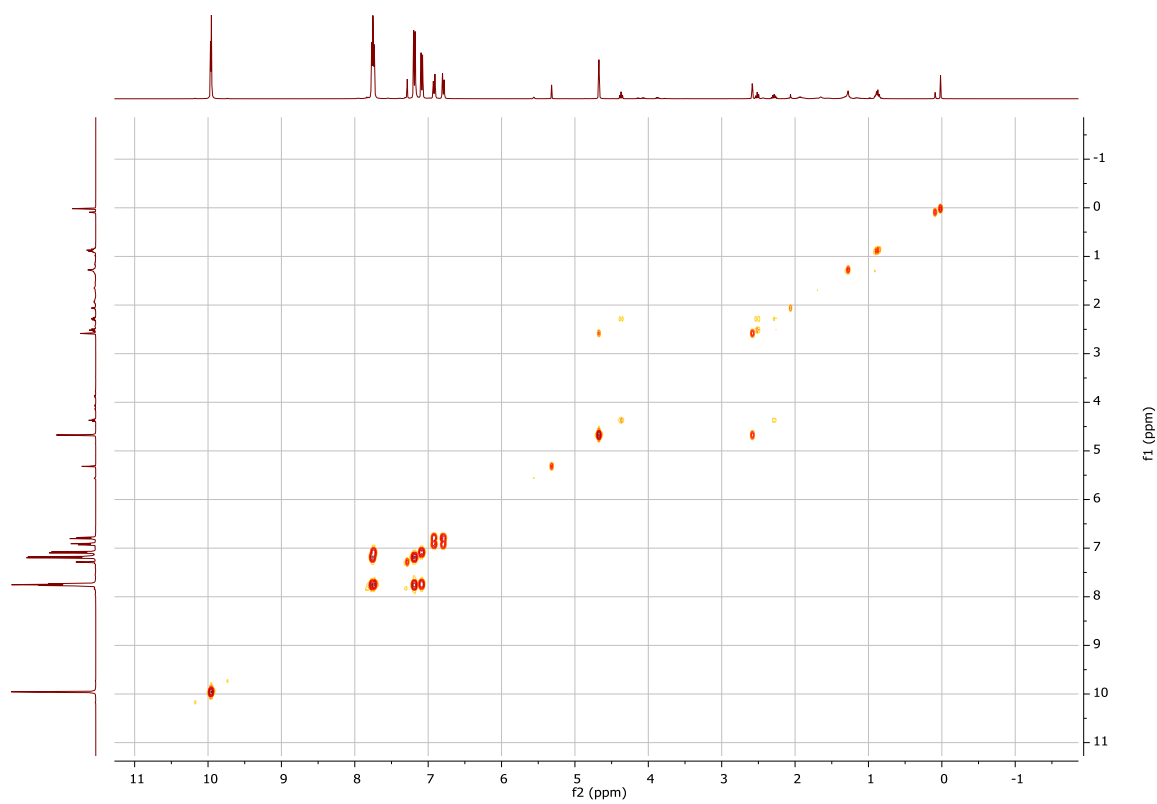
Figure S56. ^{1}H-^{1}H COSY spectrum of **129-[G$_0$']** in CDCl$_3$ recorded at room temperature (400 MHz).
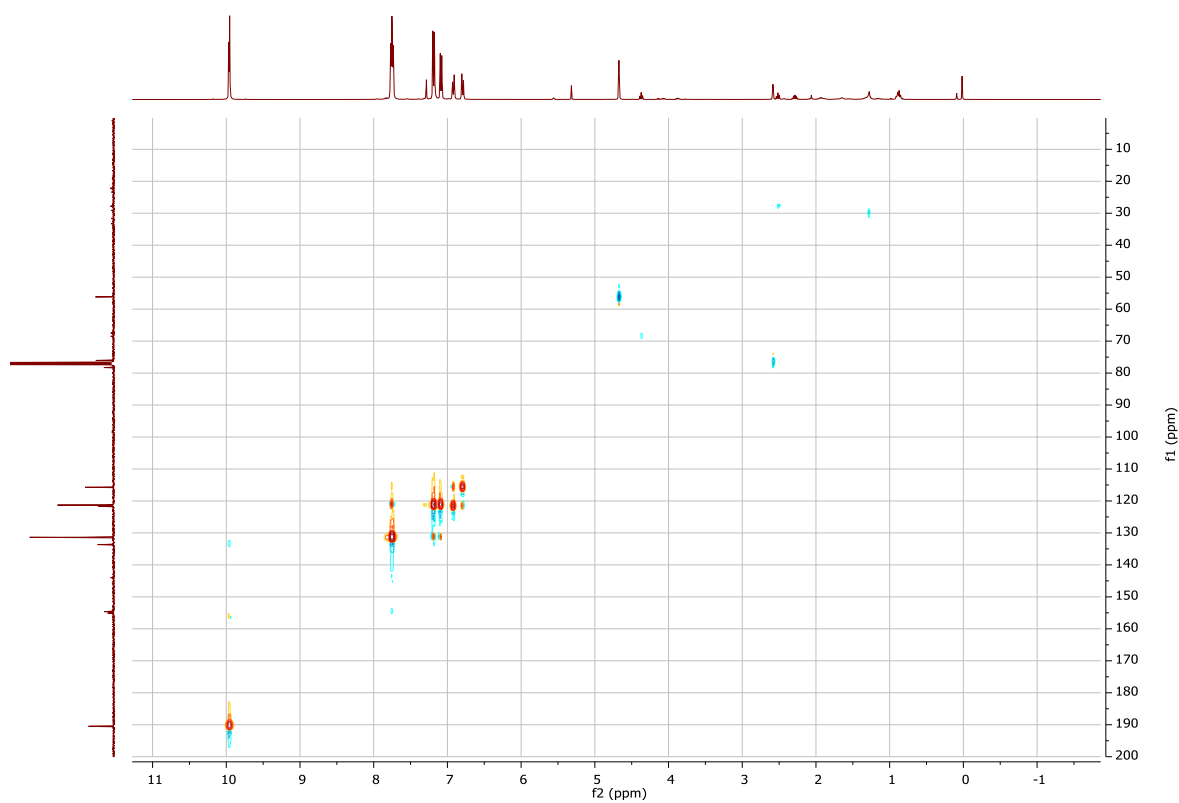
Figure S57. ^{1}H-^{13}C{^{1}H} HSQC spectrum of **129-[G$_0$']** in CDCl$_3$ recorded at room temperature (400 MHz, 101 MHz).
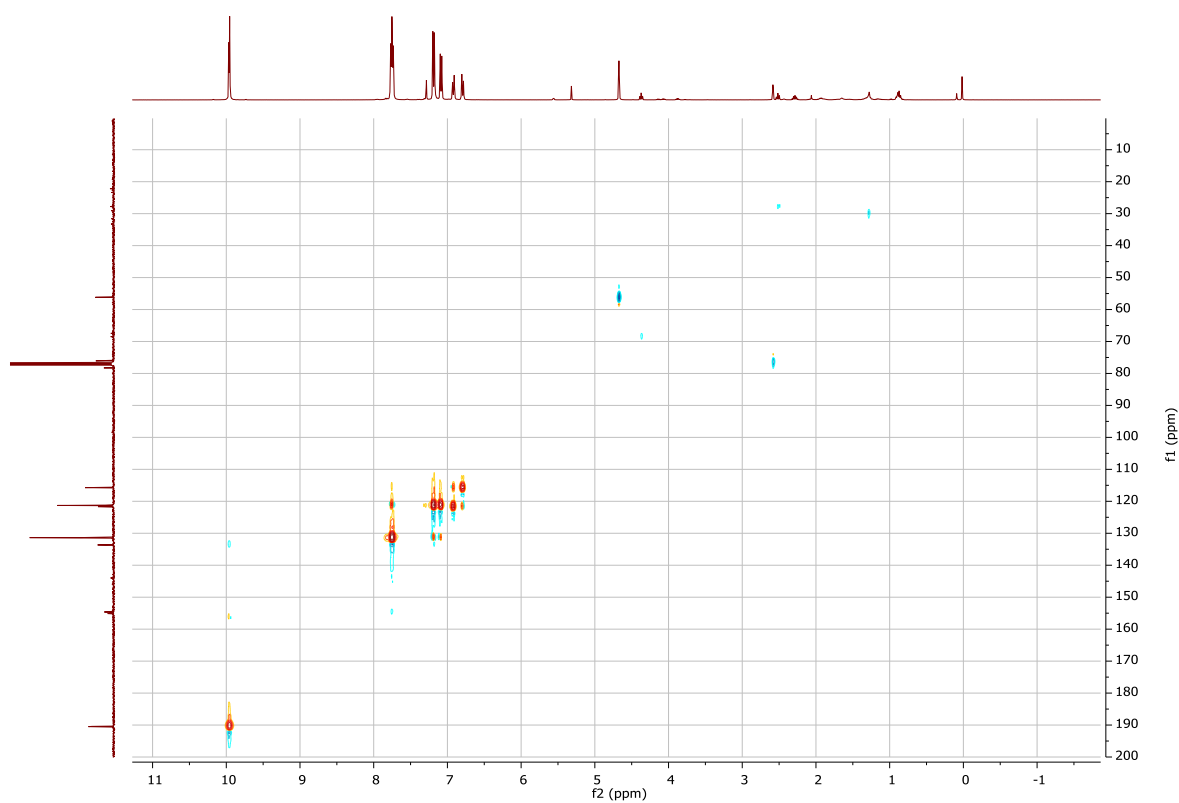
Figure S58. ^{1}H-^{13}C{^{1}H} HMBC spectrum of **129-[G$_0$']** in CDCl$_3$ recorded at room temperature (400 MHz, 101 MHz).
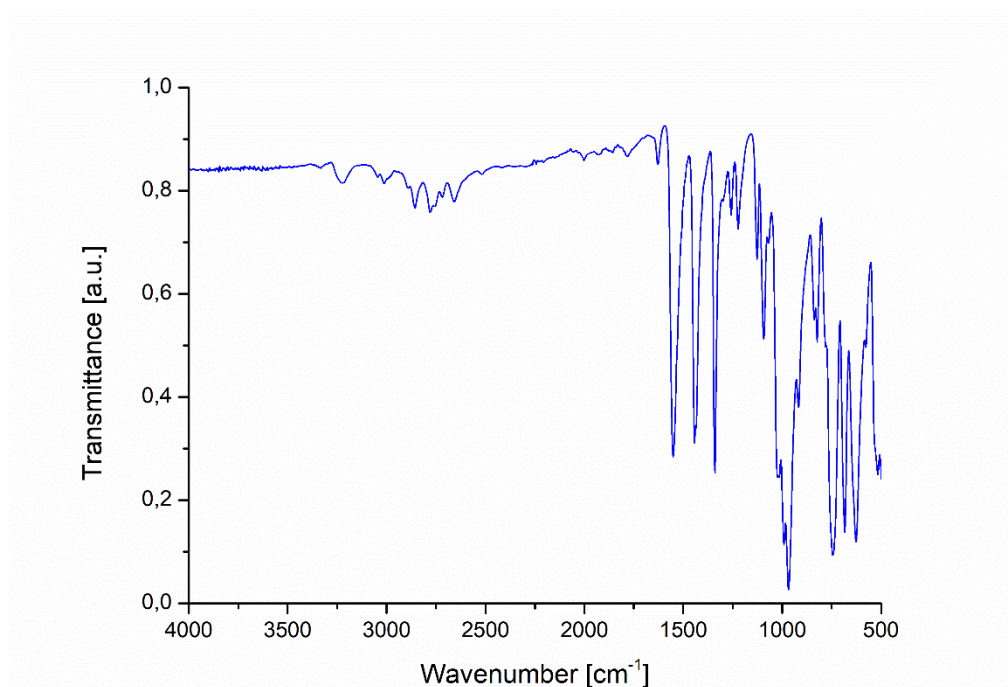
Figure S59. FT-IR spectrum of **129-[G$_0$']**.

1.13. Acetylene dendron 134-[G₁]

Figure S60. ^{1}H NMR spectrum of **134-[G₁]** in CDCl₃ recorded at room temperature (400 MHz).

Figure S61. ^{13}C{^{1}H} NMR spectrum of **134-[G₁]** in CDCl₃ recorded at room temperature (101 MHz).
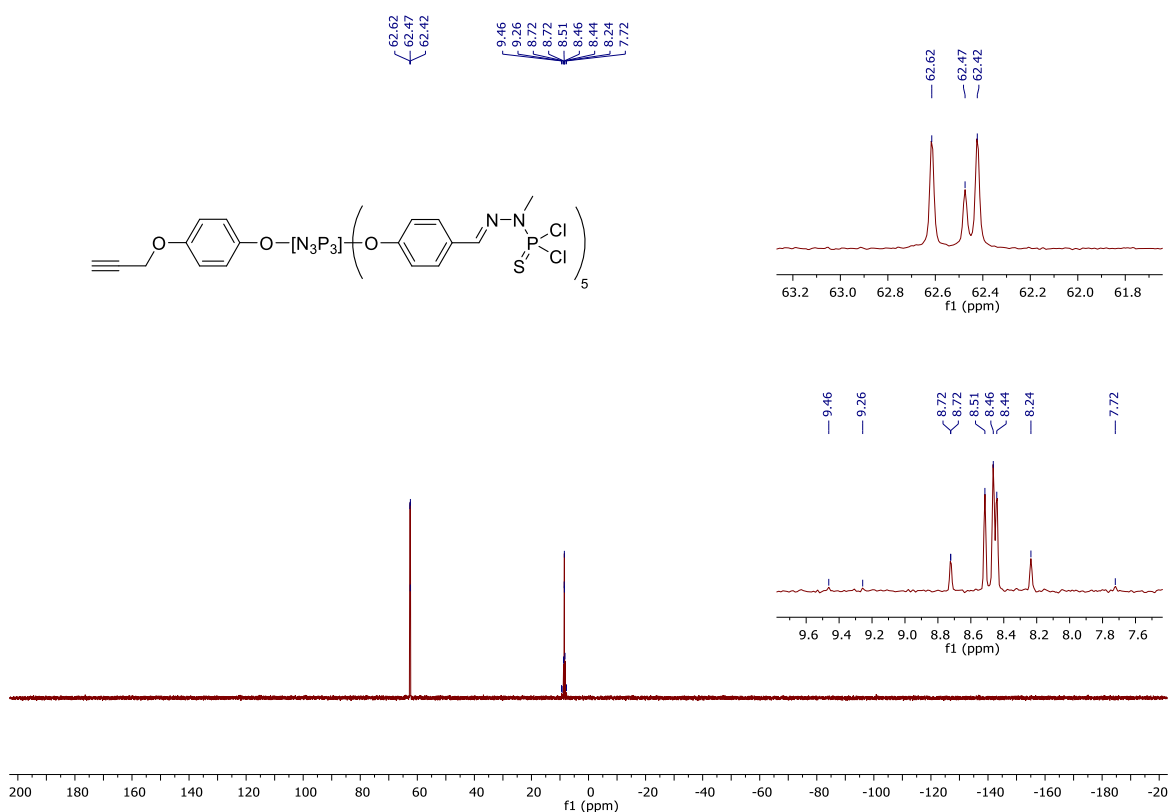
Figure S62. $^{31}P\{^1H\}$ NMR spectrum of **134-[G₁]** in CDCl₃ recorded at room temperature (162 MHz).
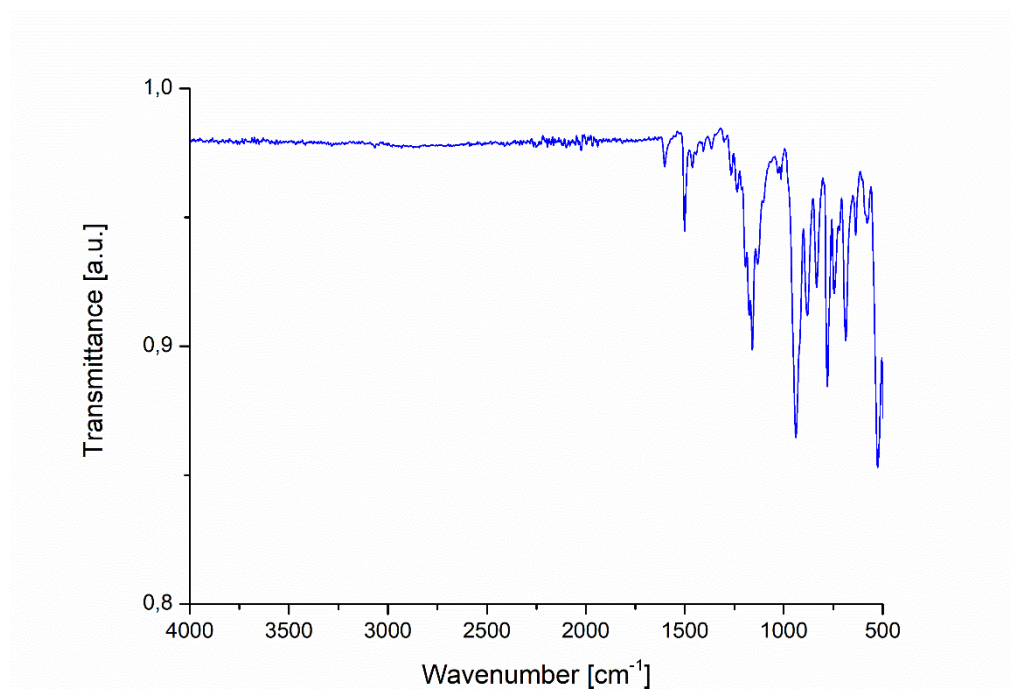
Figure S63. FT-IR spectrum of **134-[G₁]**.

1.14. Surface modification of 133-[G$_1$]

1.14.1. 2-(2-(2-methoxyethoxy)ethoxy)ethylmethanesulfonate 139
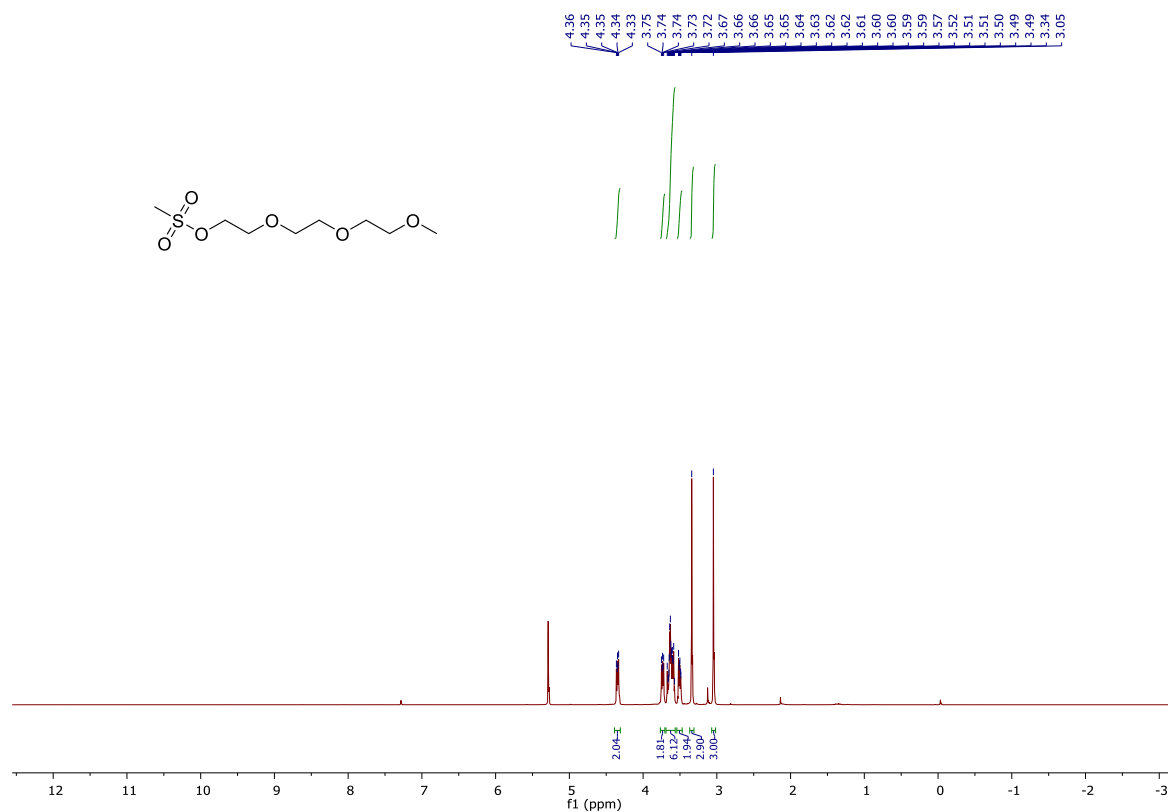
Figure S64. ^{1}H NMR spectrum of (2-(2-methoxyethoxy)ethoxy)ethyl methanesulfonate **139** in CDCl$_3$ recorded at room temperature (300 MHz).
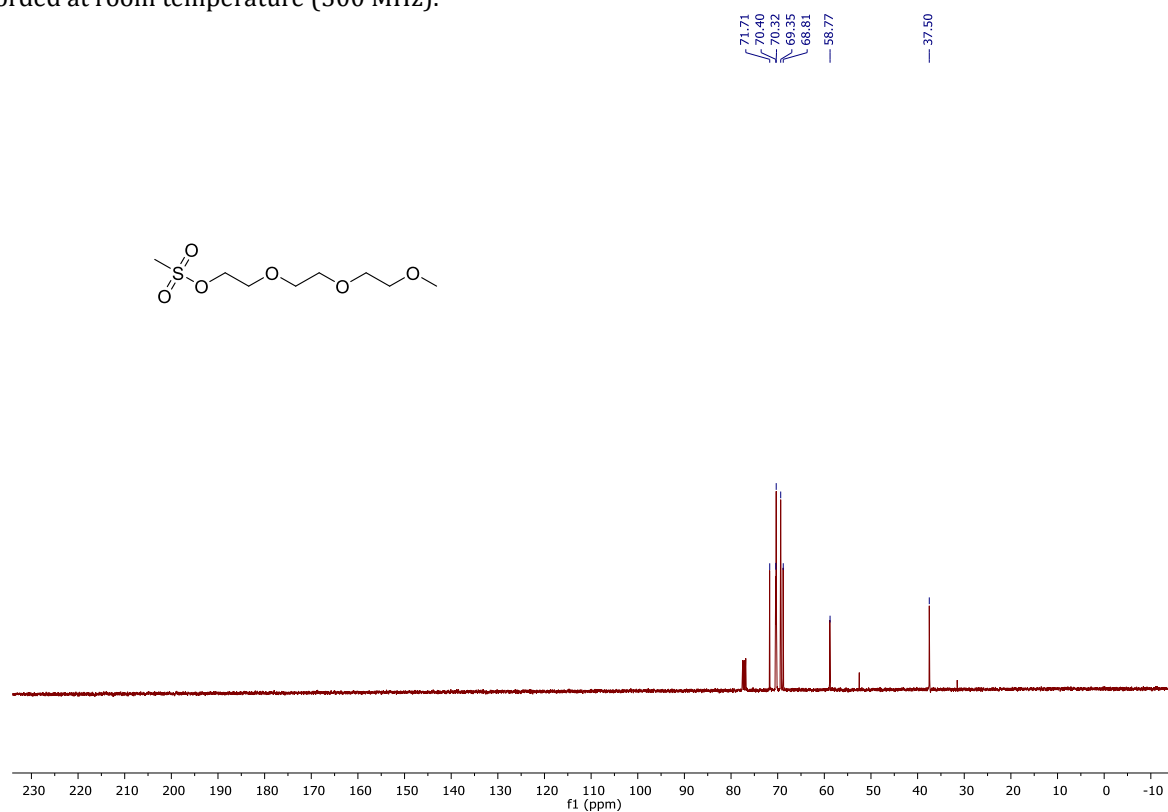
Figure S65.^{13}C{^{1}H} NMR spectrum of (2-(2-methoxyethoxy)ethoxy)ethyl methanesulfonate **139** in CDCl$_3$ recorded at room temperature (75 MHz).

1.14.2.   4-(2-(2-(2-methoxyethoxy)ethoxy)ethoxy)phenol 140
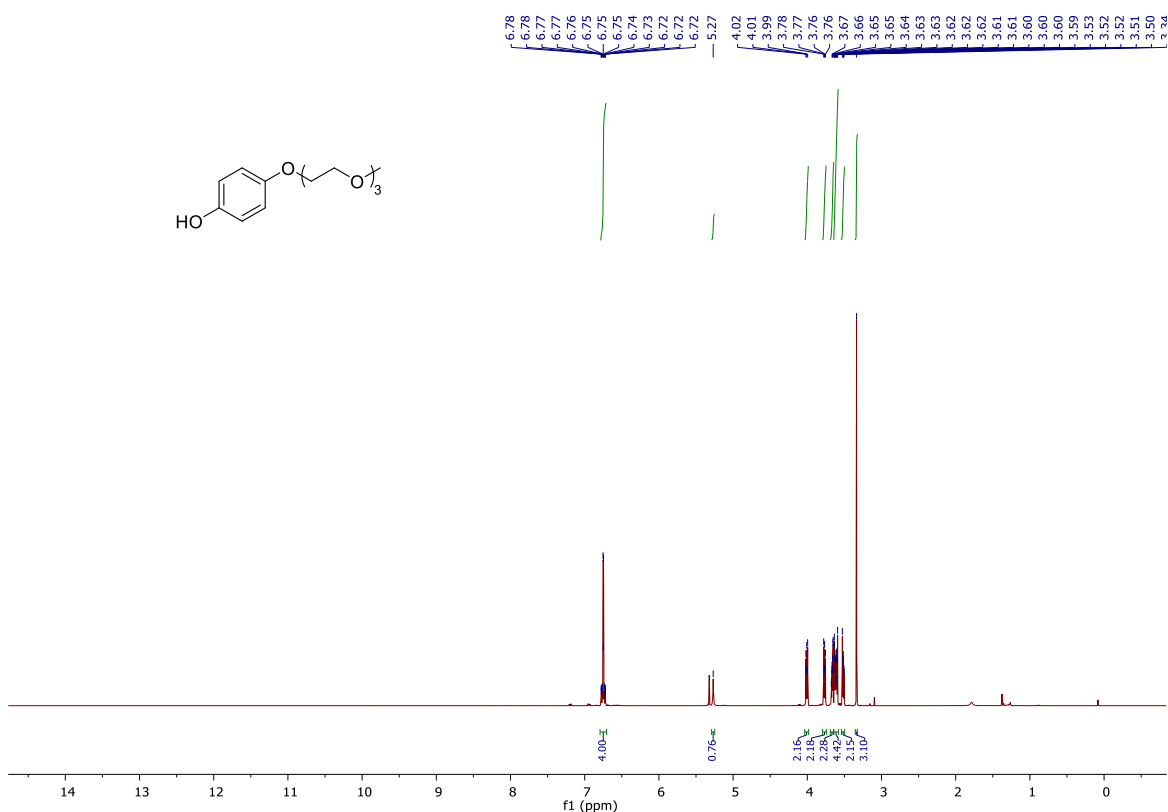
Figure S66. ^{1}H NMR spectrum of 4-(2-(2-(2-methoxyethoxy)ethoxy)ethoxy)phenol **140** in DCM-d_2 recorded at room temperature (400 MHz).
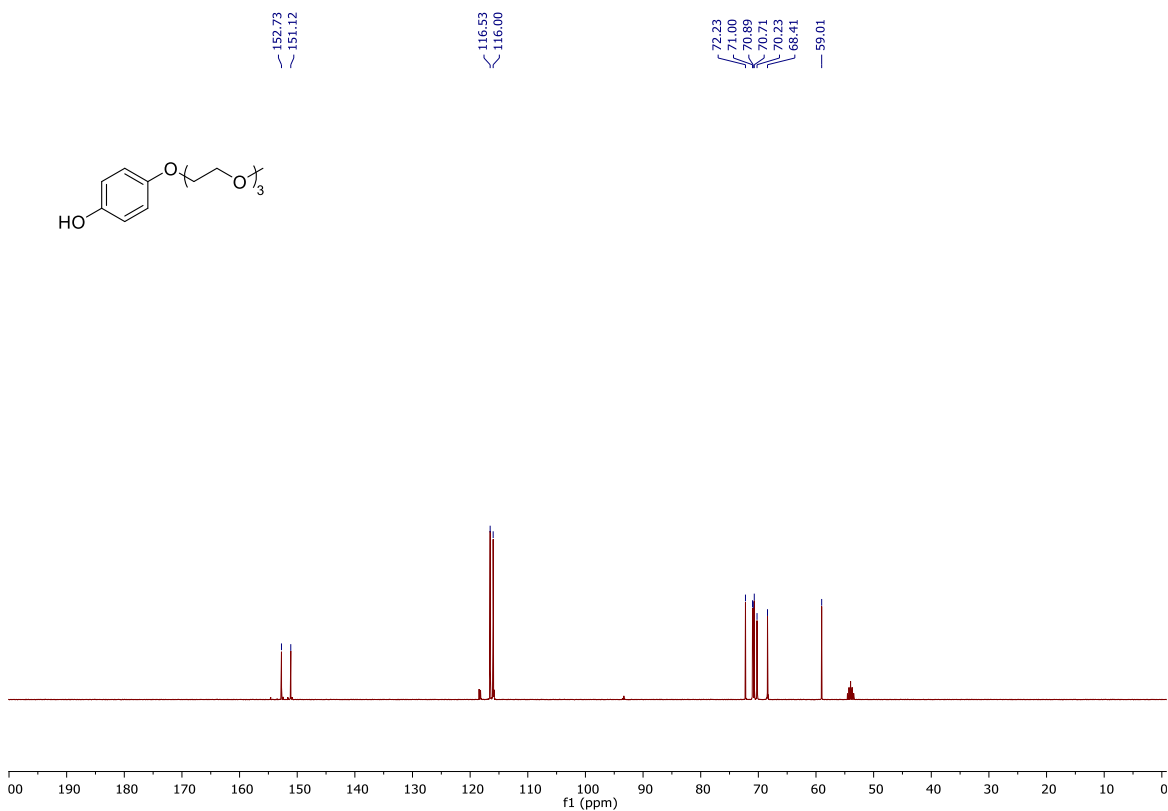
Figure S67. ^{13}C{^{1}H} NMR spectrum of of 4-(2-(2-(2-methoxyethoxy)ethoxy)ethoxy)phenol **140** in DCM-d_2 recorded at room temperature (101 MHz).

1.14.3. Azide dendron 141-[G₁]-PEG
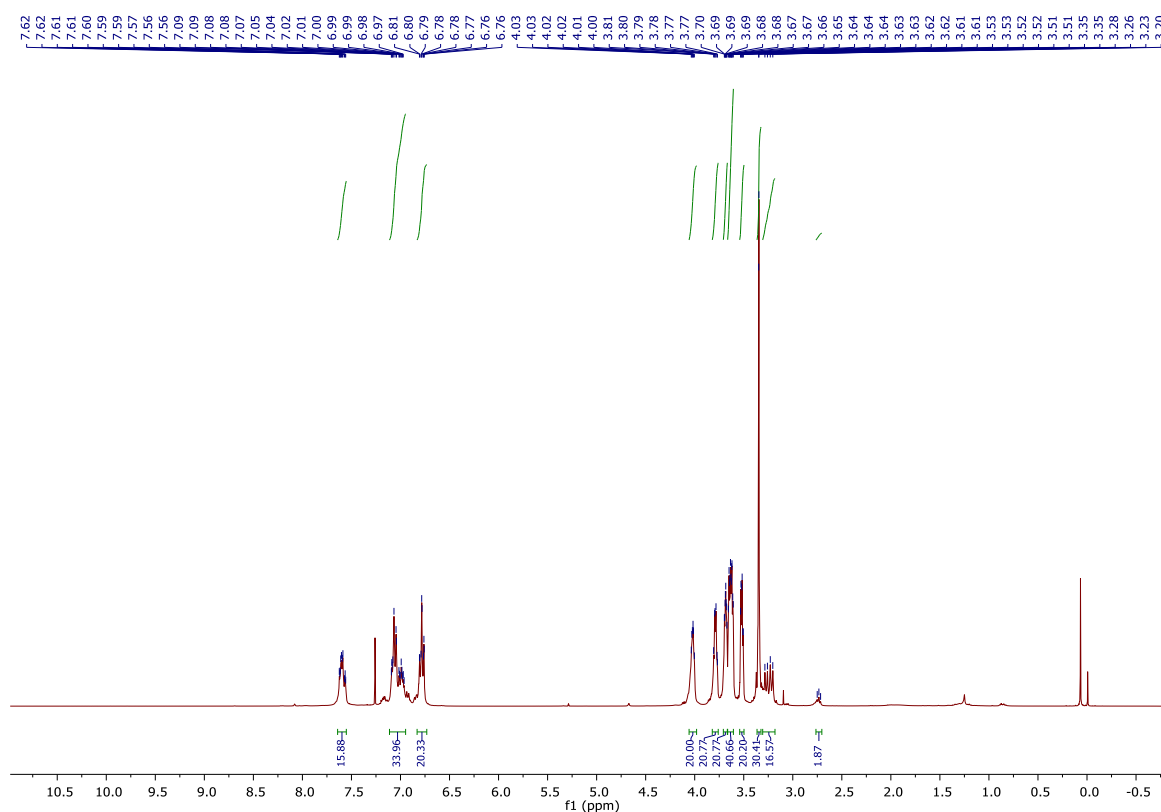
Figure S68. ¹H NMR spectrum of **141-[G₁]-PEG** in DCM-d₂ recorded at room temperature (400 MHz).
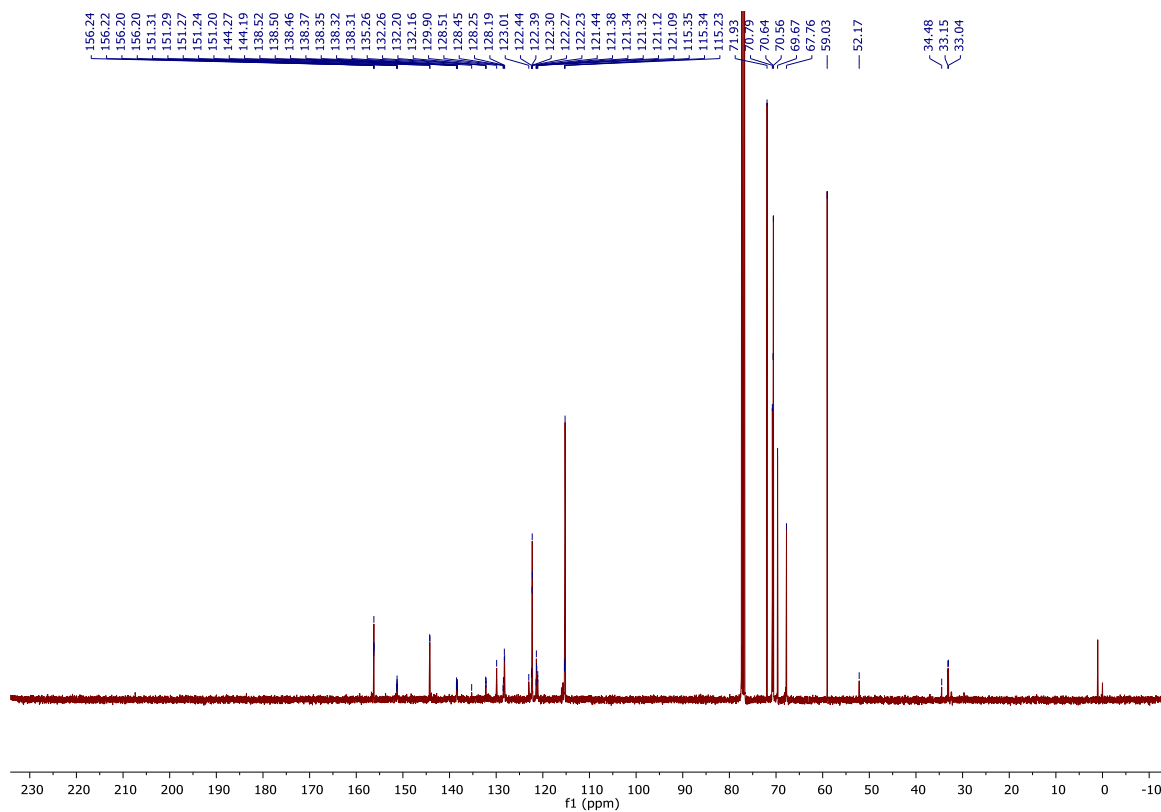
Figure S69. ¹³C{¹H} NMR spectrum of **141-[G₁]-PEG** in DCM-d₂ recorded at room temperature (101 MHz).
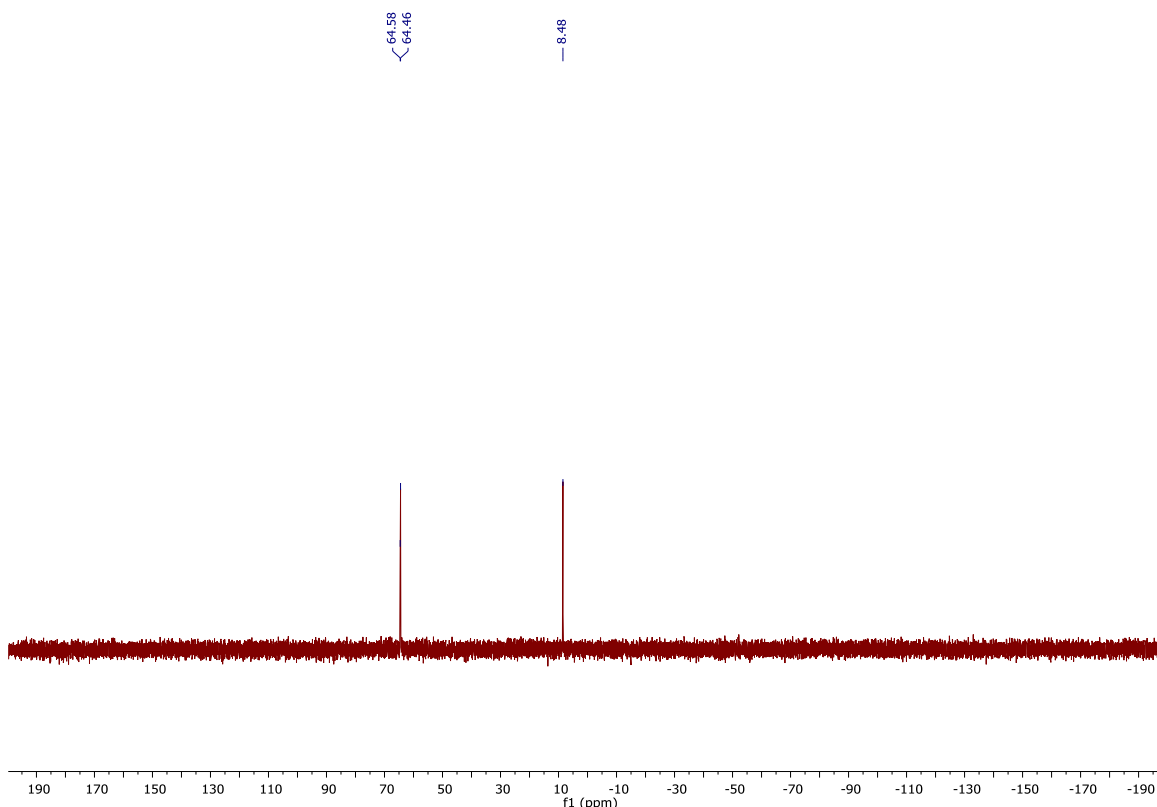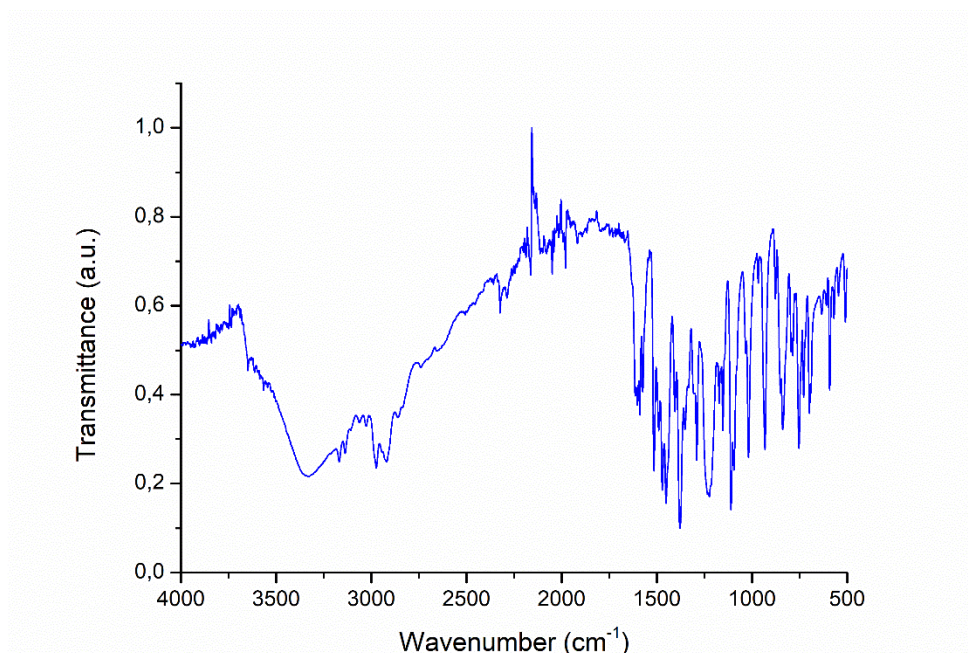
Figure S70. $^{31}P\{^1H\}$ NMR spectrum of **141-[G$_1$]-PEG** in DCM-d$_2$ recorded at room temperature (162 MHz).
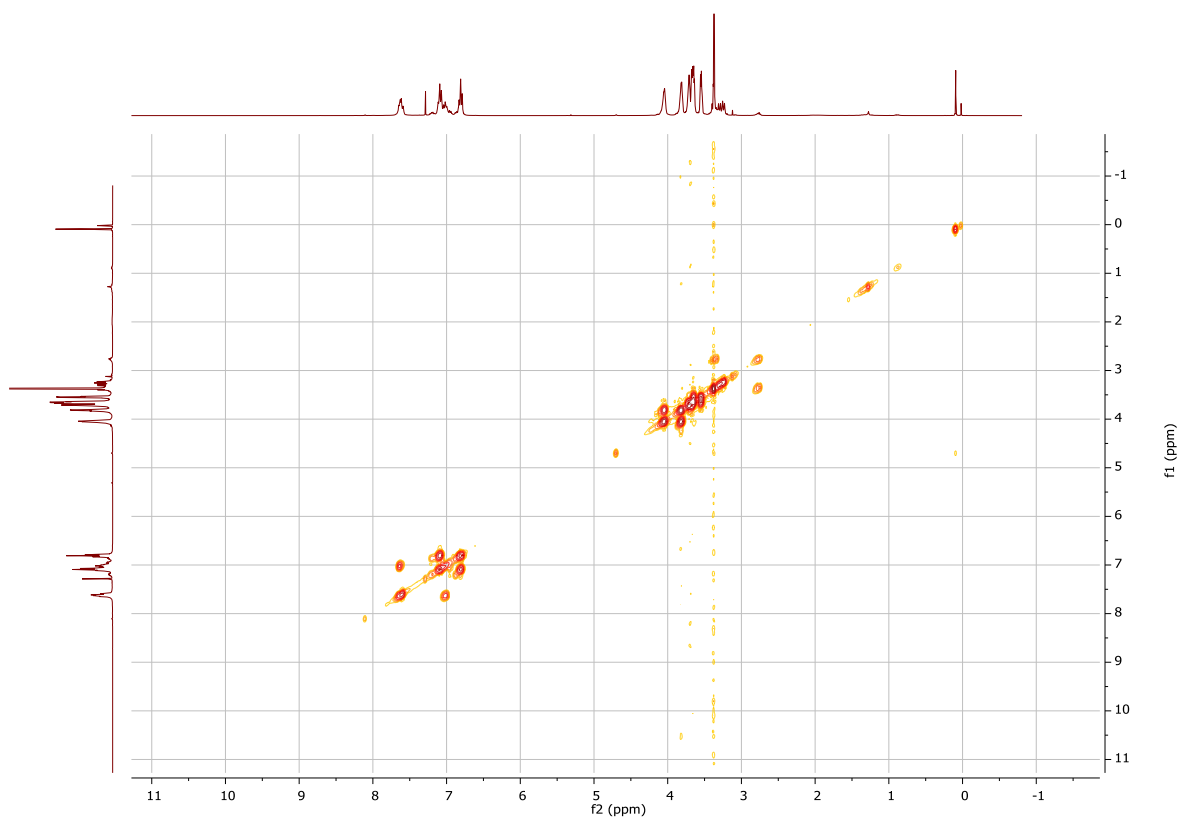
Figure S71. ^1H-^1H COSY spectrum of **141-[G$_1$]-PEG** in CDCl$_3$ recorded at room temperature (400 MHz).
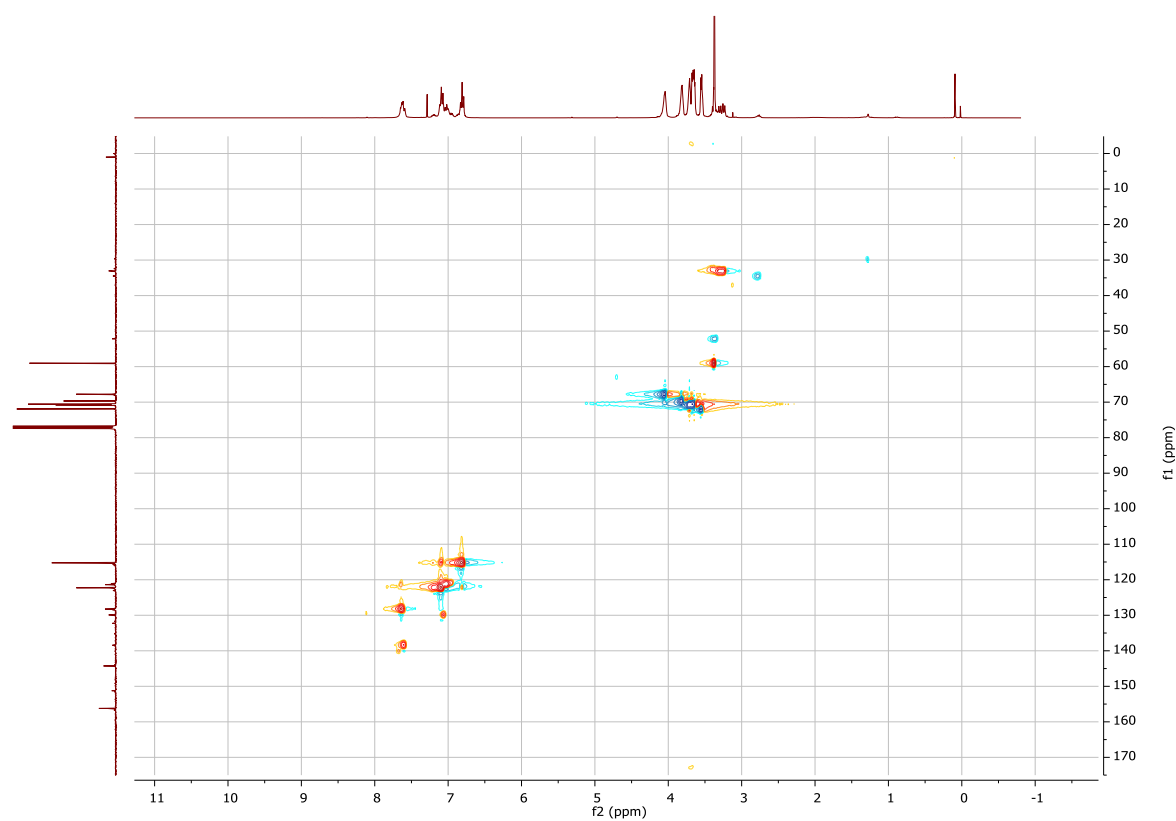
Figure S72. ^{1}H-^{13}C{^{1}H} HSQC spectrum of **141-[G$_1$]-PEG** in CDCl$_3$ recorded at room temperature (400 MHz, 101 MHz).
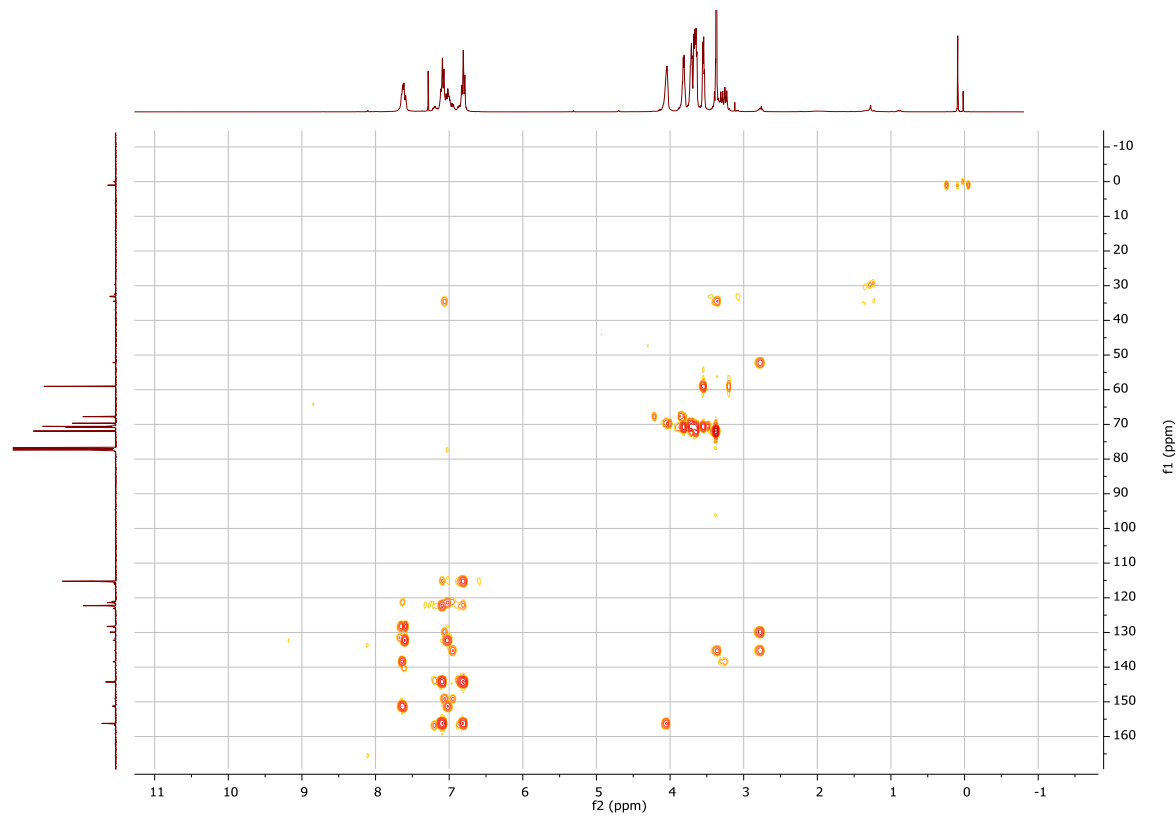
Figure S73. ^{1}H-^{13}C{^{1}H} HMBC spectrum of **141-[G$_1$]-PEG** in CDCl$_3$ recorded at room temperature (400 MHz, 101 MHz).
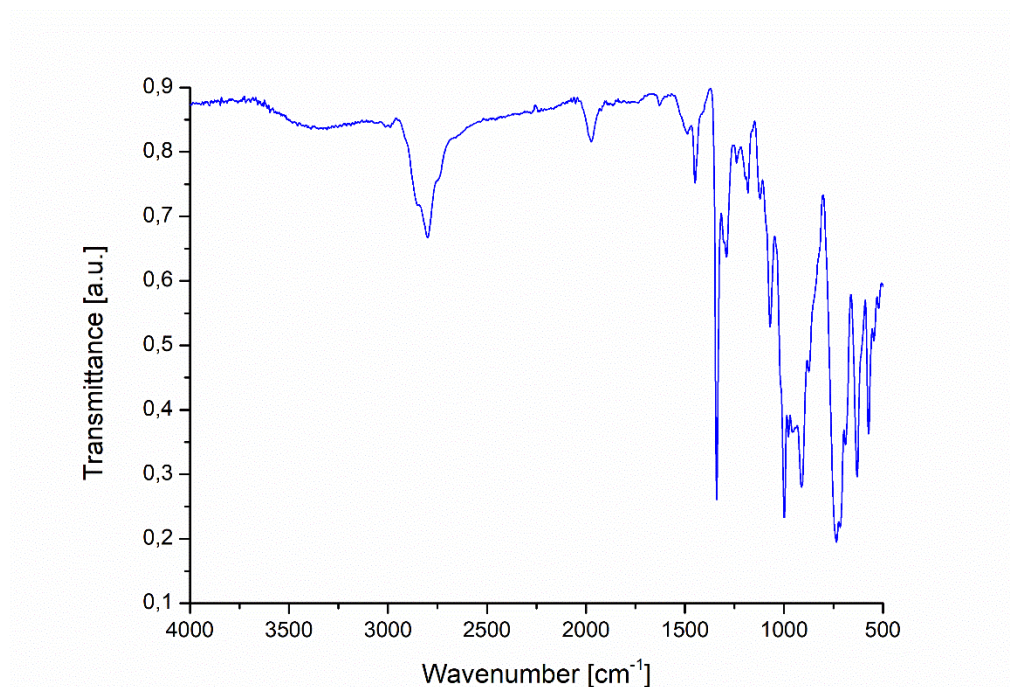
Figure S74. FT-IR spectrum of **141-[G$_1$]-PEG**.

2. Synthesis of polyphosphorhydrazone dendrimers

2.1. Dendrimer 142-[G$_0$'][G$_1$]-PEG
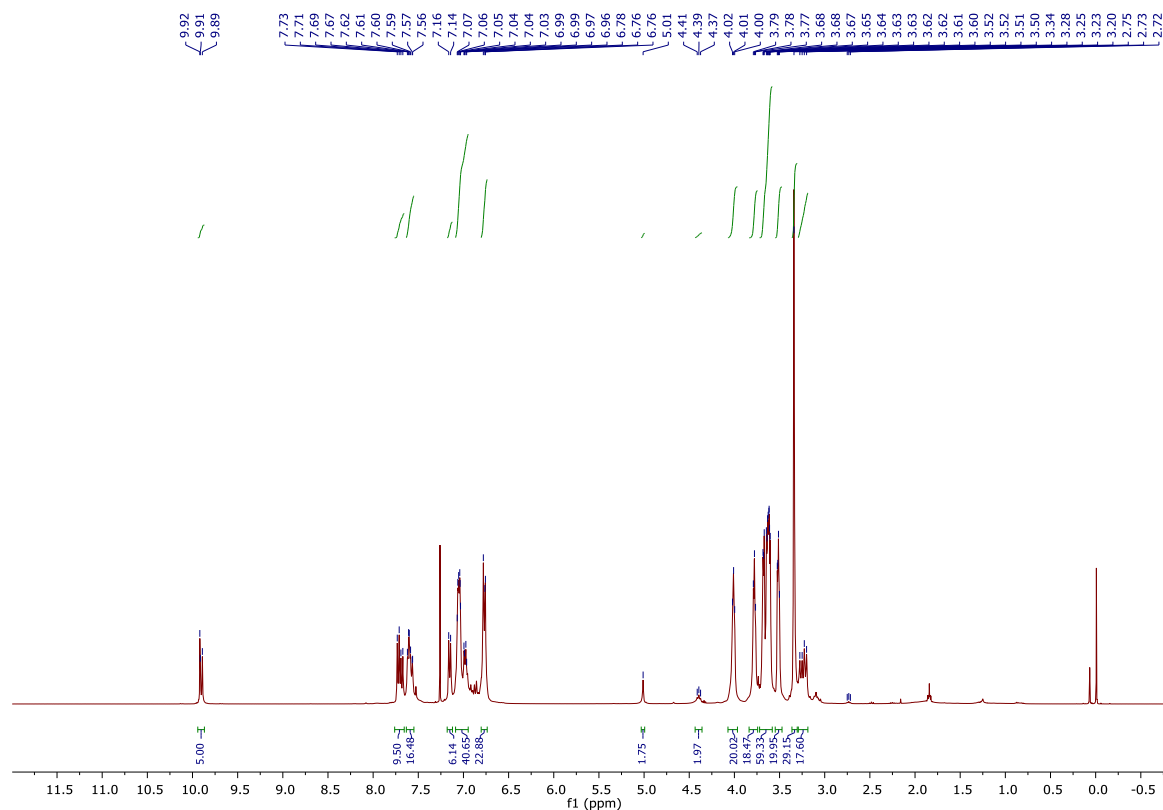
Figure S75. ^{1}H NMR spectrum of **142-[G$_0$'][G$_1$]-PEG** in CDCl$_3$ recorded at room temperature (400 MHz).
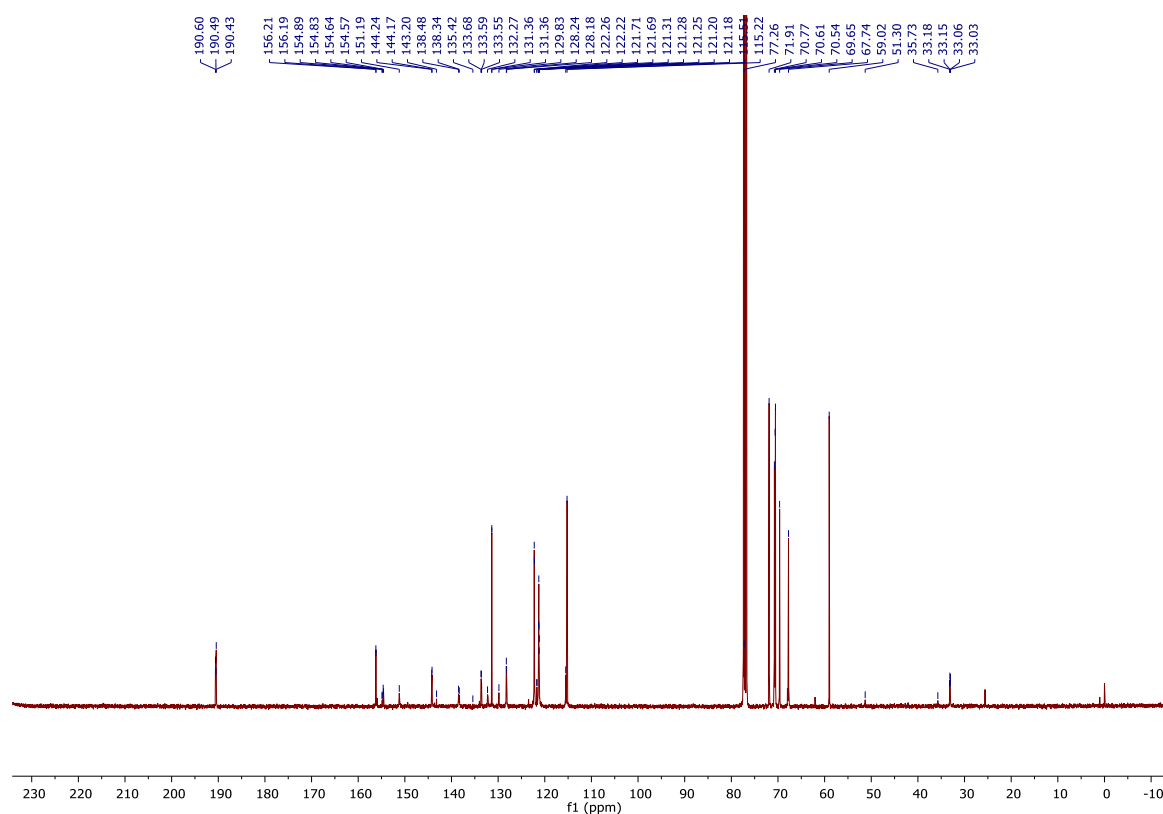
Figure S76. ^{13}C{^{1}H} NMR spectrum of **142-[G$_0$'][G$_1$]-PEG** in CDCl$_3$ recorded at room temperature (101 MHz).
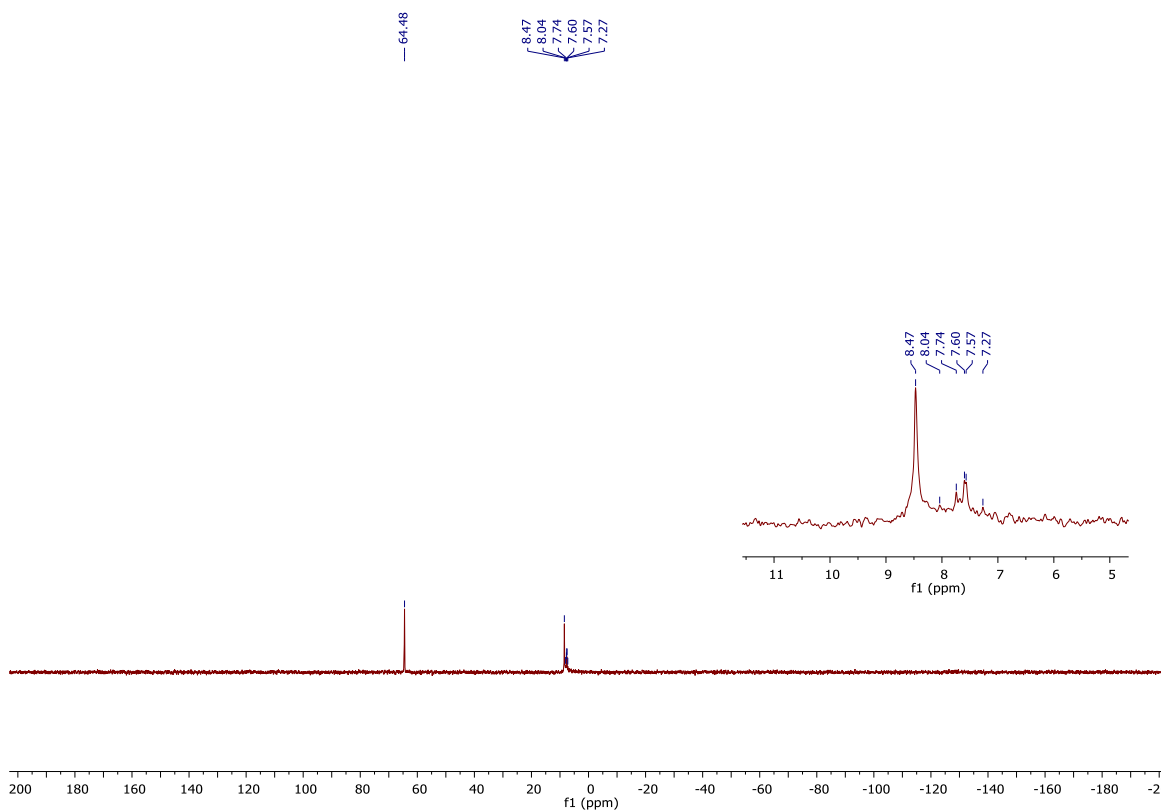
Figure S77. $^{31}P\{^1H\}$ NMR spectrum of **142-[G$_0$'][G$_1$]-PEG** in CDCl$_3$ recorded at room temperature (162 MHz).
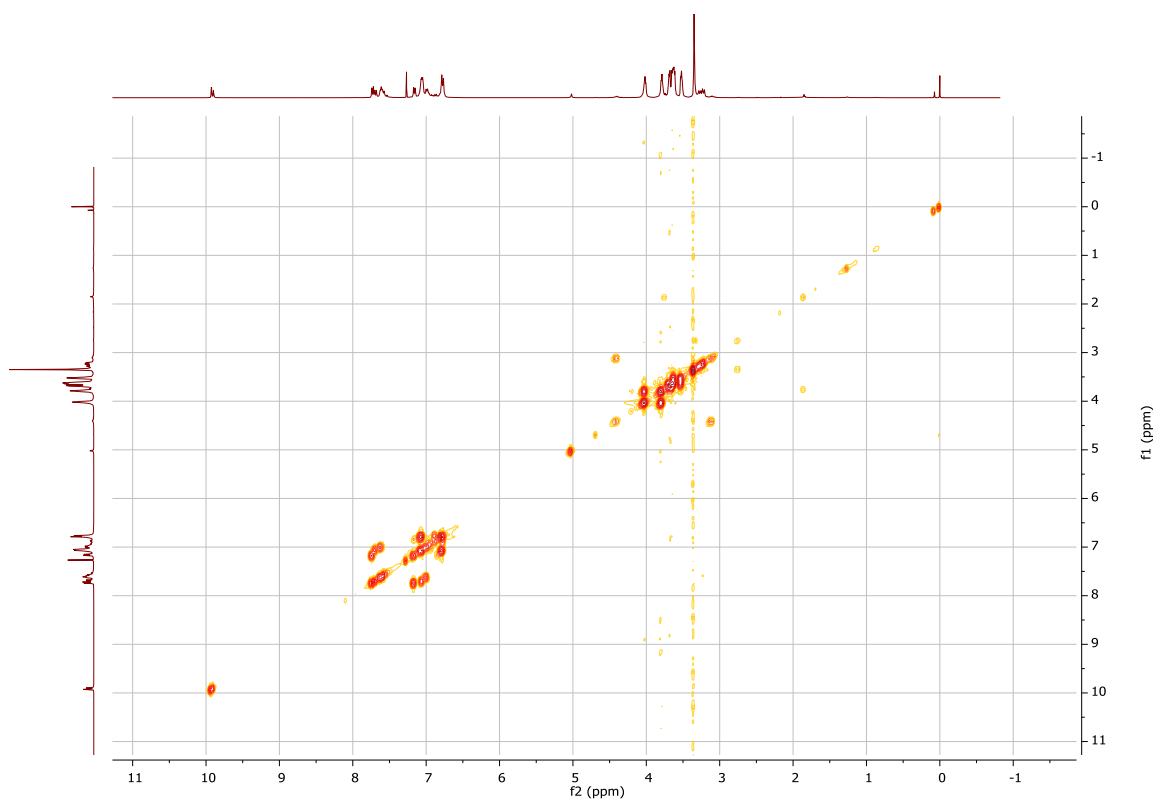
Figure S78. ^1H-^1H COSY spectrum of **142-[G$_0$'][G$_1$]-PEG** recorded in CDCl$_3$ at room temperature (400 MHz).
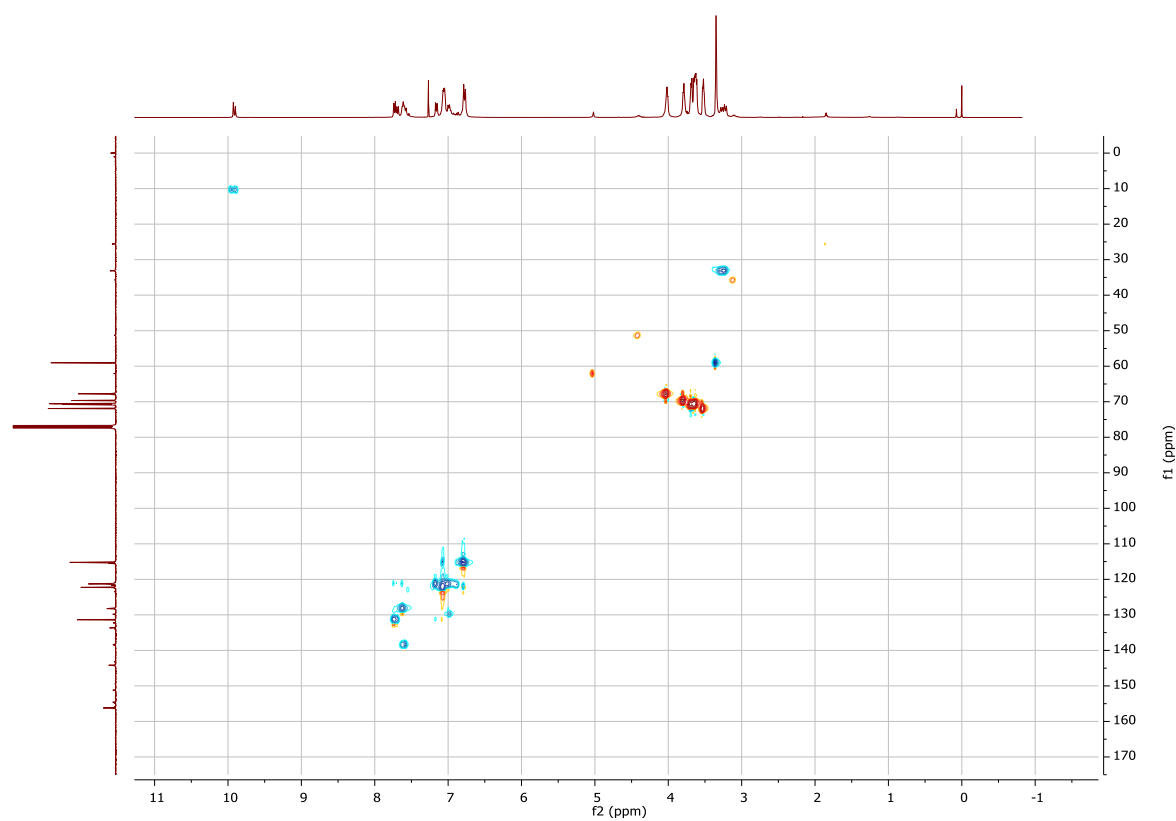
Figure S79. ^{1}H-^{13}C{^{1}H} HSQC spectrum of **142-[G$_0$'][G$_1$]-PEG** recorded in CDCl$_3$ at room temperature (400 MHz, 101 MHz).
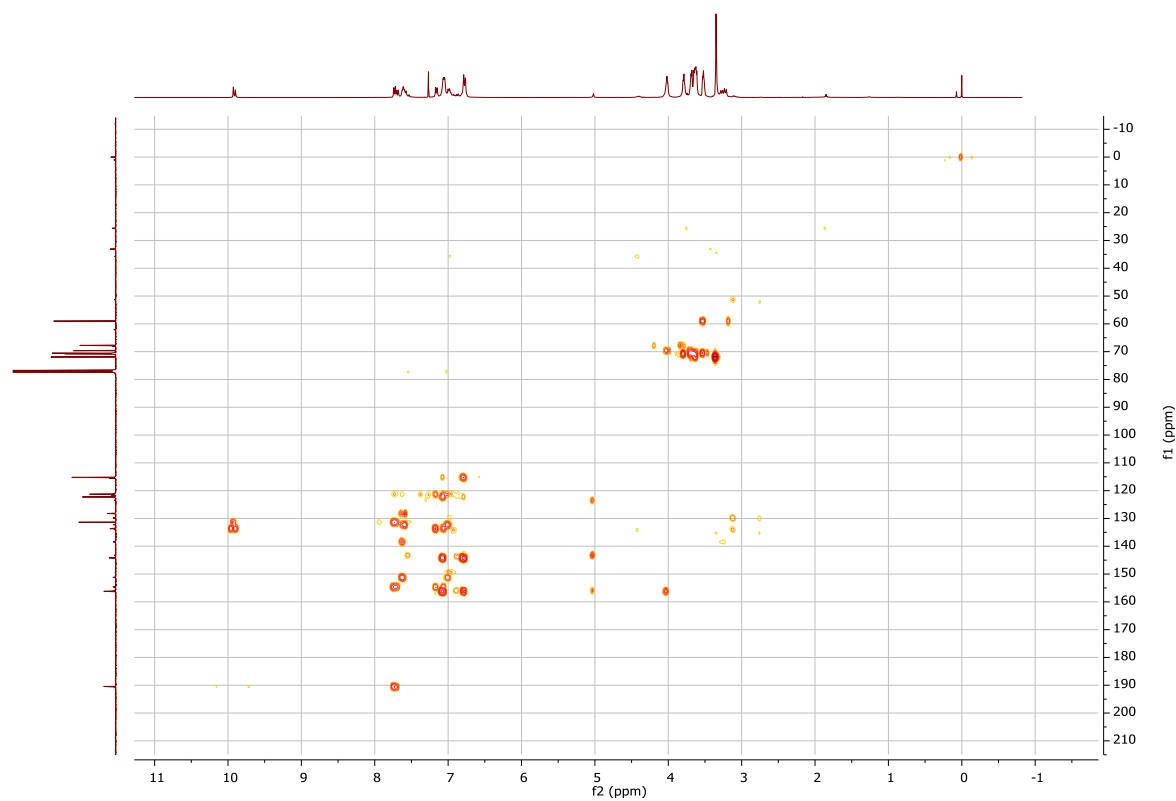
Figure S80. ^{1}H-^{13}C{^{1}H} HMBC spectrum of **142-[G$_0$'][G$_1$]-PEG** recorded in CDCl$_3$ at room temperature (400 MHz, 101 MHz).
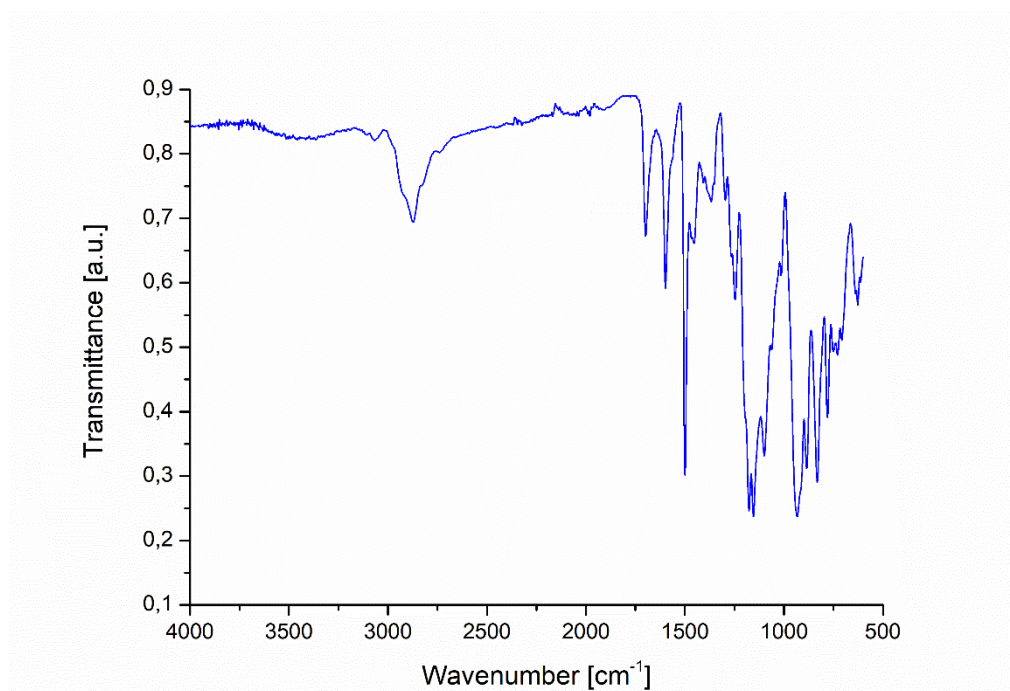
Figure S81. FT-IR spectrum of **142-[G$_0$'][G$_1$]-PEG**.

2.2. Dendrimer 143-[G₁][G₁]-PEG
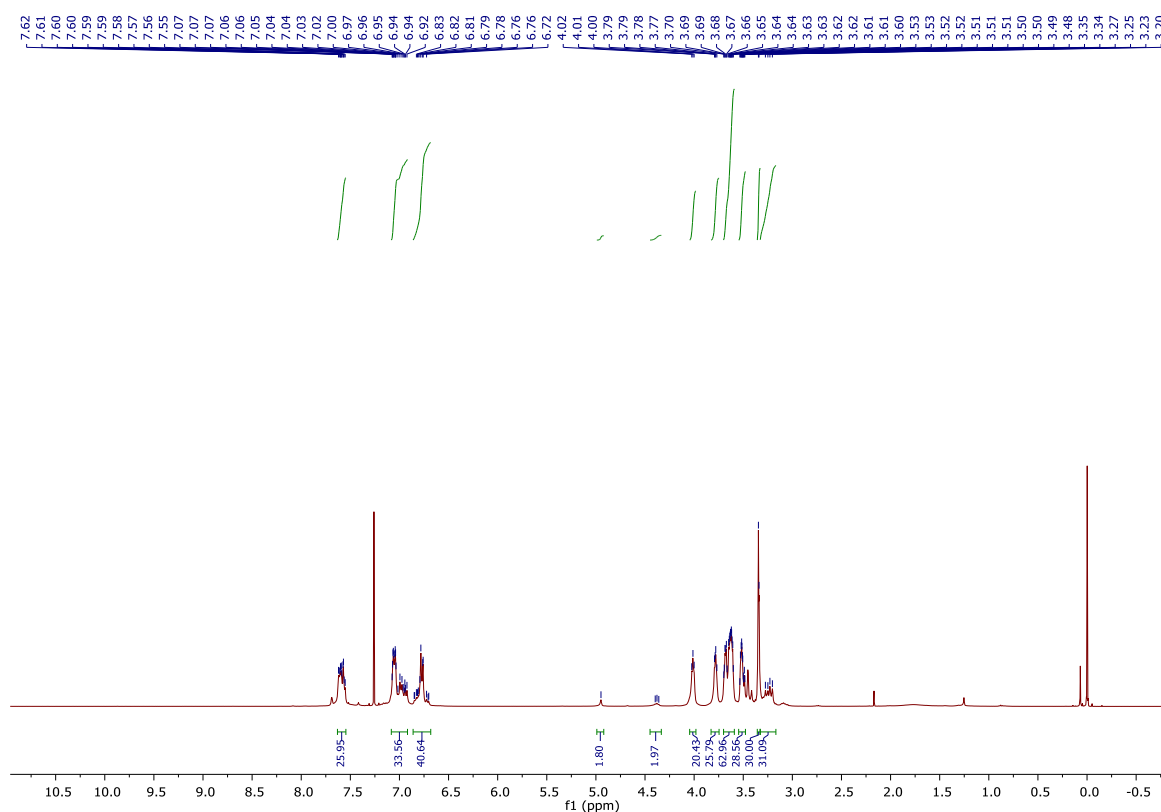
Figure S82. ¹H NMR spectrum of **143-[G₁][G₁]-PEG** in CDCl₃ recorded at room temperature (400 MHz).
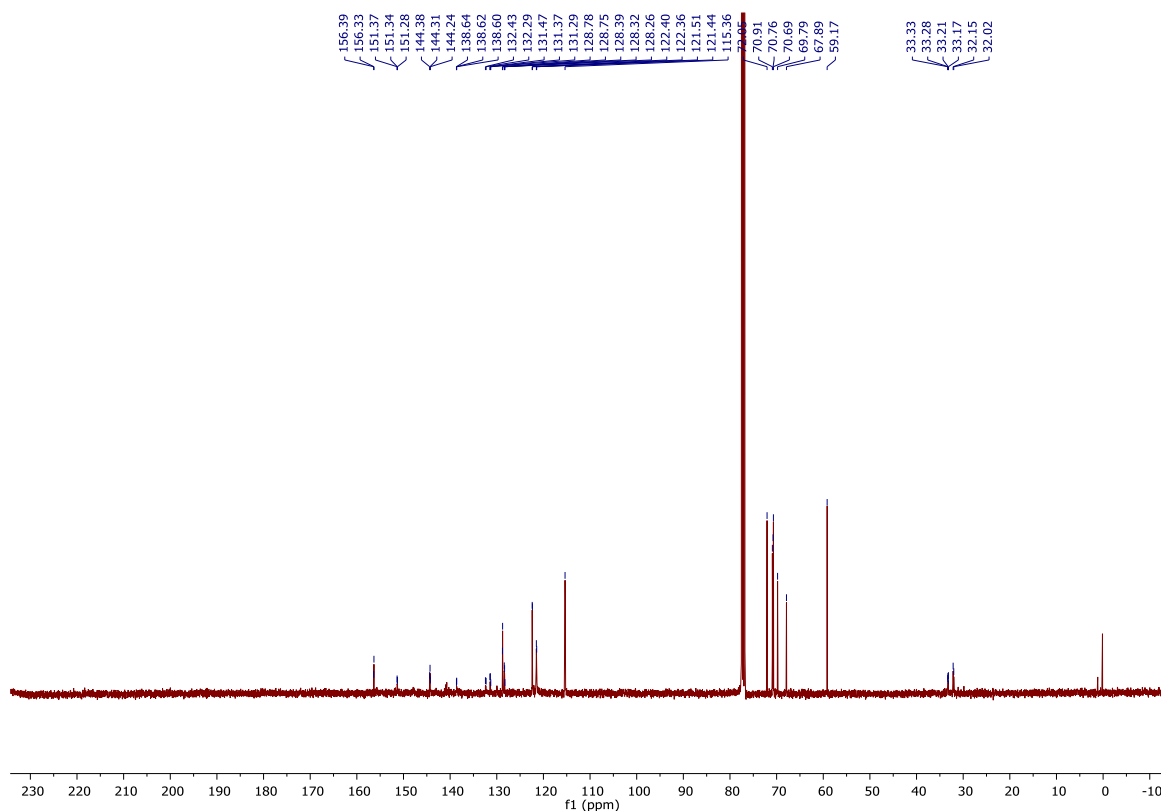
Figure S83. ¹³C{¹H} NMR spectrum of **143-[G₁][G₁]-PEG** in CDCl₃ recorded at room temperature (101 MHz).
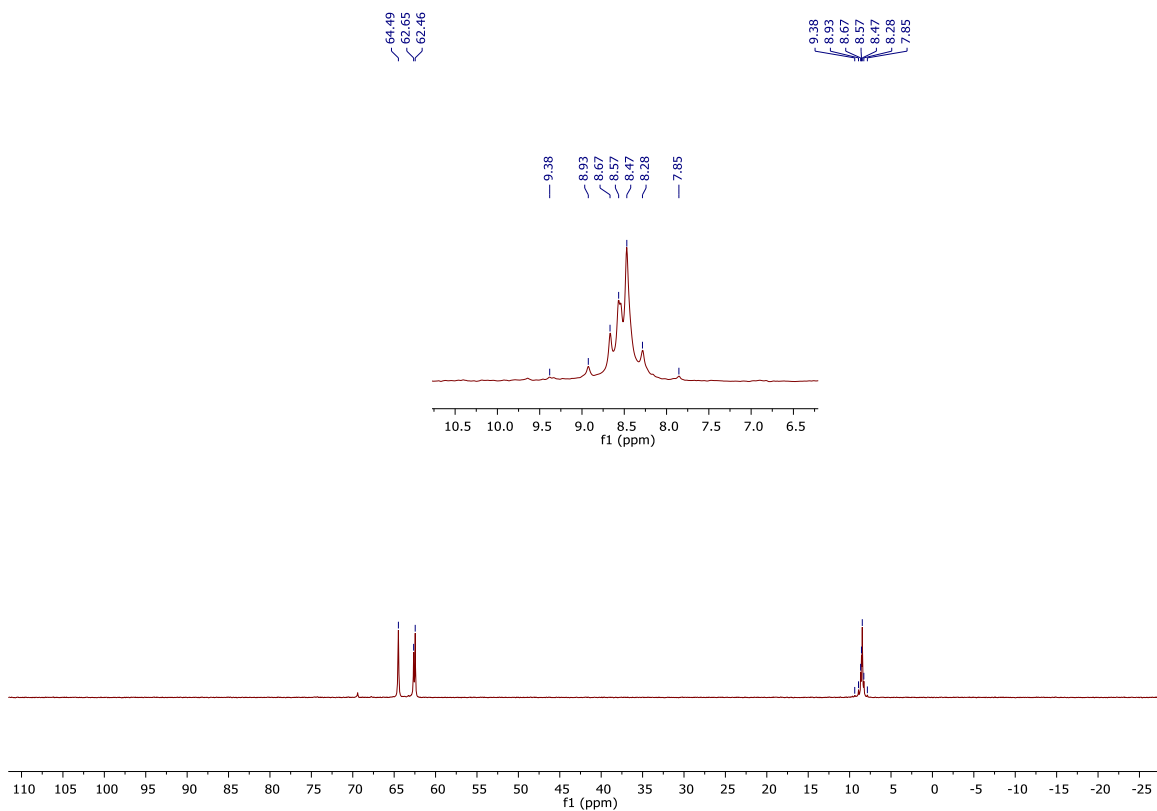
Figure S84. $^{31}P\{^1H\}$ NMR spectrum of **143-[G$_1$][G$_1$]-PEG** in CDCl$_3$ recorded at room temperature (162 MHz).
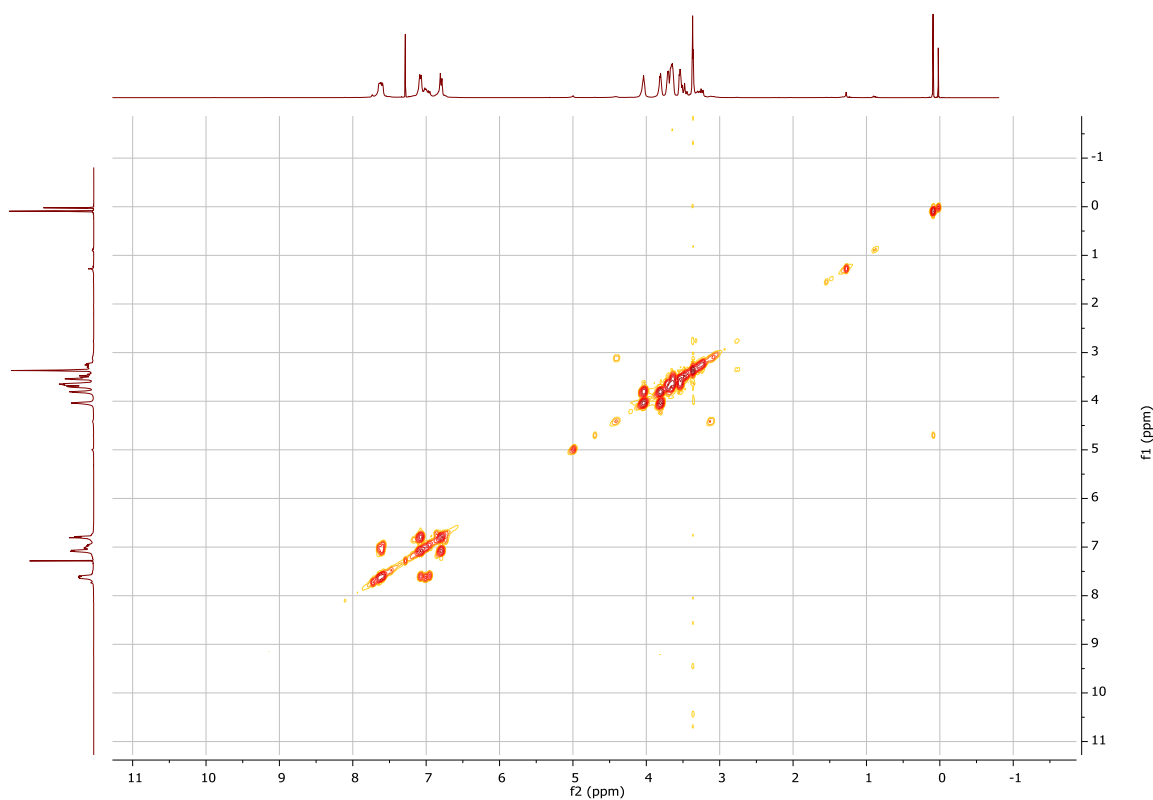
Figure S85. ^1H-^1H COSY spectrum of **143-[G$_1$][G$_1$]-PEG** in CDCl$_3$ recorded at room temperature (400 MHz).
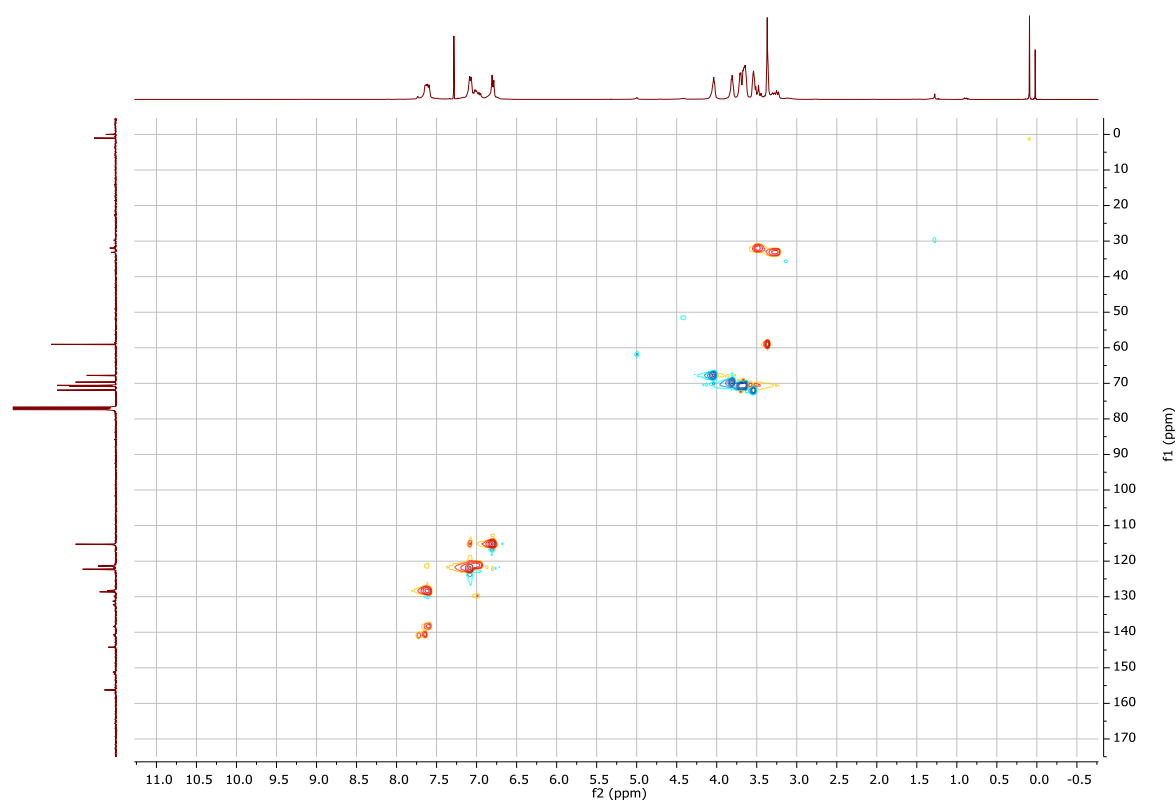
Figure S86. ^{1}H-^{13}C{^{1}H} HSQC spectrum of **143-[G₁][G₁]-PEG** in CDCl₃ recorded at room temperature (400 MHz, 101 MHz).
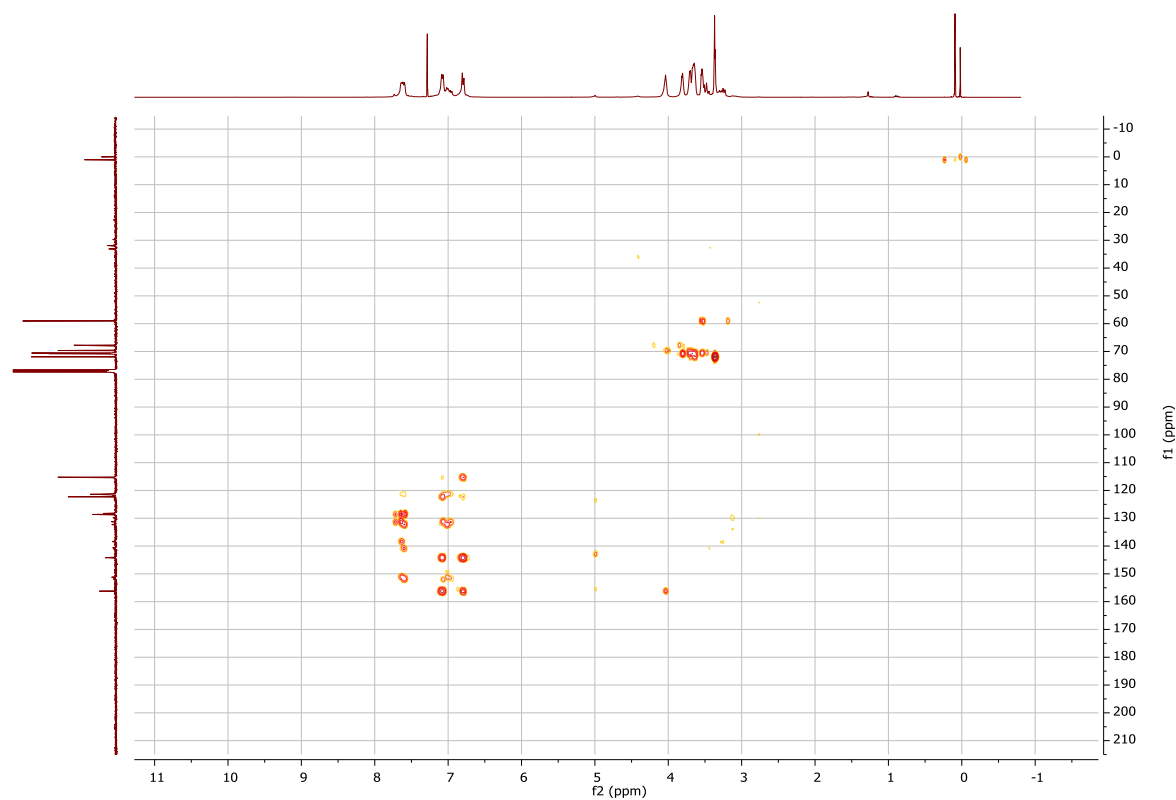
Figure S87. ^{1}H-^{13}C{^{1}H} HMBC spectrum of **143-[G₁][G₁]-PEG** in CDCl₃ recorded at room temperature (400 MHz, 101 MHz).
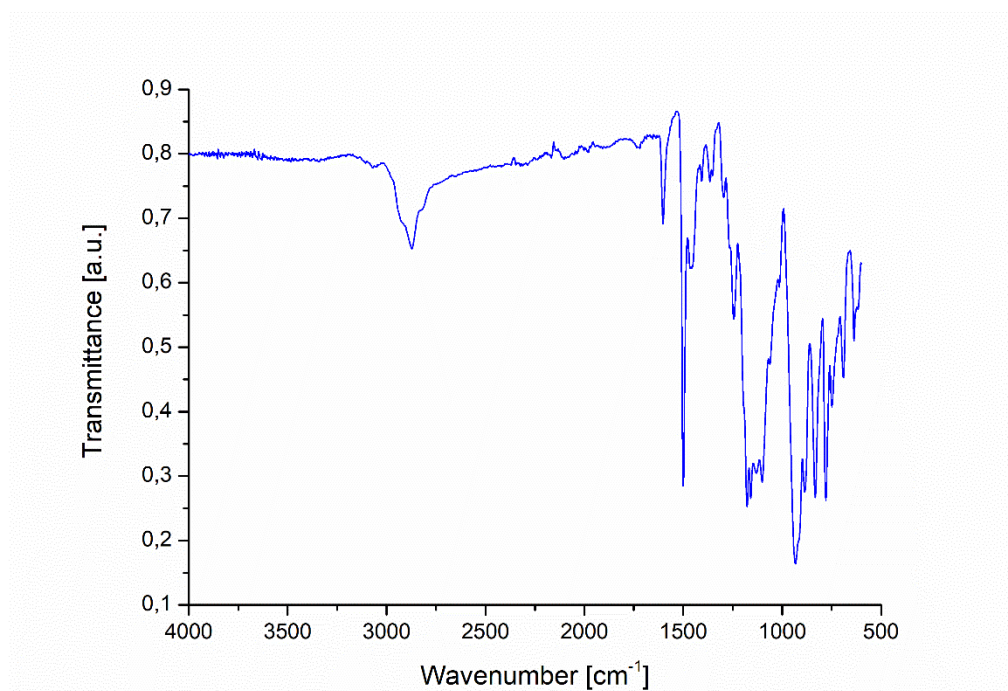
Figure S88. FT-IR spectrum of **143-[G$_1$][G$_1$]-PEG**.

3. Synthesis of unsymmetrical NHC ligands

3.1. *N*-mesitylethylenediamine 146
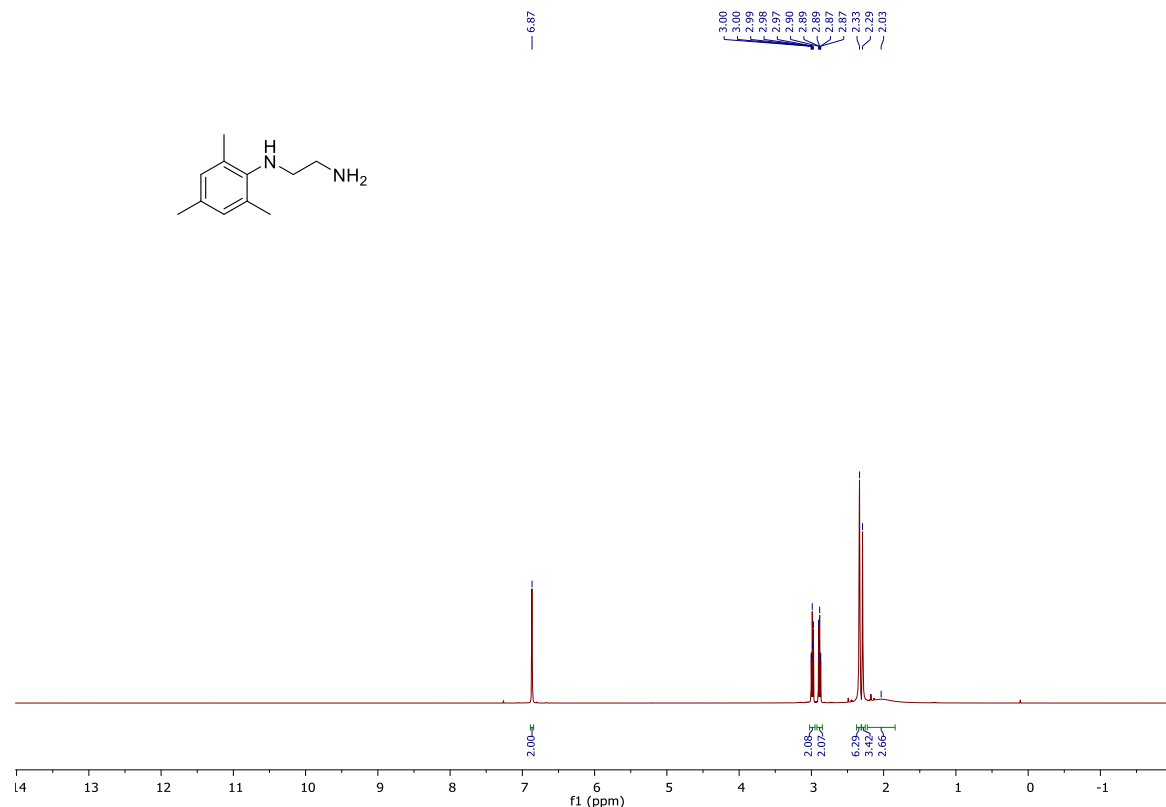
Figure S89. ^{1}H NMR spectrum of *N*-mesitylethylenediamine **146** in CDCl$_3$ recorded at room temperature (400 MHz).
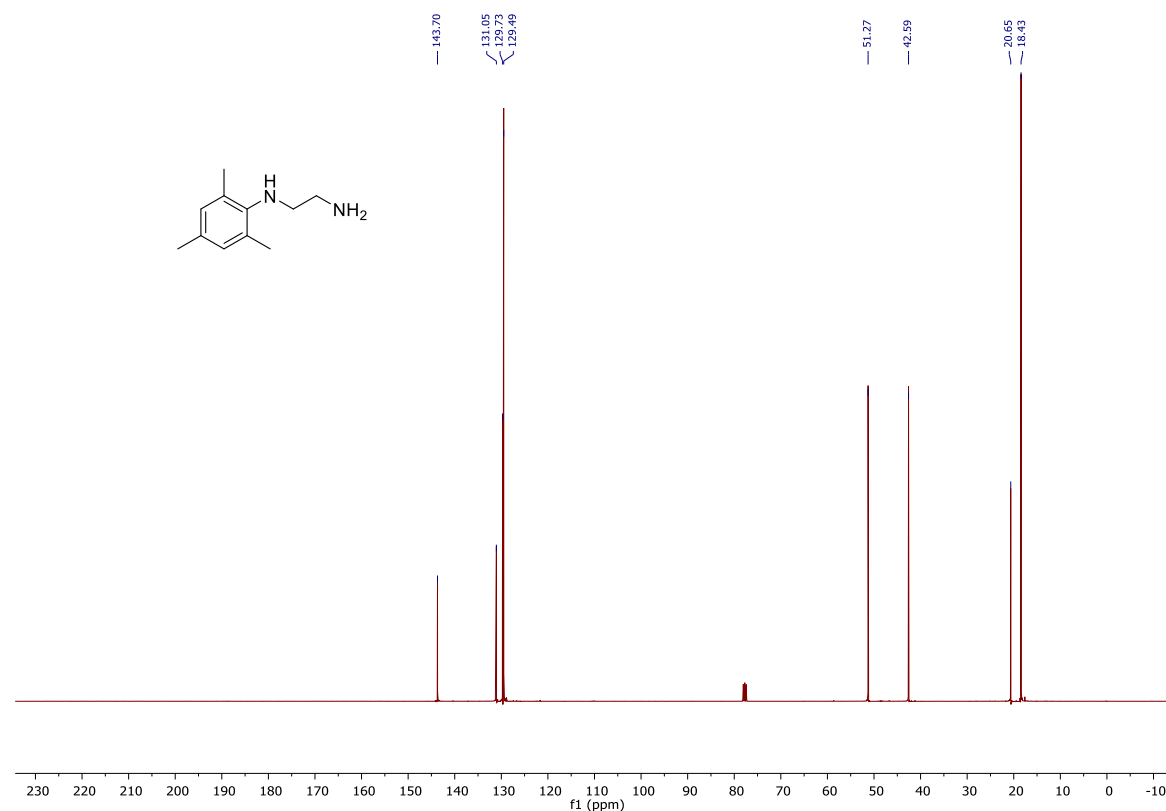
Figure S90. ^{13}C{^{1}H} NMR spectrum of *N*-mesitylethylenediamine **146** in CDCl$_3$ recorded at room temperature (101 MHz).

3.2.   4-(((2-(mesitylamino)ethyl)amino)methyl)phenol 148
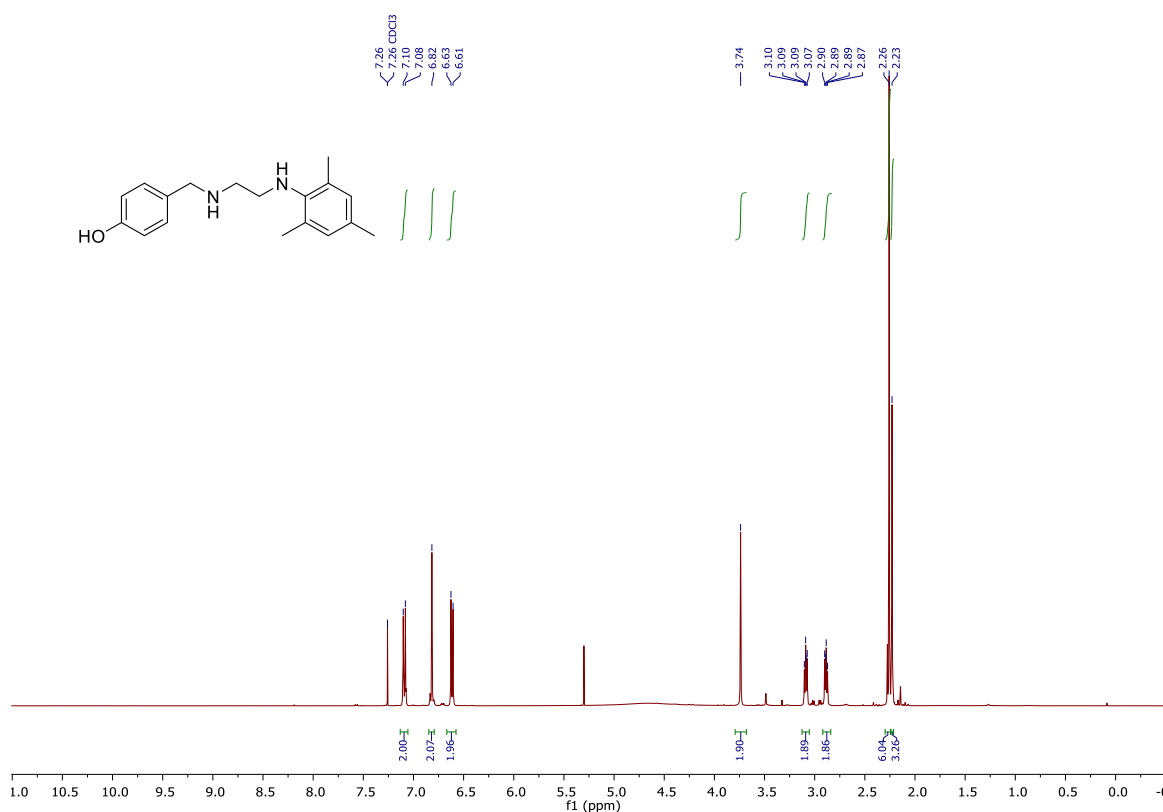
Figure S91. ^{1}H NMR spectrum of 4-(((2-(mesitylamino)ethyl)amino)methyl)phenol **148** in CDCl$_3$ recorded at room temperature (400 MHz).
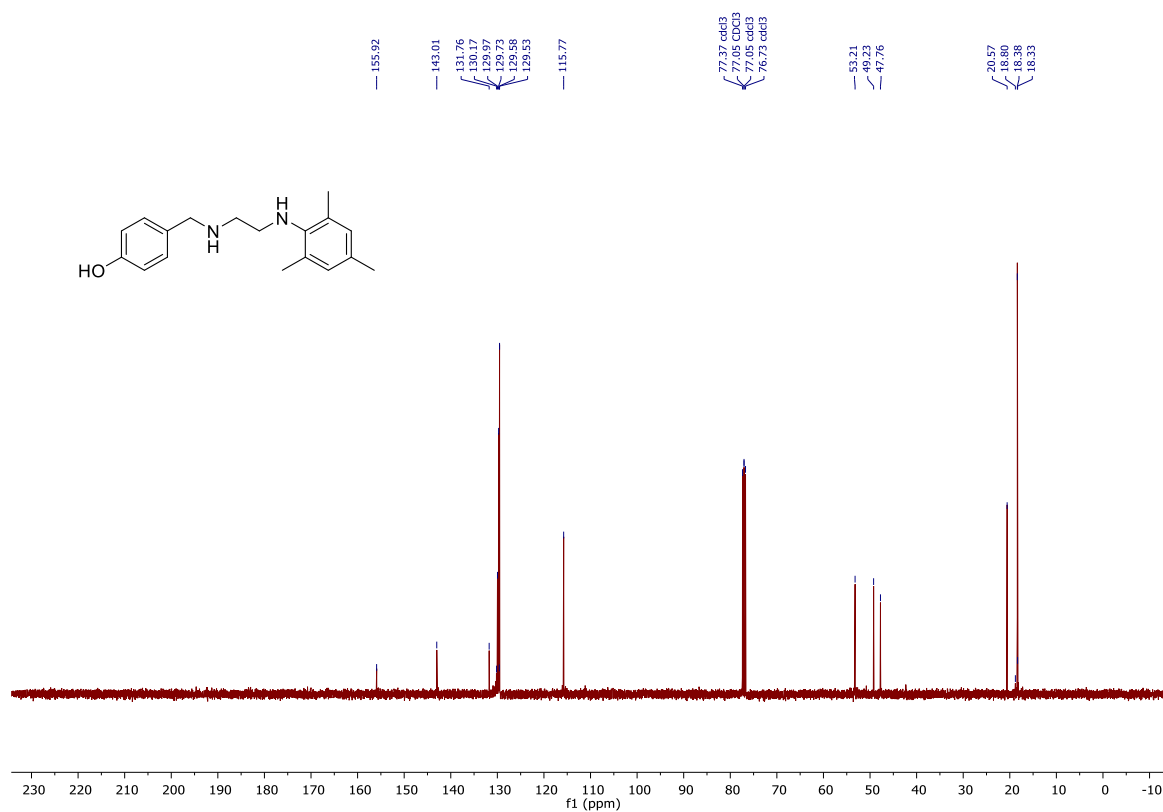
Figure S92. ^{13}C{^{1}H} NMR spectrum of 4-(((2-(mesitylamino)ethyl)amino)methyl)phenol **148** in CDCl$_3$ recorded at room temperature (101 MHz).

3.3. 1-(4-hydroxybenzyl)-3-mesityl-4,5-dihydro-1*H*-imidazol-3-ium chloride 149
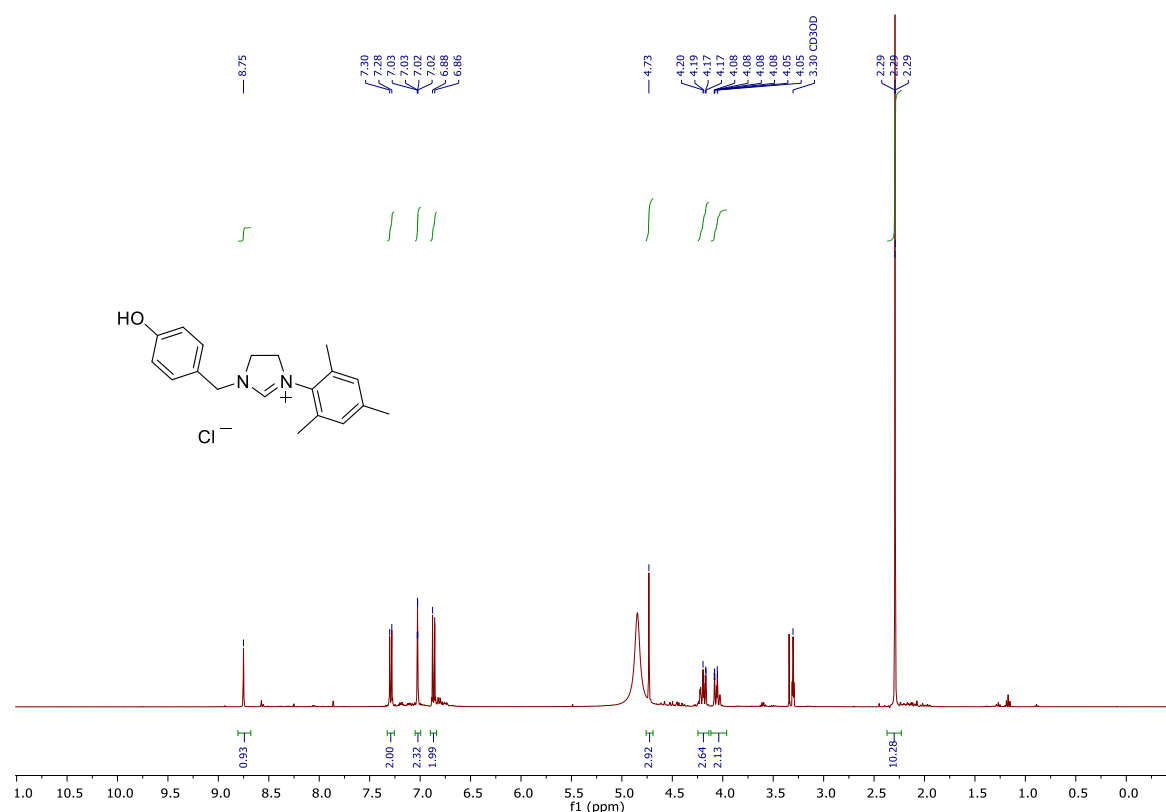
Figure S93. ¹H NMR spectrum of 1-(4-hydroxybenzyl)-3-mesityl-4,5-dihydro-1*H*-imidazol-3-ium chloride **149** in MeOD recorded at room temperature (400 MHz).
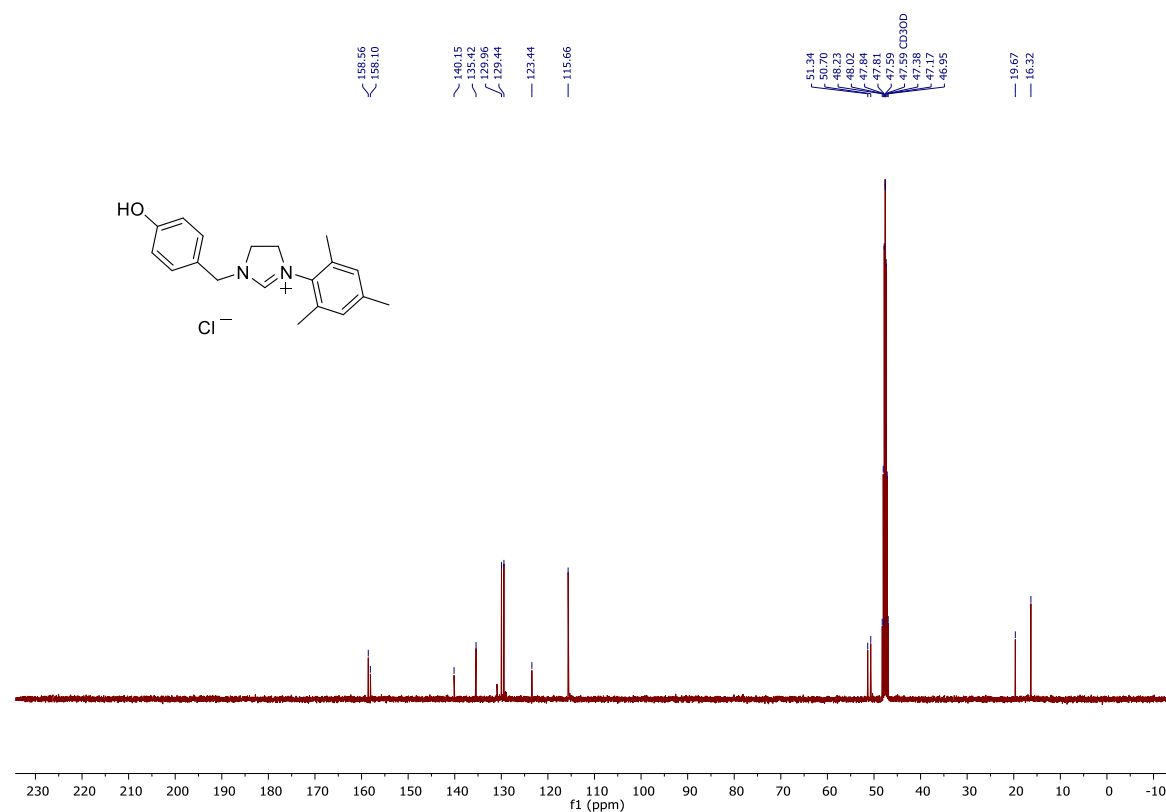
Figure S94. ¹³C{¹H} NMR spectrum of 1-(4-hydroxybenzyl)-3-mesityl-4,5-dihydro-1*H*-imidazol-3-ium chloride **149** in MeOD recorded at room temperature (101 MHz).
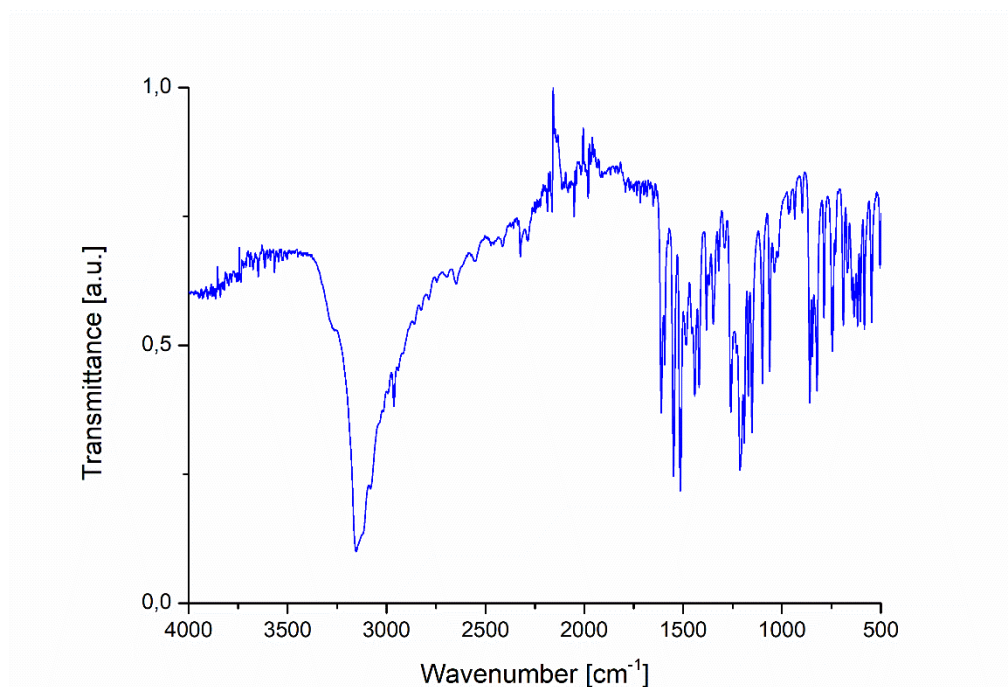
Figure S95. FT-IR spectrum of 1-(4-hydroxybenzyl)-3-mesityl-4,5-dihydro-1*H*-imidazol-3-ium chloride **149**.

Single Mass Analysis
Tolerance = 3.0 mDa / DBE: min = -1.5, max = 300.0
Element prediction: Off
Number of isotope peaks used for i-FIT = 3
Monoisotopic Mass, Even Electron Ions
100 formula(e) evaluated with 1 results within limits (up to 50 closest results for each mass)
Elements Used:
C: 0-100   H: 0-200   N: 0-5   O: 0-3

Mass	Calc. Mass	mDa	PPM	DBE	Formula	i-FIT	i-FIT Norm	Fit Conf %	C	H	N	O
295.1814	295.1810	0.4	1.4	9.5	C19 H23 N2 O	1582.8	n/a	n/a	19	23	2	1

Figure S96. HRMS of 1-(4-hydroxybenzyl)-3-mesityl-4,5-dihydro-1*H*-imidazol-3-ium chloride **149**.

3.4.   4-(hydroxymethyl)phenol 150
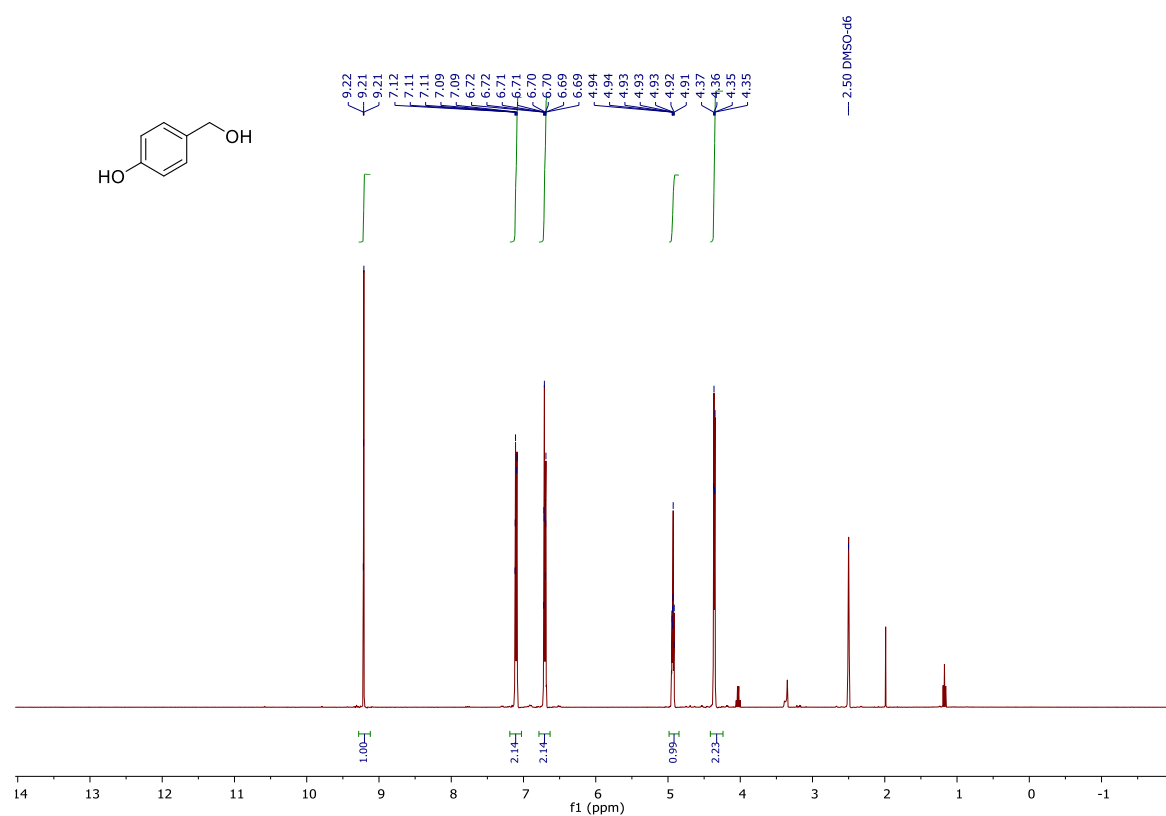
Figure S97. ^{1}H NMR spectrum of 4-(hydroxymethyl)phenol **150** in DMSO-d_6 recorded at room temperature (400 MHz).
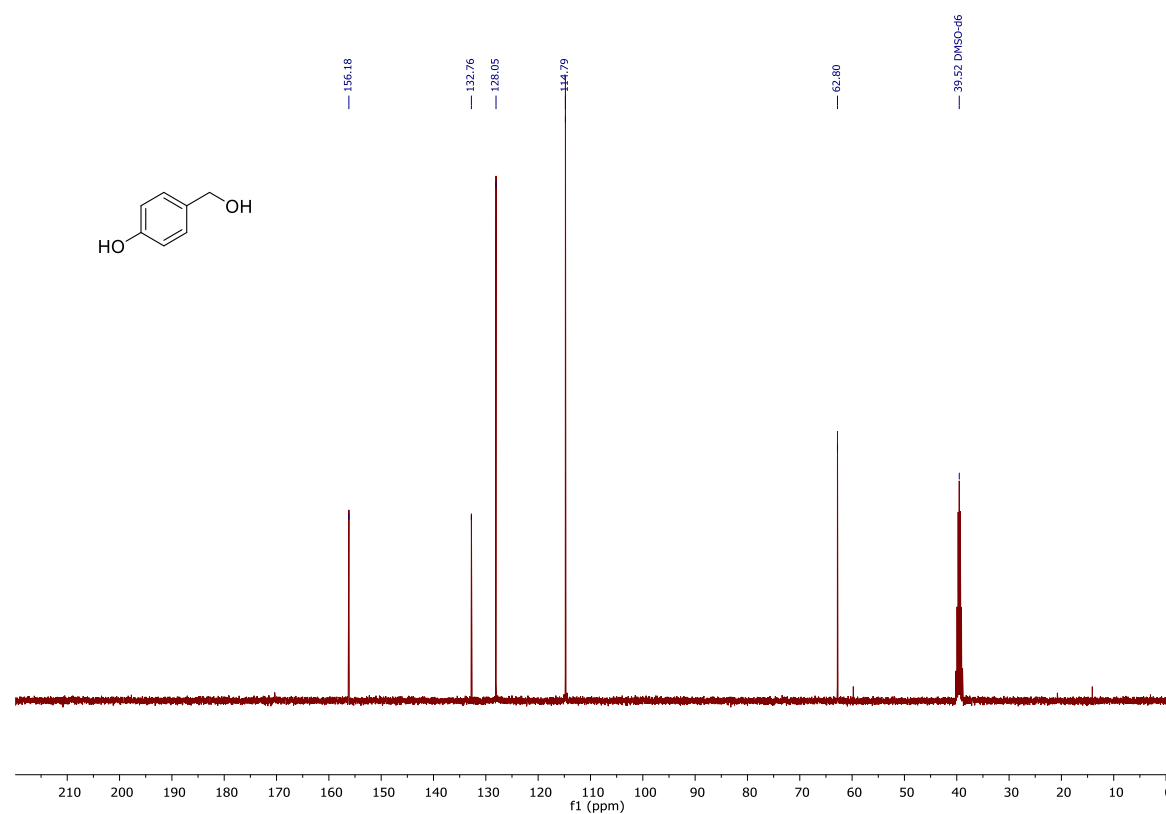
Figure S98. ^{13}C{^{1}H} NMR spectrum of 4-(hydroxymethyl)phenol **150** in DMSO-d_6 recorded at room temperature (101 MHz).

3.5. 4-(iodomethyl)phenol 151
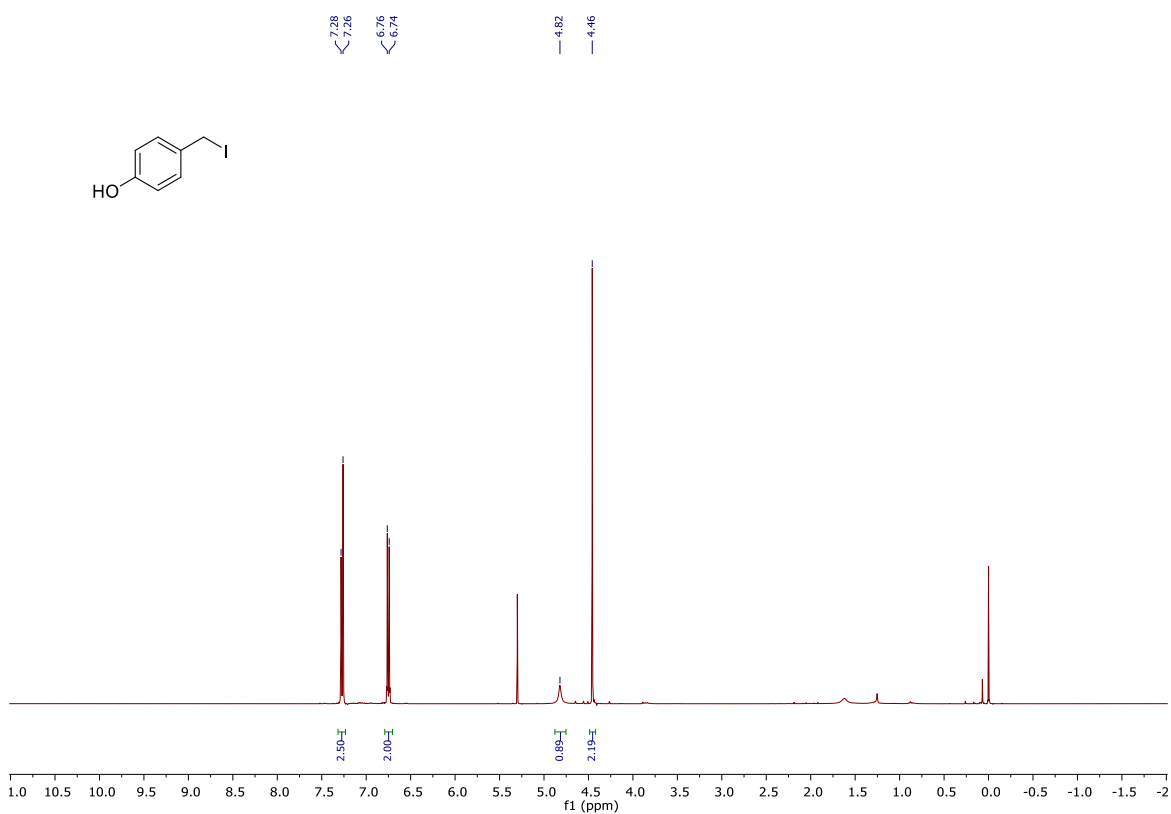
Figure S99. ¹H NMR spectrum of 4-(iodomethyl)phenol **151** in CDCl₃ recorded at room temperature (400 MHz).
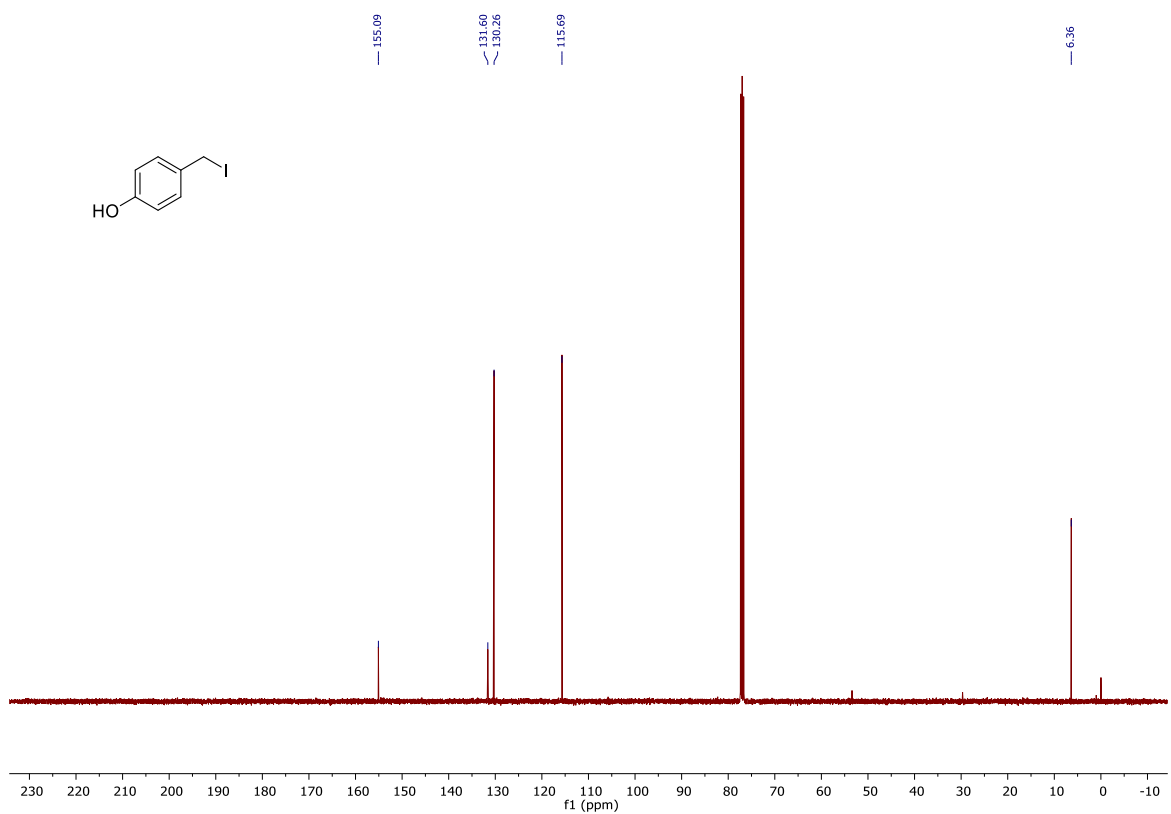
Figure S100. ¹³C{¹H} NMR spectrum of 4-(iodomethyl)phenol **151** in CDCl₃ recorded at room temperature (101 MHz).

3.6. 1-mesityl-1*H*-imidazole 152

Figure S101. ¹H NMR spectrum of 1-mesityl-1*H*-imidazole **152** in CDCl₃ recorded at room temperature (400 MHz).
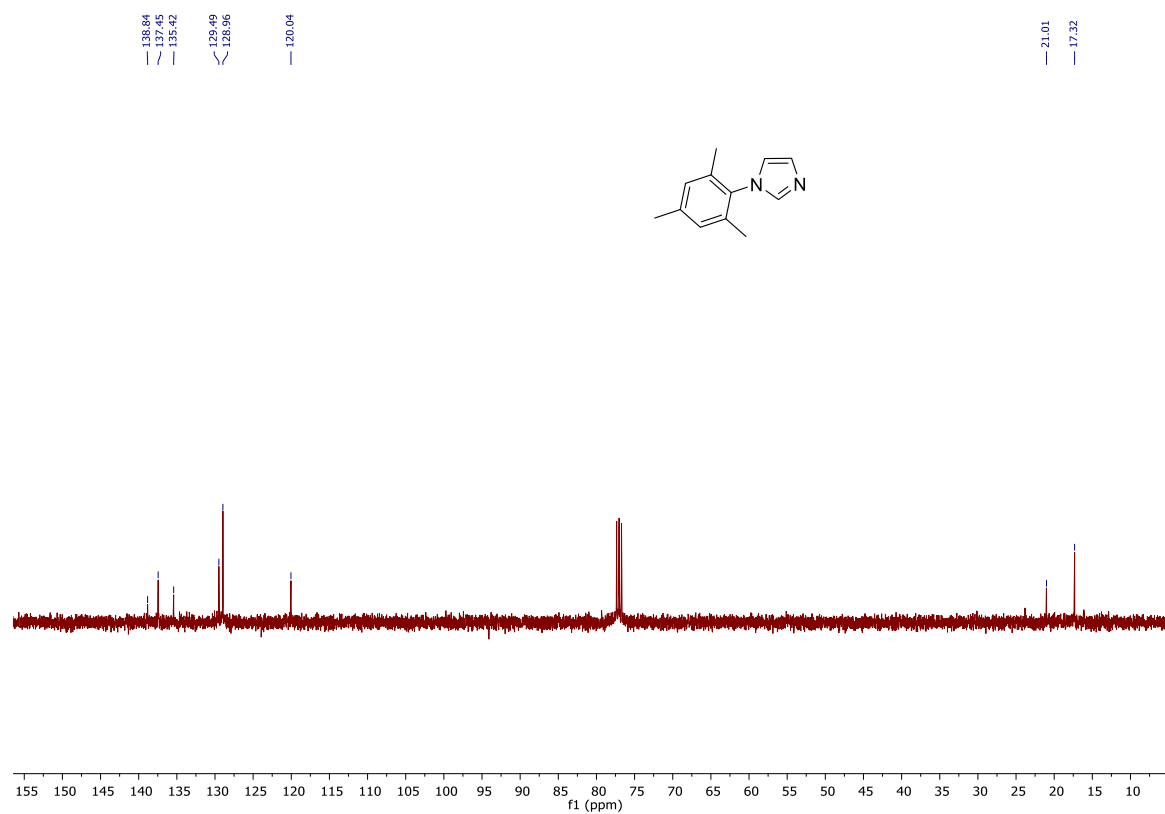
Figure S102. ¹³C{¹H} NMR spectrum of 1-mesityl-1*H*-imidazole **152** in CDCl₃ recorded at room temperature (101 MHz).

3.7.   1-(4-hydroxybenzyl)-3-mesityl-1*H*-imidazol-3-ium iodide 153
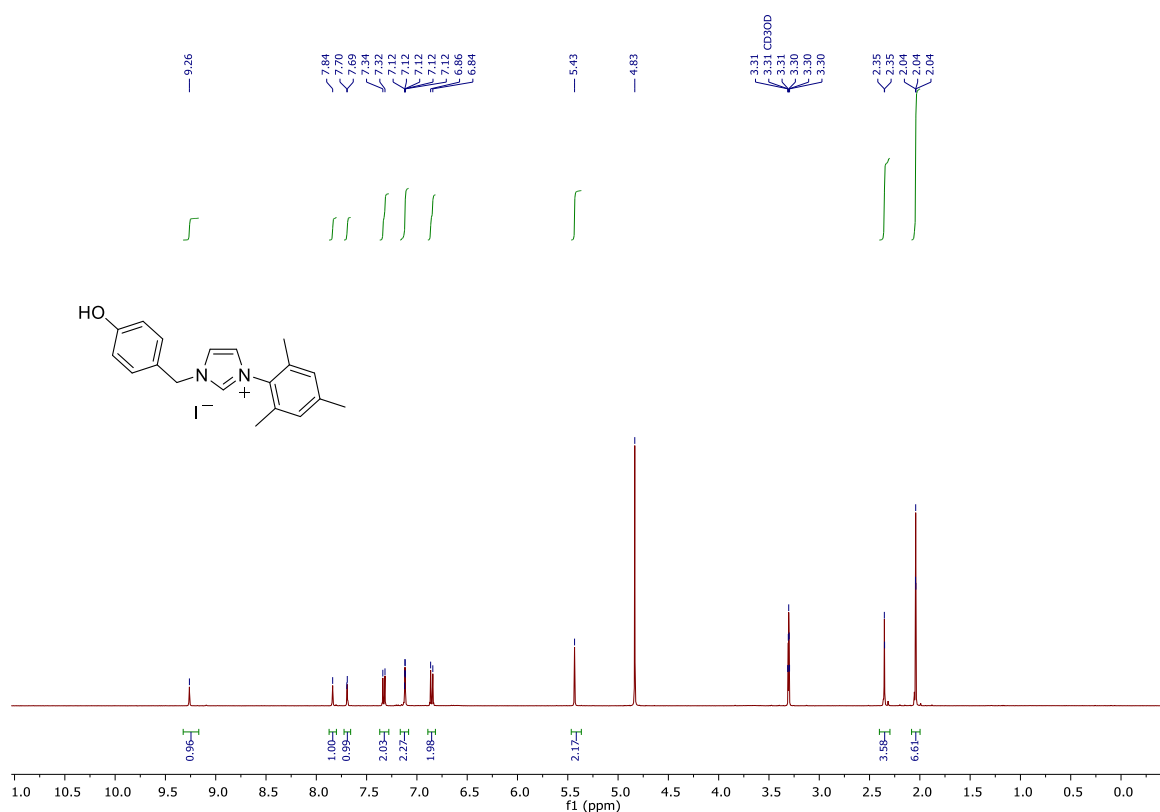
Figure S103. ¹H NMR spectrum of 1-(4-hydroxybenzyl)-3-mesityl-1*H*-imidazol-3-ium iodide **153** in MeOD recorded at room temperature (400 MHz).
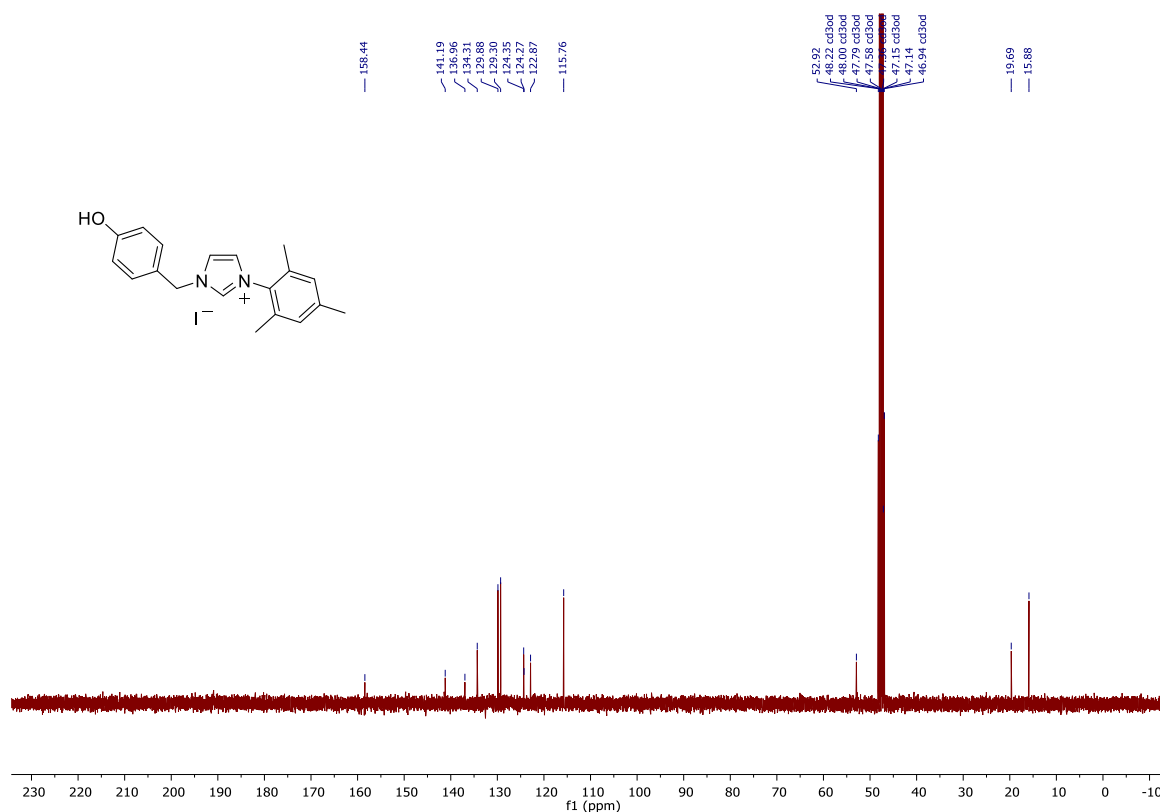
Figure S104. ¹³C{¹H} NMR spectrum of 1-(4-hydroxybenzyl)-3-mesityl-1*H*-imidazol-3-ium iodide **153** in MeOD recorded at room temperature (101 MHz).
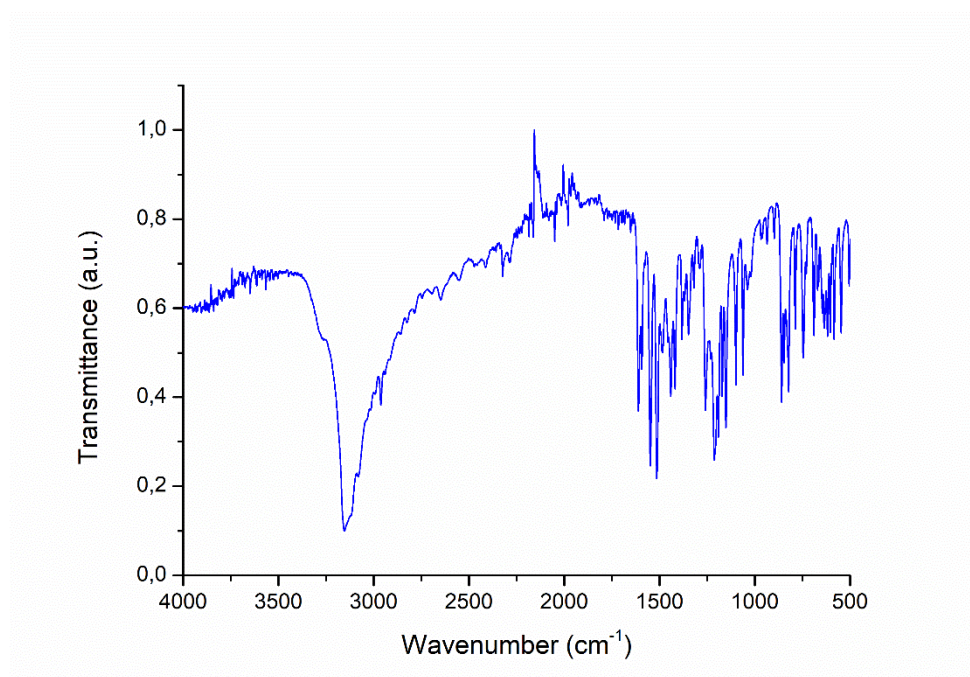
Figure S105. FT-IR spectrum of 1-(4-hydroxybenzyl)-3-mesityl-1*H*-imidazol-3-ium iodide **153**.

Single Mass Analysis
Tolerance = 3.0 mDa / DBE: min = -1.5, max = 300.0
Element prediction: Off
Number of isotope peaks used for i-FIT = 3
Monoisotopic Mass, Even Electron Ions
99 formula(e) evaluated with 1 results within limits (up to 50 closest results for each mass)
Elements Used:
C: 0-100   H: 0-200   N: 0-5   O: 0-3

Mass	Calc. Mass	mDa	PPM	DBE	Formula	i-FIT	i-FIT Norm	Fit Conf %	C	H	N	O
293.1657	293.1654	0.3	1.0	10.5	C19 H21 N2 O	1476.9	n/a	n/a	19	21	2	1

Figure S106. HRMS of 1-(4-hydroxybenzyl)-3-mesityl-1*H*-imidazol-3-ium iodide **153**.

4. Synthesis of Ru-NHC complexes

4.1. Ru36
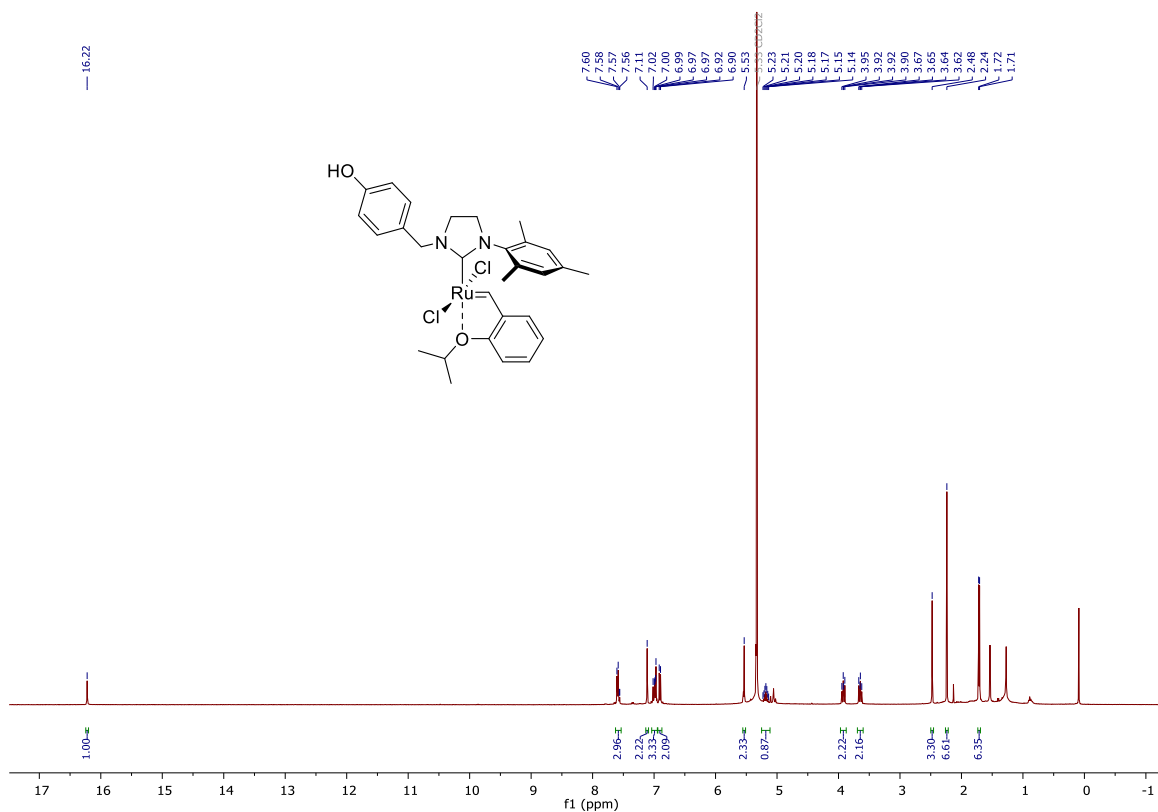
Figure S107. ^{1}H NMR spectrum of **Ru36** in DCM-d_2 recorded at room temperature (400 MHz).
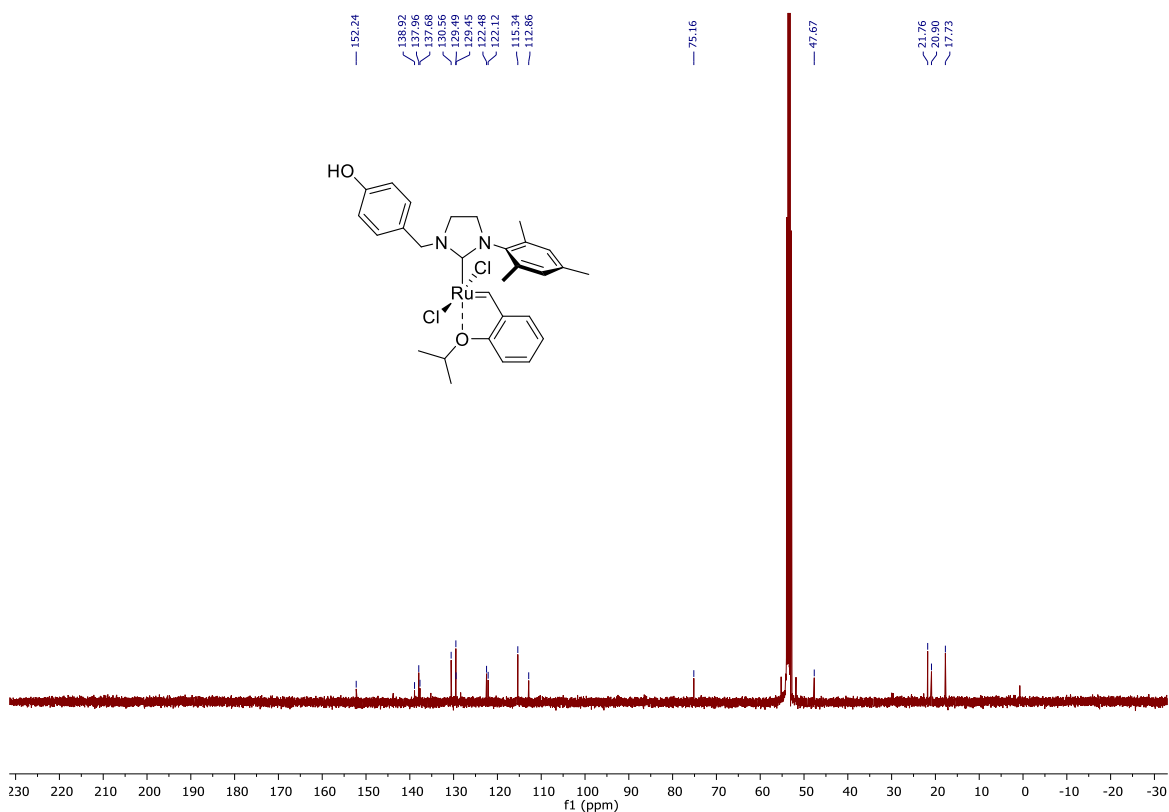
Figure S108. ^{13}C{^{1}H} NMR spectrum of **Ru36** in DCM-d_2 recorded at room temperature (101 MHz).

4.2.   Ru38
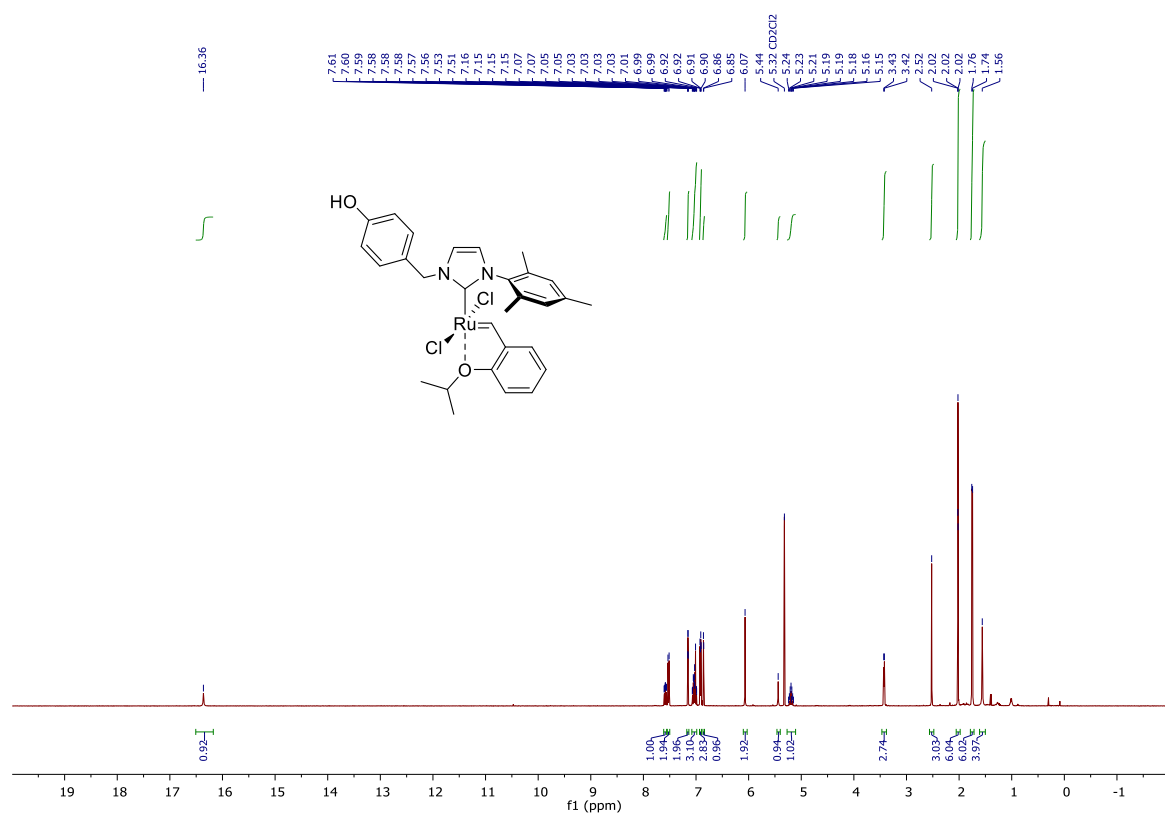
Figure S109. ^{1}H NMR spectrum of **Ru38** in DCM-d_2 recorded at room temperature (400 MHz).
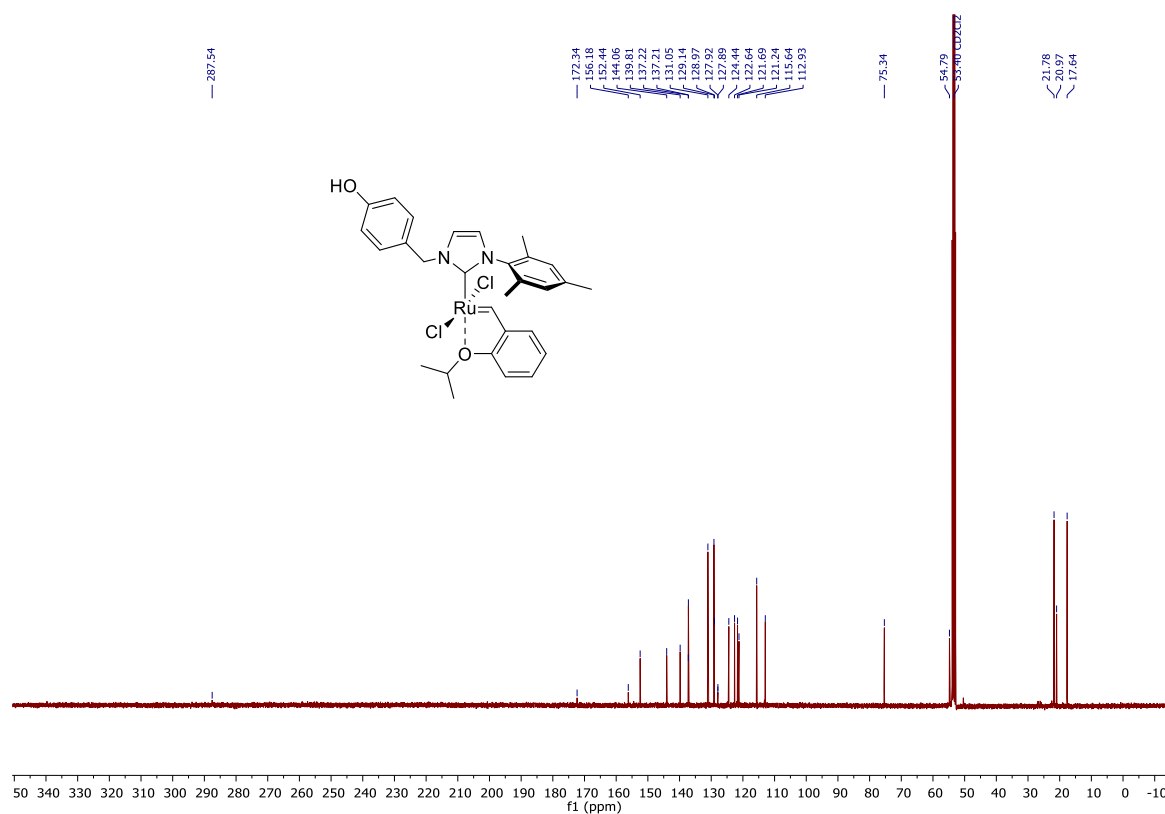
Figure S110. ^{13}C{^{1}H} NMR spectrum of **Ru38** in DCM-d_2 recorded at room temperature (101 MHz).

Figure S111. FT-IR spectrum of **Ru38**.

Figure S112. Elemental analysis of **Ru38**.

4.3. Ru41
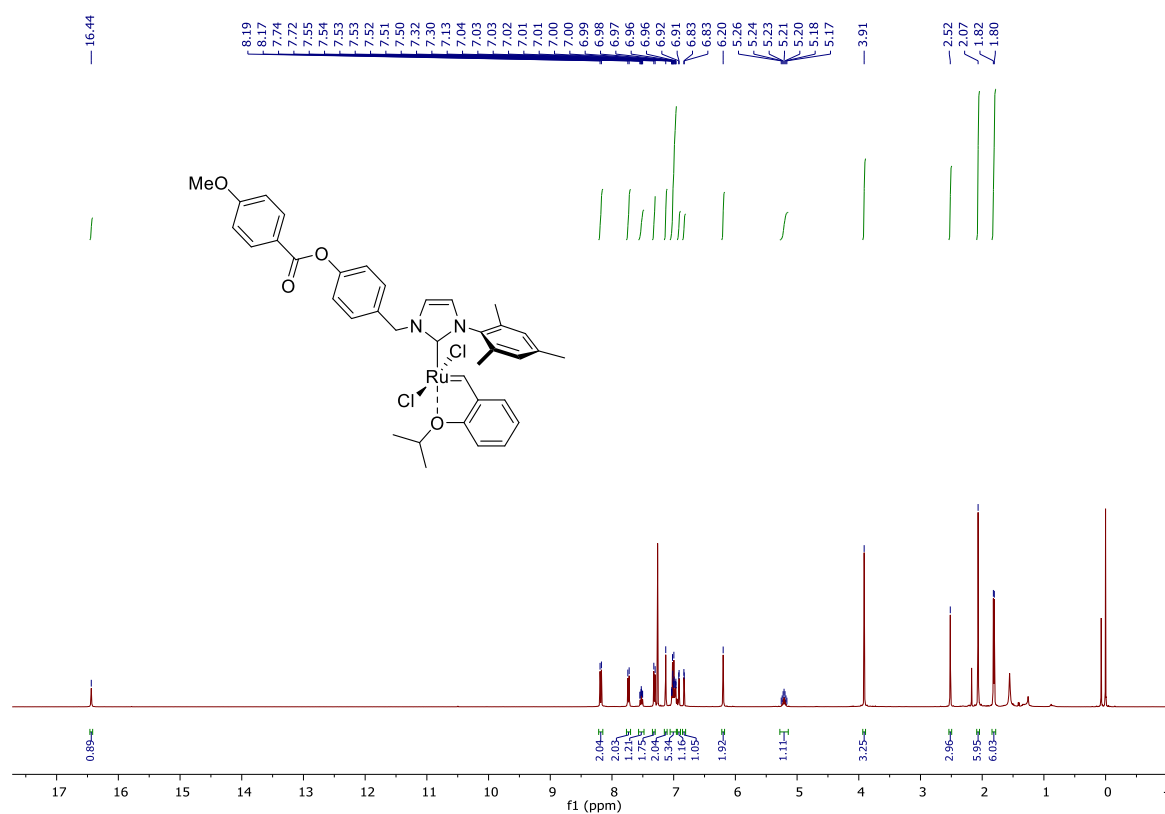
Figure S113. ^{1}H NMR spectrum of **Ru41** in CDCl$_3$ recorded at room temperature (400 MHz).
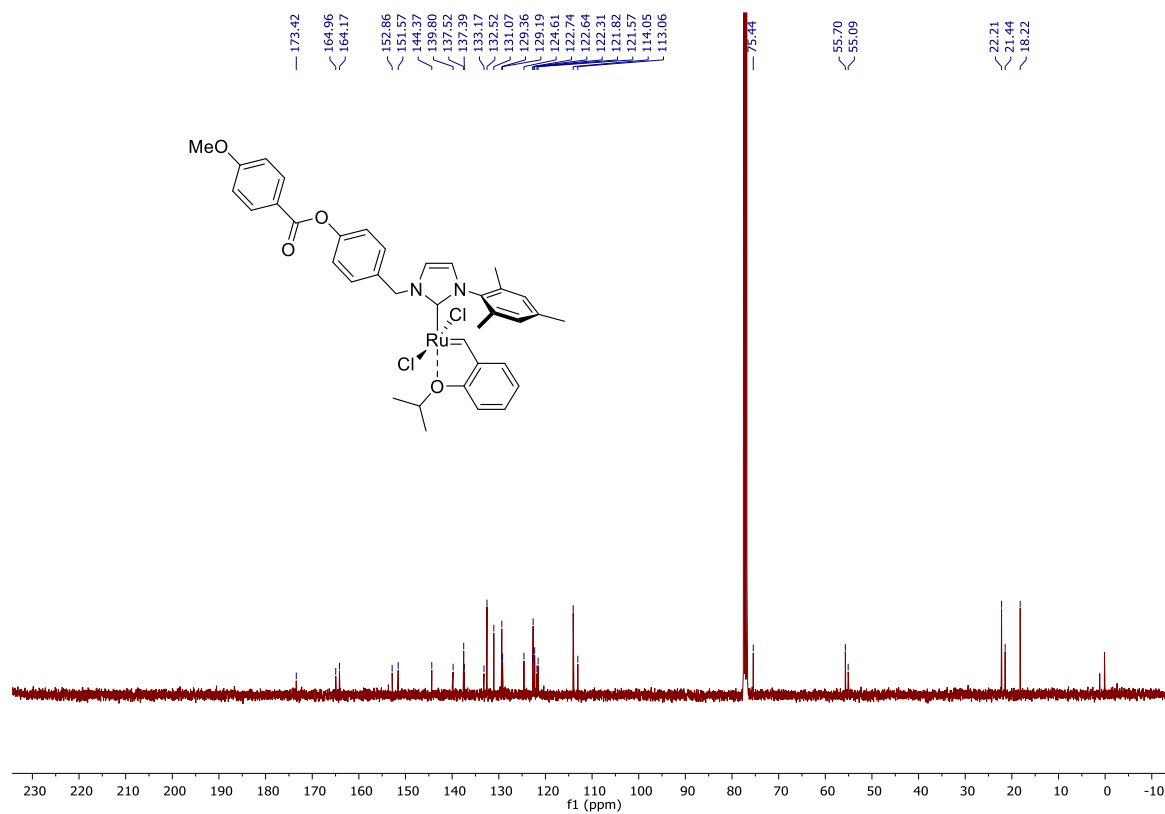
Figure S114. ^{13}C{^{1}H} NMR spectrum of **Ru41** in CDCl$_3$ recorded at room temperature (101 MHz).
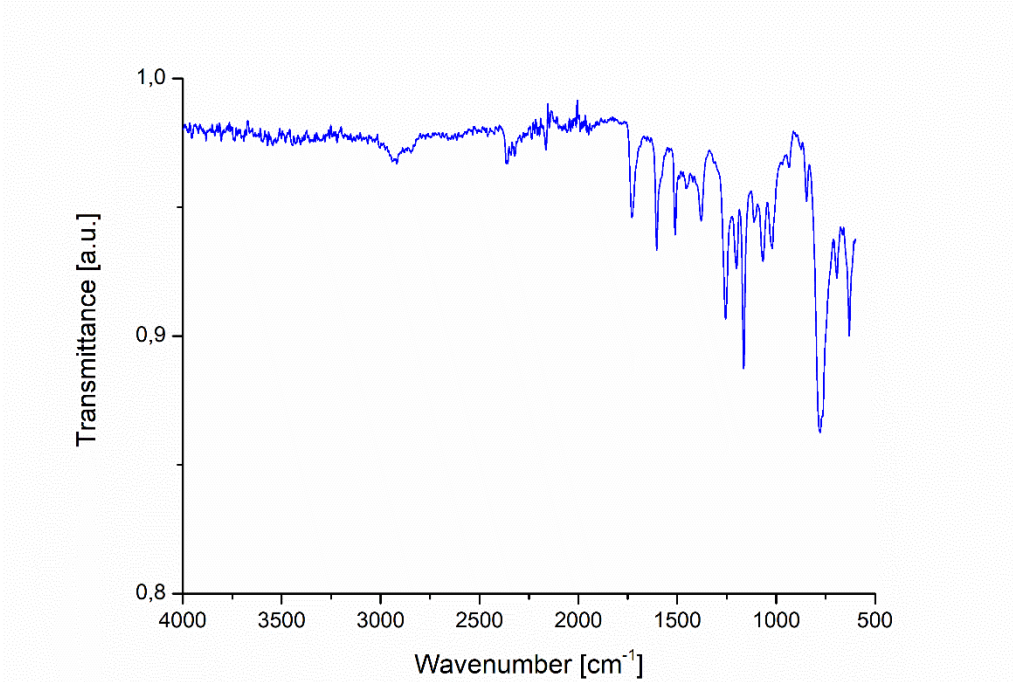
Figure S115. FT-IR spectrum of **Ru41**.

Meas. m/z	#	Ion Formula	m/z	err [mDa]	err [ppm]	mSigma
677.196030	1	C37H39N2O4Ru	677.194783	-0.2	-0.3	107.8
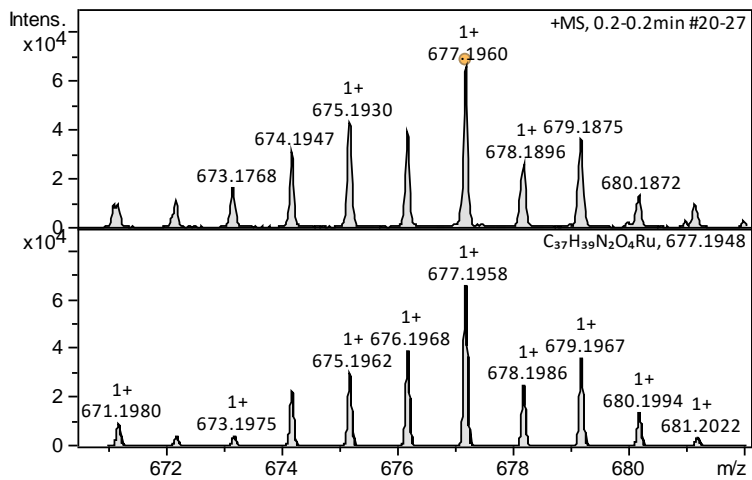
Figure S116. HRMS of **Ru41**.

5. Synthesis of (Al)MIL-101-NH₂
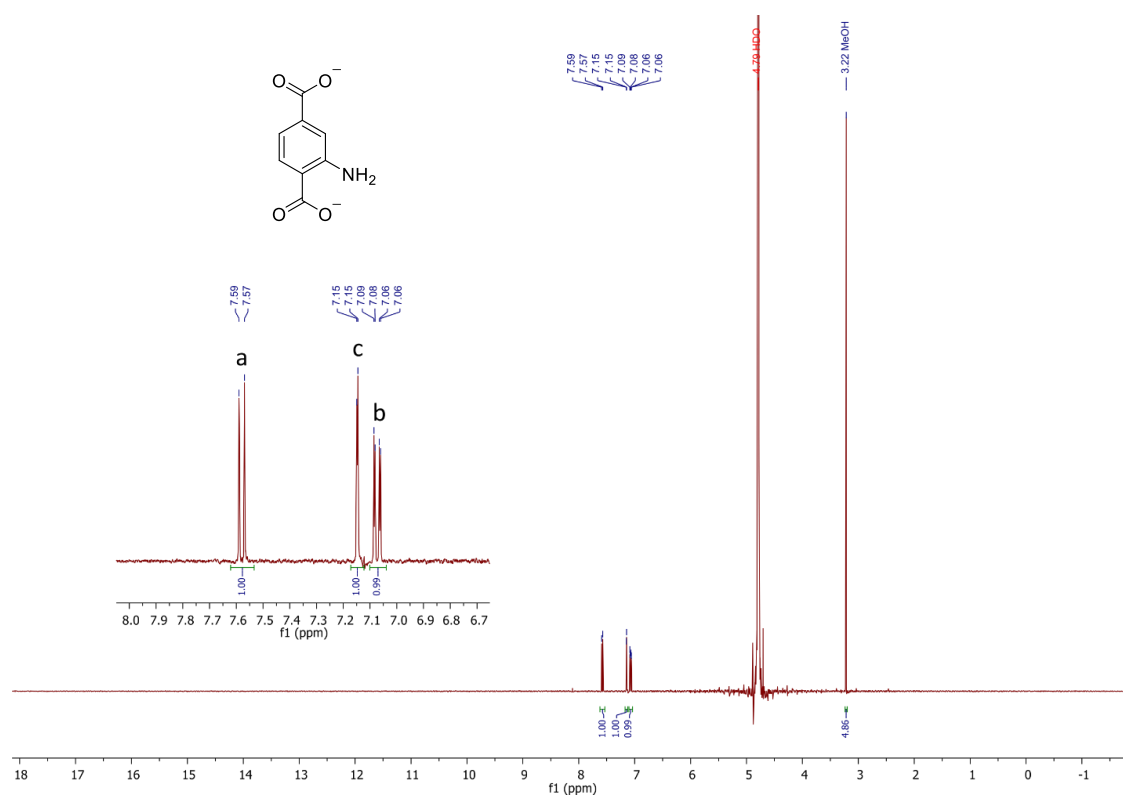
Figure S117. ¹H NMR spectrum of **(Al)MIL-101-NH₂** MOF digested in 4% w/w NaOD/D₂O recorded at room temperature (400 MHz).

6. Synthesis of dimeric structures for the immobilization attempts of Ru-NHC complexes on dendrimers

6.1. (2-benzylidene-1-methylhydrazineyl)phosphonothioic dichloride 155
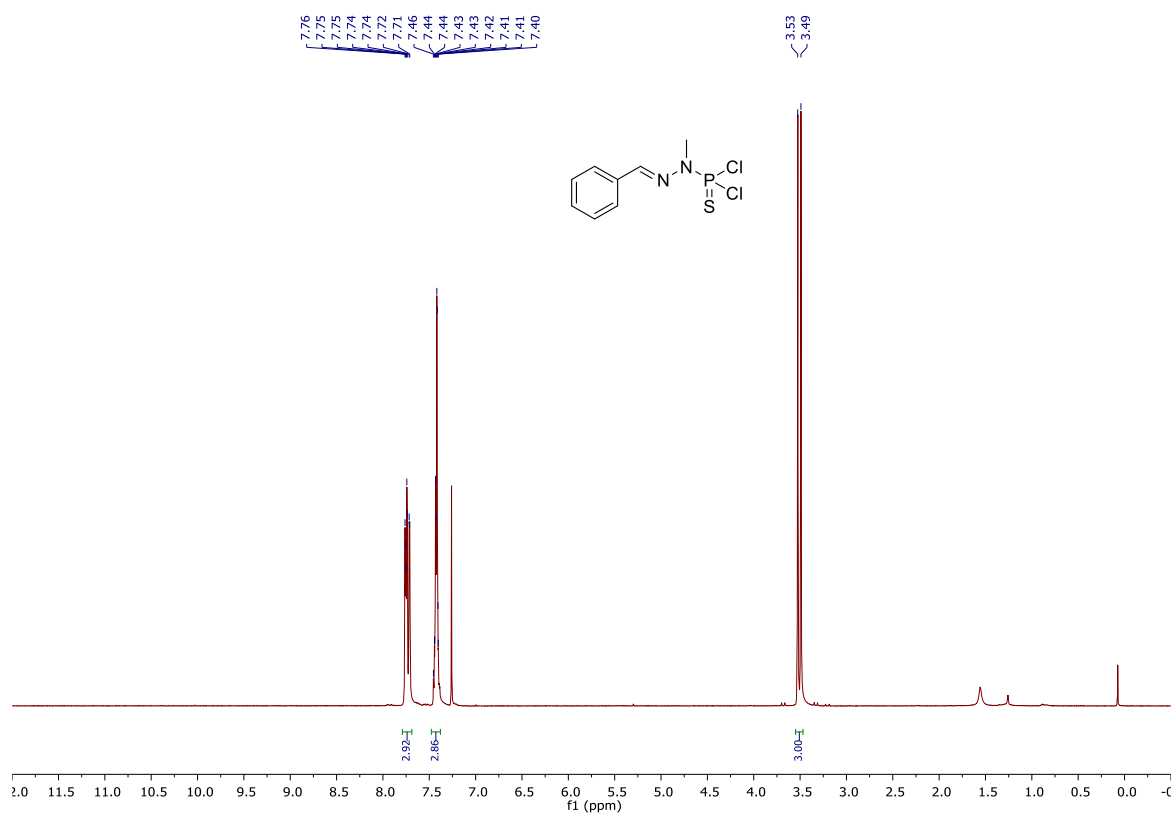
Figure S118. ^{1}H NMR spectrum of (2-benzylidene-1-methylhydrazineyl)phosphonothioic dichloride **155** in CDCl$_3$ recorded at room temperature (400 MHz).
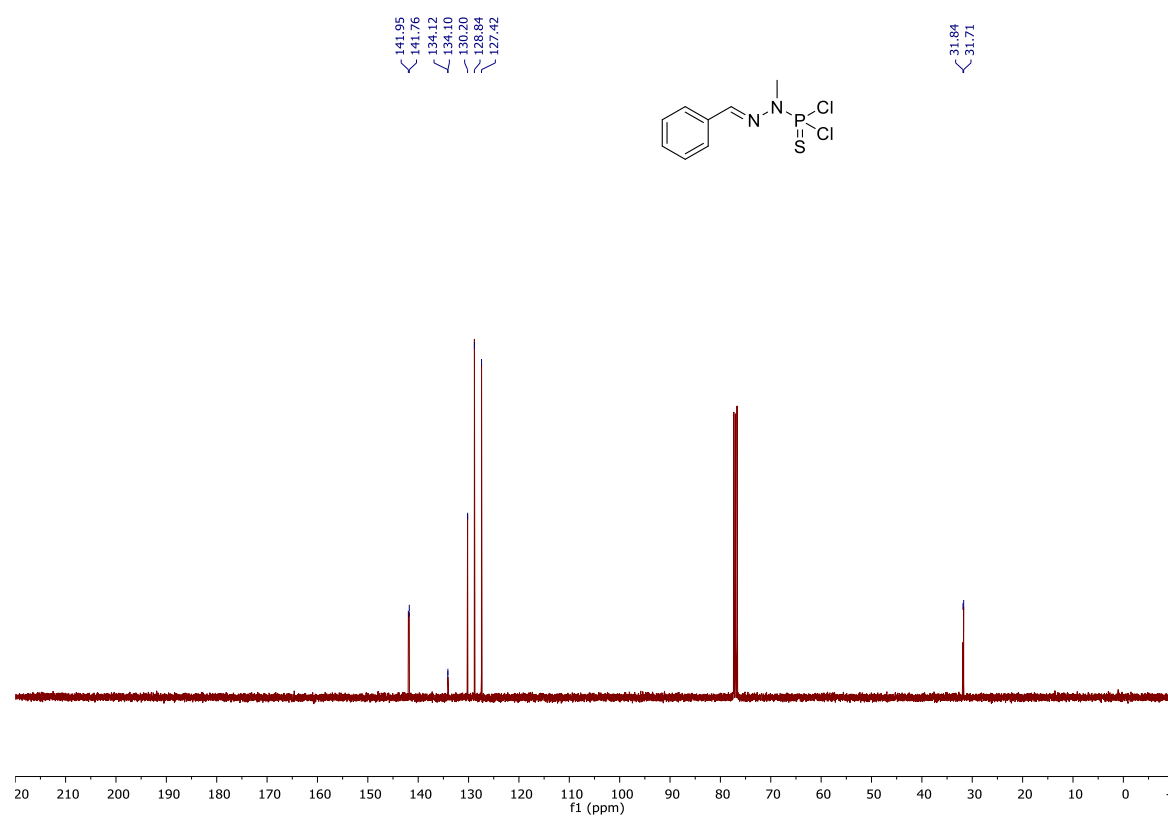
Figure S119. ^{13}C{^{1}H} NMR spectrum of (2-benzylidene-1-methylhydrazineyl)phosphonothioic dichloride **155** in CDCl$_3$ recorded at room temperature (101 MHz).
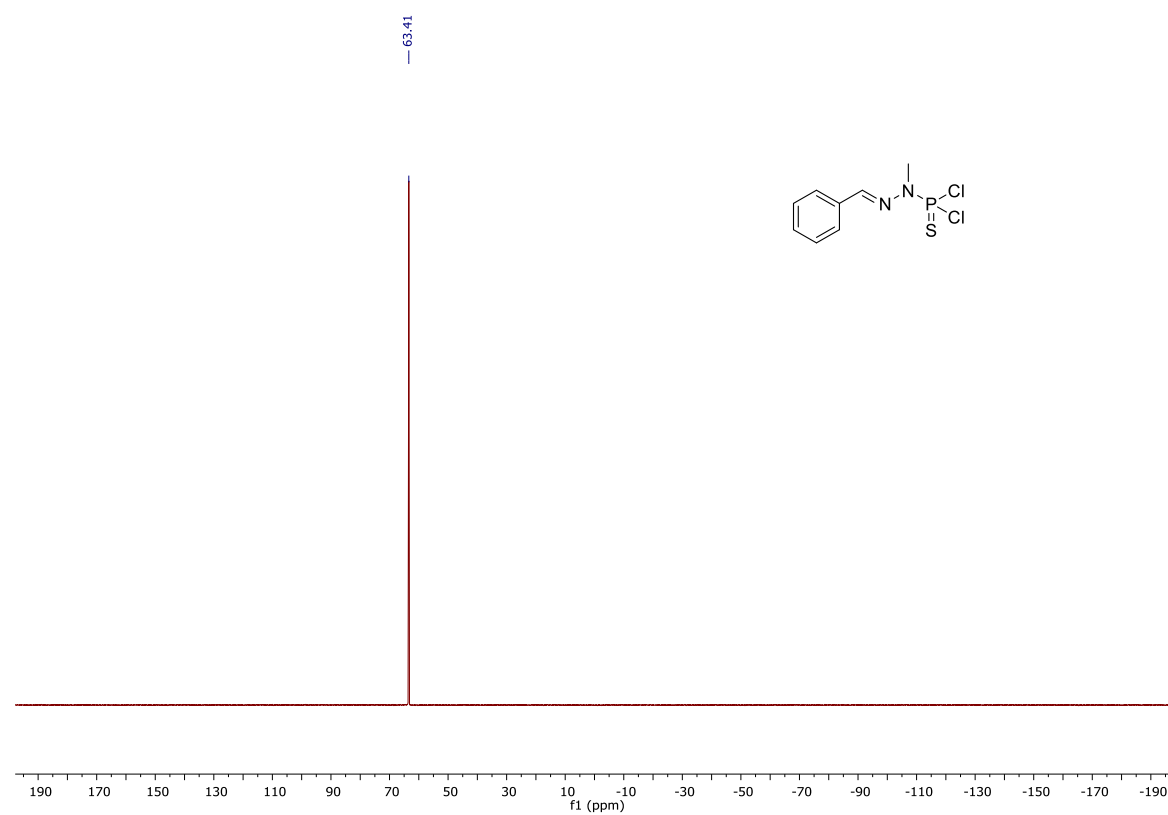
Figure S120. ^{31}P{^{1}H} NMR spectrum of (2-benzylidene-1-methylhydrazineyl)phosphonothioic dichloride **155** in CDCl$_3$ recorded at room temperature (162 MHz).
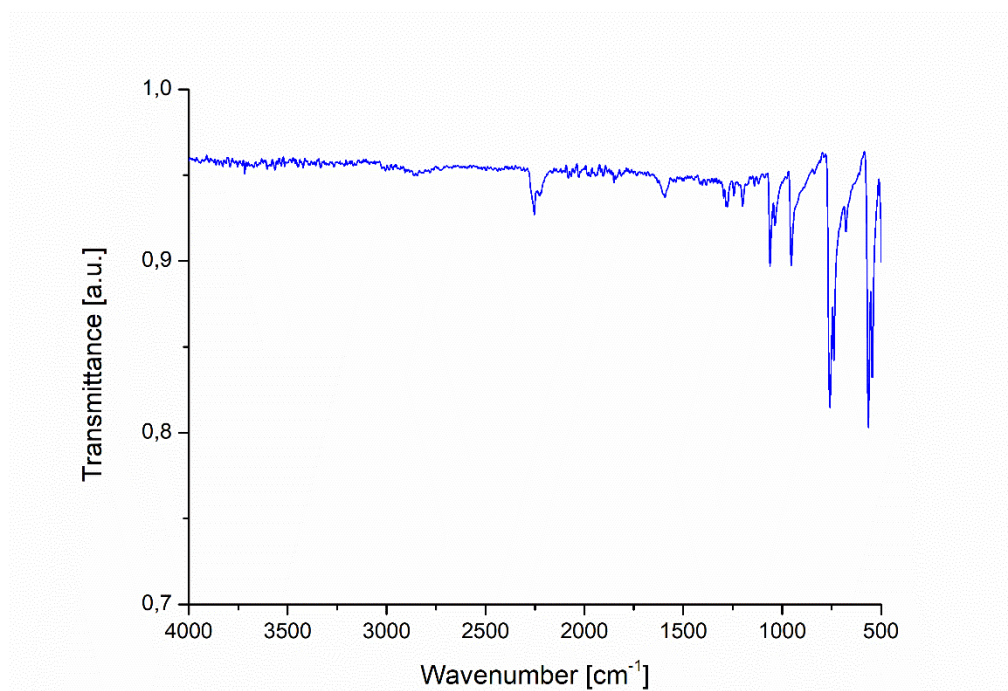
Figure S121. FT-IR spectrum of (2-benzylidene-1-methylhydrazineyl)phosphonothioic dichloride **155**.

6.2. Di-*tert*-butyl 4,4'-(((2-benzylidene-1-methylhydrazineyl)phosphorthioyl)-bis(oxy))dibenzoate 161
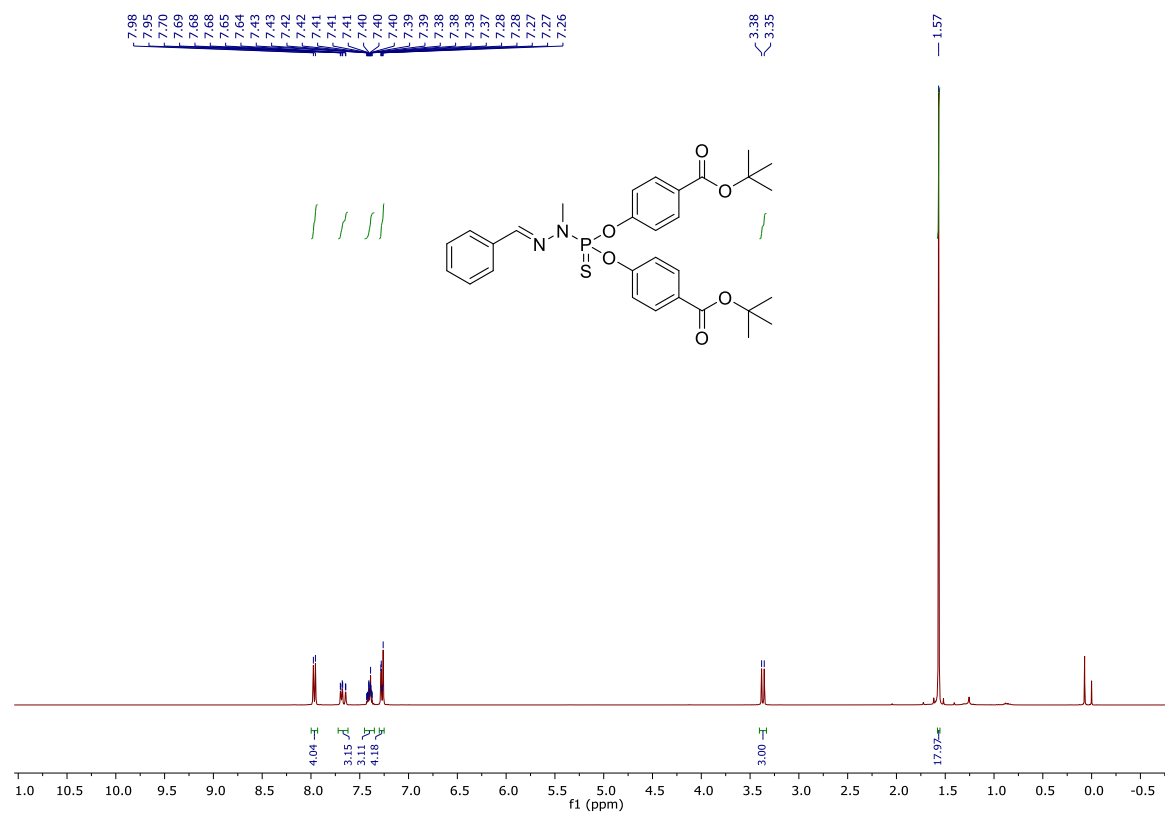
Figure S122. ^{1}H NMR spectrum of di-tert-butyl 4,4'-(((2-benzylidene-1-methylhydrazineyl)phosphorthioyl)-bis(oxy))dibenzoate **161** in CDCl₃ recorded at room temperature (400 MHz).
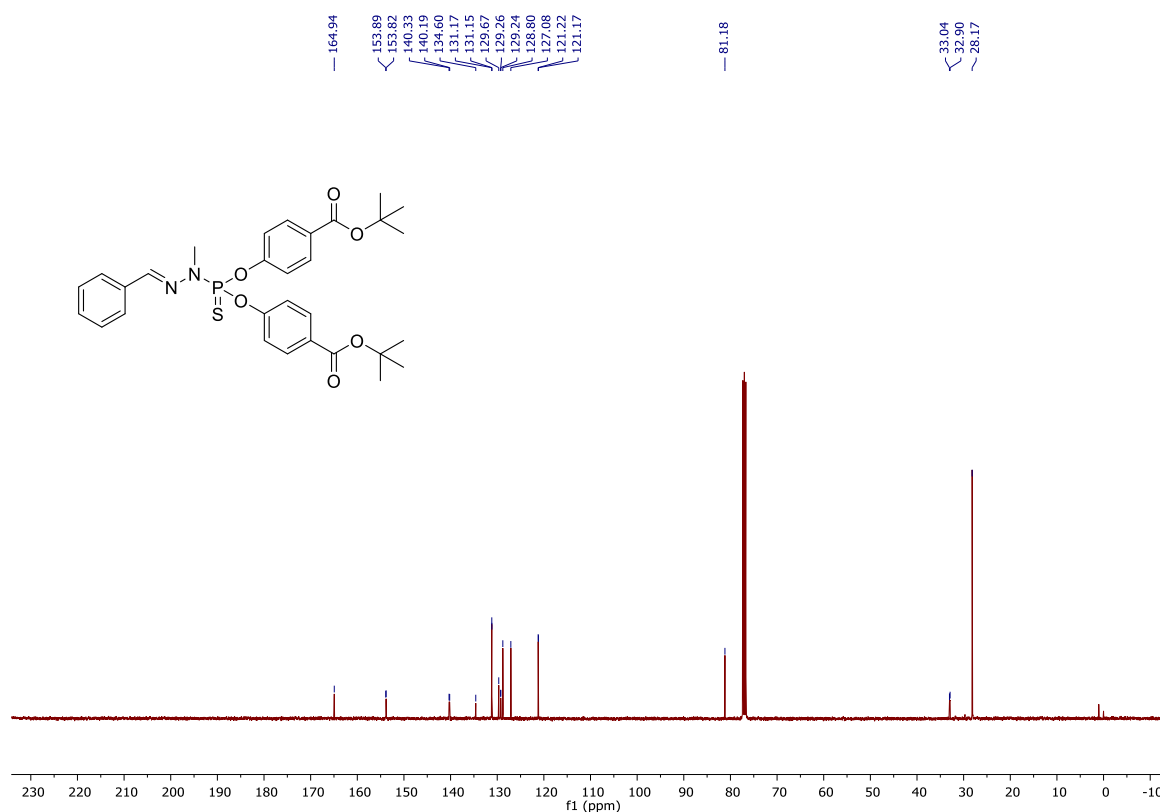
Figure S123. $^{13}C\{^1H\}$ NMR spectrum of di-tert-butyl 4,4'-(((2-benzylidene-1-methylhydrazineyl)phos-phorthi-oyl)-bis(oxy))dibenzoate **161** in CDCl$_3$ recorded at room temperature (101 MHz).
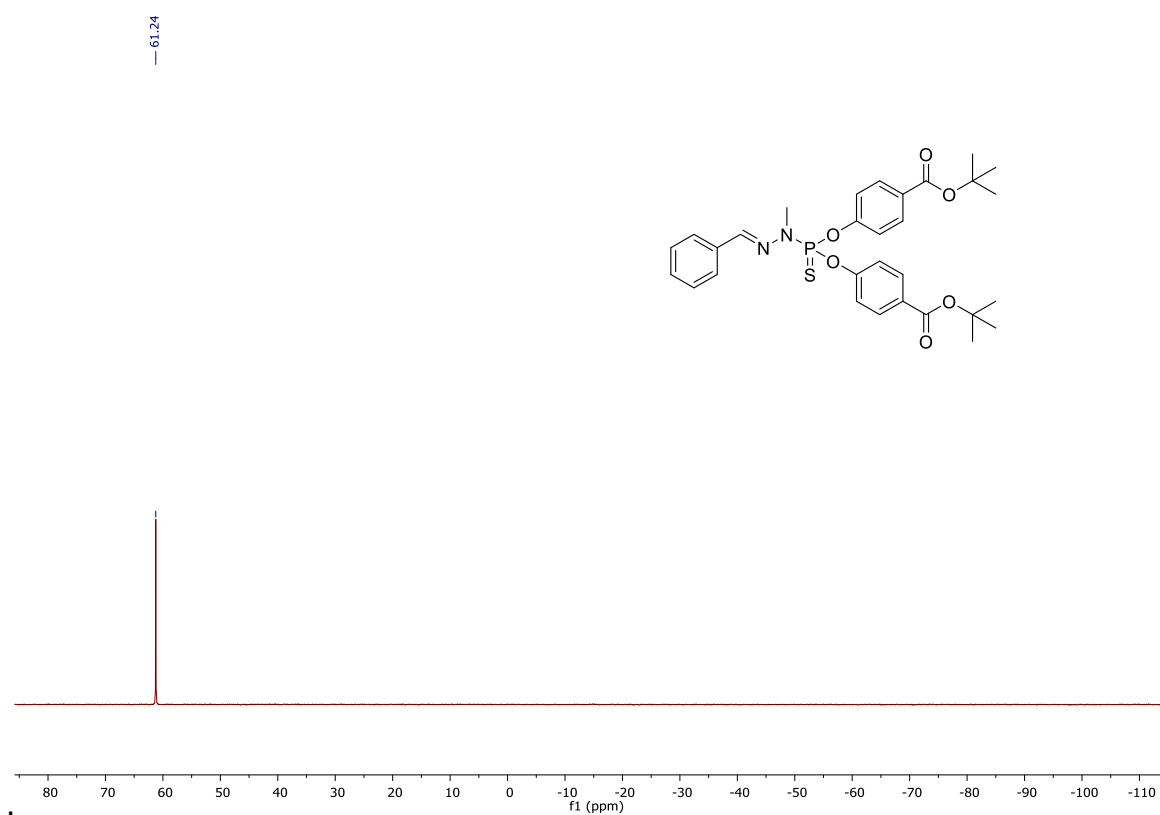
Figure S124. $^{31}P\{^1H\}$ NMR spectrum of di-tert-butyl 4,4'-(((2-benzylidene-1-methylhydrazineyl)phos-phorthioyl)-bis(oxy))dibenzoate **161** in CDCl$_3$ recorded at room temperature (162 MHz).
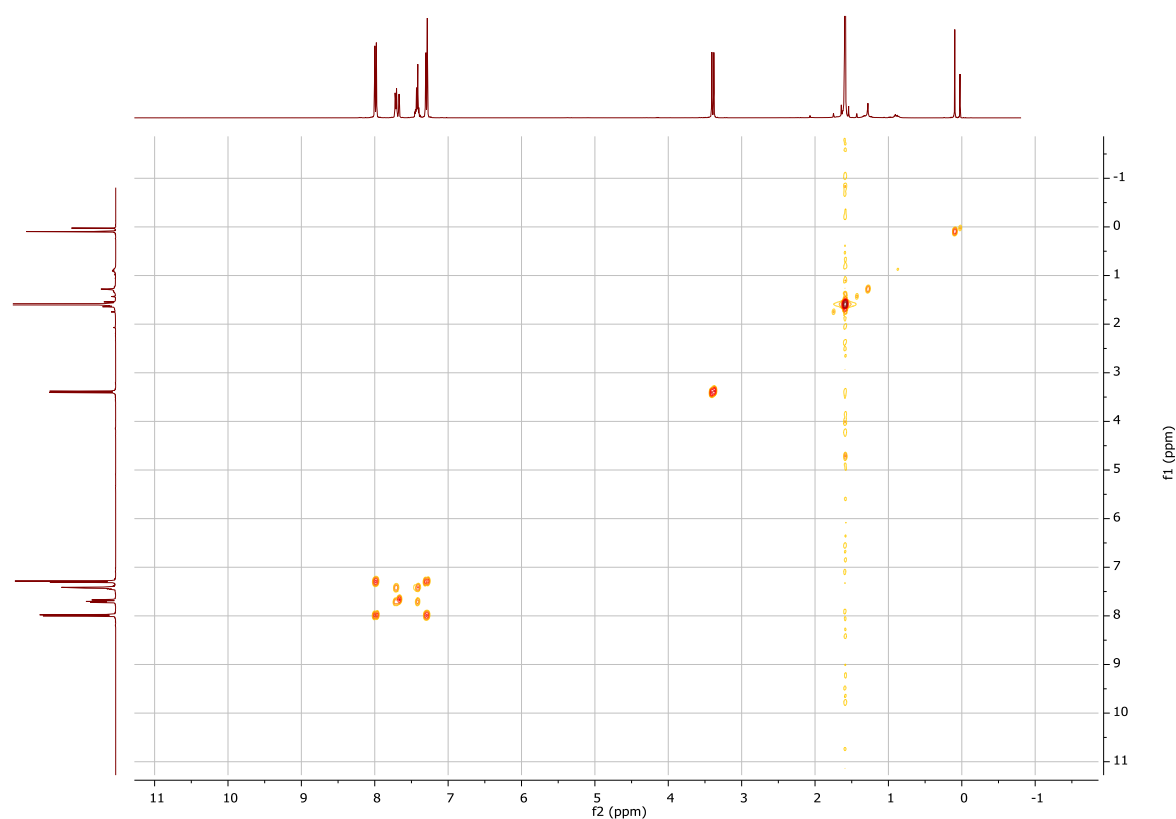
Figure S125. ^{1}H-^{1}H COSY spectrum of di-tert-butyl 4,4'-(((2-benzylidene-1-methylhydrazineyl)phosphorthioyl)-bis(oxy))dibenzoate **161** in CDCl$_3$ recorded at room temperature (400 MHz).
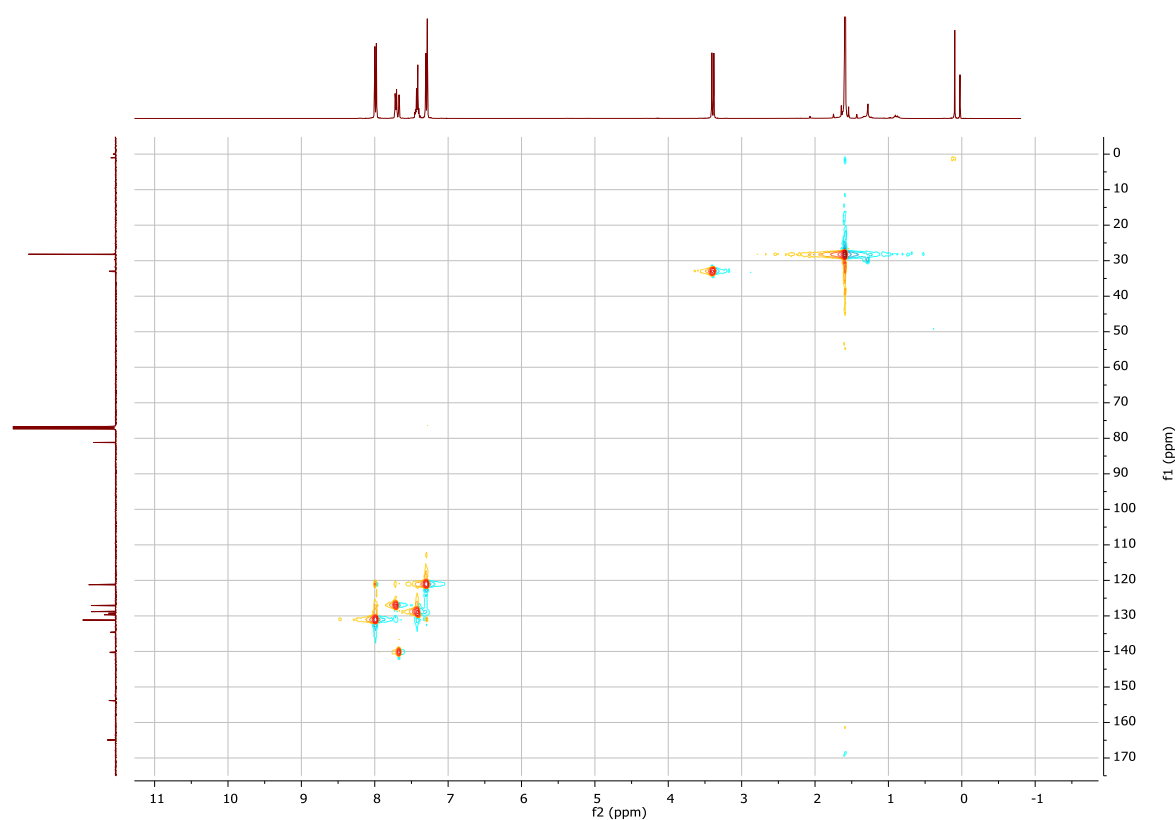
Figure S126. ^{1}H-^{13}C{^{1}H} HSQC spectrum of di-tert-butyl 4,4'-(((2-benzylidene-1-methylhydrazineyl)phosphorthioyl)-bis(oxy))dibenzoate **161** in CDCl$_3$ recorded at room temperature (400 MHz, 101 MHz).
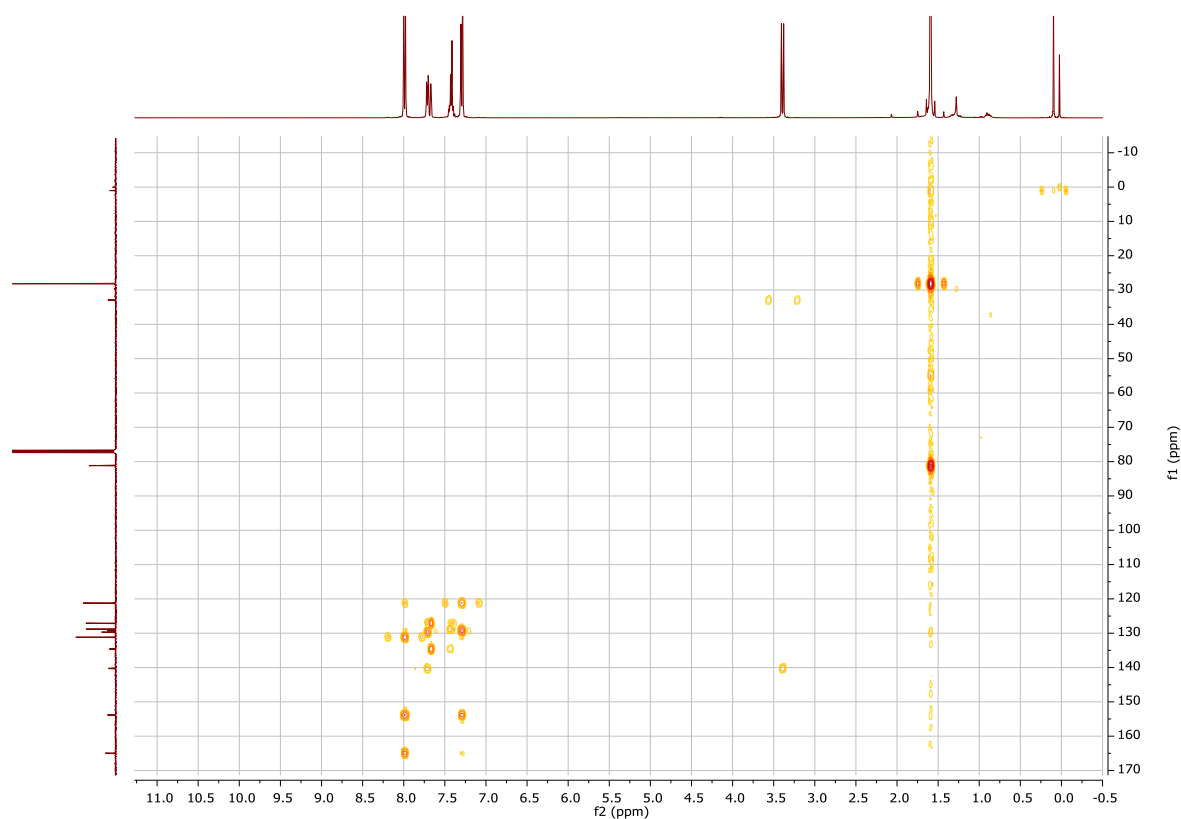
Figure S127. ^{1}H-$^{13}C\{^{1}H\}$ HMBC spectrum of di-tert-butyl 4,4'-(((2-benzylidene-1-methylhydra-zineyl)phosphorthioyl)-bis(oxy))dibenzoate **161** in CDCl$_3$ recorded at room temperature (400 MHz, 101 MHz).
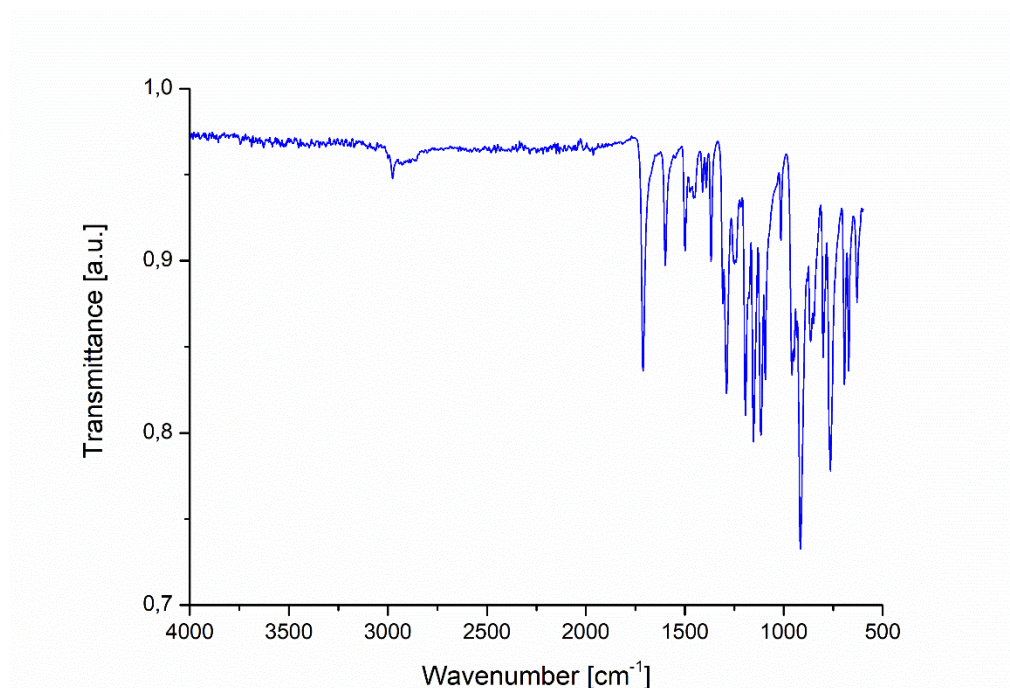
Figure S128. FT-IR spectrum of di-tert-butyl 4,4'-(((2-benzylidene-1-methylhydrazineyl)phosphorthi-oyl)-bis(oxy))dibenzoate **161**.

Meas. m/z	#	Ion Formula	m/z	err [mDa]	err [ppm]	mSigma
605.182661	1	C30H35N2NaO6PS	605.184565	1.9	3.1	9.4
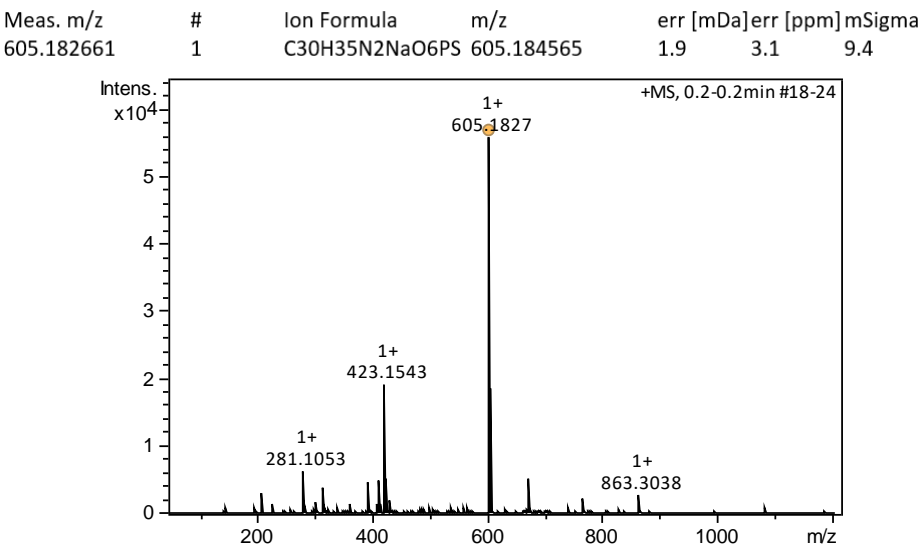
Figure S129. HRMS of di-tert-butyl 4,4'-(((2-benzylidene-1-methylhydrazineyl)phosphorthioyl)bis-(oxy))dibenzoate **161**.

Codi SAQ	Ref. mostra	%C	%H	%N	%S
23AE038/013	JCS-171	61,98	6,17	4,54	5,23

Figure S130. Elemental analysis of di-tert-butyl 4,4'-(((2-benzylidene-1-methylhydrazineyl)phos-phorthioyl)bis-(oxy))dibenzoate **161**.

6.3.   4,4'-(((2-benzylidene-1-methylhydrazineyl)phosphorothioyl)-bis(oxy))dibenzoic acid 162
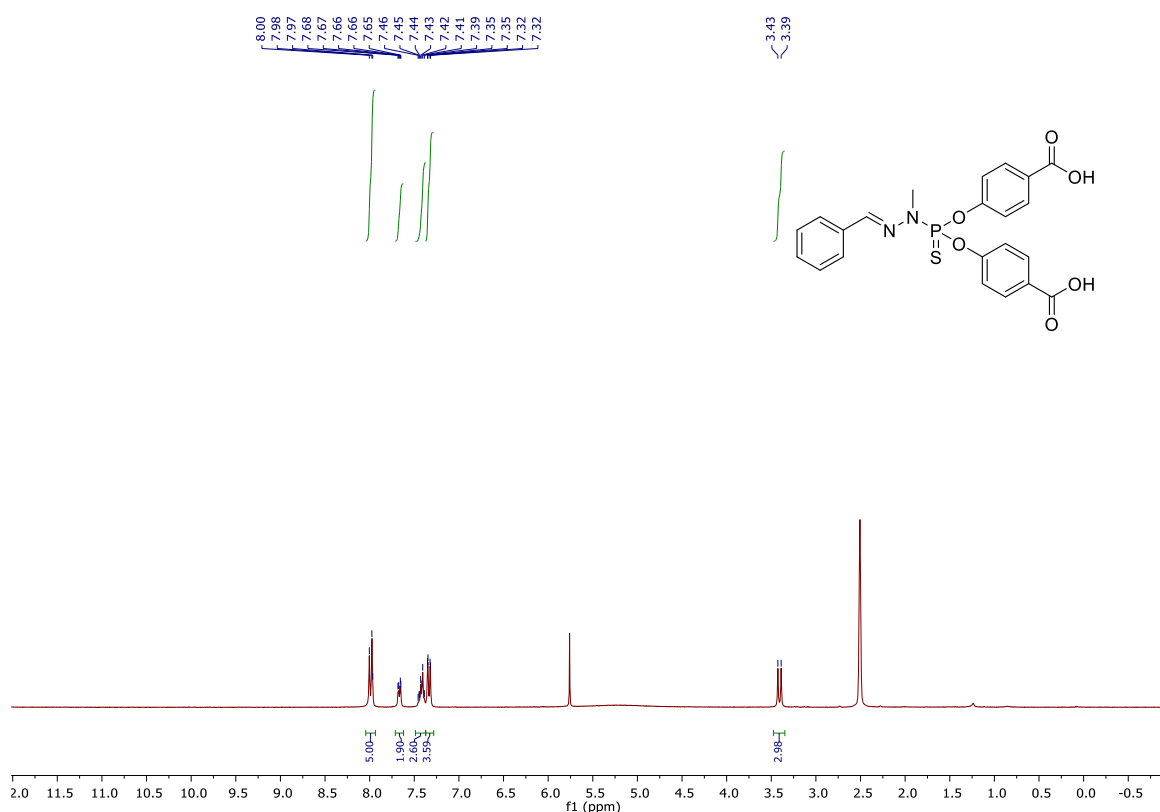
Figure S131. ¹H NMR spectrum of 4,4'-(((2-benzylidene-1-methylhydrazineyl)phosphorothioyl)bis-(oxy))-dibenzoic acid **162** in DMSO-d_6 recorded at room temperature (300 MHz).
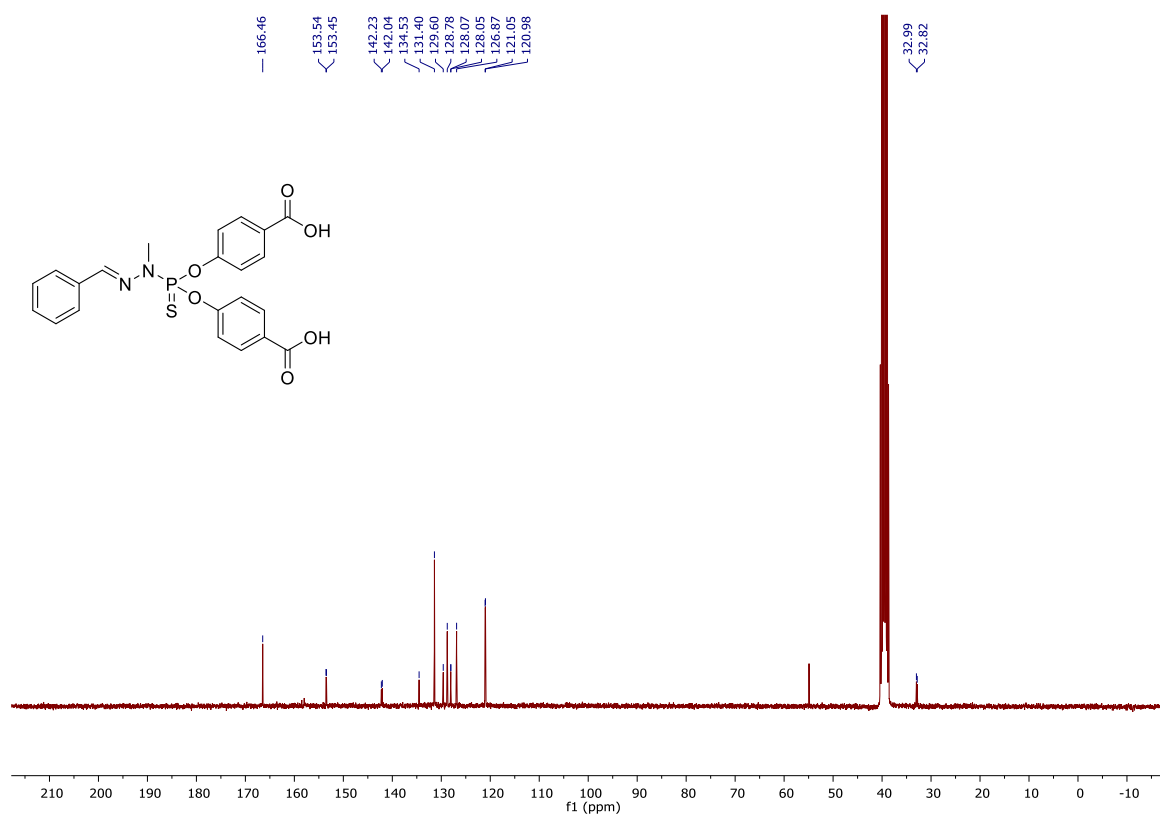
Figure S132. ¹³C{¹H} NMR spectrum of 4,4'-(((2-benzylidene-1-methylhydrazineyl)phosphorothioyl)-bis-(oxy))dibenzoic acid **162** in DMSO-d_6 recorded at room temperature (75 MHz).
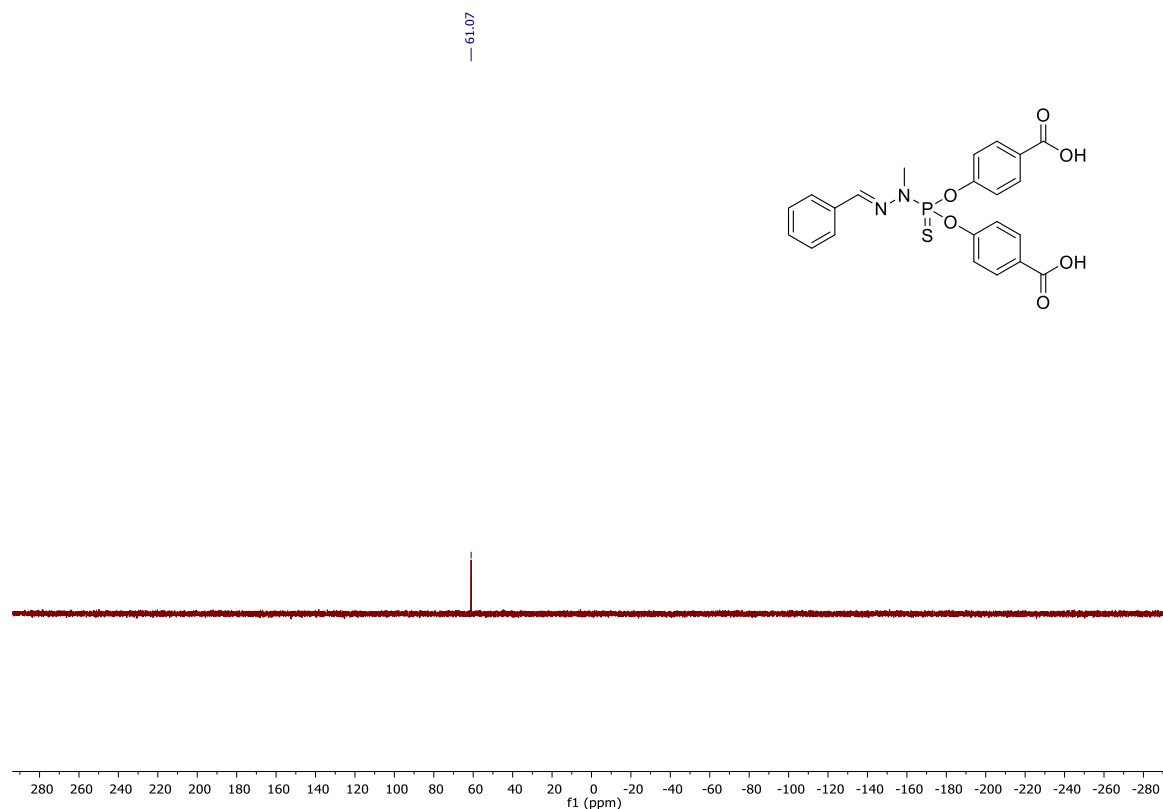
Figure S133. $^{31}P\{^{1}H\}$ NMR spectrum of 4,4'-(((2-benzylidene-1-methylhydrazineyl)phosphorothioyl)-bis-(oxy))-dibenzoic acid **162** in DMSO-d_6 recorded at room temperature (121 MHz).
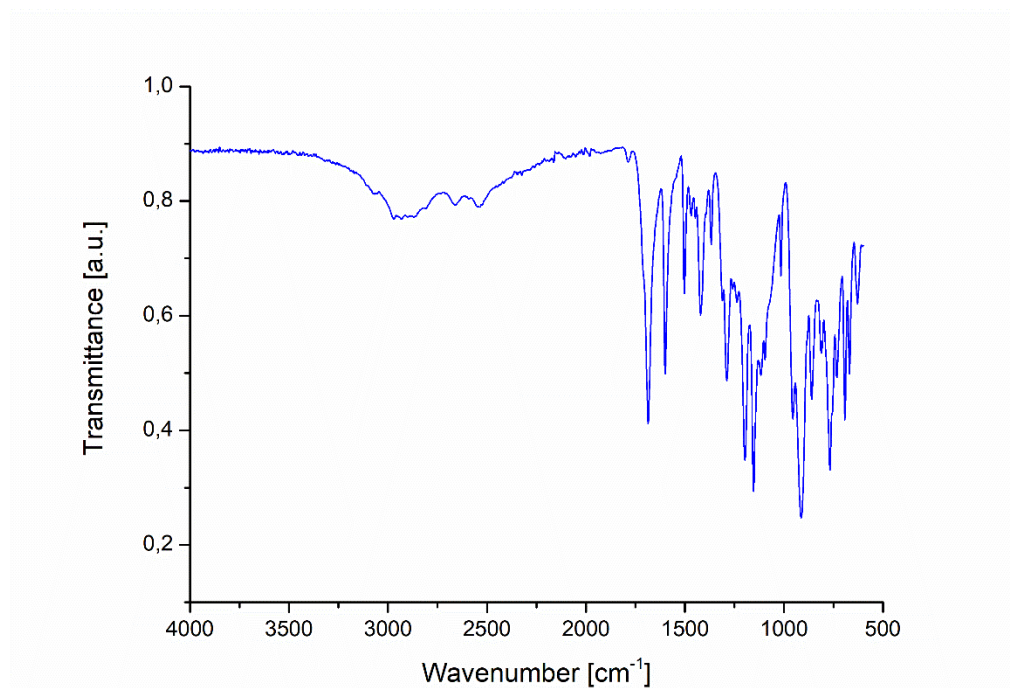
Figure S134. FT-IR spectrum of 4,4'-(((2-benzylidene-1-methylhydrazineyl)phosphorothioyl)-bis(oxy))-dibenzoic acid **162**.

Meas. m/z	#	Ion Formula	m/z	err [mDa]	err [ppm]	mSigma
493.057569	1	C22H19N2NaO6PS	493.059365	1.8	3.6	10.2
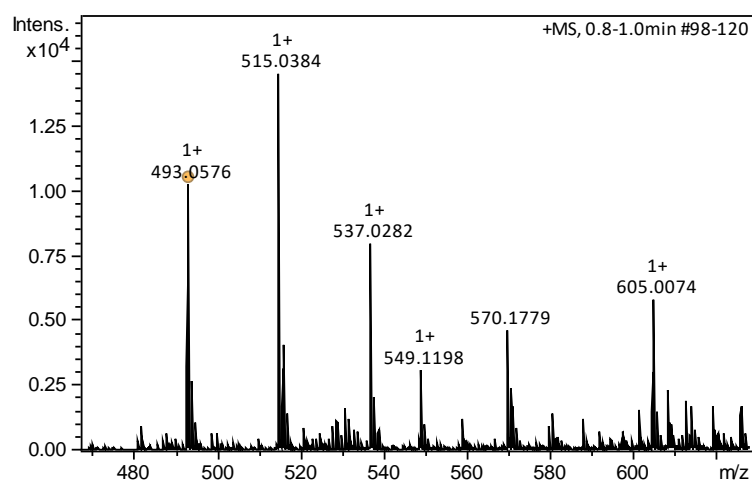
Figure S135. HRMS of 4,4'-(((2-benzylidene-1-methylhydrazineyl)phosphorothioyl)-bis(oxy))-dibenzoic acid **162**.

7. Synthesis of [Ru(*p*-cymene)Cl₂]₂-based complexes
7.1. (4-bromophenoxy)(*tert*-butyl)dimethylsilane 168
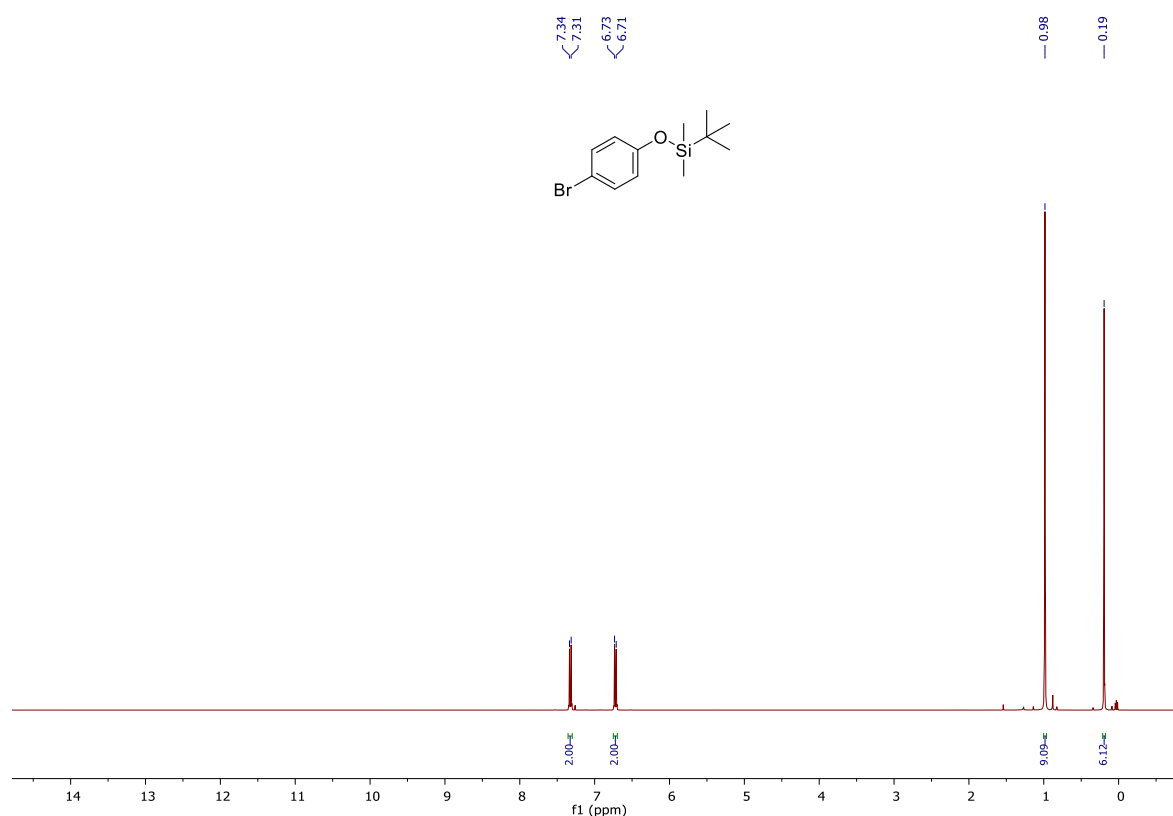
Figure S136. ^{1}H NMR spectrum of (4-bromophenoxy)(tert-butyl)dimethylsilane **168** in CDCl₃ recorded at room temperature (400 MHz).
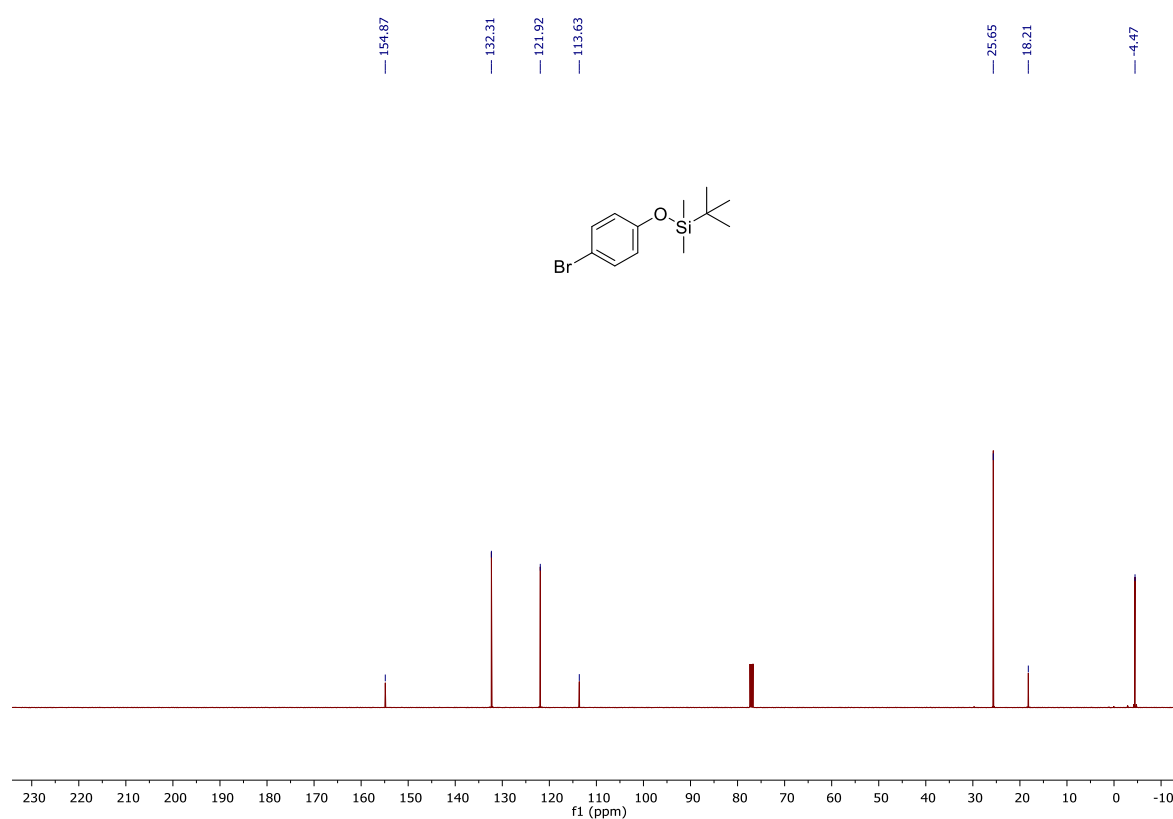
Figure S137. ^{13}C{^{1}H} NMR spectrum of (4-bromophenoxy)(tert-butyl)dimethylsilane **168** in CDCl₃ recorded at room temperature (101 MHz).

7.2.   (4-((*tert*-butyldimethylsilyl)oxy)phenyl)diphenylphosphane 169
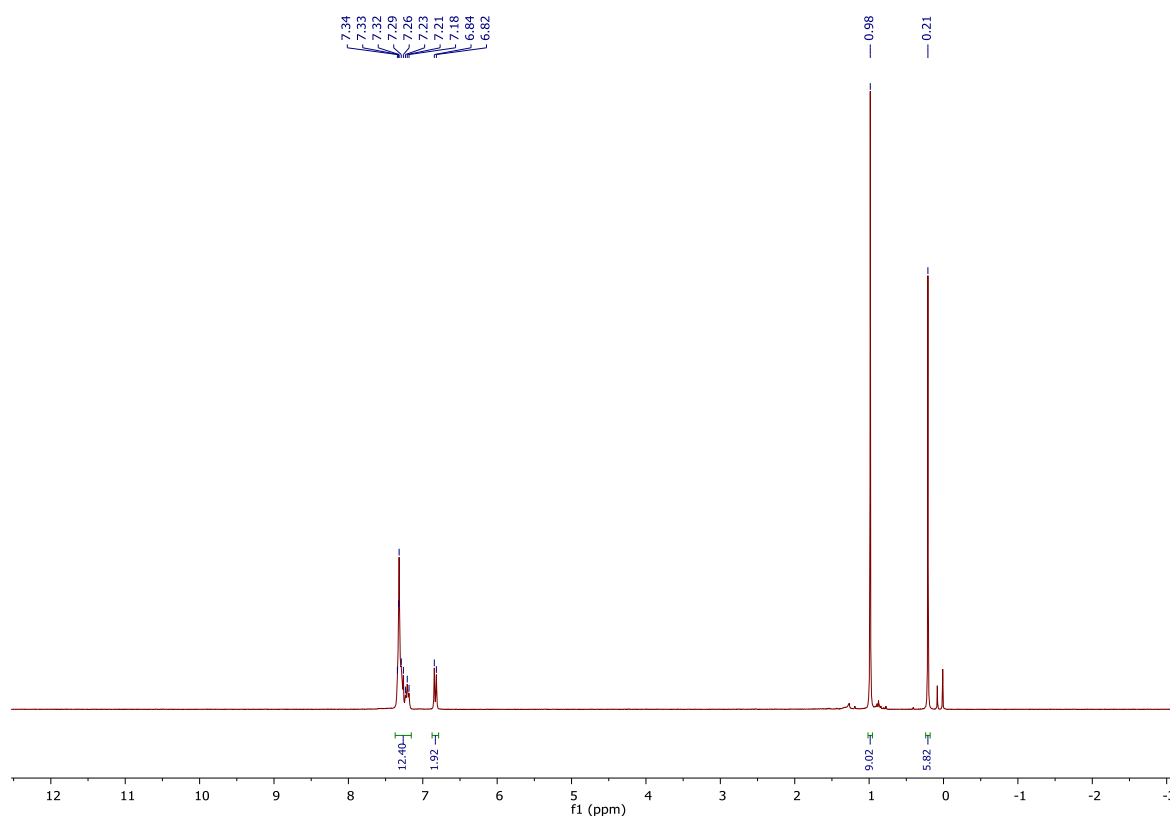
Figure S138. ¹H NMR spectrum of (4-((tert-butyldimethylsilyl)oxy)phenyl)diphenylphosphane **169** (400 MHz).
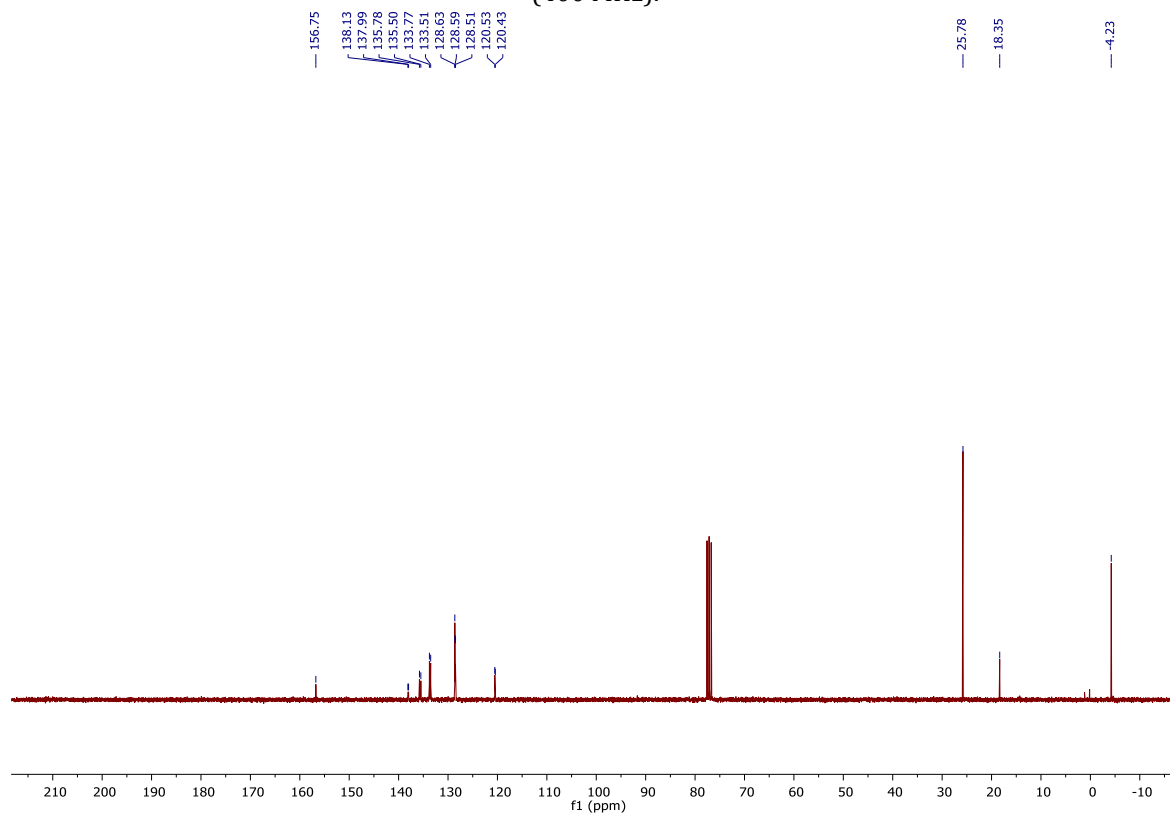
Figure S139. ¹³C{¹H} NMR spectrum of (4-((tert-butyldimethylsilyl)oxy)phenyl)diphenylphosphane **169** (101 MHz).
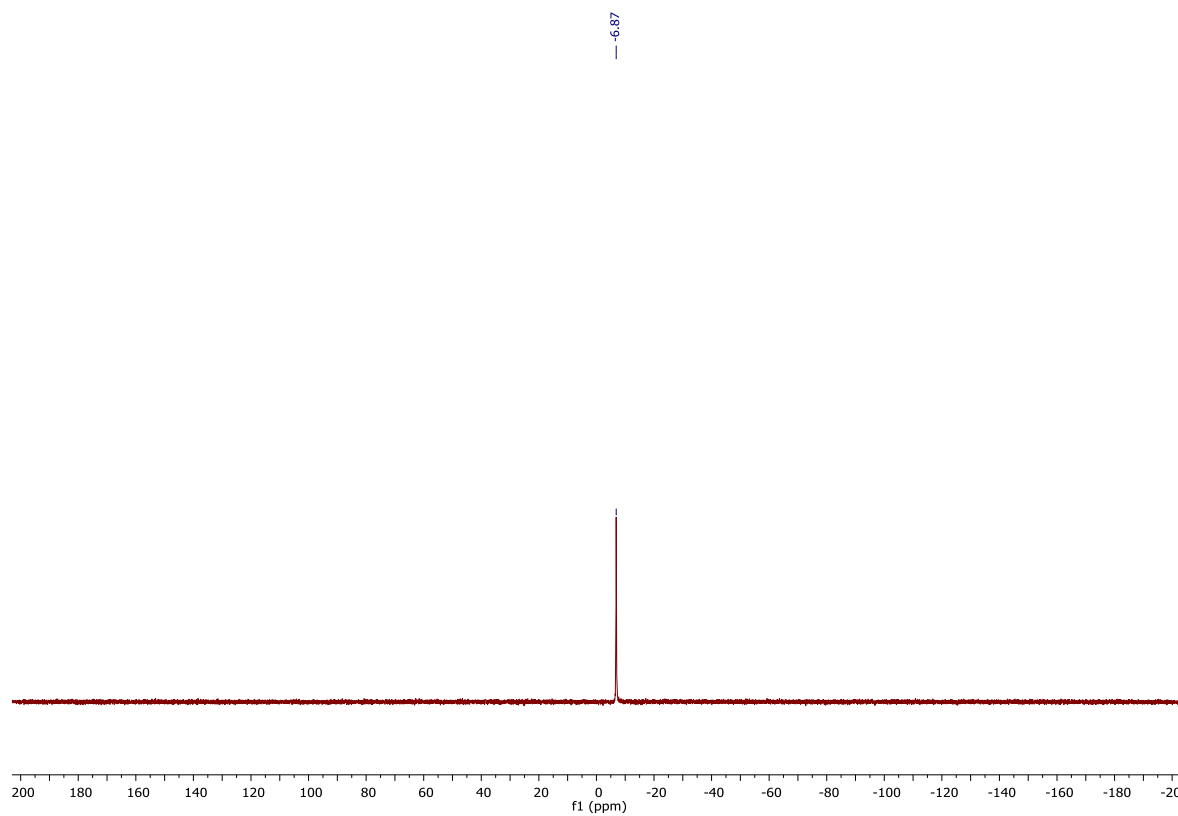
Figure S140. ³¹P{¹H} NMR spectrum of (4-((tert-butyldimethylsilyl)oxy)phenyl)diphenylphosphane **169** (161 MHz).

7.3.   4-(diphenylphosphoryl)phenol 170
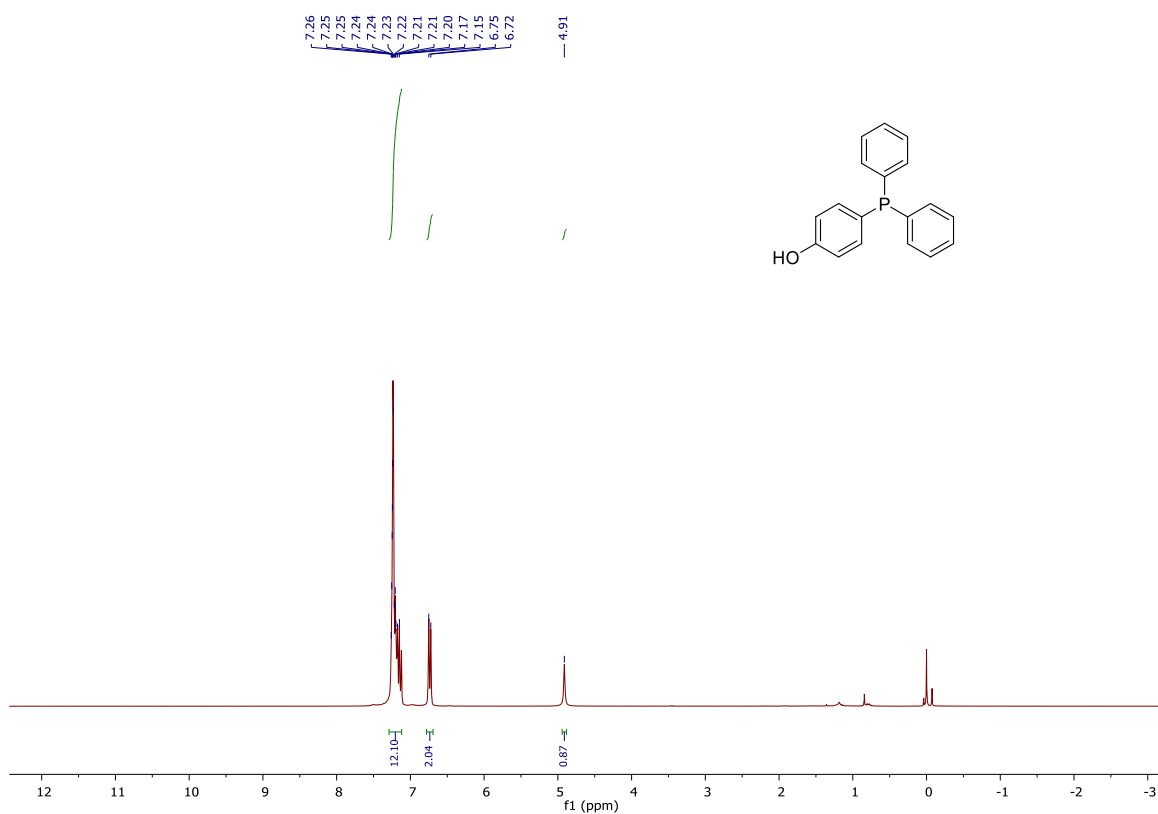
Figure S141. ^{1}H NMR spectrum of 4-(diphenylphosphoryl)phenol **170** in CDCl$_3$ recorded at room temperature (400 MHz).
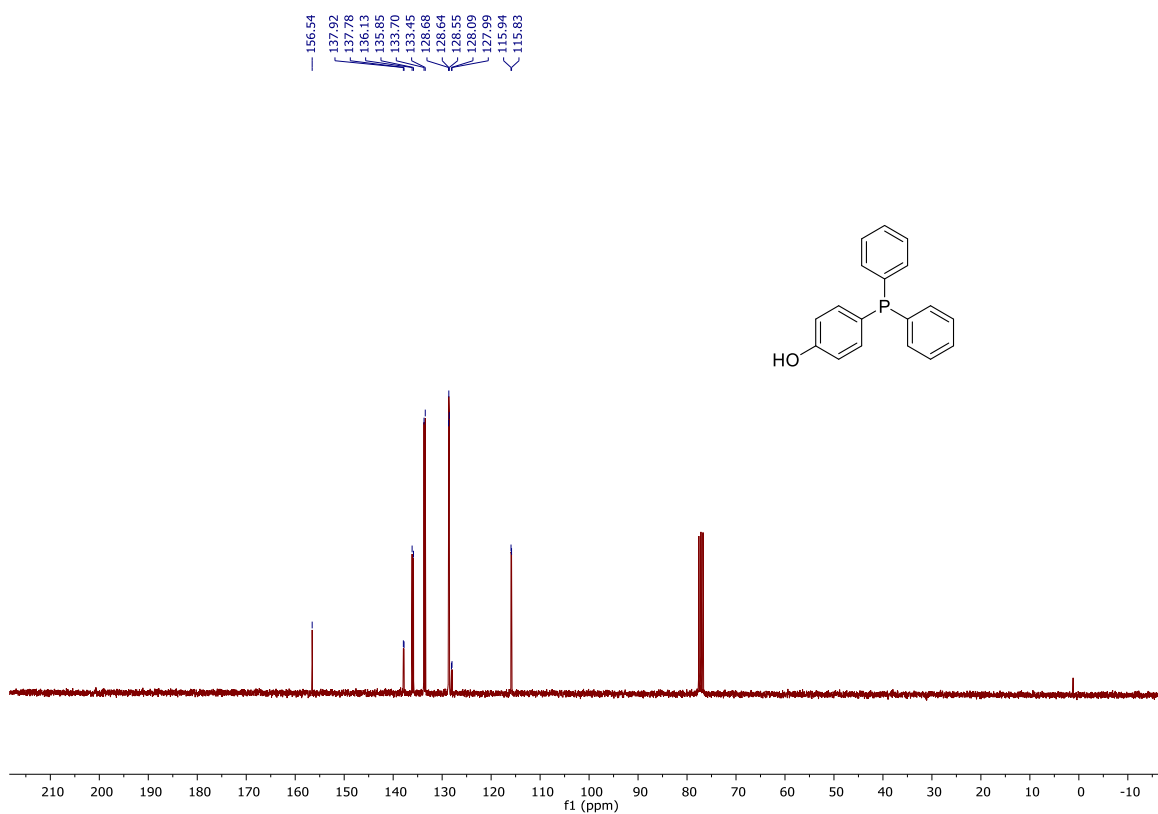
Figure S142. ^{13}C{^{1}H} NMR spectrum of 4-(diphenylphosphoryl)phenol **170** in CDCl$_3$ recorded at room temperature (101 MHz).
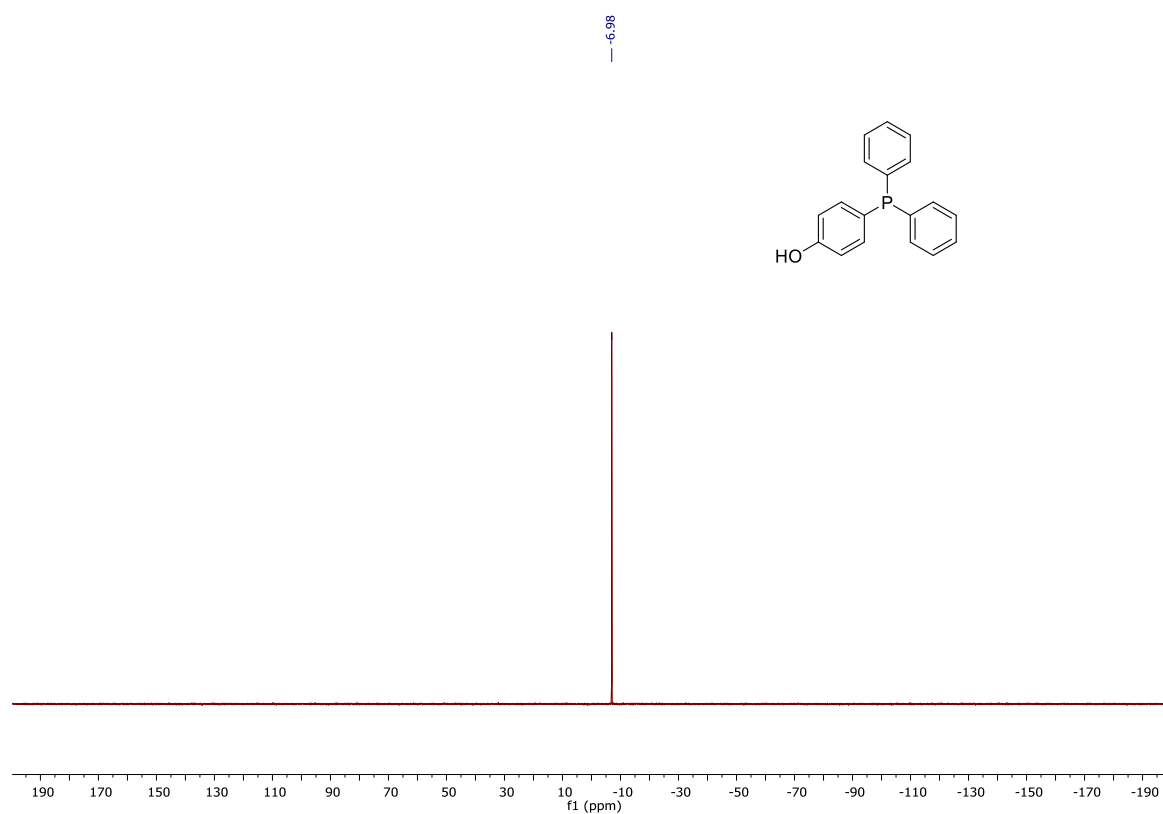
Figure S143. ^{31}P{^{1}H} NMR spectrum of 4-(diphenylphosphoryl)phenol **170** in CDCl$_3$ recorded at room temperature (162 MHz).

7.4.   Dendrimer 171-[G₁][G₁]-PEG
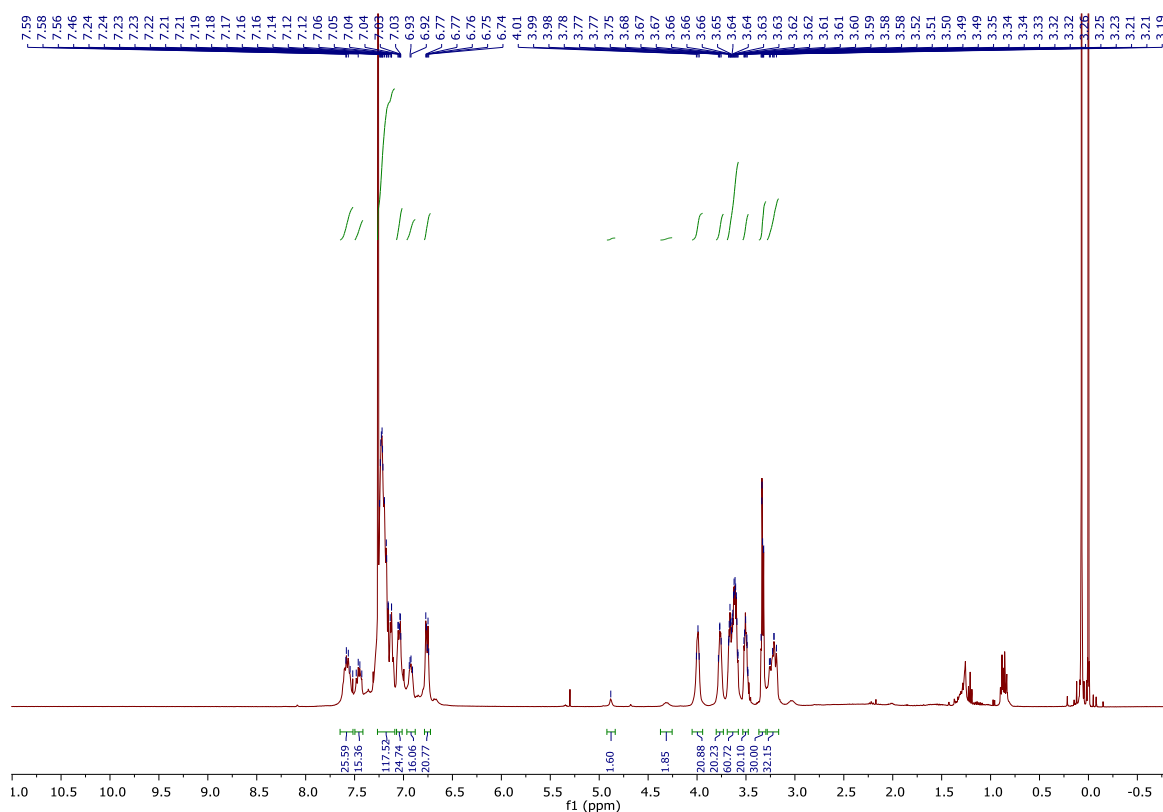
Figure S144. ¹H NMR spectrum of **171-[G₁][G₁]-PEG** in CDCl₃ recorded at room temperature (400 MHz).
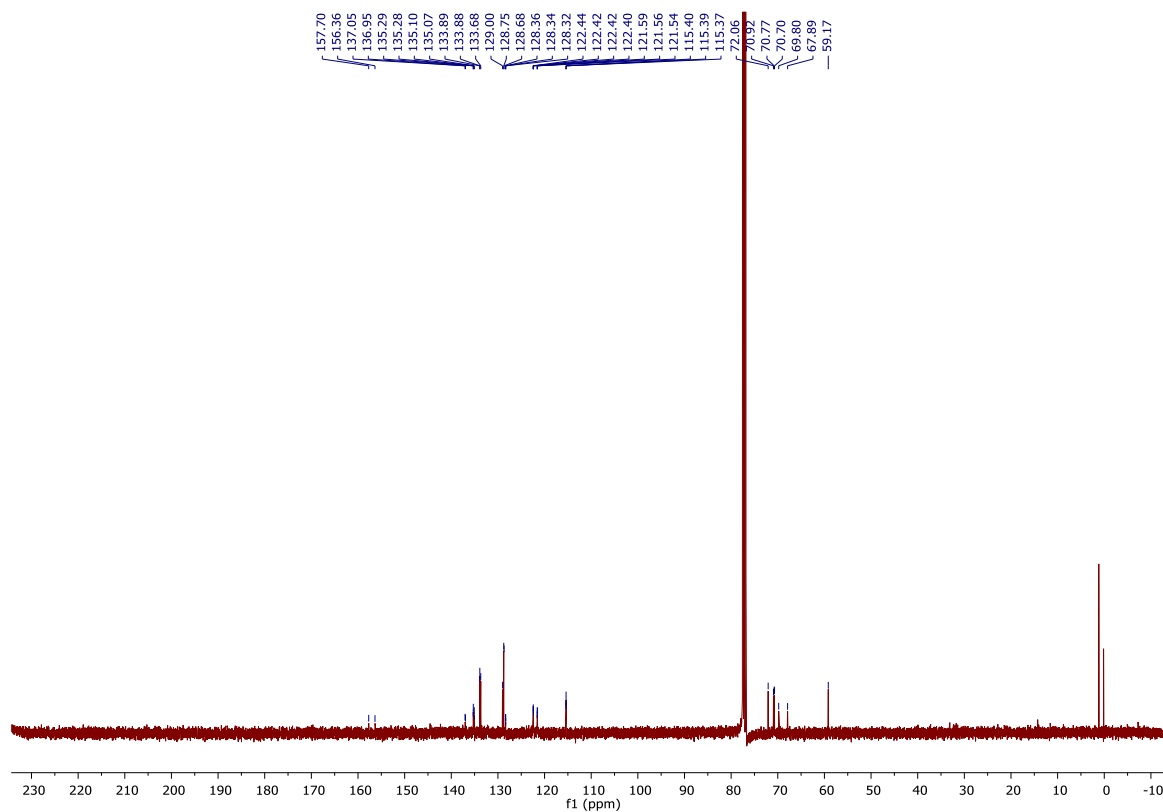
Figure S145. ¹³C{¹H} NMR spectrum of **171-[G₁][G₁]-PEG** in CDCl₃ recorded at room temperature (101 MHz).
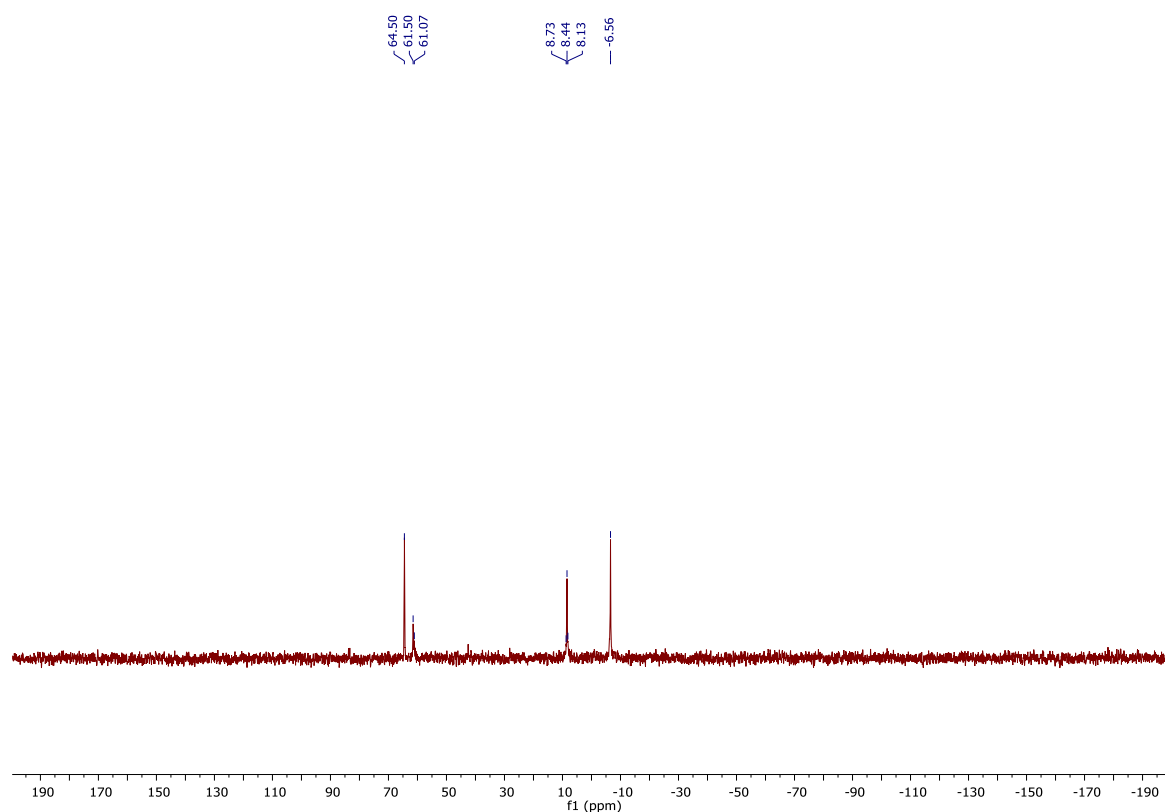
Figure S146. ^{31}P{^{1}H} NMR spectrum of **171-[G₁][G₁]-PEG** in CDCl₃ recorded at room temperature (162 MHz).

Figure S147. ^{1}H-^{1}H COSY spectrum of **171-[G₁][G₁]-PEG** in CDCl₃ recorded at room temperature (400 MHz).
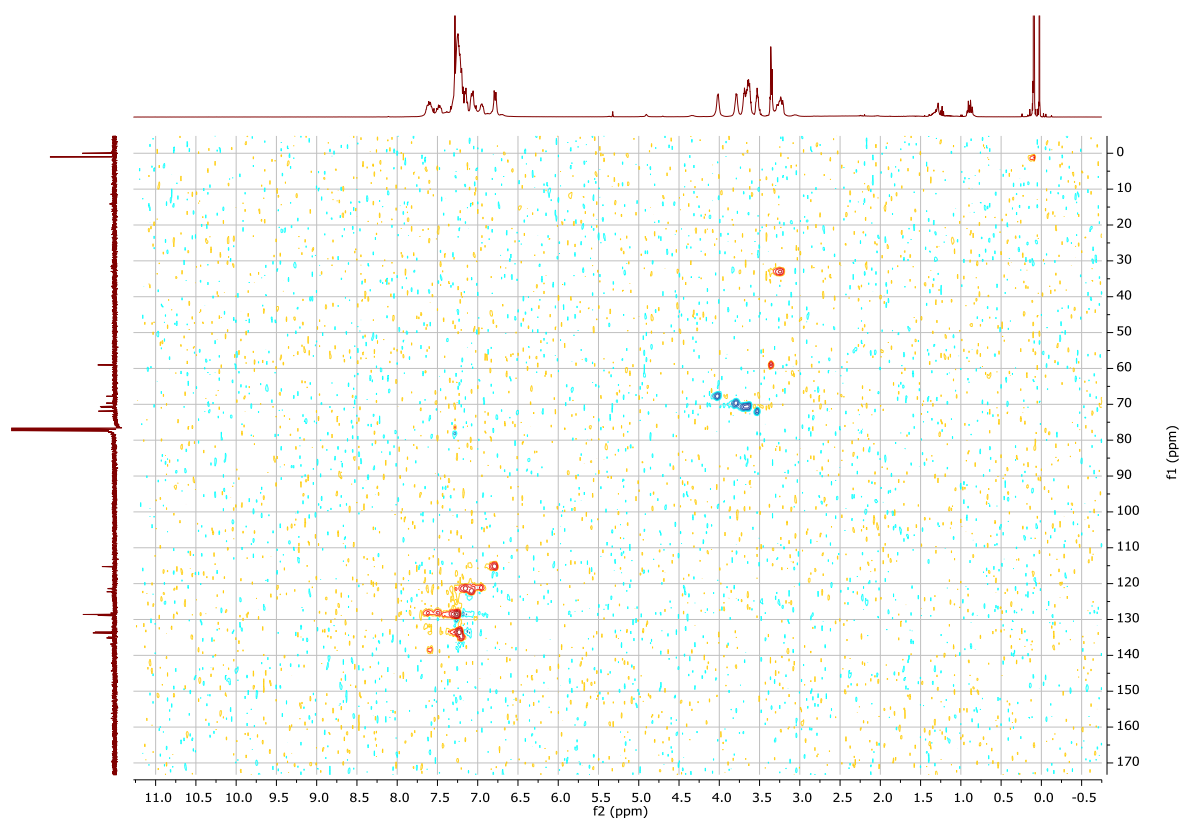
Figure S148. ^{1}H-^{13}C{^{1}H} HSQC spectrum of **171-[G$_1$][G$_1$]-PEG** in CDCl$_3$ recorded at room temperature (400 MHz, 101 MHz).
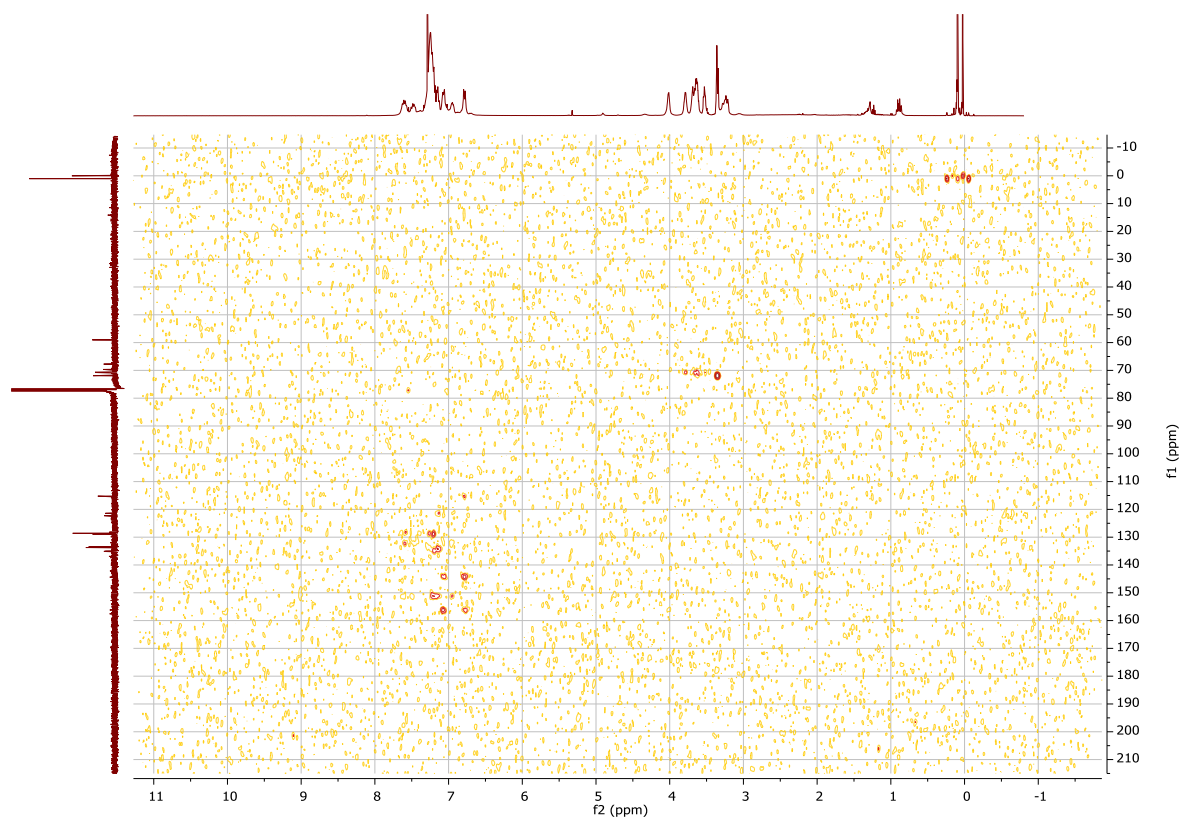
Figure S149. ^{1}H-^{13}C{^{1}H} HMBC spectrum of **171-[G$_1$][G$_1$]-PEG** in CDCl$_3$ recorded at room temperature (400 MHz, 101 MHz).
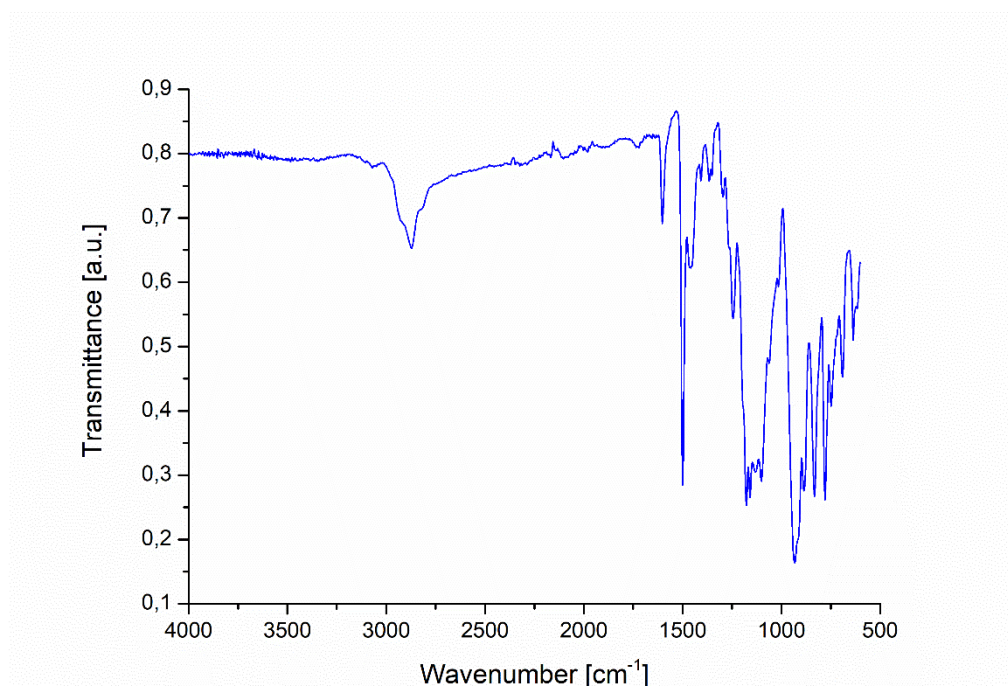
Figure S150. FT-IR spectrum of **171-[G₁][G₁]-PEG.**

7.5. Dendrimer 173-Ru@[G₁][G₁]-PEG
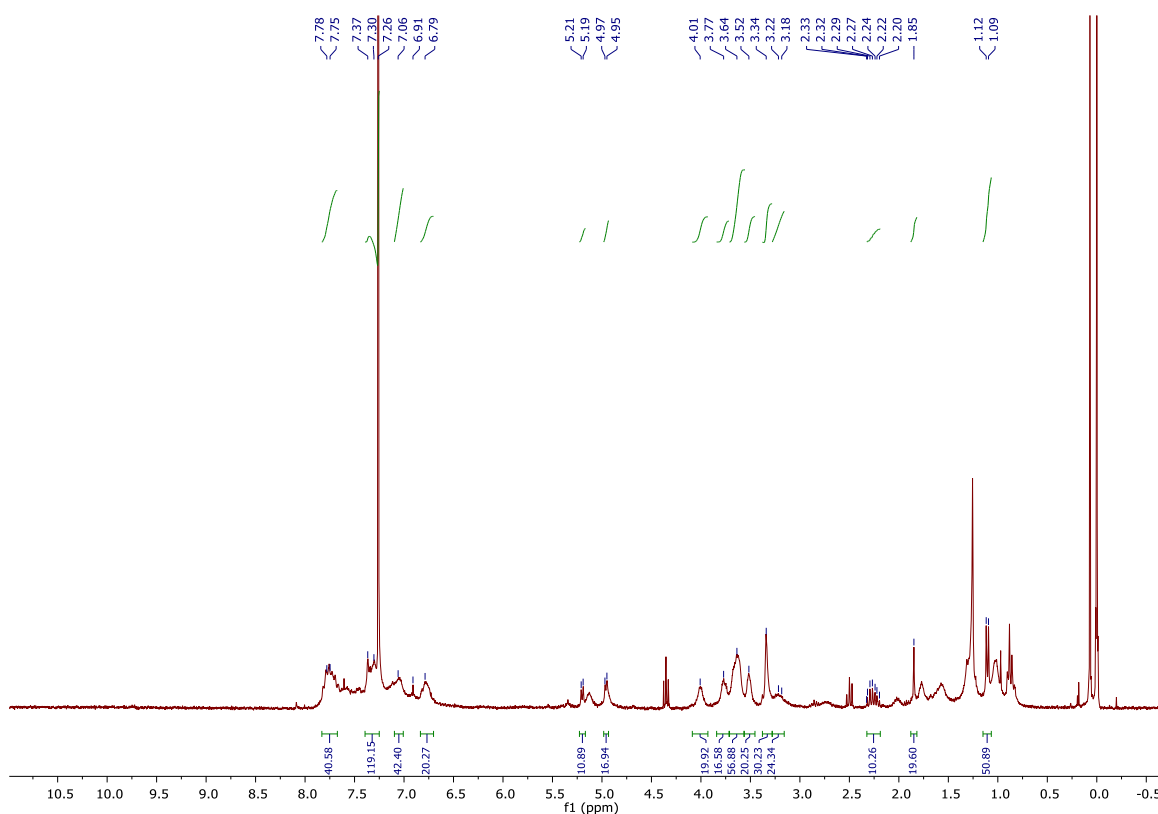
Figure S151. ¹H NMR spectrum of **173-Ru@[G₁][G₁]-PEG** in CDCl₃ recorded at room temperature (400 MHz).
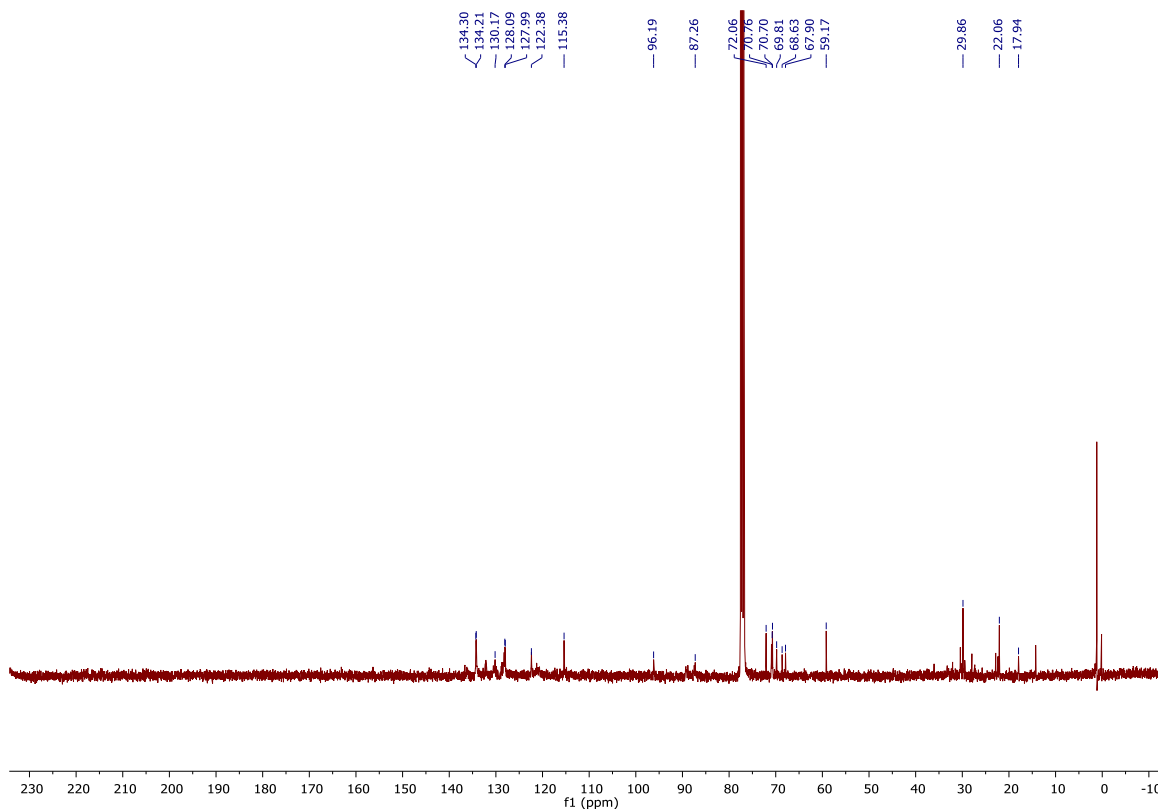
Figure S152. ¹³C{¹H} NMR spectrum of **173-Ru@[G₁][G₁]-PEG** in CDCl₃ recorded at room temperature (101 MHz).
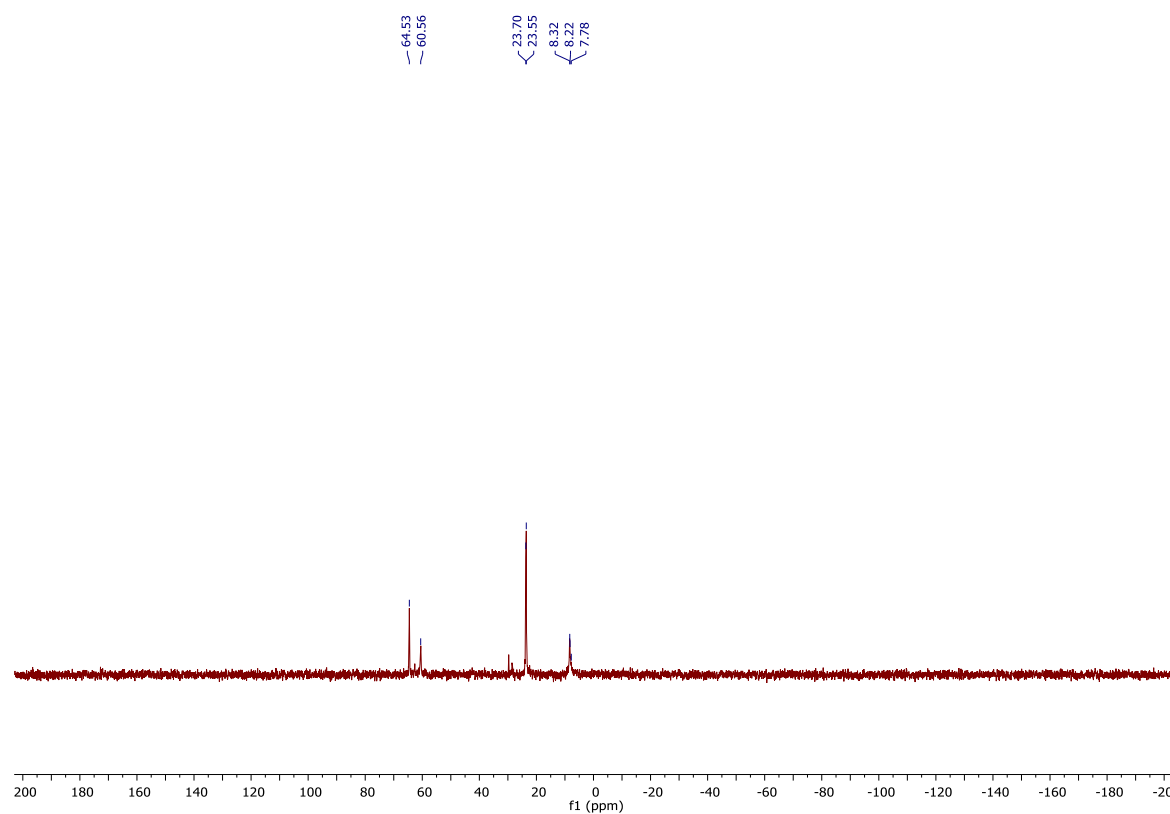
Figure S153. $^{31}P\{^1H\}$ NMR spectrum of **173-Ru@[G$_1$][G$_1$]-PEG** in CDCl$_3$ recorded at room temperature (162 MHz).
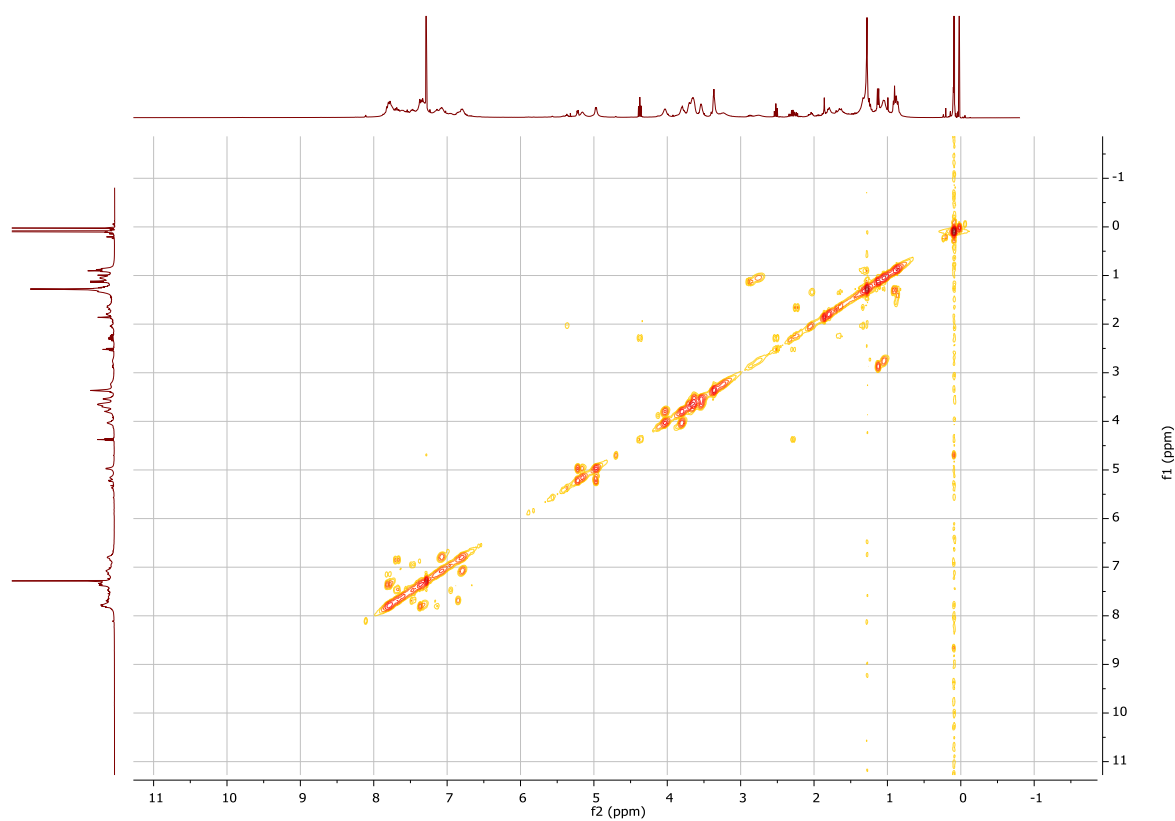
Figure S154. ^1H-^1H COSY spectrum of **173-Ru@[G$_1$][G$_1$]-PEG** in CDCl$_3$ recorded at room temperature (400 MHz).
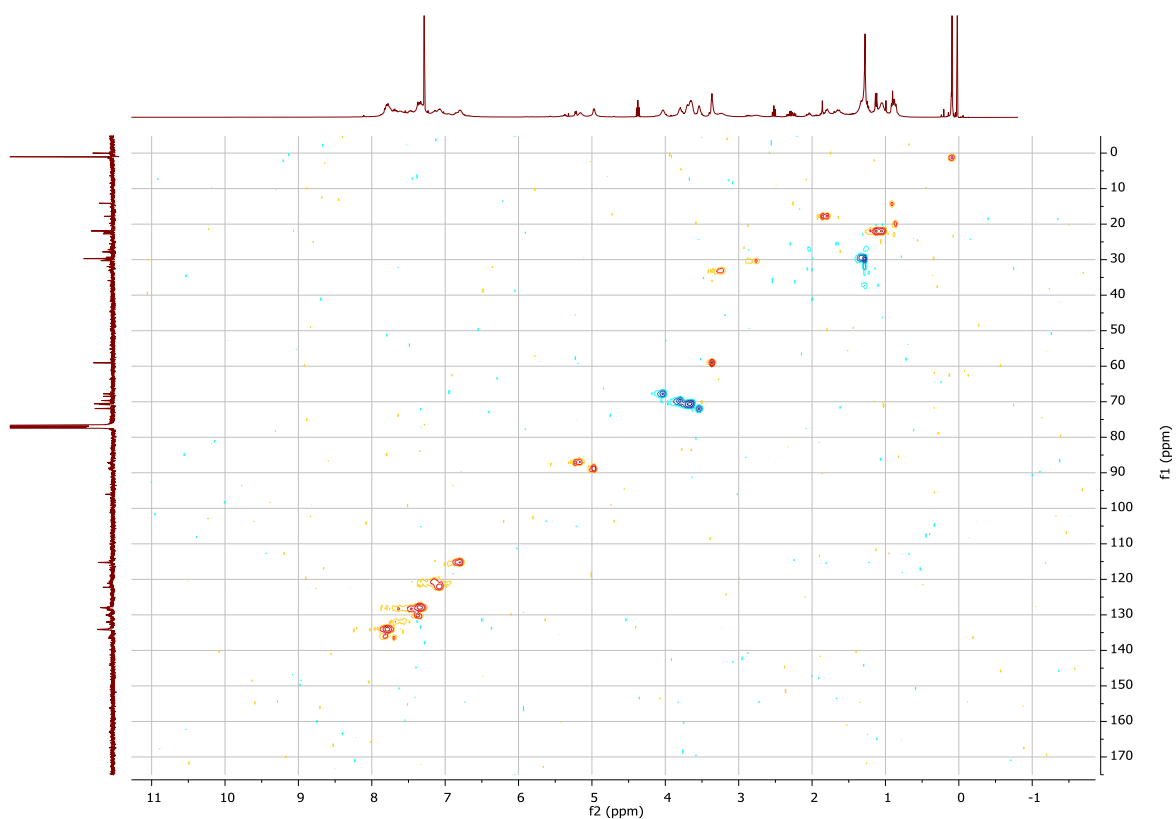
Figure S155. ^{1}H-^{13}C{^{1}H} HSQC spectrum of **173-Ru@[G$_1$][G$_1$]-PEG** in CDCl$_3$ recorded at room temperature (400 MHz, 101 MHz).
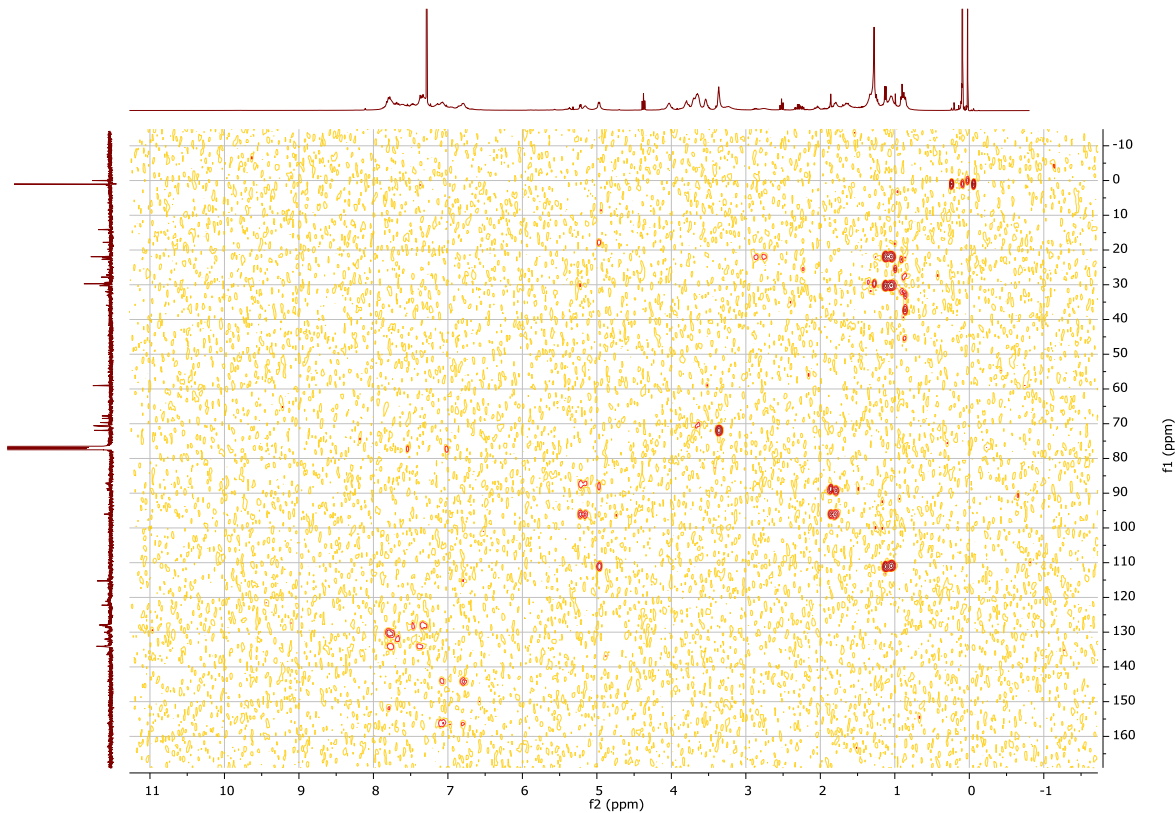
Figure S156. ^{1}H-^{13}C{^{1}H} HMBC spectrum of **173-Ru@[G$_1$][G$_1$]-PEG** in CDCl$_3$ recorded at room temperature (400 MHz, 101 MHz).
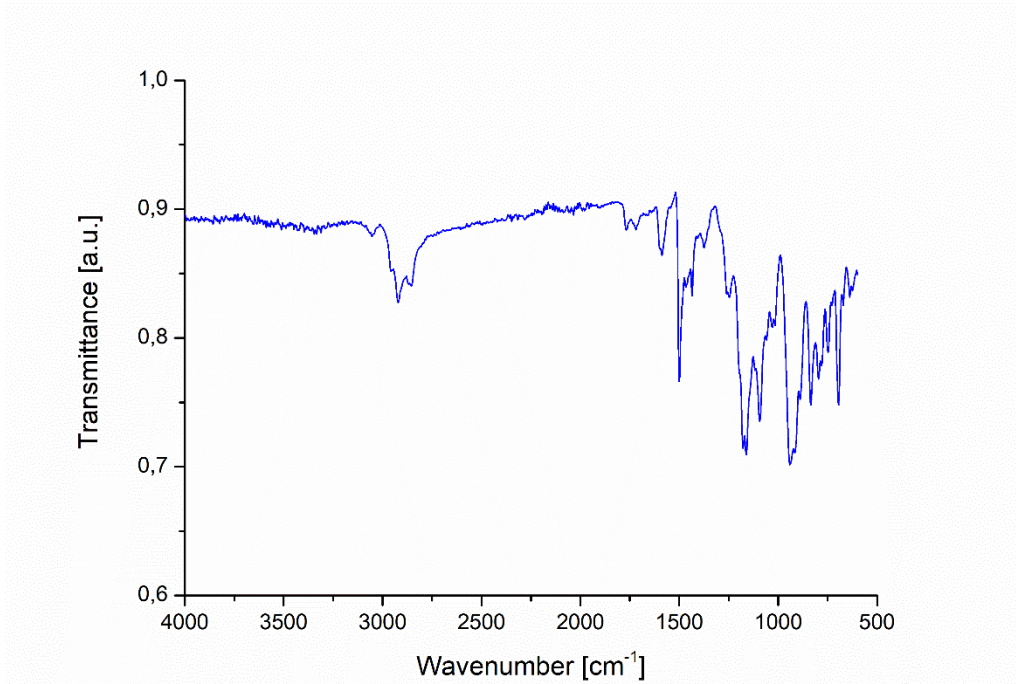
Figure S157. FT-IR spectrum of **173-Ru@[G₁][G₁]-PEG**.

Codi SAQ	Ref. mostra	%C	%H	%N	%S
23AE038/024	JCS-201	54,37	5,50	2,69	2,24

Figure S158. Elemental analysis of **173-Ru@[G₁][G₁]-PEG**.

Mostra	Codi SAQ	Ru (% (p/p))	%rsd
JCS-201	23EAt095/001	9,1	--

Figure S159. ICP analysis of **173-Ru@[G₁][G₁]-PEG**.

7.6. Diphenyl(4-methoxyphenyl)phosphine 175
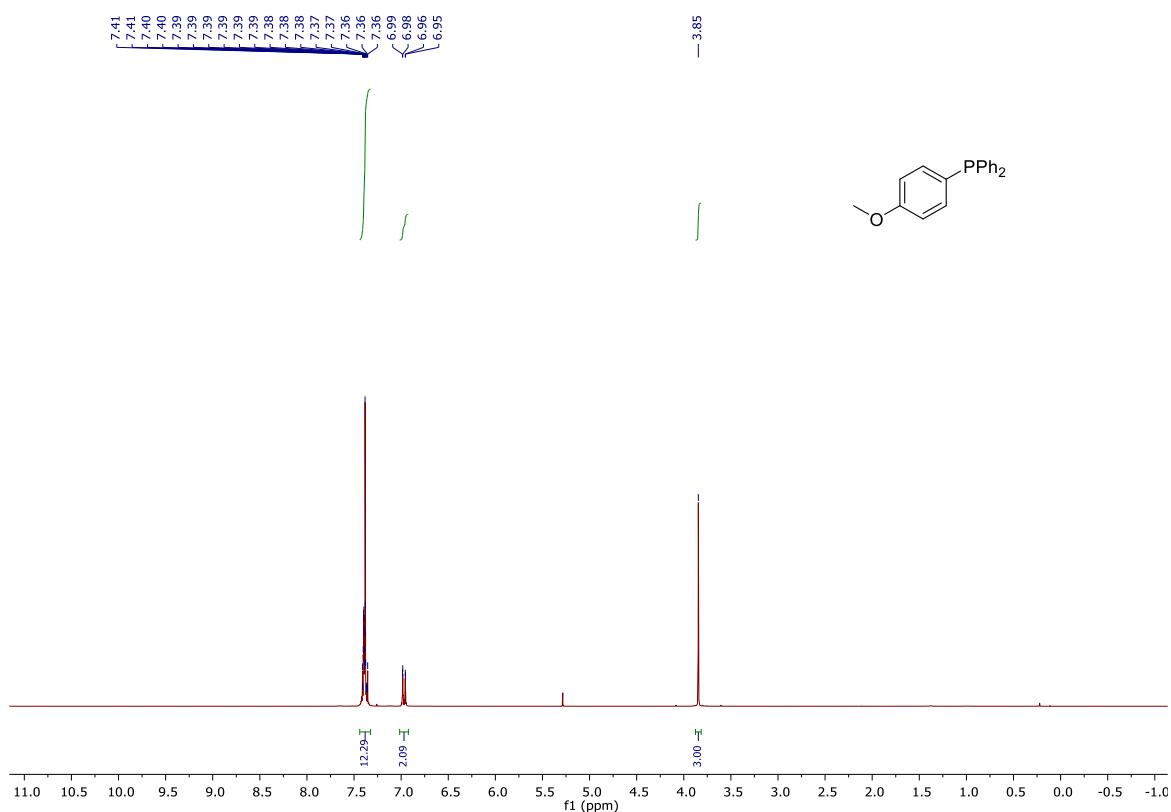
Figure S160. ¹H NMR spectrum of (4-((*tert*-butyldimethylsilyl)oxy)phenyl)diphenylphosphane **175** in CDCl₃ recorded at room temperature (400 MHz).
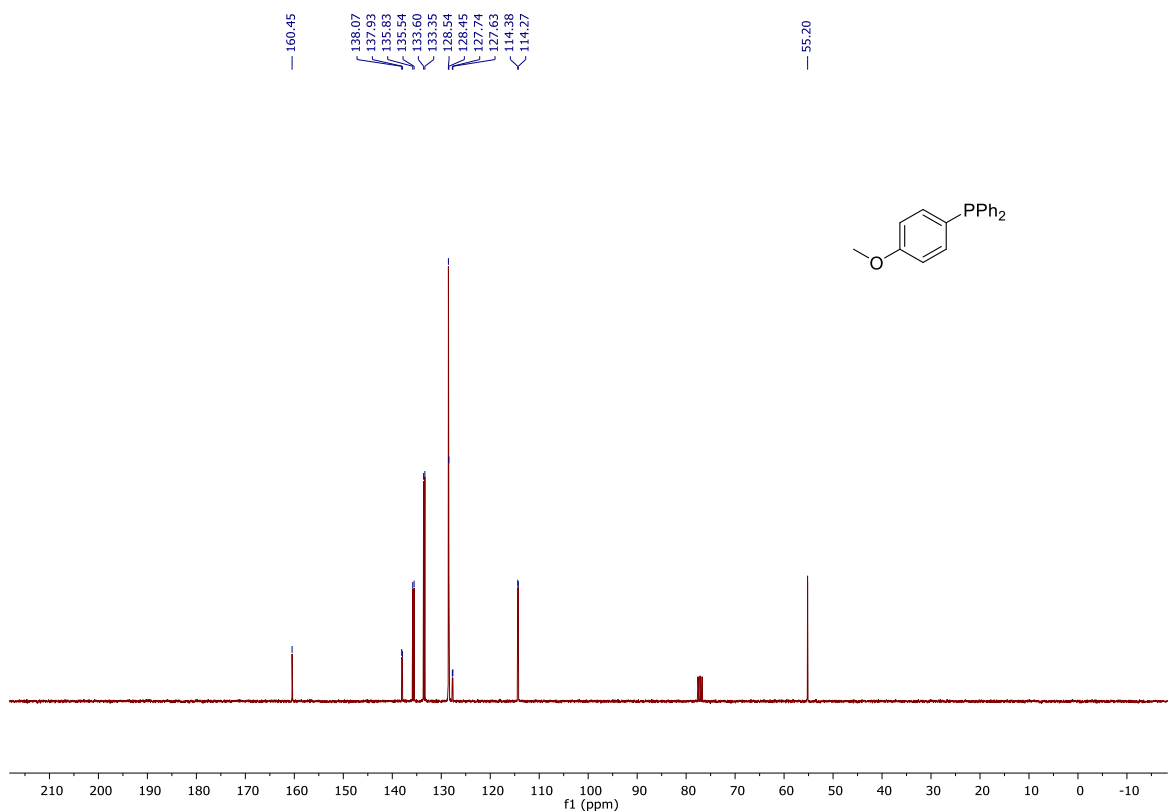
Figure S161. ¹³C{¹H} NMR spectrum of (4-((*tert*-butyldimethylsilyl)oxy)phenyl)diphenylphosphane **175** in CDCl₃ recorded at room temperature (101 MHz).
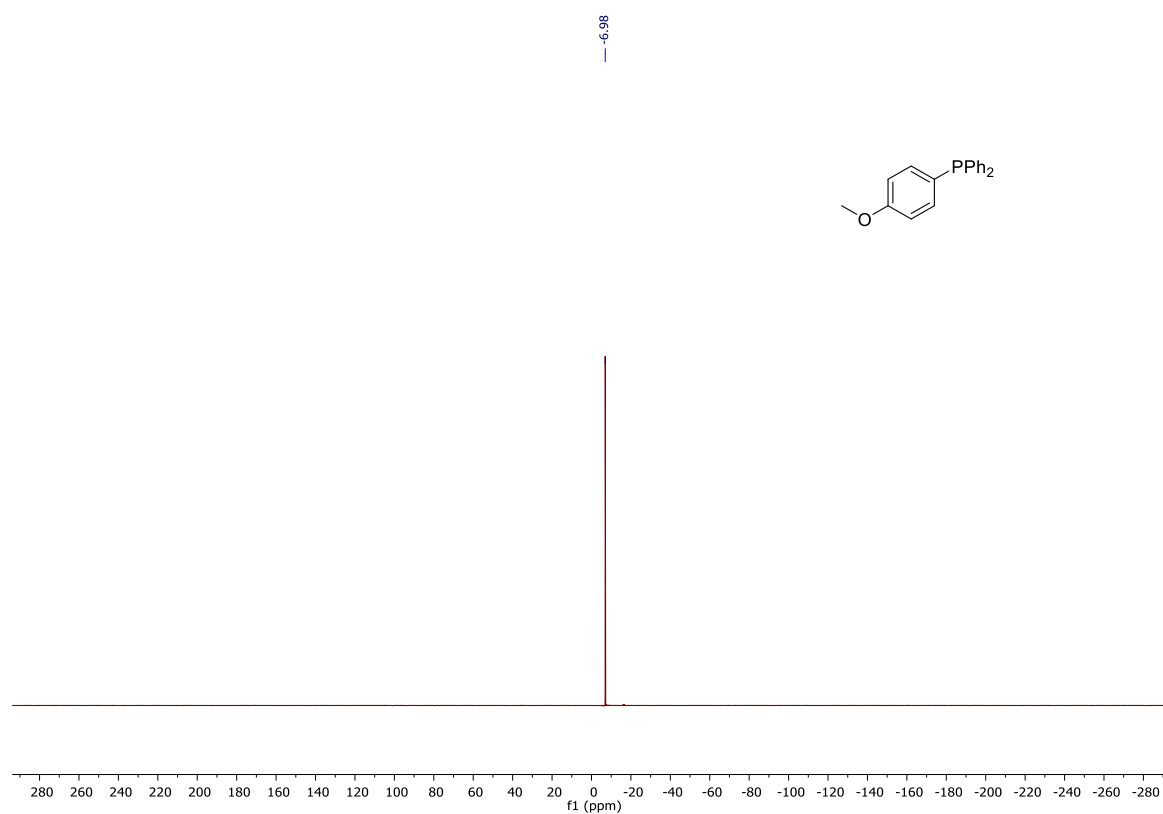
Figure S162. ^{31}P{^{1}H} NMR spectrum of (4-((*tert*-butyldimethylsilyl)oxy)phenyl)diphenylphosphane **175** in CDCl$_3$ recorded at room temperature (161 MHz).

7.7. Ru43
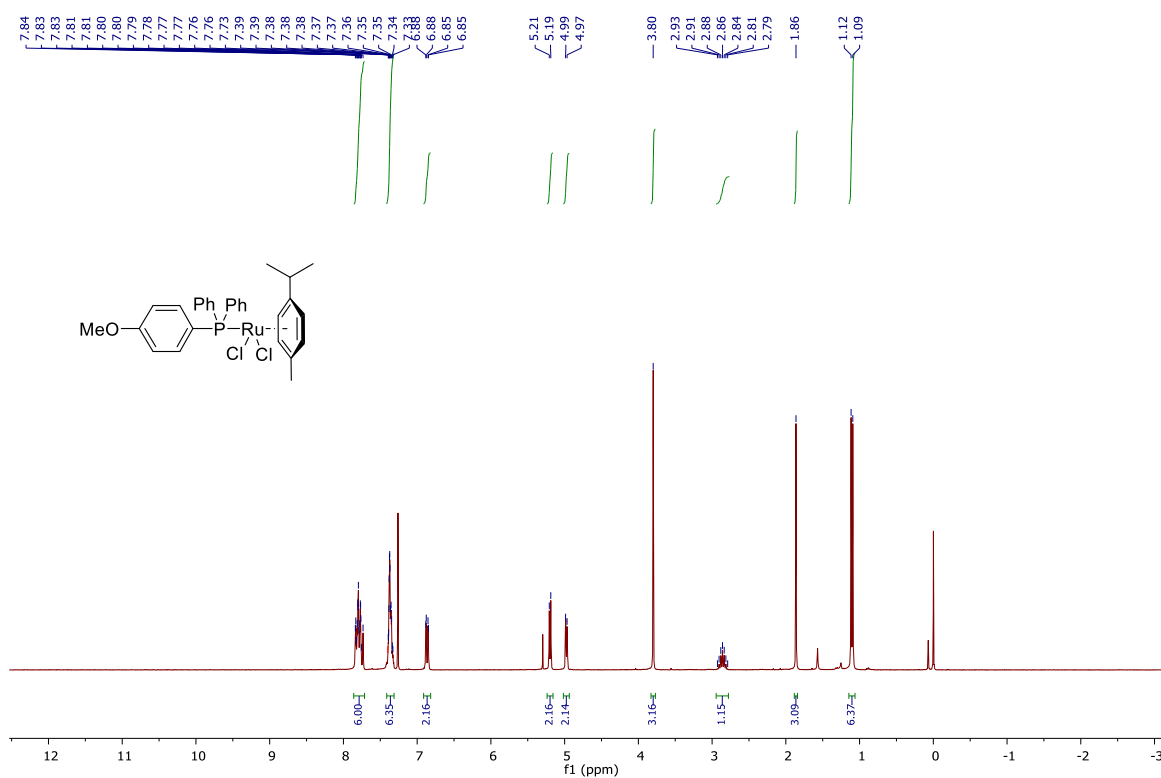
Figure S163. ¹H NMR spectrum of **Ru43** in CDCl₃ recorded at room temperature (400 MHz).
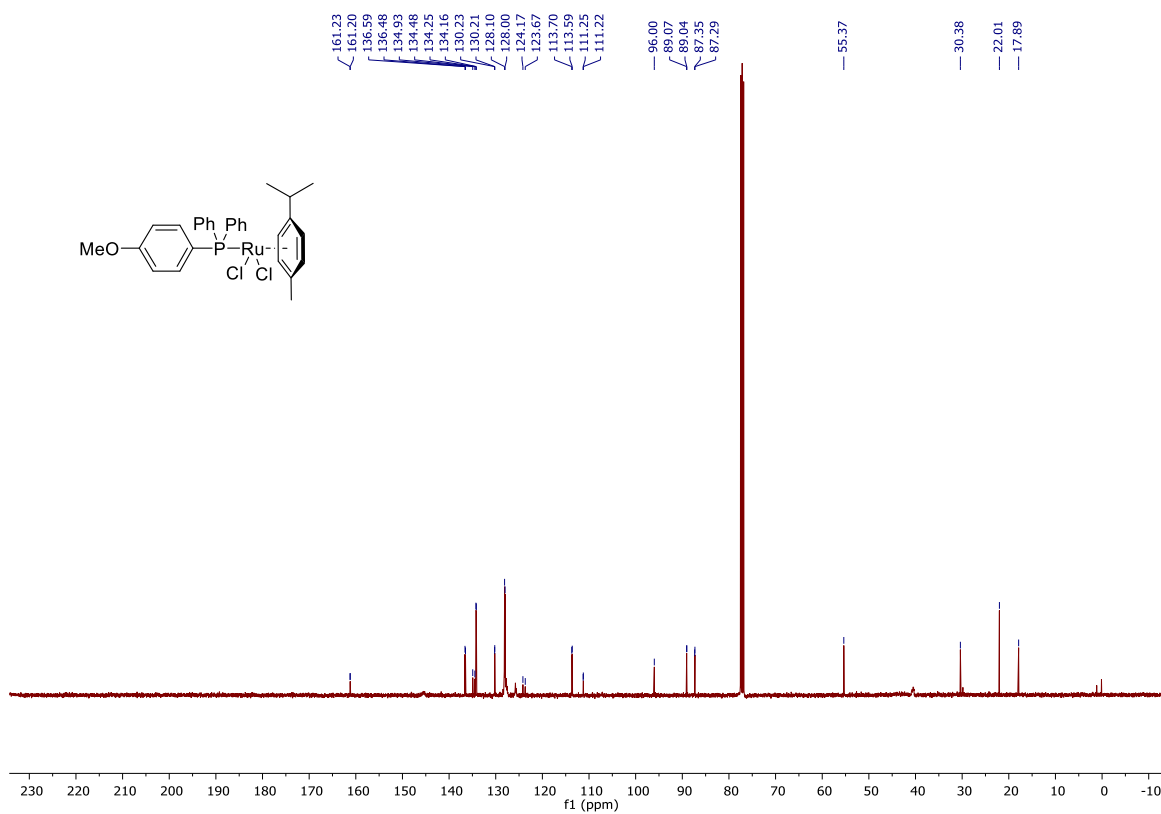
Figure S164. ¹³C{¹H} NMR spectrum of **Ru43** in CDCl₃ recorded at room temperature (101 MHz).
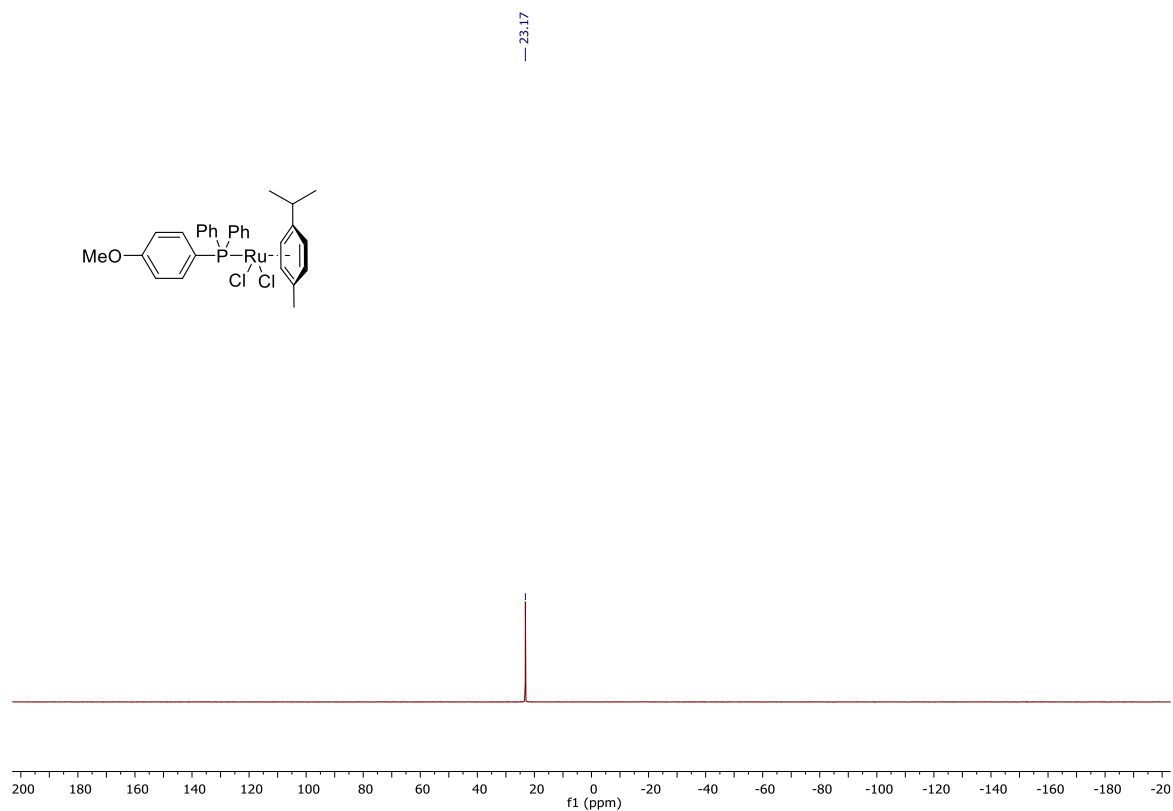
Figure S165. $^{31}P\{^1H\}$ NMR spectrum of **Ru43** in CDCl$_3$ recorded at room temperature (162 MHz).
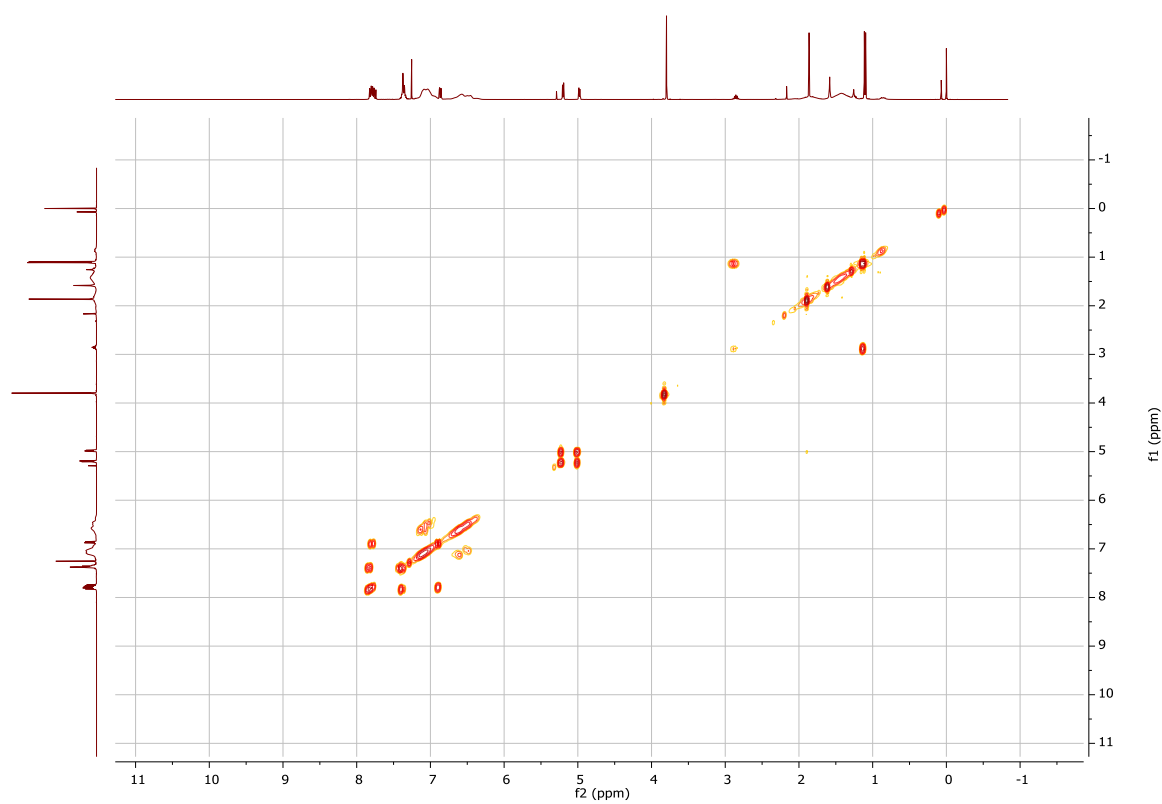
Figure S166. ^1H-^1H COSY spectrum of **Ru43** recorded in CDCl$_3$ at room temperature (400 MHz).
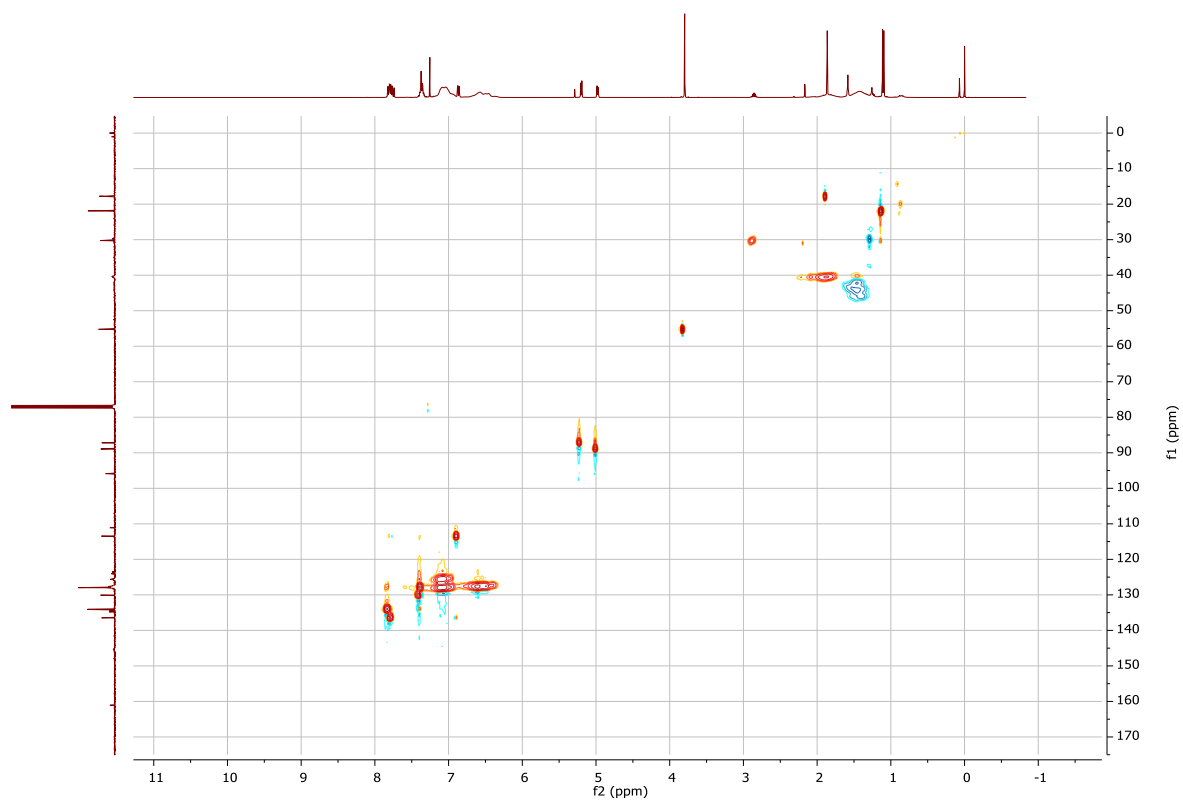
Figure S167. ^{1}H-^{13}C{^{1}H} HSQC spectrum of **Ru43** recorded in CDCl$_3$ at room temperature (400 MHz, 101 MHz).
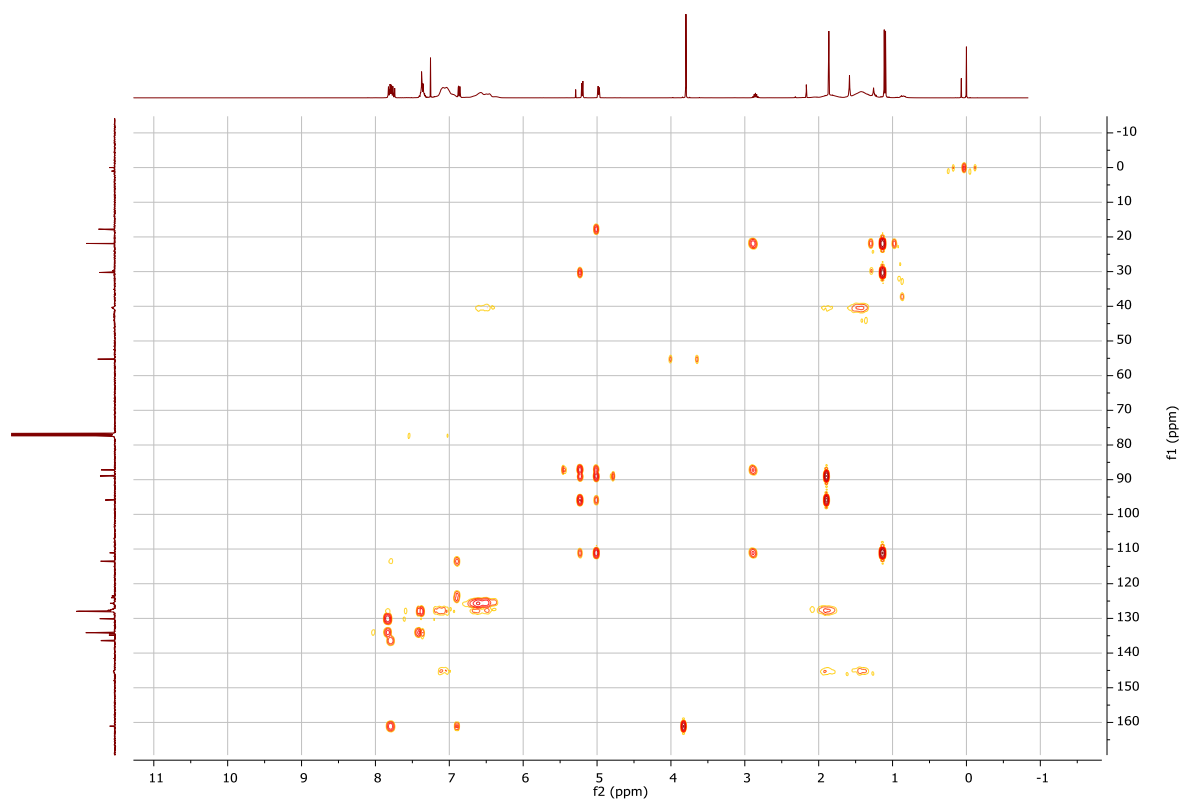
Figure S168. ^{1}H-^{13}C{^{1}H} HMBC spectrum of **Ru43** recorded in CDCl$_3$ at room temperature (400 MHz, 101 MHz).
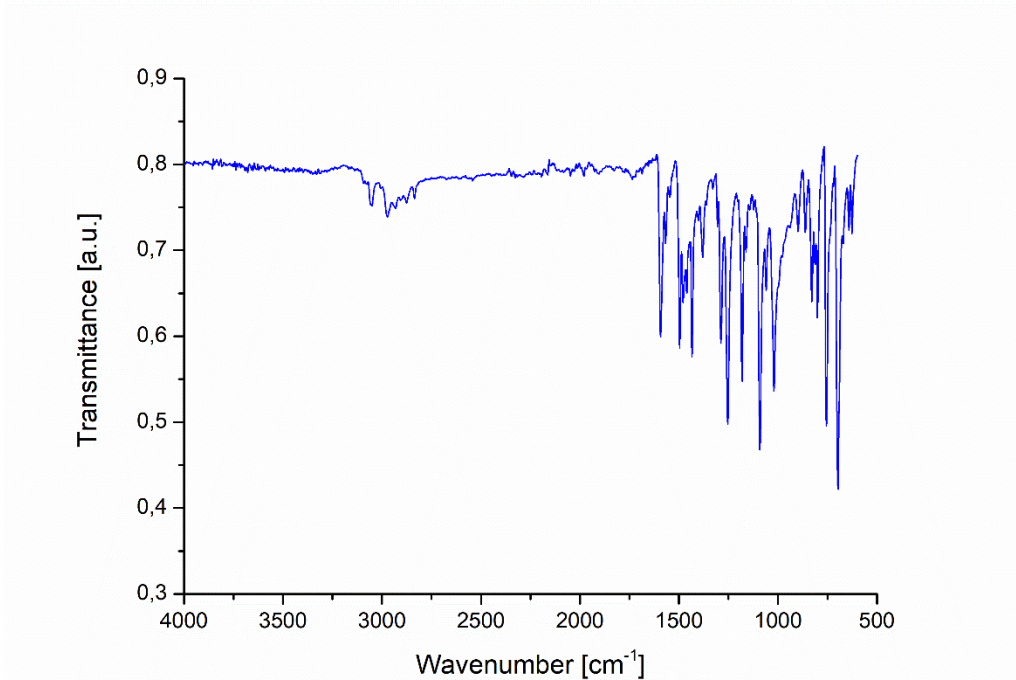
Figure S169. FT-IR spectrum of **Ru43**.

Meas. m/z	#	Ion Formula	err [mDa]	err [ppm]	mSigma
563.084629	1	C29H31ClOPRu	-0.2	-0.4	8.1
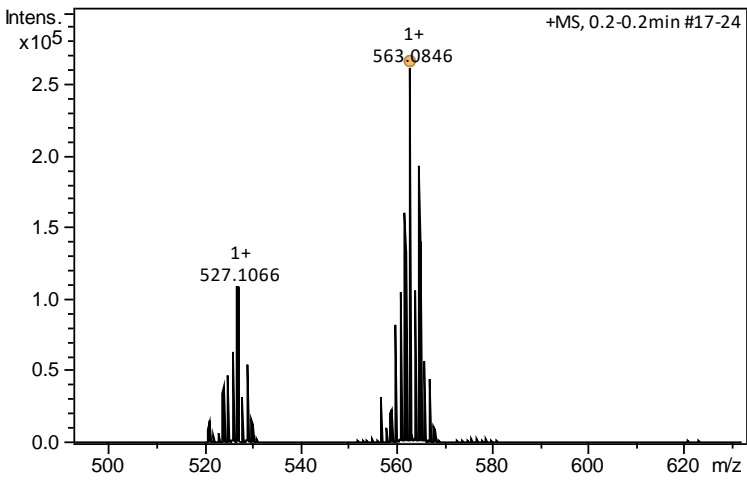
Figure S170. HRMS of **Ru43**.

Codi SAQ	Ref. mostra	%C	%H	%N	%S
23AE038/022	JCS-210	55,65	5,05	<0.1	<0.1

Figure S171. Elemental analysis of **Ru43**.

7.8.   *O,O*-bis(4-(diphenylphosphanyl)phenyl)(2-benzylidene-1-methyl-hydrazineyl)phosphonothioate 176
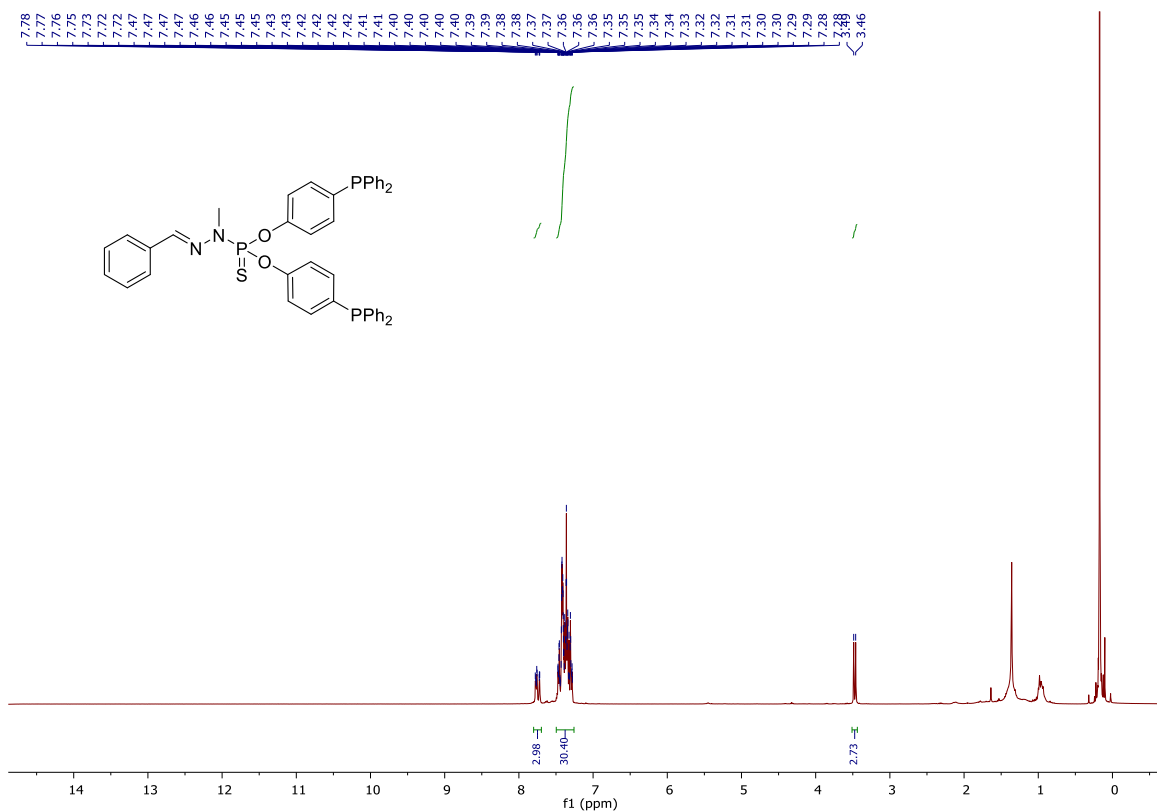
Figure S172. ¹H NMR spectrum of compound *O,O*-bis(4-(diphenylphosphanyl)phenyl)(2-benzylidene-1-methyl-hydrazineyl)phosphonothioate **176** in CDCl₃ recorded at room temperature (400 MHz).
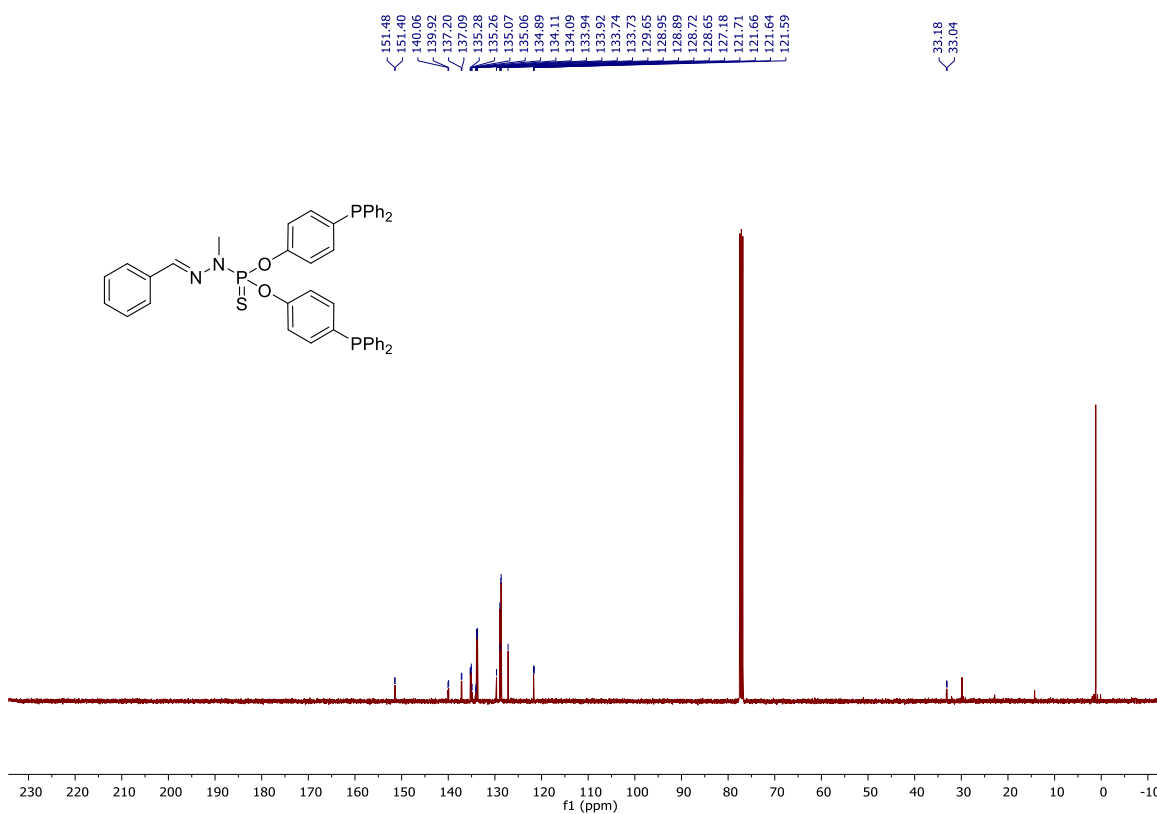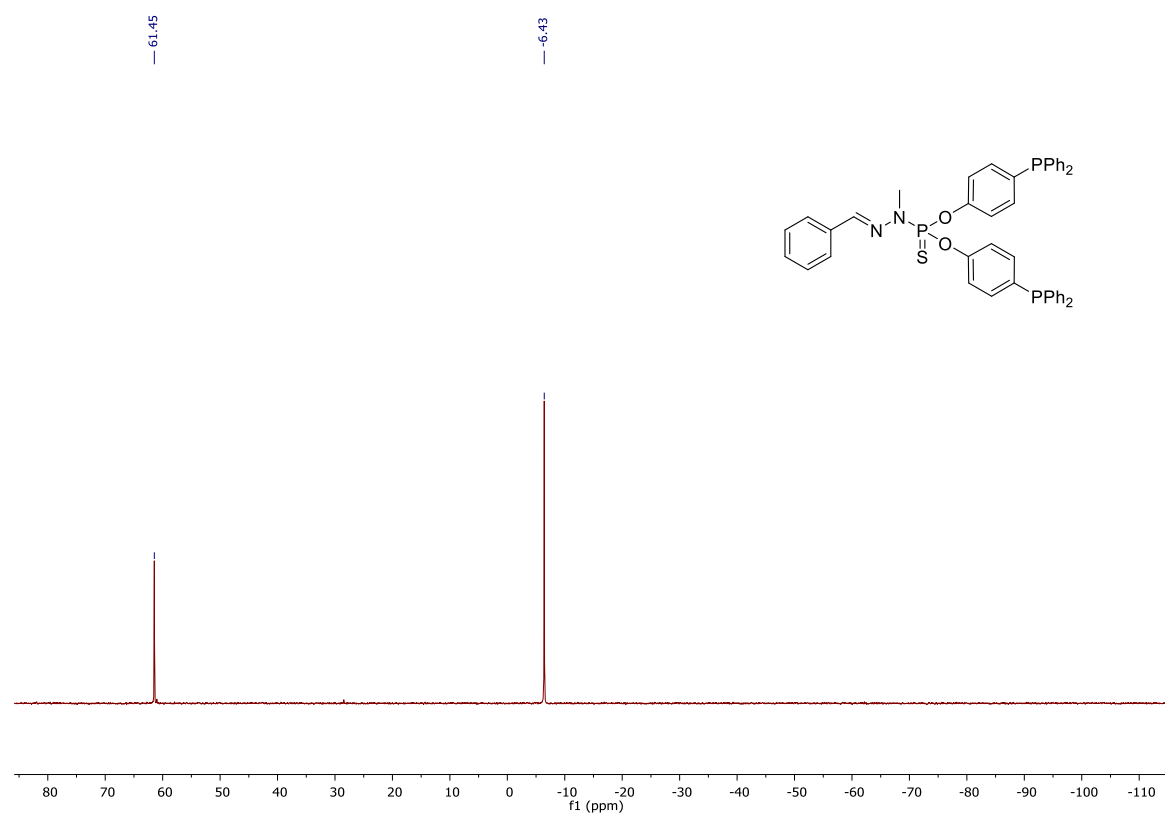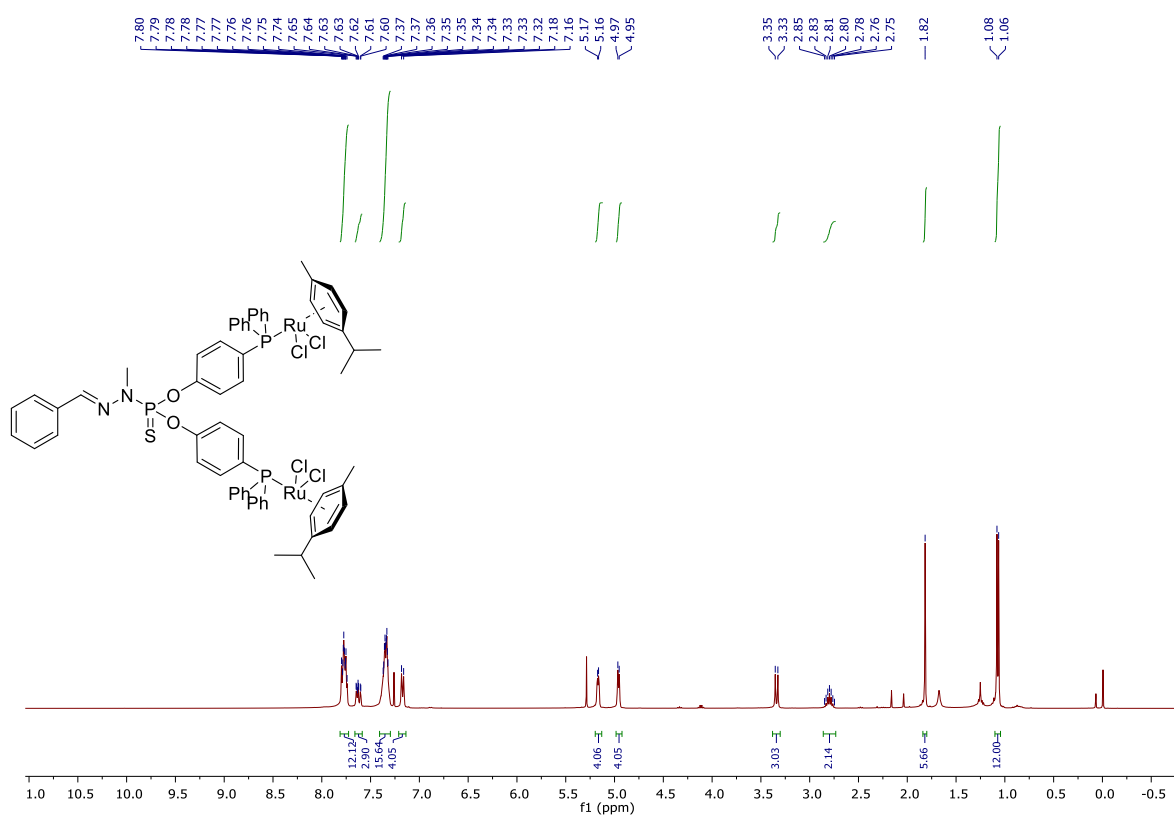

Figure S173. ¹³C{¹H} NMR spectrum of *O,O*-bis(4-(diphenylphosphanyl)phenyl)(2-benzylidene-1-methyl-hydrazineyl)phosphonothioate **176** in CDCl₃ recorded at room temperature (101 MHz).

Figure S174. $^{31}P\{^1H\}$ NMR spectrum of *O,O*-bis(4-(diphenylphosphanyl)phenyl)(2-benzylidene-1-methylhydrazineyl)phosphonothioate **176** in CDCl$_3$ recorded at room temperature (162 MHz).

7.9. Ru44

Figure S175. ^{1}H NMR spectrum of **Ru44** in CDCl$_3$ recorded at room temperature (400 MHz).
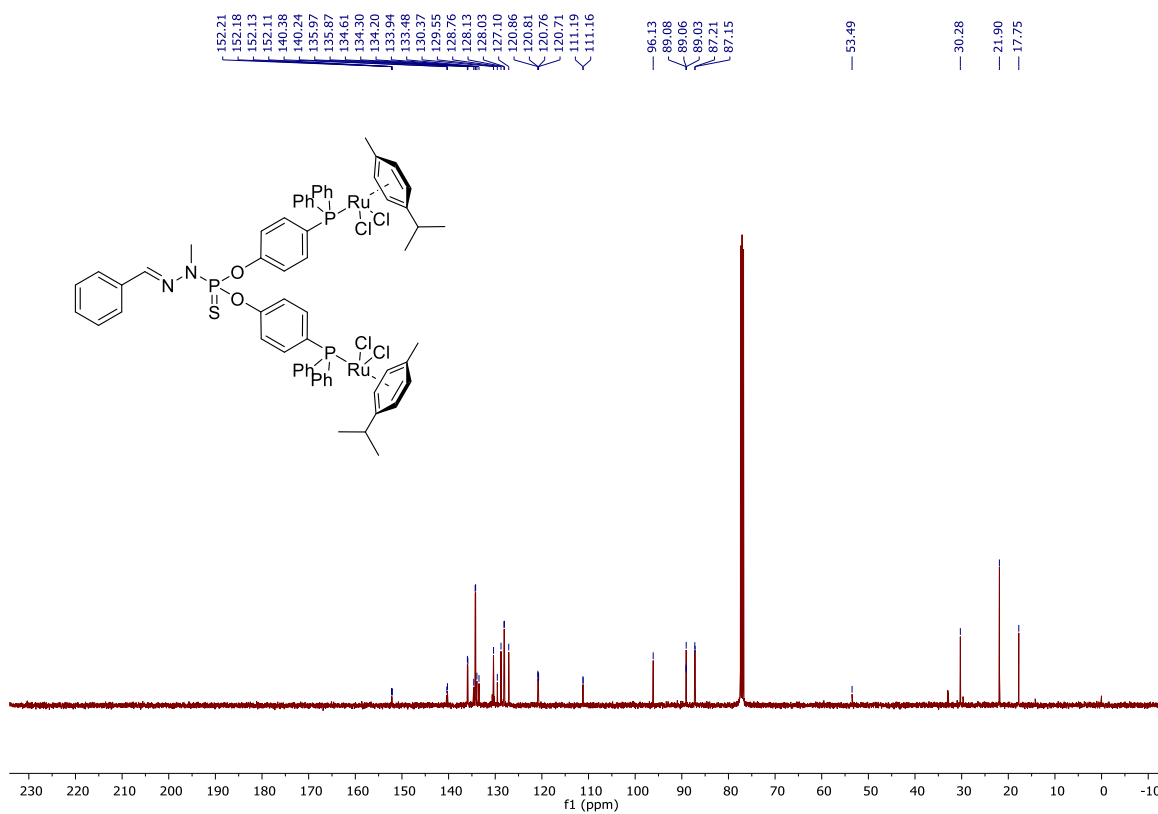

Figure S176. ^{13}C{^{1}H} NMR spectrum of **Ru44** in CDCl$_3$ recorded at room temperature (101 MHz).
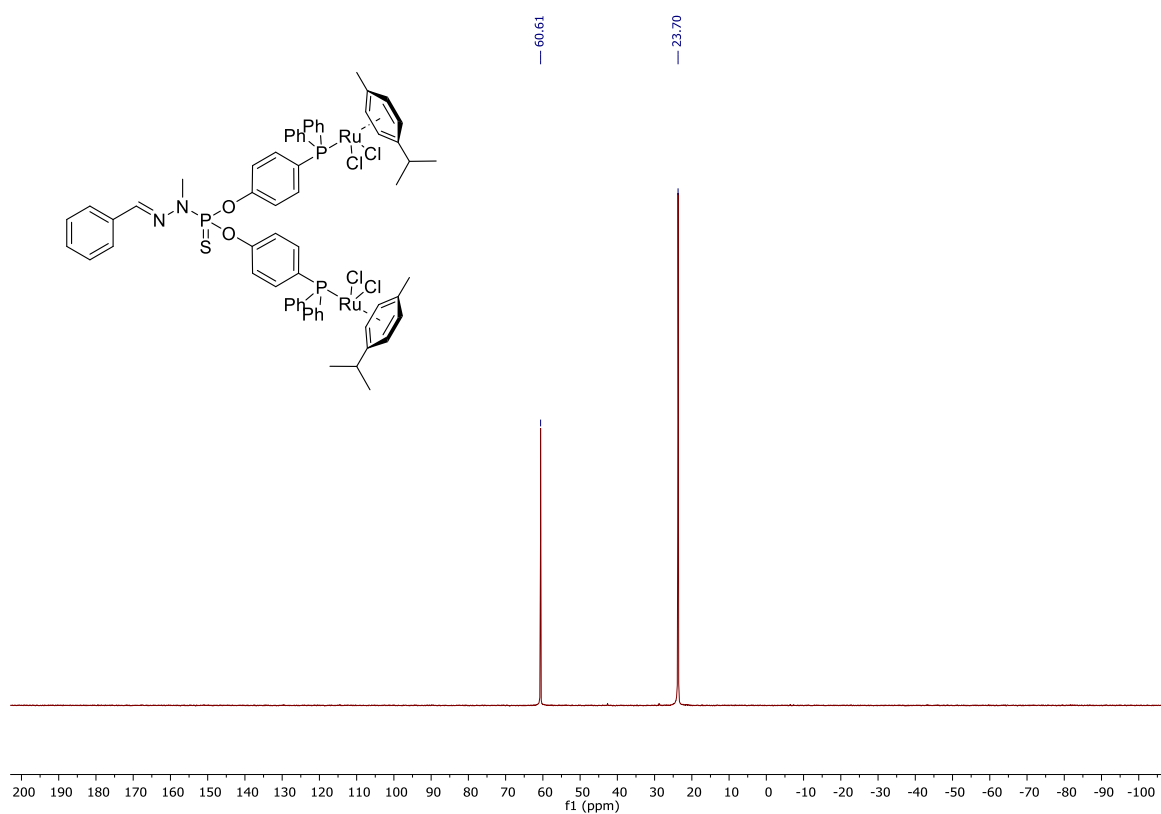
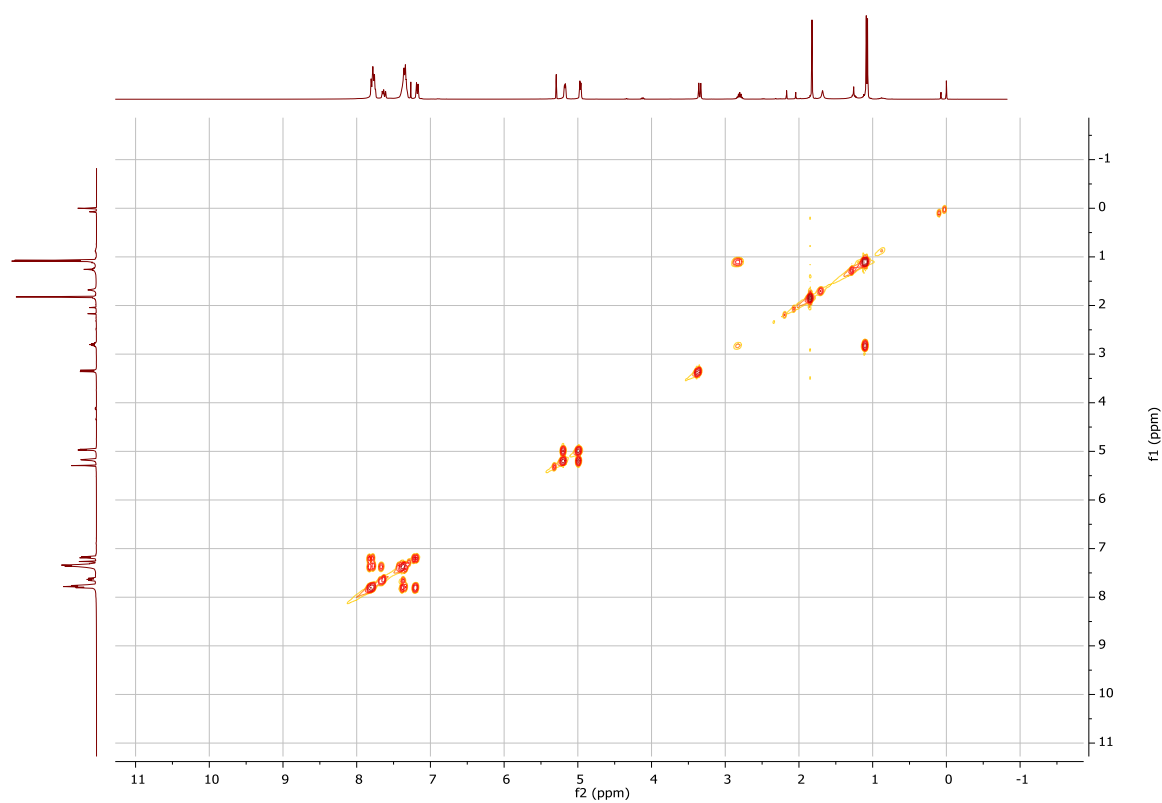**Figure S177**. $^{31}P\{^1H\}$ NMR spectrum of **Ru44** in $CDCl_3$ recorded at room temperature (162 MHz).

Figure S178. ^1H-^1H COSY spectrum of **Ru44** in $CDCl_3$ recorded at room temperature (400 MHz).
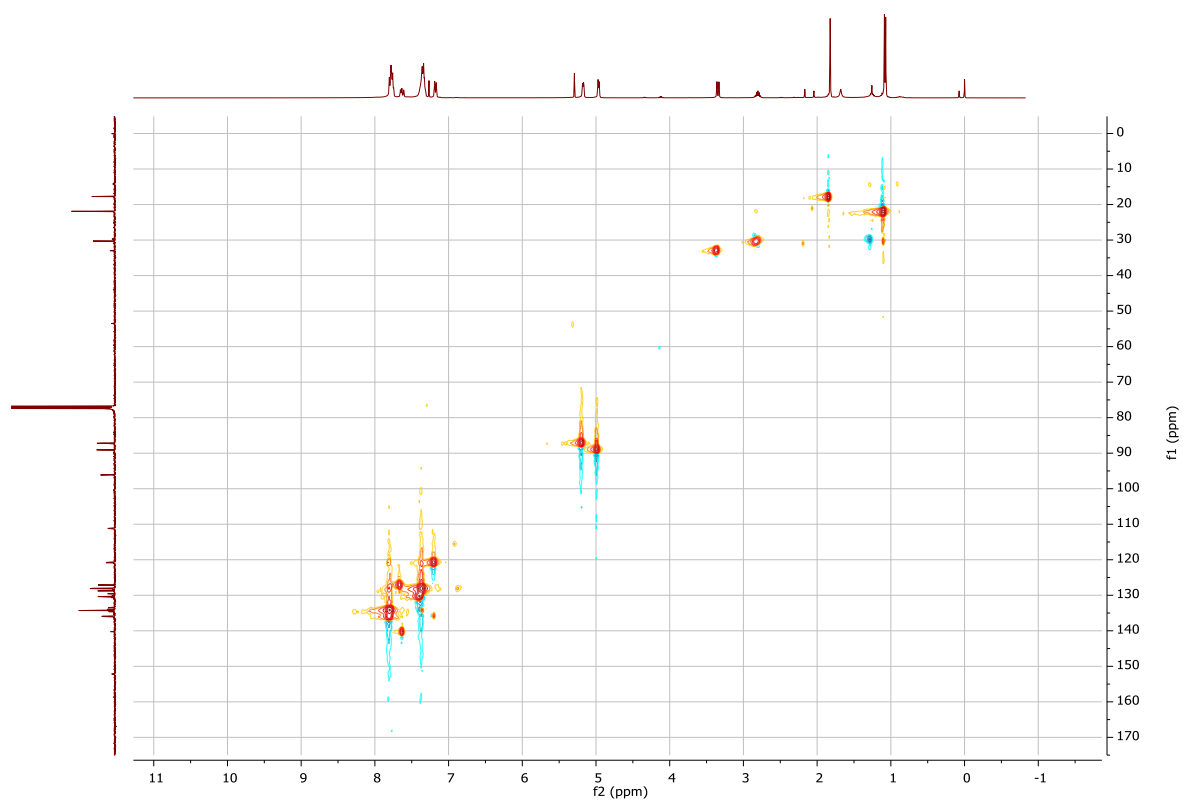
Figure S179. ^{1}H-^{13}C{^{1}H} HSQC spectrum of **Ru44** in CDCl$_3$ recorded at room temperature (400 MHz, 101 MHz).
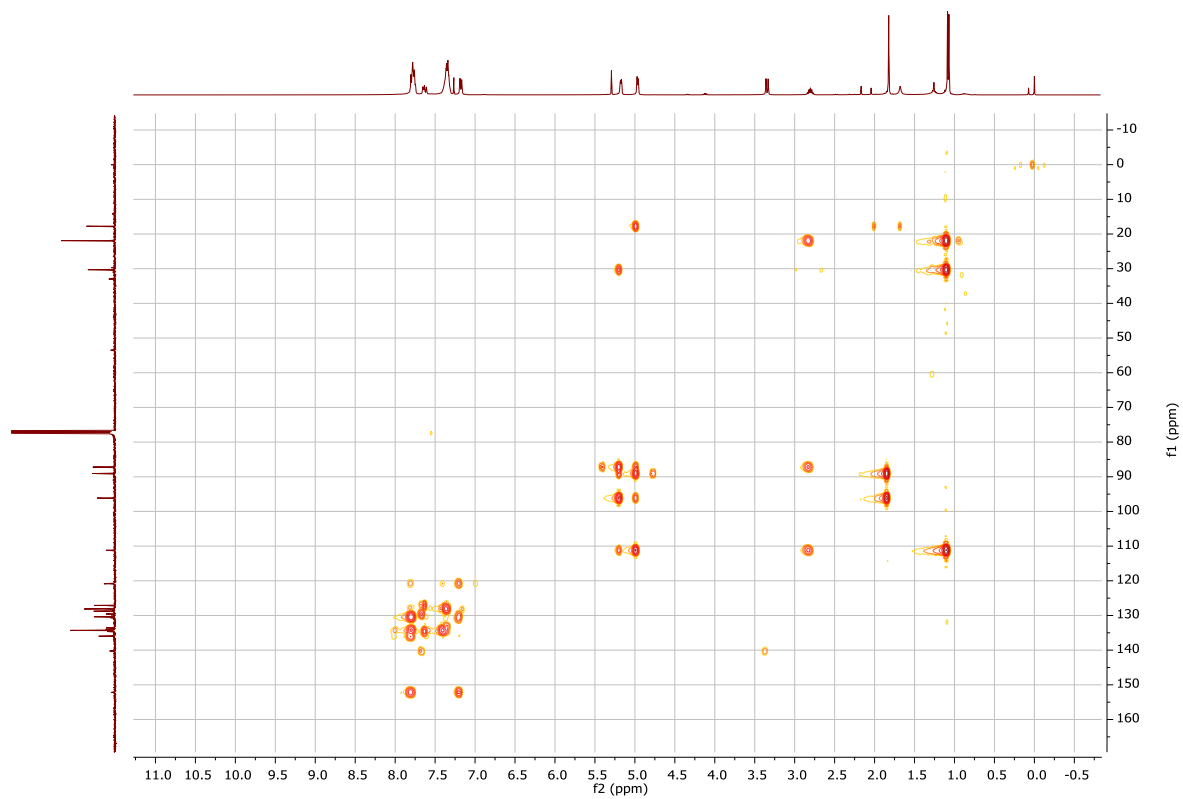

Figure S180. ^{1}H-^{13}C{^{1}H} HMBC spectrum of **Ru44** in CDCl$_3$ recorded at room temperature (400 MHz, 101 MHz).

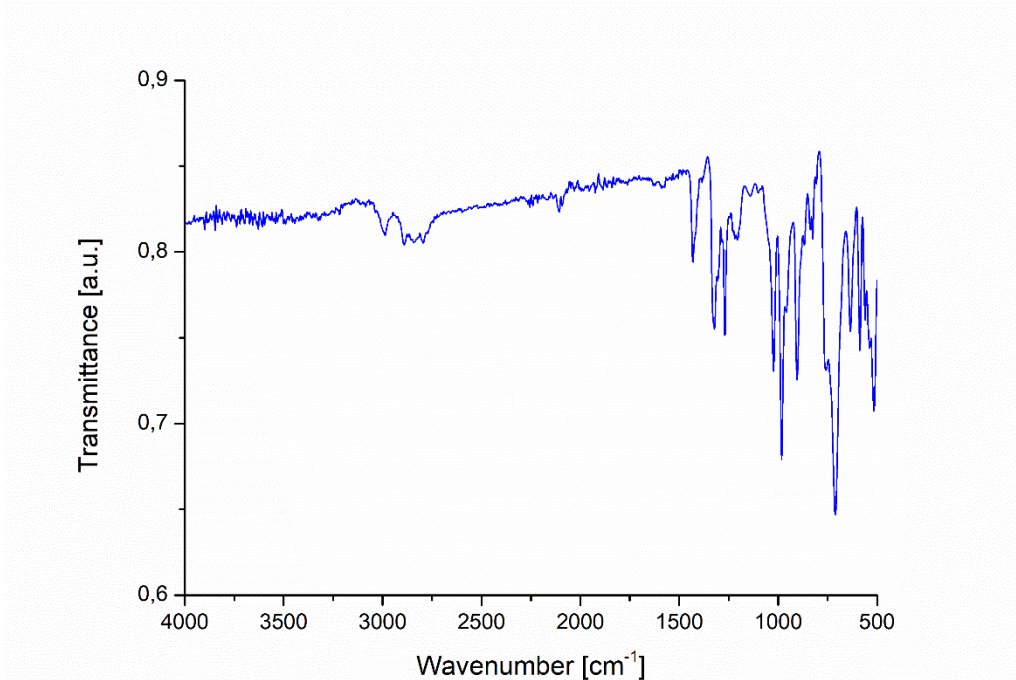**Figure S181**. FT-IR spectrum of **Ru44**.

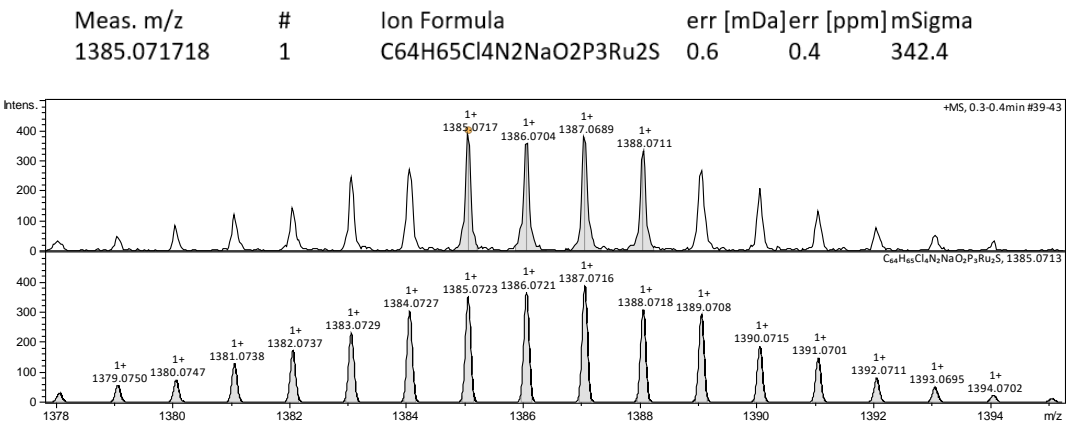| Meas. m/z	#	Ion Formula	err [mDa]	err [ppm]	mSigma
1385.071718	1	C64H65Cl4N2NaO2P3Ru2S	0.6	0.4	342.4

Figure S182. HRMS of **Ru44**.

Codi SAQ	Ref. mostra	%C	%H	%N	%S
23AE038/023	JCS-207	52,04	4,61	1,59	1,89

Figure S183. Elemental analysis of **Ru44**.